Environmental
Studies
Revolving
Funds

065

# Proceedings of the International Workshop on Wave Hindcasting and Forecasting

Canada

March 1987

The Environmental Studies Revolving Funds are financed from special levies on the oil and gas industry and administered by the Canada Oil and Gas Lands Administration for the Minister of Energy, Mines and Resources, and by the Northern Affairs Program for the Minister of Indian Affairs and Northern Development.

Environmental Studies Revolving Funds

Report No. 065

February 1987

# PROCEEDINGS OF THE INTERNATIONAL WORKSHOP ON WAVE HINDCASTING AND FORECASTING

**HALIFAX, NOVA SCOTIA**

**SEPTEMBER 23-26, 1986**

LeDrew Environmental Management Ltd.
158 Water Street
St. John's, Nfld.

Scientific Advisor: V.R. Swail

The correct citation for this report is:

Proceedings of the International Workshop on Wave Hindcasting and Forecasting, Halifax, Nova Scotia, September 23-26, 1986. Environmental Studies Revolving Funds, Report Series No. 065. Ottawa. 370 p.

Published under the auspices of the

Environmental Studies Revolving Funds

ISBN 0-920783-64-3

## WORKSHOP ORGANIZING COMMITTEE

Val R. Swail, Chairman
Atmospheric Environment Service

Volker Barthel
National Research Council

Michael E. Coolen
Mobil Oil Canada Ltd.

G. Ken Sato
Canada Oil and Gas Lands Administration

J. Ron Wilson
Fisheries and Oceans Canada

Brian Wright
Gulf Canada Resources Inc.

## WORKSHOP SPONSOR

Environmental Studies Revolving Funds

## AUTHOR INDEX

## TABLE OF CONTENTS

**ACKNOWLEDGEMENTS**

The organizers are indebted to many people who contributed to the successful completion of the workshop. Our gratitude is extended to the Bedford Institute of Oceanography for making their facility available to participants. Many people from that Institute helped in the smooth operation of the various sessions, and particular note is made of the assistance received from Ms. Betty Rumley, Mr. Francis Jordan and Mr. Bob Walker. A most interesting after-dinner presentation was made by Mr. Marvin McDill on behalf of Canada's Challenge for America's Cup. The Committee expresses its thanks to all those who served as Session Chairmen and rapporteurs. Our appreciation is extended to the workshop participants who not only diligently attended the heavy schedule of sessions, but also contributed the healthy discussion that is the earmark of success for such a gathering.

## INTRODUCTION

The International Workshop on Wave Hindcasting and Forecasting was held at the Bedford Institute of Oceanography in Dartmouth, Nova Scotia, from September 23 to 26, 1986. The workshop objectives were:

- to review relevant ESRF funded work;
- to exchange information on wave hindcasting/forecasting research; and
- to discuss priorities for future ESRF funding.

The need for this workshop flowed from a number of studies commissioned by the Environmental Studies Revolving Fund (ESRF is a program jointly administered by the Departments of Energy Mines and Resources, and Indian Affairs and Northern Development). These studies addressed industry needs for reliable forecasts and hindcasts in the Canadian offshore. The workshop was planned as a forum to discuss the results obtained from this and other current work with emphasis on establishing priorities for further research.

Papers were solicited from around the world so as to bring together the current knowledge on wave forecasting and hindcasting. The workshop itself was scheduled to permit ample time for discussion following presentations; one half the workshop time was spent in discussion sessions. One evening was laid aside for a poster/display session and five presentations were available for viewing. At the completion of all presentation sessions, the last half day of the workshop was spent in a general consideration of future research needs and priorities. This discussion was stimulated by rapporteurs' presentation of their notes on the earlier sessions.

A total of eighty people from seven countries attended the workshop. In all, thirty-three papers were presented, covering most aspects of wave forecasting and hindcasting, including: measurement, operational forecasting, model development and evaluation, shallow water effects, and theory. The discussion sessions were lively and informative with strong viewpoints freely expressed and debated. By the end of the week, most issues had received thorough consideration and on several topics a consensus emerged as to the direction which research efforts should take.

The following pages contain all but three of the presentations (at the time of publication abstracts only were available for papers B-2, C1-2 and F-5), plus the rapporteurs' session reports and the record of the concluding discussion. The material presented in the poster/display session is included in Appendix 1, while Appendix 2 presents the names and affiliations of all participants.

In summary, the workshop was a notable success, especially in light of the recent downturn in offshore hydrocarbon exploration activity. The discussion generated at the workshop and, in particular, the various recommendations made will, hopefully, serve both government and industry as a useful guide for further research.

# THE CANADIAN ATLANTIC STORMS PROGRAM (CASP):

# AN OVERVIEW

C. Anderson[1] and R.W. Shaw[2]
Bedford Institute of Oceanography

Dartmouth, Nova Scotia, B2Y 4A2

## 1. INTRODUCTION

The Canadian Atlantic Storms Program (CASP) is a multi-disciplinary research program whose primary objectives are (1) to gain an enhanced understanding of the mesoscale structure and dynamics of, and (2) to improve the forecasting of, east coast Canadian winter storms and their oceanic response. The program involves a field observation phase, carried out in the winter of 1985-86, and an analysis phase comprised of analytical and numerical modelling studies. The analysis phase draws upon the CASP field observations for motivation and validation, and will extend through 1989.

CASP is a joint program of the Atmospheric Environment Service (AES, Environment Canada), and the Atlantic Oceanographic Laboratory (AOL, Department of Fisheries and Oceans) at the Bedford Institute of Oceanography (BIO). Investigators from Canadian universities and from the private sector are also participants.

This paper is an overall description of CASP. The scientific objectives and field programs are presented for the meteorological and oceanographic components of CASP in Sections 2 and 3, respectively. Data management and analysis are described in Section 4. The participants and funding sources of CASP are listed in Appendix A. More detailed information is available from the CASP reference documents listed in Appendix B.

## 2. METEOROLOGICAL COMPONENT

In order to forecast Atlantic winter storms more accurately, better understanding is needed of their three - dimensional structure and processes. The meteorological component of CASP seeks to understand these storms through the analysis and interpretation of high- resolution observations from enhanced surface and upper air (rawinsonde) observing networks, aircraft, radar, satellites, ships

1. Atlantic Oceanographic Laboratory

2. Atmospheric Environment Service

and meteorological buoys. The area of greatest interest in the field program were the Nova Scotia/Sable Island area and the Avalon Peninsula/Hibernia area, although specialized observations actually extended as far as the north shore of the St. Lawrence River, Labrador and, when CASP was studying the same storm as the U.S. Genesis of Atlantic Lows Experiment (GALE), to the eastern half of the United States.

During the two month field phase, there were sixteen Intensive Observing Periods (IOP's) in which a representative population of storms was sampled. Ten of the 16 storms tracked south and east of Halifax providing the opportunity to examine mesoscale structures such as precipitation bands, freezing precipitation, rain/snow boundaries, cold fronts and areas of heavy snow. This section describes some of the special observing systems that were used.

a) Surface and Upper Air Observing Systems

During Intensive Observation Periods, rawinsonde ascents occurred as frequently as every 3 hours at 12 sites, including six established specifically for CASP. The location of these sites and of some of the other observing systems is shown in Figure 2.1.) These ascents gave vertical profiles of wind, temperature and humidity up to height of 30 km in the atmosphere. In addition to the land sites, the Fisheries and Oceans Canada research vessel, GADUS ATLANTICA, made 67 soundings in 17 days, using a single observer and the new CLAS semi-automatic sounding system. In all, there were approximately 900 special rawinsonde releases during CASP. During two storms, U.S. weather reconnaissance aircraft released dropsondes in the CASP area.

During each storm, additional surface observations of temperature, wind and significant weather were made by regular surface observers, DND ships and by a special team of volunteer climatological observers who communicated their observations to the CASP Operations Center in Bedford, Nova Scotia via computer terminals attached to their telephones.

Detailed mesoscale meteorological information near the surface were obtained from two arrays of 10 metre towers called MESONETs; one along the length of Sable Island, and the other in a triangular arrangement on mainland Nova Scotia. These towers continually and automatically logged wind velocity, temperature, humidity, and turbulence at 5 minute intervals. Selected stations in the mainland array radioed data directly to the CASP Operations Center in Bedford. In addition to the tower observations, during IOP's Airsonde ascents were made at each array to obtain vertical soundings over a deeper layer. These devices consisted of a balloon which was tracked visually (as far as possible) for wind information which carried aloft a package which sensed temperature and humidity.

b) Aircraft

Aircraft played an important part in CASP. There were two dedicated solely to the project: a Canada Center for Remote Sensing DC-3, and a National Aeronautics Establishment Twin Otter. Both aircraft were based at CFB Shearwater and were equipped with sophisticated devices for sampling cloud and precipitation particles and measuring air temperature, humidity and turbulence. During CASP, these aircraft flew 100 hours into selected parts of storms to observe the detailed structure and processes occurring within them.

In addition to the above aircraft, AES ice reconnaissance aircraft made vertical soundings over the Gulf of St. Lawrence and east of Newfoundland, and DND Aurora patrol aircraft recorded in-flight wind and temperature which was later forwarded to the CASP Operations Center.

c) Radar

As shown by Figure 2.1, there were three weather radars at Halifax, Sable Island and Trepassey, Newfoundland. Those at Halifax and Trepassey were able to scan the storm by varying the elevation angle of the antenna and record on magnetic tape the intensity of the radar return (interpretable in terms of precipitation intensity) in three dimensions. From these records, horizontal and vertical sections and height-time displays can be made of the storm at selected locations and be used in conjunction with data from other observing systems. During the field phase itself, radar displays were used for short-term forecasting and for guiding the research aircraft.

d) Satellites

Satellite observations were also used extensively during the field observing phase of CASP for short-term forecasting and for guiding the movement of the research aircraft. In the post-CASP analysis phase, archived satellite imagery and sounding information will be available.

One satellite display that was particularly useful during the field phase was McIDAS (Man-computer Interactive Data Acquisition System) which was developed by the University of Wisconsin. It is capable of displaying visible and infrared images from the GOES satellite upon which can be superposed meteorological fields such as isobars and precipitation type. Another display, RAINSAT, displayed infrared temperature and visible brightness from satellite observations. From these two fields and climatological considerations, RAINSAT then estimated the probability of precipitation.

e) Special Surface Observations

In addition to the two research aircraft based at Shearwater, a special surface observing site was located there to test several new sampling devices. An upward looking radiometer, using six channels at microwave frequencies, was used to remotely sense the vertical profiles of liquid water, water vapour and temperature. The observations from this instrument could be compared with those from an on-site Beukers Loran-C Navsonde upper air sounding system. A two-dimensional precipitation probe used laser technology to measure the size distribution of precipitation particles between 0.15 and 9.6mm and provide information on precipitation type and amount with time resolution of up to 1 second. Measurements with this instrument will supplement those from the Halifax weather radar.

f) CASP Forecast Center

At the same time as the extensive field observations were taking place, two very important types of activities were taking place at the CASP Forecast Center which, with the CASP Logistics Center, formed the CASP Operations Center in Bedford, N.S. The Operations Desk was staffed by experienced forecasters who provided special forecasts making use not only of the regular meteorological observing and forecasting products, but the supplementary ones that had been established for CASP. The special forecasts were then used by the CASP logistics Center for making decisions on initiating and terminating Intensive Observing Periods, as well as the deployment of specialized observing systems such as rawinsondes and aircraft.

The other activity carried out by the Experimental Forecast Desk, was to evaluate experimental forecast and analysis products produced by the Canadian Meteorological Center in Dorval, Quebec and by the Meteorological Services Research Branch of AES Headquarters. These special products included the Regional Finite Element Model, statistical weather element forecasts, streamline analyses, McIDAS, RAINSAT, a parametric wave model, freezing spray model and a storm surge

model. Evaluation and improvements of these products will continue in the post-field phase of CASP.

## 3. OCEANOGRAPHIC COMPONENT

The scientific objectives of the oceanographic component of CASP are being pursued through a field observation program and through various modelling studies.

### a) Field Observation Program

The oceanographic field program was carried out in the winter of 1985-86. The experiment was located in the nearshore region of the Scotian Shelf east of Halifax because of its (a) relatively uniform bathymetry, (b) simplified logistics and (c) the availability of historical data from the region. The oceanographic array was in place throughout the entire meteorological field program. It was deployed in early December 1985 and recovered in early April 1986. The array was designed to resolve the "natural" oceanic vertical and horizontal scales of motion (e.g. imposed by topography or stratification) as well as the response to mesoscale atmospheric forcing. The oceanographic measurements made during the field experiment included current speed and direction (moored current meters, Coastal Ocean Dynamics Applications Radar or CODAR), temperature and salinity (moored current meters, thermister chains, CTD casts), bottom pressure (moored pressure gauges), coastal sea level, and wave height (WAVERIDER buoys) and direction (WAVEC pitch-and-roll buoys). These data were supplemented by measurements of surface meteorological conditions from a buoy moored near the centre of the array, which provided the basis for local estimates of the air-sea fluxes of energy, momentum and heat as well as useful information within the larger meteorological network.

The Scotian Shelf array of current meter/bottom pressure moorings for the CASP field experiment consisted of two primary cross-shelf lines (near Halifax and to the east off Liscomb, N.S.) and a distribution of moorings along the 100 m isobath between them (Fig. 3.1). Nested within the current/pressure moorings, was a smaller wave measurement array consisting of WAVERRIDER buoys and WAVEC pitch-and-roll buoys (Fig. 3.2). Along the shore, temporary sea level gauges were paired with the offshore moorings on the 100 m isobath, and a MINIMET meteorological buoy was located on the main (Halifax) mooring line at the 100 m isobath. In addition, CODAR installations at two shore sites bracketing the Halifax line were used to map the surface currents over the wave measurement array (Fig. 3.2).

The distribution of instruments on the Halifax mooring line (CASP moorings 1-5, Fig. 3.1) was designed to resolve the baroclinic structure of the current field. The historical density field for February based on Halifax Section data (Drinkwater and Taylor, 1982) shows that the mean position of the front between the cold, fresh Nova Scotian Current and outer shelf water intercepts the bottom and surface near the 100 and 200 m isobaths, respectively. The extra current meter and thermister chain on the outer two moorings were intended to resolve the enhanced current and density fluctuations in this regime. The farthest-offshore mooring on the Halifax line measured bottom pressure only. Reduced numbers of instruments and moorings were deployed along the Liscomb mooring line (CASP moorings 9-11, Fig. 3.1), where the bottom topography is similar to that on the Halifax line at least out to the 150 m isobath (= 80 km ofshore).

The wave measurement array (Fig. 3.2) was situated between the 25 and 100 m isobaths along the Halifax line, covering a depth range where significant shallow water influence on the dominant incoming swell waves (less than 40 m for 10 s waves) was expected. Three WAVEC pitch-and-roll buoys, placed on the 100, 50 and 25 m isobaths, enabled estimates to be made of the changes in the directional wave spectrum as the waves encountered shallow water. The six WAVERIDER buoys moored

at the 35, 70 and 100 m isobaths were intended to further resolve spatial gradients in the scalar wave energy spectrum, and to provide estimates of the degree of alongshore uniformity in the shoaling process. In addition, the current meters on the 60 and 100 m isobath moorings were intended to give local estimates of the subsurface current field, while CODAR mapped the surface currents on a 3 km grid over the wave array. Finally, the MINIMET buoy was moored near the outer WAVEC buoy to measure surface wind speed and direction, and air and sea surface temperatures. Wind observations at the coast were made at the AES Martinique Beach mesonet station.

The current/pressure and wave arrays were designed to resolve the dominant forced and "natural" scales of variability. The time scale of the mesoscale forcing (of order 1 hr) is comparable to that of a cross shelf seiche (of order 2 hrs) and represents the smallest important unit of temporal variability. Therefore, the current, pressure, and sea level sampling intervals were 30 minutes. Throughout the field program, wave spectral estimates were made for all wave buoys at hourly intervals.

The spatial resolution of the current/pressure array along the 100 m isobath ranged from 15 to 130 km, whereas the average cross-isobath spacing on the offshore lines was 15 km. The nominal spatial scale (100 km) of the mesoscale forcing was therefore easily resolved by this array. The offshore lines resolved variations associated with the large-scale shoaling of the bottom toward the coast, but as indicated by the depth profiles in Figure 3.1, significant topographic variations exist on scales of 1 to 10 km. The smallest scales are particularly important for the wave studies, since swell dissipation in shallow water may depend critically on backscatter from bottom irregularities with dimensions comparable to the swell wavelength (Hasselmann et al., 1973). Furthermore, the importance of this mechanism at a given spot is sensitive to the direction of the incoming swell. For these reasons, high-quality wave direction measurements were considered to be essential.

Another important horizontal length scale is determined by the vertical stratification of the water column. Based on wintertime hydrographic data in the upper 100 m on the Halifax Section, the internal deformation radius is estimated to be 8-10 km. Fluctuations on this scale, expected to occur in the frontal region of the Nova scotia Current, would not be resolved by the 100 m isobath moorings, although their surface expressions could be detected by CODAR. On the other hand, satellite infrared imagery of the Nova Scotia Current reveals dominant wave-like meanders with scales of order 50 km in both the along-and-cross shore directions. These features would be resolved by the array.

In summary, the array was capable of identifying most of the expected forcing and background space and time scales of Scotian Shelf variability, although some interpretations might be hampered as a result of small-scale topographic irregularities.

b) Oceanographic Modelling

The primary goal of the CASP oceanographic modelling effort is to investigate and develop advanced numerical circulation and wave models with realistic atmospheric forcing, and to test these models against observations. Initial steps in this process have been to modify a high-resolution 2-D barotropic model, presently under development by MEP for oil slick trajectory analysis, which features the calculation of the vertical current profile to account for friction and some stratification effects. This model has now been tailored to the Scotian Shelf region and was run during the CASP field program.

Experience with Scotian Shelf break studies has revealed that simple two-layer models with uniform topography in the alongshore direction are inadequate to

explain the observed baroclinic structure of the wind-driven circulation. Therefore, considerably more effort is required to investigate the use of models for the response of a weakly-stratified ocean over realistic topography to mesoscale winds. Preliminary efforts in this direction involve the formulation of a two-layer model with full 2-D topography and transient forcing field.

The BIO wave prediction model was developed by Resio (1981) in the 1970's. In its present form, it has spatial and temporal resolutions of 277 km and 3 hrs. for application in ocean-wide contexts. For continental shelf applications, a more highly-resolved regional model must be nested within the large-scale calculations in order to resolve variations on scales of 10 km or less. This also requires the implementation of open boundary conditions in the regional model to allow energy to flow in and out to the deep ocean. Work on increasing the resolution of the model is progressing.

A fundamentally more difficult problem is to incorporate shallow water effects into the wave model. This requires the addition of wave direction information to the spectral energy balance in order to account for wave refraction and propagation effects. The greatest uncertainty in this process lies in the definition of the shallow water dissipation function, which has so far avoided empirical definition due to the lack of an accurate and complete date set including wind, wave height and direction, current, and bottom topography. The CASP wave observations comprise such a data set. The theoretical modelling aspects are being pursued in conjunction with others from the international wave-modelling community.

## 4. DATA PROCESSING, MANAGEMENT, AND ANALYSIS

Quality control and archiving of the CASP data collected by the various meterological and oceanographic programs described in Sections 2 and 3 are the responsibility of each individual investigator. Overall, CASP data management is the responsibility of the meteorological and oceanographic data managers located in the Cloud Physics Division of AES, Downsview, Ontario, and the Coastal Oceanography Division, AOL, at BIO, Dartmouth, Nova Scotia, respectively. The data managers will issue a consolidated CASP data set inventory in the fall of 1986 to assist interested scientists in requesting CASP data for analysis.

Analysis of the CASP data sets has started. A series of workshops are planned for the presentation and discussion of CASP findings. The first workshop was held in June, 1986, and the second is planned for November 1986. Data analysis milestones, names of the principal investigators, and a tentative analysis timetable are contained in the CASP Analysis Plan (see Appendix B).

## 5. References

Drinkwater, K.F. and G.B. Taylor. 1982 Monthly means of temperature, salinity and density along the Halifax Section. Tech. Rept. of Fish and Aquatic Sci., #1093, 67pp.

Hasselmann, K.T.P. Barnett, E. Bouws, H. Carlson, D.E. Cartwright, K. Enke, J.A. Ewing, H. Gienapp, D.E. Hasselmann, P. Krusemann, A. Meerburg, P. Mueller, D.J. Olbers, K. Richter, W. Sell, H. Walden, 1973. Measurements of wind-wave growth and swell decay during the Joint North Sea Wave Project (JONSWAP). Dtsch Hydrogr. Z., 8, (Suppl. A8) 95pp.

Resio, D.T. 1981. The estimation of wind-wave generation in a discrete spectral model. J. Phys. Oceanogr., 11 510 - 52

Appendix A

## CASP PARTICIPANTS AND FUNDING

### A.1 Participants - Meteorology

Atmospheric Environment Service
McGill University
University of Toronto
National Aeronautical Establishment
Alberta Research Council
NOAA/National Meteorological Center
Universite du Quebec a Montreal

### A.2 Participants - Oceanography

Atlantic Oceanographic Laboratory (AOL), DFO
Marine Environmental Data Service (MEDS), DFO
Atlantic Region, Canadian Hydrographic Service (CHS), DFO
Atlantic Geoscience Centre (AGC), EMR
Dalhousie University
Memorial University of Newfoundland
Universite du Quebec a Rimouski - INRS Oeanologie
Arctic Sciences Ltd.
Centre for Cold Ocean Resources Engineering (C-CORE)
Dominion Diving Ltd.
Martec Ltd.
Meteorological and Environmental Planning Ltd. (MEP)
Seakem Oceanography Ltd.
Seimac Ltd.

### A.3 Funding - Meteorology and Oceanography

Environment Canada, Atmospheric Environment Service (AES)
Department of Fisheries and Oceans (DFO)
Office of Energy Research and Development (OERD), EMR
Environmental Studies Revolving Funds (ESRF)
National Research Council
Department of National Defense

Appendix B

## CASP DOCUMENTS

1. CASP Experimental Design Document.
2. CASP Operations Plan.
3. CASP Data Management Report.
4. CASP Analysis Plan.

These documents are available from:

R.E. Stewart
Cloud Physics Research Division
Atmospheric Environment Service
4905 Dufferin Street
Downsview, Ontario M3H 5T4

or: R.W. Shaw
Atmospheric Environment Service
Bedford Institute of Oceanography
Box 1006
Dartmouth, Nova Scotia B2Y 4A2

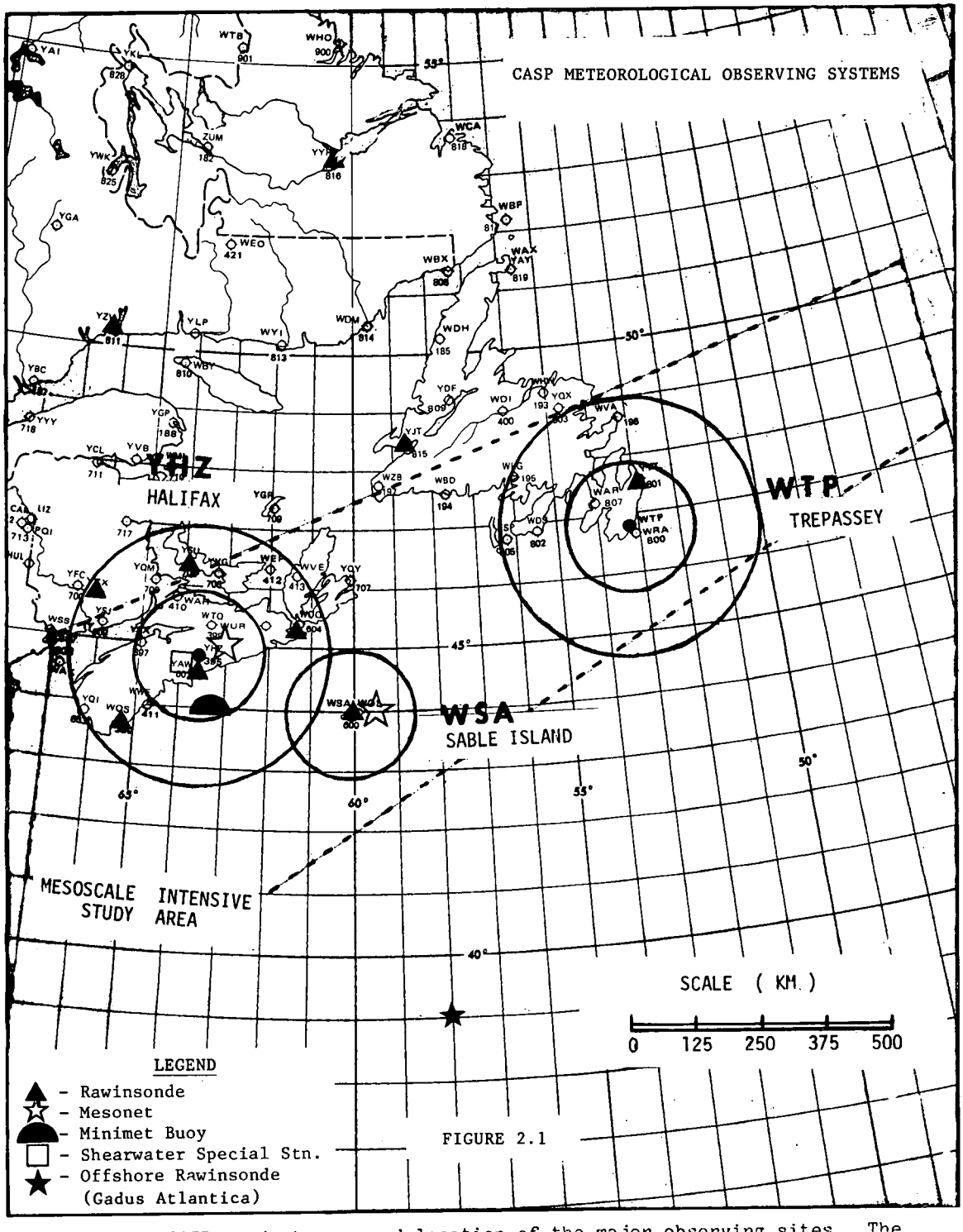


Fig. 2.1: CASP project area and location of the major observing sites. The rawinsonde sites at Maniwaki and Valcartier, Quebec are not shown. The circles indicate ranges of 125 and 250 km for the radars at Halifax and Trepassey, and 125 km for the Sable Island radar.

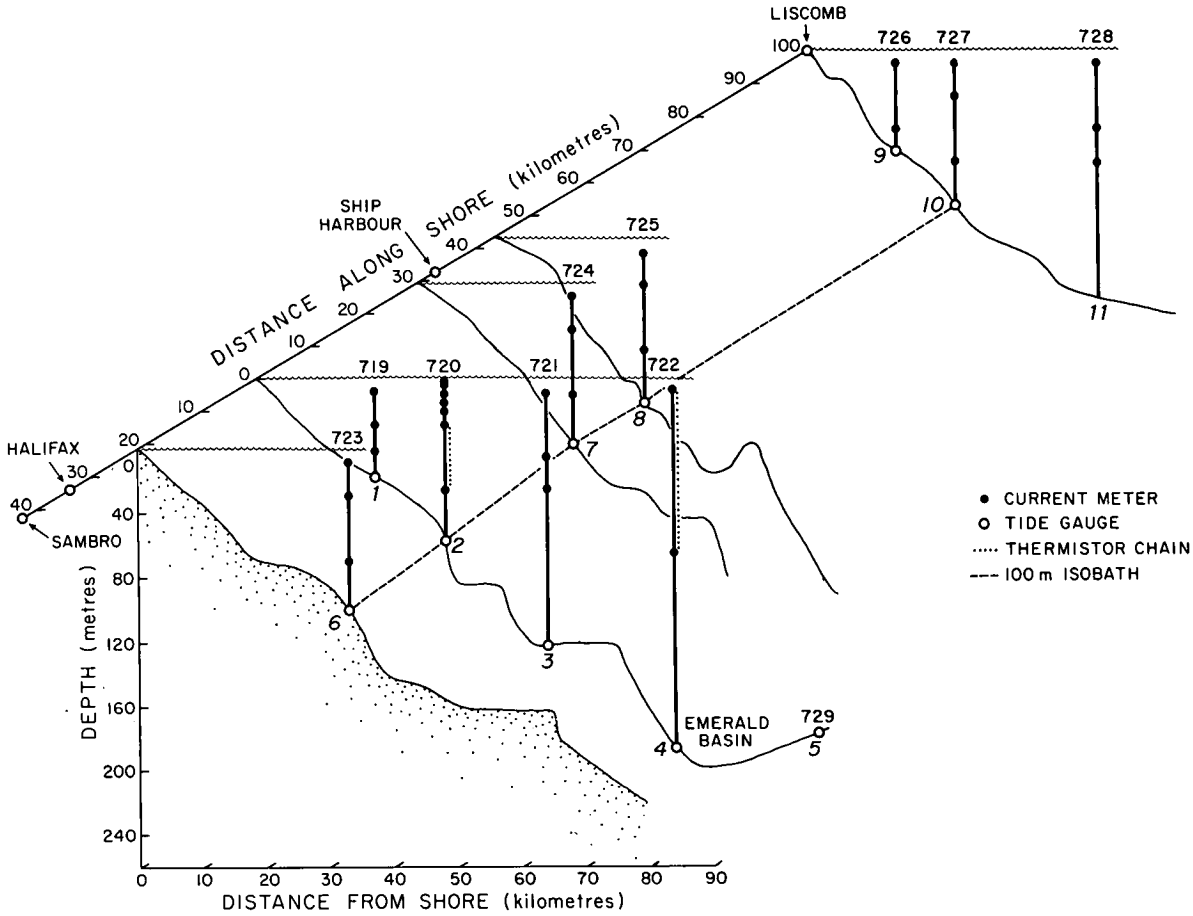


Fig. 3.1: CASP Scotian Shelf current meter/bottom pressure gauge moorings. CASP mooring designations (1-11) and BIO consecutive station numbers (719-729) are shown.

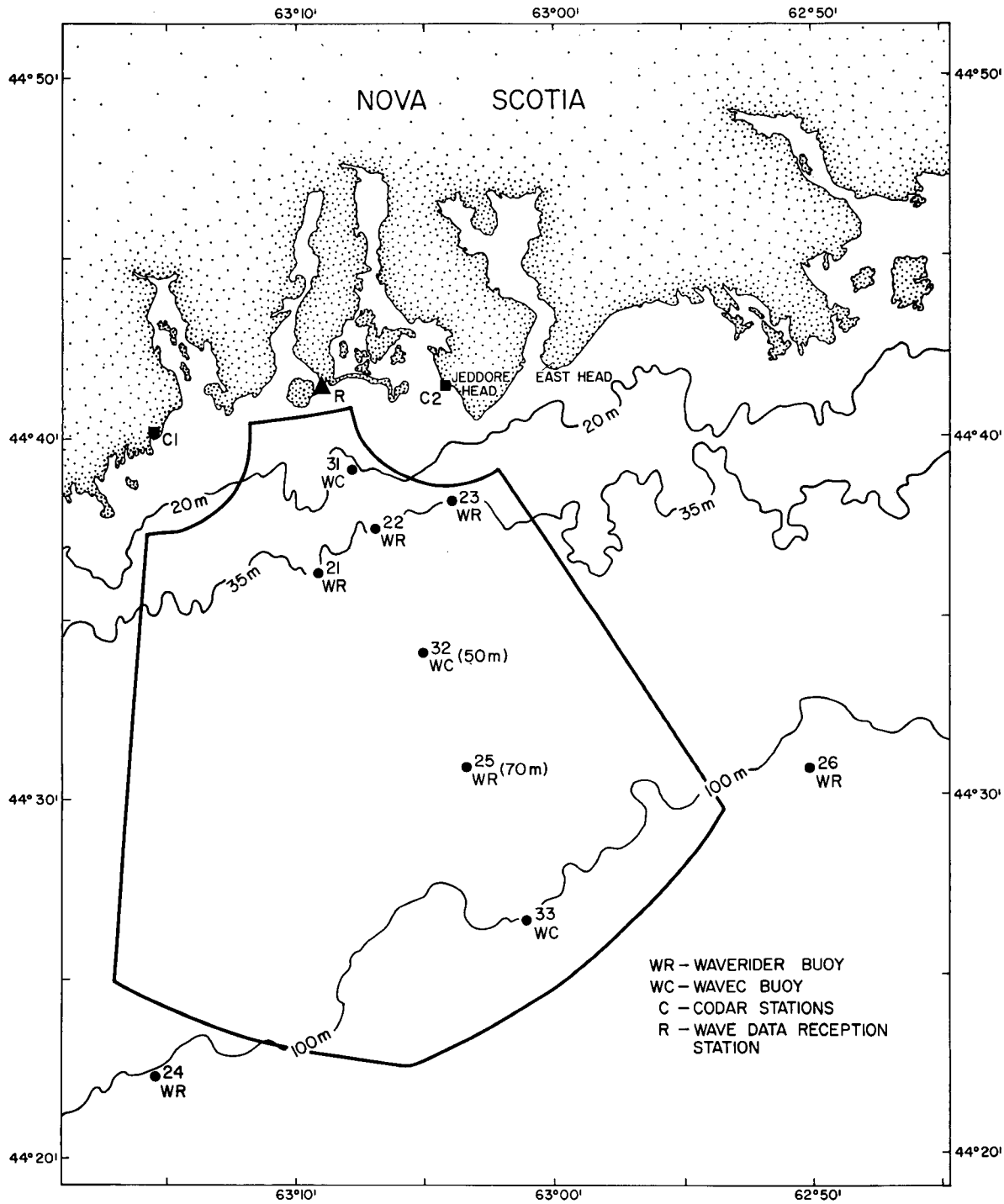


Fig. 3.2: CASP wave buoy array. Also shown are the two CASP CODAR stations and the apporximate limits of CODAR coverage.

# THE CASP ESRF WOTAN EVALUATION

Fred Dobson
Dept. of Fisheries & Oceans
Atlantic Oceanographic Lab.
P. O. Box 1006
Dartmouth, N.S. B2Y 4A2

David Lemon
Arctic Sciences Ltd.
1986 Mills Rd., RR#2
Sidney, B.C. V8L 3S1

Brian Peters
Dept. of Fisheries & Oceans
Atlantic Oceanographic Lab.
P. O. Box 1006
Dartmouth, N.S. B2Y 4A2

## Abstract

Five Wind Observation Through Ambient Noise sensors were deployed during CASP on the Nova Scotia continental shelf by Arctic Sciences, Inc. under contract to ESRF. Three were in the water from 22 November 85 to 5 April 86, and the others from 11 December 85 until 13 March 86. The objective was to test their value for estimating sea state (i.e. Beaufort number) and precipitation rate in North Atlantic winter storm conditions. They were to be calibrated against wind speed from an array of anemometers on the shore and on buoys at sea, and against precipitation rate from radars at Halifax Airport and Sable Island.

The deployment was highly successful, with a data recovery of about 90%. The analysis, including acquisition of all necessary ancillary information, is in progress now. Since the marine winds were not well-measured by the CASP surface buoys, the WOTAN experiment results, in spite of residual uncertainties in their wind speed calibrations, will considerably enhance our hindcast capability.

## Introduction

During the CASP experiment, five Wind Observation Through Ambient Noise (WOTAN) sensors were deployed on the Nova Scotia continental shelf (Figure 1). These instruments, owned (except for two belonging to the Institute of Ocean Sciences and loaned by Dr. D.M. Farmer) and deployed by Arctic Sciences, Inc. under contract to the Environmental Sciences Revolving Fund, gave a better than 90% data return during the four months they were in place: December 1985 - March 1986, inclusive. The signal they recorded was sound level (in Pa) at the sea bottom, at six separate acoustic frequencies between 4.3 and 25.0 kHz.

The purpose in deploying the WOTANS was to test them as a suitable sensor for wind speed measurements in the continental shelf environment, to investigate their ability to measure precipitation rate and, in general, to study the variability of underwater sound in the 4-20 kHz band and, indirectly, its causative mechanisms. The sites (Figure 1) were chosen to provide "additional coverage" of marine winds in the CASP offshore area: that is, to augment the land-based wind measurements of the surface mesonets on Sable Island and the N.S. mainland, and measurements from meteorological buoys at Stations 2, 5, 12 and south of Yarmouth. In fact, only one buoy: MM504 (Coastal Climate Co. "Minimet") at Station 2, provided any useful data. As a result, the WOTAN wind estimates form the bulk of the marine wind measurements made during CASP. This has proven both a boon and an embarrassment, as we will demonstrate later.

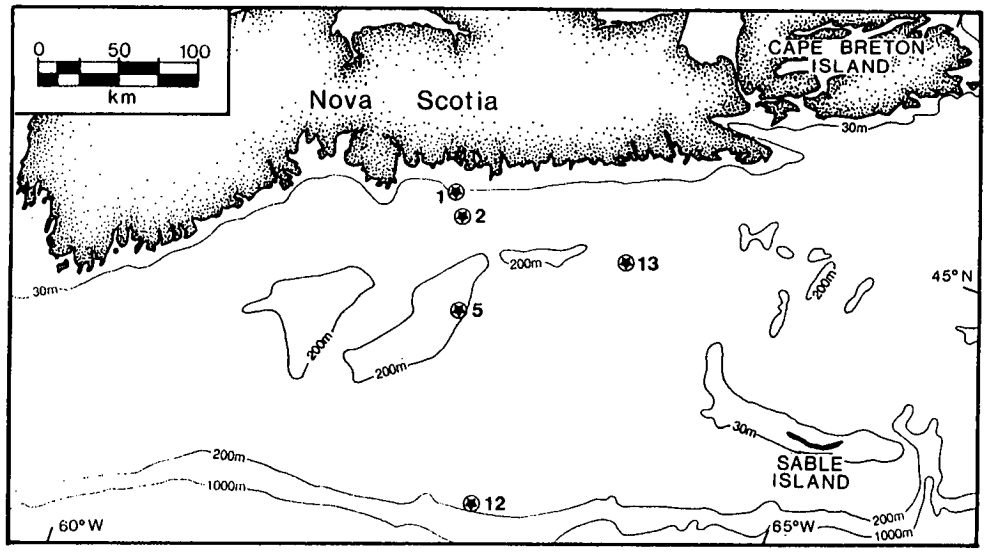


Fig. 1 Locations of WOTAN deployments for CASP (after Lemon, 1986).

## The Data Set

The particulars of the CASP WOTAN deployments are given in Table 1; all deployments cover the experiment period. The instruments were calibrated both before and after the experiment for their overall sensitivity to output from the acoustic transducers. The transducers themselves were factory-calibrated prior to deployment.

The only problem encountered was a sudden increase in background noise at Station 2, which was, by Murphy's Law, the site of the only wind buoy that worked, starting on January 14, the day before CASP began. The source of the noise has not been determined. Since post-calibration showed the electronics to be normal, and since the noise disappeared when the instrument left the water, the only likely remaining possibilities are transducer malfunctions due to pressure or temperature, or a noise source in the water. The first two possibilities will be checked out when the instrument is returned from the Arctic, where it was sent immediately after CASP (the noise source was discovered well after it was deployed under the ice).

Table 1

| Station | Depth (m) | Deployed | Recovered | No. of Channels |
|---|---|---|---|---|
| 1 | 63 | 11-12-85 | 13-03-86 | 6 |
| 2 | 93 | 11-12-85 | 13-03-86 | 6 |
| 5 | 165 | 22-11-85 | 05-04-86 | 7 |
| 12 | 225 | 22-11-85 | 09-04-86 | 7 |
| 13 | 165 | 22-11-85 | 06-04-86 | 7 |

Notes: 1. The units on Sts. 1 & 2 had six acoustic frequencies: 4.3 W, 8, 12.5, 14.5, 16.8 and 25 kHz, where "W" indicates a 2-pole, wide band-width filter instead of the standard 4-pole filter. Units 5, 12, 13 had the above channels plus a 4.3 kHz channel with a 4-pole filter.

To approach the problem we have used two strategies . First, we have "calibrated" the St. 2 WOTAN against the MM504 wind speed for the period 11-26 December 1985 (from an initial Minimet deployment which ended on December 26 in an encounter at sea with something hard). Second, we have investigated the characteristics of the noise. From looking at the noise floor at low wind speeds, it can be determined that the noise is not white: it is 50% greater at 4.3 kHz than at 25.0 kHz. From looking at the raw WOTAN data, it is clear that the presence of the noise affected not only the absolute level of the recorded acoustic signal, but also its wind speed sensitivity. This being so, no more can be done to allow for it until the unit is returned from the Arctic, and attempts can be made to reproduce the affect. One use that can be made of the noisy data is to make a wind speed calibration against MM504 for the February-March period, and then use that calibration to estimate the Station 2 wind for the 15 - 30 January period, i.e. from the beginning of CASP to the MM504 deployment date. We will try this only after the instrument's preamps have been tested for saturation at high sound levels.

Another potentially serious problem is the variation of WOTAN sensitivity with measurement site (Table 2). Although it is speculated (e.g. Lemon, 1986) that instrument depth is the cause of the differences, there could be other factors (bottom type?) at work, and therefore the observed variability must be treated as a measure of the overall uncertainty in WOTAN wind sensitivity. Choosing an average value for the sensitivity produces an uncertainty of $\pm$ 3 $ms^{-1}$ (+3.5, -2.5) at 10 $ms^{-1}$. Faced with deciding which a and b to use for which WOTAN, we chose to use calibration coefficients which were interpolated from the three sets we had (Table 2) to the depths of the CASP WOTANS.

Table 2
Variation of WOTAN Sensitivity with Deployment Site

WOTAN correlation equation is $20 \log_{10} U = a(NSL)-b$, where U is wind speed, NSL is sound pressure level in db re 1μPa.

| Investigation | Site | Depth (m) | a | b |
|---|---|---|---|---|
| Lemon et al (1984) | Continental Shelf: Queen Charlotte Sd., B.C. | 250 | 0.78 | 28 |
| Dobson et al (1986) | Continental Shelf: N.S. (CASP Station 2) | 93 | 0.84 | 33 |
| S. Vagle, IOS (1985) | Nearshore Pacific: Barkley Sound, B.C. | 15 | 0.90 | 38 |

Using these, we can predict the wind speed at each of the WOTAN locations over the CASP time period, with worst-case accuracies of $\pm$ 20-30% at 10 $ms^{-1}$, with the hope that the accuracy can be improved by future work. (In fact, some has been already done by Farmer and associates at IOS, and we may be able to improve our uncertainties by modelling the sound paths and thus correcting for depth effects.)

On making a scatter diagram of WOTAN #2 sound pressure in Pa versus wind speed, a linear relationship was found (Fig. 2a). Since all earlier work (e.g. Farmer & Lemon, 1984) is based on a linear relation between sound pressure in db and the log of the wind speed (Fig. 2b), we asked why and discovered that the log-log relation had been necessary because up until CASP all WOTANS were equipped with logarithmic preamplifiers, and since the sampled sound pressure was a time average, it was necessary to use a logarithmic relation. For CASP the preamps were linear, and so the CASP and future WOTANS can be used without the added complication of the log function. All our results will be based on the linear correlation, although in Table 2 we give our log-log slope and intercept for comparison with earlier work. Which correlation is really linear (if it is the log-log one, then our "linear" one should be Wind speed varies with (Sound level)$^{0.84}$) we cannot say at this point. If one had not seen the log-log correlations, it would be natural to start with the assumption that the linear fit was the correct one.

## Analysis to Date

Our intention is to perform sufficient processing on the WOTAN data to allow the most accurate possible estimates to be made of marine winds and precipitation at the five WOTAN sites. The precipitation analysis is the more complex and is more dependent on the availability of verification data. The analysis is being carried out at IOS Pat Bay by S. Nystuen, S. Vagle, D. Farmer and D. Lemon, and will not be discussed further here; we prefer to spend our time discussing the marine wind analysis, since it is so crucial to CASP (the functional WOTANS make up four of the seven CASP marine wind time series - not including Sable Island).

Figs. 2a and 2b show the scatter plots of vector averaged wind vs 4.3 kHz sound pressure in Pa, and log of the vector averaged wind vs 4.3 kHz sound pressure level in db re 1 volt/μPa, that is, between MM504 and Wotan #2 for the 30-day period over which both were working reliably (Nov. 27 - Dec. 26, 1985). The neutral correlation coefficients (Garrett & Petrie, 1981) were 0.96 $\pm$ 0.08 for the linear-linear plot and 0.93 $\pm$ 0.08 for the log-log plot, where the $\pm$ is a 95% confidence interval. We expect to improve on this by more intelligent use of our ship movement information; the data were simply despiked and averaged prior to being correlated (the averages brought the Minimet and WOTAN to the same sampling interval: 30 min). The correlations shown are between the 4.3 kHz sound and wind speed. Lemon (1986) suggests using the average of the 4.3 - 8 kHz correlations for each WOTAN to minimize the effects of precipitation noise (negligible in the 4.3 kHz data) and shipping noise (negligible in the 8 kHz

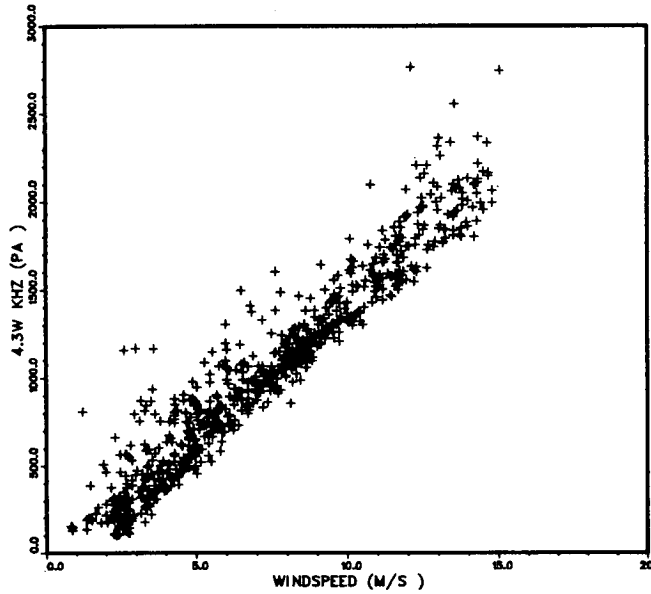


Fig. 2a Scatter plot of 4.3 kHz sound pressure level (Pa) from the WOTAN at Station 2 against wind speed ($ms^{-1}$) from Minimet buoy MM504 (at the same location), for the period Nov. 27-Dec. 26, 1985. Data despiked and averaged to give both sensors a 30-min sampling interval.

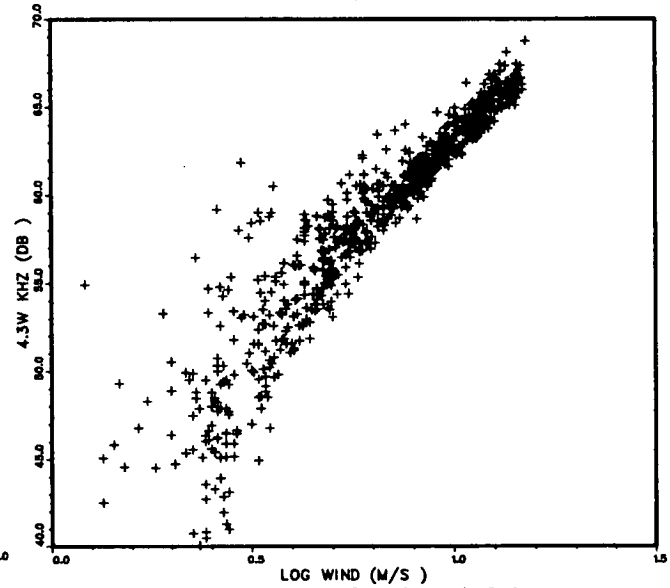


Fig. 2b As for Figure 2a, but 4.3 kHz sound level (db) against log wind speed.

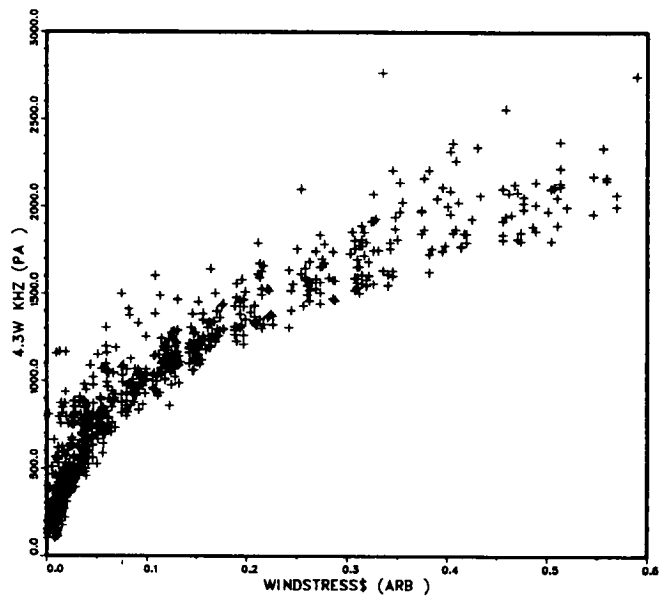


Fig. 3 As for Figure 2a, but 4.3 kHz sound level (Pa) against neutral-stability wind stress ($Nt\ m^{-2}$) computed from Smith (1981).

data). Although this does produce a visually more "realisitic" wind speed prediction, we will not implement it here; we prefer to wait for a better understanding of at least the precipitation noise, after Nystuen, Farmer & Lemon have correlated the WOTAN data with the CASP radar images of rainfall rate.

We have also computed neutral air-stability wind stress $\tau$ using (Smith, 1980, 1981)

$$\tau = \rho_a C_D U_{MM}^2$$

where

$$10^3 C_D = 0.61 + 0.063 U_{MM}$$

and correlated it (Fig. 3) with the 4.3 kHz WOTAN #2 sound pressure in Pa. As expected, a square-law curve results. To test the hypothesis that the WOTAN pressure signal is directly related to wind stress as well as wind speed, it will be necessary to search the Minimet data (which has unreliable air temperature after Feb. 5) for periods of similar wind speed for which the air stability, and hence the wind stress, were different. A correlation can then be made between a dimensionless measure of the air stability and the ratio of the square of the WOTAN wind speed to the square of the measured wind speed.

We are interested in seeing what range of wind frequencies produced useful WOTAN signals, and so have produced power and cross spectra of the MM504 wind speed and the 4.3 kHz WOTAN sound pressure for the pre-CASP period during which both were working. The power spectra (Fig. 4) are red, meaning that the short record we have (30 days = 1440 samples) is unable to define the spectral peak at its lowest frequency of 0.0234 cph (a period of 1.8 days). Ninety-five percent of the variance in the wind spectrum itself is accounted for by frequencies below 0.086 cph (a period of 0.5 days), and 25% of the total variance is at frequencies lower than 1 cycle/FFT block (a period of 1.8 days). The wind and WOTAN spectral shapes are the same within our statistical ability to estimate them.

The cross spectra between the MM504 vector average wind and the WOTAN 4.3 kHz signal (Fig. 5) indicate a sharp roll-off in coherence at 0.24 cph (a period of 4 h) and a slow drift in phase which could be interpreted as a 0.2 h lead of the WOTAN sound pressure ahead of the vector-averaged wind. We can account for one-third of the lead by allowing for a 4-min difference in sampling time caused by the differing sampled area and averaging procedures used in the two instruments.

The coherence gives a measure of the maximum wind fluctuation frequency reproduced by the WOTAN: about 0.24 cph or a period of 4 h. How this frequency varies with, for example, WOTAN depth (WOTAN 2 was at 93 m) is an open question; the most likely source of variation would be the sea surface area over which the WOTAN averages (about 30 $km^2$ for the 4.3 kHz signal at 100 m: Farmer & Lemon, 1984, and varying roughly as the square of the depth, at least to 300 m). A surface buoy, in a steady wind U, averages over a downwind strip of length $Ut_{av}$, where $t_{av}$ is the averaging time (e.g. 18 km for a 10 $ms^{-1}$ wind and a 30-min averaging time) and a width determined by the crosswind coherence length of the energy-containing fluctuations. Thus, the signals measured by the two instruments should not be expected to be fully coherent. It may be possible, using a (necessarily) crude model of the large-scale wind fluctuations in the Atmospheric Boundary Layer, to predict the observed behaviour of the coherence; the most likely scenario is that the coherence observations will provide insight into micro/mesoscale structure of the ABL.

Wille (1985) investigated noise spectra from ship traffic in the (heavily-travelled) Baltic Sea and classified them by ship density; his spectra indicate we should, at 4.3 kHz, be seeing ship noise in the range 20-60 db (10-1000 Pa). Lemon, Farmer and Watts (1984) show a ship noise "signature" indicating a double peak: the WOTAN hears strong low-frequency noise as the ship approaches and departs, but hears

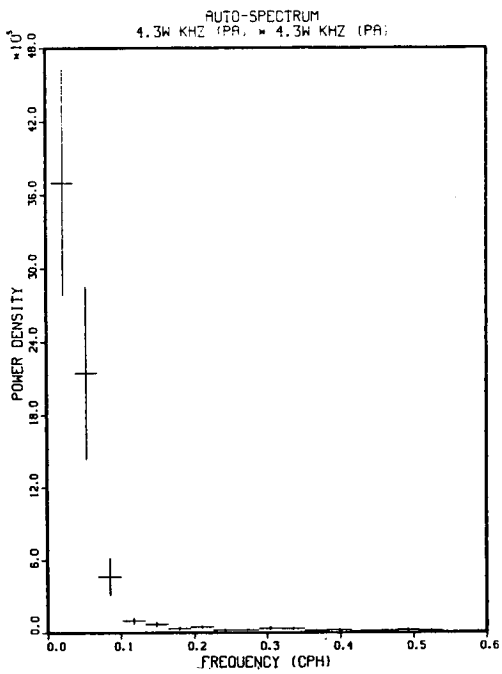


Fig. 4a Power spectrum of 4.3 kHz sound pressure level ($Pa^2Hz^{-1}$) from the WOTAN at Station 2 for the period Nov. 27-Dec. 26, 1985.

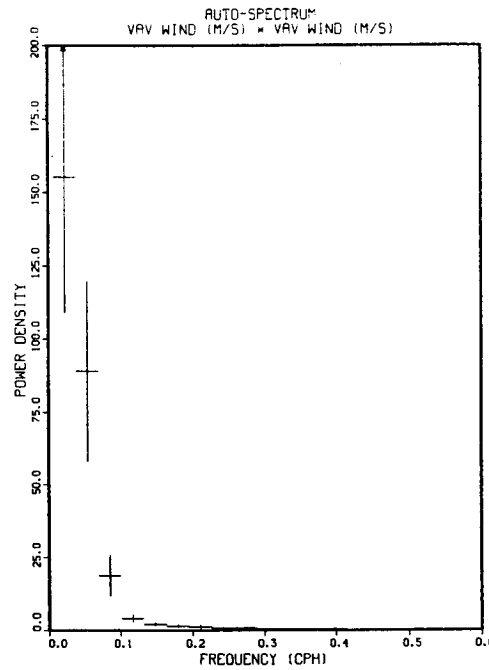


Fig. 4b Power spectrum of wind speed $(ms^{-1})^2Hz^{-1}$ from Minimet buoy MM504 at Station 2 for the period Nov. 27-Dec. 26, 1985.

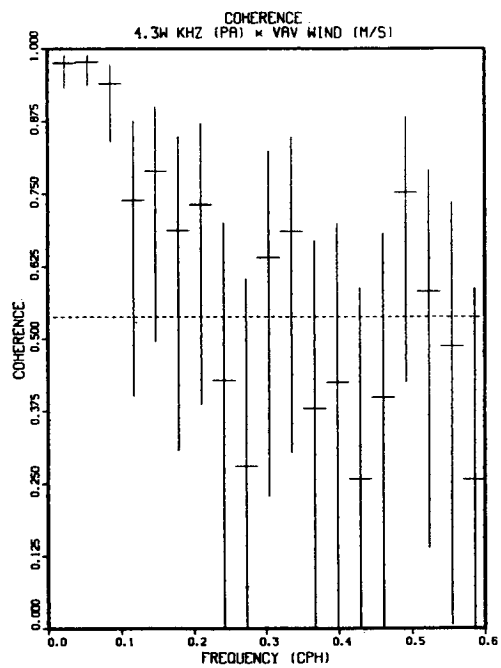


Fig. 5a Coherence between 4.3 kHz WOTAN sound pressure level (Pa) and MM504 wind speed, at Station 2 for the period Nov. 27-Dec. 26, 1985.

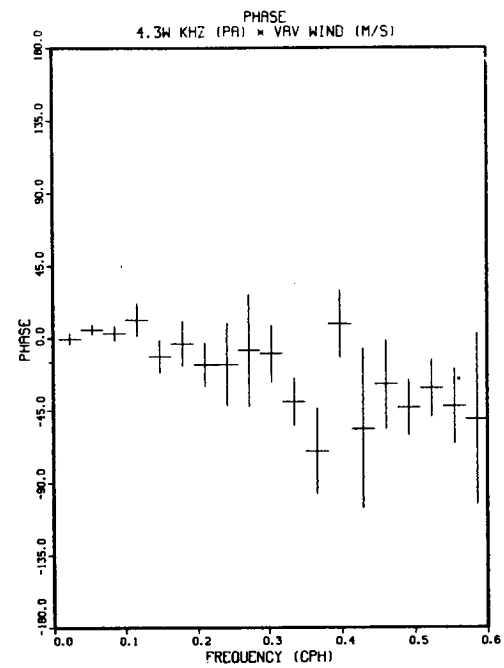


Fig. 5b Phase as for Figure 5a: positive phase means second channel leads first.

more broadband cavitation noise when the ship is closest. This signature is strongly evident (Fig. 6) in the (4.3 kHz - 16.8 kHz) composite signal. Although we can identify individual double-peaked noise spikes with the predicted passage time of particular ships, identified with Halifax Traffic Canadian Coast Guard computer files, we see no automatic way of identifying and removing them. The spikes are too highly variable and are too similar to background variability: we have, for example, identified several examples of large, wide spikes due to the simultaneous passage of as many as three ships. There has been no explicit removal of ship-induced noise from any of the WOTAN data presented here.

Conclusions

Of the five 6-channel WOTAN sensors deployed from November 27, 1985 to April 9, 1986, four gave complete data sets. Only that at Station 2 failed by becoming very noisy and unuseable as a wind sensor after January 15. The calibration constants for the Station 2 WOTAN vs wind speed from a Minimet buoy (MM504) from November 26 - December 25, 1985, when combined with those from three earlier direct WOTAN vs wind buoy calibrations, were used to estimate the depth variation of the constants, and thus to define the constants for the remaining four WOTANS. With the empirical constants time series of predicted wind speed have been produced for CASP from each WOTAN, and those time series represent 60% of the total coverage of marine wind speeds during CASP. We presently estimate the uncertainty in the WOTAN - derived wind speeds to be about $\pm$ 20%, and believe we can do better by allowing for the differing propagation paths of the sound.

The correlation of WOTAN 4.3 kHz sound pressure level with wind speed is linear, with a coefficient of 0.96 (95% confidence interval $\pm$ 0.08) between WOTAN 2 and the Minimet above it, and 0.87 (95% c.i. $\pm$ 0.08) using WOTAN 1, 4.5 nm to shoreward. Both were done on despiked, smoothed data and might be improved if a way could be found to remove ship noise. The correlation with neutral-stability wind stress computed from Smith (1981) is quadratic, as expected; we may attempt a correlation with air stability. We will also look for a correlation with wave height.

The WOTAN 2 - Minimet wind speed coherence drops below the statistically significant level at about 0.24 cph (a period of 4 hours). This is thought to be consistent with the different areas sampled by the two instruments, but the consistency should be verified by physical modelling. The power spectra of the wind from the Minimet buoy and the WOTAN 2 4.3 kHz sound are red and identical in shape, and 95% of their variance is accounted for by wind frequencies below 0.086 Hz (a period of 0.5 days).

We have been successful in identifying the noise from passing ships in the data from WOTANS 1 and 2 and find it to have the same distinctive double-peaked signature noted by Lemon et al (1984). We have not developed an automated procedure for removal of ship noise from the WOTAN wind speed estimates.

We feel the most important next step in producing a useful sea-bottom wind speed sensor is to deploy some WOTANS under wind buoys at a variety of depths in a relatively small area, and carefully determine the slope and intercept of the sound pressure level-wind speed correlation. Another important consideration is the development of a WOTAN which can report its data to shore or satellite in real time.

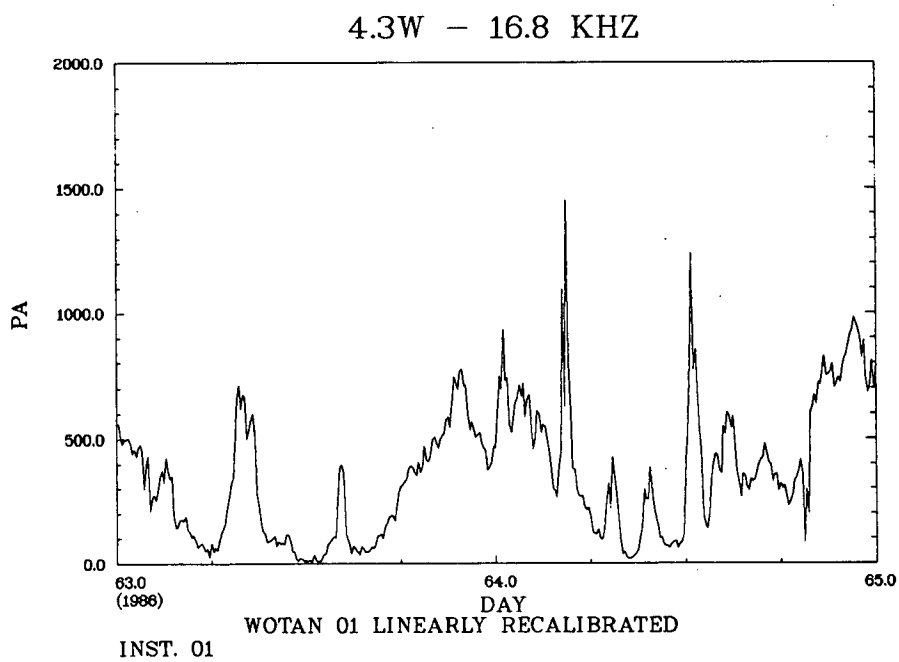


Fig. 6 Examples of ship-induced noise in the 4.3 kHz - 16.8 kHz signal from the WOTAN at Station 1 for the period 4-6 March 1986. Ship noise peaks at Day 63, hour 7 (multiple), Day 64, hour 1, 5, 7, 10, 13.

Bibliography

Farmer, D.M. and D.D. Lemon (1984). The Influence of Bubbles on Ambient Noise in the Ocean at High Wind Speeds. J. Phys. Oceanogr., 14: 1762-1778.

Garrett, C.J.R. and B. Petrie (1981). Dynamical Aspects of the Flow through the Strait of Belle Isle. J. Phys. Oceanogr., 11: 376-393.

Lemon, D. (1986). Underwater Acoustic Wind Speed Measurements during the Canadian Atlantic Storms Program. Environmental Studies Revolving Funds Report, submitted.

Lemon, D.D., D.M. Farmer and D.R. Watts (1984). Acoustic Measurements of Wind Speed and Precipitation over a Continental Shelf. J. Geophys. Res., 89: 3462-3472.

Smith, S.D. (1980). Wind Stress and Heat Flux over the Ocean in Gale Force Winds. J. Phys. Oceanogr., 10: 709-726.

Smith, S.D. (1981). Coefficients for Sea Surface Wind Stress and Heat Exchange. Report BI-R-81-19, Bedford Institute of Oceanography, Dartmouth, N.S. 31 pp.

Wille, P.C. (1985). Ambient Noise: Characteristics of the Noise Field. In Adaptive Methods in Underwater Acoustics, Ed. H.G. Urban. Reidel, Holland: 13-33.

# THE DISTRIBUTION OF SURFACE WIND OVER THE SCOTIAN SHELF

**Peter C. Smith**

**Department of Fisheries & Oceans**
**Bedford Institute of Oceanography**
**P.O. Box 1006**
**Dartmouth, Nova Scotia B2Y 4A2**
**(902) 426-3474**

## A B S T R A C T

A comparision of 10-m wind measurements indicates that the wintertime wind (stress) variance at Sable Island exceeds that at various coastal stations by a factor of three (ten). One of the objectives of CASP was to determine the horizontal scales over which these variations took place, particularly over the wave measurement array. Marine winds were measured during CASP with an array of five submerged WOTAN anemometers, including two within the wave array, (18 and 30 km offshore) and a surface anemometer buoy (MINIMET) at the offshore limit of the wave array (30 km offshore). The potential for these measurements to investigate lateral shear in surface wind over the shelf will be explored.

In addition, the horizontal variations in the vector mean wind and atmospheric turbulence near the land/sea boundary were measured during five flights of the NAE Twin Otter research aircraft in conditions of moderate to strong offshore flow under unstable and near-neutral conditions. These data indicate that changes in the mean wind speed and turbulence levels at a height of 50 m occur over scales (10 km) comparable to that of the wave array itself. This result has implications for modelling the marine boundary layer in CASP studies of fetch-limited wave growth.

## 1. Introduction

The ability to model and forecast ocean surface waves and currents driven by wind depends upon the accuracy with which the atmospheric forcing function (eg. wind stress) over the ocean is known. Typically, however, oceanographers have access to only a limited number of isolated wind measurements usually from land-based stations. This leads to uncertainty about the "appropriate" magnitude of the forcing wind and may cause significant differences between the results from separate experiments. In studies of fetch-limited wave growth, for instance, Kahma (1981), found a dimensionless growth rate of wave energy with fetch that was twice that of the JONSWAP experiment. He attributed this difference, in part, to ambiguities in the wind measurements.

Physically, the differences in wind speed and surface stress over the ocean and adjacent land masses are due to changes in friction and atmospheric stability. SethuRaman and Raynor (1980), for instance, found wind speeds measured only 5 km offshore at Long Island, N.Y. to be higher by 15-100% than those measured on the beach, which they attributed to reduced surface roughness and thermal processes at the ocean surface. Similarly, Schwing and Blanton (1984) found the mean and variance of marine winds measured at a tower 20 km off Savannah, Ga. to exceed those measured at a coastal station by factors of 2.3 and 5.1 respectively. Over

larger scales, the differences may be due, in part, to regional variations in cyclonic activity. Weisberg and Pietrafesa (1983) derived a non-diagonal transfer function between winds at Charleston, S.C. and a meteorological buoy some 300 km offshore suggesting significant spatial variations in the wind field. The seasonally-modulated gains between offshore and coastal winds reached maxima of 1.5-2.0 in winter when the kinetic energy of the offshore wind exceeded that at the coast by factors of 4-6. In a broader context, Saunders (1977) used a million ship reports to define the seasonal distributions of wind stress on $1^0 X 1^0$ squares over the eastern continental shelf of North America. His results reveal an offshore increase of roughly 50% in the magnitude of the winter mean wind stress over the Scotian Shelf but virtually no offshore variation in summer. He speculates that much of the wintertime offshore increase is associated with variations in the intensity of cyclonic activity rather than changes in friction at the underlying surface.

During the Canadian Atlantic Storms Program (CASP), the marine wind field over the Scotian Shelf was monitored continuously with an array of five submerged WOTAN anemometers (Lemon, et al, 1984), including two within the wave array (Figure 1), and a MINIMET surface anemometer buoy (Coastal Climate Co., Seattle, Wash., U.S.A.) at the offshore edge of the wave array (30 km from coast). Land-based wind measurements included those from the standard 10m towers at Shearwater Airport (7 km inland) and on Sable Island. In addition, under certain conditions, research aircraft were used to measure the distributions of wind and atmospheric turbulence at low levels in the planetary boundary layer. A primary objective of these observations was to define the horizontal scales over which variations in the marine wind field take place. In this paper, historical wind measurements from Shearwater and Sable Island will be examined to determine the offshore variability over a scale of roughly 200 km in terms of the transfer function matrix (Section 2). In Section 3, preliminary results of the airborne and fixed anemometer measurements will be presented and conclusions will be drawn in Section 4.

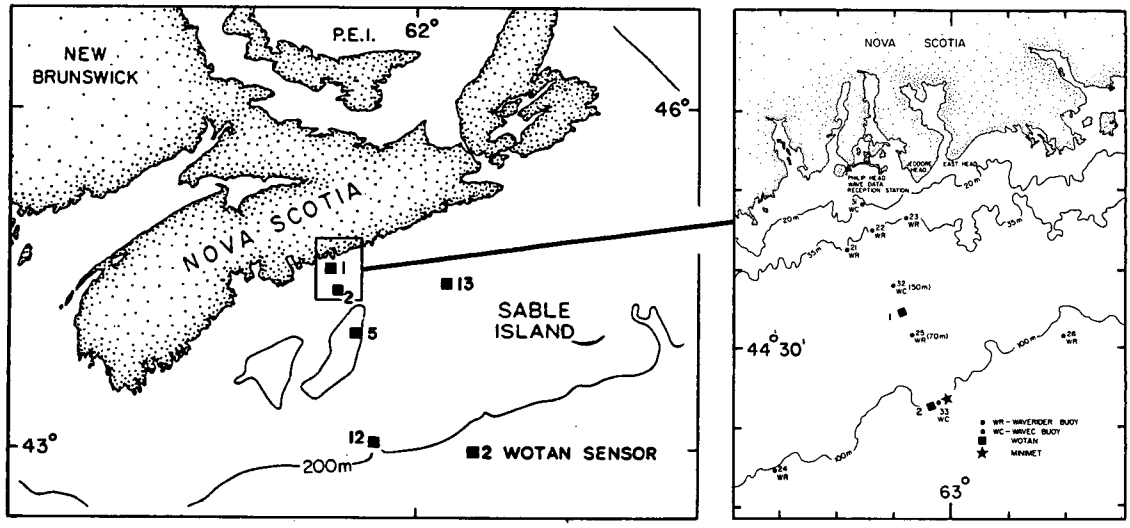


*Fig. 1 Locations of WOTAN and MINIMET anemometers during CASP. Inset shows the positions of the buoys in the BIO wave measurement array.*

## 2. Comparison of Surface Wind Measurements at Sable Island and Coastal Stations

The Atmospheric Environment Service operates a number of regular observing stations, equipped with standard (U2A) cup-and-vane anemometers at 10 m, on Sable Island and at various sites along the coast of Nova Scotia. Hourly wind observations generally consist of one- or two-minute averages of speed and direction (to the nearest ten degrees) taken at the top of the hour. For the period November 1, 1978 to December 31, 1983, the hourly data from four sites: Sable Island, Shearwater Airport (hereafter called "Halifax"), Yarmouth Airport and Sandy Cove, N.S. have been collected for analysis. (Note that the Sandy Cove anemometer, located on a headland near Halifax, is of a different type (45B), measuring average wind speed and direction over the entire hour and recording direction to only 8 points of the compass. This should not substantially affect the intercomparison of long-term statistics.) Then, since wind stress at the sea surface is the atmospheric forcing of interest, the speed data were converted to stress using Smith and Banke's (1975) formula for the 10-m neutral drag coefficient. No attempt was made to include the effects of atmospheric stratification which, according to Saunders (1977), are negligible on the seasonal time scales of interest. For convenience, the hourly stresses were resolved into cross-shore, $\tau_x(145^0T)$, and longshore, $\tau_y(55^0T)$, components. According to oceanographic convention, the direction of the wind is taken as that toward which the wind is blowing.

After examination of the full 5 - year data set, the statistics of both the mean wind stress and its variability during 1979-80 were judged to be typical of those for the entire record. Therefore, attention will be focussed on results from these two years. A comparison of the monthly vector mean wind stress at Halifax and Sable Island (Figure 2) reveals significantly larger magnitudes at Sable Island, but a fair agreement in direction. In fact, the overall (5 -year) mean stress at Sable Island (.025 Pa) exceeds that at Halifax by a factor of four, whereas the directions differ by only $5^0$. The seasonal variation evident in the monthly mean wind direction (from NW in winter, SW in summer) is caused by an annual shift in the strength and location of two principal centers of action in the atmosphere: the Azores-Bermuda High and the Icelandic Low (Blanton, et al, 1985).

Seasonal modulations are also prominent in the wind stress variability (Figure 3) as expressed by the standard deviation of the total stress vector, $\sigma = (\sigma_x^2 + \sigma_y^2)^{\frac{1}{2}}$. In winter (October-March) the standard deviations at Sable Island exceed those at the Halifax and Yarmouth coastal stations by factors of 2.5 to 3.5 which means that the variance in the offshore stress field is higher by an order of magnitude. However, the sharp increase in $\sigma$ between Halifax (7 km inland) and Sandy Cove at the coast suggests that much of the change may occur close to the land/sea boundary.

To investigate the spectral dependence of the relationship between offshore and coastal winds, frequency-dependent multiple regression analysis (Garrett and Toulany, 1982) was performed between each component of wind stress at Sable Island and the two components of stress at Halifax. In addition to providing more insight into the offshore transition in the wind field, this analysis might eventually lead to a useful operational transformation for estimating offshore from coastal winds (Weisberg and Pietrafesa, 1983). The hourly data were filtered to 3-hour intervals, using a simple running mean, and analyzed in 128-day seasonal segments commencing on November 1 (winter) and May 1 (summer) of each year. Within each segment, the data were divided into 63 overlapping (50%) blocks, demeaned and weighted with a cosine bell, prior to application of a fast Fourier transform.

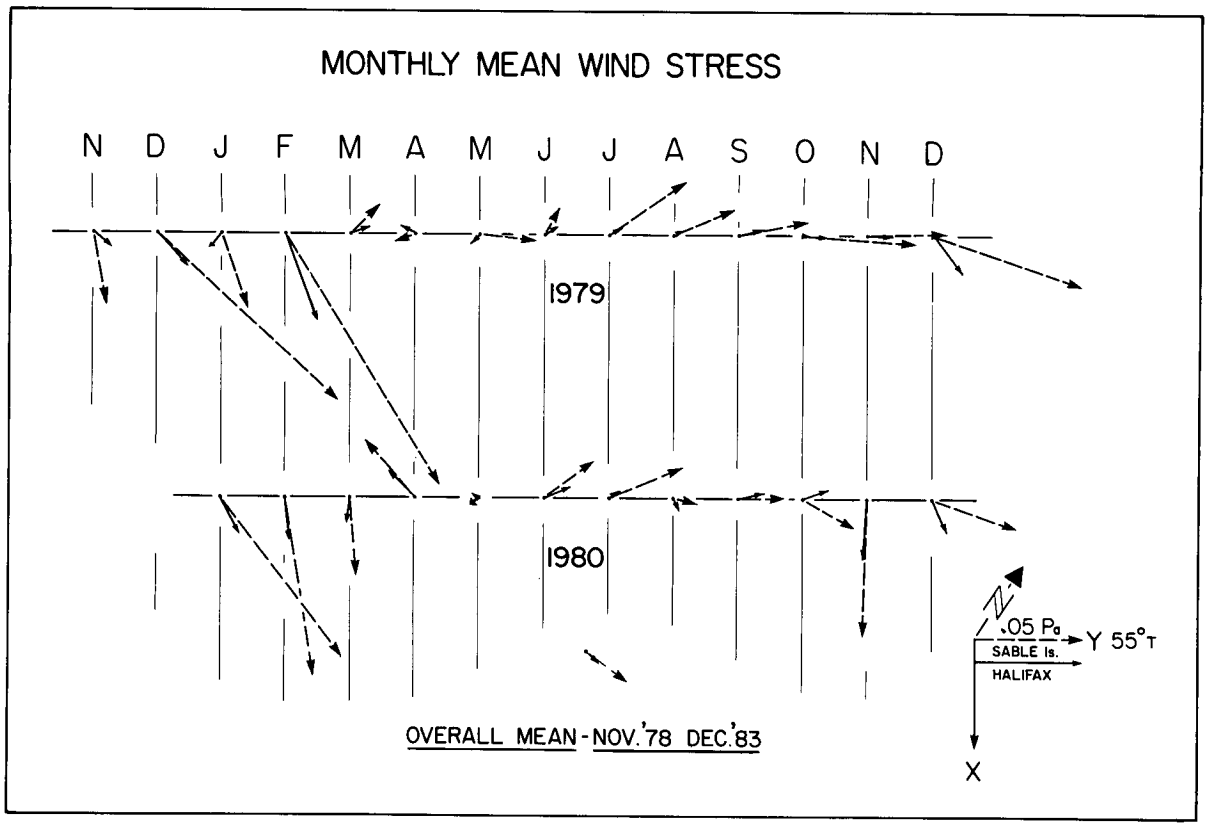


*Fig. 2 Estimates of the monthly mean wind stress at the sea surface (Smith and Banke, 1975) based on Halifax (solid) and Sable Island (dashed) winds during 1979-80. At bottom is the 5-year average stress over the period November, 1978 to December, 1983.*

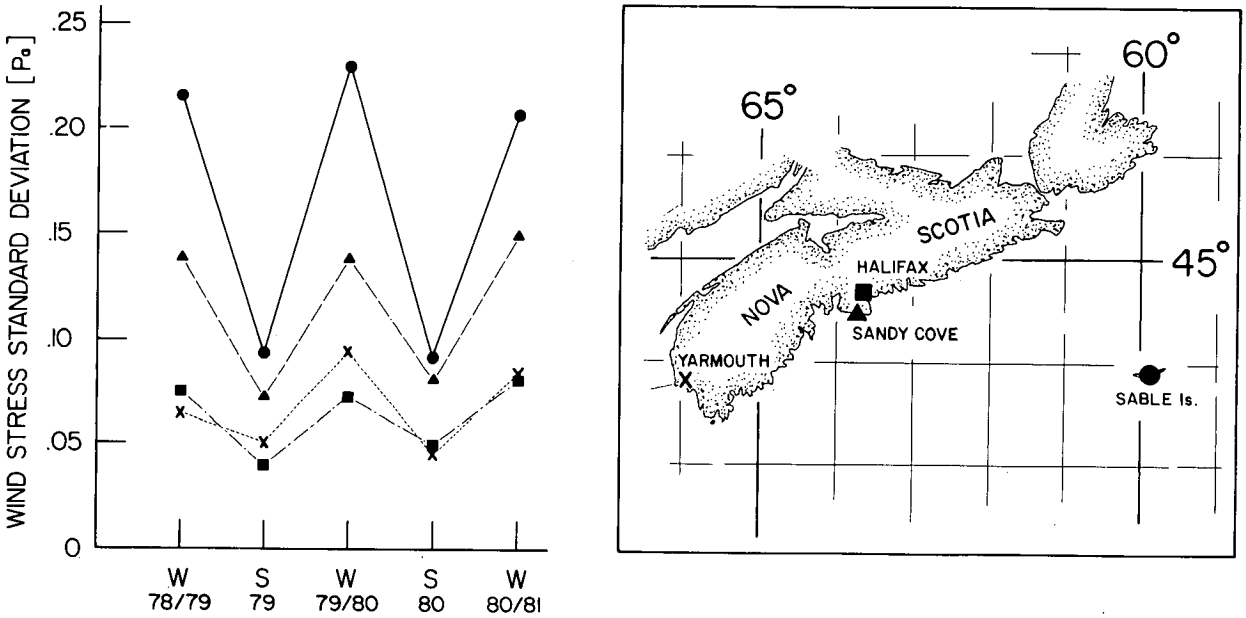


*Fig. 3 Seasonal variations of the standard deviation of the vector wind stress at Sable Island and various coastal sites. Winter values (W) cover the period from October through March; summer (S) from April through September.*

According to Welch (1967), the resulting number of degrees of freedom is 18(63)/11 = 103. The spectral and cross-spectral estimates were then used to determine the complex frequency-dependent coefficients (a, b) in a multiple regression of the form:

$$\tau_x = aX + bY + \text{noise}$$

where (X, Y) are the cross-shore and longshore components of the stress at Halifax and $\tau_x$ is the cross-shore component at Sable Island. (A similar relation holds for the longshore component, $\tau_y$). Confidence limits (95%) on the amplitudes and phases of a and b are computed according to the formulae proposed by Garrett and Toulany (1982).

Variance-conserving plots of the cross-shore component and vector wind stress spectra reveal that in winter (Figure 4a), most of the variance is concentrated in the synoptic band (2 to 10 day periods). The cross-shore component ($\tau_x$) provides the largest contribution to the variance at Sable Island whereas the two components at Halifax contribute equally in this band. As expected, the total variance at Sable Island is roughly an order of magnitude greater than at the coastal site. In summer (Figure 4b), the variance at both sites is reduced (note the scale change) and distributed somewhat more evenly through the spectrum. Although most of the energy is still in the synoptic band, there are significant contributions in the diurnal band at both Halifax and Sable Island. The diurnal constituent represents a larger fraction of the total variance at Halifax, but the fluctuations at Sable Island are stronger. In their coastal wind measurements in the South Atlantic Bight, Weisberg and Pietrafesa (1983) found a strong diurnal component, associated with the summer sea breeze phenomenon, which was absent at a buoy 300 km offshore. Those diurnal fluctuations, which were nearly rectilinear and oriented across the shoreline, served to reduce the seasonal modulation in the wind field variance. Here, however, diurnal variance is found at both coastal and offshore sites and the apparent dominance of the longshore ($\tau_y$) fluctuations at Sable Island suggests that a simple 2-D sea breeze circulation is not the cause.

The seasonal transfer functions between offshore and coastal winds may be expressed as the amplitude and phase of the maximum response of each Sable Island stress component to the two components of stress at Halifax (Figure 5). The orientation of the Halifax wind which produces this maximum response is defined by the angle

$$\theta = \tan^{-1}(b/a)$$

with respect to the X-axis, and also represents the direction for which the coherence between the two signals is greatest (Garrett and Toulany, 1982). In winter, the maximum gain in the synoptic band is roughly 3.0 for the cross-shore component and 2.5 for the longshore component. The Halifax wind which is most effective at producing cross-shore wind at Sable Island is roughly in the same direction (ie $\theta \approx 0$ ), whereas longshore wind at Sable is most coherent with Halifax wind deflected offshore by $20\text{-}30^0$. On the other hand, the longshore component at Sable Island is in phase with the most effective Halifax wind, but the phase of the cross-shore wind at Halifax leads that at Sable by an amount which increases continuously with frequency and is equivalent to roughly a 4-hour time delay over the entire range.

In summer, the gains are somewhat smaller (<2.5 in synoptic band) and exhibit a pronounced rolloff starting at periods of roughly two days. At diurnal frequencies, where significant energy exists at both sites, the amplitude of the response function reaches a minimum, suggesting that the diurnal fluctuations are not coupled. However, the orientation and phase relationships, especially in the synoptic band, appear tc be the same as in the winter season.

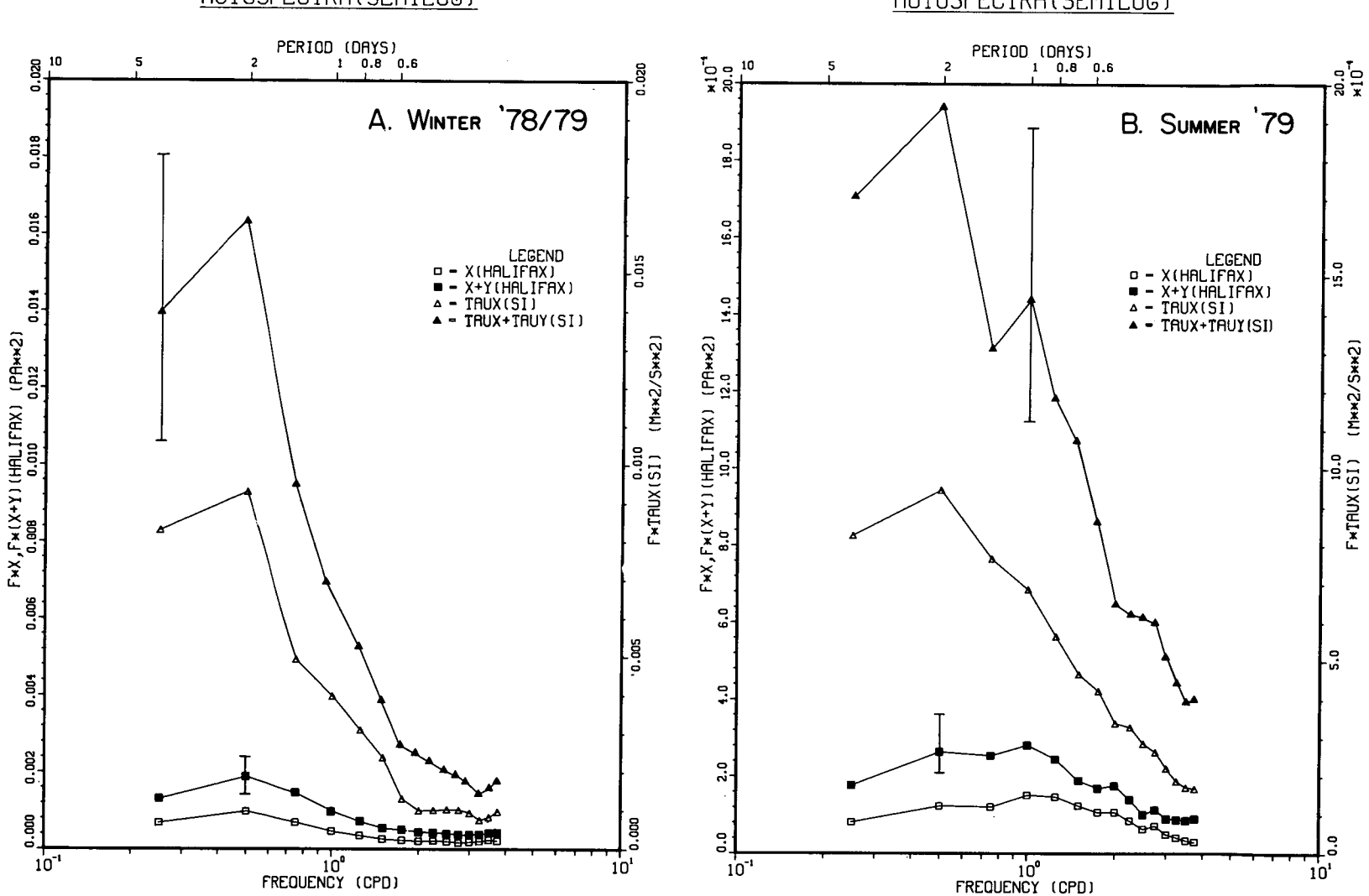


*Fig. 4 Variance-conserving plots of spectra of cross-shore component and total wind stress vector at Sable Island and Halifax during (a) winter, 1978-79, and (b) summer, 1979. Selected 95% confidence intervals are based on 103 degrees of freedom. (Jenkins and Watts, 1968).*

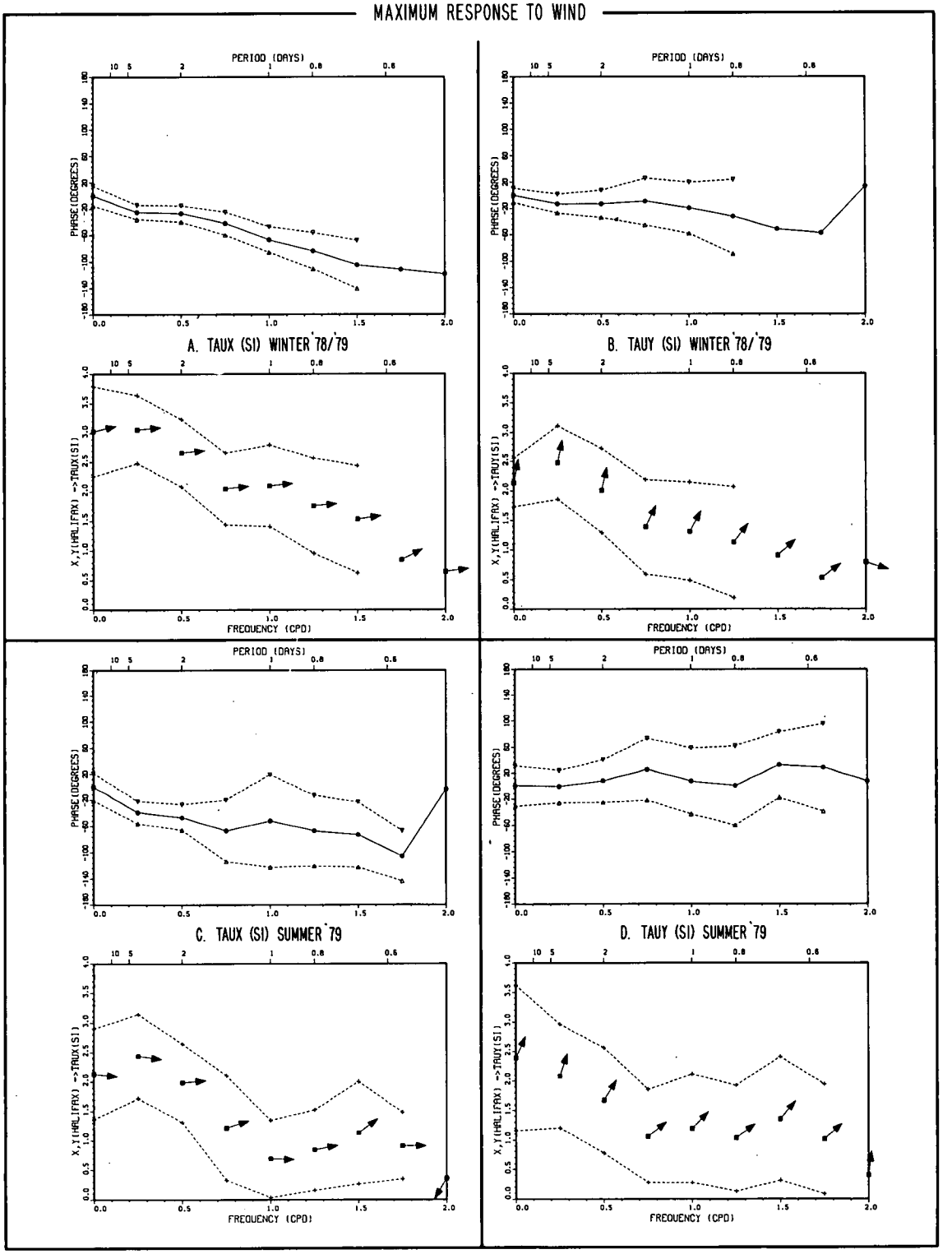


*Fig. 5 Maximum response functions, gain (lower) and phase (upper), for individual Sable Island wind stress components ($\tau_x, \tau_y$) based on the two components of stress at Halifax (X, Y). The direction, with respect to the vertical (Y) axis (55°T), of the Halifax stress which gives rise to the maximum response is indicated by arrows on gain values. Positive phase means Sable Island stress leads. Dashed curves indicate the 95% confidence intervals according to Garrett and Toulany (1982).*

Analysis of the relative contributions to the variance of the Sable Island stress components reveals that the regression on Halifax stress accounts for roughly 70% of the variance in the synoptic band in winter, but only 50% in summer. In winter, the percentage declines monotonically with frequency, whereas in summer it achieves a minimum of 10-20% in the diurnal band. As expected from the results in Figure 5, the cross-shore component at Halifax is almost entirely responsible for the variance in $\tau_x$, whereas both Halifax components make distinct contributions to the variance in $\tau_y$, especially in summer. Therefore, as in the South Atlantic Bight, the transformation matrix over the Scotian Shelf is non-diagonal.

To summarize, an examination of marine wind stress estimates based on measurements at Sable Island and several coastal sites has revealed that mean offshore wind stress and its fluctuations exceed the estimates made from coastal winds. Furthermore, a frequency-dependent multiple regression analysis has shown that, at least in winter, roughly 70% of the wind stress variance in the synoptic band may be accounted for by amplifying coastal winds by factors of 2.5-3.0 with small rotations and phase shifts. This methodology forms the basis for development of an operational transformation to represent marine surface wind stress at points of interest over the continental shelf in terms of land based measurements. One of the important questions to be addressed as part of the analysis of the CASP measurements is: How do the statistics of the wind field and hence the characteristics of the transformation matrix vary over the shelf? In this light, some of the preliminary results of airborne and fixed anemometer measurements are discussed in the next section.

## 3. Preliminary Results of Near-Surface Wind Field Measurements using Aircraft and Anemometers at Fixed Points

### a) Airborne Measurements:

As part of CASP, five low-level airborne surveys of the atmospheric boundary layer were conducted in the vicinity of the wave and current measurement arrays using the NAE Twin Otter research aircraft (Smith and MacPherson, 1986). The flight tracks were designed to measure mean wind speed and direction, the three components of atmospheric turbulence, temperature, and other atmospheric variables over the ocean and adjacent land masses. Cross-shore legs were typically 60 km in length, with an overland segment of at least 15 km, and were usually flown at a constant altitude of 50 to 70 m above the terrain.

All flights were carried out under conditions of cold, offshore advection. In these circumstances, the adjustment of the planetary boundary layer to the smoother, warmer sea surface occurs within an internal boundary layer (IBL) whose thickness increases with distance from the coast. Within the IBL, the wind speed increases due to buoyancy fluxes and reduced roughness at the sea surface, but the level of atmospheric turbulence may increase or decrease depending upon the relative importance of the contrasts in surface heating and friction (eg. Taylor, 1970). A typical cross-shore variation in (1-2 min.) average wind and direction, turbulence and air temperature at 50 m (Figure 6) reveals a 2 m $s^{-1}$ offshore increase in wind speed (which has been corrected for Doppler biases, Smith and MacPherson, 1986) coupled with a decrease in atmospheric turbulence. The latter observation implies that, in spite of weak surface heating reflected by the rise in 50 m air temperature, it is the change in surface roughness between land and sea that dictates the physics within the internal boundary layer.

In order to estimate average length scales over which the 50 m changes in wind speed and turbulence take place, data from four of the flights under similar environmental conditions were treated as an ensemble. After converting distances

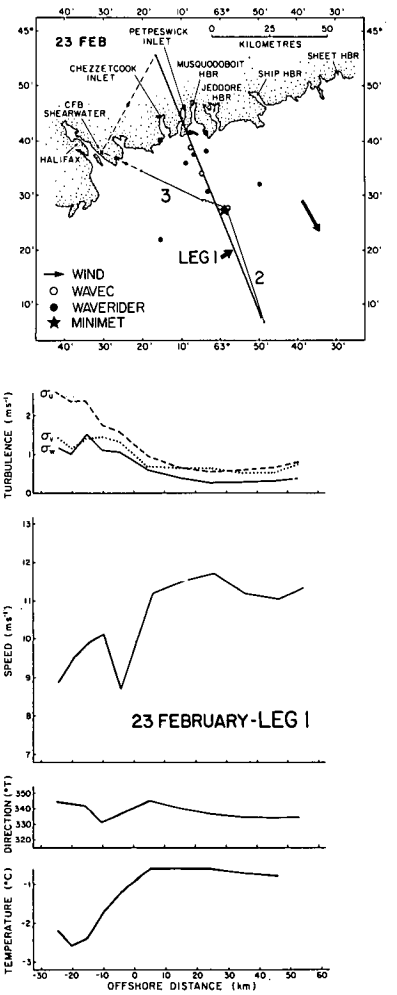


*Fig. 6 Typical cross-shore distributions of wind speed, direction, temperature and turbulence.*

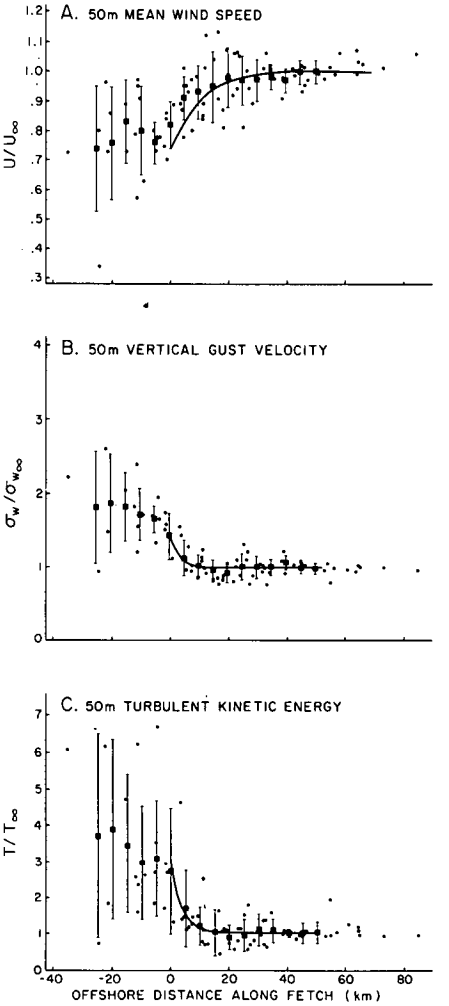


*Fig. 7 Ensemble-average ratios of local to offshore measurements. Curves are exponential fits to 10-km data.*

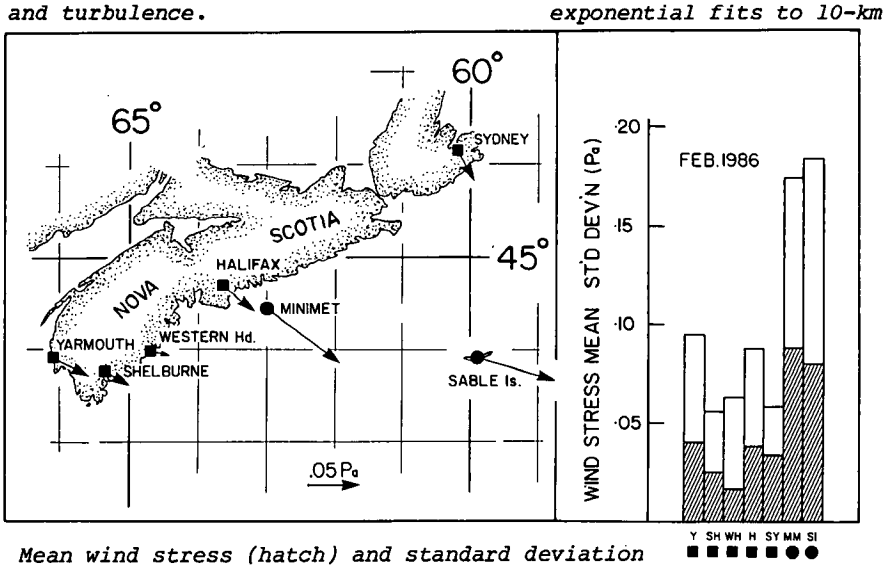


*Fig. 8 Mean wind stress (hatch) and standard deviation (blank) during February 1986. Vector means are also plotted at measurement sites (MINIMET direction rotated 25° clockwise).*

along the flight path to distances along the fetch, the 50-m data were further smoothed by averaging in 10-km overlapping bins centered at 5-km intervals from the coast. The mean wind speed, U, vertical gust velocity, $\sigma_w$, and turbulent kinetic energy, $T = \frac{1}{2}( \sigma_u^2 + \sigma_v^2 + \sigma_w^2 )$ were then normalized by their marine equilibrium values, ($U_\infty$, $\sigma_{w\infty}$, $T_\infty$), taken as the average of all observations at offshore distances (along the wind) in excess of 40 km.

In spite of the large standard deviations within each bin, the smoothed ratio, $U/U_\infty$, generally lies between 0.7 and 0.8 over land and rises gradually to 1.0 offshore (Figure 7a). An exponential least-squares-fit to the offshore variation of $(1-U/U_\infty)$ gives an e-folding scale of 9.3 km with a coastal value of $U/U_\infty = 0.73$. Similar fits to the turbulent quantities give offshore scales of 3.8 km and 3.4 km and coastal values of 1.8 and 3.3 for the quantities $\sigma_w/\sigma_{w\infty}$ and $T/T_\infty$ respectively (Figure 7b, c). Thus, under these conditions, the adjustment of the planetary boundary layer to abrupt changes in surface friction and heating over the ocean appears to be accomplished within a relatively short distance ($\leq$ 10 km) from the coast. These variations are not negligible, however, in studies of fetch-limited wave growth over the 30 km CASP wave array.

b) Measurements from Fixed Anemometers

In order to better define the spatial distribution of surface wind and stress, the CASP experimental plan called for the deployment of a number of anemometers across the shelf including two MINIMET buoys, two similar buoys manufactured by METOCEAN LTD., two experimental Hermes buoys modified by SEIMAC LTD. to carry anemometers, and the WOTAN sensors, manufactured by Arctic Sciences Ltd. of Sidney, B.C. Of this array of instruments, only one of the MINIMETs and the WOTANs (Figure 1) provided significant amounts of useful data. The others were plagued by various electrical and mechanical problems (eg leakage), which resulted in damage to or loss of the buoys.

The functional MINIMET, moored at the offshore edge of the wave measurement array 30 km from shore, was intended to measure 10-min vector average wind speed and direction, air and sea temperatures and record them internally on magnetic tape. The buoy also contained an ARGOS transmitter which relayed hourly samples of the 10-min data to shore via satellite for use by the CASP forecasters. The initial performance of the MINIMET was marred by the slow leakage of seawater into the hull, apparently caused by a collision (or vandalism) which occurred near the end of December and resulted in the loss of useful data between December 26, 1985 and January 30, 1986 when the refurbished buoy was redeployed. During the second deployment, the air temperature data were found to be unreliable due to a leaky connector between the buoy hull and sensor lead and, according to the aircraft data, the wind direction was offset by roughly $25^0$ (clockwise) apparently because of a misalignment of the anemometer vane during assembly (Smith and MacPherson, 1986). However, these problems have no bearing on the following analysis.

As before, the winds measured at Sable Island, the MINIMET buoy, and various coastal stations were used to estimate stress at the sea surface according to Smith and Banke (1975). Comparison of the February, 1986 vector wind stresses at Sable Island and the coastal sites (Figure 8) reveals the same pattern found in the winter data from 1979-80 (Figures 2 and 3) with offshore means and standard deviations exceeding those at the coast by factors 2 to 3. Furthermore, after adjustment to the reference height of 10-m using a neutral (logarithmic) boundary layer profile (Smith, 1981), the MINIMET wind stress mean and standard deviation are virtually identical to those at Sable Island. This result is also found in the March stress data (not shown). Thus, the MINIMET data confirm the hypothesis that the transition from weaker land to marine winds occurs near to the coast.

Unfortunately, attempts to further resolve the nearshore gradient in marine winds using WOTAN data has been frustrated by uncertainties in the instrument's calibration against wind speed. Previous calibration exercises have revealed that the coefficients in the formula used to relate surface wind speed to sound pressure level are strong functions of the depth at which the WOTAN is moored, especially in shallow water (F. Dobson, personal comm.). The CASP results confirmed this behaviour with the discovery that sound pressure levels at the shallowest (63-m) WOTAN near the coast were consistently higher than those measured throughout the rest of the array. When crude (interpolated) estimates of the calibration coefficients were applied to these data, the statistics of the resulting wind speeds were inconsistent with those of the nearby MINIMET and land-based measurements. Moreover, the WOTAN wind speeds tended to be highest at the inshore (shallowest) station and decrease the distance offshore (and depth). Thus, at present, the accuracy of the WOTAN wind measurements is questionable and certainly insufficient to resolve offshore variations in the marine wind field.

## 4. Conclusions

The major conclusions of this study are:

a) The mean and variance of sea surface wind stress estimates based on offshore (Sable Island) winds exceed those at coastal stations by factors of 3 and 10 respectively.

b) The transfer function between coastal (Halifax) and offshore wind stress is weakly nondiagonal with gains of order 2.5-3.0 and small phase shifts. The frequency-dependent multiple regression analysis accounts for 70% (50%) of the offshore variance in the synoptic bands during winter (summer).

c) During CASP, low-level (50-m) airborne surveys of the planetary boundary layer in conditions of cold, offshore advection revealed that the mean wind speed and atmospheric turbulence levels achieve their marine equilibrium levels at offshore scales (along the fetch) of order 10 and 4 km respectively.

d) Comparison of land-based coastal and offshore measurements with MINIMET buoy data confirm that the transition to marine winds occurs within 30 km of the coast, but WOTAN measurements across the shelf do not have sufficient accuracy to resolve this gradient.

For future CASP modelling studies of surface wave generation by wind, the most reliable estimates of the wind stress distribution will probably come from atmospheric models of the internal boundary layer, constrained by the aircraft and surface anemometer measurements.


## ACKNOWLEDGEMENTS

The author would like to thank Drs. F. Dobson and C. Anderson for many useful discussions of relevant atmospheric and oceanic physics. He is also indebted to J.I. MacPherson and the Twin Otter pilots for their support during the aircraft measurement program. This work was supported (in part) by the Federal Panel on Energy R&D (PERD).

## REFERENCES


Blanton, J.O., F.B. Schwing, A.H. Weber, L.J. Pietrafesa, D.W. Hayes. Wind Stress Climatology in the South Atlantic Bight. in Oceanography of the Southeastern U.S. Continental Shelf, ed. Atkinson et al, AGU, Washington D.C., p 10-22.

Garrett, C. and B. Toulany. 1982. Sea Level Variability due to Meteorological Forcing in the Northeast Gulf of St. Lawrence. J. Geophys. Res., 87, 1968-1978.

Jenkins, G.M. and D.G. Watts, 1968. Spectral Analysis and Its Applications, Holden-Day, San Francisco, p 82.

Kahma, K.K. 1981. A Study of the Growth of the Wave Spectrum with Fetch. J. Phys. Oceanogr., 11 1503-1515.

Lemon, D.D., D.M. Farmer, and D.R. Watts. 1984. Acoustic Measurements of Wind Speed and Precipitation over the Continental Shelf. J. Geophys. Res., 89, 3462-3472.

Saunders, P.M. 1977. Wind Stress on the Ocean over the Eastern Continental Shelf of North America. J. Phys. Oceanogr., 7, 555-566.

Schwing, F.B. and J.O. Blanton. 1984. The use of Land-and-Sea-Based Wind Data in a Simple Circulation Model. J. Phys. Oceanogr., 14, 193-197.

SethuRaman, S. and G.S. Raynor. 1980. Comparison of Mean Wind Speeds and Turbulence at a Coastal Site and Offshore Location. J. Appl. Meteorol., 19, 15-21.

Smith, P.C. and J.I. MacPherson. 1986. Lateral Variations of the Near-Surface Wind Velocity and Atmospheric Turbulence at the Land-Sea Boundary during CASP. Submitted to Atmosphere-Ocean.

Smith, S.D. 1981. Factors for Adjustment of Wind Speed over Water to a 10-M Height. BIO Report, BI-R-81-3, 29 pp.

Smith, S.D. and E.G. Banke, 1975. Variation of Sea Surface Drag Coefficient with Wind Speed. Quart. J. Roy. Meteor. Soc., 101, 665-673.

Taylor, P.A. 1970. A Model of Airflow above Changes in Surface Heat Flux, Temperature and Roughness for Neutral and Unstable Conditions. Boundary-Layer Meteorol., 1, 18-30.

Weisberg, R.H. and L.J. Pietrafesa. 1983. Kinematics and Correlation of the Surface Wind Field in the South Atlantic Bight. J. Geophys. Res., 88, 4593-4610.

Welch, P.D. 1967. The Use of Fast Fourier Transform for the Estimate of Power Spectra: A Method based on Time Averaging over Short, Modified Periodograms. IEEE Trans. Audio Electroacoust., 15, 70-73.

# WAVE FIELD PROPERTIES AND A COMPARISON OF TWO DIRECTIONAL WAVE BUOYS

Barbara-Ann Juszko, Bodo de Lange Boom, David R. Green and Robin Brown

Seakem Oceanography Ltd.,
2045 Mills Road, Sidney, British Columbia

## ABSTRACT

The performance of two directional wave buoys was assessed. The Datawell WAVEC buoy operated well, consistently provided good quality data and the derived wave direction statistics agreed with observed wave and wind directions and model results. Data from the Endeco WAVE-TRACK buoy had to be corrected with derived instrument amplitude and phase response functions and for spurious low frequency energy.

Properties of the wave field were determined using data obtained from a WAVEC buoy moored on the Grand Banks off Newfoundland. The applicability of the linear wave dispersion equation was examined and the data were shown to be affected by Doppler shifts during storms. The data were used to generate new statistics in order to describe the wave field. An apparent wave direction, obtained from a weighted averaging of the frequency dependent mean directions, showed good agreement with wind directions. Wave shape parameters were defined using the surface slope measurements. Their development through a storm described a wave profile whose forward and back face steepened with wind speed at approximately the same rate though the forward face was always steeper than the back. Both faces became more asymmetric about mean water level with wind speed. A mean wave direction was obtained from the surface slope estimates thereby providing an independent and non-spectral means of obtaining wave direction information.

## INTRODUCTION

In the past few years, increasing demand for directional wave information has led to the development of new instrumentation and analysis procedures. Two basically different designs of directional wave buoys are currently available on the market. The first is the surface slope-following buoy which includes the NORWAVE (Bergen Ocean Data), WADIBUOY (CNEXO and Nereides), and WAVEC (Datawell) buoys. The second, exemplified by the WAVE-TRACK Type 956 (ENDECO INC.) buoy, is the wave orbital-following buoy. An understanding of the operation, reliability and applicability of these two instrument types would prove useful when designing field experiments.

Two major studies have recently been conducted in Canadian waters, for which a primary goal was to assess the performance of the Datawell WAVEC and ENDECO type 956 WAVE-TRACK buoy. As these buoys provide considerably more information than "heave-only" buoys, a secondary goal was to examine their usefulness in studying wave field properties beyond the standard directional spectra.

This paper will describe the studies conducted, will provide a summary of findings with regard to the buoy assessments, and will discuss various statistics and analyses specific to directional buoy data which can further our understanding of the wave field.

## STUDY BACKGROUND

Of the two studies conducted in Canadian coastal waters employing Datawell WAVEC and ENDECO Type 956 WAVE-TRACK buoys, the first occurred along the northern coast of British Columbia from October 1982 to May 1984. The WAVEC buoy was moored in 189 m of water at 52°06.8'N and 128°57.5'W. The WAVE-TRACK was located in 156 m of water at 53°21.2'N and 130°46.7'W. Though neither buoy operated continuously over the two years, at least 10 months of data were obtained from both.

The second study was of shorter duration, February to April 1984, but was more intensive as it was designed for specific intercomparison between these two buoys as well as against a standard Waverider (Datawell), visual observations and hindcast model results. Two WAVEC buoys and one WAVE-TRACK buoy were moored in approximately 85 m of water on Newfoundland's Grand Banks off Canada's East Coast. Their positions were, respectively, 46°45.8'N and 48°48.8'W; 46°44.83'N and 48°49.75'W; and 46°45.67'N and 48°45.75'W with less than one nautical mile separating them from each other. Visual observations were obtained from a nearby manned mobile drilling unit (the West Venture operated by Mobil Oil Canada Ltd.) and model results were supplied by F.G. Bercha Ltd. of St. John's, Nfld.

The WAVEC is a slope-following buoy, approximately 2.5 m in diameter consisting of a central instrument canister to which are strapped peripheral flotation segments. The WAVE-TRACK has an inverted pendulum design composed of a surface sphere (less than 1 m in diameter) and subsurface shaft to which is attached the sensor package. The wave direction components are obtained not from East-West and North-South surface slopes as for the WAVEC, but from the angular tilt of the shaft induced by the wave orbital velocities.

Standard time series analyses methods were used to process the data to spectral components and the approach of Longuet-Higgins et al. (1963) was taken to calculate directional spectra. A second processing scheme, a Frequency Band-Pass Analysis, as described in Brainard (1982) can also be used for WAVE-TRACK data. This method, however, proved inefficient and the results of limited usefulness.

Wave field properties were studied using data obtained from one WAVEC buoy (46°44.83'N, 48°49.75'W). Standard time series analyses methods were used to obtain the spectral derived statistics. The time series of heave and surface slopes were corrected for frequency dependent instrument amplitude and phase transfer functions prior to performing any calculations in the time domain. The wave field was sampled every three hours for 34 minutes (at a rate of 1 sample every 0.78125 seconds), except during storms when continuous recording was initiated. Ensemble averaging of a maximum of 10 blocks and selected band-averaging was performed on the spectra resulting in 64 frequencies with a resolution of .005 hz for frequencies less than 0.2 hz and .01 hz at higher frequencies.

Corresponding wind measurements (every three hours) were obtained from an anemometer mounted 86 m. above mean water level on the mobile drilling unit West Venture, approximately two nautical miles from the WAVEC buoy. These data were supplied by Mobil Oil Canada Ltd. and were not corrected for anemometer height. For the non-spectral statistical analyses, two storm periods were examined: March 10-12 and March 27-31.

## BUOY ASSESSMENT

Only a summary of findings will be provided here. Details can be found in Juszko (1985) and Juszko et al. (1985).

The WAVEC buoys were generally reliable in terms of hardware, telemetry and data quality. A major concern, however, was the ruggedness of the design since the peripheral flotation segments have been dislodged or lost. Design changes to the WAVEC have since been made. As indicated by the experimental dispersion ratio (see following section), the buoy responded linearly to the wave field at all frequencies within operational range (.05 - .6 hz). Over long-term deployment, there was a 95.6% data recovery during buoy operation. An examination of the directional spectra showed results consistent with other measurements including visual observations, model results and those inferred from wind information.

The WAVE-TRACK buoy, being small, is easy to handle. However, its size limits battery capacity and the buoy cannot transmit data continuously for long periods as can the WAVEC. Its design and sensor package are quite rugged as they survived beaching on at least one occasion. During winter deployment on the Grand Banks, the exposed surfaces suffered severely from icing, a problem not observed for the WAVEC. The buoy did not respond linearly to the wave field showing spurious low frequency energy and increased noise for frequencies greater than 0.3 hz. Over long-term deployment, there was only 65.7% data recovery during buoy operation. Heave spectral results agreed well with other measurements, except as mentioned previously, at very low frequencies. Mean wave directions also agreed well in the mid-frequencies (from the spectral peak to 0.3 hz). The directional spread about the mean was generally greater for WAVE-TRACK data than WAVEC. Some of the data problems encountered may have been made more severe due to the physical conditions (e.g. icing) and the inherent large directional spreads associated with the Longuet-Higgins analysis.

## ASSESSMENT OF DOPPLER SHIFT EFFECTS

The technique developed by Longuet-Higgins et al. (1963) requires a cross-spectral analysis between the heave and two surface slope signals, in this case, the North-South and East-West slope. It can readily be shown that the heave energy values are related to the slope energies through the wave dispersion equation, such that

$$K^2 CO_{11}(f) = CO_{22}(f) + CO_{33}(f) \qquad \textbf{Eq. 1}$$

where K is the wavenumber and $CO_{11}(f)$, $CO_{22}(f)$, $CO_{33}(f)$ are the heave and two slope co-spectral estimates at frequency, f. For an example derivation of Equation 1 see Audunson et al. (1982).

The ratio, R(f),

$$R(f) = \left[ \frac{K^2 CO_{11}(f)}{CO_{22}(f) + CO_{33}(f)} \right]^{1/2} \qquad \textbf{Eq. 2}$$

can be defined as the experimental dispersion ratio and should be equal to 1.0 at all frequencies if the wave field is behaving according to linear theory and if the buoy is measuring it properly. The behaviour of R(f) was used by Audunson et al. (1982) and by Juszko et al. (1985) to assess the operational range of the buoy and the instrument response when damaged. Since the estimate of K in Eq. 2 requires an assumption on the wave phase speed, it can also be used to illustrate the influence of wind-induced (Barstow and Krogstad, 1983) or tidal (Ezraty and Cavanie, 1981) currents which produce a Doppler shift of observed wave frequencies.

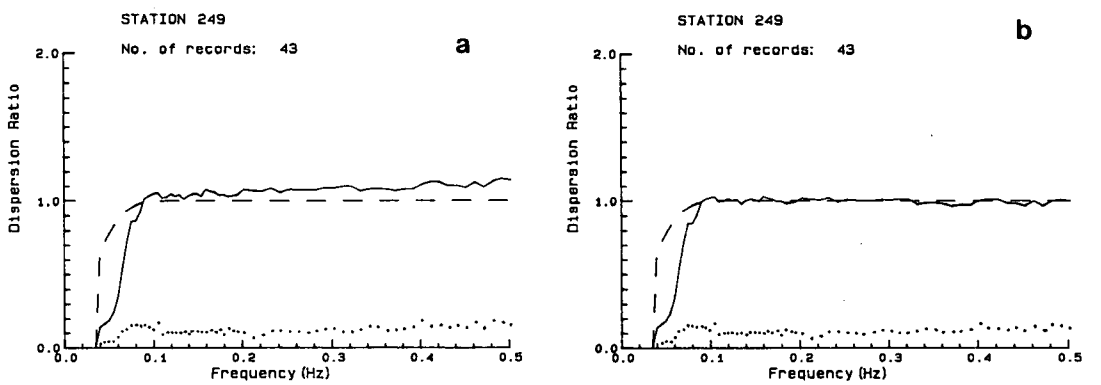


**Figure 1.** Plot of R(f) for storm records: (a) uncorrected; (b) corrected assuming a 20 cm/s current in the direction of wave travel (solid line: mean experimental values: dashed: theoretical; dotted: one standard deviation).

Figure 1 contains two plots of R(f) calculated for records taken at the peak of a storm on March 27-31. Figure 1a shows the calculated R(f) values averaged over 43 records, as well as one standard deviation about this mean. With the exception of low frequencies where water depth can influence the results, it can be seen that the ratio is greater than 1.0 at all frequencies with increased severity toward higher frequencies. Higher frequencies are more sensitive to Doppler shift effects. Figure 1b shows an applied correction assuming a Doppler shift induced by a current of 20 cm/s in the direction of wave travel. This current may be the result of an increased Stokes Drift at the height of the storm. A Doppler shift is not a function of relative heave and slope energy but only a translation of the frame of reference. Any non-linearities in the wave field would also be translated. The presence of significant Doppler shift effects would have repercussions when calculating spectral statistics as well as wave shape statistics from "heave-only" time series due, in the latter case, to the necessary wavelength assumptions. However, wave shape statistics calculated from the slope time series would not be affected.

## APPARENT WAVE FIELD DIRECTION

The most common wave direction property reported in the literature is the mean direction of wave travel for each frequency band of the spectrum. The angular spread about this mean is then calculated from one of several spreading models. Of importance for certain engineering applications, however, is a bulk estimate of the mean direction and energy of the wave field, irrespective of frequency. The peak direction, i.e. the mean direction associated with the spectral peak frequency, is often the only statistic given to characterize the bulk wave field. As the wave energy is broad-banded, the peak direction may not be representative of the wave field as a whole. Two apparent directions were derived to remedy this. They consist of a weighted averaging of the mean directions at each frequency with the weights supplied by either the energy density or by the estimate of directional spread at each frequency. Weighting by spectral density is a common procedure used to reflect the relative importance of the frequency-band and was also used by Longuet-Higgins (1957) to obtain a "Principal Direction". Weighting by directional spread, in itself a function of spectral density, allows for a greater contribution to the mean by a narrow beamed wave field.

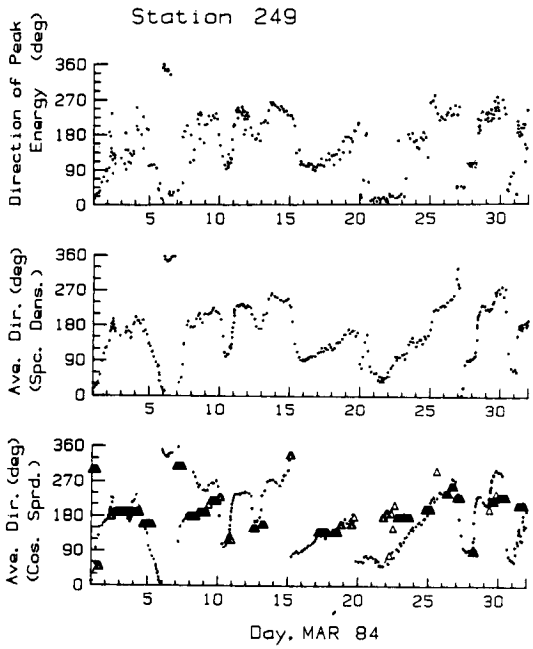


**Figure 2.** Time series plots of peak direction, average apparent direction weighted by spectral density and average apparent direction weighted by cosine spread factor. Also shown are visually observed swell directions in the region (triangles).

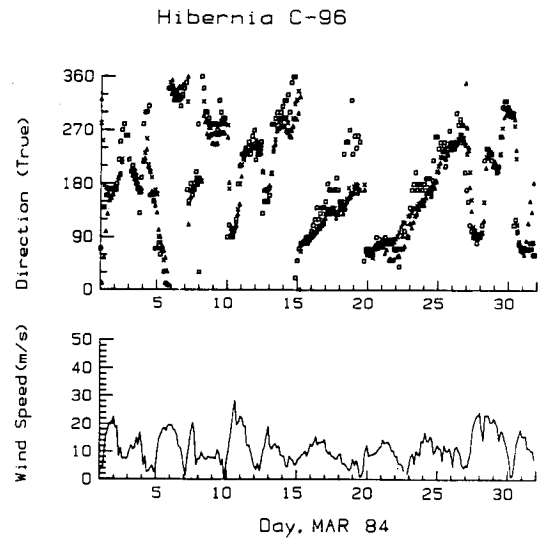


Figure 3. Time series of wind direction (squares), the spread weighted average apparent sea directions (crosses) for March 1984. Also shown are wind speeds.

Figure 2 contains time series of the peak direction (taken as "coming from") and the two different apparent directions defined above. The directional weighting is by the cosine spread parameter as defined by Hasselmann et al. (1980). Figure 3 compares the spread weighted apparent direction and an apparent "sea" direction (averaging only over periods less than seven seconds) to the direction of local winds. One would expect a better agreement between "sea" direction and local winds due to ocean response times. It can be seen in Figure 2 that both weightings leads to a reduction in the scatter when compared to peak directions. The different weightings can result in a different turning (clockwise vs counter-clockwise) of the apparent direction under veering winds (e.g. March 14-15, 26-27 - see Figure 2). Weighting by the spread tends to follow the wind more closely. This reflects the dominating influence of the low frequency spectral peak in the energy weighting and of the high to low frequency spectral development observed during storm buildups, in the spread weighting. Periods of discrepancy between wind and wave direction are usually associated with low winds and swell-dominated conditions.

## WAVE SHAPE STATISTICS

The average wave shape and how it changes with time and wind conditions, is an important consideration in both theoretical and practical applications. A zero-crossing analysis was performed on the heave time series in order to characterize each wave. The wave profile was divided into sections including front slope (trough to crest of forward or downwind face), crest front (zero-crossing to peak), trough front (trough to zero crossing) and the equivalent back face areas. The corresponding slope values were then obtained and used to calculate a resolved slope or slope magnitude (ie: sqrt($S_1^2 + S_2^2$) where $S_1$ is the North-South slope and $S_2$ is the East-West slope). As the sampling rate was too coarse to allow for wave-by-wave analysis, it was decided to average each statistic over the entire record and compare them with average statistics such as the significant wave height or spectral moments.

It is important to note that the method chosen for the calculation of the mean can result in significantly different results. A mean slope can be obtained using either of the following equations:

$$\frac{1}{N} \sum^{N} \left[(S_1^2 + S_2^2)^{1/2}\right] \qquad \text{Eq. 3}$$

$$\left[\frac{1}{N} \sum^{N} (S^2 + S_2^2)\right]^{1/2} \qquad \text{Eq. 4}$$

where N is the number of slope pairs.

Eq. 3 was used because it was conceptually more desireable to average the resolved slope when only considering properties associated with slope magnitudes. Eq. 4 has been used in the literature for calculation of the RMS slope. A linear regression between statistics calculated using both methods (Corr. Coeff. >.99) shows an approximately 18% increase in the value obtained using Eq. 4 over that from Eq. 3. Similar considerations must be taken into account when examining asymmetry parameters such as the mean horizontal asymmetry (ie. asymmetry about the zero crossing; ratio of crest front to trough front slope) indicator. There are again significant differences between a calculated mean of the ratios for each wave and the ratio of the mean derived statistic.

Figure 4 contains overlayed time series of the mean wave front slope, significant wave height and wind speed for the two storm periods in March (wind directions are the same as in Figure 3). There is an obvious co-variance between the wave slopes and both the wave energy and wind speed. It can also be observed that the wave slopes are responding to the change in the wind field faster than the total heave variance given by the significant wave height. The correlation between the mean front face slope and wind speed is shown in Figure 5. R values of 0.83 and 0.87 were found correlations between mean front slope and significant wave height and wind stress (given as wind speed squared), respectively. The results reflect an increase in wave slopes at high frequencies, almost immediately with a change in wind speed, with little contribution to the total variance by increased wave heights. There was no obvious dependence on shifts in wind direction. The maximum slopes observed during the storm ranged from 0.3 to 0.6 which are consistent with the experimental results of Kjeldsen and Myrhaug (1979) (as cited by Le Blond, 1982) who calculated a forward face steepness of 0.32 to 0.78.

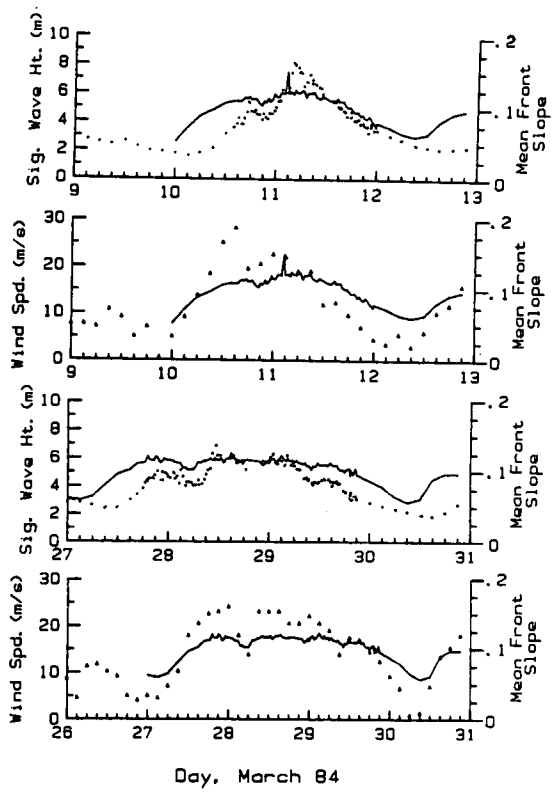


**Figure 4.** Time series of mean wave front slope (solid line), significant wave height (dotted line) and wind speed (triangles) for the two storm periods in March (1984).

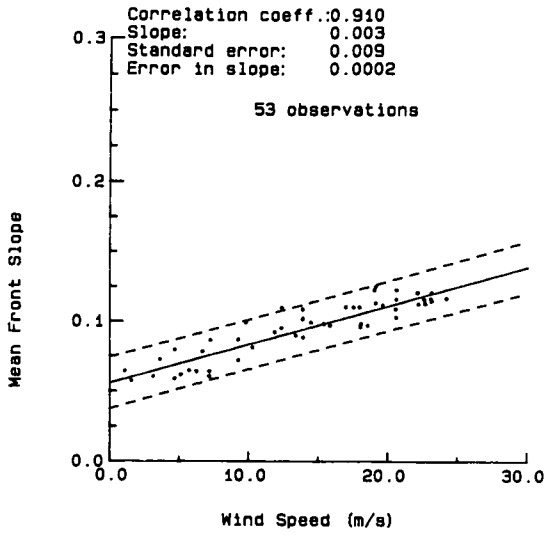


**Figure 5.** Regression of mean wave front slope and wind speed.

Figure 6 shows similar regressions of the front face horizontal asymmetry indicator against wind speed. Asymmetry indicators illustrate changes in the wave profile with the horizontal indicator reflecting changes about mean sea level in the forward or back face of the wave and the vertical indicator reflecting changes between the forward and back face. These also indicate a direct response with wind. The two plots illustrate the significant difference made by the calculation technique chosen. Figure 6a uses the ration of the record mean crest and mean trough slope. The means of the ratios (one ration for each wave profile, Figure 6b) is conceptually more acceptable though the scatter is increased due to the necessary wave-by-wave analysis required.

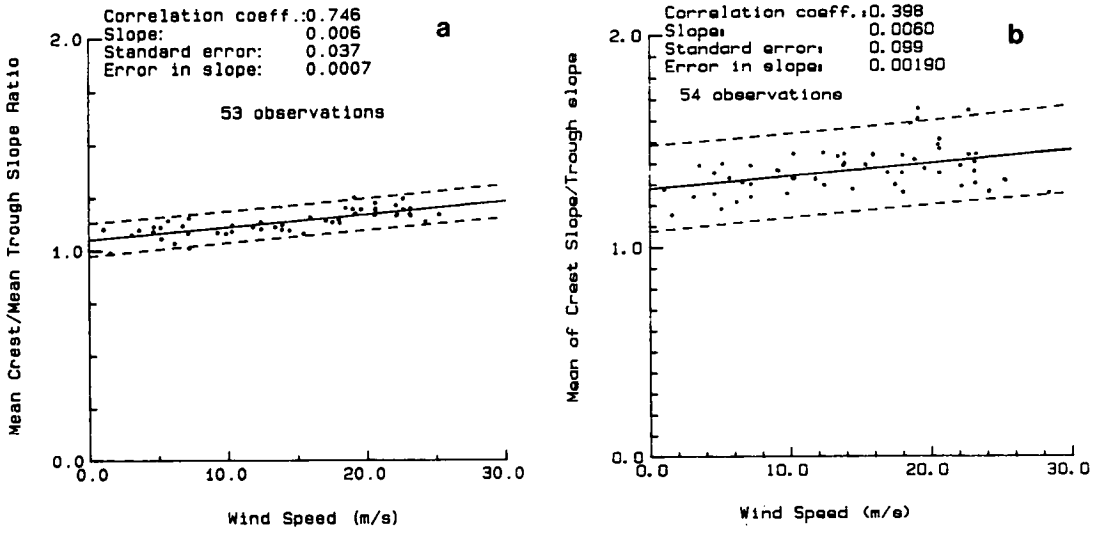


Figure 6. Regression of horizontal asymmetry indicator against wind speed for the forward face (a) mean crest/mean trough slope ratio; (b) mean of crest/trough slope ratios.

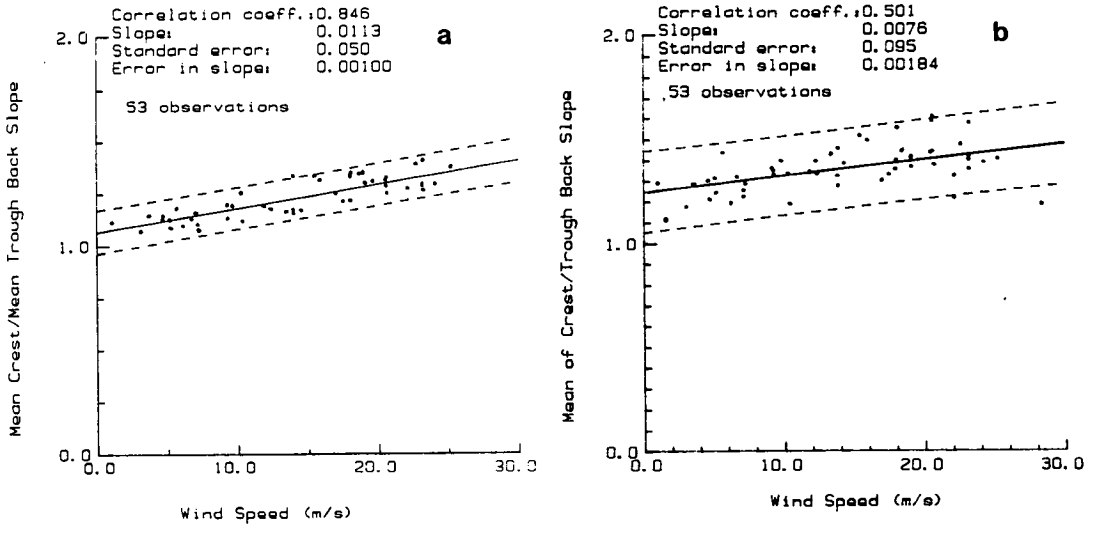


Figure 7. Regression of horizontal asymmetry indicator against wind speed for wave back face (a) mean crest/mean trough slope ratio; (b) mean of crest/trough slope ratio.

Similar statistics can be obtained using wave back slopes and the same behaviour is observed. Regression of the mean back slope against wind speed results in a Corr. Coeff. of R = 0.91 and slope of .0028. Compared with the forward face, there is slightly better correlation between the back face horizontal asymmetry parameter (see Fig. 7) and wind speed and the ratios observed were slightly larger.

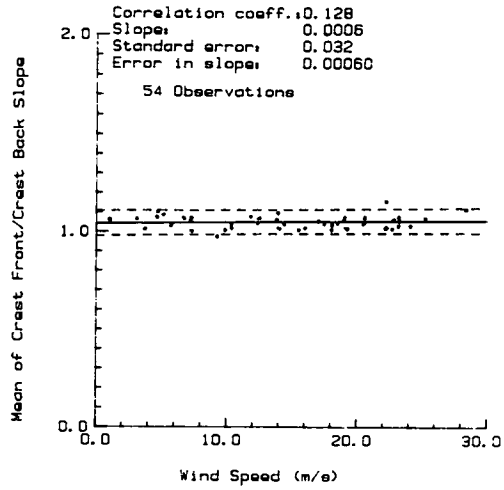


Figure 8. Regression of vertical asymmetry indicator against wind speed.

A vertical asymmetry indicator (ie. about wave peak) is given by the mean of the crest front/crest back slope ratio. A regression against wind speed, Figure 8, shows little change in the ratio with increasing winds though they are consistently greater than 1.0 reflecting a steeper forward face.

These statistics, as a whole, are describing a wave profile which develops with wind speed in such a manner that the crests are steepening relative to the troughs and the forward face and back face are steepening at approximately the same rate. They also show that the assumption of regular, symmetric waves, needed in estimates of wave steepness from a "heave-only" buoy does not apply.

Slope derived steepness values can be compared to heave derived ones. The mean slope or wave steepness parameter ($\alpha$), defined as

$$\alpha^2 = M_4/g^2 \qquad \text{Eq. 5}$$

where $M_4$ is the fourth moment of the heave spectrum and g is gravitational acceleration, has been used in order to analyze results from hindcast models in relation to wave height and wind speed (see Cummins and Bales (1980), Komen et al. (1984)). It is derived from the linear wave dispersion equation and can be used as another check on the latter's applicability.

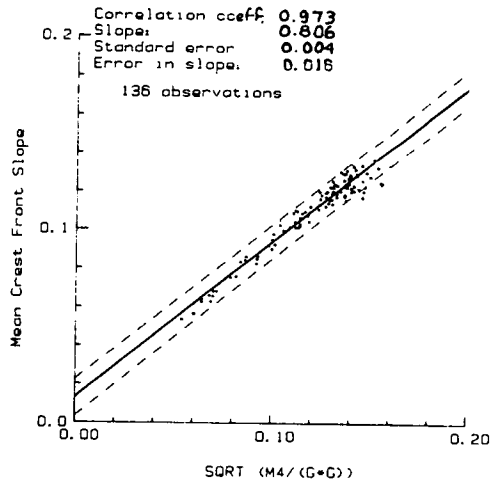


Figure 9. Regression of observed mean crest front slope against the wave steepness parameter.

Figure 9 shows a sample regression of the observed mean crest front slope against $\alpha$. The corrrelation, as expected, is very good though $\alpha$ tends to overestimate the slopes. This overestimation may reflect the unstable nature of the parameter as it is derived from the fourth moment which is very dependent on the high frequency cut-off used in the calculation.

## AVERAGE WAVE FIELD DIRECTIONS OBTAINED FROM MEASURED SLOPES

The linearized equations of motion, at the sea surface, can be written as

$$\frac{\partial u}{\partial t} = -g \frac{\partial \eta}{\partial x} \qquad \text{Eq. 6}$$

and

$$\frac{\partial v}{\partial t} = g \frac{\partial \eta}{\partial y} \qquad \text{Eq. 7}$$

where $\eta$ is the surface displacement and $u, v$ are velocities in the $x$ and $y$ plane. These equations indicate that the East-West wave slope is proportional to the $x$-component of acceleration and the North-South wave slope to the $y$-component. One can thus treat the wave slopes as any other vector quantity.

If one considers a hodographic plane of acceleration then the mean direction of the scatter ellipse is given by

$$\text{Tan } 2\phi = \frac{2 \overline{\frac{\partial \eta}{\partial x} \frac{\partial \eta}{\partial y}}}{\left(\overline{\frac{\partial \eta}{\partial y}}\right)^2 - \left(\overline{\frac{\partial \eta}{\partial x}}\right)^2} \qquad \text{Eq. 8}$$

(for example see Kundu et al. 1975) with $\phi$ also representing the mean direction of wave propagation and the overbars indicating an averaging. By rotating the co-ordinate axis to lie along $\phi$, then

$$\text{X maj} = \left[ \overline{\left(\frac{\partial \eta'}{\partial x}\right)^2} - \left(\overline{\frac{\partial \eta'}{\partial x}}\right)^2 \right]^{1/2} \qquad \text{Eq. 9}$$

$$\text{X min} = \left[ \overline{\left(\frac{\partial \eta'}{\partial y}\right)^2} - \left(\overline{\frac{\partial \eta'}{\partial y}}\right)^2 \right]^{1/2} \qquad \text{Eq. 10}$$

are measures of the scatter along the major and minor axes (primes indicate co-ordinate rotation).

The ratio R = Xmaj/Xmin provides a measure of spread in direction about the mean $\phi$. If R = 1 then there is no preferred direction to the average wave field and if $R \to \infty$ the motion is a uniform wave in the direction $\phi$. There remains a 180° ambiguity in the calculation of $\phi$.

A sample hodograph is given in Figure 10 showing considerable scatter (R = 1.4). Figure 11 contains a time series plot of the calculated direction $\phi$ and ratio R for two storm periods compared against the apparent direction derived from the spectra. The agreement is very good. Slightly better results were obtained when compared against the apparent sea directions, a reflection of the sampling bias. The larger values of R are associated with low energy, swell conditions, while lower values reflect the more confused storm conditions.

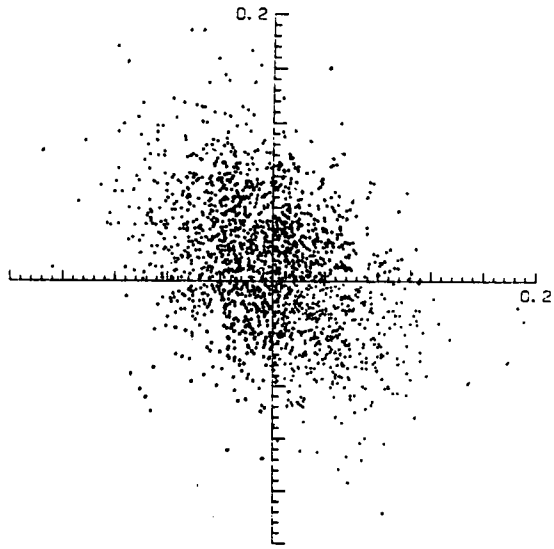


**Figure 10.** Sample Hodograph of wave slopes (R $\sim$ 1.4).

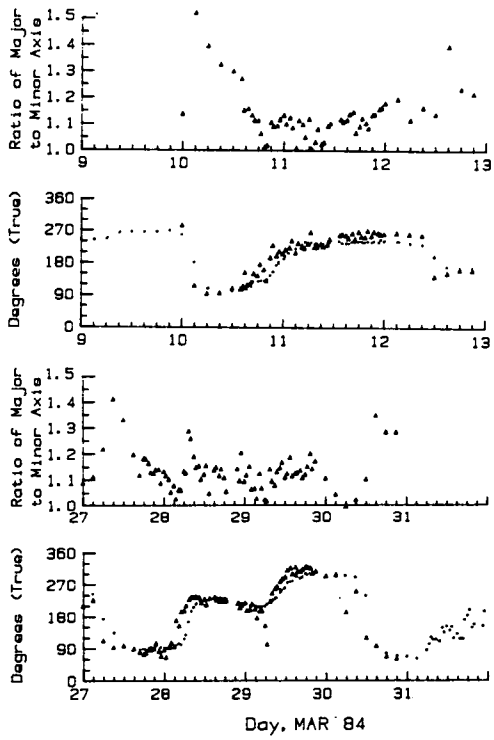


**Figure 11.** Time series of direction calculated using the hodograph method (triangles) the average apparent direction (dotted) and the ratio of the major to minor axis of the scatter ellipse.

It can be seen that very little asymmetry in the hodograph is required to resolve a mean direction purely from the slope data, indicating that this method is an alternate approach to the cross-spectral analyses for providing some wave direction information. It can be used for bulk estimates, as a check against directions obtained using a different method, and by successive filtering of the time series, provide separate frequency-band direction information (e.g. swell vs sea) with a direct estimate of the direction spread in these bands.

## SUMMARY AND DISCUSSION

This paper summarizes the directional wave buoy assessments undergone in the last few years. It was found that both the WAVEC and WAVE-TRACK buoys can be used to provide wave heave and directional information. However, the WAVEC buoy was consistently more reliable in terms of operation and data quality. This paper also introduces and illustrates various analyses that may be performed on data obtained from directional wave buoys beyond the standard spectral analyses and statistics. The calculation of a dispersion ratio, though not a new technique, was included to illustrate the potential contamination in the data due to currents. The calculation of an apparent wave field direction allows for the characterization of the mean behaviour of the wave field and the weighting can be used over selected frequency bands to describe, for example, sea and swell regimes. Single parameter descriptions are often useful in modelling and engineering applications.

The major advantage of these buoys is that they allow for the direct measurement of various wave shape statistics without having to resort to the assumptions of wavelength and wave symmetry necessary when one uses a heave signal. The analysis method, however, still suffers from bias towards high frequencies as with any zero-crossing approach. Under the experimental conditions, a direct relationship was observed between increases in mean surface slope, front or back, and crest to trough asymmetry with wind speed. This has important implications to air-sea interaction studies as the shape of the wave will influence the energy input into the sea surface by the wind. A steeper slope exposes a greater surface area perpendicular to the wind which has, possibly, been parameterized in the past by the increased drag coefficient with wind speed as cited by numerous authors (e.g. Charnock (1975), Garrett (1977), Large and Pond (1981)).

Finally, by considering the wave slopes as accelerations, one can apply standard vector analyses to the signals. One such is the hodographic analysis which provides an independent estimate of the wave direction and directional spread without requiring a concurrent heave signal nor performing any spectral calculations.

Acknowledgements

The original work was funded by the Marine Environmental Data Service (MEDS), Fisheries and Oceans and the Environmental Studies Revolving Fund Dept. of Energy, Mines and Resources of Canada. We would particularly like to thank Dr. J.R. Wilson, B. Kelly, J. Murphy and J. Minaker (MEDS), Dr. J. Buckley, Dr. R.F. Marsden (Royal Roads Military College) and J. Ransom (Mobil Oil Canada Ltd.) for providing assistance, both in equipment and personnel, data suggestions and criticisms.

References


Audunson T., S.F. Barstow and H.E. Krogstad, 1982. "Analysis of Wave Directionality from a Heave, Pitch and Roll Buoy Operated Offshore Norway". Ocean Sci. and Eng. 7 (8): 291-319.

Barstow, S.F. and H.E. Krogstad, 1983. "Directional Wave Spectra From Heave/Pitch/Roll Buoy Data". IREF 9 pp: 292-297.

Brainard, E.C., 1982. "High Resolution Directional Wave Spectra Using the F.F.T. Digital Band Pass Filter Method." Endeco Inc. (unpub.)

Charnock, H. 1975. "Wind Stress On a Water Surface" Quart. J. Roy. Meteor. Sc. 81: 639-640.

Cummins, W.E. and S.L. Bales, 1980. "Extreme Value and Rare Occurrence Wave Statistics for Northern Hemispheric Shipping Lanes". Society of Naval Architects and Marine Engineers, Spring Meeting, STAR-Symposium, Coronado, CA, June 4-6, 1980, 219-239.

Ezraty, R. and A. Cavanie, 1981. "Evaluation of Wave Direction Measurements Using a Pitch and Roll Buoy". Oceanol. Acta. 4 (2): 139-149.

Garrett, J.R., 1977. "Review of Drag Coefficients over Oceans and Continents". Mon. Wea. Review 105: 915-929.

Hasselmann, D.E., M. Dunckel and J.A. Ewing, 1980. "Directional Wave Spectra Observed During JONSWAP 1973". J. Phys. Ocean 10: 1264-1280.

Juszko, B-A., 1985. "Directional Wave Spectrum Intercomparison Study, Volume III - Intercomparison of Results." Contractor Report prepared for the Environmental Studies Revolving Fund, Dept. of Energy, Mines and Resources, Canada, 340 pp.

Juszko, B-A., R. Brown, B. de Lange Boom and D.R. Green, 1985. "A Wave Climate Study of the Northern British Columbia Coast - Volume I". Contractors Report to the Marine Environmental Data Service Fisheries and Oceans, Canada. 164 pp. plus attachments.

Kjeldsen, S.P. and D. Myrhaug, 1979. "Breaking Waves in Deep Water and Resulting Wave Forces". Off. Tech. Conf., Houston 1979. Paper OTC-3646.

Komen, G.J., S. Hasselmann and K. Hasselmann, 1984. "On the Existence of a Fully Developed Wind-Sea Spectrum". J. Phys. Ocean. 14: 1271-1285.

Kundu, P.K., J.A. Allen and R.L. Smith, 1975. "Modal Decomposition of the Velocity Field near the Oregon Coast". J. Phys. Ocean. 5: 683-704.

Large, W.F. and S. Pond, 1981. "Open Ocean Momentum Flux Measurements in Moderate to Strong Winds". J. Phys. Ocean. 11: 324-336.

Le Blond, P.H., 1982. "A Preliminary Review of Non spectral Wave Properties: Grouping, Wave Breaking and "Freak" Waves". Canadian Contractor Report. Hydrogr. Ocean Sci. 1: 66 pp.

Longuet-Higgins, M.S., 1957. "The Statistical Analysis of a Random, Moving Surface". Phil. Trans. Roy. Soc. A, 249: 321-387.

Longuet-Higgins, M.S., D.E. Cartwright and N.D. Smith, 1963. "Observations of the Directional Spectrum of Sea Waves Using the Motions of a Floating Buoy". In: Ocean Wave Spectra, Prentice-Hall Inc., Englewood Cliffs, N.Y., pp 111-136.

# WAVE CLIMATE STUDY

# NORTHERN COAST OF BRITISH COLUMBIA

**John R. Harper**
Dobrocky Seatech Ltd.
9865 West Saanich Road
Sidney, B.C. V8L 4M7

and

**Savithri Narayanan**
Dobrocky Seatech Ltd.
Topsail Road
St. John's, Newfoundland A1C 6E6

## ABSTRACT

This paper describes a wave data collection program in northern British Columbia from July 1984 to March 1985. The objective of the program was to extend the existing data base for estimating the spatial and interannual variability in the wave climate.

Minimal operational problems were experienced and data recovery rates were high (greater than 90% for satellite-transmitting buoys, the standard wave rider buoy and the meteorological station; greater than 80% for the directional wave buoy).

The wave climate shows a strong seasonal variability with a relatively quiescent summer period (June to September) with low waves ($\bar{H}_s$ <2 m) and a storm winter period (October to March) of significantly higher waves. The transition period between "summer" and "winter" is very abrupt with October being one of the stormiest months of the year.

The stormiest portion of the study region is that of Queen Charlotte Sound. The largest measured waves occurred in Queen Charlotte Sound and storm wave conditions ($H_s$ >5 m) had the highest frequency of occurrence in this area.

The trends documented in the 1984/85 measurement program were similar to those measured in 1982-1984.

## AREA DESCRIPTION

The coastal waters of northern British Columbia, which include Queen Charlotte Sound, Hecate Strait and Dixon Entrance, are one of the most productive fisheries regions in Canada (Figure 1). This part of the continental shelf contains shallow areas deeply cut by glacial troughs, and coastlines indented by many fjords. The general weather pattern for the area is characterized by strong south to southeast winds in winter, changing to weaker westerlies or calm in summer. The increased marine activities related to fishing, recreation and export, and the potential for oil and gas exploration, have generated the need for a detailed understanding of the physical oceanographic environment of this region.

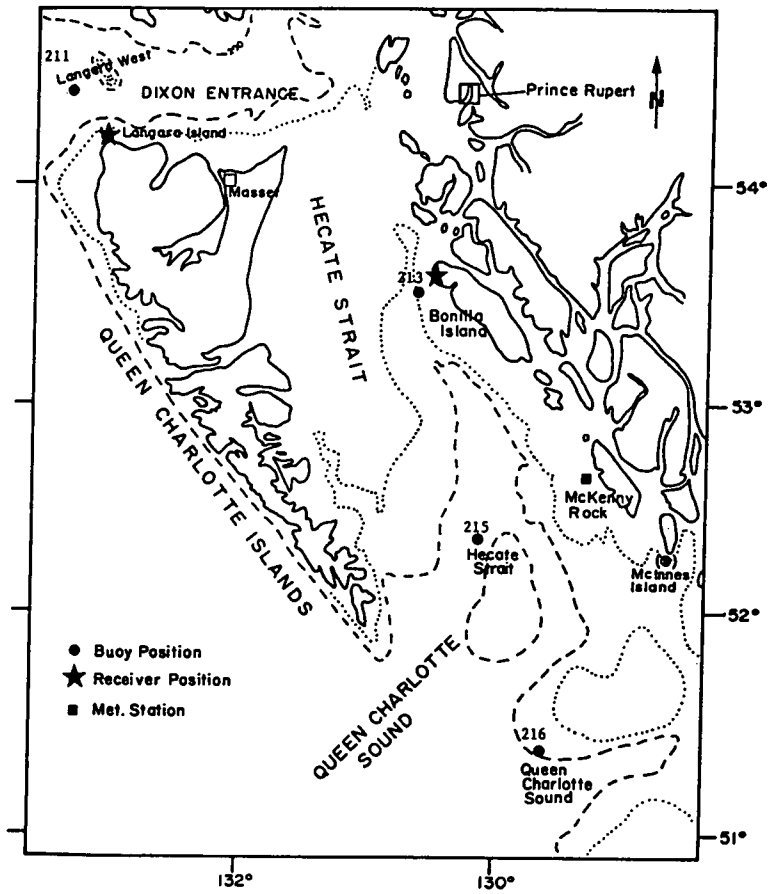


Fig. 1 Locations of Wave Study Buoys, Receivers, and Meteorological Station

## WAVE DATA

Until 1982, little wave climate data had been collected in British Columbia waters. An initial wave climate study in the waters of the northern British Columbia coast was conducted from the fall of 1982 to the spring of 1984 to establish a wave climate database, to evaluate new instrumentation and deployment techniques, to develop software for processing directional wave data, and to develop wind-wave hindcasting models for the area. That program was carried out under the direction of the Marine Environmental Data Service (MEDS) and included wave measurements from a total of seven locations and meteorological measurements from one location (Juszko et al., 1985). Data from those instruments were processed and then archived at MEDS in Ottawa, as well as being used for directional and non-directional wave analysis and interpretation.

The present wave climate study covers an extension of the initial study, over the period from June 1984 to March 1985, under support from Environmental Studies Revolving Funds (ESRF) with the following objectives:

1. to generate a longer database for waves and over-the-water winds;

2. to provide information for the seasons when data were missing during the previous year;

3. to provide an estimate of the interannual variability in the wave conditions.

This paper describes the instrumentation used during the period May 1984 to March 1985, the field program, data analysis techniques, and the wave climate (for further details, refer to DSL, 1986). The northern British Columbia wave data collection program has been extended through 1985, 1986 and 1987 under contract to Dobrocky Seatech Ltd.

## INSTRUMENTATION

Four wave data collection buoys and one satellite-transmitting weather station were operated during the study. The instrumentation, location and sampling characteristics are summarized in Table 1.

### DATAWELL WAVEC BUOY

The WAVEC system was deployed at the Langara West Station (MEDS Station 211, Figure 1) to provide wave height and direction information through measurement of the buoy's vertical acceleration and determinations of the buoy slope induced by the waves. The system utilizes a Datawell Hippy-120 heave/pitch and roll sensor and a three-axis fluxgate compass mounted in a surface-following buoy. Data were transmitted continuously from the buoy to a shore station where it was recorded in records of approximately 34 minutes in duration (at 0.78 second intervals) once every three hours. When the estimated significant wave height exceeded 4.5 m, data were recorded continuously.

### ENDECO WAVE-TRACK BUOY

A Wave-Track Model 956 system, manufactured by ENDECO, was deployed off Bonilla Island (MEDS Station 213, Figure 1). This system utilizes an accelerometer, one two-axis fluxgate compass and two tilt sensors, which consist of small mercury reservoirs with capacitance sensors that respond as inverted pendulums to movement of the mercury induced by shear in the wave orbital velocities. Data were transmitted via radio link to the Bonilla Island Lighthouse. Wave records of approximately 20 minutes in length (at 0.5 intervals) were recorded every three hours. The ENDECO Wave track buoy experienced severe electronic problems during the first few months of operation and was eventually replaced with a standard Datawell Waverider buoy.

TABLE 1

Summary of stations, instruments and sampling
A. Wave measurement systems

| Station # | Station Name | Location | Water Depth | Instrument Type | Sampling Interval | Sample Description |
|---|---|---|---|---|---|---|
| 211 | Langara West | 54°26.6' N 133°23.0' W | 285 m | WAVEC Datawell's directional wave system | 3 hours or Continuous if Hs > 4.5 m | 20 minutes at .78215 second intervals, changed to 34 minutes on 20 Oct. 1984 |
| 213 | Bonilla Island | 53°19.3' N 130°43.0' W | 159 m | ENDECO directional wave system, Wave-Track Model 956 | 3 hours | 18 minutes at 0.5 second intervals. |
| | | | | Datawell Waverider (replacement system) | 3 hours or Continuous if Hs > 4.0 m | 20 minutes of analog data |
| 215 | Hecate Strait | 52°12.0' N 130°19.7' W | 375 m | WRIPS Datawell's satellite buoy | 3 hours | Based on 34 min. at 1 second intervals, spectral data at 35 frequencies. |
| | | | | | 72 hours or Hs > 4.3 m | 34 minutes of raw data at 1 sec. intervals. |
| 216 | Queen Charlotte Sound | 51°18.2' N 129°58.3' W | 262 m | WRIPS Datawell's satellite buoy | 3 hours | Spectra at 35 frequencies. |
| | | | | | 72 hours or Hs > 4.3 m | 34 minutes of raw data at 1 sec. intervals. |

Summary of stations, instruments and sampling
B. Meteorological Station

| Station Name | Position | Height Above Sea Level | Sensor | Sampling Interval | Sample Description |
|---|---|---|---|---|---|
| McKenny Island | 52°39.1' N 129°28.3' W | 19 metres | Met One speed sensors 1 and 2 | 1 hour | Ten minute averages |
| | | | Met One direction sensors 1 and 2 | 1 hour | Ten minute averages |
| | | | Met One temperature sensors 1 and 2 | 1 hour | Instantaneous |
| | | | YSI - Sostman barometric pressure transducer | 1 hour | Instantaneous |
| | | | Wilh. Lambrecht GMBH Pernix humidity sensor | 1 hour | Instantaneous |

## DATAWELL WAVERIDER BUOY

A standard Datawell Waverider system replaced the ENDECO at the Bonilla Island site. The Waverider utilizes an accelerometer mounted in a surface following buoy, the output of which is double-integrated to obtain a wave-height time series. The heave signal was transmitted continuously to a receiving station at the Bonilla Island Lighthouse. Wave data were recorded for 20 minutes every three hours, except when significant wave height exceeded 4 m.

## DATAWELL WAVERIDER INFORMATION PROCESSING SYSTEM (WRIPS)

Datawell WRIPS systems were used at the Hecate Strait station (MEDS Station 215, Figure 1) and at the Queen Charlotte Sound Station (MEDS Station 216, Figure 1) during the program. These buoys are 1-m diameter waverider buoys, modified to include a data collection platform, GOES transmitter and ARGOS transmitter. The Data Collection Platform (DCP) digitized data from the accelerometer, computed spectral estimates and output spectral data

together with check parameters and selected summary statistics to the satellite transmission system and to an internal cassette recorder. Wave records of approximately 34 minutes duration were recorded and transmitted every three hours. Raw data were recorded every 72 hours or continuously whenever the significant wave height exceeded 4.3 m.

METEOROLOGICAL STATION

"Over-the-water" wind data were collected simultaneously with the wave data by a meteorological station on McKenney Island; the station was established approximately 19 m above sea level. Hourly records consisting of 10 minute averages of wind speed and direction data and instantaneous measurements of temperature, humidity and pressure were transmitted via GOES.

## OPERATIONS

Four cruises were required during the study: the initial deployment cruise, a scheduled servicing cruise and two contingency cruises. In general, instruments functioned well throughout the study. Loss of data resulted from three problems:

- electronic malfunction of the ENDECO Wave-Track Buoy at Bonilla Island;
- loss of the Datawell Waverider Buoy from Bonilla Island;
- failure of the WAVEC flotation components at Langara Island.

Station data recovery is summarized in Table 2. Data recovery from the Datawell WRIPS buoys averaged better than 99%, from the Datawell Waverider averaged better than 90% and from the Datawell WAVEC averaged better than 80%; no useable data was recovered from the ENDECO Wave-Track buoy. One mooring failure occurred during the program, presumably because of fishing activities (dragging) in the area.

Table 2

Monthly percentage of Station data recovery
(number of good records/expected number of records,
continuous records at non-standard times are not included)

| | Wave Data | | | | Meteorological Data |
|---|---|---|---|---|---|
| | Langara West | Bonilla Island | Hecate Strait | Queen Charlotte | McKenny Island |
| June, 1984 | 100 | | | | |
| July | 98 | 0 | 100 | 100 | 77 |
| August | 96 | 0 | 100 | 100 | 63 |
| September | 98 | 0 | 100 | 100 | 94 |
| October | 98 | 0 | 100 | 100 | 83 |
| November | 95 | 100 | 100 | 99.5 | 92 |
| December | 90 | 100 | 100 | 100 | 97 |
| January, 1985 | 48* | 52** | 100 | 100 | 90 |
| February | 0* | 100 | 100 | 100 | 97 |
| March | 94 | 100 | 100 | 100 | 97 |

* buoy flotation damaged
** buoy lost; replaced

## RESULTS

A wide variety of wave and meteorological data products were produced during the study and are available in DSL (1986). The results provide an additional 10 months of data in the ongoing northern British Columbia wave climate program and as such, provide a basis for evaluation of (a) seasonal variations in wave climate, (b) interannual variability, and (c) regional variability. Each facet of the northern British Columbia wave climate is discussed below.

### (a) Seasonal Variation in Wave Climate.

The wind patterns of the northern British Columbia region are controlled by the location and intensity of two major, semi-permanent atmospheric pressure systems (Kendrew and Kerr, 1955). The Aleutian Low, centred over the Bering Sea and the Gulf of Alaska, predominates in winter, producing strong south to southeasterly winds along the B.C. coast. The North Pacific High, centred off California, predominates in the summer, producing weak westerly and northwesterly winds. As a result of these major synoptic pressure patterns and associated wind patterns, wave conditions are strongly seasonal. Monthly mean significant wave heights and peak periods are summarized in Figure 2 and Table 3 and indicate general low wave conditions during summer months ($\bar{H}_s$ <2 m) and high wave conditions during winter months ($\bar{H}_s$ >3 m). This seasonal trend is consistent with the previous year's data (Juzko et al., 1985) and with long-term observations at Tofino, B.C. where wave heights are less than two metres during summer months and in the range of three metres during winter months (Owens, 1980).

Table 3

Monthly mean and maximum of $H_s$ (in metres) and the mean peak period (in brackets)

| | Langara West | | Bonilla Is. | | Hecate Str. | | Queen Charlotte | |
|---|---|---|---|---|---|---|---|---|
| | Max. | Mean | Max. | Mean | Max. | Mean | Max. | Mean |
| July | 3.8 | 1.3 (8.9) | No Data | | 2.4 | 0.7 (11.5) | 2.6 | 1.2 (10.4) |
| August | 6.1 | 1.9 (10.6) | No Data | | 4.5 | 1.0 (12.9) | 4.9 | 1.6 (11.1) |
| September | 4.4 | 2.0 (9.5) | No Data | | 3.7 | 1.2 (9.3) | 3.6 | 1.9 (9.6) |
| October | 7.3 | 3.3 (10.1) | No Data | | 9.0 | 2.4 (9.0) | 10.5 | 3.3 (11.7) |
| November | 9.4 | 3.8 (12.0) | 3.1 | 1.9 (10.7) | 8.3 | 2.7 (10.6) | 11.3 | 3.7 (11.7) |
| December | 8.5 | 4.1 (11.9) | 5.0 | 1.4 (7.0) | 5.8 | 1.9 (8.8) | 9.2 | 3.3 (11.1) |
| January | 6.6 | 4.1 (11.3) | 3.8 | 1.4 (6.8) | 7.7 | 2.9 (9.8) | 8.1 | 3.5 (11.8) |
| February | No Data | | 9.2 | 2.3 (7.7) | 8.8 | 2.2 (9.1) | 9.4 | 3.5 (11.1) |
| March | 6.3 | 3.7 (12.3) | 5.4 | 1.5 (7.1) | 5.3 | 1.8 (9.5) | 6.9 | 3.4 (12.0) |

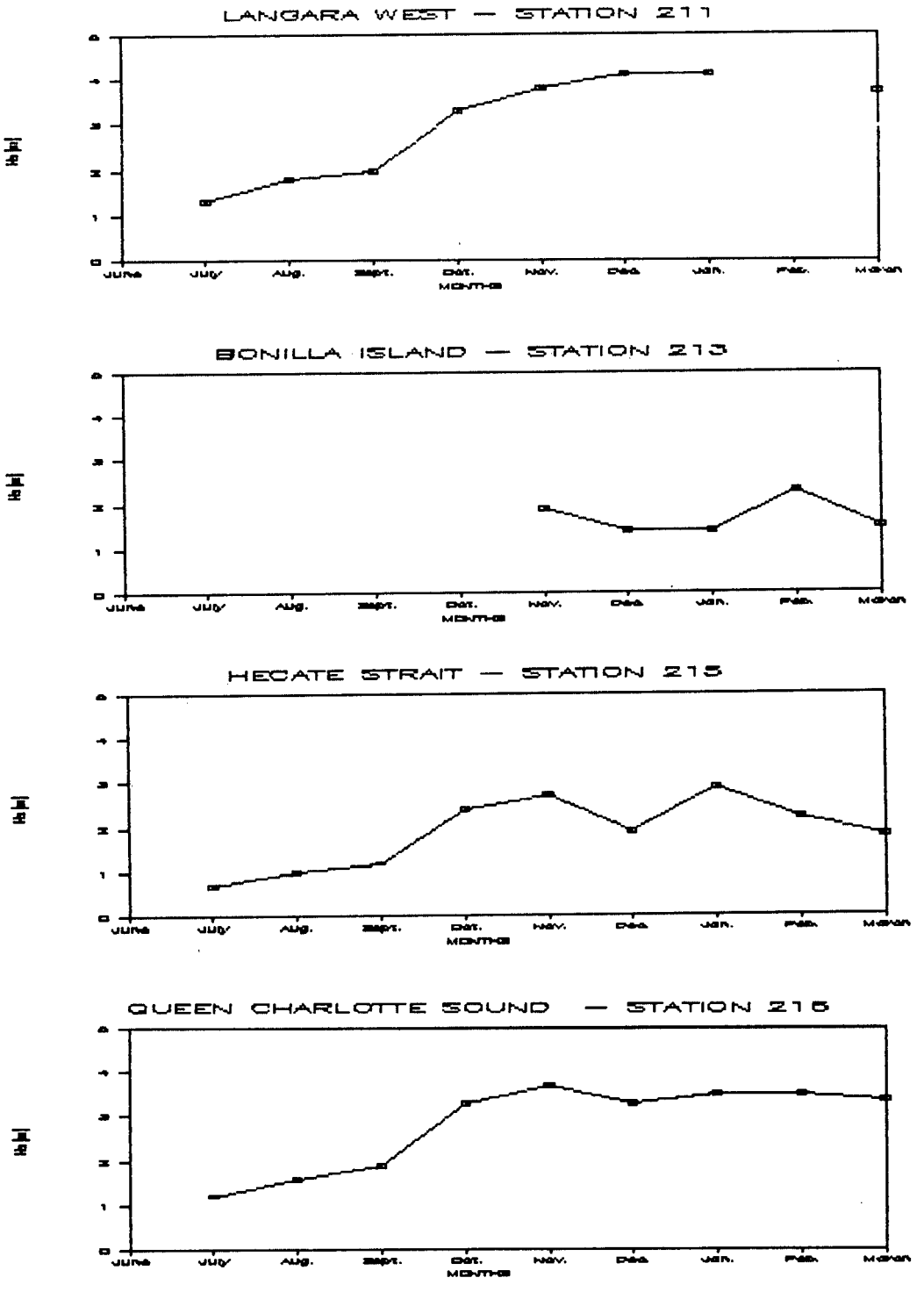


Figure 2. Monthly mean significant wave height from July 1984 to March 1985.

The monthly data plots of $H_s$ suggest that relatively abrupt changes in wave climate occur in October and that seasonal characterizations are most appropriately classified as a "summer wave climate" (May to September) and a "winter wave climate" (October to April) with very short duration transitional periods.

Of greater significance in terms of offshore operations is the frequency of storm wave events that occurred during the study (Table 4). The frequency of storm wave events ($H_s$ >5 m) increases abruptly in October and is in the range of 5 to 10% for winter months except at Bonilla Island measurement station, which is protected.

Table 4

Summary of storm wave events ($H_s$ >5 m) by season and location.

| | Langara West | | Bonilla Is. | | Hecate Str. | | Queen Charlotte | |
|---|---|---|---|---|---|---|---|---|
| | Hr | % | Hr | % | Hr | % | Hr | % |
| July | 0 | 0 | 0 | 0 | 0 | 0 | 0 | 0 |
| August | 18 | 2 | 0 | 0 | 0 | 0 | 0 | 0 |
| September | 0 | 0 | 0 | 0 | 0 | 0 | 0 | 0 |
| October | 46 | 6 | 0 | 0 | 69 | 9 | 93 | 12 |
| November | 30 | 4 | 0 | 0 | 69 | 9 | 123 | 17 |
| December | 50 | 7 | 0 | 0 | 12 | 2 | 57 | 8 |
| January | 27 | 4 | 0 | 0 | 40 | 5 | 45 | 6 |
| February | 0 | 0 | 29 | 4 | 54 | 7 | 78 | 10 |
| March | 33 | 4 | 0 | 0 | 0 | 0 | 9 | 1 |

(b) Interannual Variability

Some data are available from stations for the period of 1982 and 1983 (Juszko et al., 1985) and allow interannual comparison of the wave climate to be made. Previous data are summarized by season (Juszko et al., 1985) and are presented with the 1984/1985 data in Table 5. Conditions are comparable in the summer and fall seasons between the two data sets, with slightly more energetic conditions apparent in the 1984/85 data set. Trends are not consistent between 1983/84 and 1984/85 for the winter period; conditions were significantly more energetic in the north during 1984/85 (1983/84 $H_s$ = 3.2 m; 1984/85 $H_s$ = 4.1 m) but were less energetic in the south in 1984/85. The variance between stations during winter months emphasizes the importance of small-scale storm systems in creating regional variations in wave climate.

(c) Regional Variations in Wave Climate

The presence of the Queen Charlotte Islands strongly affects the regional wave climate by providing localized shelter from open-coast wave conditions.

Wave heights at Bonilla Island seldom exceed 3 m, even during winter months and peak wave periods are typically in the range of 7 to 8 seconds (Tables 4 and 5). The Hecate Strait and Queen Charlotte Sound stations show good correlations in mean statistics, with Hecate Strait exhibiting characteristics of a slightly more sheltered location (Table 4). Time-series of the two stations are well correlated as are storm-wave events (DSL, 1986).

Table 5

Interannual Comparison of $H_s$ (in metres) and peak period (in brackets)

| | Langara West | | Bonilla Is. | | Hecate Str. | | Queen Charlotte | |
|---|---|---|---|---|---|---|---|---|
| | 83/84[1] | 84/85[2] | 83/84 | 84/85 | 83/84 | 84/85 | 83/84 | 84/85 |
| Summer | 1.5 (9.8) | 1.5 (9.7) | ND | ND | 1.1 (12.4) | 0.8 (12.2) | 1.7 (10.8) | 1.4 (10.7) |
| Fall | 2.6 (10.7) | 3.0 (10.5) | 1.7 (8.7) | ND | 1.9 (10.7) | 2.1 (9.6) | 2.9 (11.1) | 3.0 (10.4) |
| Winter | 3.2 (11.6) | 4.1 (11.6) | 1.7 (8.6) | 1.7 (7.2) | 3.0 (10.6) | 2.3 (9.2) | 3.9 (12.2) | 3.4 (11.3) |
| Spring | 2.4 (11.2) | ND | 1.2 (8.1) | ND | 2.2 (10.9) | ND | 2.7 (11.5) | ND |

[1] 83/84: Summer = J, J, A; Fall = S, O, N; Winter = D, J, F; Spring = M, A, M
[2] 84/85: Summer = J, A; Fall = S, O, N; Winter = D, J, F; Spring = No Data

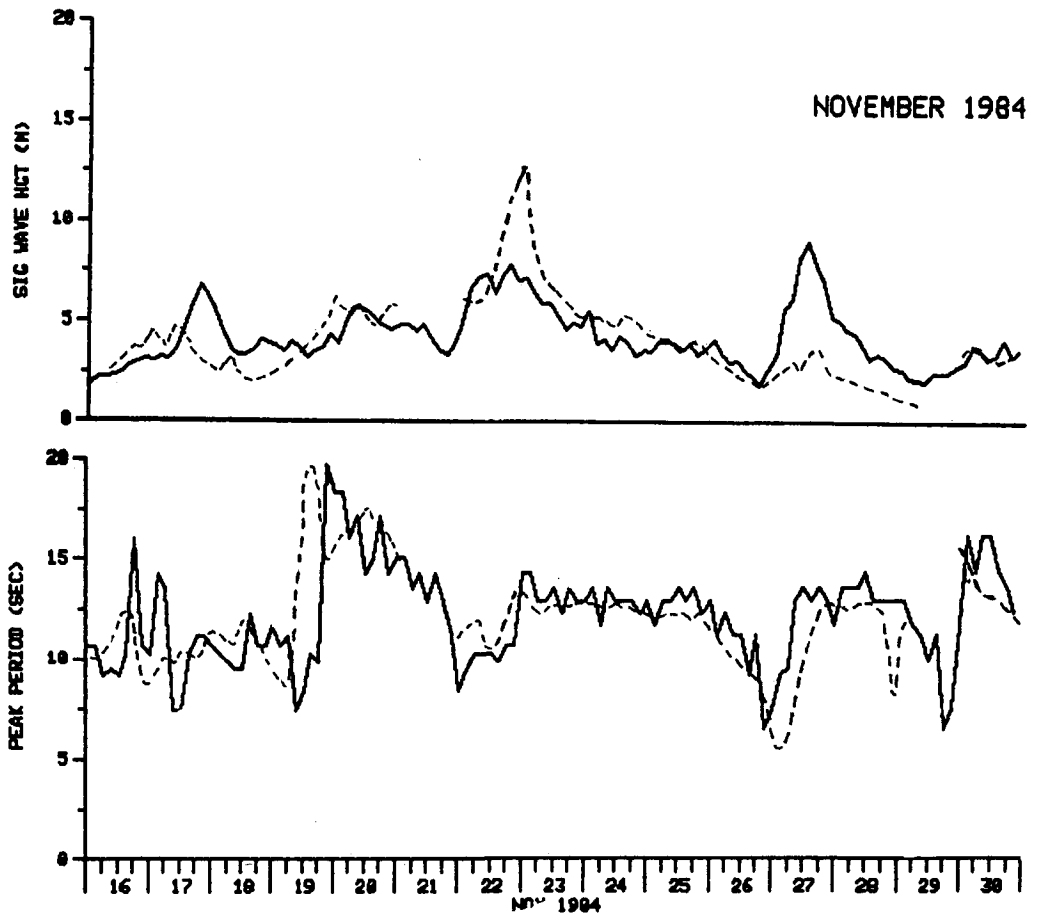


Figure 3. Time series of $H_s$ and $T_p$ for the Langara West Station (solid) and Queen Charlotte Sound Station (dashed).

The Langara West station and the Queen Charlotte station provide for an interesting comparison in that the stations are separated by approximately 400 km, but are both exposed to open Pacific swell. Seasonal statistics are relatively similar for the two periods of study indicating similar overall wave climate (Table 5). During the 1984/1985 winter storm season, mean monthly significant wave heights were consistently greater at the Langara West site (Table 3) although the severity and duration of storms were greater at the Queen Charlotte Sound site (Table 5). The largest significant and zero-crossing wave heights (11.3 m and 17.5 m, respectively) occurred at the Queen Charlotte Sound site. Figure 3 illustrates a time-series of $H_s$ and $T_p$ for the two sites for a two-week period in November 1984. While the overall trend of statistics is similar, specific events, particularly during high-energy events, do vary signficantly between the two sites.

An additional observation on wave direction, as measured at the Langara West station in 1984/1985 and the Bonilla Island station in 1982/1983, is possible. Mean monthly directions (at the peak period) for the Langara West station are consistently from due west and are out of phase with local winds, as one would expect from the swell-dominated environment. Wind and wave directions during storms are similarly only weakly correlated. Previous measurements of wave direction at the Bonilla Island station (Hodgins et al., 1985) showed a reasonable correspondence of wind and wave direction, particularly when $H_s$ exceeded 2 m; Hodgins et al. (1985) noted, however, that there is significantly more scatter in wave directions than wind directions.

## CONCLUSIONS

1. Instrumentation used during this program proved to be reliable in most cases; data recovery was generally greater than 90%.

2. The wave climate shows strong seasonal variability; data suggested that there is a "summer" period (June to September) of low waves ($H_s$ <2 m) and a "winter" period (October to March) of significantly higher waves ($H_s$ >3 m). Furthermore, the transition period from "summer" to "winter" conditions being very abrupt (i.e., October is one of the stormiest months of the year).

3. No significant interannual variations were detectable between the 1983/1984 measurement period and the 1984/1985 measurement period.

4. The stormiest portion of the study region is the Queen Charlotte Sound area, in terms of largest measured waves and duration of storms, although the Dixon Entrance area showed higher monthly mean $H_s$ during the 1984/1985 acquisition period.

## REFERENCES


Dobrocky Seatech Ltd. (DSL), 1986. Wave climate study of the northern coast of British Columbia. Prepared for the Environmental Studies Revolving Fund, Ottawa, by Dobrocky Seatech Ltd., Sidney, B.C.

Hodgins, D.O., P.M. LeBlond, D.S. Dunbar and C.T. Niwinski, 1975. A wave climate study of the northern British Columbia coast, Final Report - Volume II, Wave properties and wave prediction. Prepared for Marine Environmental Data Service, Fisheries and Oceans Canada, Ottawa by Seaconsult Marine Research Ltd., Vancouver, B.C., 71 p.

Juszko, B., R. Brown, B. de Lange Boom and D. Green, 1985. A wave climate study of the northern British Columbia coast. Prepared for Marine Environmental Data Service, Fisheries and Oceans Canada, Ottawa by Seakem Oceanography Ltd., Sidney, B.C., 164 p.

Kendrew, W. and D. Kerr, 1955. The climate of British Columbia and the Yukon Territory. Queens Printer, Ottawa. 222 p.

Owens, E.H., 1980. Coastal environments of Canada. In Short Course Lecture Notes on Basic Nearshore Processes (A.V. Bowen, ed.), National Research Council, Ottawa, 29 p.

# EVALUATION OF TWO SHALLOW WATER SPECTRAL WAVE MODELS ON SABLE ISLAND BANK, CANADA

by

Donald O. Hodgins, Ph.D.

Seaconsult Marine Research Ltd.
Vancouver, British Columbia, Canada

**Abstract**

A decoupled propagation model and a coupled discrete spectral model have been applied in shallow water around Sable Island Bank, Canada, and validated with a new directional wave dataset. The models are distinguished by the formulations of the energy balance equation, principally the terms related to wave-wave interactions and dissipation through wave breaking. The decoupled model, SPECREF, neglects nonlinear interactions and models the effects of wave breaking through the depth-dependent equilibrium range spectrum proposed by Kitaigorodskii et al. (1975). The coupled model, WAVAD, estimates the nonlinear flux due to wave-wave interactions as an integral part of the dynamic energy balance. However, it also uses an equilibrium spectrum exhibiting an $\omega k^{-3}$ form to model breaking. Hindcasts of four severe winter storms show that both models provide useful estimates of wave heights, periods and directions. RMS errors in $H_s$ were found to range from 1 to 1.25 m with S.I. of 15 to 20%. Peak period errors ranged from 1 to 2 s and error in direction from 10 to 20°. The role of the saturation spectral form was found to be very important in determining the shallow water spectral shape and tended to govern model performance.

## 1.0 The Energy Balance Equation

The transformation of ocean surface gravity waves over arbitrary bathymetry can be modelled in terms of the directional wave spectrum S (Longuet-Higgins, 1957; Karlsson, 1969). One then seeks solutions for S that represent a balance between processes that add and remove wave energy at a point (x,y) for specified boundary conditions. The governing energy balance equation may be written in wave number space as (Phillips, 1977)

$$\left[\frac{\partial}{\partial t} + (\mathbf{c_g} + \mathbf{U}).\nabla\right] S + \mathbf{R}.\nabla\mathbf{U} = Q \qquad (1)$$

where $S(\mathbf{x},\mathbf{k},\theta,t)$ = wave number spectrum, $\mathbf{k}$ = wave number, $\theta$ = direction, $\mathbf{c_g}$ = group velocity, $\mathbf{U}$ = mean current vector, $\mathbf{R}$ = radiation stress tensor (Longuet-Higgins and Stewart, 1960), $Q$ = net source term combining all energy losses and gains, $\mathbf{x}$ = (x,y) position in space, and t = time. In many locations, including Sable Island Bank, wave transformations due to interaction with background currents are negligible; then $\mathbf{u}=0$ and (1) simplifies considerably. Aside from differences in the numerical procedures for solving the propagation terms ($\partial/\partial t + \mathbf{c_g}\cdot\nabla S$) the central problem then concerns parameterization of the source terms $Q$, and specifically the importance of the nonlinear fluxes produced by wave-wave interactions. The net source terms $Q$ may be expanded as

$$Q = Q_{in} + Q_{nl} + Q_{diss} + Q_b \qquad (2)$$

where $Q_{in}$ = input energy flux due to wind, $Q_{nl}$ = energy flux due to resonant wave-wave interactions, $Q_{diss}$ = energy flux due to wave breaking (loss term) and $Q_b$ = energy flux due to wave-seabed interactions (loss term). Refraction and shoaling are accounted for in the propagation of wave energy.

Major differences between wave models result from just how the balance in (2) is computed. Two terms, in particular, are critically important: $Q_{nl}$ and $Q_{diss}$. The JONSWAP experiment (Hasselmann et al., 1973) established the fundamentally important role of $Q_{nl}$ in the overall balance; although a conservative term over all wave frequencies, it redistributes energy to both lower and higher frequencies from the central range to the right of the peak frequency $f_m$. The latter transfer, to high frequencies, provides an energy flux to the dissipation range and hence models one mechanism by which energy is lost. In general this energy flux is strong and the term is not negligible.

Few wave models include a direct formulation of $Q_{diss}$ due to the uncertainty associated with parameterizations for wave breaking in nature. Instead the process is modelled implicitly by imposing a saturation spectral form on the solution to (1) after each time step. Self-similar forms for spectra in water of arbitrary depth have been proposed (for example, by Kitaigorodskii et al., 1975; Bouws et al., 1985; Resio, 1986a); these are scaled by the local wind and/or the depth given a value for $f_m$. The shape of the predicted shallow water spectrum thus depends on the formulation adopted for this saturation limit, and on the relative importance of each term in (2) which is dictated in turn by the formulation of $Q_{nl}$, $Q_{in}$ and $Q_b$.

The two models evaluated in this study differ significantly in the calculation of $Q_{nl}$ but are otherwise similar in principle. The first, SPECREF, is described by Hodgins et al. (1986). In it the nonlinear fluxes are ignored completely ($Q_{nl}=0$) and the final balance is achieved through growth due to local wind, bottom friction, propagation, shoaling, and refraction. Dissipation is modelled with the Kitaigorodskii et al. (1975) spectral equation. The second, WAVAD, is a coupled discrete spectral model, earlier versions of which are described by Resio (1981,1982). In WAVAD the nonlinear flux $Q_{nl}$ is evaluated explicitly; this flux determines the rate at which energy is transferred to the dissipation range, and to the forward face of the spectrum. Dissipation is modelled with an equilibrium range spectrum exhibiting an $\omega f^{-4}$ dependence where $\omega=2\pi f$ with f being wave frequency. As in SPECREF refraction, shoaling, wind growth and bottom friction complete the balance equation.

The objective of this study was to evaluate the performance of two such fundamentally different models under conditions of strong wind forcing. This evaluation focusses on the practical importance of including $Q_{nl}$ in the solution of (1) under forcing conditions that are important for deriving extreme wave criteria. Evaluation of $Q_{nl}$ is computer intensive and generally one can obtain a measure of economy in shallow water wave hindcasts with a decoupled propagation model in the SPECREF class compared with coupled discrete spectral models. Alternatively one may opt for higher bathymetric resolution in the decoupled model. Thus it is important to determine both limitations in an absolute sense for either model, and any differences in relative performance.

## 2.0 Wave Database

The models were evaluated by hindcasting four storms for which shallow water measurements were made on Sable Island Bank. Nondirectional Waverider measurements in deep and shallow water were available for the first event on March 30, 1984. New directional data were collected in this study between December 19, 1984 and February 21, 1985; three storms, December 26/26, 1984, January 5/6, 1985 and January 21/22, 1985 were selected from this period for detailed hindcasting. Instrument locations and station identifiers are shown in Fig. 1 and Table 1 respectively.

The nondirectional Waverider data were sampled at 3.75 Hz for $\sim$3796 samples (16.9 min) every 3 h. In storm periods ($H_s$>4 m) continuous sampling was carried out. The data were processed to give a variance spectrum with a bandwidth of 0.00734 Hz and 16 degrees of freedom. Significant wave height $H_s$ and peak period $T_p$ were calculated from the spectra as $4\sqrt{m_o}$ and $f_m^{-1}$ respectively, where $m_o$ is the zeroeth spectral moment.

The directional data were collected with Datawell Wavec heave-pitch-roll buoys. The data were processed using the conventional analysis (Long 1980; Hasselmann et al., 1980) to yield estimates of the variance spectrum, mean wave direction $\theta_o(f)$ and the exponent s(f) of the assumed cosine-power directional spreading function (see Hodgins et al., 1986, for details). Each heave-pitch-roll record was recorded at 1.28 Hz for 2048 samples. The bandwidth of the spectrum was 0.0150 Hz giving 45 degrees of freedom.

Examples of the directional data are shown in Fig. 2 for the storm of December 26, 1984. The energy density is portrayed in 20 bands, scaled by the length of the vector and number of arrow heads, and oriented in the mean wave direction. The local wind (Fig. 1) is shown in the upper panel and the significant wave height $H_s$ is plotted in the lowest panel.

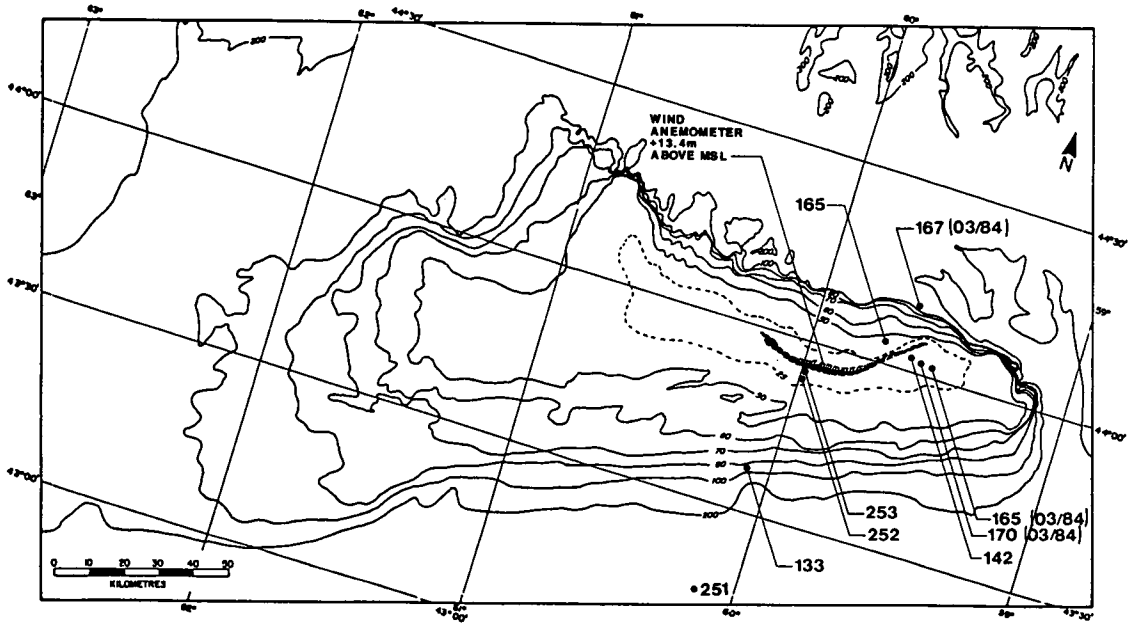


Fig. 1 Disposition of instruments on Sable Island Bank.

It can be seen here that during the early part of the storm on December 25 wave directions were closely coupled to onshore wind directions and do not differ greatly from the deeper to shallower site. As the wind shifts the high frequency energy turns with the wind but the lower frequency, energetic part of the spectrum maintains a strong southwesterly direction. Following 21 h on December 25th refraction produces a shift in direction ranging from about 10 to 30 degrees between station 252 (h=21 m) and station 253 in 12 m of water for wave periods longer than 6 s. This shift brings the wave crests more nearly parallel to the bottom contours and shoreline as the waves transform into shallow water.

These measurements are fairly typical of directional characteristics in storms 3 and 4. Reproduction of these characteristics by the numerical models is an essential test, in addition to predictions of total energy and peak period.

## 3.0 Hindcasting Strategy

The model domain for the shallow water calculations is shown in Fig. 3. For each of the four storms deep-water wave conditions were hindcast using the coupled discrete spectral model (WAVAD) run on the nested grid system shown in Fig. 4. The directional spectra from the intermediate nested grid were then used as boundary conditions for the shallow water calculations.

Table 1

Instrument Specifications

| STN. NO | INSTRUMENT | WATER DEPTH (m) |
|---|---|---|
| 165 | WR (ND) | 34 |
| 165 (03/84) | WR (ND) | 21 |
| 167 (03/84) | WR (ND) | 160 |
| 170 (03/84) | WR (ND) | 22 |
| 142 | WR (ND) | 16 |
| 133 | WR (ND) | 85 |
| 251 | WRIPS (ND) | 200 |
| 252 | WAVEC (D) | 22 |
| 253 | WAVEC (D) | 12 |

WR - WAVERIDER®
ND - NONDIRECTIONAL
D - DIRECTIONAL
WRIPS - SATELLITE BUOY
WAVEC® - HEAVE-PITCH-ROLL BUOY

NOTE: 03/84 DENOTES BUOY POSITION FOR THE HINDCAST STORM OF MARCH 29-31, 1984. ALL OTHER STATION NUMBERS PERTAIN TO THE 1984-85 FIELD PROGRAM.

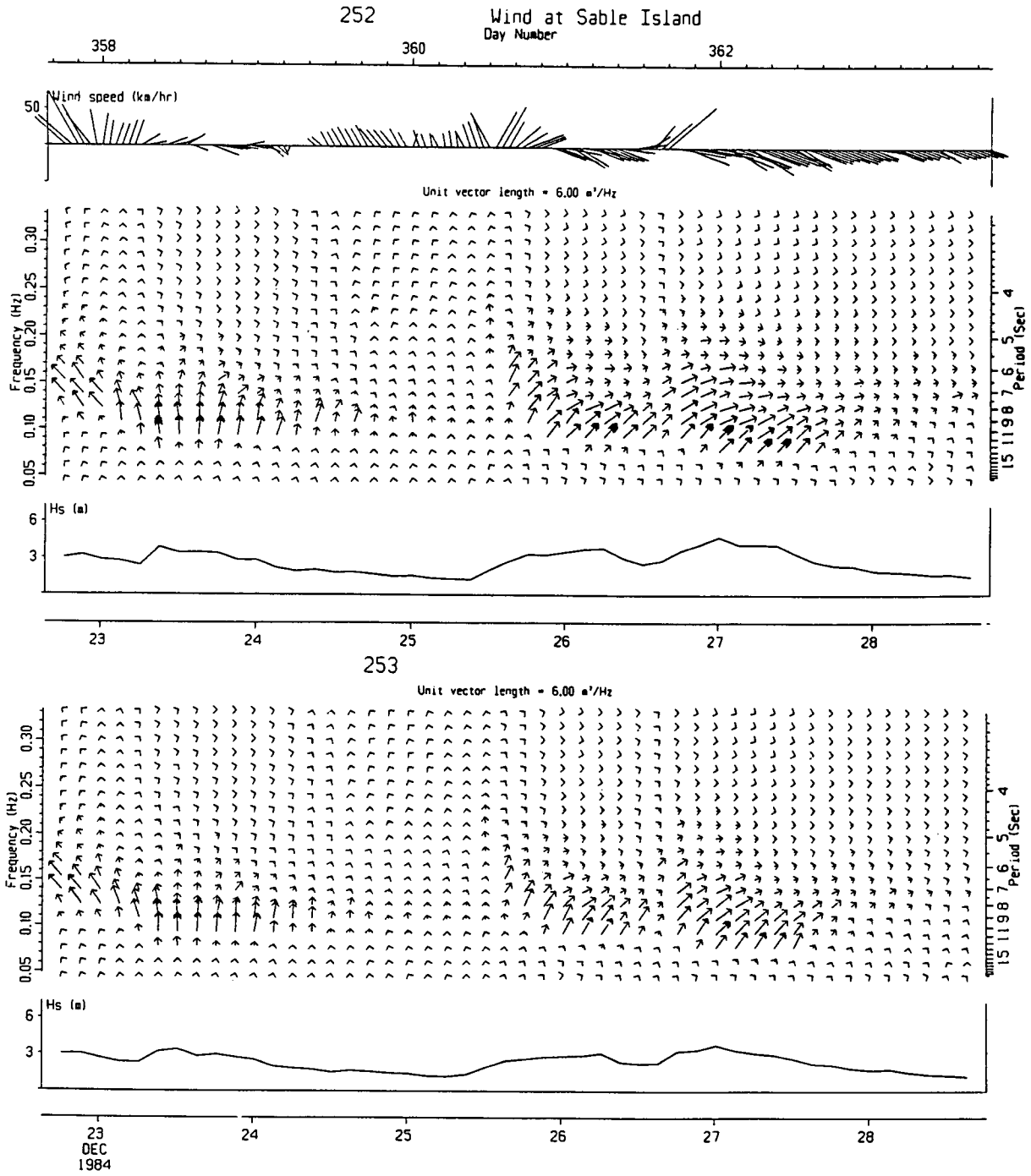


Fig. 2 Directional wave data from stations 252 and 253 in 20 frequency bands plotted against the Sable Island wind and significant wave height time-series.

Overwater wind fields were derived from 6-hourly surface weather analysis charts. Gradient winds were calculated from these pressure distributions, reduced to 10 m using a stability-dependent boundary layer model, and blended with marine observed winds.

Each shallow water model was applied with identical boundary conditions and overwater winds. Mesh sizes were selected so as to give adequate resolution of Sable Island and

local bathymetry, consistent with the theory contained in the models and computing effort. WAVAD was run on a 5 n.m. grid, whereas SPECREF was applied on a 1 n.m. mesh emphasizing the importance attached to refraction and the economy achieved in modelling each storm with a 3-h time step.

## 4.0 Model Specifications

(a) SPECREF

Equation (1) is solved to give the directional wave frequency spectrum $S(\mathbf{x}, f, \theta)$ at a specified location $\mathbf{x}$ for an arbitrary depth field resolved on a regular Cartesian grid with spacing $\Delta x = 1$ n.m. The following assumptions were invoked:

(i) The dominant source-sink mechanisms are wind input and bottom friction; the effect of nonlinear energy fluxes between different frequencies is adequately parameterized by the saturation spectrum.

(ii) Wave-current interactions are ignored ($\mathbf{U} = 0$).

(iii) Wave diffraction and wave reflection are negligible.

(iv) Energy losses due to opposing winds are negligible.

(v) Energy is limited by the depth-dependent saturation law (Kitaigorodskii et al., 1975).

Under these assumptions (1) may be restated as

$$(\partial/\partial t + \mathbf{c_g} \cdot \nabla) S = Q_{in} + Q_b \qquad (3)$$

where $Q_{in} = B.S(f,\theta)$ (wind source term),

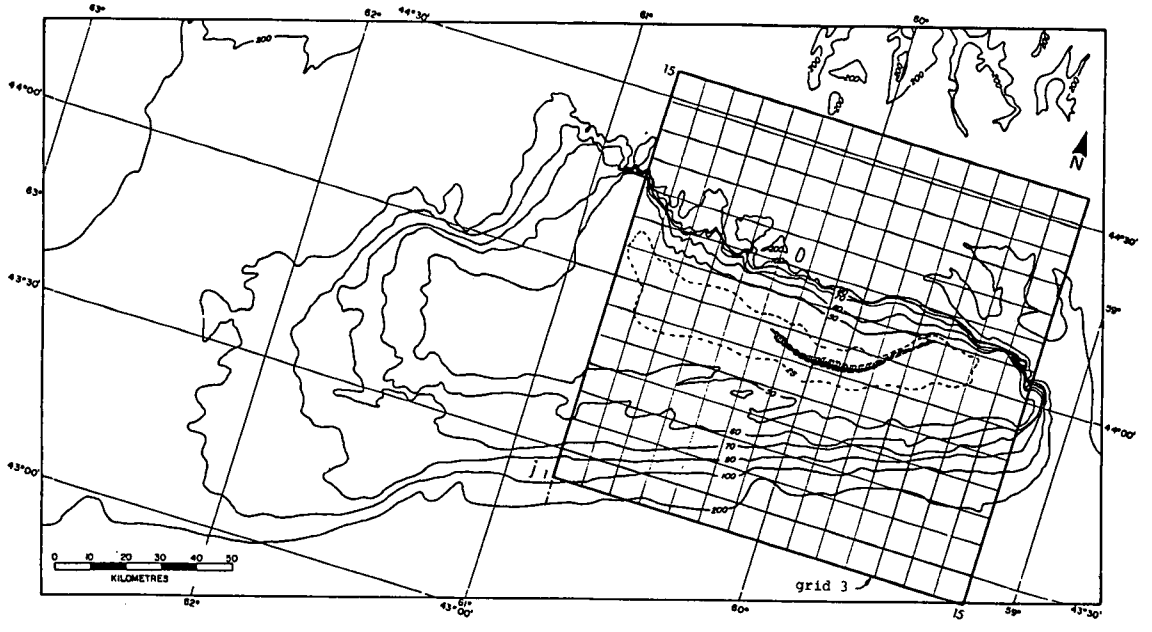


Fig. 3. Shallow water calculation domain showing the 5 n.m. grid.

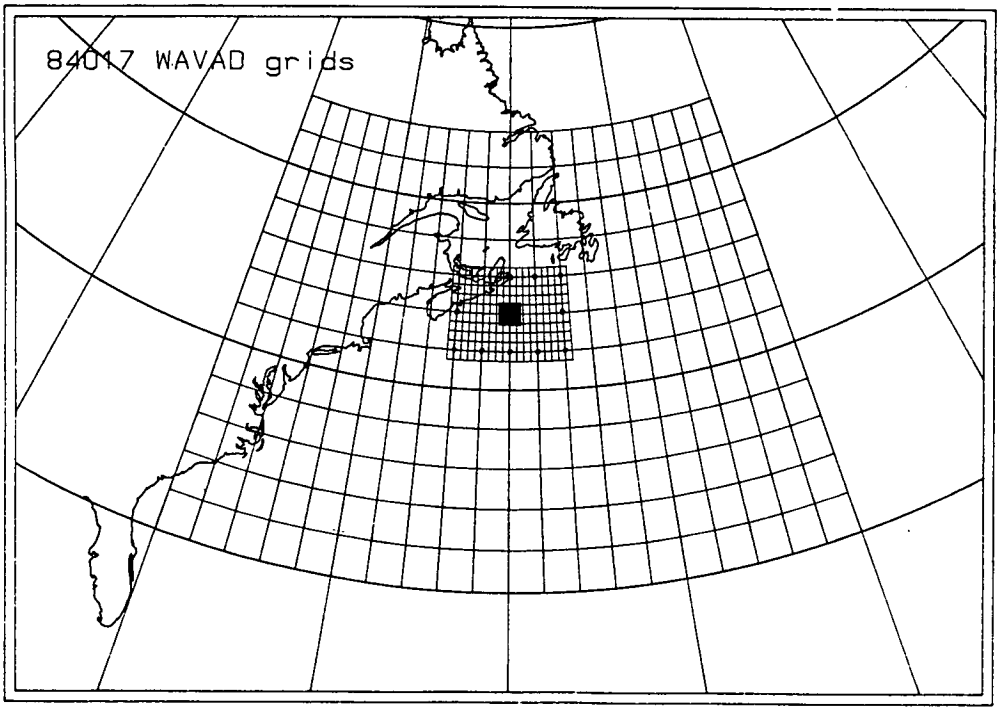


Fig. 4 Nested grid system used to hindcast the deep water wave conditions.

$$B = \begin{cases} 5f \left(\frac{\rho_a}{\rho_w}\right)\left[\frac{\mathbf{U}\cos\beta}{c} - 0.90\right], & \frac{\mathbf{U}\cos\beta}{c} > 0.90 \quad (4) \\ 0, & \frac{\mathbf{U}\cos\beta}{c} \leq 0.90 \quad (5) \end{cases}$$

with $\mathbf{U}$ = wind speed at 10 m (m/s), $\beta$ = angle between the wind and wave directions, c = wave phase speed ($gk^{-1}\tanh(kh)$), and $\rho_a$, $\rho_w$ = air and water densities respectively ($kg/m^3$).

Bottom friction is specified as:

$$\tau_b = \frac{-C_f\, gkc_g}{2\pi\omega^2 \cosh^2(kh)} .S(f,\theta) \langle u \rangle \quad (6)$$

where $C_f$ = nondimensional drag coefficient, and

$$\langle u \rangle = \left[\sum E(f) \frac{g^2k^2}{\omega^2\cosh^2(kh)} \Delta f\right]^{1/2} \quad (7)$$

and $$E(f) = \frac{S(f_i, \theta_j)}{S_o(f_i, \theta_j)} \cdot E_o(f) \quad (8)$$

with the subscript o denoting deep water, and

$$c_g = 1/2 \left[1 + \frac{2kh}{\sinh 2kh}\right] c \quad (9)$$

and solved subject to the boundary conditions $S(\mathbf{x}_b,f,\theta)$ on all open water boundaries and the fields of 10-m wind $\mathbf{U}(\mathbf{x})$ and depth $h(\mathbf{x})$. The initial condition is $S(\mathbf{x},f,\theta)=0$.

The formulation for $Q_{in}$ follows that used by Cavaleri and Rizzoli (1981) and $Q_b$ is equivalent to the method published by Collins (1972).

With $Q = 0$, (3) can be written as a homogeneous transport equation in wave energy with characteristics given by the set of wave rays radiating outward from the location $\mathbf{x}$ for all $f,\theta$. If these characteristic curves are known then the energy conservation equation may be written as

$$\frac{dS}{dt} = Q \tag{10}$$

where the time integration is along each characteristic for $(f,\theta)$. Following Longuet-Higgins (1957)

$$\frac{cc_g}{4\pi^2 f}\, S(f,\theta) = \text{constant} \tag{11}$$

as the quantity conserved along each characteristic in the absence of source-sink terms, and noting the equivalence of time-space integration given by $ds = c_g\, dt$ we have for (10)

$$\frac{d}{ds}\left(\frac{cc_g S}{4\pi^2 f}\right) = \frac{1}{c_g}\left[Q_{in} + Q_b\right] \tag{12}$$

The numerical solution is computed in two steps. First the characteristic wave rays are calculated using linear refraction theory over the specified $h(\mathbf{x})$ for a discrete set of frequencies and directions $(f_i,\theta_j,\ i=1,\ldots,I;\ j=1,\ldots,J)$. The rays are reverse-traced until they intersect an open sea boundary or land. Second, (12) is integrated along each ray for given $f_i$ and $\theta_j$ at the point of interest in shallow water using a forward stepping procedure.

The boundary conditions are supplied at the end of each characteristic ray, either from measured, hindcast or parametric directional spectra in deep water, or $S(\mathbf{x},f,\theta) = 0$ for land points.

Finally the depth-dependent saturation form proposed by Kitaigorodskii et. al. (1975)

$$E_k(f) = \alpha g^2 (2\pi)^{-4} f^{-5}\, \phi(kh) \tag{13}$$

where $\alpha$ = Phillips' equilibrium range parameter,

$$\phi(kh) = \frac{\sinh^3(kh)}{[\cosh(kh)(kh + \sinh(kh)\cosh(kh))]} \tag{14}$$

is used as an upper bound on wave energy to the right of $f_m$. To the left of $f_m$, on the forward face, energies are unbounded and are controlled there by a balance between wind input and bottom friction.

The model was applied to Sable Island Bank with 16 frequencies ranging from 0.05 Hz to 0.20 Hz in steps of 0.010 Hz and 16 directions. The B-term growth coefficient was chosen as 5, $\alpha = 0.0081$ and $C_f = 0$ (no bottom friction).

(b) WAVAD

In this model solutions to (1) are obtained for $\mathbf{U}=0$ using a fractioned step procedure (Yanenko, 1971) by recasting the governing equation as

$$\left(\frac{\partial}{\partial t} + C_g \cdot \nabla\right) S = 0 \tag{15}$$

$$\frac{\partial S}{\partial t} = Q_{in} + Q_{nl} + Q_b \tag{16}$$

Equation (15) is solved using characteristic rays, reverse propagated from each grid point at the new time level to intersect the solution for S at the previous time level. Equation (11) is then solved along each ray for given $(f,\theta)$, taking the old-time level value for S as the initial value.

In the second step the propagated spectrum at the new time level is modified to account for energy input, changes in spectral shape due to nonlinear fluxes and bottom friction losses. Wave growth is formulated as

$$\frac{\partial S}{\partial t} = B(f,\theta).S(f,\theta) \tag{17}$$

where $B = z f_m^{*2} f \cos(\theta-\beta)$ (18)

$f_m^* = f_m U/g$

$\beta$ = wind direction

$z$ = dimensionless constant

From Kitaigorodskii (1983),

$$E(f) = \frac{\alpha_u \, Ug \, f^{-4}}{(2\pi)^3} \tag{19}$$

for the equilibrium range of the wave spectrum, where E(f) is the one-dimensional spectrum obtained by integrating $S(f,\theta)$ over all directions, and $\alpha_u$ is a universal constant (0.0042). Integration of (17) with respect to f and $\theta$ with (18) and (19) substituted into it gives

$$\frac{\partial E_o}{\partial t} = \frac{RU^3}{g} \tag{20}$$

where R is a dimensionless constant of $O(3\times10^{-7})$ and $E_o$ is total energy. Equation (20) provides the change in energy due to the local wind.

Resio (1986a) has shown that at frequencies above $f_m$ the energy balance between nonlinear fluxes and wind inputs leads to an equilibrium range of the form given in (19). The consistent wave-wave interaction flux term can be written

$$\frac{\partial E_o'}{\partial t} = \frac{\varepsilon E_o'^{3} k_m^{9/2}}{\tanh^{3/4}(k_m h)} \tag{21}$$

where $E_o' = \int_{f_m}^{\infty} E(f)df$ (22)

$\varepsilon$ is a constant of $O(10_2)$ and $k_m$ is the wave number at $f_m$. This flux represents a loss to the equilibrium range.

On the forward face of the spectrum the energy gain due to wave-wave interactions can be written in terms of a fixed proportion of the total wave-wave interaction momentum flux. With the equilibrium range in (19), this leads to a net gain of wave energy through time of the form

$$\frac{\partial E_o}{\partial t} = q\, r^3 \frac{u_*^2\, c_m}{g} \qquad (23)$$

where r is the ratio of the actual equilibrium range coefficient to the "universal" value and q is a dimensionless constant.

$Q_b$ is represented in WAVAD in an equivalent manner to that used in SPECREF.

The same spectral resolution was used in WAVAD as for SPECREF (16 frequencies and 16 directions) and bottom friction was set to zero. The saturation spectrum used in WAVAD has a wavenumber dependence

$$E(k) = B'\omega k^{-3} \qquad (24)$$

where B' is a dimensional constant with units of time$^{-1}$. This spectrum provides a deep-water $f^{-4}$ equilibrium range variation, changing to an $f^{-2}$ variation in shallow water.

## 5.0 Results

Time-series comparisons of significant wave height $H_s$, peak period $T_p$ and wave direction $\bar{\theta}$ in storm 2 (December 25-27, 1984) are shown for three stations, progressing from deep to shallow water, in Fig. 5. These results, which are representative of model behaviour in all four hindcast events, show that both models capture the essential characteristics of the storm history and of the shallow water transformation of wave energy.

The station 133 comparison shows that the general character of the storm between December 25th to late on the 27th is well modelled except for the rapid decay in $H_s$ just following the second peak on December 27. There are clearly differences between the model response evidenced by the generally lower energy levels in the SPECREF predictions; this difference provides a better fit to data during the second peak but vice versa during the December 26th maximum when WAVAD is generally more accurate. Both models underpredict peak period during the first stage of the storm but give good agreement during the second.

The storm 2 shallow water comparisons in 22 m of water (station 252) show that both SPECREF and WAVAD model $H_s$ for the second growth-decay stage (Dec. 26-27) well but underestimate the first stage. In the case of SPECREF this is consistent with the station 133 results; it is harder to explain for WAVAD since energies in deeper water were well-modelled at this time. In shallow water (h = 12 m at station 253) the $H_s$ predictions are in very close agreement with measurements.

WAVAD shows a tendency here to underestimate $T_p$ at all times with perhaps an increasing error as one moves into shallower water. SPECREF provides low estimates of $T_p$ during the first stage, consistent with the boundary data, but gives a very favourable prediction at station 253 in the second stage.

The WAVAD directions in both water depths also compare favourably with measurements except late in the storm when winds have decayed to under 30 knots. There is greater variability in the SPECREF directions, linked obviously to changes in $T_p$, but this model too shows reasonable agreement with measurements. Importantly the measurements show about a 20° to 30° directional shift in wave energy between h = 22 m and h = 12 m; both models reproduce this shift in direction.

A statistical summary of model performance was compiled for all prediction-observation pairs based on systematic and unsystematic mean square errors, RMS errors and scatter indices for $H_s$, and mean errors and standard deviations of errors in $T_p$ and $\bar{\theta}$ in terms of the number of discrete frequency or direction bins by which the model predictions differ from the measurements. Scatter diagrams for $H_s$ are shown in Fig. 6 together with least-squares linear regressions of the modelled $H_s$ values onto the measured values. Histograms of errors in $f_m$ and $\bar{\theta}$ are shown in Fig. 7 and 8 respectively.

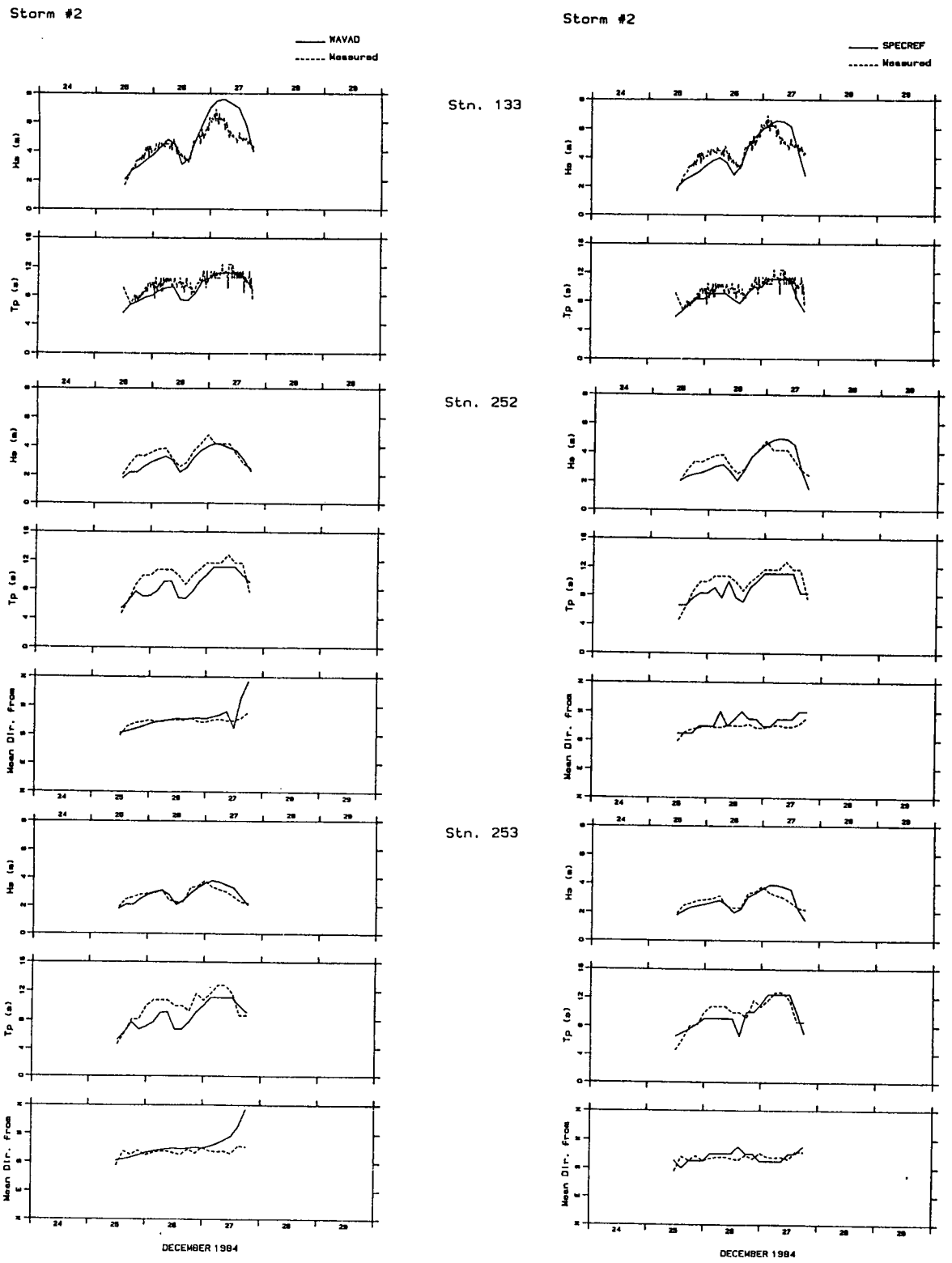


Fig. 5. Time-series of significant wave height $H_s$, peak period $T_p$ and wave direction $\overline{\theta}$ at stations 133, 252 and 253 during storm 2 (December 25-27, 1984).

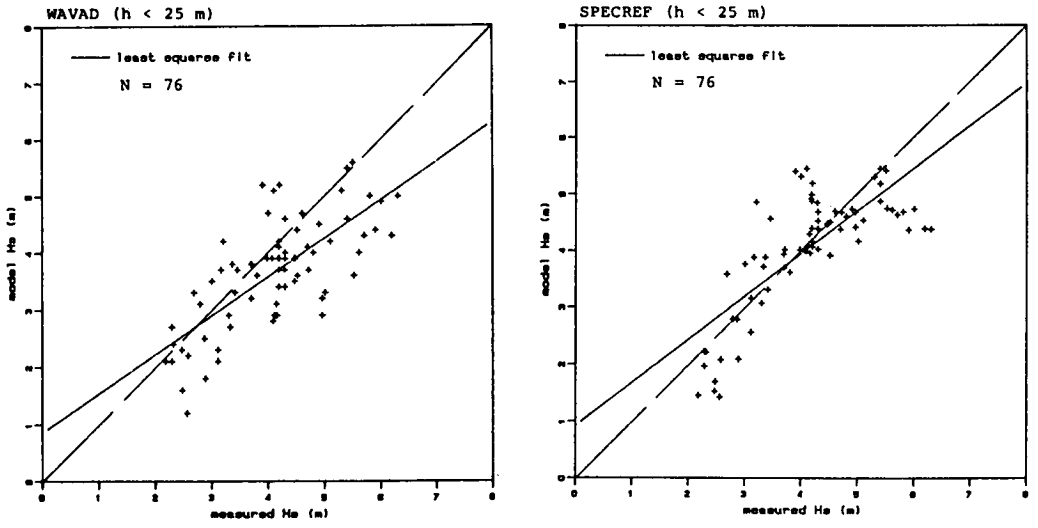


Fig. 6 Scatter diagrams of $H_s$-predicted versus $H_s$-measured in shallow water (h<25 m).

The statistics, which are summarized in Table 2, show that both models are characterized by RMS errors of about 1 m in $H_s$ and scatter indices of 15 to 20%. WAVAD shows a bias high of about 1 $\Delta$f in $f_m$ with a standard deviation of 2 $\Delta$f-bins. SPECREF is more accurate in this respect being unbiased in $f_m$ and a standard deviation of 1.6 $\Delta$f-bins. Both models exhibit mean directional errors of less than one $\Delta\theta$-bin; in the case of SPECREF this amounts to about 8° compared with 18° for WAVAD.

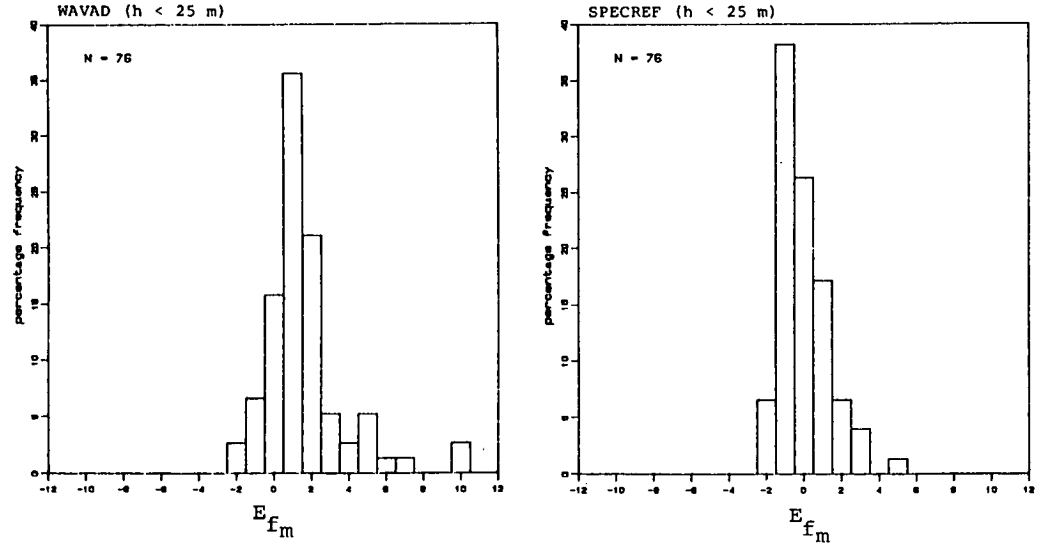


Fig. 7 Frequency histograms of the error in $f_m$ expressed in terms of the frequency discretization interval $\Delta$f.

Table 2

Statistical Summary of Wave Model Errors

| | | $H_s$ | | | | $E_{Tp}$ | | $\bar{E}_\theta$ (1) | |
|---|---|---|---|---|---|---|---|---|---|
| | | $MSE_s$ | $MSE_u$ | RMSE | SI | $\mu$ | $\sigma$ | $\mu$ | $\sigma$ |
| all data (N=139) | WAVAD | 0.70 | 0.91 | 1.27 | 0.21 | 1.24 | 2.10 | - | - |
| | SPECREF | 0.55 | 0.49 | 1.02 | 0.15 | 0.14 | 1.55 | - | - |
| h > 25 m (N=63) | WAVAD | 0.56 | 0.82 | 1.17 | 0.18 | 0.78 | 1.91 | - | - |
| | SPECREF | 0.44 | 0.50 | 0.97 | 0.14 | 0.35 | 1.76 | - | - |
| h < 25 m (N=76) | WAVAD | 0.95 | 0.44 | 1.18 | 0.18 | 1.62 | 2.17 | 0.78 | 1.08 |
| | SPECREF | 0.74 | 0.42 | 1.08 | 0.17 | -.03 | 1.33 | 0.30 | 0.68 |

(1) measured peak directions available only at stations 252 and 253 (N=54)

$\mu$ = mean

$\sigma$ = standard deviation

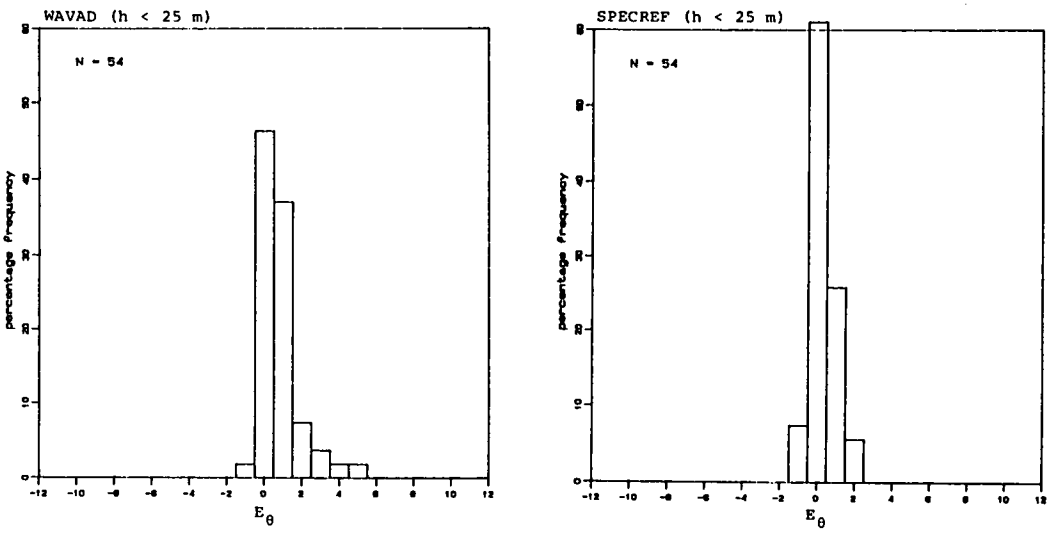


Fig. 8 Frequency histograms of the error in $\bar{\theta}$ expressed in terms of the direction discretization interval $\Delta\theta$.

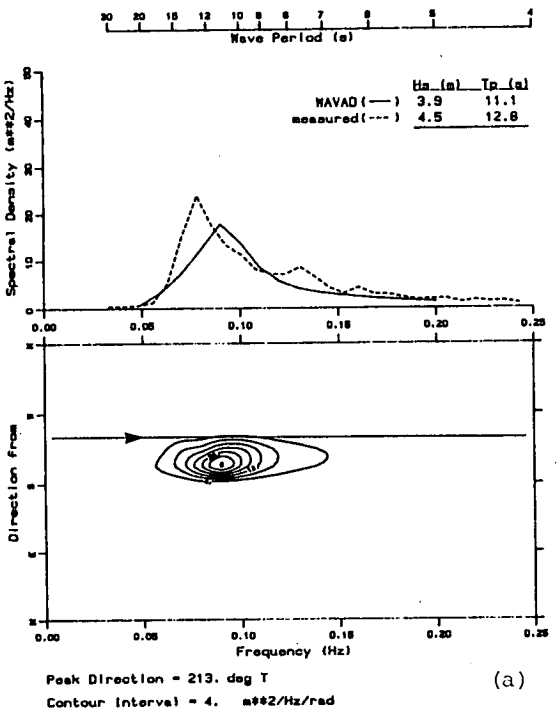


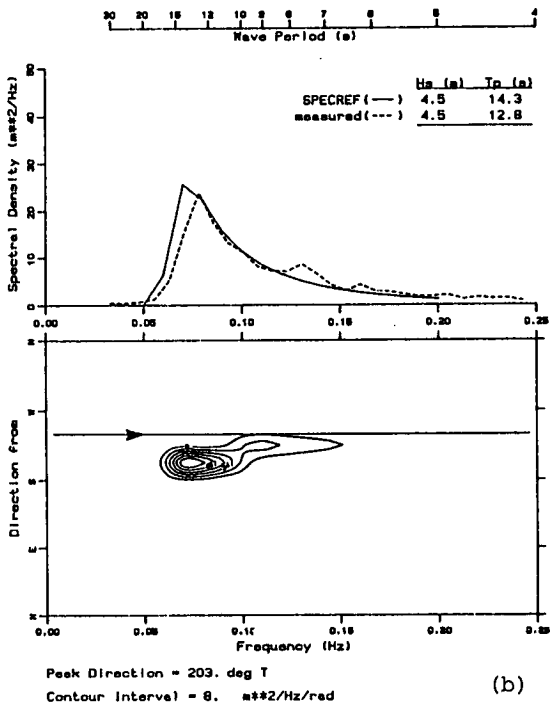


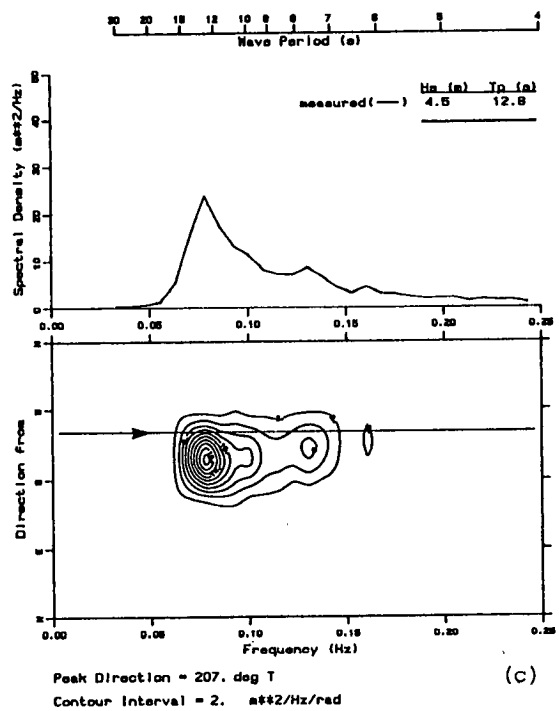


Fig. 9 Representative directional spectra from WAVAD (a), SPECREF (b), and as measured (c). The data are from station 253 at 03 GMT December 23, 1984.

Fig. 9 shows spectra for both models compared with measurements during storm 2. The tendency for WAVAD to overpredict $f_m$ is seen to result in a forward face that rises too slowly, compared with SPECREF which exhibits a shape, both above and below $f_m$, in better agreement with the measured spectrum. Each model also shows offwind directions at $f_m$ consistent with measurements. The major difference between the predicted directional spectra is seen in the shape of the high-frequency tail: SPECREF yields spectra with step-like changes in direction, whereas WAVAD spectra are more smoothly varying in direction. The modelled spectra also appear to be too directionally narrow, i.e. without sufficient spread in energy about $\theta_o$ in frequency.

## 6.0 Conclusions

Given identical deep-water boundary conditions and overwater winds we have found that the two wave models--one a decoupled propagation model and the other a coupled discrete spectral code--give very similar results for energetic sea states into water depths of about 10 m. This finding is based on comparisons of predicted and measured wave spectra from a carefully controlled directional wave database on Sable Island Bank. This is an area of relatively complicated bathymetry and sheltering. For the four storms hindcast here the decoupled

model was slightly more accurate than the coupled formation, at least in terms of wave parameters frequently used in engineering practice; both models, however, gave results that would be considered accurate enough for engineering use.

The reason for the similarity in behaviour of the two models lies in the dominant role of the saturation spectrum in the overall energy balance. For the storm conditions modelled here the wave spectra appear to be governed by an equilibrium range for frequencies higher than $f_m$, resulting from a balance between energy input from the boundaries and locally by the wind, and the losses due to bottom friction and wave breaking. By virtue of setting $C_f = 0$ (no bottom friction) we have argued that the primary balance is, in fact, between propagating wave energy, wind growth and wave breaking.

Each model incorporates a semi-empirical saturation spectrum to represent this equilibrium range. In SPECREF this spectrum is given by a Phillips' $f^{-5}$ equilibrium form modified by the depth-dependent function given in (14). The Phillips' parameter has been treated as a constant. Resio (1986a, 1986b) has derived the $\omega k^{-3}$ relation given in (23) which is used in WAVAD. Since predicted energy levels for frequencies above $f_m$ generally exceed the equilibrium range values, then the performance of each model in terms of total energy depends strongly on the location of $f_m$, the changes in energy on the forward face, and the precise level of the saturation curve.

In SPECREF $f_m$ was allowed to change as the waves propagated into shallow water, specifically as the saturation level decreased with depth, $f_m$ could shift to a lower frequency given by the intersection of the saturation curve with the forward face of the spectrum. Since no energy was transmitted to the forward face from central frequencies by virtue of ignoring the nonlinear flux due to wave-wave interactions, energy in frequencies below $f_m$ was largely fixed by the boundary conditions. This constraint produced the characteristically steep forward face of the SPECREF spectra (Fig. 9), giving satisfactory agreement with measurements.

The peak frequency $f_m$ was fixed in WAVAD equal to a value given by spatial interpolation of the deep water boundary conditions. This provided an $f_m$ that was virtually constant during the transformation process. The energy in frequencies above $f_m$ was thus governed by the equilibrium range function, and below $f_m$ by local wind growth and the pumped transfer of energy due to wave-wave interactions. This difference in the behaviour of $f_m$ and growth on the forward face compared with SPECREF explains, for the most part, the differences noted in spectral shape, specifically, the more gradually sloped forward face and small bias in $f_m$ to higher frequencies.

Thus we find that despite profound differences in the physics governing wave growth and transformation into shallow water in the two models, the term $Q_{diss}$, which is perhaps the least well understood term in the balance equation, exerts a large influence on the final results. Both models examined here, and indeed all models in first or second generation classes (see e.g. SWAMP, 1985), make use of an equilibrium range to limit energy above $f_m$. This equilibrium range depends upon one or more empirical constants even though the form of the equation may be based on a flux balance derived on dimensional grounds or from a consideration of the collision integral for four resonantly interacting waves (Kitaigorodskii, 1983; Resio, 1986a). As a result, large differences in model performance should not be expected under sea states at, or approaching, saturation provided that $f_m$ is largely correct, that the equilibrium range is well-calibrated, and that the energy balance on the forward face is approximately correct.

It appears that generalization of spectral wave models based on the energy balance equation (1) depends upon better paramaterization of the $Q_{diss}$ term. In this respect discrete spectral models that incorporate energy fluxes due to wave-wave interactions are better formulated than the decoupled codes are to take advantage of methods to calculate $Q_{diss}$ directly.

## 7.0 Acknowledgements

This work was supported by the Environmental Studies Revolving Funds Study Number 313-07-08, Canada.

## 8.0 References


Bouws, E., H. Gunther, W. Rosenthal and C.L. Vincent, 1985. Similarity of the Wind Wave Spectrum in Finite Depth Water. Part 1: Spectral Form. J. Geophys. Res., 90, 975-986.

Cavaleri, L. and P.M. Rizzoli, 1981. Wind Wave Prediction in Shallow Water: Theory and Applications. J. Geophys. Res., 86, 10961-10973.

Collins, J.I., 1972. Prediction of Shallow-Water Spectra. J. Geophys. Res., 77, 2693-2707.

Hasselmann, K., T.P Barnett, E. Bouws, H. Carlson, D.E. Cartwright, K. Enke, J.A. Ewing, H. Gienapp, D.E. Hasselmann, P. Kruseman, A. Meerburg, P. Mueller, D.J. Olbers, K. Richter, W. Sell and H. Walden, 1973. Measurements of Wind-Wave Growth and Swell Decay During the Joint North Sea Wave Project (JONSWAP). Deutschen Hydrographische Zeitschrift, Reihe A., Nr. 12.

Hasselmann, D.E., M. Dunckel and J.A. Ewing, 1980. Directional Wave Spectra Observed During JONSWAP 1973. J. Phys. Oceanogr., 10(8), 1264-1280.

Hodgins, D.O., C.T. Niwinski and D.T. Resio, 1986. Comparison and Validation of Two Shallow Water Spectral Wave Models. Environmental Studies Revolving Funds Report, Ottawa.

Karlsson, T., 1969. Refraction of Continuous Ocean Wave Spectra. ASCE J. Waterways, Harbours, Coastal Engng. Div., 95 (WW4), 437-448.

Kitaigorodskii, S.A., V.P. Krasitskii and M.M. Zaslavskii, 1975. On Phillips' Theory of Equilibrium Range in the Spectra of Wind-Generated Gravity Waves. J. Phys. Oceanogr., 5, 410-420.

Kitaigorodskii, S.A., 1983. On the Theory of the Equilibrium Range in the Spectrum of Wind-Generated Gravity Waves. J. Phys. Oceanogr., 13(5), 816-827.

Long, R.B., 1980. The Statistical Evaluation of Directional Spectrum Estimates Derived from Pitch/Roll Buoy Data. J. Phys. Oceanogr., 10, 944-952.

Longuet-Higgins, M.S., 1957. On the Transformation of a Continuous Spectrum by Refraction. Proc. Camb. Phil. Soc., 53, 226-229.

Longuet-Higgins, M.S., and R.W. Stewart, 1960. Changes in the Form of Short Gravity Waves on Long Waves and Tidal Currents. J. Fluid Mech., 8, 565-583.

Phillips, O.M., 1977. Dynamics of the Upper Ocean. 2nd Ed. Cambridge U. Press, London.

Resio, D.T., 1981. The Estimation of Wind-Wave Generation in a Discrete Spectral Model. J. Phys. Oceanogr., 11, 510-525.

Resio, D.T., 1982. Wave Prediction in Shallow Water. Proc. 14th Annual Offshore Tech. Conf., OTC 4242, Vol. 2, 147-152.

Resio, D.T., 1986a. Wave Transformations Related to Nonlinear Fluxes. Part 1: Theory. Submitted to ASCE J. Waterway, Port, Coastal and Ocean Engineering.

Resio, D.T., 1986b. Wave Transformations Related to Nonlinear Fluxes. Part 2: Field Comparisons. Submitted to ASCE J. Waterway, Port, Coastal and Ocean Engineering.

SWAMP Group, 1985. Ocean Wave Modeling. Plenum, New York, 256 pp.

Yanenko, N.N., 1971. The Method of Fractional Steps. Springer, 160 pp.

## B-2 Forecasting Wave Conditions Under the Influence of Currents and Bottom Topography

*Yung Y. Chao*

Each year, many shipmasters are faced with dangerous situations when they attempt to navigate in coastal areas where ocean surface waves interact with local bottom topography and surface currents. A well known hostile environment of this kind is the Columbia River Bar on the west coast of the United States where the heights of swell coming from the Pacific can be doubled by combined effects of strong ebb tidal currents and submarine shoals. Hundreds of search and rescue missions are conducted yearly by the Coast Guard. In spite of this effort, a number of mariners are lost each year. In order to assist marine forecasters in predicting wave conditions at potentially dangerous sites, a numerical model which incorporates refraction of ocean wave spectra by two-dimensional bottom topography and surface currents has been developed. the model, which uses as input spectral wave data from an operational global wave forecast model, is based on a wave action balance formulation and a ray backward tracing techniques. The model is designed to simulate the wave conditions at the entrance to the Columbia River where an intensive field observation program has been conducted. Comparisons of the model output with observed data indicate good agreement between the two.

# A SECOND GENERATION SHALLOW WATER RESIO WAVE MODEL

Will Perrie[1], Wolfgang Rosenthal[2] and Bechara Toulany[1]

[1]Department of Fisheries and Oceans
Bedford Institute of Oceanography
P.O. Box 1006, Dartmouth, N.S. B2Y 4A2

[2]GKSS-Forschungszentrum
Max-Planck-Strasse
D-2054 Geesthacht, West Germany

## Abstract

Starting with a standard second generation deep water discrete spectral wave model, as defined by SWAMP (1982), we implement the extensions of deep water wave Phillips saturation range concepts that have been made both to finite depth, and to the entire spectral range. the so-called Kitaigorodskii factor is applied to the spectral shape functions, for growth and saturation range, and therefore implicitly for swell and Philips' $\alpha$ function as well. Concomitantly, the deep water dispersion relation, phase and group velocities, are replaced by appropriate depth dependent versions.

The resultant model is calibrated via SWIM (1985), and shown to be competitive.

## Introduction

Some years ago, the Marine Environmental Data Service acquired the discrete spectral prediction model for wind generated waves on water, described by Resio (1981). This is a model for surface waves on deep water. Geometries like Sable Bank or Georges Bank off Nova Scotia in water less than 120 m are not correctly represented by this model but are clearly important offshore areas. A detailed presentation of shallow water adaptions made, appears in Perrie (1986). An expansion of this report is in preparation.

Modifications of the model start with the Kitaigorodskii, Krasitskii and Zaslavskii (1985) extension of the Phillips saturation range concepts for deep water wave conditions to finite depth. A further generalization to the entire spectral range is due to Bouws, Gunther, Rosenthal and Vincent (1985). Thus the self-similar deepwater JONSWAP (1973) shape is extended to finite depth, in accordance with the shallow water TMA spectra.

The so-called Kitaigorodskii factor,

$$\phi_{k(\omega_H)} = \frac{k(\omega,H)^{-3} \quad \partial k(\omega,H)/\partial f}{k(\omega,\infty)^{-3} \quad \partial k(\omega,\infty)/\partial f}$$

*where H is the depth, g, the gravitational acceleration, f, the frequency, $\omega = 2\pi f$, and $\omega_H = 2\pi f \sqrt{H/g}$, scales growth and saturation shape functions, and thus implicitly modifies swell and Phillips' $\alpha$ function. The deep water dispersion relation is replaced by the more general*

$$\omega^2 = gk \tanh kH$$

*and similarly for phase and group velocities. Dissipation is modelled following JONSWAP, refraction, following Golding (1983).*

*SWIM (1985) concerns two hypothetical experiments and one North Sea severe storm hindcast with the objective of understanding shallow water physics and its numerical modelling. The original intercomparison models are BMO, of the British Meteorological Office presented in Golding (1983), GONO, of the Royal Netherlands Meteorological Institute and described by Janssen, Komen and de Voogt (1984), and HYPAS, a model of the Hamburg wave group and documented in Gunther and Rosenthal (1984). These are set up for the North Sea and have been intercompared earlier on a quasi-operational basis without dramatic conclusion.*

*Each has a different approach to modelling shallow water waves, relates differently to the SWIM tests, and generally behaves acceptably. For hypothetical tests 1 and 2, explanation of model response can be related to shallow water physics within the model. For the hindcast, test 3, the interaction of processes is too complicated for a detailed discussion of mechanisms.*

*The interesting and unique aspect presented here is that a discrete spectral model has been modified using the same methods as applied in HYPAS, a hybrid parametric model, to enable the latter to handle shallow water waves, as implied by Kitaigorodskii et al. (1985) and Bouws et al. (1985), and results are strikingly alike.*

*SWIM Intercomparison*

*Details of the tests are documented in SWIM (1985). Fig. 1 describes SWIM test 1, where as in SWAMP (1982) we scale via friction velocity and nondimensionalize via $x_* = xg/U_*^2$ and $E_* = Eg^2/U_*^4$. Models are run to stationarity. Deep water is 120 m and appears in SWAMP (1982) and Perrie and Toulany (1985).*

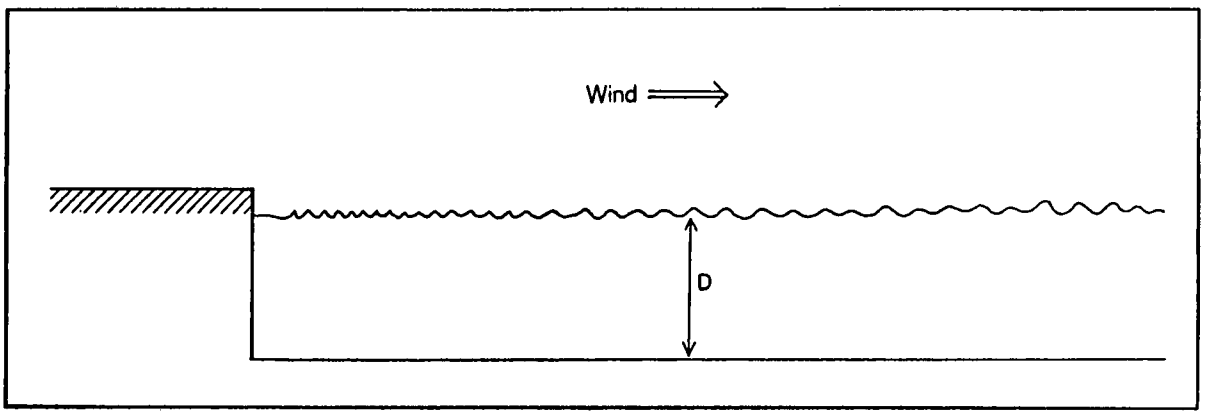


*Fig. 1 Configuration of test 1: a constant offshore wind blowing over constant depth D basin.*

*Notice BIO-Resio and HYPAS in Fig. 2 with respect to rate of growth of energy, E, with fetch and reduction of wave energy with finite depth, as opposed to BMO and GONO.*

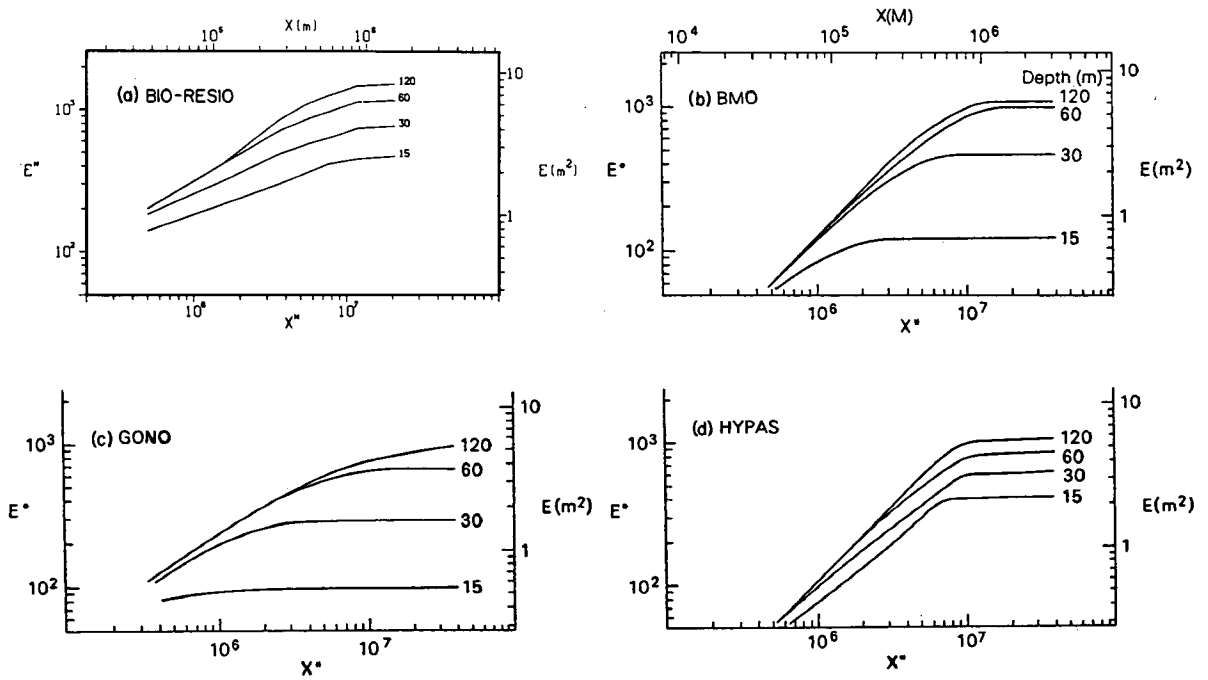


*Fig. 2 Plots of wave energy E(m²) against fetch X(m) in the depth-dependent (D=120,60,30,15 m) fetch-limited geometry of test 1 for a) BIO-Resio, b) BMO, c) GONO, d) HYPAS.*

*Similarity in scaling spectral shape functions by the Kitaigorodskii factor represents enhanced dissipation due to wave breaking at finite depth in BIO-Resio and HYPAS. $f_p$ is not assumed depth dependent. $S_{BOT}$ is strong in BMO and GONO, influencing E and $f_p$ and, via the deep water diagnostic relation, implying an increase in $f_p$ with decreasing depth. This is shown in Fig. 3, the asymptotic spectra of the models (infinite duration and fetch).*

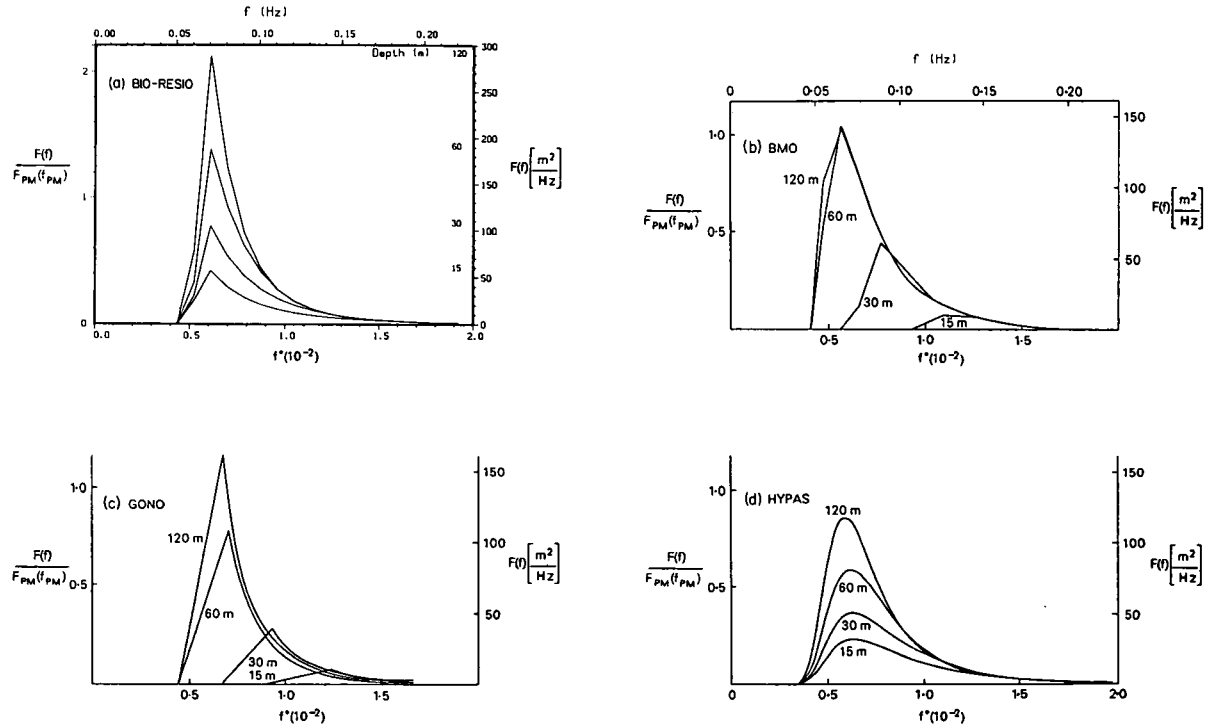


*Fig. 3 The fully developed wave energy spectra as a function of depth as in Fig. 2 plotted against frequency as in SWIM (1985).*

*Notice the hyper-high energy levels that characterize BIO-Resio, as in Perrie and Toulany (1985), which are the mark of the growth and saturation shape functions within the model and which influence all else, like $f_p$.*

*The strong dissipation within HYPAS and BIO-Resio is tantamount to quasi-equilibrium mainly dependent on depth. Whether in the presence of no advective divergence as in SWIM test 1, or in the presence of large advective divergence as in SWIM test 2, concerning onshore winds and sloping continental shelf-type bottom topography, these two models respond similarly. Plots in the latter case of large advective divergence, are almost exactly as in Fig. 3.*

*The test of a model is always in the complex interactions of processes of a real geophysical system. The chosen period, 20-26 November 1981, provided reliable wave measurements, and relevant wind fields could be realistically numerically analyzed and reconstructed. SWIM (1985) presents a discussion of the meteorological situation, wind data processing, measured wave data, and the operational characteristics of the models. Fig. 4 shows how significant wave height $H_S$, and period $T_{01}$, vary with time for the four models at FULMAR in the central North Sea.*

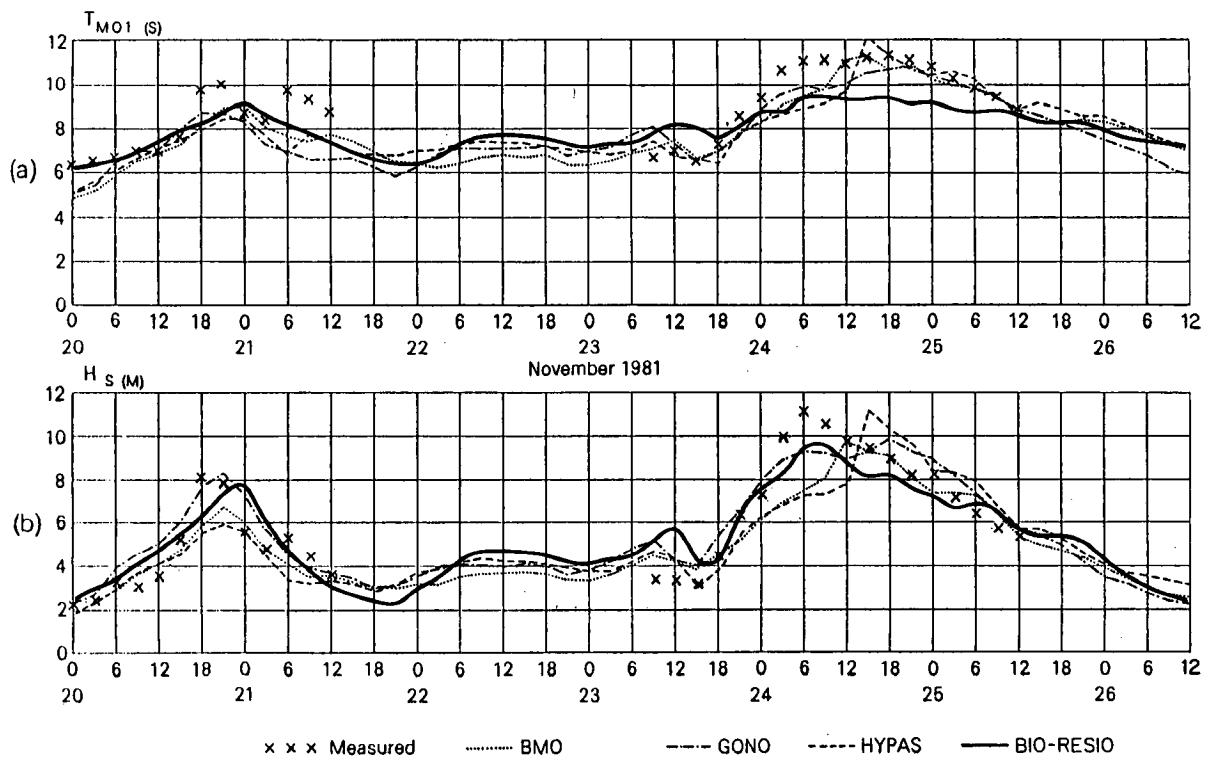


*Fig. 4 Time series of a) Mean zero-upcrossing period $T_{M01}$ (sec.); b) significant wave height $H_S$ (m); for FULMAR for the four models. Refraction and $S_{BOT}$ are neglected in BIO-Resio.*

*For the first storm, GONO and BIO-Resio reach comparable $H_S$, with BMO and HYPAS failing to match the observed rapid growth between 15Z and 18Z on the 20th. The former two models, although more successful in fitting the peak grew excessively early in the day, which could be anticipated from their growth characteristics in Fig. 2.*

*The second storm shows GONO and BIO-Resio once more giving values comparable with the peak. All models reach the peak values later than in reality and GONO and HYPAS were too high during the entire decay phase. The behavior of the models regarding period $T_{01}$ was much closer, although all were too low at the peak of the first storm, and all do the second peak reasonably, with BIO-Resio reflecting its hyper-high energy levels by being somewhat low. Otherwise growth rates are slow and decay rates reasonable.*

*Subsequent wind analysis showed the modelled winds off by 2.5 m/s and 20° in early hours of the 24th. Thus it was impossible for the wave models to match longer fetch, higher energy, north-westerlies of the second storm, which were actually present.*

*Overall statistics for FULMAR are in Table 1. The predominant over-estimate of GONO, the under-estimates of HYPAS and BMO, and the 'middling' behavior of BIO-Resio are evident.*

**Table 1**

**Verification Statistics for FULMAR**

| Model | $\frac{N}{\overline{H_S}\ (m)}$ $\overline{T_{01}(S)}$ | Model Depth (m) | RMS Height Error (m) | Scatter Index | No. of +ive Errors | No. of -ive Errors |
|---|---|---|---|---|---|---|
| BMO | 31 | 82 | 1.1 | 20 | 11 | 20 |
| GONO | 6.1 | 80 | 0.9 | 14 | 23 | 8 |
| HYPAS | 9.0 | 75 | 1.5 | 24 | 12 | 19 |
| RESIO-BIO | | 75 | 0.6 | 10 | 16 | 15 |

$N$ denotes number of observations

$\overline{H_S}$ denotes mean of observed significant wave heights

$\overline{T_{01}}$ denotes mean of observed periods

$$\text{Scatter Index} = \frac{\text{RMS error}}{\text{mean obs}} \times 100$$

*Conclusions*

*As in SWIM (1985), hypothetical experiments are seen to allow a diagnostic probing of BIO-Resio relative to other models. Differing evolutions and equilibria may be related to underlying physics within the model.*

*The hindcast, on the other hand, represents an ongoing challenge. Although all models are successful in giving various levels of wave energy, some shortcomings are clear, such as excessive growth rates in GONO and BIO-Resio. Ultimate separation of modelling processes is more difficult. Although models have different theoretical spectra, all correctly describe windsea, for example. Interaction of physical mechanisms blurs individual processes to the extent that ultimate analysis is not possible.*

*CASP may give the correct collection of detailed data for this sort of insight into model performance. It is apparent that an extraordinarily specific observation set is necessary, in order to achieve meaningful understanding of physical processes.*

*References*


*Bouws, E., H. Gunther, W. Rosenthal and C.L. Vincent. 1985. Similarity of the wind wave spectrum for finite depth water, Part 1. Spectral form. J. Geophys. Res., **90**, C1, 975-986.*

*Golding, B.W. 1983. A wave prediction system for real time sea state forecasting. Quart. J.R. Met. Soc., **109**, 393-416*

*Gunther, H., and W. Rosenthal. 1984. A shallow water surface wave model based on the TEXEL-MARSEN-ARSLOE (TMA) wave spectrum. Proc. 20th Congress IAHR, Moscow, 1983.*

*Janssen, P.A.E.M., G.J. Komen and W.J.P. de Voogt. 1984. An operational coupled hybrid wave prediction model. J. Geophysics Res., 89, C3, 3635-3654.*

*Hasselmann, K., T.P. Barnett, E. Bouws, H. Carlson, D.E. Cartwright, K. Enke, J.A. Ewing, H. Gienapp, D.E. Hasselmann, P. Kruseman, A. Meerburg, P. Muller, D.J. Olbers, K. Richter, W. Sell and H. Walden. 1973. Measurements of wind-wave growth and swell decay during the Joint North Sea Wave Project (JONSWAP). Deut. Hydrogr. Z., A12.*

*Kitaigorodskii, S.A. V.P. Krasitskii, and M.M. Zaslavskii. 1975. On Phillips theory of equilibrium range in the spectra of wind-generated gravity waves. J. Phys. Ocean., 5, 410-420.*

*Perrie, W. 1986. Making of a shallow water wave model. In press in Can. Tech. Rep. Hydrogr. Ocean Sci..*

*Perrie, W. and B. Toulany. 1985. Assessing a wave model a la SWAMP. Can. Tech. Rep. Hydrogr. Ocean Sci., No. 61, vi + 78 pp.*

*Resio, D.T. 1981. The estimation of wind-wave generation in a discrete spectral model. J. Phys. Ocean., 11, 510-525.*

*SWAMP (J.H. Allender, T.P Barnett, L. Bertotti, J. Bruinsina, V.J. Cardone, L. Cavaleri, J.J. Ephraums, B. Golding, A. Greenwood, J. Guddal, H. Gunther, K. Hasselmann, S. Hasselmann, P. Joseph, S. Kawai, G.J. Komen, L. Lawson, H. Linne, R.B. Long, M. Lybanon, E. Maeland, W. Rosenthal, Y. Toba, T. Uji, W.J.P. de Voogt. 1985. Sea Wave Modelling Project: An intercomparison study of wind-wave prediction models, Part 1 - Principle results and conclusions. Poc. IUCRM Symp. on Wave Dynamics and Radio Probing of the Ocean Surface, Miami, Plenum Press.*

*SWIM (E. Bouws, J.J. Ephraums, J.A. Ewing, P.E. Francis, H. Gunther, P.A.E.M. Janssen, G.J. Komen, W. Rosenthal and W.J.P. de Voogt) 1985. Quart. J.R. Met. Soc.. **111**, 1087-1112.*

# MODELLING THE CASP WAVE DATA SET

Fred Dobson and Will Perrie

Bedford Institute of Oceanography
P.O. Box 1006
Dartmouth, Nova Scotia
B2Y 4A2

## Abstract

During CASP, wave spectra were collected from six Waverider buoys and three directional Wavec buoys. Other data included wind, temperature, humidity, air pressure and precipitation from arrays of towers on the Nova Scotia mainland and on Sable Island, wind turbulence and velocity from aircraft flying over the wave buoy array, radiosonde data from an enhanced array of mainland and Sable Island stations, wind speed and water temperature from a buoy at the seaward end of the wave buoy array, wind speed from five sea bottom acoustic devices (WOTAN), surface current velocities and wave spectra from land-based radar (CODAR), and deeper current velocities from arrays of current meters.

Preliminary analysis will stratify the data against various dimensionless variables such as wave age, the ratio of intrinsic wave phase velocity to wind velocity; slope, the ratio of rms wave height to wavelength; fetch, the ratio of observed fetch to a scale parameter depending on the source of the wave field; the ratio of wavelength to water depth, etc.

Modelling strives to verify the self-similar k(wavenumber)-space "TMA" shallow water wave spectra of Bouws, Gunther, Rosenthal and Vincent (1985) and make an accounting for the nonlinear dynamics involved. It also studies the influence of the bottom boundary layer, refraction and currents. Finally, it tries to infer the fetch and duration evolution of the spectrum when constrained to finite depth.

## Introduction

During the Canadian Atlantic Storms Program (CASP: 15 January - 15 March, 1986) a large set of wave height and direction spectra were collected from a 9-element array (six Datawell Waveriders belonging to MEDS and three Wavecs, two from MEDS and one from BIO, on a 25 km line to the SSE from Martinique Beach, N.S.). A specially-designed, autonomously-operating data logging system provided, usually within 30 minutes of run time, power and directional spectra and status information from all nine sensors. A nearly complete (~90%) hourly time series of wave conditions at the array was accumulated.

In addition to the wave data, a great deal of relevant meteorological (Shaw, 1986) and oceanographic (Anderson, 1986) information was collected and archived. CODAR maps, by C-CORE, of surface currents over the array will allow inclusion of wave advection; bottom modification measurements were made from BIO's "RALPH" in 15m of water; currents and tides were measured at and offshore from the array; wind speeds were measured at two locations in the array and three offshore by WOTAN sensors (see Dobson, Lemon & Peters, 1986); a Coastal Climate "Minimet" buoy measured wind velocity and sea temperature at the outer end of the array; and AES meteorological mesonets on Sable Island and on the N.S. mainland provided wind velocity and air temperature among other variables; a greatly enhanced

meteorological observation network provided, and will provide, mesoscale-density analyses, from a variety of numerical models, of selected storms during the 16 CASP "Intensive Observation Periods".

All this has provided us with a unique opportunity to analyze the propagation, growth, evolution and decay of the waves produced by North Atlantic storms and their behaviour in deep and shallow water on the continental shelf of the East coast. We have measured not only the waves themselves, but also their causative mechanisms with unprecedented resolution in time and space over a three-month period, including 16 individual IOP's and an almost full range of North Atlantic winter conditions. All instruments have been calibrated before, during and after the experiment period, and so we will be producing estimates not only of the physical quantities themselves, but also of the errors associated with each.

The first part of this presentation will concentrate on exploring the observations themselves, and the second on discussing the modelling techniques we are applying to explain them in terms of the causative mechanisms.

## The Wave Spectra

Six power spectra and three directional spectra were produced for each hour. The Waverider power spectra were completed only after the individual time series, sampled once every 1.75 s, were calibrated, despiked and de-gapped when possible; the number of blocks averaged after the FFT to obtain the spectrum ranged from 3 to 17 (the FFT's were done with a 50% overlap, after a "Hanning" (cosine) window was applied). All this was done automatically by a Personal Computer at the Martinique Beach receiving site prior to (automatic) transmission to BIO.

The Wavec directional power spectra were computed by Datawell Wavec (Direc) receivers, which were then interrogated by the Martinique PC for storage and transmission to BIO. In addition, the original time series from all the buoys were stored at the Martinique site on 60 Mbyte "streamer" tapes.

It is these wave spectra, and quantities derived from them, which will be discussed here. Because our analysis is far from complete, the discussion will be confined to the power, and not the directional spectra, for two meteorological conditions: offshore and onshore winds, in both cases steady in direction over the previous 12 hours so that the conditions which produced the spectra may be considered stationary.

## Offshore Winds

The simplest case of all is offshore winds; they produce wave growth which is purely a function of the offshore distance, or fetch, of the sensor and component of the wind velocity in the wave direction. Clear-cut examples were not common, due to the complexity of the weather systems producing the winds. A few examples were found, and the resulting wave spectra follow the classic JONSWAP pattern (Hasselmann et al., 1973). The largest spectra, with the lowest peak frequency, occur at the longest-fetch sites. At shorter fetches, the spectra become progressively smaller, and their peaks occur at progressively lower frequencies. The spectral peaks at short fetches do not stay within the envelope formed by the long-fetch spectra; they typically exceed it by a factor of about two, indicating that the growing waves "overshoot" their equilibrium amplitude by a factor of about 1.5. For two clear-cut cases the variation of dimensionless peak frequencies $f_m U/g$ with dimensionless fetch $xg/U^2$ (see Table 1) indicates slightly lower peak frequencies for the longer fetches (dimensionless fetches of $3 \times 10^3$) in CASP; the variation of dimensionless wind speed U/Cp, where Cp is the wave phase speed at the spectral peak, with dimensionless fetch produces slightly lower dimensionless speeds at the same longer fetches than those presented in Donelan et al. (1985). Neither finding should be given much weight until we can scrutinize the entire data set.

Table 1

CASP Offshore Winds Parameterizations: 2 Cases

a) 21z 24-1-86 $U_{MB}$ = 12ms$^{-1}$ 15z Dir. NNE
6ms$^{-1}$ 21z $\bar{U}$ = 10ms$^{-1}$

| St$^n$ | $x^{2.}$ (km) | $\tilde{x}^{3.}$ | $f_{peak}$ | $\tilde{f}^{4.}$ | $\tilde{f}^{5.}_{JS}$ | $C_p^{6.}$ | U/Cp | $(U/Cp)^{7.}_{MD}$ |
|---|---|---|---|---|---|---|---|---|
| 24 | 36.8 | 3.6 x 10$^3$ | 0.23 | 0.23 | 0.23 | 6.8 | 1.5 | 1.6 |
| 25 | 22.4 | 2.2 x 10$^3$ | 0.24 | 0.24 | 0.29 | 6.5 | 1.5 | 1.8 |
| 26 | 28.8 | 2.8 x 10$^3$ | 0.25 | 0.26 | 0.27 | 6.2 | 1.6 | 1.7 |
| 32 | 17.6 | 1.7 x 10$^3$ | 0.28 | 0.29 | 0.3 | 5.6 | 1.8 | 1.9 |
| 21 | 12.8 | 1.3 x 10$^3$ | 0.32 | 0.33 | 0.32 | 4.9 | 2.0 | 2.0 |
| 22 | 8 | 0.8 x 10$^3$ | 0.34 | 0.35 | 0.4 | 4.6 | 2.2 | 2.3 |
| 23 | 8 | 0.8 x 10$^3$ | 0.35 | 0.36 | 0.4 | 4.5 | 2.2 | 2.3 |
| 31 | 5 | 0.5 x 10$^3$ | >0.35 | | | | | |

b) 12z 6-3-86 $U^{1.}_{MM}$ = 5ms$^{-1}$ 6z
10ms$^{-}$ 12z $\bar{U}$ = 8ms$^{-1}$
Dir. N

| St$^n$ | $x^{2.}$ (km) | $\tilde{x}^{3.}$ | $f_{peak}$ | $\tilde{f}^{4.}$ | $\tilde{f}^{5.}_{JS}$ | $C_p^{6.}$ | U/Cp | $(U/Cp)^{7.}_{MD}$ |
|---|---|---|---|---|---|---|---|---|
| 24 | 35 | 5.4 x 10$^3$ | 0.225 | 0.18 | .25 | 6.9 | 1.2 | 1.6 |
| 25 | 20 | 3 x 10$^3$ | 0.25 | 0.2 | .28 | 6.2 | 1.3 | 1.8 |
| 26 | 22.5 | 3.5 x 10$^3$ | 0.26 | 0.21 | .26 | 6 | 1.3 | 1.7 |
| 32 | 16 | 2.5 x 10$^3$ | 0.31 | 0.25 | .25 | 5 | 1.6 | 1.8 |
| 21 | 11 | 1.7 x 10$^3$ | 0.36 | 0.3 | .3 | 4.3 | 1.9 | 1.9 |
| 22 | 9.5 | 1.5 x 10$^3$ | 0.38 | 0.3 | .31 | 4.1 | 2.0 | 1.9 |
| 23 | 8 | 1.2 x 10$^3$ | >0.4 | | | | | |
| 31 | 5 | 0.8 x 10$^3$ | >0.4 | | | | | |

**Notes**
1. MM means from MiniMet wind buoy at station 33, 25.6 km from shore.
2. $x$ means largest fetch within ±20° of the wind direction.
3. $\tilde{x} = xg/U^2$
4. $\tilde{f}_p = f_p U/g$
5. JS means from Hasselmann *et al.* (1973), JONSWAP paper.
6. $C_p = g/2\pi f_p$
7. MD means from Donelan *et al.* (1985), Lake Ontario paper.

## The Separation of Sea from Swell

For offshore winds (i.e. SWIM case I: SWIM, 1985), all our spectra have two peaks: a high-frequency one from wind-driven waves and a low frequency peak from onshore travelling swell. (In fact, many of the spectra in onshore winds also have two peaks, particularly for northeasterly storms, but more on that later.) The problem we face is, given so many spectra, how do we teach a machine to distinguish between sea and swell?

The fraction $\mu$ of the wind speed in their direction at which the waves move is

$$\mu = \vec{U}\cdot\vec{k}/\omega$$

which is >1 for wave growth and <1 otherwise. For a "fully-developed" wave field,

$$f_p = f_{(\mu=1)} \text{ (fully-developed).}$$

Therefore, to include the entire wind-driven part of the spectrum, we should treat as sea all spectral peaks for which $f_p > Ff_{(\mu=1)}$ where $0 > F > 1$. We obtain F by assuming the JONSWAP self-similar spectral form (Hasselmann & Hasselmann, 1981), which is 1/100 of its peak value at $f/f_p \simeq 0.7$ (so, by definition, does the nonlinear transfer source function, which determines the position of the front face). Therefore, our swell/sea dividing line is

$$f_{swell/sea} = 0.7\, f_{(\mu=1)} = 0.7\, g/2\pi U_c$$

where $U_c$ is the component of the wind in the wave direction.

## Onshore Winds

The case of onshore winds -this is approximately SWAMP case VIB (SWAMP (1982, 1984), Perrie & Toulany (1985))- is the most complex and therefore the most challenging. It is also one of the things which makes the CASP data set unique. A typical low pressure area, intensifying off Cape Hatteras and travelling northeastwards to pass Nova Scotia, generates a band of waves to the right of its path which can travel with the storm for 1,000 km or more, depending on the difference between the group velocity of the waves and the velocity of the storm. As the storm winds reach the wave array they generate a local sea from the northeast or southwest, depending on whether the storm passes west or east of us. With the passage of the storm comes the waves generated over the long fetch. The resulting spectra show two peaks: sea from the local wind direction, and swell from the south; the peak frequency of the sea then moves to progressively lower frequency as the waves develop over the fetch provided by the moving storm. If the storm passes inland, swell becomes fully-developed sea if the storm moves slowly enough to maintain its southerly winds long enough. If the storm passes offshore, the northeasterly winds give way to north and northwest winds and fetch-limited growth begins in a direction opposing the swell.

## Swell

The swell/sea from the south and southwest is never absent; it normally determines the magnitude, direction and frequency of the maximum peak in our spectra. We will be examining it extensively and trying various modelling techniques to investigate propagation from deep to shallow water, including refraction and dissipation. The main points to be made now are, first, that there is clear evidence of strong attenuation as the waves approach shore, and second, that refraction is observed in the right sense and varies in the right direction with frequency.

We will be beginning our investigation by checking the observed onshore attenuation of our spectra, and other aspects, with the TMA spectral analysis and concomitant conclusions. It is clear in our initial examples that a) the onshore amplitude attenuation is not accompanied by a frequency upshift, and b) our array, designed with the TMA attenuation rate in mind, is observing approximately the same rate. Since we believe the majority of the attenuation is due to wave breaking, we should have an ideal

data set for investigating this part of the wave energy (and momentum) balance. At least we can constrain the existing formulations.

Sea

The behaviour of the incoming wind-driven spectra is very different, for onshore winds, from the fetch-limited case discussed earlier. As the onshore (or alongshore, for a "nor'easter") winds increase with the approaching storm, high-frequency peaks begin to be seen in the spectra from all instruments in the array. But instead of a progression of peak frequency with fetch, as for offshore winds, all spectra peak at the same frequency, and no one instrument can be guaranteed to be the largest at a particular hour until low enough peak frequencies are reached for shallow-water attenuation to take effect. In fact, the peak amplitude at each station shows great variability, and we hope we can relate it to mesoscale wind field variability using small-scale meteorological models and the dense meteorological observations available during the CASP IOP's. We will investigate some of the variability directly using the wind speed data from the WOTAN sensors in and up-fetch from the array.

Wave Model Building

Kitaigorodskii, Krasitskii and Zaslavskii's (1975) modelling of the equilibrium range by $k^{-3}$ for deep and shallow water is the precursor to the TMA analysis. Associated deep water scaling for Pierson-Moskowitz, JONSWAP, and (almost) Donelan, Hamilton and Hui (1985) is the frequency equivalent to $k^{-3}$. Bouws, Gunther, Rosenthal and Vincent (1985, 1986) postulated that finite depth spectra be self-similar in frequency space and obtainable via Kitaigorodskii et al's (1975) " $\Phi$ factor" from the deep water spectral form and achieved good agreement with data without considering bottom roughness. Furthermore, with nondimensional wavenumber $\kappa = k(f_m) \cdot U_{10}^2/g$, they scale spectral parameters and remove explicit depth dependence obtaining results equivalent to the deep water values of Hasselmann, Ross, Muller and Sell (1976), within the range of TMA data.

Thus, there exists a description for finite depth wind wave spectra and for prognostic scaling relations for spectral parameters. However, the assumed quasi-equilibrium does not give rate of growth with fetch or time. We hope to see this in our data.

An update of third generation modelling is given by Hasselmann and Hasselman (1985), Hasselmann, Hasselmann, Allender and Barnett (1985), and Resio (1986). Further discussion of the first cycle WAM (the WAve Modelling group supported by the European Community) models is presented in Komen (1986 a, b) and Janssen and Komen (1986). Fig. 1 shows the asymptotic infinite fetch and duration one-dimensional energy spectra for SWIM (1985) test 1. It indicates that there actually is some difference between these current shallow water WAM models and second generation models, including the BIO-Resio model described in Perrie, Rosenthal and Toulany (1986).

The CASP data set should allow us to do a careful hindcast study with these WAM models, similar to the WAM model study of Cardone for three hurricane cases in the Gulf of Mexico described in Komen (1986 b). With Bechara Toulany, we hope to have preliminary analyzed wave observations and computed the driving surface stress field by the end of the year, performing the WAM model wave field calculation in 1987. CASP data is, of course, very valuable in verifying ongoing modifications and improvements to third generation WAM models, allowing comparison of model interactions with real data.

Second generation wave modelling is still a viable endeavour, and we have a rather standard, discrete spectral shallow water wave model of this genre, described in Perrie and Toulany (1985); Perrie (1986); Perrie, Rosenthal and Toulany (1986) and Resio (1981). The model is small, fast, of proven ability via SWIM (1985) tests and thus useful in situations of limited computer resources and experimentation, for example, data assimilation. The shallow water modelling follows Bouws, Gunther, Rosenthal and Vincent (1985) and Gunther and Rosenthal (1984). Thus, a limited hindcast study of a portion of the CASP data would test TMA assumptions and analysis.

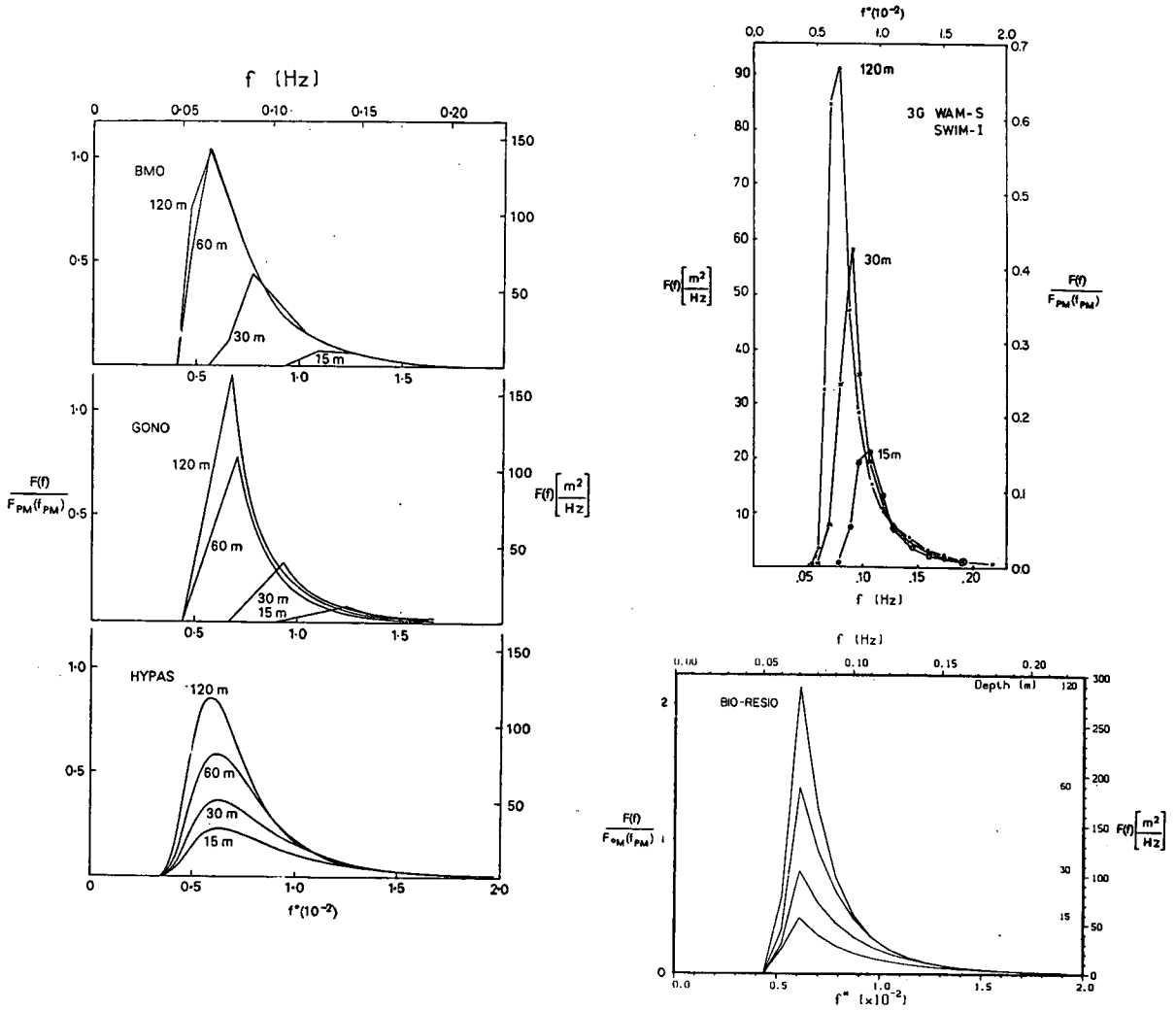


Fig. 1 The fully-developed wave energy spectra as a function of depth plotted against frequency for BMO, GONO, HYPAS: the models of SWIM (1985), and BIO-Resio, and WAM-S, the third generation model.

Bibliography

Anderson, C. (1986). The Oceanographic Component of the Canadian Atlantic Storms Program (CASP). Proceedings, ESRF Workshop on Wave Hindcasting and Forecasting; Sept. 23-26, 1986, B.I.O.

Bouws, E., Gunther, H., Rosenthal, W. and Vincent, C.L. (1985). Similarity of the wind wave spectrum for finite depth water, Part I. Spectral form. J. Geophys. Res., **90** C1, 975-986.

_____(1986). Similarity of the wind wave spectrum for finite depth water, Part II. Statistical relations between shape and growth stage parameters. Submitted.

Dobson, F., Lemon, D. and Peters, B. (1986). The CASP ESRF WOTAN evaluation. Proceedings, ESRF Workshop on Wave Hindcasting and Forecasting; Sept. 23-26, 1986, B.I.O.

Donelan, M., Hamilton, J. and Hui, W. (1985). Directional Spectra of Wind-Generated Waves. Phil. Trans. R. Soc. Lond. A, 315: 509-562.

Gunther, H. and Rosenthal, W. (1984). A shallow water surface wave model based on the TEXEL-MARSEN-ARSLOE (TMA) wave spectrum. Proc. 20th Congress IAHR, Moscow, 1983.

Hasselmann, K. et XV al. (1973). Measurements of Wind-Wave Growth and Swell Decay during the Joint North Sea Wave Project (JONSWAP). Deutsch. Hydrogr. Zeit., Reihe A (8), 12: 95 pp.

Hasselmann, K., Ross, D.B., Muller, P. and Sell, W. (1976). A parametrical wave prediction model. J. Phys. Ocean., 6, 201-228.

Hasselmann, S. and Hasselmann, K. (1981). A symmetrical method of computing the nonlinear transfer in a gravity wave spectrum. Hamb. Geophys. Einzelschriften, Reihe A, 52: 170 pp.

Hasselmann, S., Hasselmann, K., Allender, J.H. and Barnett, T.P. (1985). Computations and parameterizations of the nonlinear energy transfer in a gravity-wave spectrum. Part II: Parameterizations of the nonlinear energy transfer for application in wave models. J. Phys. Ocean., 15, 1378-1391.

Hasselmann, S. and Hasselmann, K. (1985). Computations and Parameterizations of the nonlinear energy transfer in a gravity-wave spectrum. Part I: A new method for efficient computations of the exact nonlinear transfer integral. J. Phys. Ocean., 15, 1369-1377.

Janssen, P.A.E.M. and Komen, G.J. (1986). A shallow-water extension of the 3-G WAM model. Venice WAM Workshop Tech. Note, June 1986.

Kitaigorodskii, S.A., Krasitskii, V.P. and Zaslavskii, M.M. (1975). On Phillips' theory of equilibrium range in the spectra of wind-generated gravity waves. J. Phys. Ocean., 5, 410-420.

Komen, G.J. (1986 a). A third generation ocean wave model. Proceedings, ESRF Workshop on Wave Hindcasting and Forecasting; Sept. 23-26, 1986, B.I.O.

Komen, G.J. (1986 b). Recent results with a third generation ocean wave model. Symp. on Measuring Ocean Waves from Space. Johns Hopkins University.

Perrie, W. and Toulany, B. (1985). Assessing a Wave model a la SWAMP. Can. Tech. Rep. of Hydrogr. Ocean Sc., No. 61, vi + 78 pp.

Perrie, W. (1986). Making of a shallow water wave model. In press in Can. Tech. Rep. Hydrogr. Ocean Sci.

Perrie, W., Rosenthal, W. and Toulany, B. (1986). A second generation shallow water Resio wave model. Proceedings, ESRF Workshop on Wave Hindcasting and Forecasting; Sept. 23-26, 1986, B.I.O.

Resio, D.T. (1981). The estimation of wind-wave generation in a discrete spectral model. J. Phys. Ocean., 11, 510-525.

Resio, D.T. (1986). Wave transformations related to nonlinear fluxes. ASCE J. Waterway, Port, Coastal and Ocean Eng. to appear.

Shaw, R. (1986). The Canadian Atlantic Storms Program: Meteorological Component. Proceedings, ESRF Workshop on Wave Hindcasting and Forecasting; Sept. 23-26, 1986, B.I.O.

SWIM (Bouws, E., Ephraums, J.J., Ewing, J.A., Francis, P.E., Gunther, H., Janssen, P.A.E.M., Komen, G.J., Rosenthal, W. and de Voogt, W.J.P.) (1985). Quart. J.R. Met. Soc., 111, 1087-1112.

# THE METEOROLOGICAL OFFICE OPERATIONAL SEA STATE FORECASTING SYSTEM

P. E. Francis

Meteorological Office, Bracknell, United Kingdom

## 1. Introduction

The advent of the oil exploration and production industry in the North Sea during the 1970's marked the introduction of dedicated off-shore services in the Meteorological Office. Initially the requirement for forecasts of sea state, (eg wave heights and periods, perhaps broken down into wind sea and swell), was met by the use of empirical growth curves, married to surface winds also empirically derived from numerical weather prediction (NWP) model fields. In order to supply a better service, and to enable the growth in demand to be met, a numerical model for sea state forecasting was developed during the mid-1970's. In 1976 a coarse grid model was operationally introduced, covering the Northern Hemisphere oceans. A higher resolution model, with depth dependent terms, covering the European continental shelf was subsequently used operationally from 1977. Research into better procedures to model the physics of wave generation and decay lead to subsequent improvements and an increase in spectral resolution. By 1979 the models were in a form that remained stable for a few years, eventually described in a published article, Golding (1983).

In 1982 the Office took delivery of a CDC Cyber 205 vector processer, the related increased computing power having a two-fold effect on the sea state forecasting system. Firstly a new NWP model was introduced, with an explicitly represented boundary layer. This model is capable of calculating much improved surface winds for later use in the wave models. Secondly, the opportunity was taken to increase both the spatial and spectral resolution of the wave models, thus leading to improved hindcasts and forecasts.

Most recently, in July 1986, versions of the original model extended in geographical coverage, and eventually to include some carefully assessed improvements in the physical processes, were introduced for operational use. These improvements are reported below. Table 1 contains a summary of model coverage and resolution during the entire period of operational use.

## 2. The model

Details of the physics and mathematics of an earlier version of the present operational model can be found in Golding (1983). In summary it is sufficient to state here that the model is a so-called "second generation" spectral model, incorporating an empirical representation of non-linear wave interaction processes, as well as the basic features such as wave growth, propogation and decay. In the European Waters version there are additional shallow water processes such as dissipation by bottom friction, refraction, and depth dependant group velocities. The new latitude - longitude versions of the model have essentially the same formulation as that described by Golding.

Experience from prolonged operational use, plus more detailed evidence from carefully conducted hindcast studies, the SWIM Group (1985), the WHIST Report (1986) had indicated that two physical processes in the model needed close attention and possible revision. The directional relaxation of the wave spectrum in rapidly changing wind situations had always been a weak feature of the model, revealed for instance in the 'Hurricane' case of the SWAMP study, the SWAMP Group (1985).

Table 1: Basic structure of operational models from 1976 to the present.

| Period | Model area | Spatial resolution | Spectral resolution |
|---|---|---|---|
| Aug. 1976 - Oct. 1979 | Northern oceans, to approx. 20°N | 300 km at 60°N on a polar stereographic projection | 12 directions x 6 frequencies |
| July 1977 - Oct. 1979 | European continental shelf to approx. 20°W | 50 km at 60°N on a PS projection | 12 x 6 (with shallow water processes) |
| Oct. 1979 - Sept. 1982 | Both models as above | Both models as above | 12 x 11 |
| Sept. 1982 - June 1986 | Northern oceans | 150 km at 60°N on a PS projection | 16 x 14 |
| Sept. 1982 - June 1986 | European continental shelf | 25 km at 60°N on a PS projection | 16 x 14 (with shallow water processes) |
| Sept. 1982 - June 1986 | Mediterranean Sea | 50 km at 60°N on a PS projection | 16 x 14 |
| July 1986 to date | Global | 1.5° lat. x 1.875° long. | 16 x 13 |
| July 1986 to date | European waters (incl. Med. and Baltic) | 0.25° lat. x 0.4° long. | 16 x 13 (with shallow water processes) |

A new formulation for directional relaxation, with rate of change of spectral energy density through direction being a function of frequency, has since been investigated, programmed and tested. Introduction into the operational model awaits full testing in conjunction with the other new feature, namely a more balanced growth and dissipation formulation. The existing formulation had been seen to result in two main shortcomings, namely insufficient growth in short fetches, and insufficient dissipation in long fetches. These features have now been overcome by increasing the exponential growth rate and replacing the original dissipation scheme by one suggested in Komen et al (1984). Before introduction into the operational suite these new formulations are presently being tested in hindcast studies based on the SWIM storms, the SWIM Group (1985). A general improvement in both energy levels and directional distribution is expected.

Other changes implemented, or planned for implementation, with the global model are great circle corrections in the advection routine (probably not necessary in the European Waters version), a variable ice boundary, and use of pre-computed 'look-up' tables for the required final wind sea spectrum, generated by the empirical non-linear energy re-distribution process.

## 3. The operational system

The main forecast runs are performed each day, based on 00 UTC and 12 UTC data times. Since there is not enough high quality measured wave data available to enable a starting field to be defined directly, it is necessary to generate such a field by using the models in hindcast mode, ie using wind fields which closely resemble the actual physical situation. Such winds are obtained from the NWP model during its assimilation phase, ie while it is running forward in time and relaxing towards the available atmospheric measurements. Such wind fields are of a high quality, as can be seen by reference to the statistics given in a latter section of this paper. The Global NWP model has 2 assimilation steps every 12 hours, the regional NWP model has 4. It can thus be seen that the surface wind fields used in the hindcast cycle have the benefit of all possible wind measurements that are reported.

The resulting starting fields are permanently archived since there are many applications for the information that they contain. This is discussed in more detail in a later section. The winds themselves are nominally valid at a height of 19.5 m, since this is the level at which the basic wave model formulation was fixed. In reality the winds are taken direct from the lowest level of the NWP model, at a pressure height of 0.997 $P_*$, where $P_*$ is (over the sea at least) the mean sea level pressure. The NWP models are generally discussed in a paper by Gadd (1985).

The Global model is run for a forecast period of 5 days, the regional model for a period of 36 hours. Presently the necessary boundary conditions for the regional model are taken from an earlier run of the Global model, since for operational reasons the finer resolution forecasts are required earlier. The total elapsed time for the suite of programs including linking the results to a front-end processor, is 20 minutes per 12 hour cycle.

The results of the integration are complete two-dimensional wave energy density spectra at each grid point. Since this represents a vast amount of data to further process, and since experience from many years of supplying customer services has shown that such detail is not operationally required, the spectra are compressed to a one-dimensional form (by integrating over directions) before transfer to the front end processor. A mean direction for each frequency is also calculated, thus an 8-fold reduction in data volume is achieved.

Once the data are stored on the front-end processor, several pathways are followed in order to make maximum use of the information. Routine verification is performed, using measured wave data received on the global telecommunications system (GTS) sponsored by the World Meteorological Organisation (WMO). This procedure is discussed later on in some depth. The hindcast (starting) fields are permanently archived, forming a data-base from which a variety of customer enquiries can be answered. To date nearly 9 years of hindcast data, everytwelve hours, have been archived. Examples of customer enquiries can be found in the fields of climatology, insurance claims, pollution investigations, coastal erosion, harbour design etc. A recent paper, Francis (1986), describes the possible climatological applications in more detail.

Direct access to the spectral data set is used to prepare material for real-time users who require high resolution time series information at individual grid points, or information on the 1-dimensional spectrum, or mean directional data. Examples of such users are the authorities responsible for coastal defences, who routinely receive tabulations of forecast wave height and wind speed for low lying areas of coast, liable to flooding in high sea states. An example of such output is shown at Table 2.

Most operational output however comes from a data set which is constructed in a more compressed format, ie consisting of significant wave height, direction and period, broken down into wind sea and swell components. This data set is formatted exactly similarly to those containing products of the NWP model forecast runs. In this way a common suite of access programs, chart drawing packages and encoding routines is possible. This common products suite of programs in very versatile, enabling access, extraction and interpolation to most common map projections, for any specified area or even for single points. The ships routeing service based at Bracknell receive hardcopy charts for any oceanic area of current interest, while the off-shore industry forecasters at the London Weather Centre are in receipt of North Sea charts via a computer to computer link. The uses of the forecast data, and of the hindcast archives, are fully discussed in Ephraums (1985).

After a WMO announcement of the global model much interest was evident from national meteorological centres, both within Europe and world-wide. The Meteorological Office has subsequently agreed to release encoded (WMO FM47-V GRID) bulletin of sea state forecast data on the GTS. Global coverage will be by means of 10 bulletins with a $2\frac{1}{2}^{o}$ x $2\frac{1}{2}^{o}$ resolution, using a GRID code facility that avoids the encoding of land areas. In the European area the higher resolution products will be available in 2 bulletins with a grid size of $1\frac{1}{4}^{o}$ x $1\frac{1}{4}^{o}$. It is hoped that this product service will be available to national meteorological centres by 1 October 1986.

Table 2: Example of single point time-series forecast tabulation

For Transmission to Wessex Water Authority

Initial Data Time 12 Z 20/2/84 Location 50.5 N 2.6 W

| HOURS AFTER DATA TIME | WIND SPEED | WIND DIRECTION DEG. (FROM) | TOTAL WAVES HEIGHT M. | TOTAL WAVES PERIOD SEC. | WIND-SEA HEIGHT M. | WIND-SEA PERIOD SEC. | SWELL HEIGHT M. | SWELL PERIOD SEC. | SWELL DIRECTION DEG. (FROM) |
|---|---|---|---|---|---|---|---|---|---|
| 0 | 17.9 | 167 | 1.3 | 6.0 | 0.6 | 3.5 | 1.1 | 8.3 | 214 |
| 3 | 21.5 | 148 | 1.5 | 5.3 | 1.1 | 4.1 | 1.1 | 9.9 | 220 |
| 6 | 20.3 | 173 | 2.1 | 5.3 | 1.9 | 4.9 | 1.0 | 10.2 | 210 |
| 9 | 16.3 | 230 | 2.1 | 5.8 | 1.7 | 5.0 | 1.3 | 8.2 | 191 |
| 12 | 17.7 | 227 | 2.3 | 6.4 | 1.5 | 4.8 | 1.8 | 9.4 | 215 |
| 15 | 18.0 | 237 | 3.5 | 7.7 | 2.1 | 5.6 | 2.8 | 10.5 | 212 |
| 18 | 18.6 | 231 | 3.7 | 8.1 | 2.1 | 5.6 | 3.1 | 11.2 | 206 |
| 21 | 20.9 | 244 | 4.4 | 8.7 | 2.8 | 6.5 | 3.4 | 12.8 | 203 |
| 24 | 32.6 | 237 | 4.3 | 8.3 | 3.1 | 6.4 | 3.1 | 13.8 | 202 |
| 27 | 22.3 | 231 | 4.7 | 8.4 | 3.3 | 6.6 | 3.3 | 13.0 | 198 |
| 30 | 25.4 | 252 | 3.9 | 8.0 | 2.4 | 5.7 | 3.0 | 13.1 | 207 |
| 33 | 24.0 | 257 | 4.2 | 8.8 | 2.3 | 5.8 | 3.5 | 13.3 | 205 |
| 36 | 20.2 | 264 | 3.8 | 8.4 | 1.8 | 4.8 | 3.3 | 13.1 | 206 |

4. Forecast verification

An essential part of the operational system is the routine verification of hindcast and forecast values against such data as are available at Bracknell on the GTS. In view of the wide spread of quality within ship based sea state observations, the operational system currently uses only fixed position stations for verification purposes. These stations include ocean weather ships, oil production platforms, and moored buoys. Care is taken to assess whether the visual estimates contained in the verification data base are of a sufficient quality for use. A gross quality control procedure removes most of the incorrect reports. Verification of the hindcast data is performed every 6 hours, while forecast products are compared with measurements at T+6, 12, 18, 24 and 36 hours for the European model, and at T+12, 24, 36, 48, 72, 96 and 120 hours for the global model. At the time of writing 22 locations are used in the European model and 28 in the global model. Efforts will be made to pursuade more national services to put their measured wave data onto the GTS, thus increasing the size of the verification data base. The bulk of the present global verification data come from American and Japanese data buoys, with a few Atlantic weather ships, and buoys off South America and Oman.

In Table 3 are some summary sea-state verification statistics for the month of July 1986, the month in which the new forecasting system became operational.

Table 3: Summary error statistics for sea state, July 1986

| | Global Model | | | | | | European Model | | | | | |
|---|---|---|---|---|---|---|---|---|---|---|---|---|
| | Significant wave ht.(m) | | | Wave period (sec) | | | Significant wave ht.(m) | | | Wave period (sec) | | |
| Time | N | mean | SD | N | mean | SD | N | mean | SD | N | mean | SD |
| T+0 | 3410 | 0.0 | 0.7 | 3116 | -1.1 | 2.0 | 1329 | 0.1 | 0.5 | 1346 | 0.0 | 1.9 |
| 12 | 1709 | 0.1 | 0.7 | 1570 | -1.2 | 2.0 | 672 | 0.1 | 0.5 | 683 | 0.0 | 1.9 |
| 24 | 1708 | 0.1 | 0.7 | 1570 | -1.2 | 2.1 | 672 | 0.1 | 0.6 | 682 | 0.0 | 1.9 |
| 36 | 1711 | 0.1 | 0.7 | 1573 | -1.2 | 2.1 | 672 | 0.2 | 0.6 | 681 | 0.0 | 1.9 |
| 72 | 1709 | 0.1 | 0.8 | 1570 | -1.2 | 2.1 | | | | | | |
| 120 | 1711 | 0.0 | 0.9 | 1571 | -1.2 | 2.2 | | | | | | |

Where N = number of comparisons, error = modelled - measured, SD = standard deviation.

There values show the model performance in a broad, generalised picture. The model does not yet contain the projected improvements outlined in section 2, in particular the great circle correction term could have a significant impact. Furthermore, lacking detailed information on how individual buoy records are processed in order to obtain wave period, it is possible that comparing measured periods with $Tm_{02}$ from the model (ie $Tm_{02} = (m_o/m_2)^{\frac{1}{2}}$) is not a correct procedure, and that some other estimator of period should be used.

No discussion of wave model performance is complete without a consideration of the errors of the wind fields used to drive the model. In Table 4 are some summary statistics of wind errors at the same locations used for the data in Table 3. It should be remembered that what are being compared are mostly buoy wind measurement at fairly low heights, say 5-10 m; platform winds corrected to 10 m; and model wind values at 20-30 m.

Table 4: Summary error statistics for surface wind speed, July 1986

| | Global Model | | | European Model | | |
|---|---|---|---|---|---|---|
| Time | Number of Measurements | Mean error ($ms^{-1}$) | Standard deviation ($ms^{-1}$) | Number of Measurements | Mean error ($ms^{-1}$) | Standard deviation ($ms^{-1}$) |
| T+0 | 3626 | -0.4 | 2.8 | 1524 | 0.4 | 1.9 |
| 12 | 1816 | 0.1 | 2.6 | 771 | 0.4 | 2.2 |
| 24 | 1815 | 0.0 | 2.7 | 772 | 0.3 | 2.2 |
| 36 | 1815 | 0.1 | 2.9 | 770 | 0.5 | 2.4 |
| 72 | 1815 | 0.1 | 3.3 | | | |
| 120 | 1814 | -0.1 | 3.5 | | | |

Where error = modelled - measured

It is apparent that surface winds from the limited area NWP model tend to be stronger than those from the global model. Never-the-less the quality of these winds is very high, from both NWP models, contributing without doubt to the virtually unbiased wave forecast errors.

In addition to routine operational verification, several investigations involving closer examination of both operationally produced data and data from carefully controlled hindcasts (ie using specially produced wind fields) have been performed. Informative accounts of this work are to be found in Houghton (1984) (looking at model performance up to 1982), the SWIM Group (1985) and the WHIST report (1986). Such investigations have led to the improvements outlined earlier in section 2.

## 5. Future developments

Further development of the Meteorological Office operational sea state forecasting system, at least over the next five years, will centre around two main areas of work. As part of the general WAM Group activity the Office is actively investigating possible methods for the assimilation of wave data into models, anticipating the large increase of such data when several ocean observing satellites are launched at the end of this decade. Early work, based on the techniques used for assimilating data into the NWP models, is proving to be promising. Much progress however will depend on a realistic simulation of the technique on a large scale, perhaps using whatever contemporary data (oceanographic and meteorological) can be gathered from the SEASAT and JASIN data banks.

On a smaller scale the European regional model, which includes depth dependent effects, would almost certainly benefit from the inclusion of some of the effects due to tidal depth variation and tidal currents. Such effects are important in shallow areas, especially the English Channel and Southern North Sea. Since the Office also runs an operational storm surge forecast model, Procter et al (1983), which produces grid point values of surface elevation and depth integrated current, the opportunity will be taken to assess the likely

benefits of using the available data. A unified model would also probably be beneficial to the calculation of the storm surge since surface roughness, defined perhaps by wave age, is a contributor to the momentum exchange process that has to be modelled.

References:


Ephraumns, J. J., (1985), "Applications of wave and surge models". The Meteorological Magazine, 114, pp 282-291.

Francis, P. E., (1986), "Numerical wave models as a source of data for marine climatology". Advances in underwater technology, ocean science and offshore engineering. Volume 6, Oceanology. (SUT) pp 157-168

Gadd, A. J., (1985), "The 15-level weather prediction model". The Meteorological Magazine, 114, pp 222-226.

Golding, B., (1983), "A wave prediction system for real-time sea state forecasting". Q.J.R. Meteorol. Soc., 109, pp 393-416.

Houghton, I., (1984), "A long time-series verification of hindcasts from the Meteorological Office wave model archive". The Meteorological Magazine, 113, pp 317-328.

Komen, G. J., Hasselmann, S. and Hasselmann, K., (1984). "On the existence of a fully developed wind-sea spectrum'. J. Physic. Ocean, 14, pp 1271-1285.

Procter, R. and Flather, R. A., (1983), "Routine storm surge forecasting using numerical models: procedures and computer programs for use on the CDC CYBER 205 at the British Meteorological Office". Wormley Institute of Oceanographic Sciences, Report No. 167 (unpublished).

The SWAMP Group, (1985), "Sea Wave Modelling Project (SWAMP). An intercomparison study of wind wave prediction models. Part 1. Principal results and conclusions". Ocean Wave Modelling, Plenum Press, 256 pp.

The SWIM Group, (1985). "A shallow water intercomparison of three numerical wave prediction models (SWIM)". Quart. J. R. Met. Soc., 111, pp 1087-1112.

The WHIST Report (1986), Francis, P. E., Ephraums, J. J., Bracher, C. H. and Thomas, J. P. "A wave hindcast study (WHIST)". Final report by the Meteorological Office to the Dept. of Energy. To be published in the Department's Offshore Technology series.

## C1-2 Development of a Global Scale Ocean Wave Forecasting Model for Marine Guidance

*Dinorah Esteva and Hong Chin*

As part of the continuing effort to improve the quality of marine guidance over the high seas, a newly developed global scale ocean wave forecasting model was placed in an experimental operational evaluation mode at the National Meteorological Center (NMC) in Washington, D.C. in early November, 1985. This particular model contains provisions for including the effects of a number of recent advances in wind-wave theory; these include local wind sea spectral growth through a modified SAIL II, nonlinear mechanism as indicated by the Joint North Sea Wave Project (JONSWAP) results (Hasselmann et al., 1973), independent development of directional bands as suggested by the results of the Sea Wave Modelling Project (SWAMP) experiments, and spectral overshoot in high frequency bands as discussed by Mitsuyasu (1969) and measured by Barnett and Wilkerson (1967). Forecasts of wave elevation directional frequency spectra and summary statistics at aproximately 6,000 grid points located between 70S and 75N are generated at three hour intervals to 72 hours. Fields of equivalent winds at a height of 19.5m above the sea surface are derived from the 1000 mb and surface fields of the NMC atmospheric global spectral model using a modified two layer boundary model described by Cardone (1969).

Comparisons of model outputs using NDBC data buoy measurements as a standard show the model to be underforecasting significant wave heights slightly where the Navy's Global Spectral Ocean Wave Model (GSOWM) tends to overforecast, and the combined sea and swell forecasts of NMC's modified Bretschneider model tend to vary from above the GSOWM results to below the new model results over a 48 hour forecast period. In addition to periodic wind field updates, numerical experiments are also underway to incorporate satellite-derived measurements into wave model restart fields. Preliminary results of hindcast tests using September 1978 SEASAT measurements provide an encouraging basis for the possibility of assimilating satellite data into wave models. Present modelling objectives include the incorporation of significant wave height measurements derived from GEOSAT altimeter data.

# INCREMENTAL ENHANCEMENT OF WAVE FORECASTING CAPABILITIES BY AN OPERATIONAL SPECTRAL WAVE MODEL

Lally, S.K.*, N.M. Stevenson+, and D.C. Fu+

*Oceanroutes Canada
1496 Bedford Hwy
Bedford, NS B4A 1E5

+Oceanroutes Inc.
3260 Hillview Ave.
Palo Alto, California 94304

## ABSTRACT

Over the past ten years, OCEANROUTES INC. has developed portable, regional Spectral Wave Models, capable of operations in both hemispheres. These wave models were developed to aid the operational forecaster in providing site specific forecasts to the offshore industry. They have been used on a twice daily basis for offshore forecasting since 1976. Verification results indicate that an intelligent forecaster working with the model will produce a more accurate forecasts than the forecaster or the model alone.

This paper will describe the development of the spectral wave model with particular emphasis on the adaption of the model to the Canadian East Coast. An advantage of the model is the capibility for an on-site user to modify the wind fields to reflect local conditions and adjust the timing of frontal passages.

Verification results for the Canadian Model and those used in the North Sea and the NW Australian Shelf will be presented. An independent Australian study show dramatic improvement in forecast skill when forecasters use the spectral model.

The paper will discuss the model's capability of coupling deep water spectra with a shallow water model for design studies. Further, it will discuss the use of the model output in real-time vessel motion prediction.

## INTRODUCTION

The Canadian East Coast Spectral Wave Forecasting Model has evolved from a limited area model developed for the Gulf of Alaska and refined during applications in the North Sea, off the East Coast of the U.S. and in the Indian Ocean. This evolution has led to the development of a central core, which, by the generation of an appropriate grid, can be modified for worldwide use.

Each model is very adaptive and can be used both in the hindcast and forecast mode. OCEANROUTES' Spectral Wave Models are used operationally for site-specific forecasting in the North Sea and the Southern Australia - Bass Strait region. The Australian and North Sea models have been in continuous use since their inception, with continuous upgrading in coding, wave propagation, spreading and decay terms.

The Spectral Wave Model (SWM) provides the meteorologist with the means of simultaneously predicting the development of sea and swell in terms of frequency, direction and height at a large number of locations. Experience has shown that a meteorologist aided by the model is consistently superior to the meteorologists's unaided prediction, especially of swell, at time periods greater than 24 hours.

OCEANROUTES' spectral wave models are based on the premise that ocean conditions can be represented as the summation of large numbers of individual wave components. These components, expressed in terms of energies, are calculated at fixed grid points in discrete time steps. Wave generation, propagation and dissipation are calculated along the actual paths of the waves. The wind data required as input to the model is derived from atmospheric models such as a planatary boundary layer model. For each forecast period, generally at each synoptic period (00/12Z), a matrix showing the distribution of wave energy with respect to direction and frequency is obtained, and from this matrix specified wave parameters can be readily derived for selected grid points. For computational convenience, the spectral energies are calculated at geographically fixed grid points at discrete increments of time and modifications to spectral shapes are calculated along the actual paths of the ocean waves. Predictions are made by employing a combination of `grid' and `ray' techniques. Ray and grid approaches are coupled to take advantage of the strengths of both techniques.

The actual physical process of how a wind generates surface-water waves is extremely complex. Fortunately, the process of wind-wave evolution can be modeled implicitly by the relatively simple equation of radiative transfer

$$\frac{\delta E(f,\Theta,\vec{x},t)}{\delta t} + \vec{C_g}(f,\Theta) \cdot \nabla E(f,\Theta;\vec{x},t) = G(f,\Theta;\vec{x},t;E,U) \tag{1}$$

where

$$E(f,\Theta,\vec{x},t) = \int_{f-\Delta f/2}^{f+\Delta f/2} \int_{\Theta-\Delta\Theta/2}^{\Theta+\Delta\Theta/2} S(f,\Theta,\vec{x},t)\, df\, d\Theta \tag{2}$$

E is a representation of the wave energy contained within the two-dimensional spectral band ($\Delta f, \Delta\Theta$) centered at ($f,\Theta$). $S(f,\Theta;\vec{x},t)$ is the spectral energy density of the wave component at frequency f propagating from direction $\Theta$. $\vec{C}$ is the corresponding group velocity, and U is the horizontal surface wind vector. $\vec{x}$ is the horizontal position vector, and t is time.

$G(f,\Theta;\vec{x},t;E,\vec{U})$ is a source function that represents all processes that either aid or inhibit spectral development. It should be noted that G is a function of the entire wind and wave field. The processes represented by G include momentum transfer at the air/sea interface, white capping, and other dissipative mechanisms. Omitting the functional arguments for brevity, we can express G as

$$G = (A + BE)\left[1 - \left(\frac{S}{S_\infty}\right)^2\right] - DE \tag{3}$$

The A and B terms were derived originally by Inoue (1967). $A(f,\Theta,\vec{U})$ is the Phillips resonance growth term, (Phillips, 1957, 1958, 1960, 1977) proportional to the atmospheric turbulence pressure spectrum. It accounts for the initial excitation and growth of wind waves on the ocean surface induced by the random pressures associated with the overlaying atmospheric turbulence. $B(f,\Theta,\vec{U})$ is a wind driven instability feedback mechanism of the type introduced by Miles (1957, 1959) and modified by Phillips (1957, 1966). This mechanism produces an energy transfer at the air/sea interface to the spectral component $(f,\Theta)$ that is proportional in part to the curvature of the mean wind profile at the elevation where the wind speed matches the phase velocity of the wave. $A(f,\Theta,\vec{U})$ produces initial linear growth, while $B(f,\Theta,\vec{U})$ induces subsequent growth that is exponential in character.

Waves cannot grow forever as evidenced by wave breaking and other types of dissipation. For purposes of establishing an upper limit on wave growth, we invoke the concept of a fully developed sea. It is assumed that if the wind blows uniformly in speed and direction over a sufficiently large area and for a sufficiently long period of time, the wave spectrum will attain the fully developed form of Pierson and Moskowitz (1964). This fully developed form is represented by $S_{\Delta_0}$. The D term represents the dissipation of spectral wave energy density components traveling against the wind. This accounts for the fact that some spectral components will not receive energy from the wind when wind opposes wave propagation; hence, the relevant dissipation must be included.

At each time step, equation (1) is solved numerically in two stages: the advective transport of wave energy represented by the $C_g \cdot \nabla E$ term is performed, and the separate contribution from the source/sink terms represented by G is calculated. The wave field is represented by a field defined at the discrete grid points and time-steps of the model. At each point, $S(f,\Theta)$ is divided into equi-angular directional bands (i.e. 30, 15, etc.) and numbered clockwise from the north. For the North Sea version of the SWM, 16 frequency bands of varying widths are used. ***** The frequency bandwidths are chosen to allow broad coverage of the important frequencies without sacrificing detail in that part of the spectrum where higher resolution is required. The Northwest Australian Shelf version of the SWM is subject to long southerly fetches, and therefore has two additional low-frequency bands for a total of 18 frequencies.

The energy propagation algorithm is one of the strong points of the OCEANROUTES' Spectral Wave Model. We have adopted the viewpoint, for our treatment of propagation, that represents the spectral density of all locations closest to the grid point in question for all frequencies in the range $[f - \frac{\Delta f}{2}, f + \frac{\Delta f}{2}]$ and directions of propagation in the range $[\Theta - \Delta\Theta/2, \Theta + \Delta\Theta/2]$. A Monte Carlo program is used to calculate interpolation coefficients for wave energy propagation as a function of the frequencies, bandwidths, direction of travel, grid spacing, and time-step. These coefficients indicate what fraction of the energy at a given point at $(f,\Theta)$ will go to each downstream point for the same $(f,\Theta)$ component at the next time-step, or conversely, where the propagated energy arriving at a given point came from and, therefore, how much energy arrived.

The resultant propagation algorithm preserves the group velocity of wave-front and wave-back propagation for plane waves and for point sources of energy. Furthermore, the scheme spreads wave energy radially in a physically reasonable manner, as extensive testing of the method in a numerical wave tank has proven. The grid spacing in any given SWM may be chosen from a range of 10 to 150 nautical miles, thereby allowing a selection of grids which considers all areas that have influence on wave conditions at the specific offshore areas of interest. The North Sea grid covers an area that is approximately 3,000,000 square miles, while the grid for the Northwest Australian Shelf covers almost 60,000,000 square miles. The larger Australian grid is required to accurately model the generation of southerly swell over rather long fetches originating in the southern Indian Ocean. The grid system of the two models are shown in Figures 1 and 2. The grid for the Canadian East Coast Model is shown in Figure 3.

All control tables used by the models and in their development, including the locations of the grid points, the land/sea boundary table, the allowable fetches in all directions from each grid point, the wave propagating coefficients, and so on, are computer generated for speed and accuracy.

Significant wave heights, which are required for comparisons with most observations, are determined by

$$H_S = 4\sigma = 4\, E^{1/2} \qquad (4)$$

where the square of $\sigma$ is the variance of the process and E is proportional to the total energy of the wave field at the point.

Mean wave period is determined by

$$T_o = \left(\frac{M_o}{M_2}\right)^{\frac{1}{2}} \tag{5}$$

where 0, 2 subscripts denote the zero and second spectral moments.

Grid Spacing and Time-Step Considerations

A number of considerations interact synergistically in the choice of the model grid spacing and time step. In the first place, the grid system must cover the relevant geographical region from which spectral wave components may reach the area of interest or significantly affect that region. The geography of the ocean basin and the climatology of common/extreme weather patterns and storm tracks define the extent of the coverage necessary.

Given this coverage, it would seem a priori desirable to have as fine a grid spacing as possible in order to increase the model's spatial resolution. However, if the distance between grid points is much less than the resolution of the input wind fields that drive the model, the final model spatial resolution will be a function of wind field resolution and not that of the grid spacing. In this case, unnecessarily fine grid spacing results in excessive computing costs with no added benefit. Model output cannot be expected to be much better than the meteorological input. On the other hand, a grid system too coarse to accurately model small, tight storm systems or very sharply defined fronts will miss or average out their sometimes very pronounced effects which can be quite localized in time and space.

OCEANROUTES' models designed or implemented to date have had grid spacings ranging from a high of 150 nautical miles (Australian/Indian Ocean model) to a low of 30 nautical miles (both the North Sea fine grid model and the western Mediterranean Sea model). Thus, fitting a given number of grid points into a given geographical region yields a particular grid spacing - a spacing which also must be consistent with the climatology and meteorological data resolution for that region.

It should be pointed out as a footnote to this discussion that the choices made in the Spectral Wave Model System are not necessarily unchangeable. Should our studies during the system design stage of this project indicate that a finer grid spacing is required and that the developmental and operational costs are acceptable, such modifications are relatively easy and straightforward to implement. As an example, if sixteen frequencies are included in the deep-water model, a 1.5 hour time-step will be required for a 40 nautical mile grid spacing, and a 1.2 hour time-step would be required for a 30-35 nautical mile spacing.

SPECIAL FEATURES

The principal advantage of OCEANROUTES' regional model is that wind fields can be edited by the local meteorologist, thus permitting consideration of local effects and small-scale features not reflected in the larger basin models. This means that the local meteorologist can, on site, with the use of a terminal and modem, can modify the model to adjust the timing of frontal passages and other local phenomena.

WAVE MODEL OUTPUTS

The primary output of such a model is an energy spectrum at each grid point in the ocean area being modeled. The wave spectrum is specified through the energy matrix that defines the distribution of energy (directional energy). Additional outputs are all derived from the wave spectrum. These include (but are not limited to):

1. The total significant wave height, period, and direction.
2. The estimated significant swell height, period, and direction for all swell trains present.

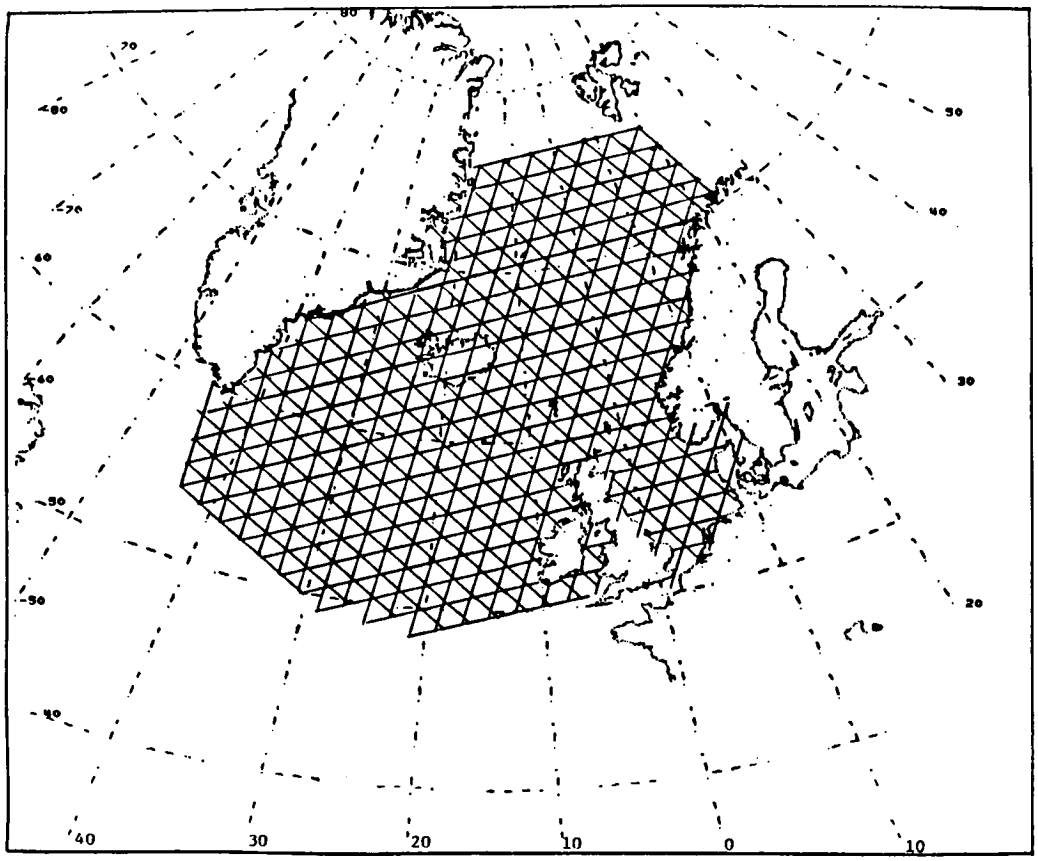


Figure 1. OCEANROUTES' Spectral Ocean Wave Model grid system for the North Sea.

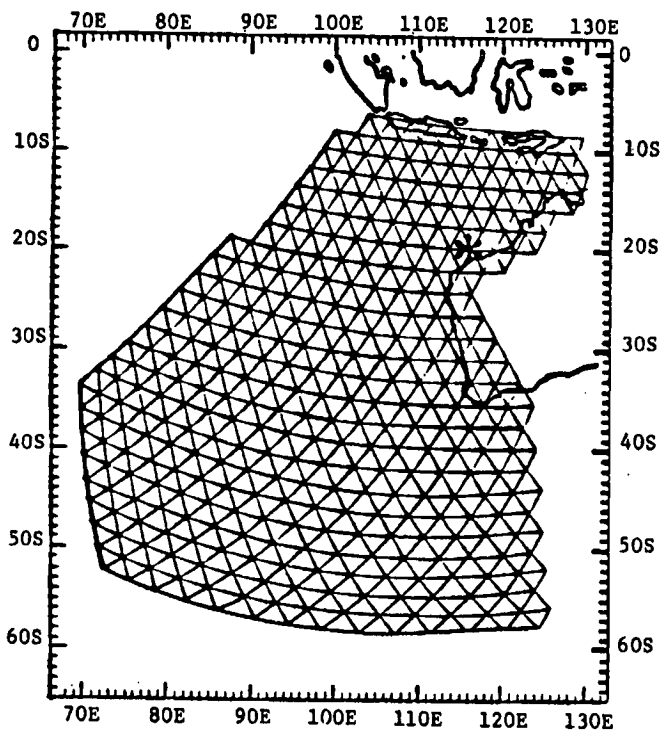


Figure 2. Australian/Indian Ocean Spectral Wave Model Grid.

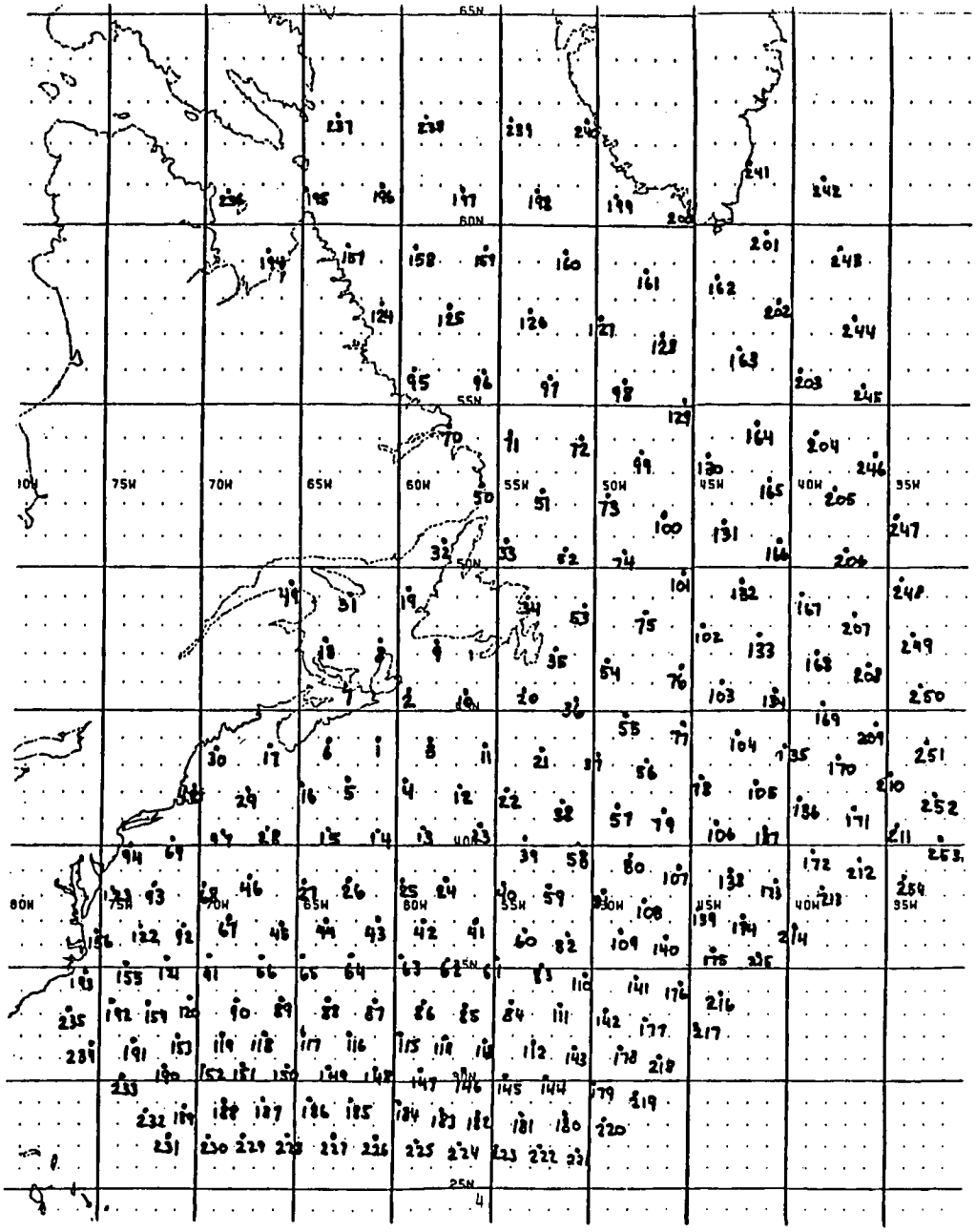


Figure 3 Canadian East Coast Model Grid

3. Maximum probable wave heights for a given observing period and probability of exceedence.
4. Other statistical properties of the wave field.
5. Significant and maximum probable heave, pitch, and roll for vessels in the wave field (given properties of the vessels.
6. Forces, moments, and total loading on fixed structures.
7. Operational windows for various offshore operations.
8. Optimum vessel headings for minimum motions.

## VERIFICATIONS

### Canadian East Coast Model

Testing, evaluation, and verification of the Canadian East Coast Model took place in the winter of 1984/85 (Lally 1985). The model was verified at two grid points, one near Sable Island (44N 61W) and the other in the Hibernia field (46.86N 49.21W). These points were chosen as the most representative ones in the major drilling sites off Nova Scotia and Newfoundland. At that time, there were three stationery rigs operating near each grid point, which were taking continuous observations. The Hibernia wave rider was also in operation for part of the verification period. Weather observations and wave rider reports from all six rigs and the Hibernia wave rider were analyzed and compared to the wave model forecast.

Time history plots for December 1984 were produced and each peak in the plot was analyzed as a hindcasting event. The time history plot for Sedco 709 is shown in Figure 4a and b.

As an example we have chosen the second hindcast event Dec. 6 to 8, 1984. The major wave generation event during this period came from a low which began to deepen South of Nantucket on December 6 at 12Z (Figure 5a). By December 7 at 12Z the low had tracked up through southern New Brunswick and was located at Anticosti Island with a central pressure of 972 mb (Figure 5b). The low continued to deepen as it sped through Southeastern Labrador and into the Labrador Sea on December 8th.

Significant wave heights of 7 to 8 metres has developed over the Sable Island area by December 7 at 12Z (Figure 6a and b). Figure 6a is the contoured significant wave height output from the Spectral Wave Model and figure 6b is the actual significant wave height analysis from the MetOc Centre. The charts show an excellent correlation especially south of Newfoundland where a high of over 8 metres was analyzed and in the Sable Area of our interest. As shown in the time history plots, the timing of the peak wave height was excellent. The observed combined wave height at Sedco 709 (figure 4a) was nearly equal to the forecast wave height whereas the characteristic wave height from the Sedco 709 wave rider is significantly higher than the forecast and observed values. Sedco 709 was located east of Grid Point 1 at N W, it is therefore realistic to expect the peak values of the significant wave height to be higher than at the grid point in this situation.

The verification report recommended that land/sea/ice tables be introduced into the model and that land/sea boundaries be reevaluated in the Newfoundland/Gulf of St. Lawrence areas.

A wave model with 30 degrees resolution has been recognized as too crude and may cause serious shortcoming (Lazanoff and Stevenson 1975). Therefore, a 15 degrees resolution has been recently implemented in the Canadian East Coast model. Also, since the verification in 1984/85, the model has been upgraded to run on a larger computer and processing time has been reduced by one half. The model shows improved verification in evaluations made to date.

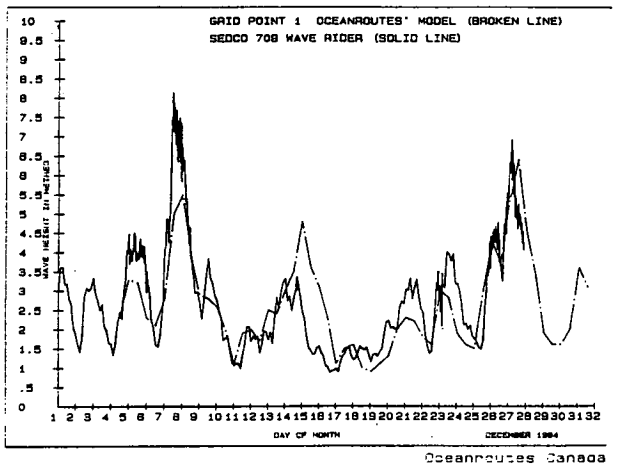


(a)

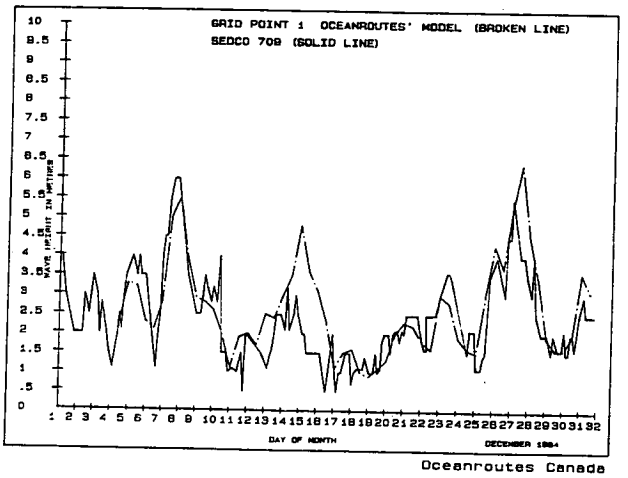


(b)

Figure 4

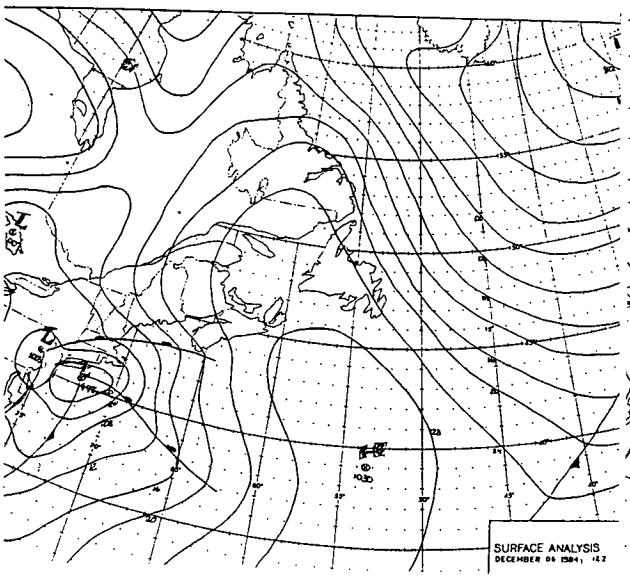


(a)

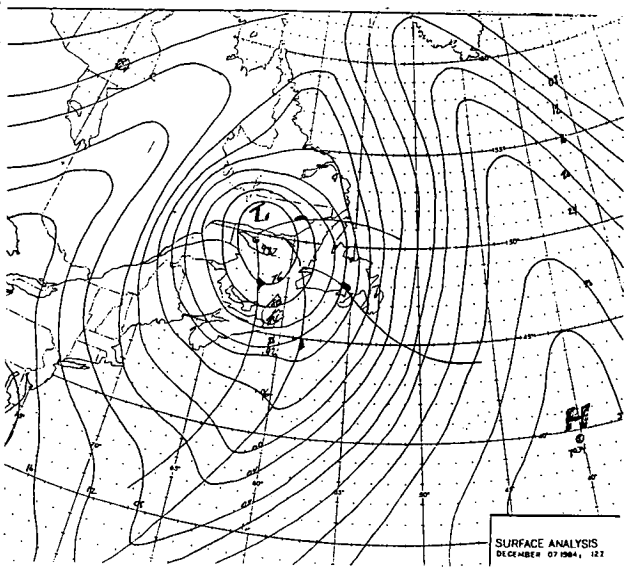


(b)

Figure 5

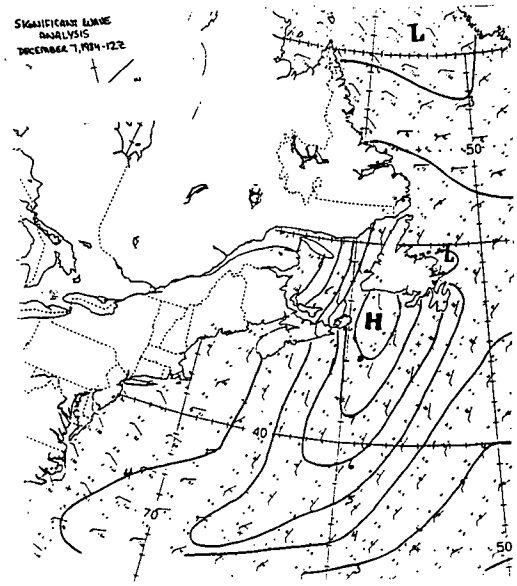


(a)

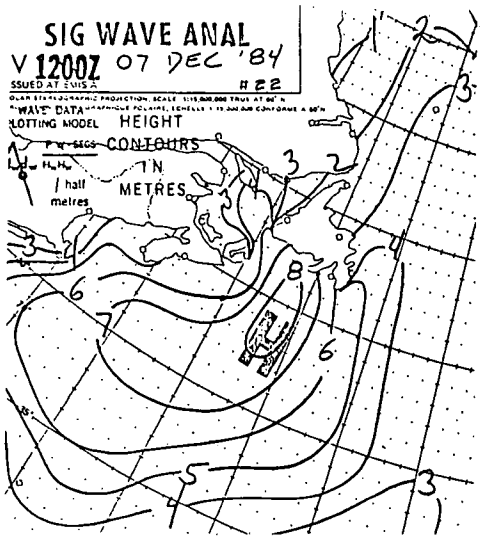


(b)

Figure 6

BRAE 12 GMT 29 MAR 86 FORECAST

HS = 7.6 FEET
= 2.3 METERS
TS = 7.2 SECONDS

WIND SPEED = 12 KNOTS
WIND DIR = 179 DEG

| PERIOD | DIRECTION (FROM) 0 | 150 | 180 | 210 | 240 | 270 | TOTAL |
|---|---|---|---|---|---|---|---|
| 4.0 | 0 | 2 | 3 | 1 | 1 | 0 | 7 |
| 5.5 | 0 | 6 | 9 | 5 | 2 | 0 | 22 |
| 6.5 | 0 | 9 | 16 | 10 | 3 | 0 | 38 |
| 7.5 | 2 | 6 | 22 | 16 | 4 | 1 | 51 |
| 8.6 | 5 | 1 | 28 | 20 | 5 | 3 | 62 |
| 9.7 | 8 | 0 | 16 | 19 | 5 | 9 | 57 |
| 10.9 | 4 | 0 | 2 | 5 | 8 | 21 | 40 |
| 12.0 | 0 | 0 | 1 | 1 | 9 | 35 | 46 |
| 12.8 | 0 | 0 | 0 | 0 | 7 | 47 | 54 |
| 13.8 | 0 | 0 | 0 | 0 | 3 | 55 | 58 |
| 15.0 | 0 | 0 | 0 | 0 | 1 | 47 | 48 |
| 16.3 | 0 | 0 | 0 | 0 | 0 | 20 | 20 |
| 18.0 | 0 | 0 | 0 | 0 | 0 | 3 | 3 |

HS (METERS) FOR EACH DIRECTION:
HS= .4 .8 1.3 1.1 .7 1.1

SHIP HEADING = 312 DEGREES TRUE NORTH
HVS= 1.499 FT PTS= .527 DEG RLS= .646 DEG

Figure 7

Forecast for Brae, North Sea where 'HVS' is heave, 'PTS' pitch and 'RLS' roll.

North Sea and Australian (Indian Ocean Models)

The model has consistently achieved excellent results in the North Sea and an independent assessment of the Australian model shows improved accuracy in wave forecasting as a result of the introduction of OCEANROUTES' Australian Spectral Wave Forecasting Model. In 1982, Woodside Offshore Petroleum Pty. Ltd. commissioned an independent assessment of the offshore forecasting service by R.K. Steedman and Associates (Tate 1983). They studied the period from June 1981 to February 1982 which happened to coincide with the introduction of the Indian Ocean Spectral Wave model for routine operations.

During the period November 1979 to July 1980, preceding the introduction of the model, forecasts of the total wave within + or - .6m on 54.1% of occasions. These results were compared with the results obtained during the assessment for Woodside, using a sample t-test, and it was found that there was a significant improvement in accuracy at the 95% confidence level. It was also noted (Tate 1983) that results for individual months varied between 36.7% and 61.3% during the 1979/80 period and between 46.9% and 88.9% during the 1981/82 period.

Other verifications since that date have confirmed that the Australian (Indian Ocean) model has become a valuable forecasting aid in the preparation of wave forecasts for deep water locations off Western Australia, both in improving forecasts in general and in the particular case of the onset and intensity of high wave episodes.

OTHER APPLICATIONS

1. The wave spectra predicted by SWMs can be used to drive the Oceanroutes' shallow water model to account for wave breaking, refraction, shoaling, wave growth limited by water depth and land sheltering effects. Other physical processes which occur in shallow water (Vincent 1982, Forristall et al 1985) can be included if necessary. Oceanroutes had applied this to estimate shallow water wave spectra along a pipeline corridor on the Northwest Australian Shelf. The model is operational and has been used to forecast spectra during a pipelaying and other real-time operations. The model was described briefly by Fu (1985A). The scouring model in conjunction with the shallow water model can be used to estimate the hydrodynamic forces on a pipeline buried in the bed. The stability of a pipeline depends on wave height and wave period, but is also very sensitive to wave direction and bathymetry (Fu 1983).

2. Conducting and planning upcoming works on offshore vessels, offshore managers and/or engineers are more interested in wave induced motions than wave conditions on vessels, since every ship has its own characteristics.

The Oceanroutes' system of vessel motion responses consisting of SWM and transfer functions can predict the spectral responses, from which, heave, pitch, roll, surge, sway, yaw and boom-tip motions can be derived. SWM for both O/R deep and shallow water available since 1976 (Silveria et al 1978), have been supported the prediction of wave-induced motions. An example of vessel motion predictions for a semi-submersible for Brae, North Sea is shown in figure 7 (Fu, 1985B).

One type of transfer function is the response amplitude operators (RAO) for semi-submersibles and drill ships. RAO is defined as the ratio of the amplitudes of the vessel motion responses to wave. Usually, RAOs are determined by physical model test. RAOs can vary to account for their change in load systems for derrick barges during their lifting operations (Rawstron et al 1978).

3. A nested model is under development in conjunction with a coarser grid model. this model will be useful when a smaller scale grid is needed, such as tropical cyclones and predictions over shallow water. (Stevenson, 1984)

REFERENCES:


Forristall, G.Z. and A.M. Reece, "Measurements of wave attenuation due to a soft bottom: The SWAMP Experiment", Journal of Geophysical Research, Vol 90, No. C2, 1985.

Fu, D.C.,"Wave model abnormalities detected by field measurements", 19th Annual Congress, CMOS, Montreal, June 12-14, 1985A.

Fu, D.C.,"Wave refraction and current analyses along a pipeline corridor in the Arabian Gulf", prepared for Brown and Root, Inc., 1983.

Fu, D.C., "Vessel motion prediction system users' manual for Brae", Oceanroutes Internal Report, 1985B.

Inoue, T. 1967. "On the growth of the spectrum of a wind generated sea according to a modified Miles-Phillips mechanism and its application to wave forecasting." New York University Geo. Sci. Lab. TR-67-5.

Lally, S.K., "Verification of the Canadian East Coast Spectral Wave Model", Oceanroutes Canada, Internal Publication, 1985.

Lazanoff, S.M. and N.M. Stevenson, "An evaluation of a hemispheric operational wave model", Fleet Numerical Weather Central Technical Note 75-3, Monterey, CA, 1975

Miles, J. W. 1957. "On the generation of surface waves by shear flows," Journal of Fluid Mechanics, 3, pp. 185-204.

Miles, W. J. 1959. "On the generation of surface waves by shear flow, Part II". Journal of Fluid Mechanics 6, pp. 568-582.

Phillips, O. M. 1957. "On the generation of waves by turbulent wind," Journal of Fluid Mechanics, 2, pp. 417-445.

Phillips, O. M. 1958. "The equalibrium range in the spectrum of wind generated waves," Journal of Fluid Mechanics, 4, pp. 426-434.

Phillips, O. M. 1960. "On the dynamics of unsteady gravity waves of finite amplitude, Part I," Journal of Fluid Mechanics, 9, pp. 193-217.

Phillips, O. M. 1966. "On the dynamics of the upper ocean." Cambridge University Press, 261 pp.

Phillips, O. M. 1977. "The dynamics of the upper ocean." Cambridge University Press, 2nd edition.

Pierson, W. J. and L. Moskowitz. 1964. "A proposed spectral form from fully developed wind sea based on the similarity theory of S. A. Kitaigorodskii." Journal of Geophys. Res. Vol. 69.

Rawstron, P.J.M. and G.J.B. Blight, "Prediction of weather downtime for derrick barges", OTC Paper 3150, 1978.

Silveria W.A. and C.S. Skees, "Application of spectral techniques to forecasting wave conditions and wave-induced vessel motions", OTC 3280, 1978.

Tate, A.J., "An operational spectral wave forecasting model" - North West Shelf, Australia, Offshore China '83,Guangzhau, China, Nov. 22-26, 1983.

Vincent, C.L., "Shallow water wave modeling", preprints 1st International Conference, Meteorology and Air/Sea Interaction of the Coastal Zone, the Hague, American Meteorological Society, 87-95, 1982.

# THE OPERATIONAL WAVE FORECASTING PROGRAM OF THE CANADIAN FORCES METEOROLOGICAL AND OCEANOGRAPHIC (METOC) CENTRE, HALIFAX, N.S.

W. G. Lumsden

Meteorological and Oceanographic Centre
F.M.O. Halifax, N.S.

and

R. K. Cross

National Defense Headquarters
Ottawa, ON

## 1. INTRODUCTION

The Canadian Forces Meteorological and Oceanographic (METOC) Centre has been actively involved in the analysis of and the provision of sea state forecasts since the late 1960's. The meteorologists preparing these analyses and forecasts are employees of the Atmospheric Environment Service who have been seconded to the Canadian Forces Weather Service (CFWS). The intent of this paper is to give those involved either in the operational aspect of or in research activities related to the provision of sea state information, an overview of the METOC Centre program.

The primary function of the METOC Centre's sea state program is to support Canadian Forces and NATO naval activities in the northwest Atlantic. These activities include surface, sub-surface and air operations. Naval areas of interest include such things as ship routing, replenishment at sea, antisubmarine wafare, search and rescue, amphibious operations, flight operations off of ships, mine hunting and ship design.

## 2. ANALYSIS PROGRAM

The analysis program consists of four analyses per day at 0000Z, 0600Z, 1200Z and 1800Z. The analysis domain is shown in Figure 1. All ship reports of wind and sea state information are automatically plotted and subjectively checked for consistency and validity. One can readily see in Fig 1 that the distribution of data is relatively poor; thus, a completely objective analysis would be difficult. To complete the analysis the analyst uses the previous six hour analysis, the 12 hour sea state forecast valid for that analysis time and the isobaric analysis to effectively produce a real-time hindcast for the data sparse areas.

The plot model as shown in Fig 2 has both wind wave and swell wave information and the combined wave is calculated and plotted. It is the combined wave that is actually analyzed. Historically we have labelled this chart as a 'Significant Wave Analysis', where in fact it is or has become a 'Combined Wave Analysis'. Fig 3 depicts a completed analysis, the arrows depict the direction and type of the predominant wave. The straight arrow depicts wind waves and the crooked arrow indicates swell.

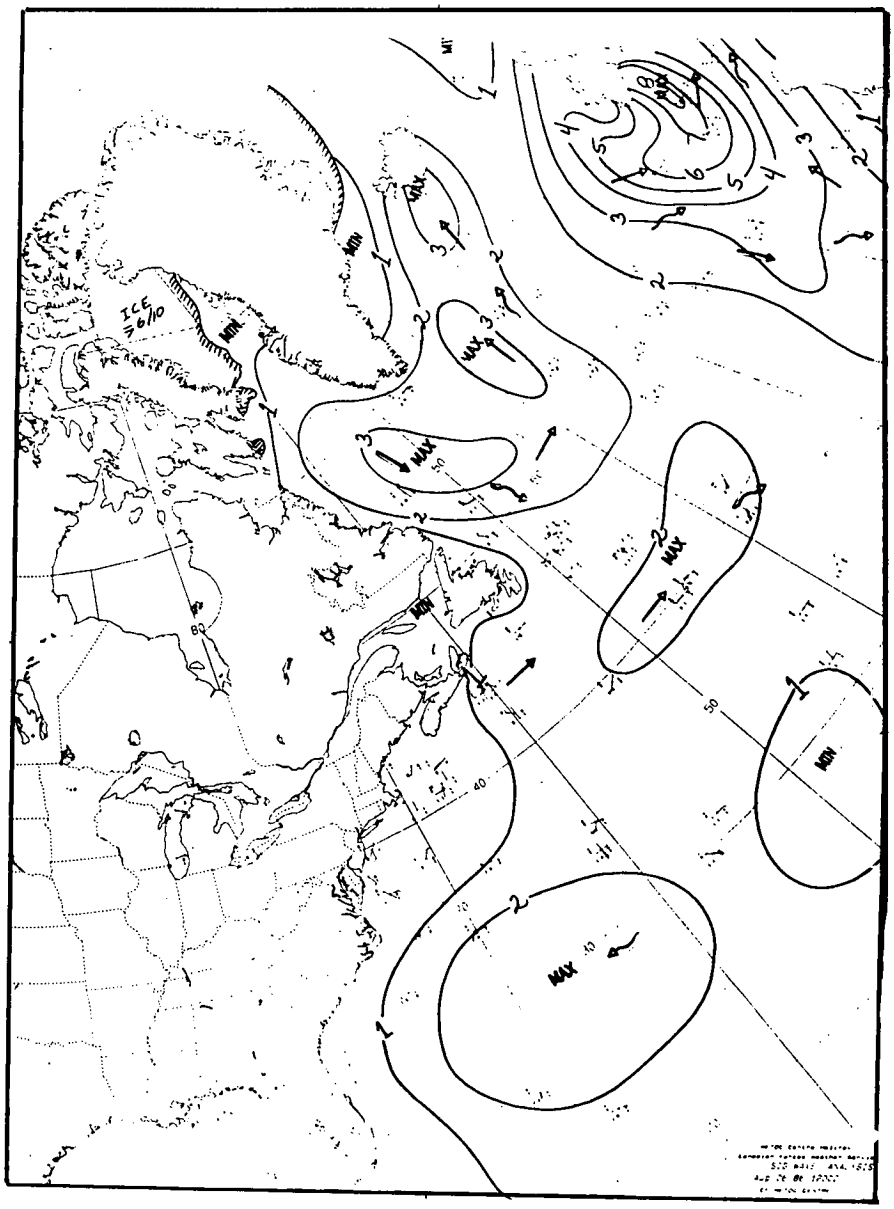


(Figure 1)

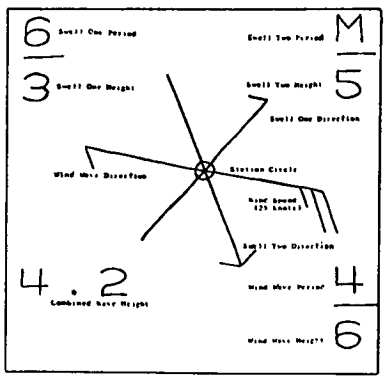


(Figure 2)

## 3. FORECAST PROGRAM

The forecast program consists of twice daily forecasts for 12, 24 and 36 hours based on the 0000Z and 1200Z analyses and the meteorological forecast products based on these analyses. The key to any sea state forecast is analysis of the current wind regime and an accurate prognosis of how the surface winds are going to evolve with time. The first step after the actual analysis of the wind fields and current sea states is the production of a 12 hour isobaric prognosis. This prognosis is then used as an underlay of the sea state analysis in order to determine the wind and fetch domains for the period leading up to forecasts' valid time. Particular emphasis is placed on recognizing/conserving the energy in present wave fields and extrapolating forward in time. The Bretschneider nomogram is the primary tool used for forecasting sea, while Suthons's nomogram is used for handling swell.

The sequence for the 24 and 36 hour prognoses is much the same. The isobaric patterns are forecast and the preceeding prognosis and isobaric pattern are used as underlays in producing the new product. Once again a heavy emphasis is placed on maintaining patterns and decaying significant sea state areas carefully. Fig 4, a 12 hour prognosis, depicts the present format of the wave forecast products. This product is very similar to the analysis product, contours are drawn at one metre intervals and areas of high and low sea states are indicated as such with a 'H' for high and a 'L' for low and the predominant waves in an area use arrows as per the WMO accepted format.

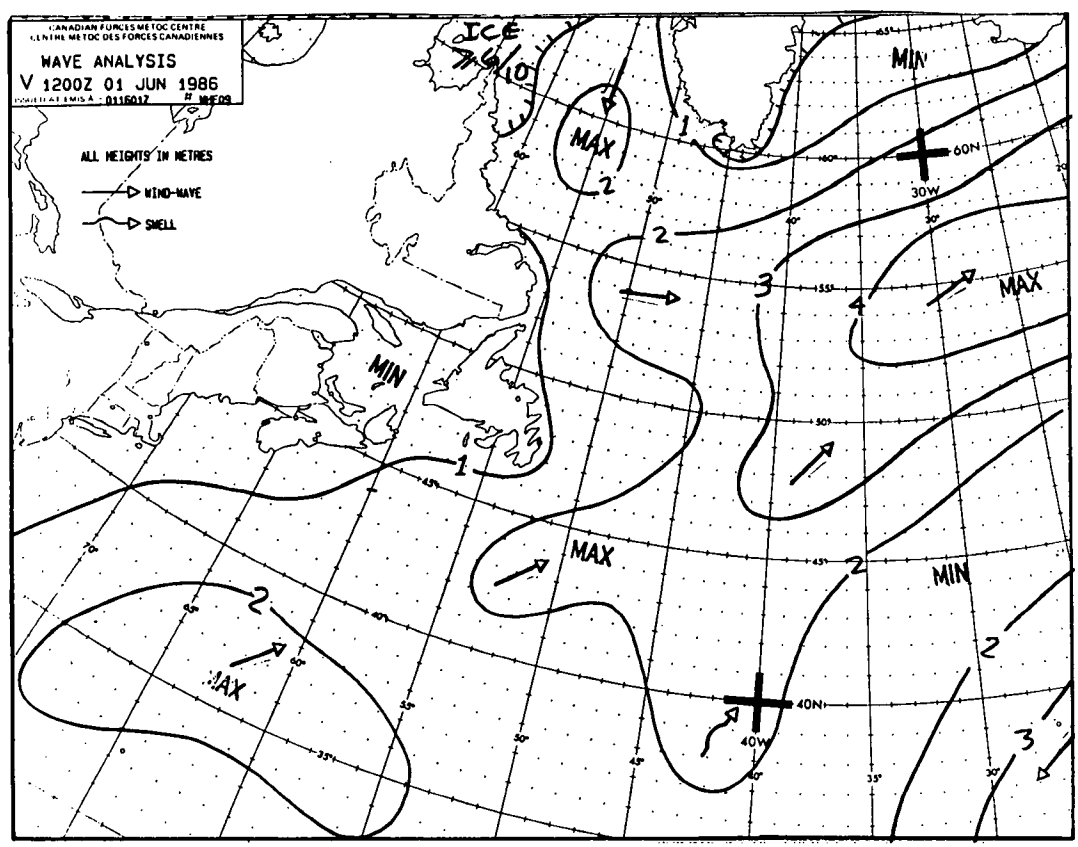


(Figure 3)

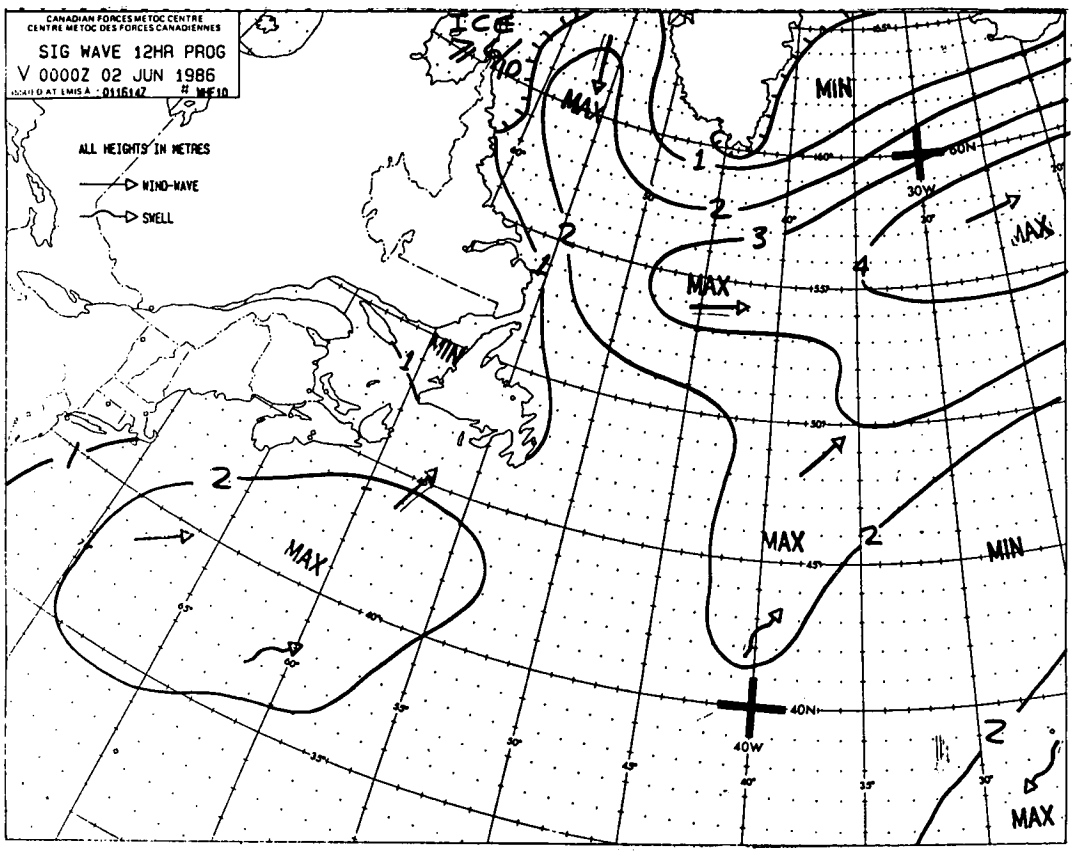


(Figure 4)

4. VERIFICATION

In 1983 a semi automated verification system was implemented which provides data on our performance. The system provides data for the centre point of each five degree latitude/longitude square over the entire forecast domain as well as five sub-sections. Daily and monthly statistics of mean height, bias, mean absolute error and root mean square error are produced. The daily statistics are provided for both 00Z and 12Z forecast products for each of the 12, 24 and 36 hour forecasts. Fig 5 provides examples of the annual results.

5. DISTRIBUTION

METOC's sea state products are distributed on the AES regional facsimile network and on the CF radiofacsimile broadcast system. The radiofacsimile broadcast commonly known as CFH is an open broadcast operating four HF frequencies (4271, 6330, 10,536 and 13,510 Hz) and one LF frequency (1225 Hz). A modest investment provides users access to this system.

(Figure 5A)

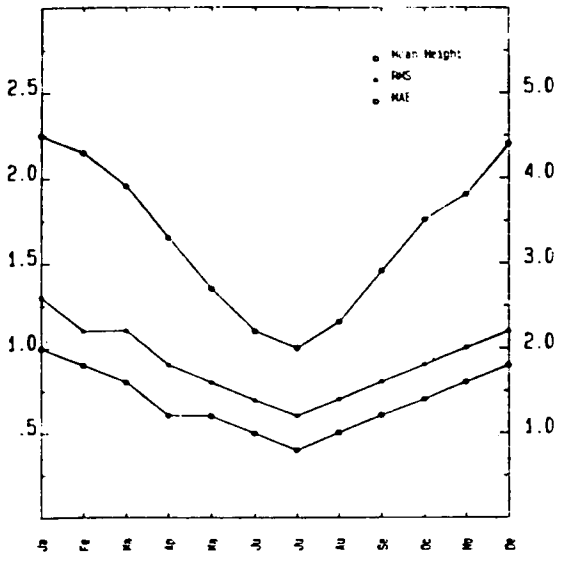


Wave Statistics (1985)

(12 Hr) Total Zone

(Figure 5B)

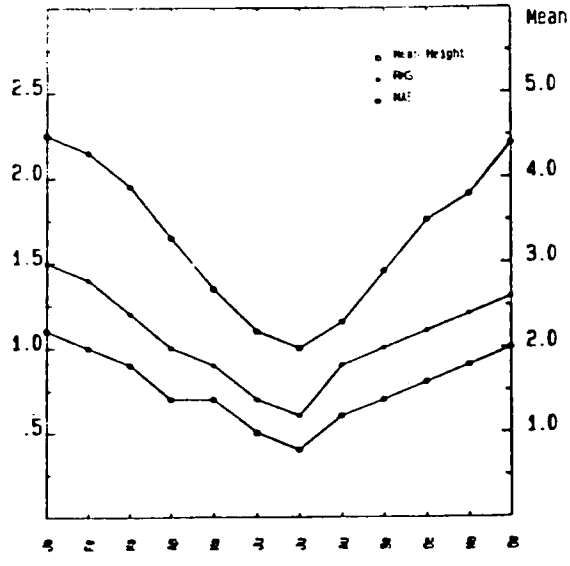


Wave Statistics (1985)

(24 Hr) Total Zone

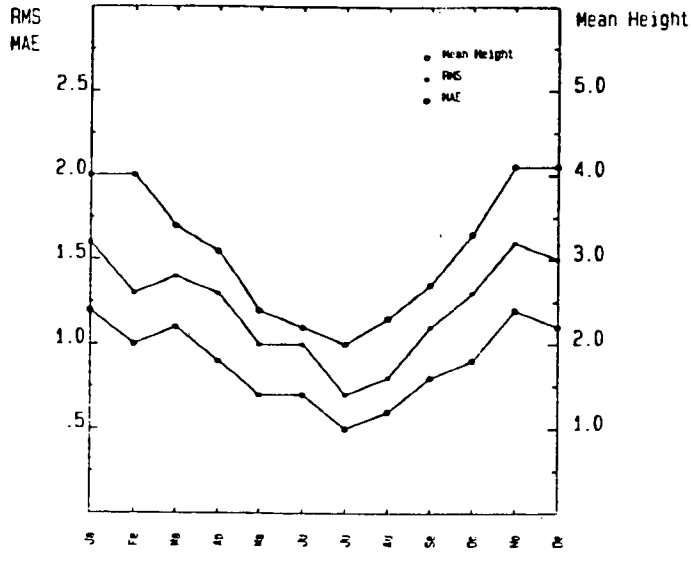


Wave Statistics (1984)

(36 Hr) Total Zone

(Figure 5C)

## 6. ARCHIVE

An archive of all 00Z and 12Z analyses was started in June 1971 and a continuous set held at the Centre. All analyses for that period up to and including December 1985 have been microfilmed. A positive microfilm copy of these analyses is available on loan to any researcher who has a requirement. The actual analyses are only kept for a three year period; copies of these can also be made available.

## 7. PARAMETRIC MODEL

The Parametric Wave Model which was developed for the Atmospheric Environment Service, by the MEP Company under contract, was an effort, at least in part, to computerize the operational procedure used at the METOC Centre; thus, the parametric approach. No attempt will be made here to explain the model since a following paper will do so. The model output is routinely available to the operational forecaster but unfortunately the output arrives too late to be considered for the analysis or the 12 hour forecast. It is of marginal use for the 24 hour forecast and arrives in plenty of time for consideration in preparation of the 36 hour forecast.

Although received too late for consideration in the actual products, the model output does provide valuable guidance to operational staff, particularly junior forecasters. The process of evaluating why the model has over-or-under developed a feature provides valuable training experience.

## 8. FUTURE DEVELOPMENTS

Since the METOC Centre is an operational centre, we are not actively involved in any model development. Spectral model output would certainly be desirable; however, that is outside our mandate. We do however plan to introduce an objective wave analysis routine which will incorporate all ship sea state observations. It would be desirable to use the Parametric Wave Model's zero hour output as the first guess field but this data is not available early enough. Therefore, we will be using either the model's 12 hour forecast or the METOC's 12 hour forecast as the first guess field.

# THE AES PARAMETRIC OCEAN-WAVE FORECAST SYSTEM

K.A. Macdonald* and S. Clodman

Meteorological Services Research Branch
Atmospheric Environment Service
Downsview, Ontario

## Introduction

In December 1985, the Atmospheric Environment Service (AES) implemented into its operational forecasting program, a numerical ocean-wave forecasting model. This parametric model, developed by the Meteorological Services Research Branch through contracts with the MEP Company, is based upon the Bretschneider wave forecast equations which relate key wave parameters (significant wave height, period and speed) to the surface wind field. Discrimination is maintained between developing, wind generated sea waves and decaying swell waves based upon the wave-wind speed differential. Forecasts are produced twice daily for large portions of the northwest Atlantic and northeast Pacific Oceans and are distributed in chart format via digital fascimile to support the wave forecasting programs of AES forecast centres and the Canadian Forces Meteorological and Oceanographic (MetOc) Centres.

This paper will begin with a brief review of the Bretschneider theory, upon which the parametric model is based, followed by a description of how this theory is applied within the model. There will also be an explanation for why the AES chose the parametric approach for its first numerical ocean-wave forecast system. Results from several evaluation studies will be presented which have identified many characteristics of the model's forecasts and sources of recurring errors will be explained. Finally, there will be a case study to illustrate typical model performance.

## Model Theory

The theory of the parametric wave model is based upon the Bretschneider (1952, 1960, 1973) theory which related wave parameters (significant height of developing and fully developed wind waves, height of decaying swell waves, direction of wind waves and swell, and period of wind waves and swell) to the surface wind field. The original Bretschneider theory assumes constant wind velocity (both direction and speed) in space and time. The stepwise ray procedure, which the model uses and will be described here, is a later adaptation to allow computation with varying wind velocity. The existing MetOc procedure calculates the wave using similar principles, as described in Morgan (1971).

Bretschneider, along with most other theorists, recognized two main episodes in the wave lifetime - generation and decay. During generation a wind wave is being built up by the wind. During decay the wind has decreased and there is a declining swell wave. However, the average period, wave length and speed continue to increase throughout the wave lifetime.

The Bretschneider (1973) equations (nomogram in Bretschneider (1970)) for height H and period T, in constant units are:

$$H = 0.283\ g^{-1}\ U^2\ \tanh\ (0.0125\ X^{0.42}) \qquad (1)$$

$$T = 7.54\ g^{-1}\ U\ \tanh\ (0.077\ X^{0.25}) \qquad (2)$$

---

* Presently at Maritimes Weather Centre, Atmospheric Environment Service, Bedford, N.S.

where $X = g\,U^{-2}x$ is a nondimensional fetch composed of a constant wind speed U, the total fetch x and the acceleration due to gravity g; H is the significant wave height, which is the average of the highest 1/3 of the waves and T is the significant period representative of those 1/3 of the waves. So for example, for a wind speed of 10 m $s^{-1}$ acting over a fetch, x, of 1000 km, (1) and (2) give a significant wave height of 2.65 m with a period of 6.8 s, while a wind speed of 30 m $s^{-1}$ acting over the same fetch results in a significant wave height of 14.3 m with a period of 14.1 s. As the fetch increases, H and T increase at first rapidly and then more slowly towards the limit $H_m = 0.283\ g^{-1}U^2$ and $T_m = 7.54\ g^{-1}\ U$. If the actual fetch is kept constant, H increases as the square of U while U is relatively small; however, it increases only a little faster than linearly for large U. As the wind becomes stronger, it takes a longer fetch to approach $H_m$ and $T_m$.

For (1) and (2) to be valid, the duration, t, of the wind must be sufficiently long. If t is too small then H and T are duration-dependent rather than fetch-dependent. In this event, a time-dependent equivalent fetch $x_e$ must be computed and substituted for x in (1) and (2). This $x_e$ represents the movement of the wave front with the group velocity $dx_e/dt$. At t = 0, x = 0 and $dx_e/dt$ increases from 0 at t=0 to about 0.6U as an asymptotic limit. For example if U = 10 $ms^{-1}$, t = 60h, then $x_e$ = 1000 km. If $x_e$ increases beyond x then the wave becomes fetch-dependent and x is again used in (1) and (2). Venkatesh (1975) gives the method for computing $x_e$.

The decay period is determined by the nomogram in Bretschneider (1952). The height, $H_D$, at the end of the decay period depends upon the height, H, at the beginning of the decay, the decay fetch distance and the generation fetch distance. Table 1 provides a comparison of wave decay. Thus it can be seen that the decay proceeds rapidly at first and then more slowly. On the other hand, Table 1 also shows the wave period increases as the wave decays. Simultaneously the phase speed, i.e., the speed of apparent wave motion, and the group speed, i.e., the speed at which the wave energy is translated, increase in like proportion. Thus swell waves usually advance ahead of generating waves.

Table 1 Wave Decay

| H (m) | T (s) | Generation Fetch (km) | Decay Fetch (km) | $H_D$ (m) | $T_D$ (s) |
|---|---|---|---|---|---|
| 5 | 10 | 1000 | 500 | 3 | 11 |
| 5 | 10 | 1000 | 1500 | 2 | 12 |
| 5 | 10 | 1000 | 7000 | 1 | 13 |

If the water is not very deep, bottom effects on the wave become significant. These effects alter the height (reduce it), period (increase it) and the direction of motion (turn it towards shore) of the wave. Since the parametric wave model uses only deep water theory it is not necessary to understand these effects in detail. One should, however, appreciate the limit of validity of the deep water assumption.

Suppose the depth is D and the significant wave height is H. Then $D < 12\ H$ implies shallow effects are non-negligible and $D < 5\ H$ implies that such effects are dominant. For small to moderate values of H, shallow water effects are unimportant for ocean forecasting. However, large waves over shallow water areas (e.g., Grand Banks) or shoals can be a problem. If H = 15 m, a depth as large as 180 m will result in some bottom effects. Hence caution should be applied near the continent and over the Grand Banks, as the forecast waves will occasionally be inaccurate.

## Model Description

Two domains for the parametric model have been established, One corresponds to the Halifax MetOc Centre's forecast region in the northwest Atlantic. The other is somewhat larger than the region of responsibility of the west coast forecast offices (MetOc Centre

Esquimalt and CFFC Comox). These two domains are shown in Figure 1. Each grid point on the 381-km grids shown in this figure represent a target point, defined as a point at which forecasts of significant wind wave height, major swell height, combined wave height, and period and direction of waves and swell are calculated. In computing the waves and swell, 24 rays are extended from each target point at 15 degree intervals. These rays terminate when they reach land or when they reach the ray grid boundaries shown in Figure 2. The Atlantic version also recognized sea ice by terminating rays when they reach the ice edge as represented by the boundary of 6/10 or greater ice coverage.

The rays represent a discrete set of potential lines of fetch for each target point. In order to develop waves the model requires the wind to be known at all points along the ray. This wind data is supplied to the model from the Canadian Meteorological Centre (CMC). Up to the 0-h forecast time analyzed winds are used and after that winds generated by the CMC's atmospheric spectral forecast model are accessed. Presently the winds that are used are identified as being for the 1000 mb level, however, this is somewhat misleading. The 1000 mb wind analyses depend heavily on reported ship data, hence in areas where there are reports the 1000 mb winds are representative of the ship winds. Where there is a lack of ship data the analyzed winds are influenced most by the first guess field which is a forecast. It, like forecasts for the later projections, is a forecast for the 1000 mb level. When the 1000 mb level is above the lowest computational level of the NWP model, linear interpolation to 1000 mb is performed. However, when the 1000 mb level is below the model's lowest computational level, rather than extrapolate outside the model's vertical domain, the winds default to their value on the lowest computational level (currently sigma = 0.991 or approximately 80 m). In either case it is important to realize that the winds being used by the wave model are not for the 10 m or 19.5 m level as would be desirable, but instead are for a somewhat higher, but variable level.

The CMC wind data is provided on a 42.3 km grid at 6-hourly intervals. Cubic spline interpolation is applied to obtain the wind at any given point in space and time along each ray. Since the wave model is interested only in the wind component along a ray, wind speeds are set to zero if the wind angle differs by more than 25 degrees from the ray direction. Potential wave generation regions are then defined as regions (in space and time) along each ray where the wind speed component is greater than 5.14 m $s^{-1}$ (10 kts).

In order to model the generation of waves along each ray, a moving fetch procedure (Wilson, 1963; Venkatesh, 1975) is used: thereby taking into account both the space and time variability of the wind. The method is a stepwise numerical integration of the parametric wave equations (Bretschneider, 1952, 1970) relating significant wave height and period to a steady wind velocity (on the ray), acting over a small fetch (up to 74 km) for a short duration (up to 2 h). This procedure is carried out over each generation region of each ray; and the wave arriving at the target point closest to the forecast time is selected as the forecast for that ray.

If a generating region extends to the target point, then the wave developed over that region can be considered to be a sea wave reaching the target point. On the other hand, if the sea wave propagates out of a generating region before reaching the target point, two conditions can arise. First, if wind speeds persist slightly below the speed that yields the generated wave height, the sea waves are carried along unchanged on the assumption that these winds will be able to support the waves that have been developed. If, further along, the wind speeds increase, further generation of the sea waves takes place. The second condition occurs if wind speeds decrease significantly to the point where they cannot maintain the waves that have been developed. In this case the sea waves become swell waves and are allowed to decay along the remaining distance of the ray to the target point; that is the decrease of wave height and increase of period are computed as a function of decay distance and minimum fetch (Bretschneider, 1952; Venkatesh, 1975).

The highest single wind wave and the highest single swell wave reaching the target point from the 24 rays become the forecast for that point. For each of these waves the model will have calculated the significant wave height and the period of this significant wave. The direction of propagation of each wave is given by the direction of the ray over which it was generated. At each target point a combined wave height, defined as the

Figure 1

Atlantic and Pacific domains of the Parametric Wave Model.
Model target points indicated by circles on a 381 km grid.

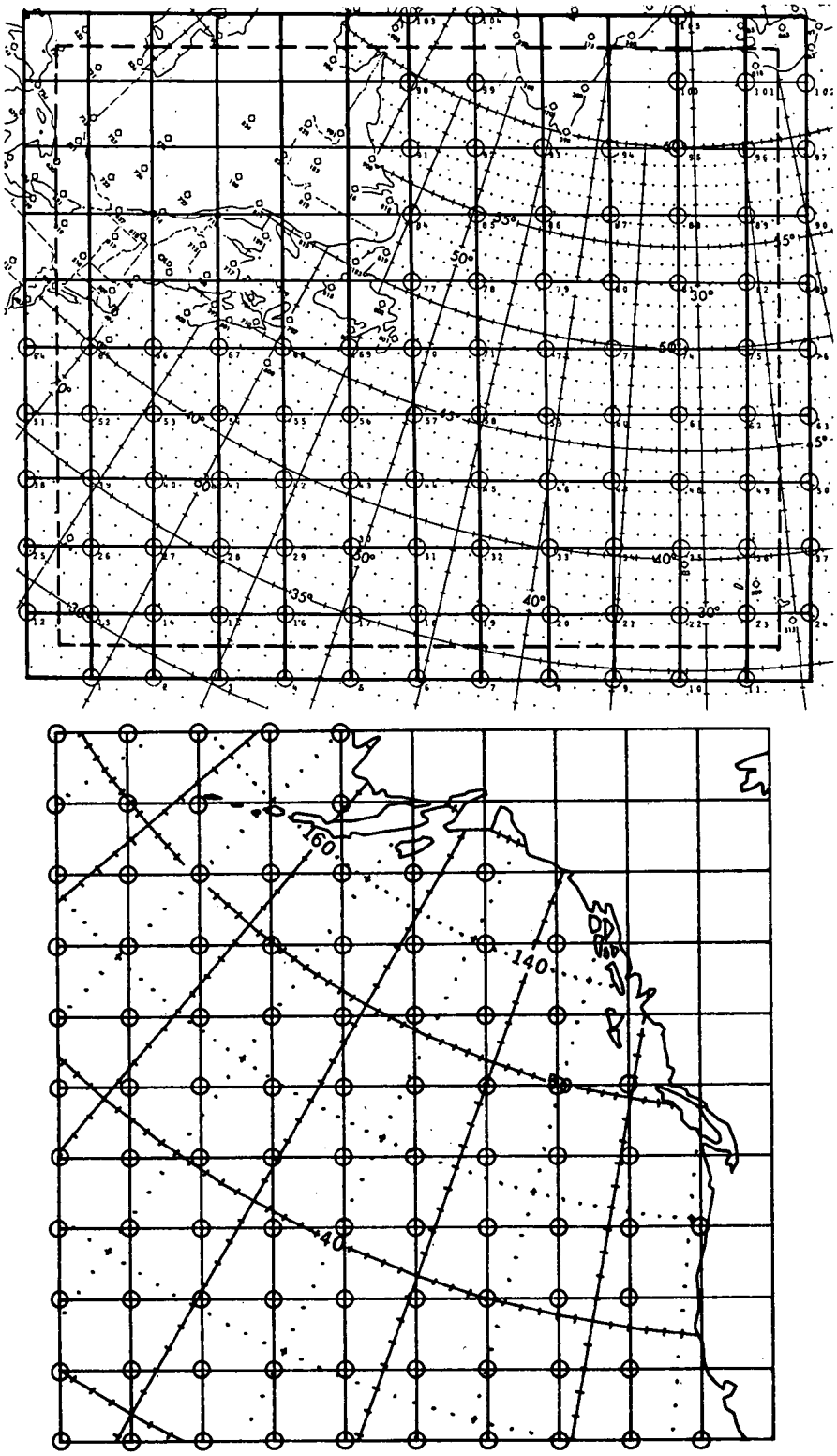

Figure 2

Wave generation domains of the Parametric Wave Model

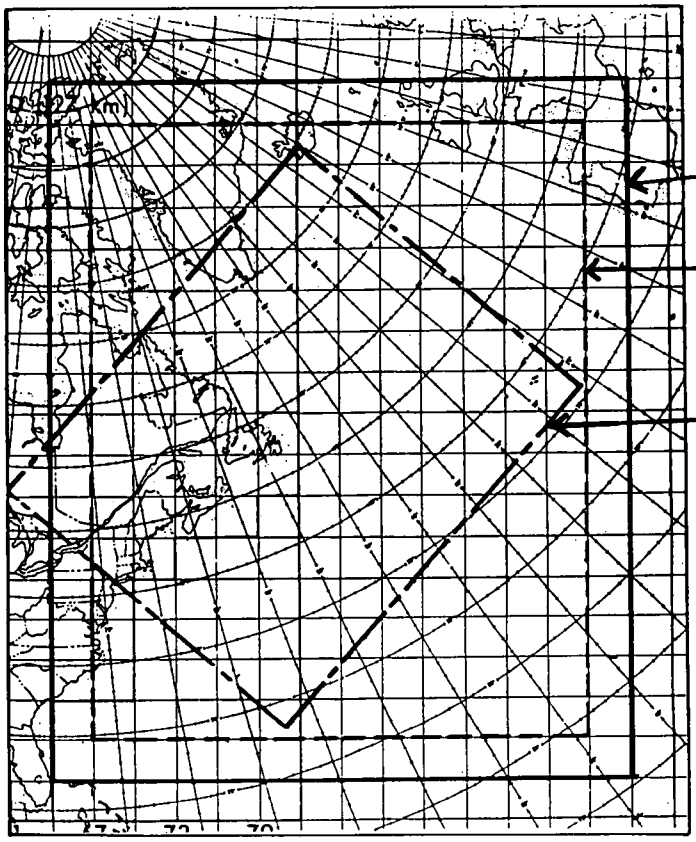


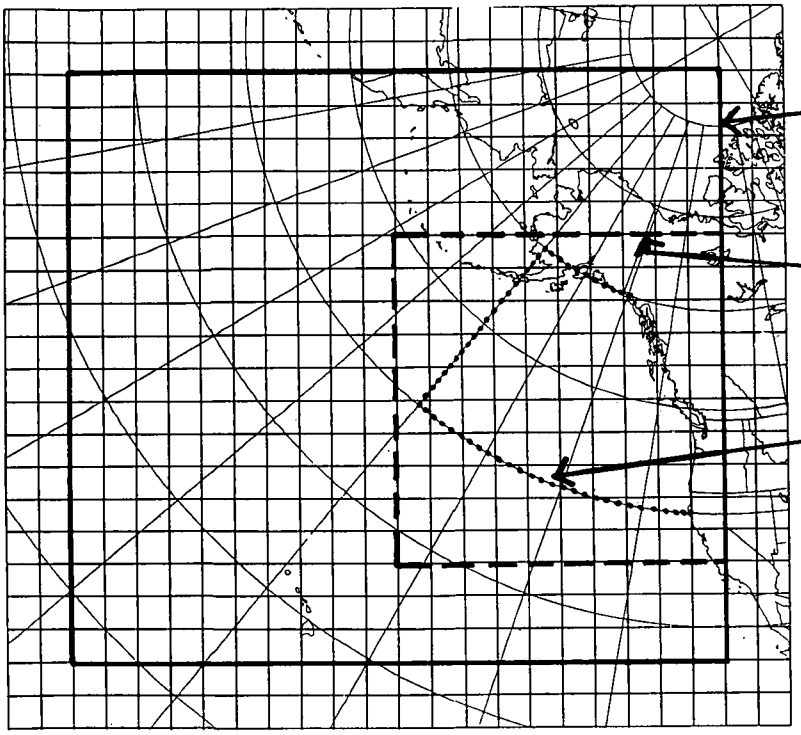

square root of the sum of the squares of the wind wave and the swell wave heights, is also calculated.

It is important to point out that the only inputs to the model are the wind fields from the CMC. Sea conditions reported in the synoptic reports of ships are not considered. Thus a wave chart produced by the forecast system and labelled as a 0-h analysis is not an analysis of the reported sea conditions, but instead represents the computed (hindcast) sea conditions based upon the historical 1000 mb wind data.

Sources of Error

Forecasts generated by the parametric wave model will, at times, be inaccurate. There are a variety of potential sources for such inaccuracies, the most important of which are listed below:

- inaccuracies in the wind speed and direction data supplied to the model, i.e., analysis and forecast errors;
- inadequacies of the wind input data at representing actual wave generating conditions, i.e., the fact that the winds are not for the surface level and that they do not adequately account for factors such as low level atmospheric static stability;
- inaccuracies in the definition of the fetch, possibly due to inadequate information on the location of sea ice;
- inadequacies in the SMB theory itself in translating wind velocity into wave buildup;
- inadequacies in the Bretschneider theory for wave decay;
- inaccuracies in dealing with non-constant conditions, i.e., errors arising from the application of the Wilson moving fetch approach;
- the failure to account for shallow-water effects;
- perceived inaccuracies resulting from comparisons with inaccurate wave observations.

While any or all of these potential sources of error could come into play for a particular wave forecast, in general, each occurs under particular, often recognizable, situations. This has been evident from many of the model evaluations which have been performed and will be described in a following section.

Why the Parametric Approach?

Development work on the ocean-wave model began in 1981. At that time there were several factors which led to the decision to develop a parametric model, vis-a-vis a more elegant spectral model. The MetOc Centre in Halifax had been preparing wave forecasts subjectively since the early 1970's using a parametric (Bretschneider nomogram) approach. Its forecasters had become quite skilled at the procedure and several informal intercomparison studies had shown that the MetOc product was the best wave forecast being issued for the Canadian East Coast. In introducing a numerical wave model into the operational forecasting environment it was desirable to select a model which would approach the forecasting problem in a similar, albeit more comprehensive manner, than the forecaster. In this way the forecaster would be in a better position to interpret the model solutions and make subjective adjustments to the forecasts as necessary. In fact, original plans called for quite a sophisticated work station to be developed to allow the forecasters to manipulate the wind data being supplied to the model and to permit graphical adjustments to the model's forecasts. Unfortunately the AES's computer and communications facilities have not yet evolved to a state where this is practical.

In the future, when the forecasters are accustomed to incorporating a numerical solution into their wave forecasts, it might then be appropriate to replace the parametric model with a more sophisticated spectral model. Presently however, there is little demand

from users of the MetOc product for the more comprehensive wave information available from a spectral model and there is no clear evidence that spectral models produce superior significant wave height forecasts. The AES plans to conduct some intercomparison studies in the upcoming year to determine if in fact better forecasts are available from a spectral model.

## Model Performance

A number of evaluations of the parametric wave model have been performed both before and after it became operational. The first tests were done during March 1984. At that time an objective verification was performed in which the model's forecasts of combined wave height were compared against available ship reports of sea conditions. During the winter of 1984-85 an operational test of the model was carried out at which time forecasts for the Atlantic domain were transmitted in "near-real-time" to the Halifax MetOc Centre. MetOc used the model's forecasts in their wave forecast program and also objectively verified the forecasts against their own subjective wave analyses. During this same trial, the model's forecasts were made available to the AES's Maritimes Weather Centre and they evaluated the forecasts over their area of responsibility (the Scotian Shelf).

Since the model became operational it has been assessed by many of the forecast offices which receive it including the Halifax MetOc Centre, the AES Pacific Weather Centre and CFFC Comox. All of the objective verifications have been supplemented by extensive subjective assessments of forecast and analysis charts resulting in the identification of a number of model performance characteristics which will be summarized below.

### i) Overall Assessment

The principle finding of the evaluations has been that the ocean-wave forecast system performs quite satisfactorily, producing reasonable looking patterns of wave heights consistent with the wind fields supplied to the model. Objective verification statistics such as mean absolute and root mean square errors usually suggest that the model's forecasts are slightly inferior to the subjectively prepared forecasts. However, subjective comparisons often find that the model is superior in maintaining temporal and spatial continuity in its forecasts.

### ii) Wind Errors

Most of the errors associated with the wave model forecasts can be traced back to errors in the driving wind field. On average, the wave model displays an overforecasting bias; a bias which grows with forecast projection time. The use of 1000 mb winds to represent the surface wind field introduces a natural overestimation of wind speeds. This wind bias itself has been noted to grow with forecast projection time; possibly resulting from a known characteristic of the operational CMC NWP Spectral model to overdevelop both low and high pressure centres leading to exaggerated pressure gradients.

One of the most noticeable of the wave model's characteristic errors is to overdevelop waves in the warm sector of baroclinic developments, particularly when these are well developed systems and the pressure gradients are strong. In the low levels of the atmosphere these regions are statically quite stable and hence the windspeeds at 1000 mb can be significantly stronger than at the surface. There have been several examples where the observed winds were 35 to 40 kts yet the Spectral model indicated $>$ 50 kts.

On the other hand, in cold northwesterly outbreaks from the continent, when the lower levels of the atmosphere tend to be very unstable, windspeeds supplied to the wave model were usually underestimated. MetOc meteorologists, as a result have noted a recurring error on the part of the wave model to underdevelop seas in these cold outbreak situations.

### iii) Overforecasting Combined Wave Heights

On a few specific occasions it was apparent that combined wave heights were

overestimated due to a shortcoming in the logic of the wave system used to differentiate between the wind driven sea wave and the decaying swell wave. On these occasions, a particular wave generating region resulted in a sea wave arriving at a target point along one ray, while on an adjacent ray the same wave was identified as swell, the result of a small difference in wind speed or direction. The period and height of these two waves were usually very similar and so the combined wave height would be approximately 40% too large.

iv) Rapid Swell Decay

MetOc meteorologists using the wave model output have frequently noted situations in which the swell carried by the model was too low. Two factors are believed to account for this. The Bretschneider (1952) decay nomogram is less sophisticated than the generation nomogram in that fewer of the factors which influence wave decay are considered. In particular, the wind and wave fields present over the decay region are not taken into account. If winds, although not strong enough to support a generated sea, continue to have a component in the direction of the wave propagation then decay will take place more slowly than if the winds act to oppose the waves. The wave model does not recognize this effect and in many of the cases identified by MetOc as having swell waves which were too low, the winds were in fact "following" the waves.

The second factor accounting for the MetOc observation illustrates a tutorial application of the wave model. In several of the cases in which the wave model was critized for having too little swell, careful re-examination led to the conclusion that it was the subjective analysis and perhaps the reported data that were unreasonable. In most of these cases, swell was being identified both by the analyst and the reports, when in fact the phonomenon was wind generated and supported sea waves. The wave model was therefore useful in identifying a recurring weakness in the subjective analyses.

v) Underestimated Wave Regions

Contoured combined wave height charts from the wave model frequently depict relative minima in the height field which are exaggerated. That is, in observed regions of low wave heights, the model forecasts even lower heights. This problem is common near the centre of slow moving low pressure systems and just behind cold fronts. The problem arises because, in these regions of large cyclonic curvature in the isobaric field, there is often no wind component along any of the rays emanating from a target point. Effectively the wave model is not allowing for the directional dispersion of the waves. Presently the wind direction must be within 25° of ray direction in order to have any speed component at that point. Experiments to widen this threshold angle are now being planned in the hopes of reducing the problem of exaggerated wave height minima.

Case Study

The case study which follows was extracted from the 1984-85 operational test period for the purpose of illustrating the predictive skill, and some of the above-mentioned characteristic errors of the model.

The model run was made about 6 h after 0000Z 26 February 1985 (referred to as time-zero, T + 0). Analyzed wind fields from the preceding 72-h period were used to generate a T + 0 significant-wave prediction. Forecast wind fields from the CMC Spectral NWP model provided wind information for the subsequent 36-h period, i.e., out to 1200Z 27 February 1985 (T + 36). The case study discussion will begin with a description of the synoptic weather situation followed by a study of the wave model forecasts and the verifying analyses.

i) Synoptic Situation

Two surface weather analyses charts, one for T + 0 and the other for T + 36, appear in Figure 3 and will be used to illustrate the main synoptic features and their evolution. At T + 0 there was a quasi-stationary 982 mb low near the southern tip of Greenland.

Associated with this low, there was a strong northwesterly flow across the Davis Strait-Labrador Sea region. To the south, a developing, fast-moving storm centre was passing over the Grand Banks. At T + 0 the centre of the storm was 986 mb and it was moving eastward at 50 kts under the influence of a strong zonal upper flow. The historical position of the centre is shown at 6-h intervals.

In the next 12 h the storm deepened rapidly, with the central pressure dropping 21 mb between T + 0 and T + 12. Meanwhile it maintained its 50 kt eastward motion. After T + 12 the storm turned northward quite suddenly, slowed to about 20 kts, and further deepening was minimal. This progression can be seen from the historical positions given on the T + 36 analysis.

During this 36-h period of the storm's evolution the configuration of the pressure pattern also underwent changes. At T + 0, the low as elongated in the east-west direction resulting in a long west-southwest fetch in the warm sector. As the storm decelerated and turned northward, the east-west trough disappeared and a north-south trough became established. As a result, the southwesterly generation region was lost and a southerly generation region east of the low and a northwesterly one to the west became established.

ii) Wave Model Forecasts

The four wave model forecasts produced from the 00Z February 26 run (T + 0 through T + 36 at 12-h intervals) are presented in Figure 4. The verifying analyses (Figure 5) were prepared in real-time by MetOc meteorologists from the ship data which was available at the time.

At T + 0 the model predicted a combined-wave maximum of about 8 m south of Greenland resulting from the northwesterly flow across the Labrador Sea. During the subsequent 24 h this maximum changed very little as the generation region remained stationary; in the meantime 3 to 4 m of swell propagated south eastward from the generation region. The verifying analysis substantiates the prediction; however, it must be pointed out that no reports are available in the area.

Of greater interest is the wave pattern associated with the developing storm starting out south of Newfoundland. At T + 0, the wave model predicted up to 10 m seas associated with the long west-southwesterly fetch of the warm sector where winds of 45 kts were reported. The verifying analysis would suggest this maximum may have been overestimated, due no doubt to the stable flow. It can also be pointed out data is sparse at this time and the wave model prediction did not violate any of the available data.

As the storm moved eastward a new generation region developed, the result of the very strong southerly winds which evolved southeast of the low centre. On the wave model forecasts a new maximum can be seen to develop at T + 12 ahead of the primary maximum and, during the subsequent 24 h, this moved northward along the edge of the chart, while wave heights increased. The verifying analyses substantiate this evolution both in magnitude and location.

During this same period the warm sector southwesterly generation region was virtually eliminated as the storm which had been dominated by an east-west trough, adjusted to a north-south trough orientation. As a result the east-northeastward propagating wind waves generated by the model were largely converted to swell which travelled out of the model domain by T + 36.

Meanwhile, on the back side of the storm, at T + 0, a strong northwest flow generation region was just beginning to develop. By T + 12 a relative maximum "ridge" line is apparent on the wave model's combined wave prognosis and by T + 24 a separate 9 m maximum centre appears supported by 65 kt northwesterly winds. During the final 12-h period the northwest flow generation region associated with the storm aligns with the northwest flow originating from the Greenland low and a wave height maximum in excess of 10 m is predicted at T + 36.

Figure 3
CMC Surface Analyses
at the start (T + 0) and end (T + 36) of the forecast period

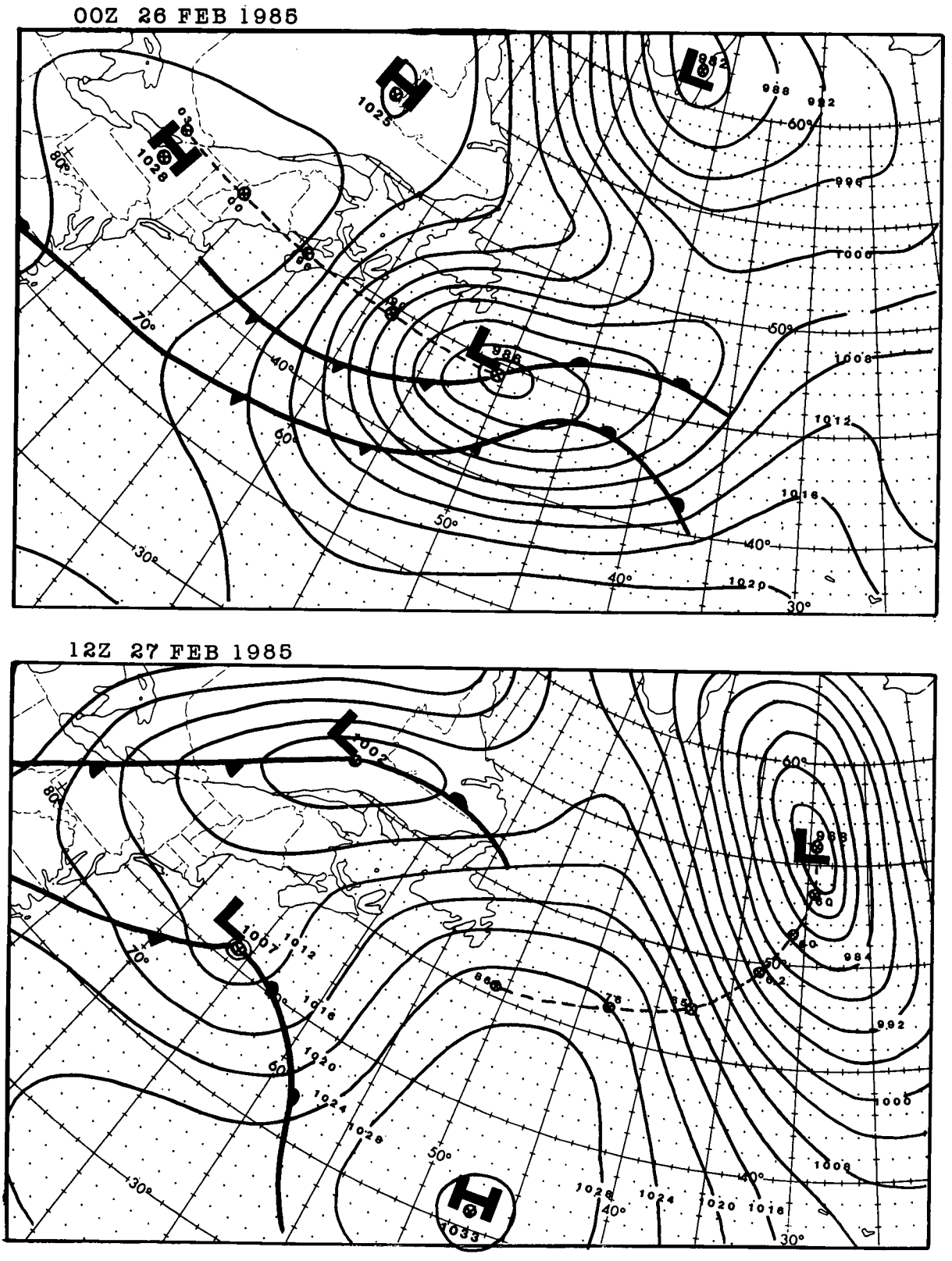

**Figure 4**
**Parametric Wave Model Prognoses**
**12-h intervals from T + 0 to T + 36**

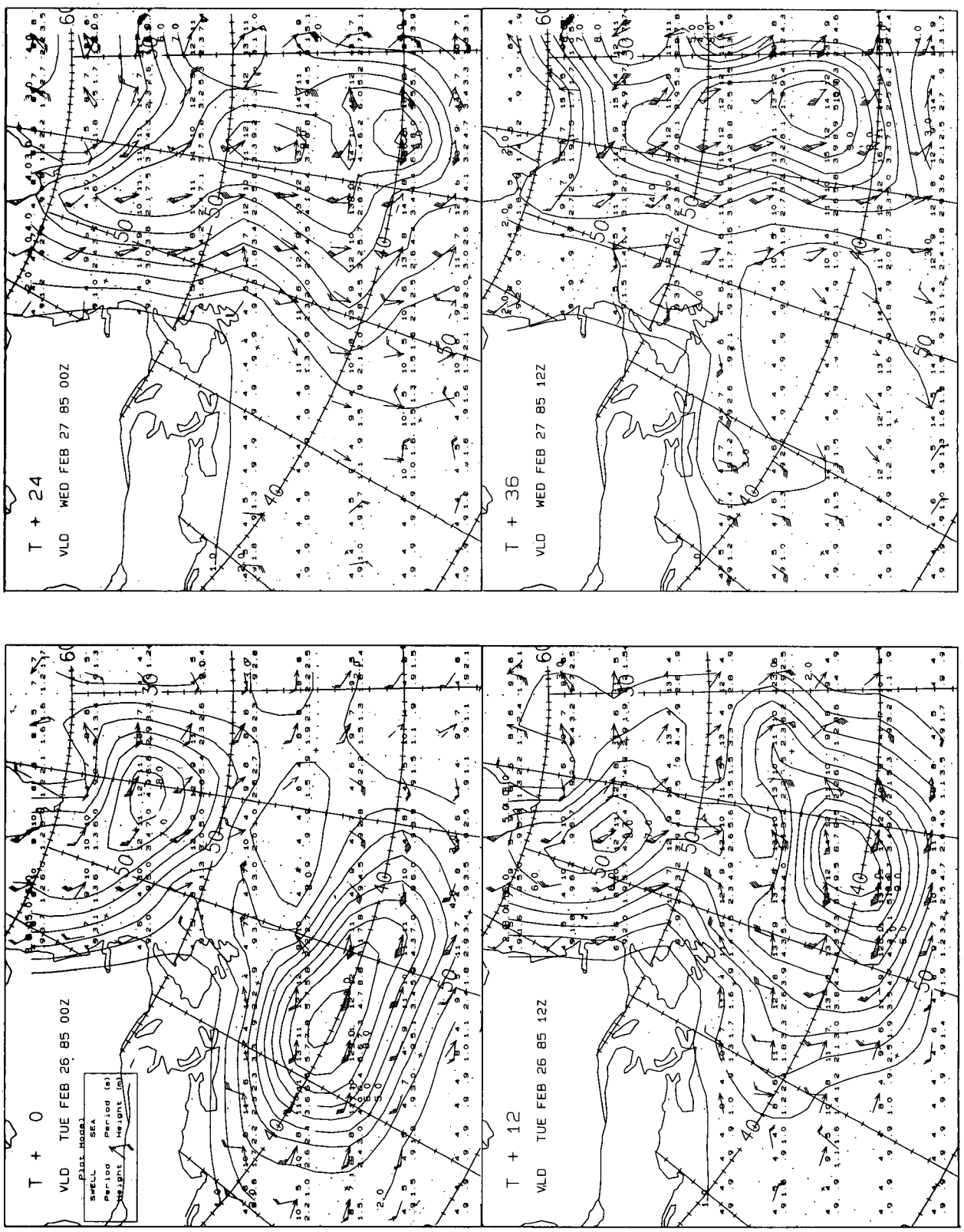

Figure 5
Verifying MetOc Subjective Wave Analyses
Times correspond to the Wave Model Prognoses shown in Figure 4.
Dots represent the location of wave observations.

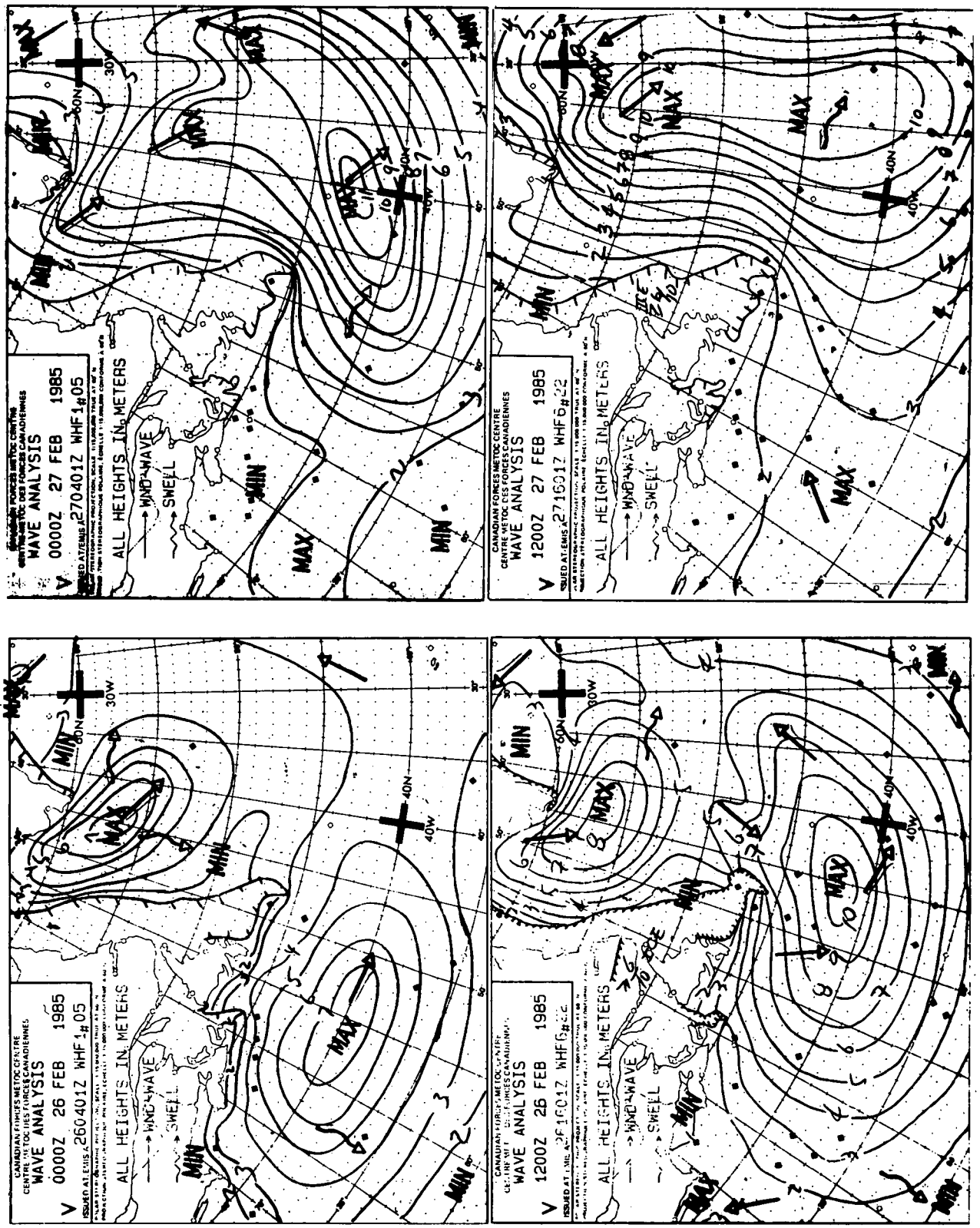

The final wave height pattern at T + 36 verifies extremely well on the MetOc analysis. The evolution, however, as indicated by the T + 12 and T + 24 charts, is somewhat different. While the model showed one maximum, associated with the westerlies, moving out of the region and a second maximum being generated in the northwesterlies, the analyses treat this as one maximum in which the direction of wave propagation gradually changed as the wind field became reoriented. The limited amount of ship data does not provide support to one scenario more than the other, but looking at the wave model in isolation, it can be said that it has produced a synoptically realistic wave forecast in a rapidly changing synoptic situation.

Summary

The parametric ocean-wave model described here essentially computerized the Bretschneider wave forecasting procedure which has long been the method used by operational meteorologists in Canada. By using a moving fetch procedure the model is able to integrate the effects on waves of wind conditions over a 3 to 5 day period; a much more thorough assimilation than can be achieved by manual techniques.

Evaluations have revealed that the system is able to produce realistic wave height forecasts which are consistent with the generating wind fields which are supplied. However, the wind fields do have certain inadequacies which impact on the wave model. On average, because the wind forecasts are not for the surface level, they are biased towards being too strong. This translates into an overforecasting bias on the part of the wave model. Specific overforecasting is most often observed in warm stable flow situations, such as in the warm sector of baroclinic developments, when the difference between the forecast wind field and the actual surface wind is a maximum. Winds, however, are sometimes underestimated, most noticeably in cold, unstable flows such as occur in Arctic outbreaks from the North American continent.

During the past year, new wind data have become available at CMC. They are now producing a "surface wind" which is obtained using an appropriate boundary layer longarithmic profile and is intended to be representative of the 10 m winds. They are also producing winds for the sigma = 0.998 level (approximately 17 m) using linear extrapolation from the spectral model's computational levels. During the Canadian Atlantic Storms Program (CASP) this latter wind was used to drive an experimental version of the parametric wave model, however, the results have yet to be assessed. Nevertheless we are confident that as new and improved wind inputs become available forecasts from the wave model will likewise show improvement.

While most of the wave system's forecast errors can be traced to inaccuracies in the wind input, there are several system deficiencies as well. On some occasions a single significant wave will be identified as both a wind wave and a swell wave resulting in an overestimated combined wave height. In other situations wave heights may be underestimated because the system fails to account adequately for the directional dispersion of waves. Further experimentation and tuning of model parameters should lead to improvements in these areas.

A final problem which is evident is the simple wave decay algorithm which the model uses. Because it fails to take into consideration the wind field influencing a decaying wave, it frequently decays swell waves too rapidly under a "following" wind situation.

**Acknowledgements**

The development of the Parametric Ocean-Wave System was made possible through funding from the Panel on Energy Research and Development (PERD). Much of the development work was done under contract by the MEP Company, Markham, Ontario.

The authors wish to thank the many meteorologists who have studied and evaluated the model during its development and since its implementation. Particular thanks go to Mr. Wayne Lumsden, Officer-in-Charge of the Canadian Forces MetOc Centre, Halifax. Finally, the authors are indebted to Mrs. Freda Edwards for typing the manuscript.

**References:**

Bretschneider, C.L., 1952: "The Generation and Decay of Wind Waves in Deep Water". Trans Amer. Geophys. Union, Vol. 33, No. 3.

Bretschneider, C.L., 1970: "Forecasting Relations for Wave Generation". Univ. of Hawaii, Look Lab, Vol. 1, No. 3.

Bretschneider, C.L., 1973: "Prediction of Waves and Currents". University of Hawaii, Look Lab, Vol. 3, No. 1.

Meteorological and Environmental Planning Ltd., 1982: "Development of an Ocean Wave Forecasting System". Prepared for Atmospheric Environment Services under DSS Contract 01SE.KM601-1-1174.

Morgan, M.R., 1971: "The Analysis and Forecasting of Sea and Swell Conditions in Deep Water". Atmos. Env. Svc., Tech. Memo 763.

Venkatesh, S. 1975: "Deep Water Wind-Wave Relationships - A Series Solution Approach". Environment Canada - AES, Canadian Meteorological Research Reports (CMRR 5/75).

Wilson, B.W., 1963: "Deep Water Wave Generation by Moving Wind Systems". Amer. Soc. Civ. Eng., Trans. Paper No. 3416, Vol. 128.

# A SENSITIVITY STUDY OF SPECTRAL WAVE GROWTH ALGORITHMS

V. J. Cardone and J. A. Greenwood

Oceanweather Inc., Cos Cob, Connecticut

## INTRODUCTION

There has been a significant increase in the implementation of discrete-type spectral wave prediction models both for operational wave forecasting systems and for hindcasting applications. Additional interest in wave models has been stimulated by the prospect of routine global remote sensing of marine surface winds and surface wave properties from microwave sensors to be mounted on future polar orbiting satellites.

Operational spectral wave prediction models appear to differ mostly in the formulation and behavior of the source term algorithms used to compute duration-wise spectral growth. Following the terminology adapted by the group of modellers who participated in the SWAMP (1985) wave model intercomparison program, source term treatments can generally be grouped into three classes or generations.

First-generation source term algorithms generally emphasize the atmospheric input source terms, neglect the nonlinear source term entirely, and treat the saturation range of the spectrum parametrically. Second-generation source term algorithms include an explicit source term to represent wave-wave interactions, but the parameterizations employed are valid only for restricted classes of spectral shapes. Recently, third-generation source term algorithms have been introduced which incorporate very accurate representations of the wave-wave interaction source term and explicit representations of the dissipation source term, and which model evolution of the rear face of the spectrum through local source term balancing. Third-generation algorithms are considerably more expensive computationally than first- or second-generation models, but may be implemented in practical models on supercomputers.

In this study, the behavior of a calibrated first-generation (ODGP) and second-generation (SAIL) source term algorithm is systematically compared with that of a tuned third-generation (Hasselmann et al., 1985) algorithm for both hypothetical and realistic wave regimes. The hypothetical cases consist of fetch- and duration-limited wave growth under homogenous winds (as in SWAMP test case 2), and adjustment of the wave spectrum following an abrupt wind shift (SWAMP test case 7). The realistic cases consist of hindcasts of several intense historical Gulf of Mexico hurricanes, in which the same wind field input for each hurricane was used for all wave models.

The results suggest that tuned variants of each model can provide very skillful hindcasts of integrated properties of the spectrum, such as significant wave height. The skill is so high in fact that residual errors in winds and sampling errors in wave measurements continue to obscure effects related to differences in model physics. We conclude with recommendations on the accuracies required of wind fields and wave measurements for meaningful validation of wave models.

## SOURCE TERM CLASSES

Following SWAMP (1985), spectral wave prediction models are differentiated by their source

term treatment. In so-called first-generation (1G) treatments, the input source term is generally represented as

$$S_{in} = A + BF$$

where A represents an excitation mechanism such as the model proposed by Phillips (1957) to describe resonance of surface wave components with atmospheric turbulent pressure fluctuations. BF represents energy transfer to waves through coupling of the mean shear flow in the marine atmospheric boundary layer to surface wave components. In 1G models, an equilibrium spectrum, usually the Pierson-Moskowitz (P-M), is used to limit growth of total wave energy and to shape the tail (high-frequency part) of the spectrum, thereby avoiding the need for a dissipation source term for wind waves. $S_{nl}$ either is not considered or plays a minor role relative to $S_{in}$. Some 1G models perform very well, as discussed below, because their linear and exponential growth rates are not taken directly from theory, but have been tuned based upon observations of net wave growth in simple duration- or fetch-limited situations, or upon trial hindcasts of more complicated wave regimes.

In second-generation (2G) source term treatments, the nonlinear source term plays the dominant role in the evolution of the spectrum because it greatly exceeds in magnitude $S_{in}$ in the forward face of the spectrum. Since a rigorous representation of $S_{nl}$ is not possible in a discrete model at current computer speeds, the $S_{nl}$ source term in 2G models is described in terms of a few parameters, and is valid only for a restricted class of spectral shapes. Most 2G models have retained the simplified 1G model treatment of the high-frequency part of the spectrum in terms of a saturation range rather than attempt an explicit balancing of source terms. The $S_{in}$ term in 2G models is usually taken from the Bight of Abaco field experiment (Snyder et al., 1981), which provides growth rates about a factor of 5 smaller than those used in 1G models.

As demonstrated in SWAMP, 2G models have not provided significant improvements over well-tuned 1G models, and this has led to the development of a third-generation (3G) model (Hasselmann et al., 1987). The 3G model retains an empirical wind input source function and a dissipation source function based upon a general white-capping dissipation model (Hasselmann, 1974). The nonlinear source term is specified through the discrete interaction operator parameterization (Hasselmann et al., 1985), which contains the same number of degrees of freedom as used to specify the discretized spectrum, and is structured in the same way as the exact Boltzman integral. The computational efficiency of this form over the full integral is achieved by restricting the integration to only two elementary interaction configurations, as determined from a large number of tests with the exact integral, to describe the essential features of $S_{nl}$.

## WAVE MODELS

The basic structure of the representatives of each model class compared in this study is given schematically in Table 1. The ODGP (1G) model was first described by Cardone et al. (1976) and more recently by MacLaren Plansearch (1985 and 1986). The ODGP model has been tested against a broad range of wave regimes and has undergone few changes over the last decade. The only substantive variant of ODGP is ODGP2, in which the equilibrium range obeys an $f^{-5}$ law uniformly, with the equilibrium range coefficient, $\alpha$, dependent upon non-dimensional total energy, $\epsilon$, following Resio's (1981) correlation. ODGP2 provides virtually the same skill as ODGP in hindcast of storm peak sea states. However, the equilibrium range relaxation allowed by the $\alpha - \epsilon$ correlation in ODGP2 provides somewhat improved results during storm decay.

The SAIL2 (2G) model source term treatment was described by Greenwood et al. (1985). The currently operational version was tuned to provide essentially the same growth rate as ODGP in pure duration-limited growth under the action of winds of constant speed and constant directional veering (assumed slew rate of 10 degrees per hour). The algorithm was tuned through the mechanism used to model the transition between pure wave growth and the imposed limit to growth.

The source term treatment of the 3G-WAM model is described by Hasselmann et al. (1987). The model tuning is described by Komen et al. (1984). In practical applications, the directional resolution of the discretized spectrum has been limited to 12 directions, while

the 1G and 2G models use 24 directions. The WAM model has undergone more limited application than 1G and 2G models. A review of recent applications is given in this volume by Komen and Zambresky (1986).

## DURATION GROWTH

Figure 1 (a, b) compares the duration-growth of total energy and peak frequency in the format used to display the SWAMP model results. The spread of growth curves exhibited in SWAMP is shown on the plots. The duration growth curves (of energy) of ODGP2, SAIL2, and EXACT-NL (which follows 3G-WAM closely up to the P-M limit) are seen to lie in the middle of the range of SWAMP results, close to the curves of the SAIL and GONO models (not shown).

## FETCH GROWTH

Figure 2 (a - d) compares the fetch-wise growth of non-dimensional total variance (scaled by friction velocity), scaled peak frequency, peak enhancement factor and equilibrium range level ($\alpha$) for the three models (20 m/sec wind speed). Two sets of curves are given for the 3G model (from Hasselmann et al., 1985), one based upon the exact nonlinear interaction source term and the second based upon the discrete-interaction approximation to the nonlinear source term.

The fetch-wise growth of ODGP2 indicates lower energy levels than 3G-WAM at all fetches calculated (the ODGP2 and SAIL2 fetch runs were restricted to 1200 km), and this energy shift appears to be consistent with the reduced equilibrium range level in ODGP2 relative to 3G-WAM. The variations of peak enhancement and non-dimensional peak frequency with non-dimensional fetch for ODGP2 are remarkably close to those of the 3G-WAM.

The fetch-wise growth of energy for SAIL2 is faster than that of 3G-WAM despite the lower energy in the equilibrium range. The faster migration of peak frequency of SAIL2 relative to 3G-WAM is apparently responsible. The peak enhancement of SAIL2 fetch-limited spectra is comparable to that of 3G-WAM.

## SWAMP CASE 7A

The characteristics of wave growth in a turning wind are probably more relevant to the behavior of wave models in most naturally occurring wave regimes. SWAMP case 7 was designed to examine the response of the two-dimensional wave spectrum following a sudden 90-degree wind shift. In subcase 7A, the wind shift was imposed after duration growth in a stationary wind had shifted the peak frequency to exactly twice the fully developed peak frequency. In subcase 7B, the wind shift was imposed at the time of full development.

Figure 3 compares the two-dimensional spectrum (energy density is non-dimensionalized by the peak density of the wind sea at the wind shift; frequency is non-dimensionalized by the peak frequency of the wind sea at the wind shift) for the ODGP2, SAIL2, EXACT-NL and 3G-WAM models at 6 hours after the wind shift for SWAMP case 7A (wind speed 20 m/sec). The ODGP2 and SAIL2 spectra resemble the 3G-WAM spectrum more so than the EXACT-NL, while differences in detail between ODGP2, SAIL2, and 3G-WAM tend to be comparable to the differences between the EXACT-NL spectrum and the 3G-WAM spectrum.

## HURRICANE CASES

The 3G-WAM has recently been tested against three historical Gulf of Mexico hurricanes (Hasselmann et al., 1987). The wind fields used for these tests were the same as had been used previously to drive the ODGP and SAIL2 models in some of the same storms. Table 2 gives all possible comparisons of peak significant wave height at available measurement sites.

All models were applied to hurricane Camille, a storm which was important in the development and tuning of the ODGP model (and hence of SAIL2). All models evidently provide skillful hindcasts of peak sea states at the deep-water measurement sites. Time histories of measured and hindcast significant wave height at these sites for the recent 3G-WAM run and the original ODGP run (Cardone et al., 1976) are compared in Figures 4 and 5. It is interesting to note the resemblance between models of the residual differences

between hindcast and measured time series at both sites, strongly suggesting that some factor besides model physics is the principal limit of hindcast skill. That factor is most likely wind field errors. The wind fields used probably fail to resolve small-scale spatial features and to adequately resolve temporal variability (Camille's intensity was modelled as steady in the 36-hour period before landfall). Frequency spectra associated with peak sea states at stations 1 and 2 were very similar for all model runs (not shown).

## SUMMARY HINDCAST SKILL

Table 3 provides a summary of the most readily available statistical measures of hindcast skill in specification of storm peak significant wave heights for the three models under consideration. All statistics reflect a mix of tropical and extratropical storms. The SAIL2 and WAM statistics include also hindcasts of a group of recent North Sea cyclones (WHIST) evaluated at deep-water measurement locations. For most of the hindcasts which formed this data base, wind fields were prepared by application of detailed post-analysis of historical data, often with considerable manual override of objective analysis methods. Under these circumstances, the indicated members of each wave model class are able to provide skillful hindcasts of peak storm sea states.

## CONCLUSIONS

On the basis of the results of this study and our broad range of experience with 1G and 2G models considered, we have formed the following conclusions and recommendations.

1. The skill of the 3G-WAM wave model in specifying integrated properties of the spectrum and spectral shape, in wave regimes associated with typical tropical and extratropical storms, has been demonstrated to be at least comparable to that of finely tuned 1G and 2G models. 3G-WAM therefore may be used in practical applications if computing resources allow.

2. Finely tuned 1G and 2G models and 3G-WAM, when adapted with comparable spatial and spectral resolution and when driven by high-quality historical wind fields, provide specification of peak significant wave height in Northern Hemisphere tropical and extratropical storms with mean errors of about 0.5 m and scatter index of 10% - 15%. There is evidence that in these situations the residual differences between measurements and hindcasts is caused by wind field deficiencies and variability in wave measurements derived from records of typical length.

3. It follows from conclusion 2 that the results of many studies carried out with tuned 1G and 2G models remain generally valid. Most such studies need not be repeated with 3G-WAM. Examples include the ODGP hindcast study of deep-water extreme wave criteria associated with Gulf of Mexico hurricanes, the recently conducted extreme wave climate studies for Hibernia and Venture, and the 28-year long-term wave climate study for the Norwegian Sea (Eide et al., 1985) carried out with SAIL2. In addition, 1G and 2G models which have demonstrated considerable skill in real-time forecasting applications may continue to be used.

4. 3G-WAM provides the most suitable model context for further investigation and refinement of source term specification. Areas where better understanding of growth-dissipative processes could lead to model improvement include: $S_{in}$ - clarification of the differences between wind speed scaling and friction velocity scaling; the effects, if any, of mesoscale gustiness, atmospheric stability, stage of wave development and swell on the atmospheric input to wind-waves; $S_{ds}$ - a more quantitative theory is needed in order to remove one of the last areas of empirical tuning from 3G-WAM; $S_{nl}$ - small differences between the exact calculation and the discrete-interaction approximation remain and may affect model performance in some situations.

5. There remain some naturally occurring wave regimes where differences between tuned 1G, 2G, and 3G wave models may be rather larger than suggested by validation studies reported thus far. These include sea states excited by tropical cyclones which propagate at speeds greater than about 15 m/sec; seas excited by subtropical monsoonal wind regimes (e. g., South China Sea, Indian Ocean); rare occurrences of nearly fully-developed seas at wind speeds greater than 20 m/sec; and most shallow-water wave

regimes. Except in such regimes, further validation studies can reveal little about the relative advantages of model nuances or physics unless wind fields and wave measurements satisfy the following criteria:

| Wind Field Errors | Mean | Scatter (Index) |
|---|---|---|
| Wind speed | +/- 1 m/sec | 10% |
| Wind direction | +/- 5° | 10° ($\sigma$) |
| Significant wave height | +/- .25 m | 5% |
| Peak frequency | +/- .5 sec | 5% |
| Wave direction | +/- 5° | 10° ($\sigma$) |

REFERENCES


Cardone, V. J., W. J. Pierson, and E. G. Ward. 1976. Hindcasting the directional spectrum of hurricane generated waves. J. of Petrol. Tech., 28, 385 - 394.

Eide, L. I., M. Reistad, and J. Guddal. 1985. Data base of computed wind and wave parameters for the North Sea, the Norwegian Sea and the Barents Sea, every six hours for the years 1955 - 1981 (in Norwegian). Det Norske Meteorologiske Institutt, Oslo.

Greenwood, J. A., V. J. Cardone, and L. M. Lawson. 1985. Intercomparison test version of the SAIL wave model. In Ocean Wave Modeling, The SWAMP Group. Plenum Press, New York, 221 - 233.

Hasselmann, K. 1974. On the spectral dissipation of ocean waves due to white capping. Bound.-Layer Meteor., 6, 107 - 127.

Hasselmann, S., K. Hasselmann, J. H. Allender, and T. P. Barnett. 1985. Computations and parameterizations of the nonlinear energy transfer in a gravity-wave spectrum; Part II: Parameterizations of the nonlinear energy transfer for application in wave models. J. of Phys. Oceanog., 15, 1378 - 1391.

Hasselmann, S., K. Hasselmann, P. A. E. M. Janssen, G. J. Komen, L. Bertotti, A. Guillaume, V. J. Cardone, J. A. Greenwood, M. Reistad, and J. A. Ewing. 1987. The WAM Model; a third-generation ocean wave prediction model. In preparation.

Komen, G. J. and L. Zambresky. 1986. A third-generation ocean wave model. Presented at International Workshop on Wave Hindcasting and Forecasting, September 23 - 26, Halifax, Nova Scotia.

Komen, G. J., S. Hasselmann, and K. Hasselmann. 1984. On the existence of a fully developed wind-sea spectrum. J. of Phys. Oceanog., 14, 1271 - 1285.

MacLaren Plansearch Ltd. 1985. Evaluation of the Spectral Ocean Wave Model (SOWM) for supporting real-time wave forecasting in the Canadian east coast offshore. Report submitted to the Atmospheric Environment Service.

MacLaren Plansearch Ltd. 1986. CASP wave forecasting operational test. Report prepared for the Environmental Studies Revolving Funds (ESRF) under Contract #702-30-08. In press.

Phillips, O. M. 1957. On the generation of waves by turbulent wind. J. Fluid Mech., 2, 417 - 445.

Resio, D. T. 1981. The estimation of wind-wave generation in a discrete spectral model. J. of Phys. Oceanog., 11, 510 - 525.

Snyder, R. L., R. W. Dobson, J. A. Elliot, and R. B. Long. 1981. Array measurements of atmospheric pressure fluctuations above surface gravity waves. J. Fluid Mech., 102, 1 - 59.

SWAMP (Sea Wave Modeling Project) Group, 24 authors. 1985. Ocean Wave Modeling. Plenum Press, New York, 256 pp.

Table 1

STRUCTURE OF SPECTRAL MODELS USED IN COMPARISON STUDY

| MODEL | Source $S_{in}$ $\lvert\theta\omega\rvert\leq 90°$ | Source $S_{nl}$ | Source $S_{ds}$ $90<\lvert\theta\omega\rvert<180$ | Saturation rear face | Saturation forward face | Direc. Relax | Propagation | Discretization |
|---|---|---|---|---|---|---|---|---|
| 1G ODGP | A + BF | - | $-Df^4F$ | 1: $\alpha g u_* f^{-4}$ | P-M | Explicit | Interpolatory | 15f x 24d |
| | | | | 2: $\alpha(\epsilon)g^2f^{-5}$ | P-M | | | |
| 2G SAIL2 | B · F | JONSWAP | | $\alpha(\epsilon)g^2f^{-5}$ | Mod Ochi | Explicit | Interpolatory | 15f x 24d |
| 3G WAM | B · F | DIA | | Implicit | P-M | Implicit | Finite Difference | 26f x 12d |

Table 2

COMPARISONS OF PEAK SIGNIFICANT WAVE HEIGHT
IN HINDCASTS WITH IDENTICAL WIND INPUT

| STORM | SITE | MEASURED (M) | HINDCAST ODGP | HINDCAST SAIL | HINDCAST WAM |
|---|---|---|---|---|---|
| CAMILLE | ODGP STN1 | 13.6 | 13.2 | 13.3 | 13.5 |
| | ODGP STN2 | 7.9 | 8.2 | 9.6 | 9.0 |
| ANITA | EB04 | 5.4 | - | 4.7 | 4.8 |
| | EB71 | 6.6 | - | 7.6 | 7.7 |
| | EI133 | 6.0 | - | 5.2 | 5.1 |
| FREDERICK | 42003 | 8.9 | 9.3 | - | 9.3 |

Table 3

PEAK HS HINDCAST ERRORS REPORTED IN LARGER DATA SETS
WITH 1G, 2G, AND 3G WAM MODELS

| | 1G ALL CASES | 2G ALL CASES | 3G HURR. | 3G WHIST |
|---|---|---|---|---|
| N | 60 | 23 | 7 | 52 |
| MEAN DIFFERENCE (M) | .1 | .7 | .1 | .3 |
| SCATTER INDEX | 12% | 15% | 9% | 15% |

ODGP 60 COMPARISONS IN 19 STORMS (REECE AND CARDONE, 1982)
SAIL 23 COMPARISONS IN 3 HURRICANES, 1 GRAND BANKS, 5 WHIST STORMS
WAM 59 COMPARISONS IN 3 HURRICANES, 6 WHIST STORMS

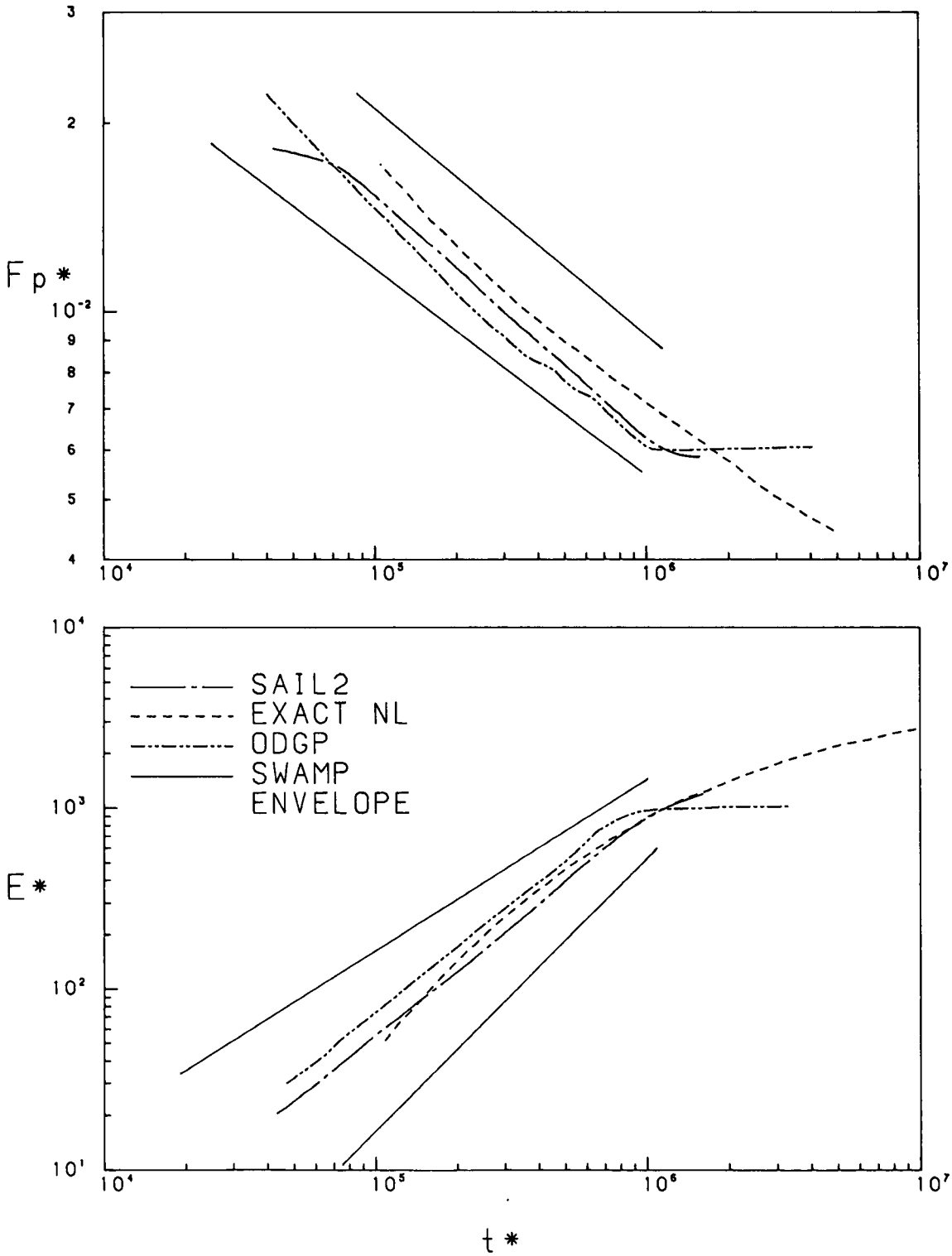


Figure 1. Non-dimensional duration-limited growth curves for total energy E*, and peak frequency F* (non-dimensionalization by friction velocity) for indicated models (EXACT-NL from SWAMP, 1985) and envelope of curves for all SWAMP models.

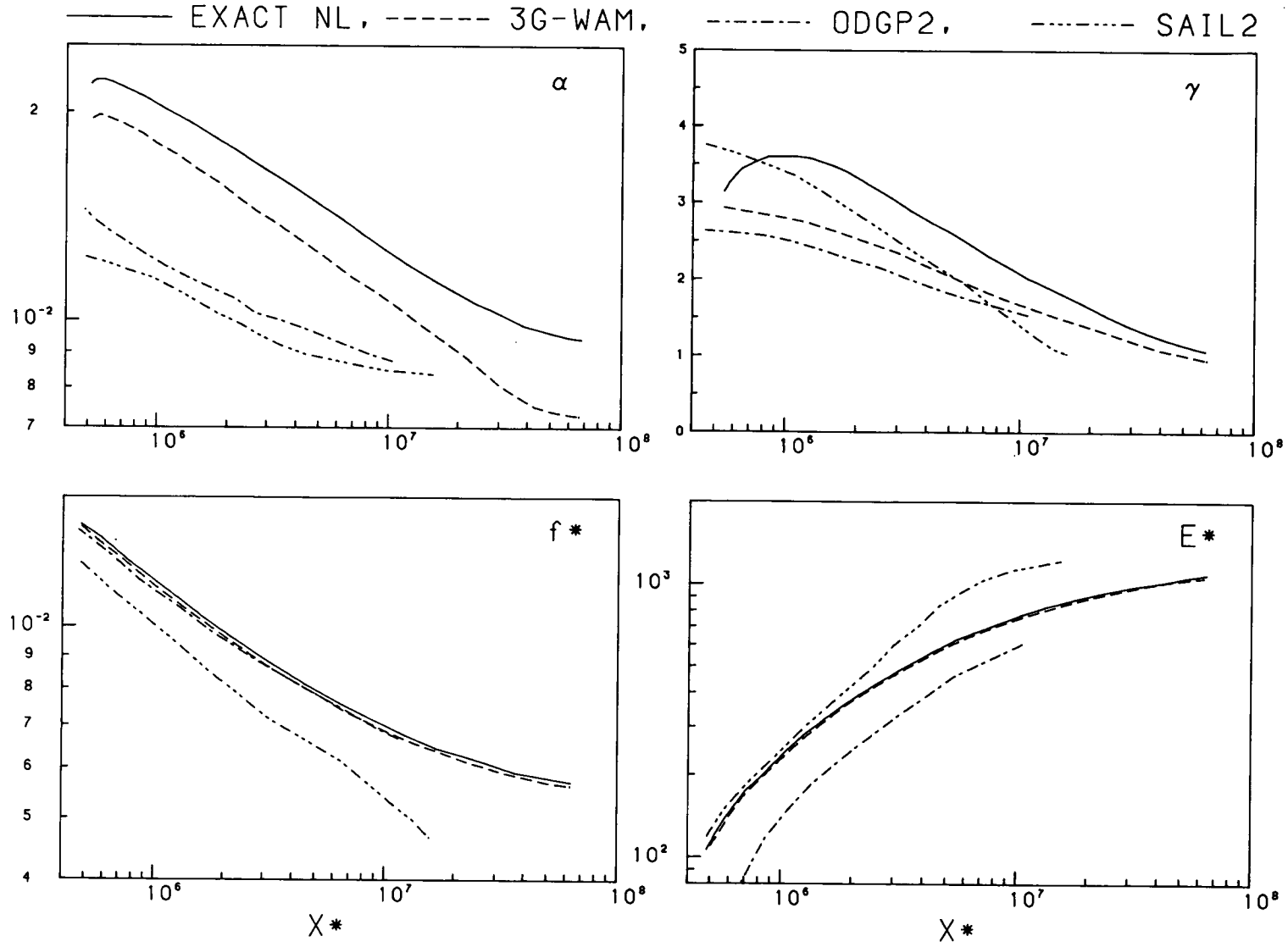


Figure 2. Comparison of fetch-growth curves for spectral variable non-dimensional total energy, peak frequency, peak enhancement and equilibrium range coefficient. Results for EXACT-NL and discrete-interaction approximations from Hasselmann et al. (1985).

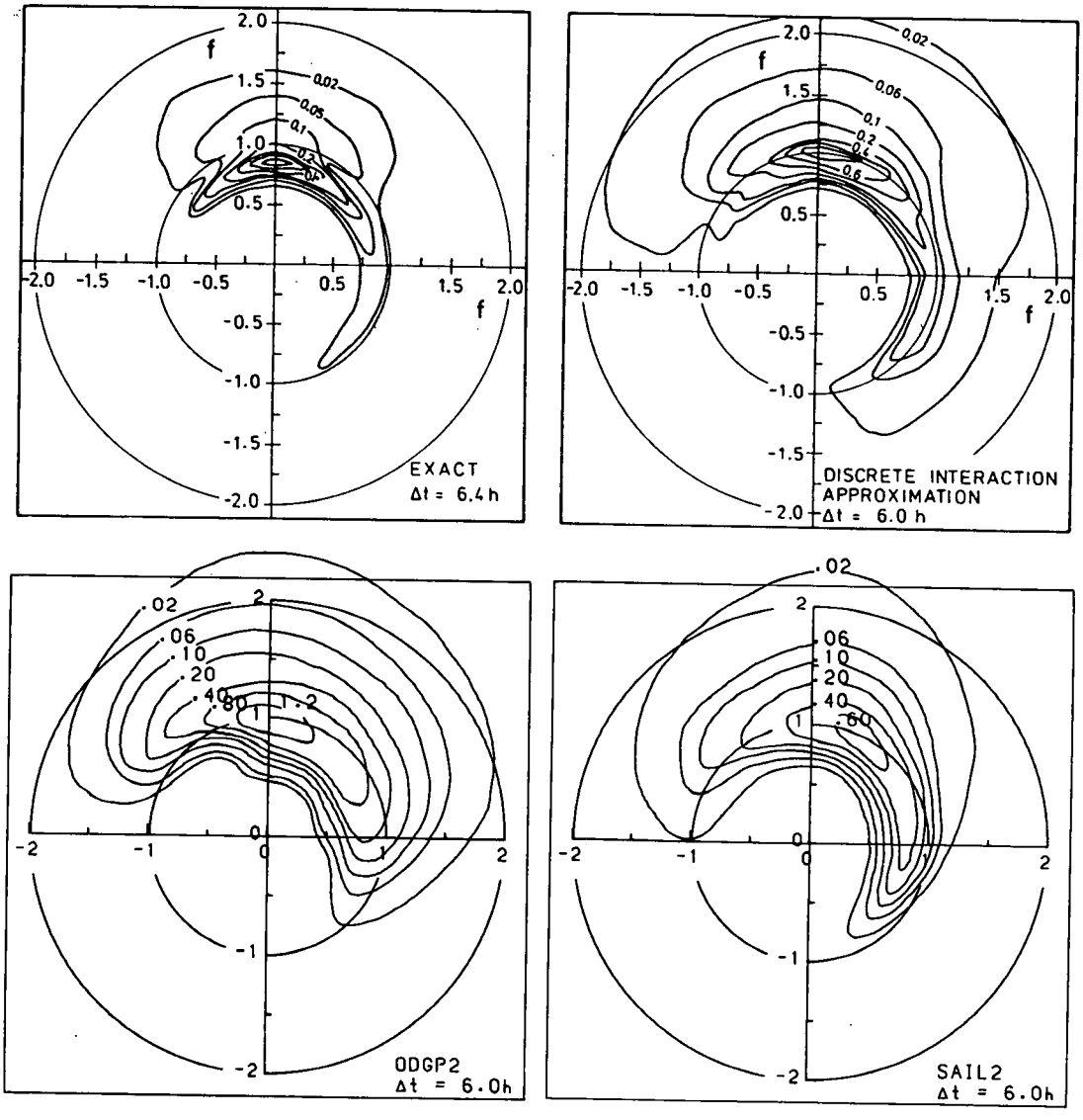


Figure 3. Response of two-dimensional wave sprectrum to sudden 90-degree change in wind direction at 6 hours after wind shift from westerly to southerly (direction toward which) as in SWAMP Case 7A. Results for EXACT-NL model and describe interaction approximation (3G-WAM) from Hasselmann et al. (1985).

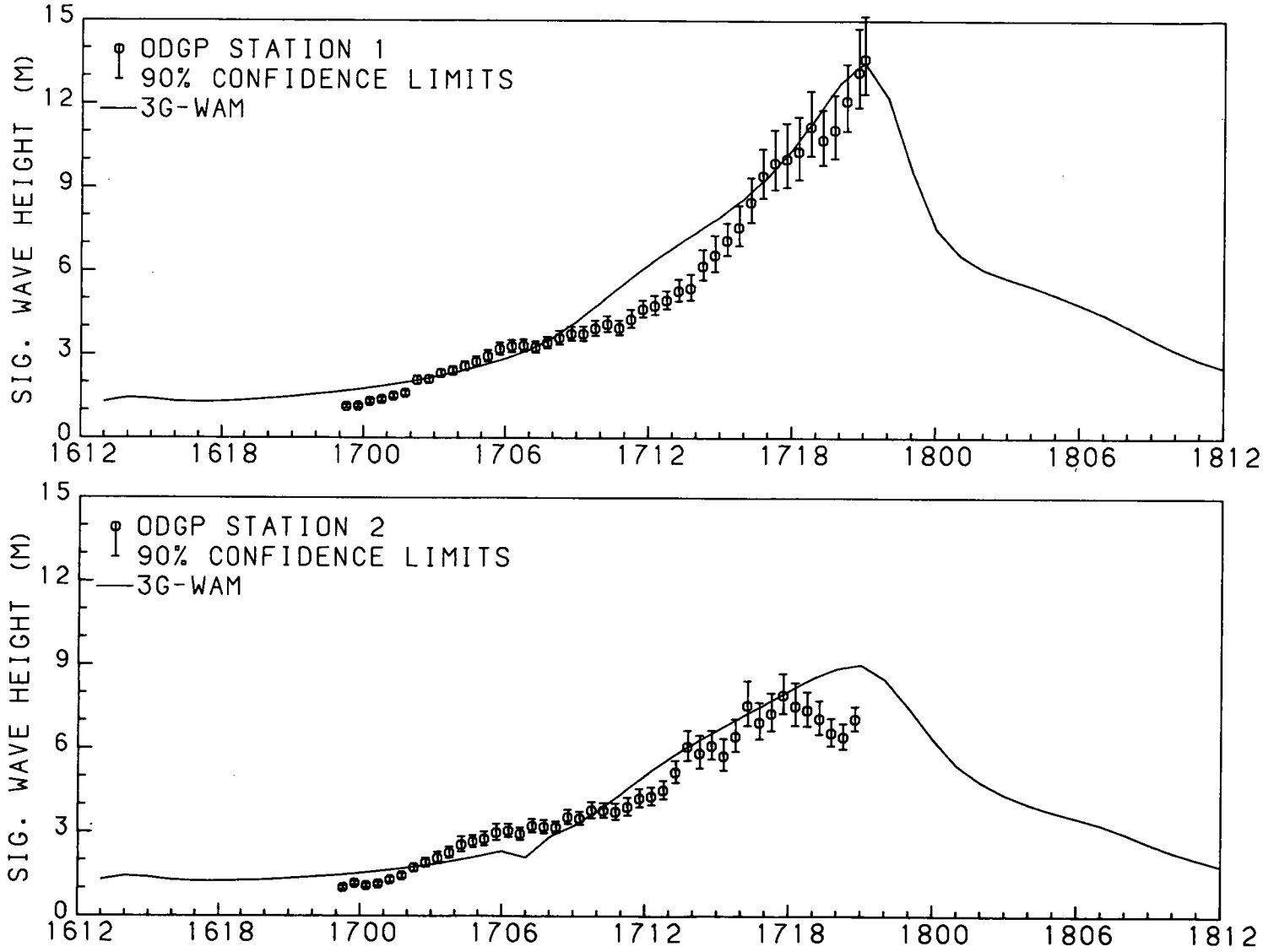


Figure 4. Comparisons of measured and 3G-WAM model hindcast of significant wave height at deep-water measurement sites in hurricane Camille (after Hasselmann et al., 1987).

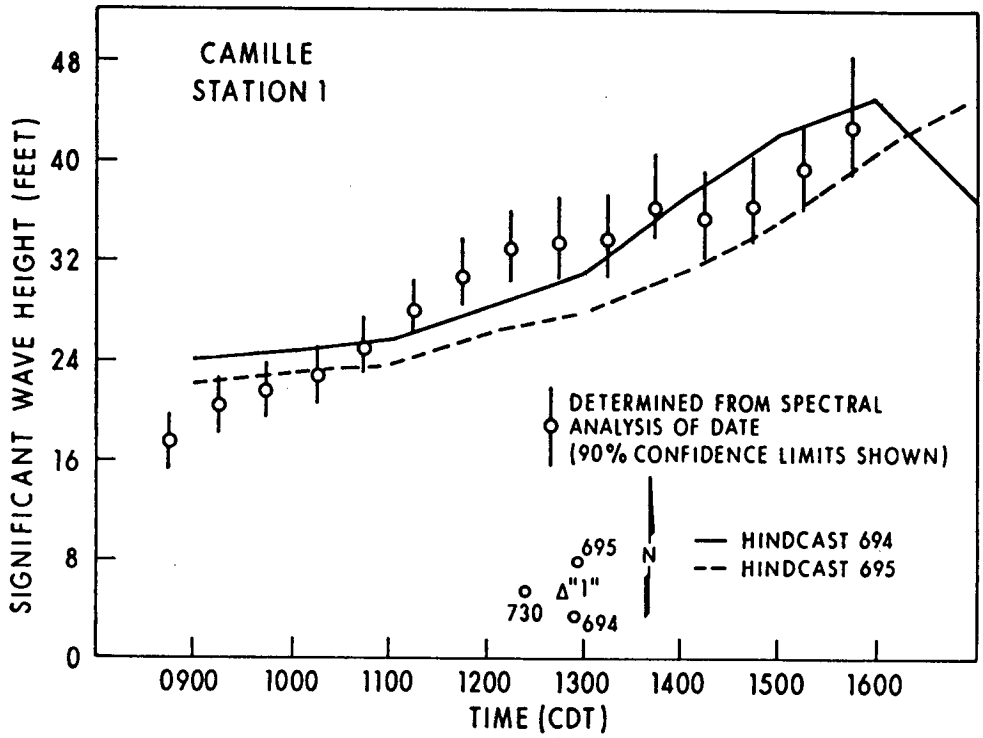


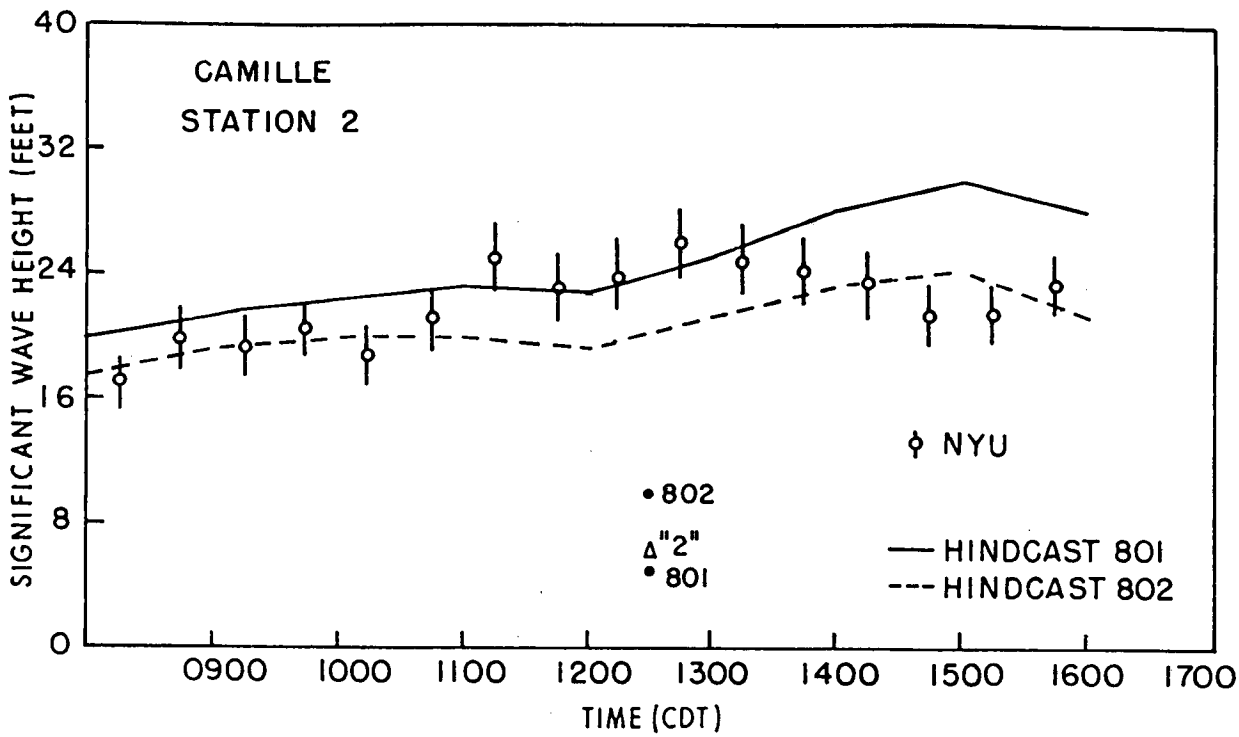


Figure 5. Comparison of measured and ODGP model hindcast of significant wave height at deep-water measurement sites in hurricane Camille (after Cardone et al., 1976).

# OCEAN WIND AND WAVE MODEL COMPARISION WITH GEOSAT SATELLITE DATA

R.L. Pickett[1], D.A. Burns[1], R.D. Broome[2]

[1]Naval Ocean Research and Development Activity, NSTL Station, MS 39529 USA
[2]Planning Systems, Inc., 115 Christian Lane, Slidell, LA 70458 USA

ABSTRACT

By comparing operational wind and wave models to GEOSAT satellite data, we found that on 10 March 1986, Canada had the best skill score for a regional wind analysis, NOAA had the best score for a global wind analysis, the Netherlands had the best score for a regional wave analysis, and the U.S. Navy had the best score for a global wave analysis.

## I. INTRODUCTION

The U.S. Navy is evaluating operational wind and wave models to determine if present Navy models need improvements. The evaluation program consists of intercomparing models. The technique is similar to that reported by Cavaleri et al, (1982) and Resio and Vincent (1982), except they used hypothetical wind and wave fields. By contrast, we used observed wind and wave fields recorded by the GEOSAT satellite.

For this evaluation, we compared 6 operational wind and 8 operational wave model analyses to GEOSAT satellite observations for one day (10 March 1986). We tested wind model analysis from Canada, the Netherlands, the Federal Republic of Germany, Japan, the U.S. Navy, and the U.S. National Oceanic and Atmospheric Administration (NOAA). We tested wave model analysis from Canada (both military and civilian) the Netherlands, the Federal Republic of Germany, Japan, the U.S. Navy, NOAA, and a private U.S. company (Offshore and Coastal Technology).

## II. METHOD

### A. Model Data

To obtain the above model output, we requested all participants send us their analyzed (not forecasted) wind and wave fields for 0000, 0600, 1200, 1800, and 2400 GMT on 10 March 1986. We received the results in a variety of forms, such as magnetic tape, gridded charts, and contoured charts. Next, we saved and edited the GEOSAT wind and wave fields. Finally, we matched the model and GEOSAT fields by computer, if we received magnetic tapes, or by hand, if we received charts.

### B. GEOSAT Data

The GEOSAT satellite was launched in March 1985, and uses a RADAR altimeter to estimate wind speeds and wave heights. The altimeter is a narrow-beam, downward-looking, short-pulse RADAR that bounces signals off the ocean's surface. Since the signals are stored aboard the satellite until it passes over the ground station, wind and wave data are unavailable for 3 to 16 hours after they are sampled. Table 1 summarizes the satellite's characteristics (from Kilgus et al.,1984).

Table 1. GEOSAT satellite characteristics.

| | | |
|---|---|---|
| ORBIT: | ALTITUDE | 800 KM |
| | LATITUDE INCLINATION | 108 DEG |
| | PERIOD | 101 MIN |
| | GROUND SPEED | 6.6 KM/S |
| | REPEAT CYCLE | 3 DAYS |
| RADAR: | FREQUENCY | 13.5 GHZ |
| | MAX. OCEAN SPOT SIZE | 25 KM |
| | EFFECTIVE SPOT SIZE | 2 TO 7 KM |

Since the satellite is in near polar orbit, and the reflection spot is small, wind and wave coverage consists of narrow, north and south tracks. These tracks cover the earth at about 3000 km spacing near the equator, and converge near the poles (see Figure 1).

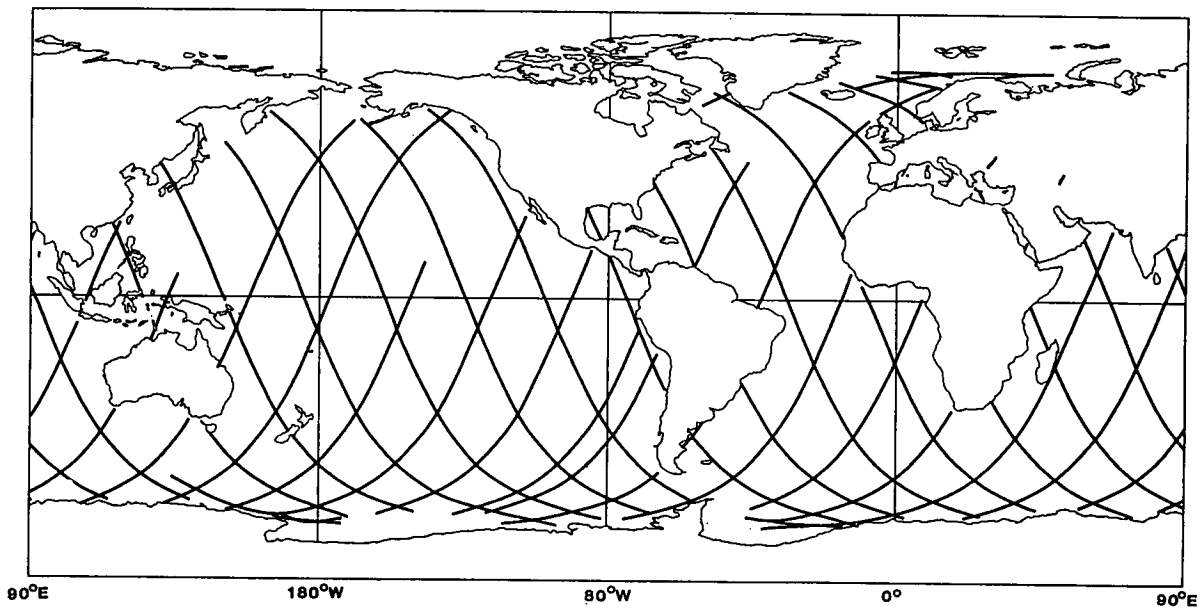


Figure 1. Track of GEOSAT satellite on ocean's surface during test day of 10 March 1986. Gaps result from editing.

Significant wave heights are estimated along these tracks by measuring the leading-edge slope of the returning pulse. High seas spread the return pulse, and hence reduce its slope.

Wind speeds are estimated indirectly. A surface reflection coefficient is calculated from the return pulse magnitude. The pulse is absorbed at the ocean surface by capillary waves and foam, and these factors depend on wind speed. Ground processing is then used to relate the reflection coefficient to surface wind speed.

The satellite was designed to measure significant wave heights within 10% (waves greater than 5 m), or 0.5 m (waves smaller than 5 m), and to estimate wind speeds within 1.8 m/s (Kilgus et al.,1984). To check this accuracy, we first edited the GEOSAT data (to eliminate transmission errors, islands, and ice), and then matched times and locations to the NOAA buoy network. Figures 2 and 3 compare GEOSAT wind speeds and wave heights to those recorded by the NOAA buoys (within 30 min and 50 km) during our test. The mean buoy-GEOSAT wind differences was -0.8 m/s, and the standard deviation of the difference was 2.2 m/s. The mean wave difference was 0.1 m and the standard deviation was 0.4 m.

There are several sources for the scatter in Figures 2 and 3. For example, buoys average over time (8 min for wind, 20 min for waves), whereas the satellite averages over space (maximum of 25 km, but most of the return comes from the center 2 to 7 km). Also, the satellite sensor errors (1.8 m/s wind, 0.5 m wave height) shown as shaded areas on the plots are independent of the buoy sensor errors (1 m/s wind, 0.5 m wave height). All these sources of scatter are mixed in Figures 2 and 3. In spite of these error sources, however, these few buoy-satellite comparisons suggest that GEOSAT is useful for model verification.

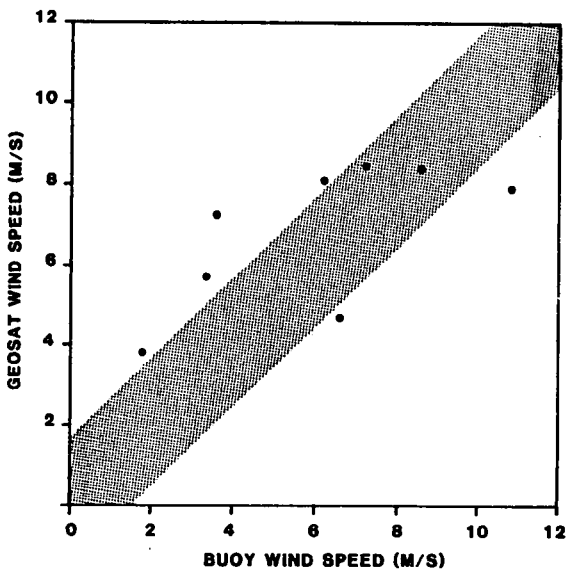


**Figure 2. Comparison of wind speeds recorded by NOAA buoys and GEOSAT satellite. Satellite observations were within 30 min and 25 km of matching buoy observation. Shaded band is satellite design accuracy.**

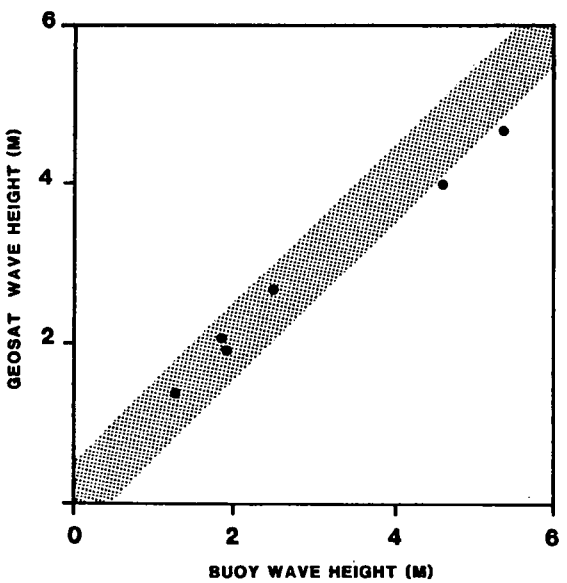


**Figure 3. Comparison of significant wave heights recorded by NOAA buoys and GEOSAT satellite. Satellite observations were within 30 min and 25 km of matching buoy observation. Shaded band is satellite design accuracy.**

C. Comparison Data.

To use the above satellite data, we selected those wind and wave points on the 10 March 1986 GEOSAT tracks that were within 1.5 hours of model analysis times. Next, if we were provided magnetic tapes, we computer scanned all model values for GEOSAT values that were within 50 km. If we were provided contour charts, the process was more subjective. We plotted GEOSAT tracks on the model output and read off overlapping points.

The matched sets of data pairs from the satellite and models were then arranged in tables (see sample in Table 2), by separating them into three classes: light, moderate, and heavy. Class boundaries were selected so that nearly equal numbers of satellite observations occurred in each class. This was done to eliminate any advantage of a model forecasting the most probable class.

Comparing a class row and column sum in these tables, shows if that class occurred as often in the model as it was observed. A column sum that is larger than the row sum for the same class, indicates the model overpredicted that class. The opposite is also true: a smaller column sum, relative to a row sum, means the model underpredicted that class (Panofsky and Brier, 1965).

Table 2. Distribution of pairs of U.S. Navy model (wind model at top, wave model at bottom) and GEOSAT satellite data for 10 March 1986. Data pairs are within 1.5 hours and 50 km of each other. Table values are in percent.

**NAVY GLOBAL WIND MODEL**

| GEOSAT | LIGHT | MEDIUM | HEAVY | SUM |
|---|---|---|---|---|
| LIGHT | 36 | 7 | 4 | 47 |
| MEDIUM | 14 | 7 | 14 | 35 |
| HEAVY | 3 | 0 | 15 | 18 |
| SUM | 53 | 14 | 33 | 100 |

SKILL SCORE = .35

NUMBER OF OBSERVATIONS = 138

LIGHT=0 to 6M/S MEDIUM>6 to 10M/S HEAVY>10M/S

**NAVY GLOBAL WAVE MODEL**

| GEOSAT | LIGHT | MEDIUM | HEAVY | SUM |
|---|---|---|---|---|
| LIGHT | 27 | 11 | 1 | 39 |
| MEDIUM | 12 | 17 | 7 | 36 |
| HEAVY | 2 | 2 | 21 | 25 |
| SUM | 41 | 30 | 29 | 100 |

SKILL SCORE = .48

NUMBER OF OBSERVATIONS = 243

LIGHT=0 to 2M MEDIUM>2 to 3M HEAVY>3M

An overall skill score was also calculated from the tables. To calculate this score, table values were combined into a single number defined by:

$$SS = (R-E)/(T-E)$$

where:

SS = skill score
R = number of times model results agreed with GEOSAT (sum of observations on major diagonal),
E = number of times model results agreed with GEOSAT due to chance (formula given below),
T = total number of model-GEOSAT pairs.

E was calculated by multiplying each column sum by the row sum for that class, adding these column-row products, and dividing by T.

The above skill score ranges from 1, when all model-GEOSAT pairs agree (all pairs fall on the diagonal), to 0 when the number of pairs agreeing is expected by chance.

## III. RESULTS

A summary of the wind model results are shown in Table 3 (units are meters per second), and a summary of the wave model results are shown in Table 4 (units are meters). At the request of some participants, the names of countries and agencies are not given in the table. The left side of each table shows regional models, and the right side shows global models. In the bottom row, as a reference for the model-GEOSAT statistics, are the buoy-GEOSAT means and standard deviations.

**Table 3. Differences between wind models and GEOSAT satellite data on 10 March 1986. The statistics of the differences and the skill score (defined in text) are given for both regional and global models. Differences between NOAA buoys and GEOSAT are listed in the bottom row.**

| | REGIONAL | | | | GLOBAL | | | |
|---|---|---|---|---|---|---|---|---|
| | MEAN (M/S) | ST.DEV. (M/S) | NUM. OBS. | SKILL SCORE | MEAN (M/S) | ST. DEV. (M/S) | NUM. OBS. | SKILL SCORE |
| MODEL A | | | | | | | | |
| MODEL B | 1.1 | 3.4 | 47 | 0.3 | | | | |
| MODEL C | | | | | | | | |
| MODEL D | 2.2 | 2.8 | 87 | 0.2 | | | | |
| MODEL E | 1.1 | 3.7 | 62 | 0.2 | | | | |
| MODEL F | 1.0 | 2.4 | 14 | | | | | |
| MODEL G | 1.7 | 3.6 | 66 | 0.3 | 1.1 | 3.9 | 138 | 0.4 |
| MODEL H | 0.1 | 3.1 | 71 | 0.3 | -1.1 | 2.8 | 74 | 0.5 |
| MODEL I | | | | | | | | |
| BUOYS & TOWERS | | | | | -0.8 | 2.2 | 8 | |

Table 4. Differences between wave models and GEOSAT satellite data on 10 March 1986. The statistics of the differences and the skill score (defined in text) are given for both regional and global models. Differences between NOAA buoys and GEOSAT are listed in the bottom row.

| | REGIONAL | | | | GLOBAL | | | |
|---|---|---|---|---|---|---|---|---|
| | MEAN (M) | ST. DEV. (M) | NUM. OBS. | SKILL SCORE | MEAN (M) | ST. DEV. (M) | NUM. OBS. | SKILL SCORE |
| MODEL A | | | | | | | | |
| MODEL B | 1.8 | 1.6 | 38 | 0.0 | | | | |
| MODEL C | -0.2 | 1.5 | 67 | 0.3 | | | | |
| MODEL D | 0.0 | 1.1 | 87 | 0.6 | | | | |
| MODEL E | 0.5 | 1.0 | 62 | 0.4 | | | | |
| MODEL F | 0.3 | 0.4 | 14 | | | | | |
| MODEL G | 0.4 | 0.7 | 81 | 0.6 | 0.2 | 0.8 | 243 | 0.5 |
| MODEL H | -0.7 | 1.2 | 129 | 0.2 | -0.1 | 0.9 | 393 | 0.3 |
| MODEL I | -0.1 | 1.3 | 58 | 0.4 | | | | |
| BUOYS & TOWERS | | | | | 0.1 | 0.4 | 6 | |

Each model entry covers one row in the table. The row contains the mean difference of the matching data pairs (model minus GEOSAT), the standard deviation of these differences, the number of data pairs, and the skill score calculated by the formula given above.

To estimate variability in Tables 3 and 4, we ran Navy wind and wave model comparisons with GEOSAT on two other days. We found day-to-day variability on the order or $\pm$ 0.1 for means, $\pm$ 0.3 for standard deviations, and $\pm$ 0.1 for skill scores.

Even though we were requested not to list all the names in the above model-GEOSAT comparison tables, we decided to list the best performers. Based only on our evaluations for 10 March 1986 they are: Canada had the best skill score for a regional (North Atlantic) wind chart, NOAA had the best score for a global wind chart, the Netherlands had the best score for a regional (North Atlantic) wave chart, the U.S. Navy had the best score for a global wave chart.

## IV. CONCLUSIONS

Our first conclusion is that satellites are the ideal way to validate wind and wave models. When GEOSAT data are properly edited, the satellite provides reasonably accurate global data. In addition, new satellites will be launched soon that will scan side-to-side so that the whole ocean surface is covered instead of a narrow path like GEOSAT. As a result of such data, all wind and wave models should improve.

Our second conclusion is that, considering how little data are routinely available to these operational models, they did fairly well. Most model differences from GEOSAT were not that much larger than the buoy differences from GEOSAT.

Third, we think that model-satellite comparisons such as those presented here should be automated and run routinely. This would provide a operational method for continually testing relative model performance, or for evaluating new models or data assimilation techniques.

Fourth, from our ratings there seems to be no clear relationship between advanced model physics and operational performance. The Navy wave model, for example, does not use the latest physics, yet it had a high skill score. These models are probably data limited rather than physics limited.

Finally, we need to repeat this test on another day. A repeat test will enable us to see if the results in the above tables are consistent, or if some models perform better in certain seasons. Since GEOSAT will be turned off and moved to another orbit during October and November 1986, we hope to do a repeat test soon.

## REFERENCES

1. Cavaleri, L., G.J. Komen and W. de Voogt, 1982. Sea Wave Modeling Project, Netherlands Meteorological Institute, De Bilt, Holland, 300 pp.

2. Kilgus, C.C., J.L. MacArthur and P.V.K. Brown, 1984. Remote Sensing by RADAR Altimetry, Johns Hopkins APL Technical Digest V5, #4, pp. 341-345.

3. Panofsky, H.A., and G.W. Brier, 1965. Some applications of statistics to Meteorology. Penn. State. U., 224pp.

4. Resio, D.T. and C.L. Vincent, 1982. A comparison of various numerical wave prediction techniques. Society of Petroleum Engineers Journal, October, pp. 764-774.

# A COMPARISON OF HINDCAST STUDIES WITH
a) A COUPLED DISCRETE WAVE MODEL,
AND
b) A COUPLED HYBRID WAVE MODEL.

Lars Ingolf Eide,
Norsk Hydro.

Magnar Reistad,

Johannes Guddal,
The Norwegian Meteorological Institute.

## 1. INTRODUCTION.

The present study was designed to assess the role of different wave models chosen for the provision of wave data for statistical use. Since the hindcast technique seems to have reached a break-through in marine data provision, branches of hindcast procedures appear, such as long-term continuous hindcasting, stormy season hindcasting, selected storms, annual extreme storms.

The reference material for this study is an extensive 30 years continuous hindcasting of wave parameters. The input wind vector fields were computed objectively from successive air pressure fields. A 2. generation, discrete type wave model, "WINCH", was applied, see Cardone, V., et al. 1983.

Alternatively, the wave model "NOWAMO", Haug, O., 1968, modified 1986, (unpubished), was applied for the years 1980-84, and we compare co-located result wave parameter distributions from the two models through that period, referred to nearly colocated measurement data distributions as shown on map figure 1.

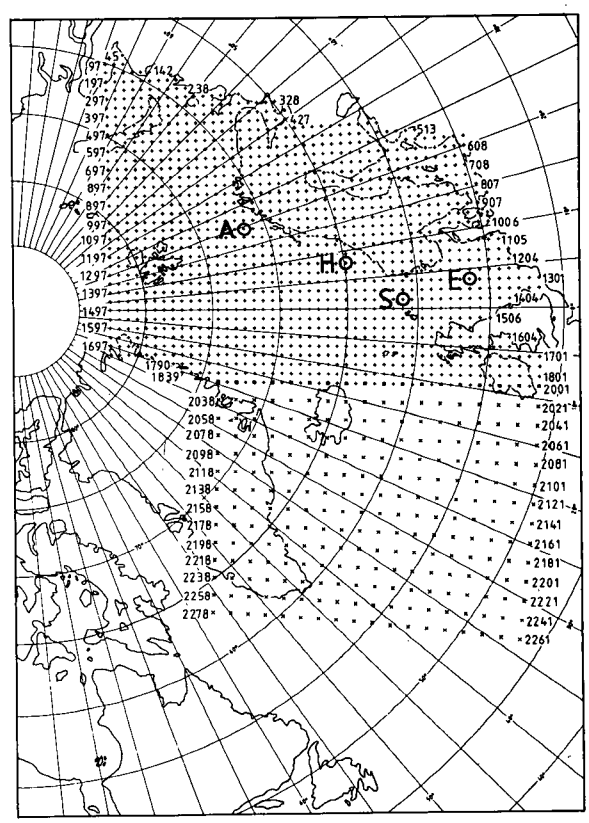


Figure 1. Model area and verification sites.
A = AMI
H = Haltenbanken
S = Statfjord
E = Ekofisk

## 2. HINDCAST STUDY ORGANIZATION.

The organization of a hindcast study project will deal with many problems and limitations, like
- basic input data collection, checking, processing.
- computer economy, which has a lead on the choice of area extension and model resolution.
- unknown performance of numerical model applied.
- rational archiving of output results, from integrated parameters (significant wave heights) to full 2-dimensional wave energy spectra ( energy density in frequency-directional bins).

While some questions are settled directly from economical/practical limitations, others are solved through "trial and error". The organization of the present study is illustrated on figure 2, and came forth as a result of experience gained from 2 previous study attempts. Through these, less successful studies, error sources were revealed and assessed, and ideas came how to compensate for them in the most efficient and economical way.

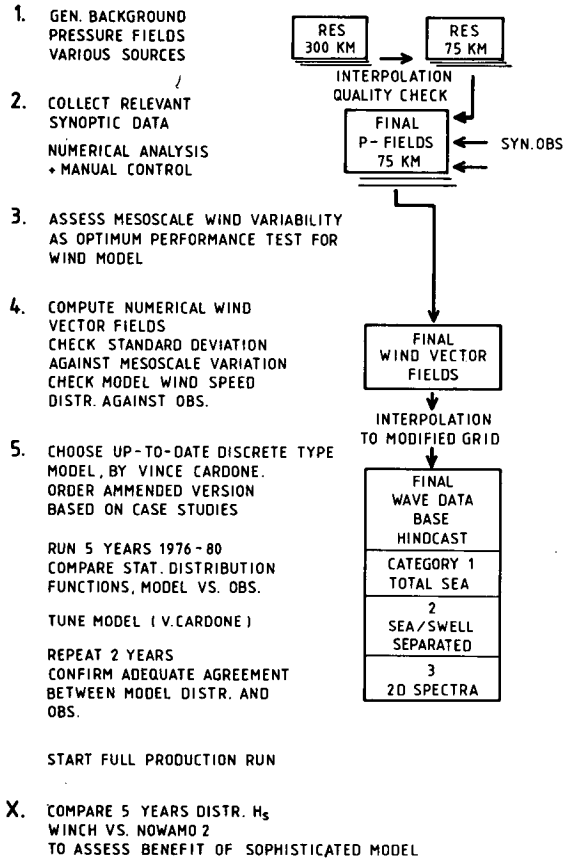


Figure 2. Organizational diagram for a wind/wave hindcast study project.

A few comments help to understand the diagram. The basic input fields of surface air pressure are established in 3 steps :
- organization of "background air pressure fields", either from previous programs or other sources. Interpolation to optional resolution (6 hrs.,75 km).
- collection of all available synoptic data from various sources covering the area of extent (fig. 1).
- numerical objective analysis by letting synoptic observations influence and correct background fields.

Next come the production and quality assessment of wind fields. Wind data procedures are described in the next section, and quality assessments are done by comparisons with in-situ observations. The wind sampling variability has been studied and was proved to be of the order of 30% of the model/observation scattering.

The wave data production run was started with a preliminary 5 years hindcast 1976 to 1980. Statistical distribution functions of $H_s$ were compared at 4 locations with wave rider measurements. After a moderate tuning of the wave model, a second preliminary hindcast of 2 years now confirmed model data distributions very low-biased from observations, and the final production run 1955 - 85 was carried out. Output data were archived according to 3 categories:
- "total sea" parameters,
- split wind sea and swell parameters,
- 2-dimensional wave energy spectra.

Figure 3 shows resulting hindcast distributions compared to observed ones for $H_s$ and $T_p$. Figure 4 shows an area contouring of the mean annual occurrence of wave heights exceeding 4 m.

The reference data base is described in Eide, Reistad, Guddal, 1985.

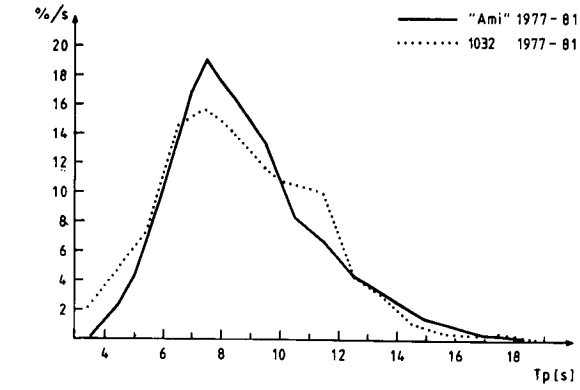


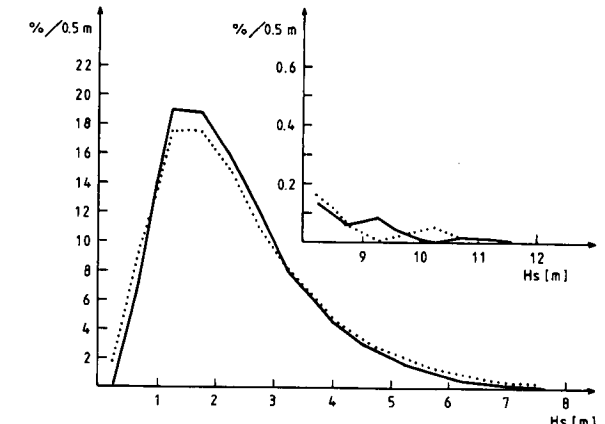


Figure 3. Model and observational (AMI) $H_s$ and $T_p$ distributions , from reference study.

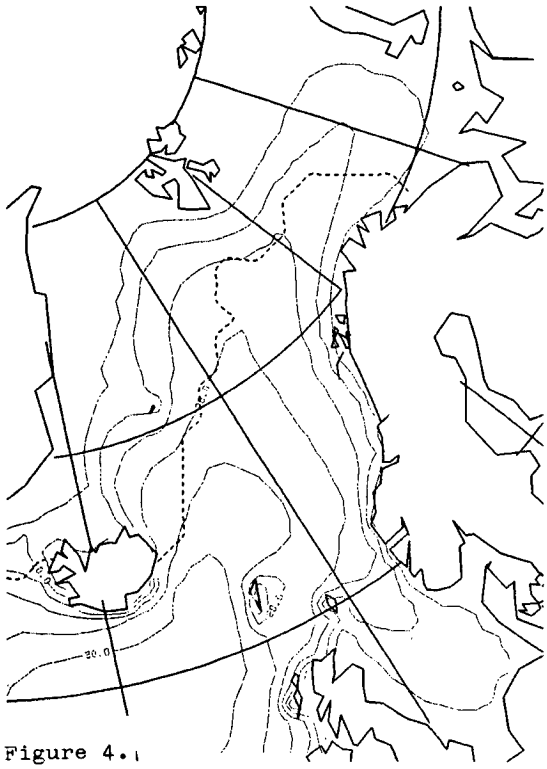

Figure 4.1

FREQUENCY OF HMO ≥ 4M
YEAR 1955-84
EQUIDISTANCE 5.0 %
----- MAX. EXTENSION OF ICE

## 3. WIND MODELLING PROCEDURES.

In mid- and high- latitudes, the wind modelling will start from the relation between air pressure fields and wind vector fields. Among different procedures, one may think of a ranking as indicated below :

A. Winds given explicitly from an operational numerical atmospheric model, including a reliable boundary layer representation.
B. Winds produced by manual "kinematic analysis, starting from geostrophic wind fields, taking into account observed winds and boundary layer stability effects.
C. Winds produced objectively, wind observations, sea surface and air temperatures taken into account for stability effects.
D. Winds computed as geostrophic winds reduced to 10m, assuming neutral stability.

These procedures require different degrees of manual intervention and correction procedures. Summarizing, table 1 shows a survey of these procedures, and their characteristics in terms of data origin, wind observation data assimilation, physical consistency in time and space, boundary layer representation, manual intervention and correction required.

TABLE 1

| WIND VERSION | DATA ORIGIN | ASSIMILATION OF OBS.WINDS | PHYSICAL CONSISTENCY | BOUNDARY LAYER REPR. | MAN INTERVENT. CORRECTION |
|---|---|---|---|---|---|
| A | Multiple layer atm model, expl. winds. | Automaticly incl. checking/rejections. | Objectively modelled. | Optimized. | Minor. |
| B | Geostroph. winds. | Manually, subjectively. | Subjectively. | Air-sea temp diff. taken into acc., subjectively. | Significant. |
| C | Geostroph. winds. | Automaticly, iterative fitting to model fields. | Inadequate. (smoothing of fields) | Neutral stability assumed. | Necessary to some extent. |
| D | Geostroph. winds. | Inadequate. | Inadequate indirectly via pressure analysis. | Neutral stability assumed. | Necessary to large extent. |

In the organization of a hindcast study, its ambition level, meaning its branch of hindcasting and optional sophistication of data, will determine firstly the choice of the wave model and from there the choice of wind calculation procedure. For instance, detailed hindcasting of the directional features of a moving storm would require an advanced wave model and version A of wind modelling. On the other hand, a long term (30 years) hindcasting aimed at statistical treatment of $H_s$ series could require a less advanced model ( like the hybrid parametric model NOWAMO) and version D of wind modelling.

The wind model actually applied in this study was developed by Reistad, 1983, with references to Brown 1974 and 1978. This procedure classifies as version D.

## 4. 2. GENERATION HYBRID PARAMETRIC AND DISCRETE SPECTRAL WAVE MODELS.

The following is more or less quoted from "SWAMP" book.

The development of a surface wave field in time and space is governed by the energy balance equation

$$\frac{\partial F}{\partial t} + \vec{v} \cdot \nabla F = S = S_{in} + S_{nl} + S_{ds}$$

where $F = F(f, \theta)$, wave energy as a function of frequency and propagation direction.

First generation models, referred to in "SWAMP" as decoupled propagation models (DP), essentially develop each individual component F independently from other components.

Second generation models reflect a revised balance given by (1) introducing the non-linear wave-wave interaction term $S_{nl}$. For a relatively slowly varying wind field, one may assume that the re-distribution of energy by $S_{nl}$ is sufficiently rapid relative to the advection term and the other source terms that a quasi-equilibrium distribution of the JONSWAP form can be applied, the energy spectrum being characterized by a single, slowly changing scale parameter like E or $f_p$.

However, for strongly non-uniform wind fields, an approximate parameterization of $S_{nl}$ is needed.

In the parametric wind sea models, the growth of the wind sea part is expressed in terms of a small set of coupled transport equations describing only a few characteristic spectral parameters. A parametric description of the wave field is appropriate only for the wind sea region. Low frequency swell components are primarily controlled by advection. Parametric models, therefore, are combined as hybrid models with standard discrete spectral representation for the swell components, and referred to as coupled hybrid models (CH).

On the other hand, coupled discrete (CD) models retain the traditional discrete spectral representation for the entire spectrum. The principal difference between the model concepts lies in the division between the discrete and the parametrical regions of the spectrum.

## 5. THE WAVE MODELS, "WINCH" (CD), AND "NOWAMO" (CH).

The "WINCH" (Waves Incident on Norwegian Coast, Hindcast) is a CD model developed by Oceanweather Inc. It is a modified version, also, from the one used in "SWAMP" study and adapted to the Norwegian Shelf. The waves are grown using a combination of the Miles-type growth and parametric growth. Non-linear energy distribution is modelled by use of a parametric reference spectrum and wave direction relaxation is explicitly taken into account.

The "NOWAMO" (Norwegian Operational Wave Model) is a CH model originally developed by Odd Haug . In the present version, its growth term is derived from the JONSWAP relations, making the scaled total wind sea energy grow through an initial growth, an intermediary phase and finally a rather sudden saturation. Figure 5 shows the duration growth curve to be well centered within the range of the "SWAMP" participants .

Both models now apply the same frequency spectrum:

$$F = \alpha g^2 (2\pi)^{-4} f^{-5} \exp(-1.25(f/f_p)^{-4}) \times (1 + 3.4\Gamma(f/f_p)^{-12} \exp(-1.0625(f/f_p)^{-16} + 1.25(f/f_p)^{-4}))$$

(see list of symbols).
"WINCH" applies the empirical relation

$$(3)\quad \Gamma = \max(0., 0.54(1 - (\varepsilon/\varepsilon_{pm})^2))$$

while in "NOWAMO" we have decided to use

$$(4)\quad \Gamma = \max(0., 0.40(1 - (\varepsilon/\varepsilon_{pm})^2))$$

This minor difference has no effect on spectral integration. It could possibly have the effect in "NOWAMO" that retained swell components become a little bit too low.

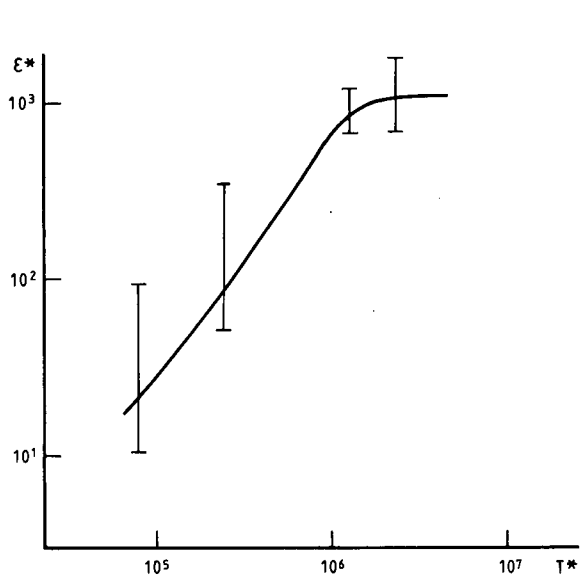


Figure 5. Growth curve of scaled total sea energy with scaled duration from "NOWAMO", shown within "range" of SWAMP participants.

The time/space resolutions of the two models are similar; 2 hours,75 km.

"WINCH" resolves the spectrum in 15 frequency bands and 24 directional sectors. "NOWAMO" uses period bands of width 2 sec. while the separation of wind sea and swell allows a "free" directional resolution.

Angular spreading functions are also different, in that "WINCH" essentially uses that of Mitsuiasu, see also Cardone, 1983. "NOWAMO" simply uses a cosine square energy distribution around the wind direction.

These are the main similarities and differences between the two models. It should turn out that the application of these models in parallel will demonstrate the effect of different treatment of swell, namely the difference in basic model concepts.

It should be emphasized that the separation of swell in "NOWAMO" allows a very cost-effective data production, since only locations (gridpoints) of actual interest enter the swell calculation. From that viewpoint, simple CH models are interesting if they can be proved to produce statistical distributions which up to some level can compete with those from a more advanced model. This might be the case for conventional $H_s$ statistics, for certain ocean basins of well described wind climatology, and for instance for selected cases of uni-directional storms.

## 6. INTERCOMPARISONS "WINCH"VS. "NOWAMO", DISTRIBUTION FUNCTIONS 1980 - 84, AND CASE STUDIES.

The intercomparison and verification sites were shown on figure 1. Figures 6 to 9 now show $H_s$ distribution functions from "WINCH", "NOWAMO" and observations. The number of events vary from site to site, since measurement data series do have "gaps". For each position, average $H_s$ and standard deviation $\sigma_{Hs}$ are given, and for the models result data, verification parameters (versus observations) "root-mean-square" (RMS) errors and correlation coefficients R are given.

The most evident feature of these diagrams is the systematic bias of the "NOWAMO" data to the low side, with a slight exception for Ekofisk. The "WINCH" data have generally average values and standard deviations very close to the corresponding observational data parameters, thus indicating general confidence to these data in extreme analysis application.

RMS errors are slightly higher for "NOWAMO" data at AMI and Haltenbanken, while correlation coefficients are in general of the same magnitude.

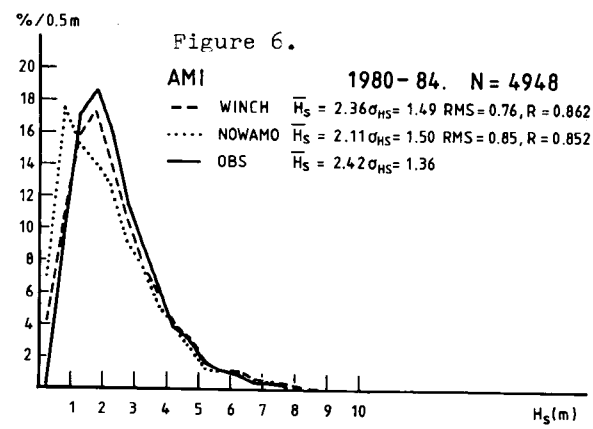


Figure 6.

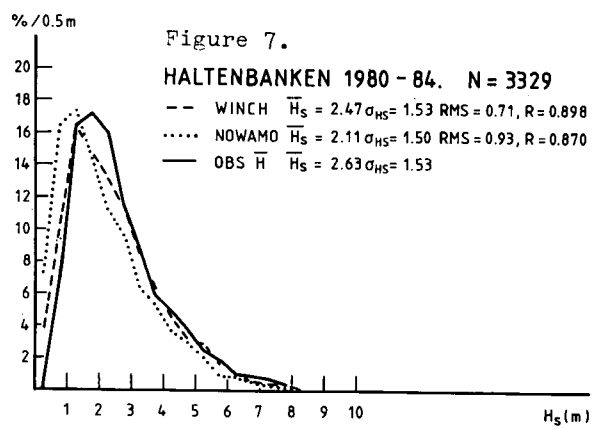


Figure 7.

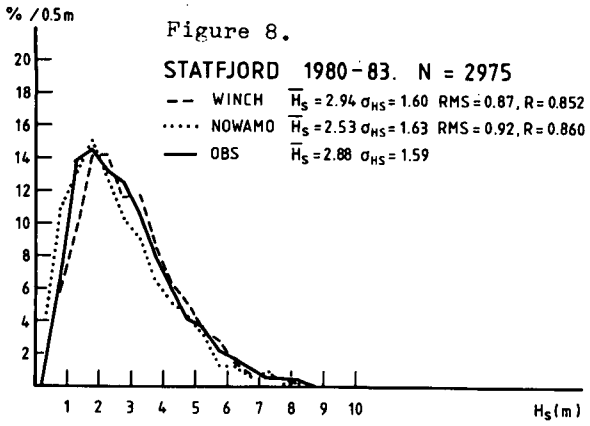


Figure 8.

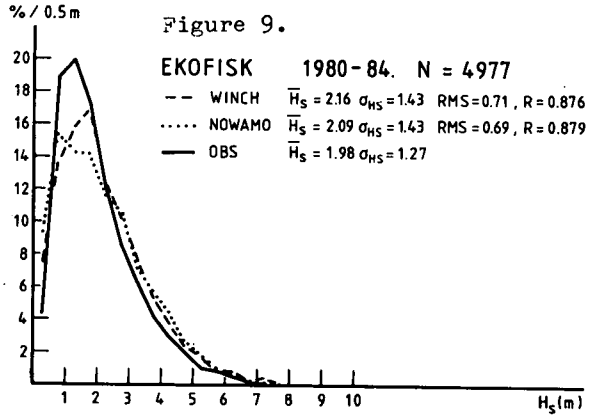


Figure 9.

We believe that the significant differences shown here, are mainly caused by the "NOWAMO" treatment of swell, particularly the discretization of swell mentioned above. This assumption is supported by the fact that the location Haltenbanken shows the largest differences in model performance, and Haltenbanken has been proved to be the most swell exposed area among the four.

As shown on figure 10, model performance can shift from one storm to another, the reason probably being errors in the wind field, or even the possibility that advanced models still have weaknesses where simple parameterization can be more lucky.

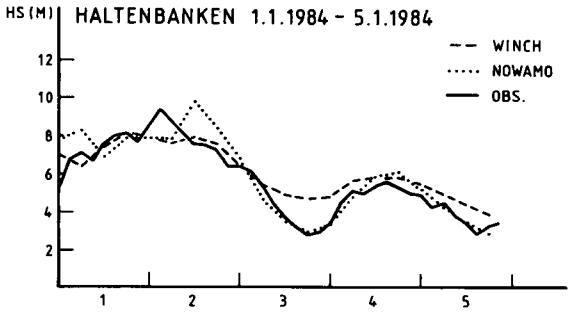


Figure 10. Case studies intercompared for $H_s$ developments through storms at Haltenbanken and Statfjord.

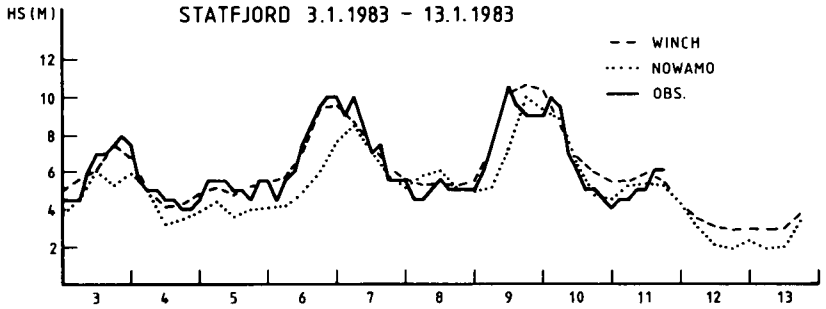

## 7. CONCLUSIONS.

If a wave hindcast study is primarily aimed at $H_s$ statistics and extreme analysis, a hybrid parametric model might be as adequate as a discrete spectral model. The reason is probably that wind field errors are normally distributed, fairly low-biased, and the tuning guarantee of parametric models prevent large biases in $H_s$ distributions.

For more detailed studies, applying results for $T_p$, $\theta_p$, separated swell, two-dimensional spectral output, advanced models are more likely to pay off. As mentioned earlier, this also calls for higher optimalization of the wind fields. Presently, wind fields of version A are barely available for more than the recent 5 years. Versions B and C are expensive, but are in principle available back to the 1940's. In our reference study, we have used the version D, with the rather advanced wave model "WINCH". It is conceivable, therefore, that the application of wind fields of version C or B, would have improved the database quality to an even higher level.


## 8. ACKNOWLEDGEMENT.

The authors are grateful to mr. Frank Cleveland for his excellent support with the graphical material.


## 9. REFERENCES.


Cardone, V.,Greenwood, J. A.:"Development and Evaluation of a Coupled Discrete Wave Prediction Model", Oceanweather Inc., Cos Cob, CT 06807, USA, 1983.

Haug, Odd: "A Numerical Wave Prediction Model", Meteorologiske Annaler, The Norw. Met. Inst., 1968.

Eide, L. I.,Reistad, M., Guddal, J.: "Database av beregnede vind og bølgeparametre for Nordsjøen, Norskehavet og Barentshavet, hver 6. time for årene 1955 - 81 (extended to 1985). The Norw. Met. Inst.,1985.

Reistad, M.:"vindmodell for hindcast". Progress report. The Norw. Met. Inst.1983.

Brown, R.A.:"Matching classical boundary layer solutions towards a geostrophic drag coefficient relation". Boundary Layer Meteorology, 7, 489 - 500, 1974.

Brown, R.A.:"Similarity parameters from first order closure and data". B.L.M., 14, 381 - 396, 1978.

SWAMP book: Hasselmann, K. et al. "Sea Wave Modelling Project". Plenum Press, New York, London 1984.


## 10. LIST OF SYMBOLS.

$H_s$ = significant wave height.
$T_p$ = "peak" spectral period.
$\theta_p$ = "peak" spectral direction.
$F = F(f,\theta)$ = spectral energy density, varying with:
$f$ = frequency.
$\theta$ = propagation direction.
$S$ = net growth source term.
$\mathcal{V}$ = component group velocity.
$S_{in}$ = wind input term.
$S_{nl}$ = non-linear wave-wave interaction.
$S_{ds}$ = dissipation term.
$\alpha = \varepsilon^{-0.23}/4.49$
$\varepsilon$ = dimensionless total energy = $Eg^2/U_{10}^4$
$U_{10}$ = wind speed reduced to 10 m level.
$\varepsilon_{pm}$ = saturation value , using Pierson Moscowitz spectrum.
$g$ = gravity acceleration constant.
$f_p$ = "peak" spectral frequency.

# WAVE HINDCAST SENSITIVITY

F. X. Penicka

Newfoundland Marine Sciences
Mount Pearl, Newfoundland

## INTRODUCTION

The Environmental Studies Revolving Funds (ESRF) initiated a hindcast sensitivity study in 1984, of the deep water wave spectral model developed by D. T. Resio and implemented for hindcasting in the Canadian East Coast waters by the Marine Environmental Data Service (in the following the model is referred to as the "Resio model"). The objective of the study was to evaluate the sensitivity of the model to variations in input wind fields and to factors such as model time step and grid spacing. Variations in the wind fields were to include errors in wind estimates, variation of the percentage of pressure based winds versus kinematic analysis winds and linear versus nonlinear interpolation of the input winds. An indication of the performance of the model under various storm conditions was to be provided by hindcasting several storms from the ESRF list of severe storms.

Because of the space and time limits on this presentation only a brief outline of the tests can be given here. Full details can be found in a report submitted to the ESRF.

The actual hindcasting for this study was done by the Marine Environmental Data Service (MEDS). In all sensitivity tests the present MEDS system was taken as a standard and the assumption was made that no a priori changes were required. For example, the regular grid and time step were employed for testing the sensitivity to input errors and the sensitivity to variable percentage of pressure based versus kinematic analysis winds. The tests were performed in such a way that none or minimum changes in the model code were required. This was achieved by accessing the MEDS hindcast procedure at various stages using an appropriate input (Figure 1) and, in the case of quadratic interpolation test, by replacing the original bi-linear interpolation program by a new program supplied by the Newfoundland Marine Sciences (NMS).

Two types of input were used in the sensitivity tests:

(a) synthetic wind fields, and

(b) wind input data prepared by the Offshore and Coastal Technologies Inc. (OCTI) for wave hindcasting in support of the ESRF Directional Wave Spectrum Intercomparison Study.

The synthetic input consisted of a uniform stationary wind to which a small perturbation, an "error", was applied, and from a hypothetical cyclonic weather system moving across the model grid. The synthetic wind fields were used to test the sensitivity of the model to errors in input wind fields and the sensitivity to grid spacing and time step.

The wind fields from the ESRF Directional Wave Spectrum Intercomparison Study provided realistic cases for testing the effect, on the hindcast wave parameters, of varying the proportion of pressure based winds and kinematic analysis winds, and for comparison between bi-linear and quadratic interpolation of input wind fields. Directional wave observations, as well as hindcasts prepared by OCTI using a more recent version of the model, were available for comparison.

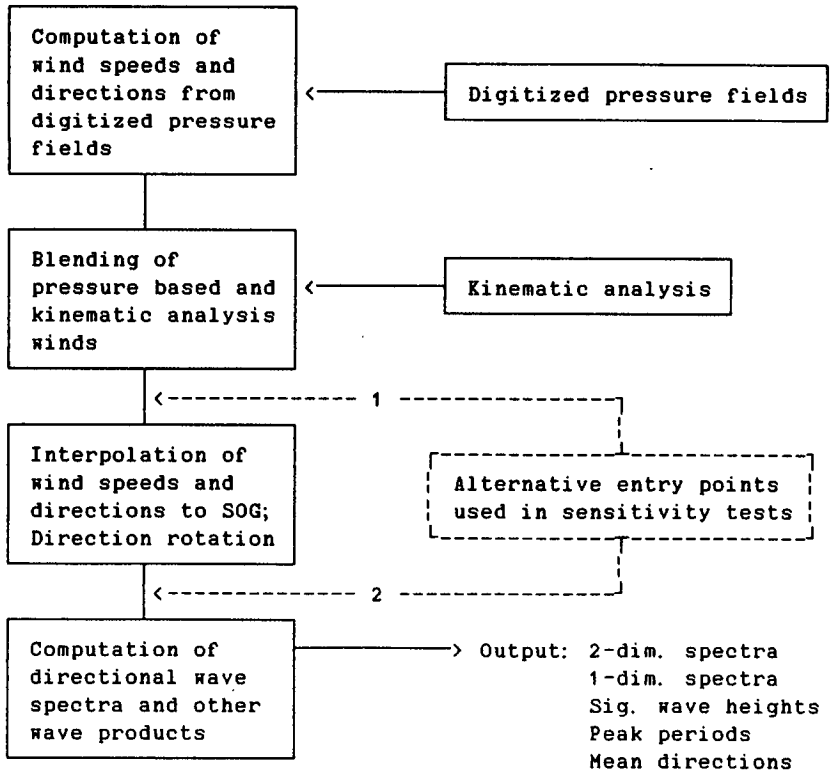


FIGURE 1: MEDS WAVE HINDCAST PROCEDURE

The primary output from the model is a set of directional wave spectra, each represented by 20 frequency bands and 16 direction bands. The secondary wave products, computed from the directional spectra, include sets of one-dimensional spectra, significant wave heights, $H_s$, peak periods, $T_p$, and mean directions at peak period, $\theta$. Only $H_s$, $T_p$ and $\theta$ were compared in the sensitivity tests. These are the parameters of greatest interest in hindcast applications and it is believed that restricting the comparisons to them did not lead to any significant loss of information at least in the windsea portion of the spectrum. The reason is that the shape of the windsea spectrum is essentially controlled by nonlinear wave-wave interaction which, in the Resio model, is parameterized in terms of $T_p$ and the Phillips equilibrium coefficient. Thus the number of degrees of freedom representing the non-directional windsea spectrum is equal 2 rather than 20 (corresponding to the 20 frequency bands).

With few exceptions the results of the sensitivity tests were processed and presented for specific sites. It was assumed that the main application of the model would be in coastal areas subject to hydrocarbon exploration. Since the MEDS version of the model does not include any shallow water effects it is not, in its present form, suitable for hindcasting waves on the Scotian Shelf. The model grid is also not optimized for the Labrador Shelf, and therefore it was assumed that the primary application area for the model would be on the Grand Banks. The comparison sites were selected accordingly. However, the results are believed to be generally applicable to any location to which the model itself is applicable.

## SENSITIVITY TO ERRORS IN INPUT WIND FIELDS

Some idea of the response of the wave model to errors in input wind fields can be obtained by examining the implicit relationships between the significant wave height (or the peak period) of locally generated windsea and wind speed. The Resio model was developed to be consistent with the fetch limited wave growth rates observed during the JONSWAP experiment. Therefore, as a first approximation, the windsea significant wave height and peak

period under the fetch limited conditions should follow empirical relationships proposed by Hasselmann et al. (1973): $H_s \sim u$, $T_p \sim u^{0.33}$. Under these conditions a small fractional (or percent) error in the input wind , $\delta_u$, would lead to a fractional error in significant wave height of approximately the same magnitude, $\delta_H \approx \delta_u$, and to a fractional error in peak period, $\delta_T \approx 0.33\delta_u$.

According to D.T. Resio (personal communication) for duration limited waves, which are more typical in open ocean situations, the significant wave height is given by $H_s \sim u^{5/7}$. Under these conditions, the fractional errors in significant wave height are expected to be $\delta_H \approx 0.7\delta_u$.

For fully developed seas the hindcast spectrum approaches Pierson-Moskowitz spectrum for which $H_s \sim u^2$ and $T_p \sim u$. Thus, under these conditions, $\delta_H \approx 2\delta_u$, and $\delta_T \approx \delta_u$.

In a real event hindcast the situation is more complex. At each time step at any individual grid point, the error in wave energy (and analogously in $H_s$ or $T_p$) is a combination of an energy error input into the wave field locally at that time step and some fraction of errors input into the same grid point and into surrounding grid points at earlier times. Even if the wind velocity is known at some location exactly (e.g. from nearby wind measurements) the hindcast waves at that point still are contaminated by errors which propagated there from the rest of the grid. Because of this interplay of local input and advection it seemed desirable to use, in these tests, a simplified wind input in which the temporal and spatial variability of the error free fields was reduced or eliminated.

The first set of tests employed the simplest possible input: a uniform stationary wind blowing from the west. Westerly (i.e. off shore) winds were selected in order to test to what extent errors in wind direction affect the hindcast waves through changes in fetch. After certain time (144 hours), sufficient to bring the wave field from zero energy into balance with the input wind field, a sequence of unbiased and biased random perturbations in speed and direction was applied to the uniform wind field. The reference wind had a speed of 40 knots (20 m/s) and the perturbations were random (in space) and normally distributed. The sequence of the perturbations is shown in the upper part of Figure 2. Each test consisted of two six-hour (input) time steps. The RMS and bias (computed over all active grid points) at the two time steps were the same but the actual perturbations at each grid point differed randomly (i.e. two different random sets were used for the two time steps). This was believed to best represent errors in actual wind estimates which may be random in both time and space. The constant change of the perturbations was also believed to make the test representative of wave growth situation which is typical of storm conditions. The RMS and bias of the input perturbations were selected after a literature review of error characteristics of wind fields used as input in wave simulations.

Figure 2 shows the time series of RMS and bias of wave parameter errors in relation to the RMS and bias of the input errors. "Error" is here a difference between a value of the parameter at a given time step and a value at the same grid point at the end of spin-up (output time step 47, i.e. after 141 hours).

A number of observations can be made on the basis of this plot:

(1) An unbiased error in the input (step 49-50) results in a positive bias in $H_s$ and $T_p$.
(2) Errors in wind direction do not have any appreciable effect on the bias in the wave height errors and only a small effect on the bias in peak period errors. They have a greater effect on the RMS of $H_s$ and $T_p$ errors, most likely through changing the fetch.
(3) Errors in wind speed produce only small and virtually unbiased errors in the wave direction.
(4) Unbiased errors in wind direction result in somewhat biased errors in wave direction. According to D.T. Resio (personal communication) the magnitude of this bias depends on the particular sequence of the input errors.
(5) There is a considerable persistance in the errors past the 12 h duration of each test. This makes difficult correlating the input and output errors.
(6) Time-wise interpolation leads to a decrease in the RMS error in the input and a corresponding decrease in the RMS error in $H_s$ as evidenced by the presence of double peaks in a number of tests.

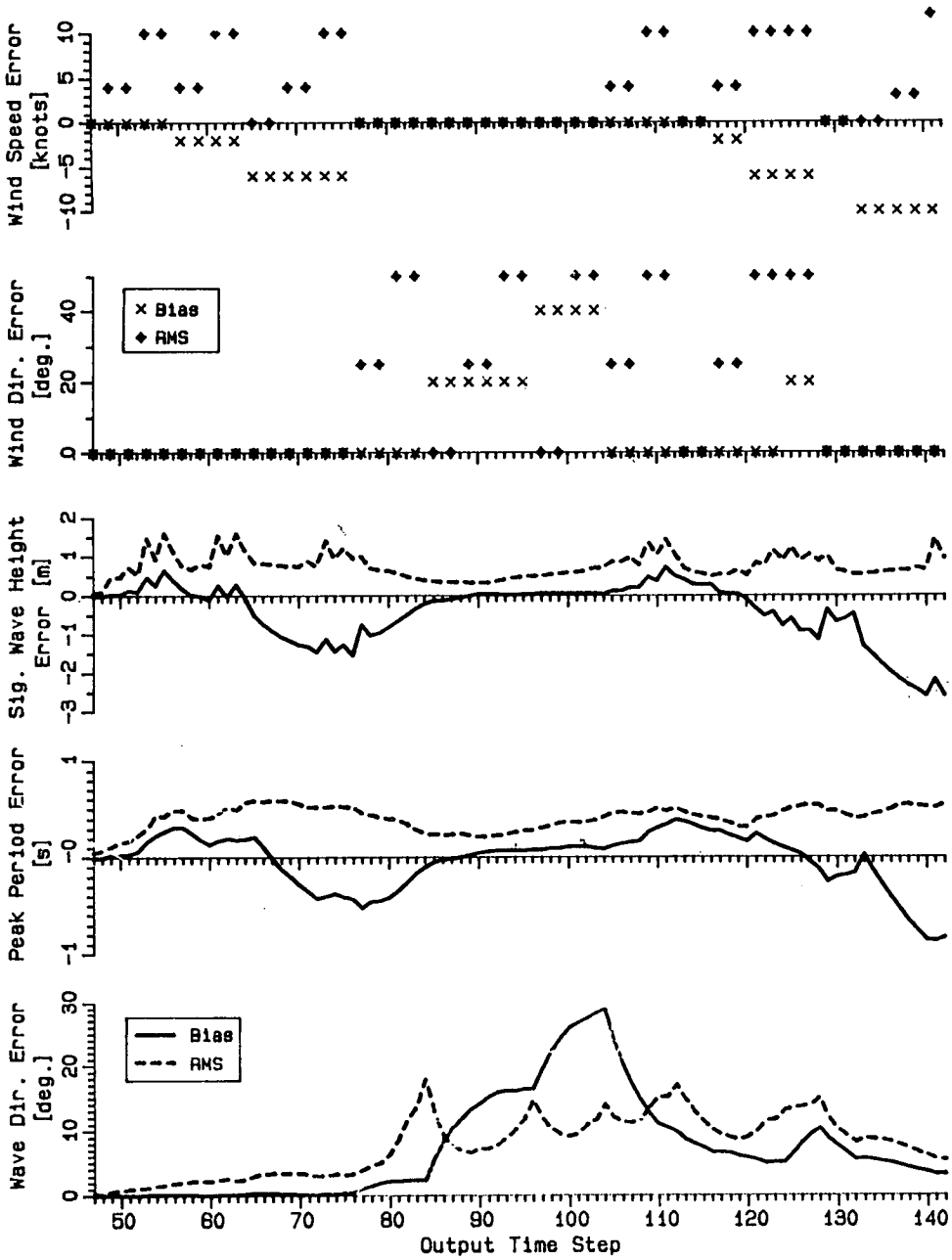


FIGURE 2: WAVE MODEL RESPONSE TO A PERTURBED UNIFORM STATIONARY WIND FIELD. BIAS AND RMS ERRORS OVER ENTIRE GRID.

Individual input and output errors were compared at several grid points. However, only two special cases are presented here. Figure 3 shows the time series of errors in wave parameters at a grid point (Station 49) at which the input errors were set to zero. It thus demonstrates the effect of advection from the surrounding area. As would be expected, in this case the output errors are primarily affected by the bias in the input errors.

Station 50 was located two grid spacings (about 150 nautical miles) from the upwind land boundary and directly downwind from Stn. 49. Therefore, the output errors at Stn. 50 should be primarily of local origin and closely correlated with the local input errors. Figure 4 shows the scatter diagram of $H_s$ vs. wind speed. The points can be fitted well with a straight line of slope 1 (%/%) which is consistent with fetch limited conditions at this station. There is a greater scatter in the $T_p$ vs. wind speed plot which may be due to the fact that only discrete values of $T_p$ are resolved. Line of slope 0.33 (%/%) applicable to the fetch limited conditions is shown for comparison.

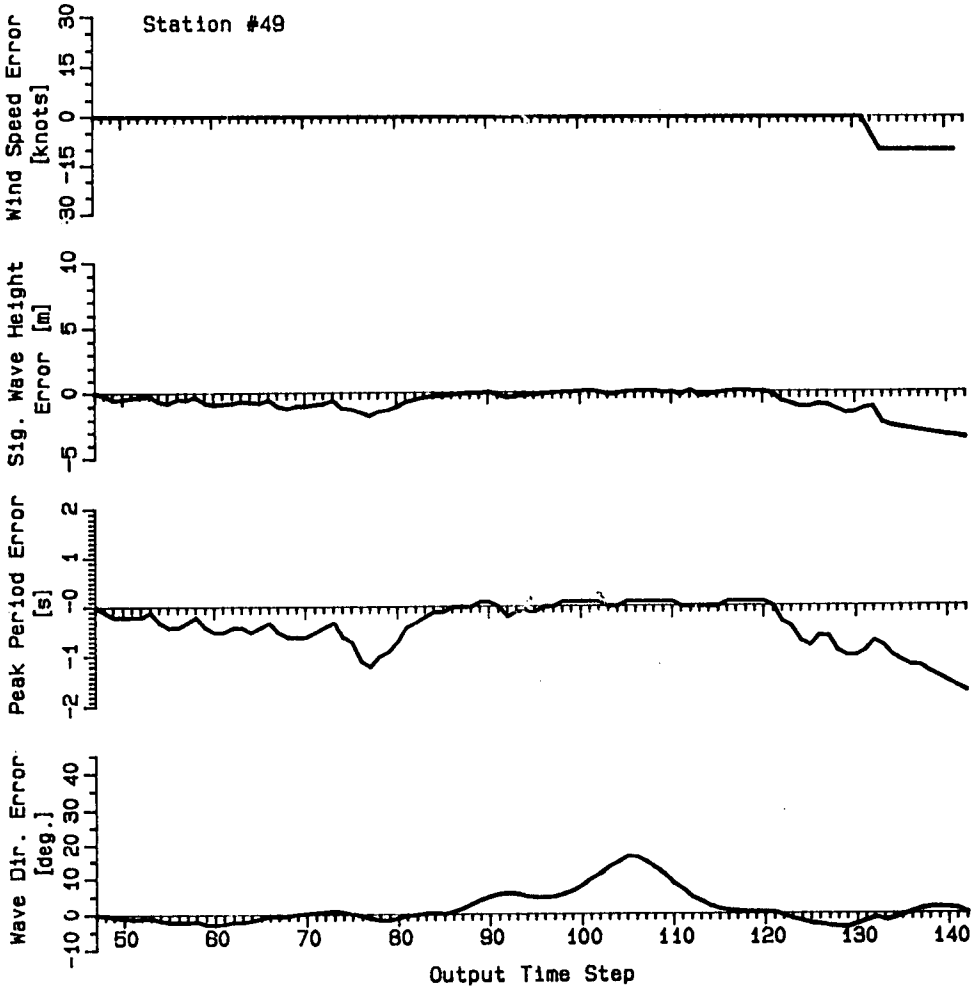


FIGURE 3: WAVE MODEL RESPONSE TO A PERTURBED UNIFORM STATIONARY WIND FIELD - STN. 49

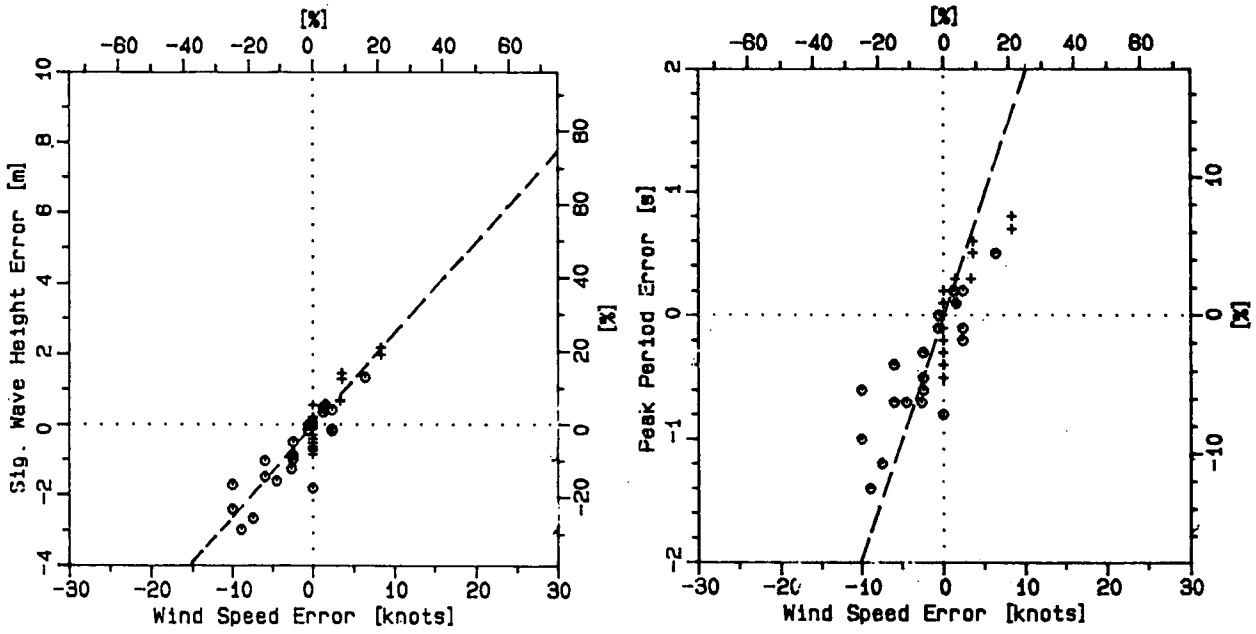


FIGURE 4: CORRELATION BETWEEN INPUT AND OUTPUT ERRORS AT STATION 50

In a real event hindcast, errors in wind estimates are not likely to be entirely random, as assumed in the previous test. The winds are determined from patterns (isobars or streamlines and isotachs) and therefore there will be some relationship between errors at adjacent grid points. Inspection of two sets of weather maps (for the same storm) prepared by two different weather offices indicated that there may be considerable differences between weather maps prepared by different analysts: in central pressures of a storm and in its track. The effect of these errors is expected to differ from that due to completely random errors. In the case of an error in central pressure the storm track and the flow pattern are unchanged but the storm is weakened or intensified. In the case of an error in the location of the storm center the flow pattern is again unchanged but shifted with respect to the unperturbed position. Thus neighbouring grid points are affected in a similar way and the total effect may be greater than that due to random errors.

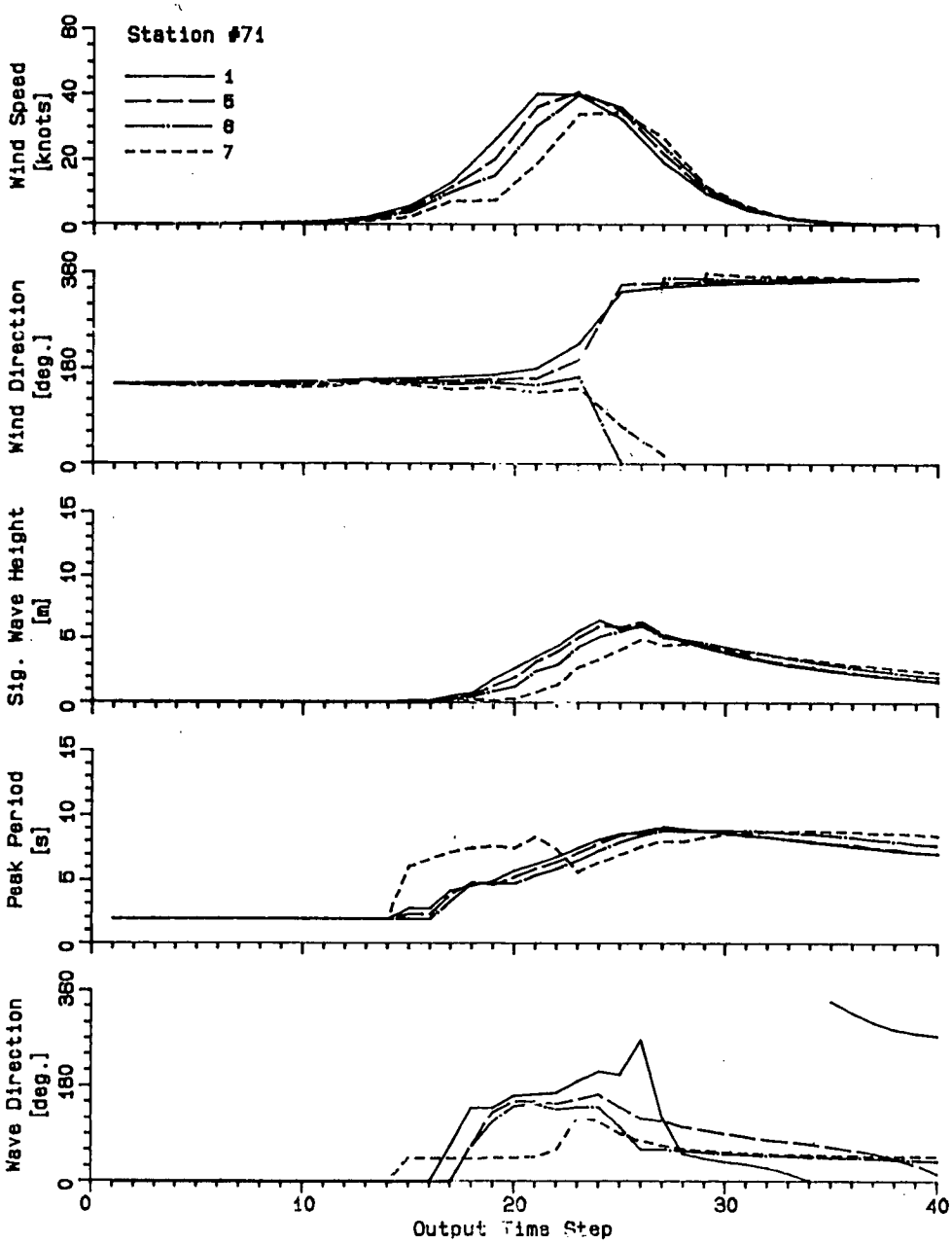


FIGURE 5: WAVE MODEL SENSITIVITY TO ERRORS IN STORM TRACK.

The second set of tests described here was intended to investigate the sensitivity of the Resio model to these two types of non-random errors. A synthetic input was again used for the sake of simplicity. The synthetic storm was caused by a low pressure system travelling in a north-easterly direction across the model grid. The storm deepened as it moved along its track until it reached about half way across the grid. After that the central pressure increased again as the storm moved out of the generating area.

In one set of tests the storm track was unchanged but the storm intensity was modified by applying random perturbations to the central pressure. Perturbations of RMS 1 mb, 1.5 mb and 2 mb were employed. The resulting errors in $H_s$ and $T_p$ paralleled those in the wind speed and the comparisons will not be presented here. More interesting was the case in which random perturbations were applied to the storm track. Figure 5 shows the comparison for the grid point closest to Hibernia (Station 71). Curves 1 correspond to the unperturbed case while curves 5, 6 and 7 correspond to the perturbed storm tracks with RMS of 0.3, 0.6, and 1.2 degrees/time step respectively. Tracks 7 and 8 passed Stn. 71 on the opposite side than tracks 1 and 5. As would be expected the main effect on the significant wave height is a shift in time of the time series curve as well as a change in the maximum $H_s$. The effect of course depends on the relative position of the hindcast site with respect to the storm track and it decreases with increasing distance.

## SENSITIVITY TO GRID SPACING AND TIME STEP

Sensitivity of the Resio model to grid spacing and model time step was tested using both synthetic storm winds and wind fields prepared for the ESRF Wave Intercomparison Study. For these tests the grid spacing of the spherical orthogonal grid normally employed by MEDS was increased and decreased by 20%. This allowed comparison of three grids of nominal spacing of 180, 150 and 120 nautical miles with, respectively, 123, 185 and 283 active grid points. A use of a finer grid would pose more severe requirements on the computer resources while providing little advantage because the technique of wind analysis incorporated in the MEDS hindcast procedure is not likely to resolve features of scale smaller than about 150 nautical miles. In order to obtain an indication of the model sensitivity to changes in fetch due to changes in boundary representation additional tests were made with the standard and the fine grids modified by including additional sea grid points along the western boundary.

In all cases using the synthetic storm input the differences between the hindcast wave parameters for the various grid spacings were small particularly during the growth stage. For hindcasts using the standard and fine grids the wave height reached virtually the same maximum while the use of the coarse grid lead to a slightly lower peak. The difference in the significant wave height was the largest during the abatement of the storm which may indicate that the change in grid spacing affected mainly the wave propagation term. However, it may have been also due to a change in fetch (during this stage the winds were from the west). On average, the differences in significant wave height were negligible for the 20% decrease in grid spacing (bias 0 m to -0.27 m, RMS difference 0.07 m to 0.13 m); the RMS difference was somewhat larger for the 20% increase in grid spacing (bias 0 m and -0.12 m, RMS difference 0.21 m and 0.31 m). The bias and RMS differences in peak period were smaller than the period resolution in all cases.

A change in grid spacing had a greater effect on significant wave heights in the real event hindcasts of a compact storm which developed very rapidly. For that storm the fine grid hindcast overestimated the maximum significant wave height, unlike the standard grid hindcast in which the peak was underestimated. In both cases the peak was shifted and the wave decay was inadequate.

The comparisons were made for grid points closest to the observation site which did not coincide for the two grids. This may explain the relatively large differences in the significant wave heights. The local winds also differed between the two grids but it is interesting to note that while the local wind speed dropped more rapidly (from about the same peak) in the fine grid case, the significant wave height during the abatement of the storm was lower in the standard grid hindcast (due to its higher peak and not due to a lower rate of decrease). On average, the use of the fine grid lead to a somewhat greater error, compared to the measurement, (bias 1.02 m, RMS error 1.11 m in the significant wave height,

-1.66 s and 1.86 s in the peak period) than the use of the standard grid (0.96 m and 0.78 m in $H_s$, -1.65 s and 1.77 s in $T_p$). The fine grid comparison point was further away from the measurement site than the standard grid point and this was most likely the reason for the worse error statistics. This storm was relatively compact and it moved rapidly, therefore strong horizontal gradients in wind speed occurred.

In the second storm comparison both hindcasts overpredicted the significant wave height during most of the storm but the fine grid lead to values closer to the observation by about half meter (bias 0.6 m versus 1.03 m). This storm developed less rapidly and was less compact than the first storm. The storm was stalled over the Grand Banks for over 30 hours and the winds remained relatively steady for long periods of time. The spatial gradients of wind speed were not as great as in the first storm and consequently both hindcast grid points were representative of the measurement site. The mean errors in peak period were comparable (bias and RMS errors approximately 2 s for both grids) but the mean wave directions differed by about 30° between the two grids.

The regular time step employed by MEDS is 3 hours. To test the sensitivity to time step hindcasts were made using 4 hour and 2 hour time steps and various grid spacings. All combinations of time step and grid spacing satisfied the Courant stability condition. In order to avoid the need for changes in the model computer code only synthetic storms, which could be digitized at the appropriate time intervals, were hindcast in these tests. With one exception the hindcast significant wave heights and peak periods increased with decreasing time step. This suggests a need for a recalibration should a time step be modified. The average change in significant wave height over the whole storm for the decrease in time step from 3 h to 2 h ranged between 0.16 m and 0.32 m, the RMS difference was between 0.16 m and 0.38 m. Changes in peak period were smaller than the period resolution. Increasing the time step to 4 h had a greater effect: up to -0.65 m in the mean and 0.46 m in the RMS difference. There were indications that a decrease in time step lead to an emphasis of the peak, and a more rapid fall off, in the significant wave height.

## EFFECT OF VARIATION IN THE PERCENTAGE OF PRESSURE BASED WINDS VERSUS KINEMATIC ANALYSIS WINDS

Wind fields used in the MEDS hindcast procedure are a blend of winds computed from surface pressure fields and winds obtained through kinematic analysis. As part of this study four blends of pressure based and kinematic analysis winds were compared: 100% : 0%, 80% : 20%, 50% : 50% and 20% : 80%.

In designing this set of tests it was realized that there was a great risk that, rather than evaluating the sensitivity of the hindcast technique, the tests might result in comparison between the skills of the analyst who produced the weather analysis charts and the skills of the analyst responsible for the kinematic analysis. An attempt was therefore made to utilize, as input, data sets as free of subjective influences as possible. Surface pressure fields were interpolated from CMC pressure analysis data, available on magnetic tape, which were produced by an objective analysis method. For kinematic analysis winds wind fields prepared by OCTI for the ESRF Wave Intercomparison Study were used. The OCTI wind fields contained 100% kinematic analysis winds in the vicinity of the comparison location and a blend of 80% kinematic analysis winds/20% pressure based winds elsewhere. These winds provided a good approximation to the actual wind conditions as evidenced by the good agreement between hindcast and observed waves in the Wave Intercomparison Study (Juszko, 1985). For the purposes of the present study, the OCTI wind fields were treated as a sample drawn from a set of kinematic analyses prepared by a number of skilled analysts. It seemed reasonable to assume that the 20% contamination by winds based on surface pressures represented less variability than would be introduced by different analysts.

The area covered by the kinematic analysis was not sufficiently large for a 0% : 100% hindcast. Therefore separate inputs were prepared by interpolating the OCTI winds over the whole area of their coverage and reducing the active region of the MEDS wave model grid to cover the same sea area as the OCTI grid. This provided 0% : 100% input consistent with the other blends. In addition, comparison could be made between the MEDS version of the Resio model and the more recent version used by OCTI in which the input and wave propagation terms were modified (Penicka et al., 1985).

The comparisons were made for two storms. In the case of the first storm (Figure 6) the wind fields containing the largest percentage of the pressure based winds resulted in wave hindcast with the lowest bias (0.58 m) and the highest RMS error (0.86 m) in significant wave height, and the highest RMS error in peak period (1.91 s). Wind fields containing the largest percentage of kinematic analysis winds lead to significant wave heights with the highest bias (0.83 m) but the lowest RMS error (0.62 m). The peak period also exhibited the lowest bias (-1.71 s) and the lowest RMS error (1.84 s) for this blend.

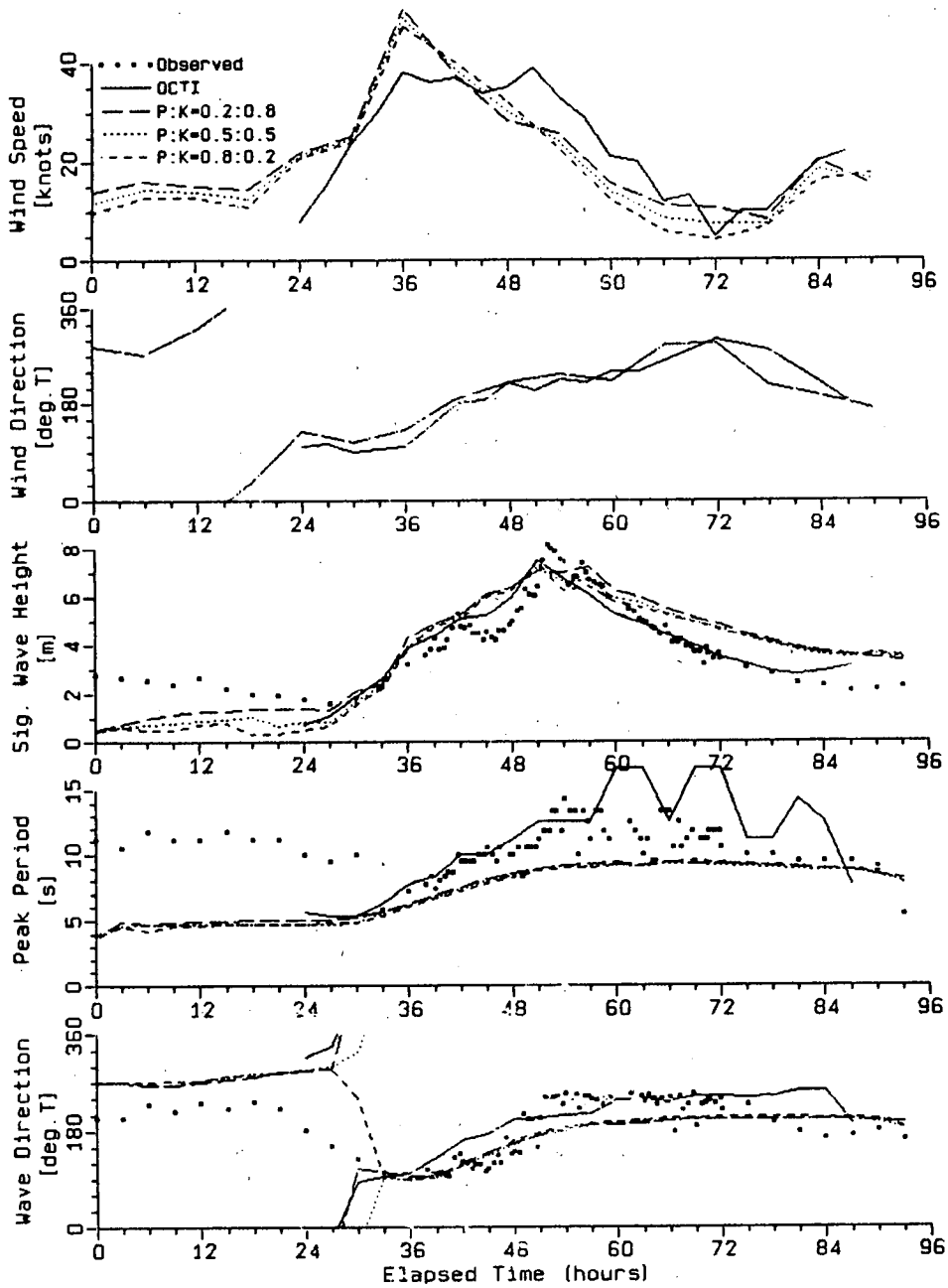


FIGURE 6: TIME SERIES OF HINDCAST AND MEASURED WAVE PARAMETERS FOR VARIOUS PROPORTIONS OF PRESSURE BASED WINDS AND KINEMATIC ANALYSIS WINDS -STORM 1

In the case of the second storm the differences in the hindcast wave parameters between the different blends were much greater particularly after the storm reached its peak. The divergence from the observed wave parameters was the greatest (more than 4 m during a part of the storm) for the inputs containing a large proportion of pressure based winds (80% and 100%). This suggests an error in the pressure analysis used to derive the winds. The blend with the highest percentage of kinematic analysis winds resulted in a hindcast with the best overall significant wave height error (bias 1.28 m, RMS error 0.8 m) and the lowest RMS error in peak period (1.83 s). However, in this case the peak period bias was larger than that of any other combination (-1.53 s). The peak period bias was the smallest in the hindcast using only pressure based winds (-1.14 s) but the other error statistics in this hindcast were substantially degraded (1.77 m bias and 1.71 m RMS error in significant wave height; and 2.17 s bias in peak period).

## QUADRATIC VERSUS BI-LINEAR INTERPOLATION OF INPUT WIND FIELDS

In the MEDS hindcast system the blend of pressure based and kinematic analysis winds is defined on a 2.5° latitude x 2.5° longitude grid and it must be interpolated to the spherical orthogonal grid employed by the wave model. This is achieved by means of bi-linear interpolation. As part of this study hindcasts of two storms were prepared using quadratic interpolation instead of the bi-linear interpolation. The quadratic interpolation was a straightforward finite difference transcription of the first six terms of the Taylor series expansion. Comparison of the hindcast wave parameters showed a negligible difference between the two interpolation methods: the mean and RMS differences were less than 0.15 m for the significant wave height and no more than 0.1 s for the peak period.

## ACKNOWLEDGEMENTS

This study was funded by the Environmental Studies Revolving Funds. All wave hindcasts were prepared by the Marine Environmental Data Service. Atmospheric input data were provided by the Canadian Meteorological Centre, wave measurement data were provided by Seakem Oceanography Ltd. Dr. J.R. Buckley was the study's Scientific Adviser. Dr. D.T. Resio reviewed parts of the study report and provided helpful criticism and suggestions.

## REFERENCES

Hasselmann, K., T.P. Barnett, E. Bouws, H. Carlson, D.E. Cartwright, K. Enke, J.A. Ewing, H. Gienapp, D.E. Hasselmann, P. Kruseman, A. Meerburg, P. Muller, D.J. Olbers, K. Richter, W. Sell, and H. Walden. 1973. Measurements of wind-wave growth and swell decay during the Joint North Sea Wave Project (JONSWAP). Dtsch. Hydrogr. Z., A8 (Suppl.), No.12, 95pp.

Juszko, B.A. 1985. Directional wave spectrum intercomparison study. Phase 4 - intercomparison of results. Draft report submitted to the Environmental Studies Revolving Funds.

Penicka, F.X., D.T. Resio, and R.D. Worsfold. 1985. Wave directional spectrum hindcasts for the ESRF Wave Directional Spectrum Intercomparison Study. Report submitted to the Environmental Studies Revolving Funds.

# THE INCORPORATION OF REAL-TIME WAVE MEASURMENTS INTO WAVE FORECASTS

Donald T. Resio

Offshore & Coastal Technologies, Inc.
Vicksburg, Mississippi, U.S.A.

## 1. INTRODUCTION

Over the past three decades our knowledge of the physics of wave generation, marine boundary layers, and synoptic scale weather patterns has steadily increased. However, our skill in wave prediction over a time interval of one to three days does not appear to have increased commeasurately with these advances. It is easy to presume that most of the problems in wave prediction are related strictly to problems in wind prediction skill. After all, if the input wind fields are poor, the calculated wave fields will also be poor. Very little of the total weather prediction budget appears to be directed toward the prediction of marine wind fields. In fact, many of today's sophisticated computer models for weather prediction do not even have built-in boundary-layer algorithms for predicting winds at a fixed reference level in marine areas. Consequently, even when top-quality, limited fine mesh (LFM) model predictions are available for an area, the predicted wind speeds and directions can be very poor for application to wave forecasting. However, this situation is changing as more groups are beginning to produce global and/or regional forecasts on an operational basis. In this light, it now seems appropriate to investigate some alternative means of improving wave forecasts. In particular, this paper will examine the possibility of incorporating real-time and delayed wave information from measurements into forecasts.

## 2. AVAILABLE DATA SOURCES

During the last decade, satellite communications have allowed measured wave data to begin to be reported to forecast centers within an appropriate time scale for incorporation into forecast models. Since such data are quite sparce over the entire globe, the value of such information may not be very substantial for global-scale forecasts; but, the information content might be quite valuable for regional and local forecasts, which can be important for scheduling certain marine operations. At present most of the real-time data comes into the forecast center in the form of wave heights and periods or non-directional wave spectra; however, continuing work in the area of directional sensors may eventually shift the balance toward more directional wave spectra.

As will be discussed in other papers presented at this conference, a new source of wave data on a global scale, via satellite measurements, appears to be emerging. The Geosat measurements of wave heights compare well with in situ measurements and can provide a large-scale global coverage over the course of a single day. Unfortunately, several problems exist in incorporating existing satellite data into wave forecasts today. First, the existing coverage is quite broad and might miss some important local factors (tropical storms, initial stages of "bombs," near coastal effects, etc.). Second, only information on wave heights is presently available on a reliable basis; therefore, information on wave periods, spectra, and directions is not available to the wave model. Third, the satellite information is not coordinated with standard reporting times, but rather arrives in terms of a continuous swath along the satellite ground path. Fourth, due to processing delays, satellite-derived wave heights are typically available only 12 to 18 hours after the measurements are made. Some or all of these shortcomings may be removed by the addition of

new satellites and new satellite technology; but they still exist as important considerations today.

## 3. THEORETICAL CONSIDERATIONS

### 3.1 Introduction

The amount of improvement in wave forecast skill obtainable via the incorporation of measured wave data should depend primarily on three factors:

(1) the number and quality of measurements available and the timeframe in which they can be made available to forecast centers;

(2) the percentage of the total forecast error correctable by incorporation of accurate wave data into initialization schemes; and

(3) the ability to incorporate appropriate information from measured wave data into wave models.

The first of these factors is important but outside of the main interest of this paper; consequently, only factors 2 and 3 will be analyzed here.

### 3.2 Analysis of Error Terms Related to Inaccurate Existing Waves in a Wave Model

As with any study of this kind, we could proceed along a purely empirical approach. However, often a theoretical framework can assist in explaining certain aspects of experimental results. Therefore, before any simulations are examined, we will develop a brief heuristic outline for the general analysis of errors in wave models. For the sake of discussion, let us partition the total forecast error into three components

$$(3.1) \quad e_{tot} = e_1 + e_2 + e_3$$

where

$e_{tot}$ is the total error for a given forecast time,
$e_1$ is the error component due to errors in wind speeds and and directions over the forecast interval,
$e_2$ is the error component due to errors in the wave field at the zero hour and its propagation/persisentce to the forecast time, and
$e_3$ is the error component due to inaccurate model simulation over the forecast interval.

Since it is extremely difficult, if at all possible, to separate terms $e_1$ and $e_3$ from each other in practice, let us assume that $e_3$ and $e_1$ can both be considered as a single term $e_1'$ (= $e_1 + e_3$). In a sense, $e_1'$ can be regarded as the component of error generated over a given forecast interval and $e_2$ can be regarded as the component of error related to past errors in the wave field. Thus, $e_2$ can be considered to represent an historical error term and is expected to depend on the amount of "memory" in a wave forecast.

At any grid point in a wave model for a particular time step, the total wave energy can be formally divided into local sea and swell. For the purpose of attempting to understand error characteristics in forecast waves, this step is important since it allows us to define separate functional relationships between each of these portions of the spectrum relative to given wind inputs and model characteristics. For local sea we have, in an conceptual framework, three definable "states" which further determine some of these functional relationships:

(1) the waves are fetch limited,
(2) the waves are duration limited, or
(3) the waves are fully developed.

For open-ocean forecasts, duration-limited growth scenarios tend to occur much more often than fetch-limited conditions, so let us begin by examining the role of existing errors in the energy content of local sea relative to future errors.

For duration-limited wave growth, using a model based on an $f^{-4}$ spectral similarity form, we have

$$(3.2) \quad E_{sea}^{n+1} = E_{sea}^{n} + Q \frac{c_m u_*^2 \Delta t}{g}$$

or

$$(3.3) \quad E_{sea}^{n+1} = E_{sea}^{n} + Q' \frac{u_*^{5/3} \Delta t}{g^{1/3}} E_{sea}^{n^{1/3}}$$

where $E_{sea}$ is the total energy in the local sea, the superscripts "n" and "n+1" refer to time steps in the model, Q and Q' are dimensionless coefficients, $u_*$ is the friction velocity, $\Delta t$ is the time increment between time steps, and g is the acceleration due to gravity. The form of equation 3.2 suggests that a positive feedback exists between errors at time step n+1 and those at time step n; however, since waves eventually become fully developed, this feedback cannot become unstable.

Let us examine a simple case in which the "true" wave height of the local sea is 4 metres at time zero and a constant, "true" wind speed of 40 knots blows for 48 hours. Figure 3.1 traces the temporal behavior of the error for a range of initial errors. As expected from equation 3.3, the error first grows with time; however, as the wave conditions approach a fully-developed state, the magnitude of error diminishes. By the end of 48 hours, no error due to erroneous initial conditions persists.

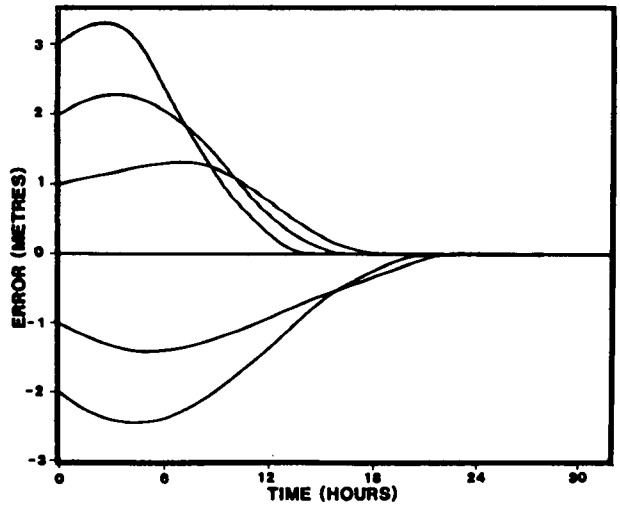


Figure 3.1. Time-wise behavior of error in wave height of local sea, assuming a "true" 40-knot wind and initial wave height of 5 metres, for various initial wave height errors.

An important point is evident in Figure 3.1. The typical time for waves to reach a fully-developed state from an initial condition of zero is only 24 to 48 hours for reasonable storm winds, say 25 to 60 knots. Given a non-zero initial condition, the time to attain a fully-developed state can be substantially less. Therefore, as is suggested by Figure 3.1, the expected improvement in wave forecast skill for local sea due to accurate wave height initialization will be largest for 6-hour and 12-hour forecast intervals and should tend toward zero for forecast intervals above 24 hours.

The above conclusion is only valid for local sea. For swell, the persistence becomes much longer and errors propagate through both space and time. Figure 3.2 shows the persistence of a wave height error following a wave train propagating away from a storm. A simple approximation to the functional form for wave energy decay can be taken as

$$(3.4) \quad E_{swell}^{n+1} \sim E_{swell}^{n} \exp(-\Delta t)$$

where $E_{swell}$ is the initial swell energy at time zero and $\Delta t$ is the model time step. This type error tends to preserve, at least roughly, a constant proportion of difference between the predicted and "true" energies. In other words, if the swell wave energy is 30 percent too high at the location to which these waves have propagated at any later time. Of course, since the wave energy is decaying, the absolute magnitude of the error will be smaller at a later time. This error term can be very important in areas outside of the central portion of a storm or even for points in the interior of a storm after the most intense part of the storm has passed.

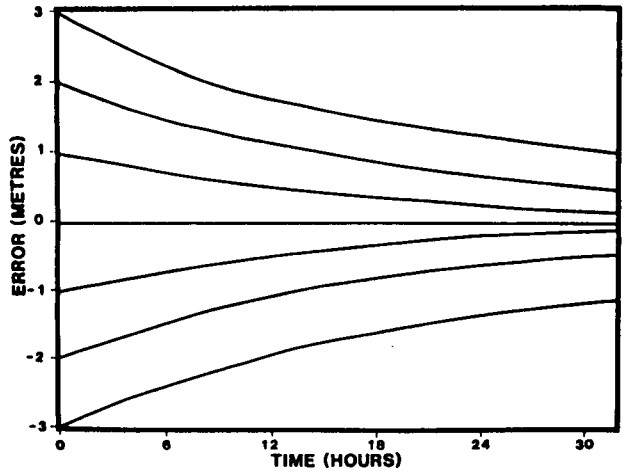


Figure 3.2. Time-wise behavior of error in wave height of swell, assuming an initial swell wave height of 6 metres, for various initial errors.

There are several reasons why the error term related to swell can be quite large and very persistent in wave forecasts. First, as previously mentioned, no negative feedback is inherent in the wave models which would tend to reduce the errors. Second, this error represents the accumulation of errors in wind fields and in modeling capabilities. And, third, our understanding of the physics of swell decay and our ability to model swell propagation are quite limited.

## 3.3 The Incorporation of Measured Wave Data into a Numerical Wave Forecast Model

The number and type of internal parameters in a wave model depends on the type of wave model used. In a first-generation discrete-spectral model, only the existing energy contents in each frequency-direction element is needed, along with wind information, to produce forecast wave conditions. In a second generation discrete-spectral model, as well as in parametric and hybrid-parametric models, information on certain wave parameters is essential to the wave prediction process.

For a first generation model in deep water, we have

$$(3.5) \quad E(f,\theta)^{n+1} = E(f,\theta)^{n} - \vec{c}_g \cdot \vec{\nabla} E(f,\theta)^{n} + S_1(f,\theta,u_*)$$

where $E(f,\theta)$ represents the energy density at frequency f and direction $\theta$, the superscripts "n" and "n+1" refer to time steps in the model, $c_g$ is the group velocity of waves with frequency f, and $S_1$ is the sum of the source terms acting on the waves. As seen in equation 3.5, the growth or decay of a given spectral element is independent of spectral parameters such as the location of the spectral peak.

In a second generation model in deep water, we have

$$(3.6) \quad E(f,\theta)^{n+1} = E(f,\theta)^{n} - \vec{c}_g \cdot \vec{\nabla} E(f,\theta)^{n} + S_2(f,\theta,u_*,\frac{f}{f_m},\frac{f}{f_{sw}})$$

where $S_2$ is the sum of all source terms in the model and $f_{sw}$ is the peak of the swell portion of the spectrum. For practical purposes the same general form for the source term is also appropriate for third generation wave models.

Measured Directional Spectra

If a full directional spectrum were available, it could be input directly into a first generation wave model; and after estimating the values of $f_m$ and $f_{sw}$, the spectrum and these parameters could be input into a second generation wave model. However, it is extremely difficult to extrapolate a directional spectrum from one location directly to other spatial points, since spectral shapes are not very linear. Consequently, other methods for extrapolation of input wave spectra need to be found for applications in both the first and second generation wave models. Of course, if sufficient measured data are available to resolve most of the important features in the wave field, an interpolation scheme can be used to obtain entire spatial fields of directional spectra and wave parameters for input into a wave model.

Measured One-Dimensional Spectra

For most ocean areas, there are very few sources of real-time directional wave spectra made available on an operational basis. If only one-dimensional spectra defined as

$$(3.7) \quad E_1(f) = \int_0^{2\pi} E(f,\theta)\,d\theta$$

are available, the energy in a wave model cannot be updated by any independent information relating to wave direction. Consequently, in an objective analysis of these cases, information on the directional distribution of energy must come primarily from the wave model. A simple updating methodology which has been found adequate in a wide range of test cases is of the form

$$(3.8) \quad E'(f,\theta)^{n+1} = E(f,\theta)^{n+1}\left[\frac{\overset{c}{E}_1(f)}{E_1(f)^{n+1}}\right]$$

where $E'(f,\theta)^{n+1}$ represents the updated energy at the $n+1^{th}$ time step and $\overset{c}{E}_1(f)$ represents the measured one-dimensional wave spectrum.

Unfortunately, even one-dimensional wave spectra are not very easy to interpolate, since the energy contents in any frequency component are so dependent on the location of $f_m$ and/or $f_{sw}$. Consequently, for updating an entire spatial field of information, it appears preferable to rely on some parametric spectral concepts. In this context, a general knowledge of the physics of wave generation, propagation, and decay can be used to provide additional information relative to the updated wave field. Following our earlier partitioning of wave energies into sea and swell, an efficient, yet flexible, parametric representation for spectral shapes has been found to be of the form

$$(3.9) \qquad E(f) = E_{sea}(f) + E_{swell}(f)$$

where

$$(3.10) \qquad E_{sea}(f) = \frac{\alpha' g u_* f^{-4}}{(2\pi)^3} \phi\left(\frac{f}{f_m}\right)$$

$$\text{with} \quad \phi\left(\frac{f}{f_m}\right) = \delta \exp\left[-\frac{(f-f_m)}{2\sigma^2}\right] \quad \text{for } f \geq f_m$$

$$= \delta \exp\left[-\left(\frac{\beta f}{f_m}\right)^{-4}\right] \quad \text{for } f < f_m$$

where $\delta$, $\sigma$, and $\beta$ are parameters definable in terms of $u/c_m$ (ratio of wind speed to the phase velocity of the spectral peak) and $\alpha'$ is a universal constant; and,

$$(3.11) \qquad E_{swell}(f) = \frac{\alpha_r g c_{sw} f^{-4}}{(2\pi)^3} \phi_{sw}\left(\frac{f}{f_{sw}}\right)$$

$$\text{where} \quad \phi_{sw}\left(\frac{f}{f_{sw}}\right) = \delta^{\exp\left[\frac{-(f-f_{sw})^2}{2\sigma_{sw}^2}\right]^{-4}} \quad \text{for } f \geq f_{sw}$$

$$= \delta_{sw} \exp\left[-\left(\frac{\beta_{sw} f}{f_{sw}}\right)^{-4}\right] \quad \text{for } f < f_{sw}$$

where $c_{sw}$ is the phase velocity of the frequency of the swell peak, and $\alpha_r$, $\delta_{sw}$, $\sigma_{sw}$, and $\beta_{sw}$ are shape parameters. For a small value of $\alpha_r$ and a large value of $\delta_{sw}$, the spectral shape approaches $\alpha$ and $\delta_{sw}$ approaches 1, the spectral shape approaches that of the local sea. Thus, the form of 3.11 can treat spectral shapes ranging from very long, low-steepness wave conditions (such as occurs after long propagation distances) to relatively high steepness waves (such as occurs when a wind drops suddenly and the wave spectrum is just beginning a transition phase away from a local sea spectral shape). Stable estimates for all of the parameters required in this formulation can be obtained from simple algorithms applied to the measured spectra.

As was the case with directional spectra, the availability of real-time spectral measurements is such that they will probably only improve wave forecasts in a local area over a short interval of time. For example, if a given point in a wave model were updated with a measured spectrum, the characteristic time that the information content would reside at that grid point is approximately

$$(3.12) \qquad \Delta t = \frac{\Delta x}{\hat{c}_{g_m}}$$

where $\Delta t$ is the characteristic time for all information at the grid point to be replaced by energy propagating into this point from other grid points, $\Delta x$ is the grid spacing in the model, and $\hat{c}_{g_m}$ is the group velocity of the spectral peak. For a typical global-scale operational wave model ($\Delta x \simeq 2.5^{\circ}$), equation 3.12 gives an estimate of 6 to 12 hours for the typical persistence limit of waves at a point. Thus, for a comparison 24 hours later, the improvement in skill at the same grid point cannot be much improved by the incorporation of even "perfectly" accurate waves at that point; however, adjacent grid points can obtain improved forecast results when the presumably more accurate waves propagate to those locations.

In the above discussion, the importance of updating a wave model with a complete spatial field of wave measurement inputs, rather than just updating the wave model at selected points, is evident. Besides the obvious effect related to the dispersion of the improved information into a large area, in some wave models, the introduction of abrupt spatial gradients can create problems related to the modeling techniques used. For example, if only one point is updated with significantly higher waves than the surrounding area, the high energy waves propagating out of this point can create significant deviations in mean wave directions at nearby points (Figure 3.3). In turn, these errors can influence the directional distribution of energy received from the wind and the directional distribution of energies gained and lost from nonlinear wave-wave interactions.

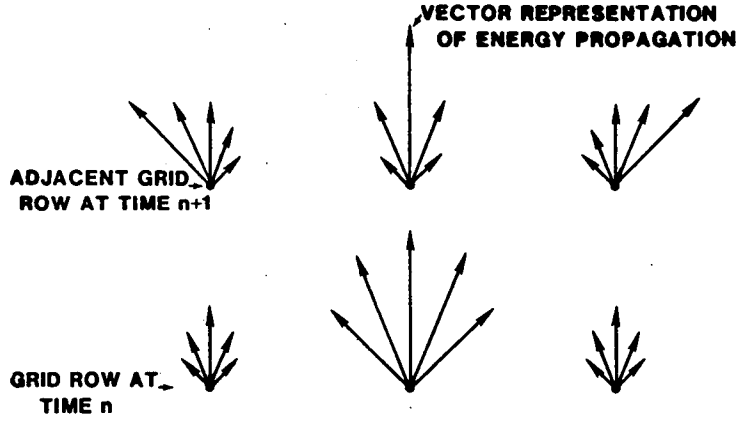


Figure 3.3. Situation in which an "updated" wave model point produces directional deviations in nearby wave model points.

In areas where interpolation is not possible on a reasonable scale, it is recommended that consideration be given to employing spatial statistical techniques for estimating smooth "updated" wave fields surrounding a point. In our own work, we have found that an inverse-square-distance weighting function seems adequate for blending independent data into a wave model with a high level of information retention at forecasts of 24 hours and greater and minimal numerical problems. Based on in-house studies of the spatial autocorrelation function associated with extratropical storms and the work of Resio (1985) on extreme wind distributions, we have developed the following form for a spatial weighting function for updating a wave model from measurements at a single point in the North Atlantic Ocean,

$$(3.13) \quad p(x) = \exp\left(-\frac{X^2}{2\sigma_x^2}\right)$$

where X is a distance measured from the measurement point to any grid point and $\sigma_x$ is approximately 80 km when used for extrapolating local sea parameters and 140 km when used for extrapolating swell parameters. In actual applications the parametric updating is of the form

$$(3.14) \quad Z'^{n+1} = Z^{n+1}(1 - p(x)) + Zp(x)$$

where $Z'^{n+1}$ is the value of the parameter after updating, $Z^{n+1}$ is the value before updating, and Z is the estimated value of the parameter based on measurements. One problem in using equations 3.13 and 3.14 occurs in areas where swell and local sea merge, i.e. in regions immediately following the peak of a storm; however, in these areas the values of $f_{sw}$ and $f_m$ converge, so this problem is not too consequential.

Measured Wave Heights

At present satellites are primarily providing information on wave heights only. This presents somewhat of a problem since one cannot independently determine how much of the total wave energy is contained in the local sea and how much is swell. Because of this, the primary source of such information must come from the wave model.

Given a partitioning of energy in the model as

$$(3.15) \quad E_{tot} = E_{sea} + E_{swell}$$

one cannot obtain separate "updating" coefficients for these different wave trains; therefore, a simple updating of the form

$$(3.16) \quad E'(f) = E'_{sea}(f) + E'_{swell}(f)$$

where $E'(f)$ uses internally consistent wave parameters such that

$$(3.17) \quad E'_{sea} = \int_0^\infty E'_{sea}(f)\, df$$

with $E'_{sea}$ as the measured energy assumed to be in the local sea, i.e.

$$(3.18) \quad E'_{sea} = E_{sea}\left[\frac{\hat{E}_o}{E_o}\right]$$

and

$E_{swell}(f)$ uses internally consistent wave parameters such that

$$(3.19) \quad E'_{swell} = \int_0^\infty E'_{swell}(f)\, df$$

with $E'_{swell}$ as the measured energy assumed to be swell, i.e.

$$(3.20) \quad E'_{swell} = E_{swell}\left[\frac{\hat{E}_o}{E_o}\right].$$

## 4. SIMULATIONS OF WAVE FORECAST SKILL IMPROVEMENT DUE TO INCORPORATION OF MEASURED WAVE DATA

There are at least two different ways to obtain estimates of the improvement in the skill of wave forecasts due to the incorporation. The most straightforward way is to obtain a large set of wave data and forecast winds and have at it, running the model with and without updating via the wave measurements. This method is quite laborious and requires a rather substantial data set over a long period of time for proper evaluation. A second method involves an evaluation of the set of error probabilities from functional relationships among predicted wave model results assuming certain characteristics of wind errors and modeling errors. Since this research effort did not have access to a large set of wave data and forecast winds, the latter method will be used here.

A simple stochastic treatment of the forecast error in the wave heights of the local sea can be gained by allowing a sequence of winds with a specified stochastic error term to operate on the local grid point,

$$(4.1) \quad H^{n+1} = N^n + \phi_G(H^n, u_* + \varepsilon_{u*}, \theta_u + \varepsilon_\theta)$$

where $\phi_G$ is the local wave generation mechanism, $\varepsilon_{u*}$ is the random error component in the friction velocity over time step n, $\theta_u$ is the wind direction, and $\varepsilon_\theta$ is the random error component in the wind direction. Assuming open-ocean conditions with minimal fetch limited effects, this reduces the problem of evaluating the wave forecast skill to an analysis at a single point. In this context it is easy to run a single point hindcast with "true" winds and with winds including a stochastic error term and compare the results with and without updating the results after every 24 hours with the "true" wave height, which in this case is obtained from the parallel simulation with no wind errors. This assumes that the wave model itself contributes only a small error relative to the effect wind error on the predicted waves; however, if we want to examine the effects of model errors we can expand 4.2 to the form

$$(4.2) \quad H^{n+1} = H^n + \phi_G(H^n, u_* + \varepsilon_{u*}, \theta_u + \varepsilon_\theta, \varepsilon_m)$$

where $\varepsilon_m$ is an error component due to model inaccuracies. For the parallel simulation with the "true" winds the $\varepsilon_m$ term is retained.

The behavior of $\varepsilon_{u*}$, $\varepsilon_\theta$, and $\varepsilon_m$ have been at least partially answered in past studies. For the purposes of discussion here, $\varepsilon_{u*}$ is assumed to have a long-term gaussian distribution with standard deviations of 2.0 m/sec at 12 hours, 2.5 m/sec at 24 hours, 3.0 m/sec at 36 hours, and 3.5 m/sec at 48 hours; and $\varepsilon_u$ and $\varepsilon_m$ are also assumed to have long-term gaussian distributions with constant standard deviations of $10^o$ and 0.5 metres, respectively. (Note: No negative values of wind speed or $H^n$ are allowed.)

Table 4.1 shows the results of a simulation covering one year of time, based on an actual wind speed sequence from Sable Island (Figure 4.1). As can be seen here, there is substantial improvement in only the 12-hour forecast for local sea. If we assume that the error in wave height measurements is about 10 percent of the wave height, we obtain Table 4.2.

TABLE 4.1 Root Mean Square Errors in Simulated Local Seas With and and Without Incorporating "Perfect" Wave Height Information

| | Forecast Interval (hours) | | | |
|---|---|---|---|---|
| | 12 | 24 | 36 | 48 |
| No Updating | 1.1 | 1.3 | 1.5 | 1.6 |
| Updating | 0.6 | 1.2 | 1.5 | 1.6 |

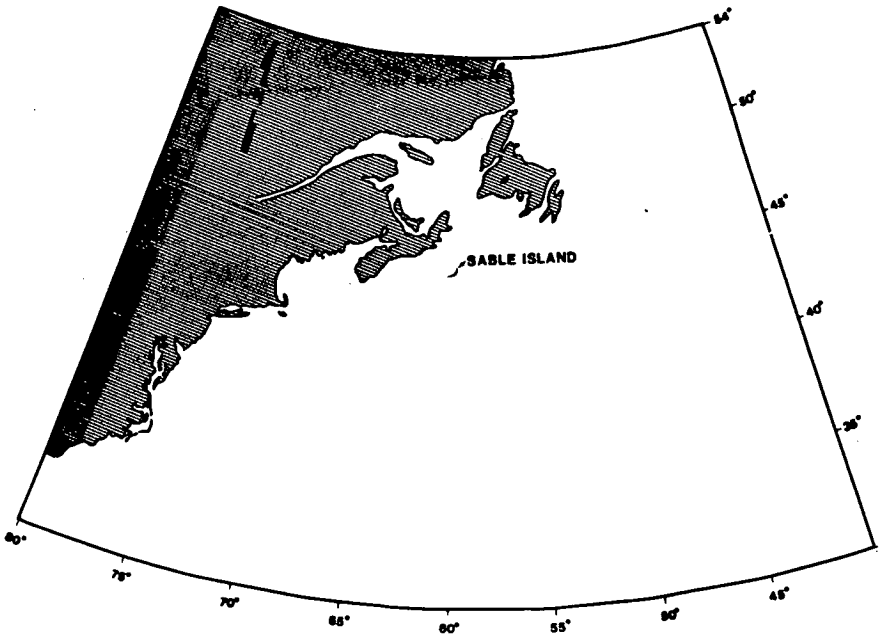


Figure 4.1. Map showing location of Sable Island area.

TABLE 4.2 Root Mean Square Error in Simulated Local Seas With and Without Incorporating Wave Height Information With Inherent 10% Random Error

| | Forecast Interval (hours) | | | |
|---|---|---|---|---|
| | 12 | 24 | 36 | 48 |
| No Updating | 1.1 | 1.3 | 1.5 | 1.6 |
| Updating | 0.8 | 1.3 | 1.5 | 1.6 |

Since estimation of expected swell errors involve large-area wave simulations, the probabilistic treatment of swell is considerably more difficult than the treatment of local sea; however, if we adopt a somewhat simplified approach to the problem we can at least obtain a rough estimate of the expected improvement in swell forecast skill obtainable by incorporating measured waves. To this purpose, let us assume that the swell height in the absence of wave measurements can be estimated by the relation

$$(4.3) \quad H_{sw}^{n+1} = H_{sea}^{*} + \phi_d(H_{sea}^{*}+\epsilon_H, m+\epsilon_m, d+\epsilon_d)$$

where $H_{sea}^{*}$ represents the local sea in the wave source area, $\phi_d$ is the decay over distance d as estimated in model "m." The terms $\epsilon_H$, $\epsilon_m$, and $\epsilon_d$ refer to errors in the initial wave height, the modeled physics, and the decay distance. The error in $H_{sea}^{*}$ can be estimated from the results of the previous simulation; but, one can only guess at the terms $\epsilon_m$ and $\epsilon_d$. Here they are assumed to be normally distributed (in terms of percentage deviations) around the modeled values, such that the sum of both error terms contributes an additional error of 10 percent of the swell height at a grid point.

If wave information is available over an entire field at the zero hour for the forecast, the only remaining error will be the $\epsilon_m$ term over the forecast interval plus any error in wave height measurement and estimated group velocity. In this case, using the assumption that $\epsilon_m = 0.1\ H_{sw}$, we can estimate the errors as a simple function of the estimated swell height.

Tables 4.3 and 4.4 give the results of simulated swell height forecasts, based on equation 4.1. The "true" values were estimated by assuming $\epsilon_H = \epsilon_m = \epsilon_d = 0$ in these simulations.

TABLE 4.3 Root Mean Square Errors in Simulated Swell Heights With and Without Incorporating "Perfect" Wave Height Information

| | Forecast Interval (hours) | | | |
|---|---|---|---|---|
| | 12 | 24 | 36 | 48 |
| No Updating | 0.8 | 1.0 | 1.1 | 1.2 |
| Updating | 0.2 | 0.4 | 0.5 | 0.6 |

TABLE 4.4 Root Mean Square Errors in Simulated Swell Heights With and Without Incorporating Wave Height Information With Inherent 10% Random Error

| | Forecast Interval (hours) | | | |
|---|---|---|---|---|
| | 12 | 24 | 36 | 48 |
| No Updating | 0.8 | 1.0 | 1.1 | 1.2 |
| Updating | 0.3 | 0.5 | 0.6 | 0.6 |

Table 4.5 presents the comparative rms error estimated for combined sea and swell assuming perfect wave measurements. This table suggests that even for intervals longer than 24 hours a significant increase in skill (primarily due to better estimates of swell heights) can be obtained by incorporating measured wave data. For the 12-hour forecast, the improvement in both local sea forecasts and swell forecasts contribute to a dramatic reduction in the rms skill. It should also be noted that, since the improvement in swell prediction is persistent, even if data such as satellite-derived wave heights become available 12 hours after real time, considerable improvement in wave prediction should still be possible.

TABLE 4.5 Root Mean Square Errors in Simulated Combined Sea and Swell With and Without Incorporating "Perfect" Wave Height Information

| | Forecast Interval (hours) | | | |
|---|---|---|---|---|
| | 12 | 24 | 36 | 48 |
| No Updating | 1.4 | 1.6 | 1.9 | 2.0 |
| Updating | 0.6 | 1.3 | 1.6 | 1.7 |

## 5. SUMMARY OF RESULTS

This study has attempted to present a theoretical/statistical framework for examining possible improvements in wave forecasts via the incorporation of wave measurements at the zero hour of the forecast. The results obtained suggest that a short-term gain in the accuracy of local sea predictions is realized; however, by 24 hours, this gain becomes almost neglegible. The gain in accuracy of swell predictions is also substantial in the short term; but, unlike the situation of local sea, this gain appears to persist for long intervals when an entire field of wave data, rather than a single point, is used to update the wave forecast model.

Other portions of this paper discuss various methods for incorporating measured wave data into wave models. It seems that methods to accomplish this are in a very formative stage, and it is recommended that further study into these methods be initiated.

As a final note, I feel that it is appropriate to point out that it is not always possible to evaluate the real value of something (such as an improved forecast skill) simply on a statistical basis. In this same context one might conclude that life boats on a ship only marginally improve the survivability of passengers. The point is that, even if they are only successfully used once, they are worth the investment in them. Similarly, if improved wave forecasts affect critical decisions involving lives and/or critical operations only once, the investment in these new techniques should be justifiable.

## 6. REFERENCES

Resio, D. T., 1985: A new technique for the estimation of extreme wind speeds. Proc., Int'l. Workshop on Offshore Winds and Icing, Halifax, Nova Scotia.

# REAL-TIME SPECTRAL WAVE FORECASTING MODEL TEST DURING CASP

B.M. Eid[1], V.J. Cardone[2], J.A. Greenwood[2] and J. Saunders[1]

1. MacLaren Plansearch Limited, Halifax, Nova Scotia, Canada
2. Oceanweather Inc., Cos Cob, Connecticut, U.S.A.

## ABSTRACT

This paper describes the work funded by the Environmental Studies Revolving Funds (ESRF) to set up and test a regional spectral ocean wave model for providing real-time wave forecasting during the Canadian Atlantic Storm Program (CASP).

The study consists of three phases. The first phase involves setting up the forecast procedure which includes:

(1) selection of a suitable operational wave model and modifications to the model for CASP application (including shallow water algorithm and using the Canadian Meteorological Centre (CMC) NWP model winds as input);

(2) accessing the CMC real-time wind data; and

(3) acquiring access to other necessary data such as wind/wave observations, ice cover data, etc.

The second is the forecasting phase which involves production of real-time forecast of directional spectral wave parameters during CASP field program. The third, verification phase of the study involves the evaluation of the model predictions against measurements which include both wind and wave data collected from both deep and shallow water sites.

Two versions of the model were run using two different input wind fields (one with CMC surface winds and the other using input winds produced from reanalysis of the LFM/NGM pressure fields in a man-machine forecast system). Time series comparisons and verification statistics are presented for the above two models. The model predictions are assessed and recommendations are made for improvement of wind and therefore, wave specifications.

## 1.0 INTRODUCTION

The Canadian Atlantic Storm Project (CASP) intensive field program was carried out from January 15 to March 15, 1986 offshore the East Coast of Canada. CASP main objective was to provide a better understanding and forecasting of east coast winter storms. In addition, CASP has provided a unique data base for numerical modelling studies for storm evolution and meteorological and sea state predictions.

This study was funded by the Environmental Studies Revolving Funds (ESRF) to produce and evaluate real-time wave forecasts from a regional spectral wave model which includes shallow water effects, for the duration of the CASP field experiment. (For details see MacLaren Plansearch (1986)).

The main objectives of this study are: (1) to identify wind and wave forecasting procedures, i.e. identify an appropriate spectral ocean wave model to be run in real-time during CASP and provide real-time data which is required as input to the wave model; (2) to provide real-time wave forecasting during CASP; and (3) to assess the model predictions.

Part of this study involved the acquisition of real-time wind fields from the Canadian Meteorological Centre (CMC) Numerical Weather Prediction (NWP) Operational Model suitable for input to the wave forecast model. The next step was to run a real-time test of the wave model during the CASP period for operational use and for evaluation of the model contribution to improving the wave forecasting in Canadian Waters.

A large amount of data on marine environment was collected during CASP, including measurements of winds and waves. These data were collected, checked, quality controlled and used for verification of both wind and wave predictions. Field data were collected from several sources. These sources were: Bedford Institute of Oceanography (BIO), Atmospheric Environment Service (AES), Shell Canada Limited, Petro-Canada, Huskey-Bow Valley, MacLaren Plansearch, and NOAA Buoy data from National Oceanographic Data Centre.

This paper describes the work carried out under the ESRF study Number 702-30-08 which consists of three phases:

1. Set-up the wave forecast procedure. The ODGP (Ocean Data Gathering Program) Spectral Ocean Wave Model was selected for this test. A modified version of the model which includes shallow water equations describing wave propagation in the CASP-OC (CASP Oceanographic Component) area, was set-up on a VAX 11/750 computer. This phase also included arrangements to access the CMC Operational Spectral Model wind fields, extraction of gridded wind vectors at all wave model grid points and data transmission into the VAX 11/750 computer to drive the wave model. The CMC winds (given at Sigma 0.998 level) was used directly without modification as input to the ODGP model.

2. Run the wave model and produce wave forecasts in real-time during the CASP field program, Jan. 15 to March 15, 1986.

3. Evaluate the model performance by comparing model results with measured data collected during CASP field project and wave predictions from other sources such as the METOC and the ODGP operational wave model which is driven by different winds in a man-machine forecasting system. The latter model (i.e. ODGP - OPR) has been running in real-time as part of MacLaren Plansearch/Oceanweather Inc. operational forecasting system.

## 2. MODEL SET-UP FOR CASP TEST

### 2.1 SELECTED MODEL AND PROCEDURE SET-UP

The model selected for the CASP wave forecasting test is the Ocean Data Gathering Program, ODGP, which has been operational at Oceanweather Inc./MacLaren Plansearch since mid September 1983. The model is a fully directional spectral deep-water wave model.

The ODGP wave model has been adopted for use in an operational wave analysis and forecast system, on the grid system shown in Figure 1. The grid consists of a coarse grid of spacing 1.25° latitude and 2.50° longitude covering most of the North Atlantic Ocean west of 20°W, and a nested grid (fine grid) in which the grid spacing is half that of the coarse. The fine grid extends over the Scotian Shelf and the Grand Banks covering most of the CASP study area. The present model has 24 directional bands spaced 15 degrees apart and 15 frequency bands.

The ODGP wave hindcast model evolved from the SOWM (Spectral Ocean Wave Model of the U.S. Navy) about a decade ago (a detailed documentation of both the ODGP and SOWM models is given in MacLaren Plansearch (1985)) and has since been tested against a broader range of wave regimes than any other existing model. The ODGP model incorporates a relatively simple representation of the source terms in the spectral energy balance equation compared to more recent formulations. The calibration of these parameterizations has remained stable over this period, unlike most contemporary models, which appear to undergo continuous tuning.

For the present CASP application, we regard the general problem of wave climate specification in the Canadian East Coast waters as basically a three-scale problem. The largest scale requires a grid of about 100 km spacing covering most of the North Atlantic Ocean (e.g. the ODGP coarse grid). The second scale requires a gird no more than about 50 km spacing (e.g. the ODGP fine grid) to resolve large islands and capes and irregular shoreline geometry, large scale ice cover effects, and hopefully smaller scale features in the windfield. Given that the typical shelf width offshore (to depths of 50 m) in Canadian East Coast waters of interest is of order 50 km, or 1 grid spacing on the fine grid, it is appropriate that the coarse and fine grid scales be treated as deep water. The third scale should resolve the shallow shelf width explicitly on a grid of the order 1-2 km spacing (e.g. ODGP ultra-fine CASP grid).

While the time step in a wave model on the larger two scales is 1-3 hours, the time step required in current shallow water wave models for a 1 km grid is typically less than 60 seconds. Clearly the specification of a wave climate in shallow water, using a wave model with shallow water physics is a computing intensive activity to be pursued only on a regional basis as required. However, the proposed deep-water model is invaluable in that it can provide the required deep-water spectra which the shallow water models require as input.

For this study, therefore, the ODGP discrete spectral model (which based on deep water physics) is applied on a two-dimensional nested- grid system to account for the large and fine scales (Figure 1), and on a one-dimensional spatial grid extending to a 100 m contour which covers the CASP-OC measurement sites with shallow water propagation (Figure 2).

Two versions of the deep-water ODGP model were used in the present study:

(1) ODGP-CMC: ODGP model driven by the CMC wind fields (analysis and forecast at Sigma 0.998 level), and

(2) ODGP-OPR: the operational version of ODGP (which is running in real-time at Oceanweather/MacLaren Plansearch). This version is identical to the above, but driven by winds obtained from the NOAA LFM/NGM numerical weather prediction surface pressure and a man-machine analysis which incorporates the Marine Planetary Boundary Layer (MPBL) equations developed by Cardone (1969, 1978).

The results of above runs provide an excellent means of evaluation of the CMC winds and its suitability to run a wave model. The results of the ODGP-CMC at the end of the ultra-fine grid are used to run the shallow water model as described in the following sections.

## 2.2 ODGP DEEP-WATER MODEL ALGORITHM

Only a very brief summary is presented hereunder. For detailed description of the model, the reader is referred to Cardone et al (1976), and MacLaren Plansearch (1985 and 1986). The general energy balance equation for wave evolution is given by the equation:

$$\frac{\partial}{\partial t} S(f,\theta;x,t) + Cg.\ \nabla\ S = F(f,\theta;x,t) \qquad (2.1)$$

Where: $S=S(f,\theta;x,t)$ is the two-dimensional wave spectrum as a function of frequency and direction $\theta$ at a given location x and time t; $C_g=C_g\ (f,\theta)$ is the deep-water group velocity; and $F(f,\theta;x,t)$ is the source function which represents all physical processes that transfer energy from or to the spectrum.

The source function may be expressed as a sum of three terms:

$$F = F_{in} + F_{nl} + F_{ds}$$

Where: $F_{in}$ = energy input function by wind, $F_{nl}$ = non-linear transfer by wave-wave interaction, and $F_{ds}$ = energy dissipation term.

The input source function ($F_{in}$) is represented in ODGP as a function of wind speed and frequency according to the linear equation:

$$F_{in} = A + B.S$$

The A term in the above equation $=A(f_i,u)$ is a function of frequency f and wind speed u. This term represents Phillips' external turbulent pressure forcing. The B.S term corresponds to Miles' linear feedback mechanism. The term $B(f_i,u_*)$ is expressed in ODGP as a function of frequency and the friction velocity $u_*$. The energy transfer associated with the non-linear wave-wave interaction is not explicitly included in ODGP. The above terms are described in MacLaren Plansearch (1985) and also in Pierson (1982).

## 2.3 SHALLOW-WATER WAVE MODEL

In recent years, two new concepts have been introduced to describe shallow water wave transformations. The first concept follows from the theoretical finding that non-linear wave-wave interactions, which are now generally believed to play an important role in the deep water spectral energy balance, are greatly enhanced in shallow water. Over a sloping bottom these interactions, though intrinsically energy conserving, effectively act to cause attenuation of wave height, as energy transferred from the vicinity of the spectral peak to higher frequencies is lost through wave breaking in the so-called saturation range of the spectrum. The second new concept is turbulent bottom friction, which depends sensitively on bottom sediment properties and sediment transport processes.

These concepts have led to the introduction of a number of new shallow water wave prediction models, but the properties of these models vary widely and a number controversial issues which affect the quantitative performance of these models in storm situations have yet to be resolved. This had led to a number of intercomparison studies involving alternate models. Several such studies are underway in the U.S., Canada and Europe, and it appears that a much clearer picture of the relevant physics for shallow water transformation will emerge in about one year. One of the seeming consequences of the dominance of one or both of the above source terms in the process of shallow-water transformations is the recent finding that wind/wave spectra in shallow water follow a self-similar form that can be described by the so-called TMA spectrum (Bouws et al (1985)).

In the present study, a shallow water version of the ODGP model (which includes wave number scaling, shoaling, refraction, and bottom friction using Grant and Medsen (1982) model) has been nested within the coarse and fine ODGP grids over the CASP-Oceanographic array, and has run experimentally, separately from the operational system as described below. In this separate analysis/forecast run input winds are taken from CMC NWP products.

The algorithm used in the CASP shallow-water model are described in details in MacLaren Plansearch (1986).

### 2.3.1 Model Implementation

The shallow-water model is adapted on a one-dimensional (1-D) array of grid points laid out along the CASP shallow-water measurement array, so-called ultrafine grid, as shown in Figure 2. The (1-D) array extends along CASP-OC array in the direction, normal to the bottom contours, which are taken as straight lines parallel to coastline. Bottom slope was taken as constant in the ratio 1:294. Grid points were spaced at depth intervals of 7.5 m, yielding a grid spacing of 2.205 km.

Immediately following each CMC deep-water wave model run, the 1-D shallow-water model was executed separately nine times to provide wave analyses and forecasts on the 1-D shallow-water grid at six-hourly intervals between forecast projection times of 0 and 48 hours. The 1-D model is initialized from the two-dimensional wave spectrum and wind speed and direction specified at the ODGP fine-grid point located at the end of the 1-D line.

## 3. REAL-TIME APPLICATION DURING CASP

The degree of success in using an Ocean wave model in an operational sense is dependent on the timing of the output from the numerical weather prediction models, as well as the speed of running the wave model and providing forecast useful for real-time operational needs. The implementation of the ODGP/CASP model followed closely the timelines used for the ODGP-OPR model. Basically, the model was executed twice daily in a hindcast/forecast cycle for oo and 12 GMT (tau 0) initial states. In each run the T-6 and $T_o$ states were generated from the corresponding T-6 and $T_o$ wind fields (i.e. analysis winds). Values at T-6 were not immediately available from the CMC model output, instead T+6 prog values from the 12 hour previous run were used. Each run is continued forward to 48 hours, driven by CMC forecast winds. This procedure is schematically presented in Figure 3.

## 4. EVALUATION OF MODEL PREDICTIONS

### 4.1 STUDY AREA AND DATA BASE ASSEMBLY

Figure 4 depicts the study area and the locations of model grid points and evaluation sites at which field data were available during the study period. The study area is divided into four geographical regions: Region 1 covers the U.S. east coast and Georges Bank, Region 2 on the Scotian Shelf, Region 3 on the Grand and Region 4 at CASP-OC area at which the ODGP-CMC shallow water model results were compared with BIO directional wave measurements. Table 1 provides a list of the evaluation sites and the nearest ODGP grid points and data sources. In addition, the manually drawn charts of significant wave height produced at the METOC centre in Halifax, N.S. were obtained and their predictions were compared with the ODGP model results.

Winds were measured at various anemometer heights ranging from 10 to 90 m above water surface. Therefore, all observed winds, with the exception of the Minimet data, were reduced to a common 20 m neutral wind by using the procedure described by Cardone (1969) and (1978).

### 4.2 ANALYSIS AND RESULTS

The results of the models evaluation are presented in details in MacLaren Plansearch (1986). Due to the limited space available for this paper, only a very brief summary of the results and conclusions drawn are presented here.

The results of the ODGP-CMC (deep and shallow), ODGP-OPR and METOC predictions were compared against the observed field data (wind speed, direction, wave height and peak period). Time series plots were obtained (sample plots are shown in Figure 5). Linear regressions and scatter diagrams were produced (as shown in Figure 6). In addition, error statistics were calculated as shown in Table 2 for all deep water sites combined, and Table 3 for shallow water sites combined. As shown in Figure 5, a large error in the deep water model predictions had contributed to the large error in the shallow-water

predictions during the last two weeks of January. This is also clear from Table 3 where error statistics are smaller for period Feb 2 to March 15 than those obtained for the entire study period.

In addition to the above analyses, four storm events were selected for intensive evaluation of the alternate analysis and forecasts of sea-level pressure winds provided by various operational NWP products and the corresponding sea-state model predictions. The 4 storm events are listed below:

Storm #1: 19 Jan. 00 GMT to 23 Jan. 00 GMT
Storm #2: 26 Jan. 12 GMT to 30 Jan. 12 GMT
Storm #3: 15 Feb. 00 GMT to 19 Feb. 00 GMT
Storm #4: 10 Mar. 00 GMT to 14 Mar. 00 GMT

A systematic intercomparison of alternate forecasts of central pressures and position of separate low pressure systems which comprise the above 4 storms is presented here. This analysis was performed to provide an indication of differences between forecast pressure field, which may be related to differences between forecast surface wind fields and, therefore, to differences between deep-water forecasts produced from the OPR and CMC winds. The comparison is presented in terms of the mean and standard deviation between forecast and analysis central pressure, latitude and longitude of lows, stratified by forecast projection time and model (LFM/NGM, OPR, CMC), as shown in Table 4.

As shown in Table 4, the central pressure mean errors are consistently positive (i.e. over-forecast) for all models and increase with increasing forecast range. However, up to 24 hr. prog such errors for the OPR forecasts are only 1 mb, which indicates that the man-machine mix procedures are effective in improving the forecasts provided by the LFM/NGM models. The scatter in the OPR forecasts is also slightly improved relative to that of the underlying numerical forecasts. Overall, the CMC pressure errors are close to those of LFM/NGM model. This is somewhat surprising, considering the tendency for CMC surface wind forecasts to be positively biased (Table 2). However, in the case of CMC model, the sign of the central pressure error may not be as a good indicator of the relative accuracy of the forecast pressure gradient about the low centre.

The forecast mean errors of storm latitude for the LFM/NGM and OPR models are generally small and negligible. The CMC has the tendancy for northward displacement. The forecast mean errors of storm longitude are positive for all models. This statistic is believed to reflect a tendancy for the models to move low systems eastward slower than observed.

## 5. CONCLUSIONS

This paper described the work carried out to set-up and test a regional spectral ocean wave model which provided real-time wave forecasts during the two months duration of CASP. This study provided a comprehensive evaluation and statistical measures of the accuracy of the operational wave model (ODGP) which was driven by the CMC winds during CASP period. In addition, ODGP-CMC model predictions were also compared against those obtained from the same model (ODGP-OPR) when driven by an improved (man-machine mix) wind field.

The side-by-side evaluation of ODGP-CMC and ODGP-OPR provides insights into the causes of the main difference between the two models, i.e. input wind fields. Certainly, the CMC provided winds with a large positive bias, which grew with forecast projection time. This, in turn, contributed to the large errors in wave height predictions.

The ODGP operational wave model can predict sea-state accurately with a mean scatter index of 30% at T+0 to 37% at T+48 hr with RMSE in the range 0.85 to 1.07m. When driven by CMC winds, the same model predicted wave height with scatter index of 60 to 70% and RMSE of 1.88 to 1.97 m, for T+0 and T+48 hr, respectively. Peak periods were predicted with better accuracies by both models (22 to 28% S.I.). However, the mean errors in wind fields from the two models at the evaluation sites were not as large as those of wave heights. This is due to errors in the far field winds which may have contributed to the prediction of swell waves travelling from those offshore fields.

In addition, a 1-D shallow-water wave model was tested within the CASP-OC area. The accuracy of this model is a function of input spectra (obtained from the deep-water model) at the end of the 1-D array, treatment of local winds (particularly offshore winds), and shallow-water propagation algorithm. When excluding the periods when the input deep-water spectra were incorrect (i.e. the last two weeks of January), the model predicted the wave height with RMSE of 0.5 m and 35% S.I.

METOC predictions showed comparable skill to the ODGP-OPR at analysis time (T=0) where as the ODGP-OPR provided better skill in forecast mode.

## 6. REFERENCES


Bouws, E., J.J. Ephraums, J.A. Ewing, P.E. Francis, H. Gunther, P.A. Janssen, G.J. Komen, W. Rosenthal, W.J. de Voogt (1985). A Shallow Water Intercomparison of Three Numberical Wave Prediction Models (SWIM). Quart. J.R. Met. Soc., Vol. III, PP. 1087-1112.

Cardone, V.J., W.J. Pierson and E.G. Ward (1976). Hindcasting the directional spectrum of hurricane generated waves. J. of Petrol. Tech. 28, pp. 385-384.

Cardone, V.J. (1969). Specification of the wind field distribution in the marine boundary layer for wave forecasting. Report TR-69-1, Geophys. Sci. Lab., New York University. Available from NTIS AD#702-490.

Cardone, V.J. (1978). Specification and prediction of the vector wind on the U.S. Continental Shelf for application to an oil slick tragectory forecast program. Final Report, for NOAA, U.S. Dept. of Commerce, Silver Spring, Maryland, Nov. 1978.

Grant, W.D. and O.S. Madsen (1982). Moveable bed roughness in unsteady oscillatory flow. J. of Geophysical Res., 87 (C1), PP. 469-481.

MacLaren Plansearch limited (1985). Evaluation of the Spectral Ocean Wave Model (SOWM) for Supporting Real-Time Wave Forecasting in the Canadian East Coast Offshore. Report submitted to the Atmoshperic Environment Service, January 1985.

MacLaren Plansearch limited (1986). CASP Wave Forecasting Operational Test. Report prepared for the Environmental Studies Revolving Funds (ESRF) under Contract #702-30-08, (in press).

Pierson, W.M. (1982). The spectral ocean wave model (SOWM), a Northern Hemisphere computer model for specifying and forecasting ocean wave spectra. Prepared for the: David Taylor Naval Ship Research and Development Command under Contract: N00167-80-M-4781.

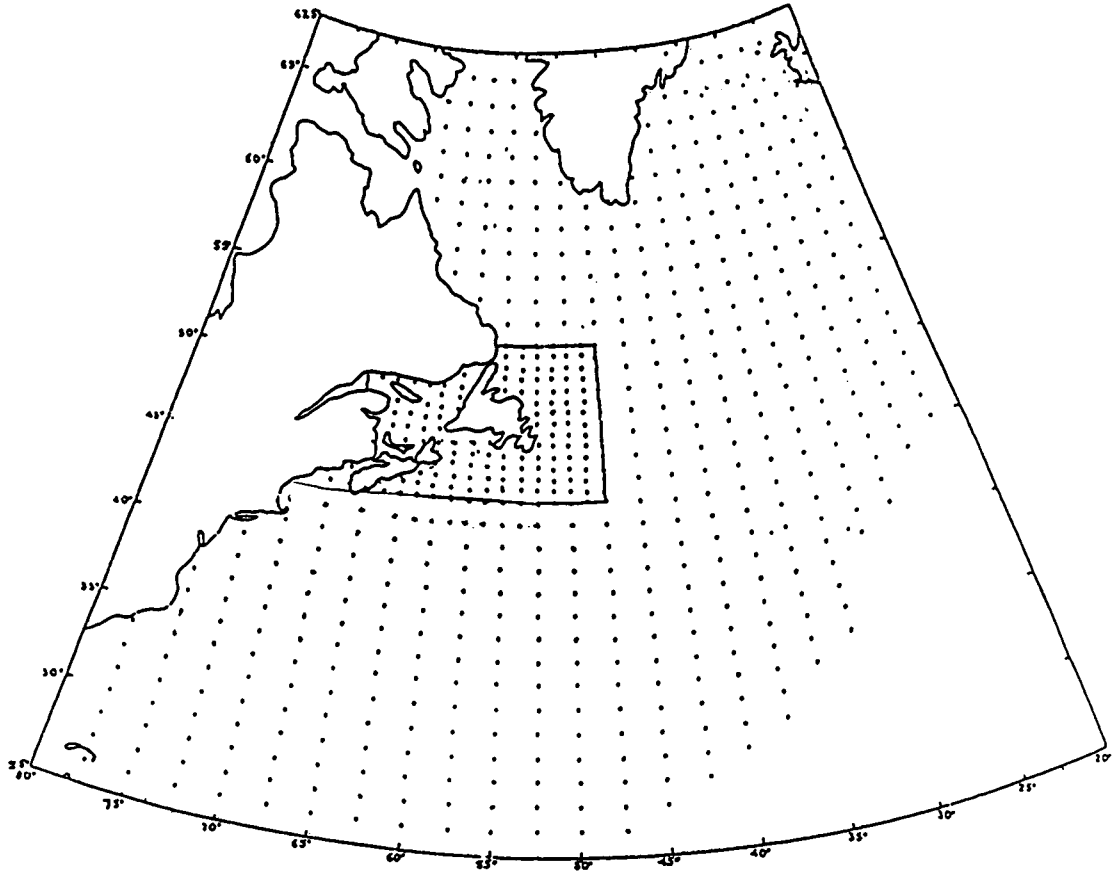

Figure 1: Operational ODGP wave forecast model grid. Coarse grid point shown at spacing of 1.25° latitude by 2.5° longitude. Domain of fine-mesh CASP grid is also shown (0.625° X 1.25°).

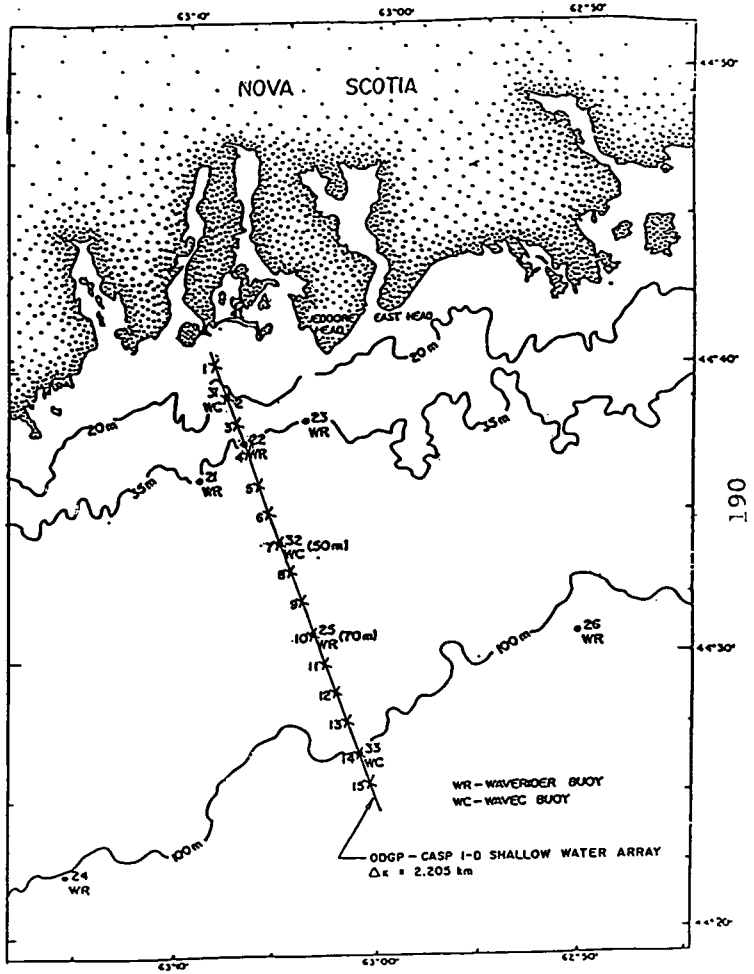


FIGURE: 2 .: CASP SHALLOW-WATER, ONE-DIMENSIONAL MODEL GRID

## OPERATIONAL ODGP/CASP WAVE FORECAST SYSTEM

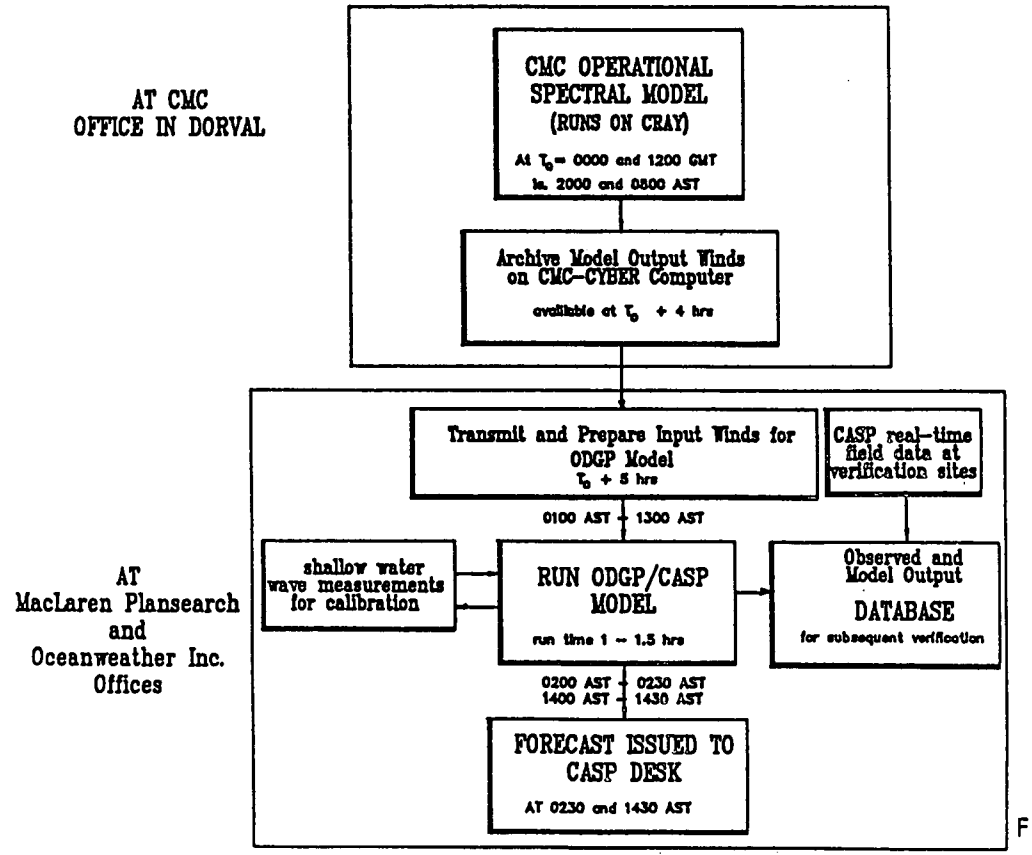


FIGURE 3

TABLE 1 EVALUATION SITES

| SITE # | LOCATION | WATER DEPTH (m) | NEAREST ODGP GRID POINT | AVAILABLE PARAMETERS | DATA SOURCE | ANEMOMETER HEIGHT (m) |
|---|---|---|---|---|---|---|
| 11 | 38°31'N<br>70°42'W | 2834 | 236 | Wind, Wave, Spectral Estimates Air, Sea Temp. | NOAA BUOY 44004 | 10 |
| 12 | 41°04'N<br>66°34'W | 85 | 277 | Wind, Wave, Spectral Estimates Air, Sea Temp. | NOAA BUOY 44011 | 10 |
| 21a | 43°51'N<br>60°38'W | 40 | 1013 | Wind, Wave, Spectral Estimates, Air, Sea Temp. | MANMAR/Waverider: R. GORILLA at Cohasset A-52. | 88 |
| 21b | 43°41'N<br>59°53'W | 105 | 1013 | Wind, Wave, Spectral Estimates, Air, Sea Temp. | MANMAR/Wavrider: SEDCO 709 and JOHN SHAW at N. Triumph B-52 | 17<br>73 |
| 22 | 43°51'N<br>58°22'W | 1516 | 1014 | Wind, Wave, Air, Sea Temp. | MANMAR: SEDCO 709 at Tantallon M-41 | 17 |
| 31a | 46°27'N<br>48°29'W | 97 | 1127 | Wind, Wave, Air, Sea Temp. | MANMAR: SDS VINLAND at Terra Nova I-97 | 83 |
| 31b | 46°41'N<br>48°25'W<br>46°51'N<br>48°10'W | 98<br>117 | 1127 | Wind, Wave, Air, Sea Temp. | MANMAR: SEDCO 710 at N. Ben Nevis M-61 and BOWDRILL 2 at Whiterose L-61 | 78<br>82 |
| 41 | 44°27'N<br>63°01'W | 100 | SW14 | 2-D Spectral Estimates, Wind Speed, Direction | WAVEC 33/Minimet* | 3 |
| 42 | 44°34'N<br>63°05'W | 50 | SW 7 | 2-D Spectral Estimates, Wind Speed, Direction | WAVEC 32/Minimet | 3 |
| 43 | 44°39'N<br>63°08'W | 25 | SW 2 | 2-D Spectral Estimates, Wind Speed, Direction | WAVEC 31/Minimet | 3 |

* One MINIMET buoy was deployed at 44°28'N, 63°00' W

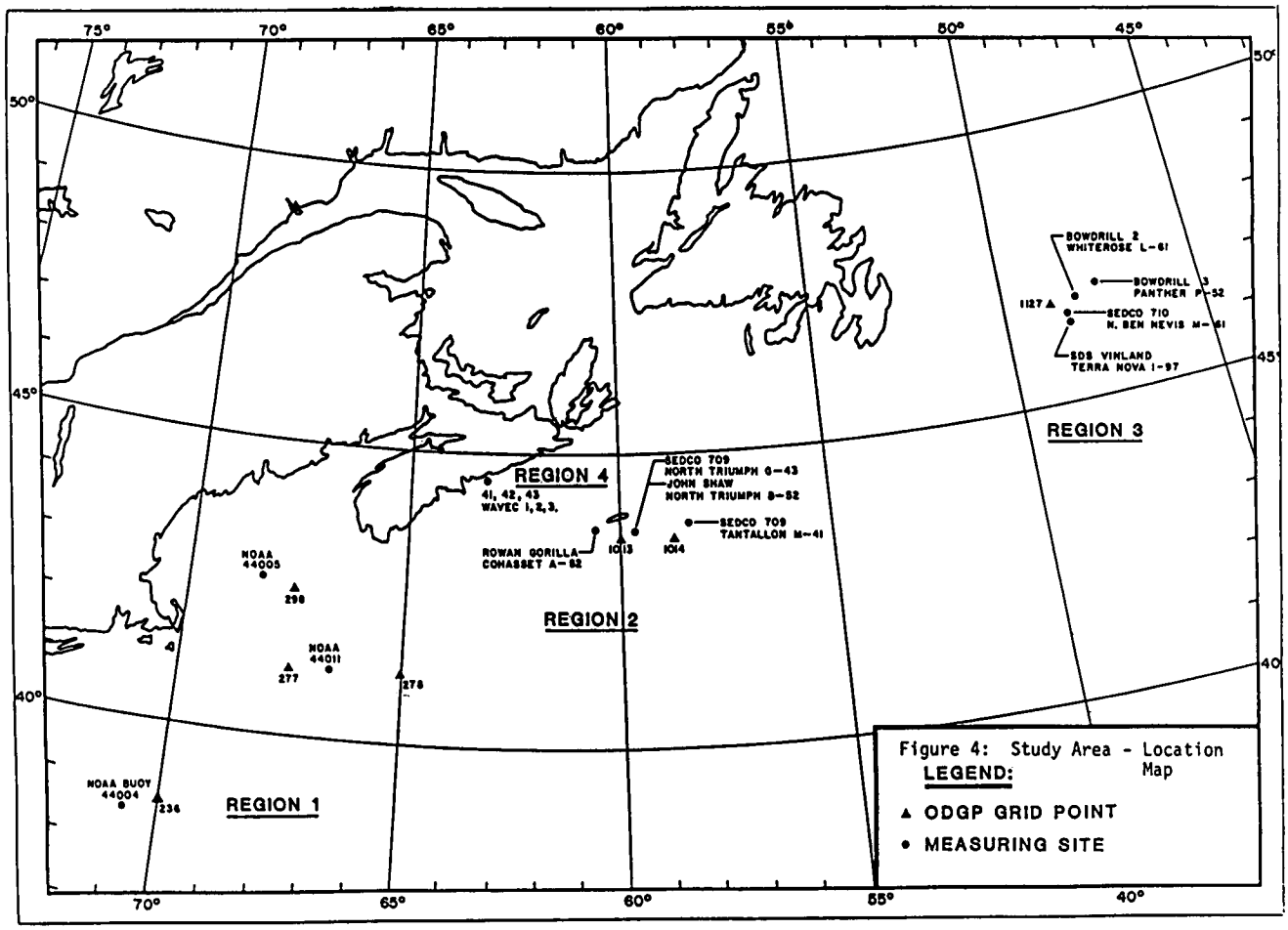


TABLE 2 ERROR STATISTICS - ALL DEEP WATER SITES

| PROG TIME (HR) | MODEL | WIND - SPEED RMSE (kts) | SI (%) | BIAS (kts) | ABS.ER. (kts) | SIGNIFICANT WAVE HEIGHT RMSE (m) | SI (%) | BIAS (m) | ABS.ER. (m) | PEAK PERIOD RMSE (sec) | SI (%) | BIAS (sec) | ABS.ER (sec) |
|---|---|---|---|---|---|---|---|---|---|---|---|---|---|
| 00 | OPR | 5.89 | 28 | -1.26 | 4.54 | 0.85 | 30 | 0.23 | 0.65 | 1.94 | 22 | -0.36 | 1.49 |
| | CMC | 7.59 | 36 | 0.91 | 5.74 | 1.88 | 65 | 1.02 | 1.33 | 2.05 | 24 | 0.49 | 2.05 |
| | METOC | | | | | 0.83 | 28 | 0.28 | 0.62 | | | | |
| 12 | OPR | 7.22 | 35 | -0.45 | 5.58 | 0.92 | 32 | 0.26 | 0.70 | 1.95 | 22 | -0.39 | 1.49 |
| | CMC | 8.17 | 39 | 2.09 | 6.09 | 1.91 | 66 | 1.10 | 1.37 | 2.04 | 24 | 0.60 | 1.56 |
| | METOC | | | | | 1.20 | 41 | 0.34 | 0.88 | | | | |
| 24 | OPR | 7.93 | 38 | -0.45 | 6.16 | 0.98 | 34 | 0.24 | 0.74 | 1.95 | 22 | -0.38 | 1.51 |
| | CMC | 8.55 | 41 | 2.54 | 6.40 | 1.96 | 69 | 1.19 | 1.43 | 2.19 | 25 | 0.72 | 1.65 |
| | METOC | | | | | 1.15 | 39 | 0.25 | 0.89 | | | | |
| 36 | OPR | 8.39 | 40 | -0.88 | 6.59 | 1.06 | 37 | 0.19 | 0.80 | 2.10 | 24 | -0.39 | 1.62 |
| | CMC | 9.32 | 45 | 2.50 | 7.00 | 1.97 | 70 | 1.21 | 1.46 | 2.38 | 27 | 0.92 | 1.75 |
| | METOC | | | | | 1.23 | 42 | 0.21 | 0.95 | | | | |
| 48 | OPR | 9.25 | 44 | -1.06 | 7.23 | 1.07 | 37 | 0.14 | 0.84 | 2.14 | 25 | -0.36 | 1.67 |
| | CMC | 9.71 | 47 | 2.88 | 7.47 | 1.97 | 70 | 1.18 | 1.47 | 2.47 | 28 | 0.95 | 1.84 |

Mean Error (Bias) - $\sum (x_1-x_2)/NPTS$

Mean Absolute Error - $\sum|(x_1-x_2)|/NPTS$

Roof Mean Square Error (RMSE) - $(\sum (x_1-x_2)^2/NPTS)^{1/2}$

Scatter Index (S.I.) - (RMSE/AVE) x 100

where: $x_1$ is the model value (i.e. forecast),
$x_2$ is the observed value
AVE is the mean of observed values and
NPTS is the number of data pairs.

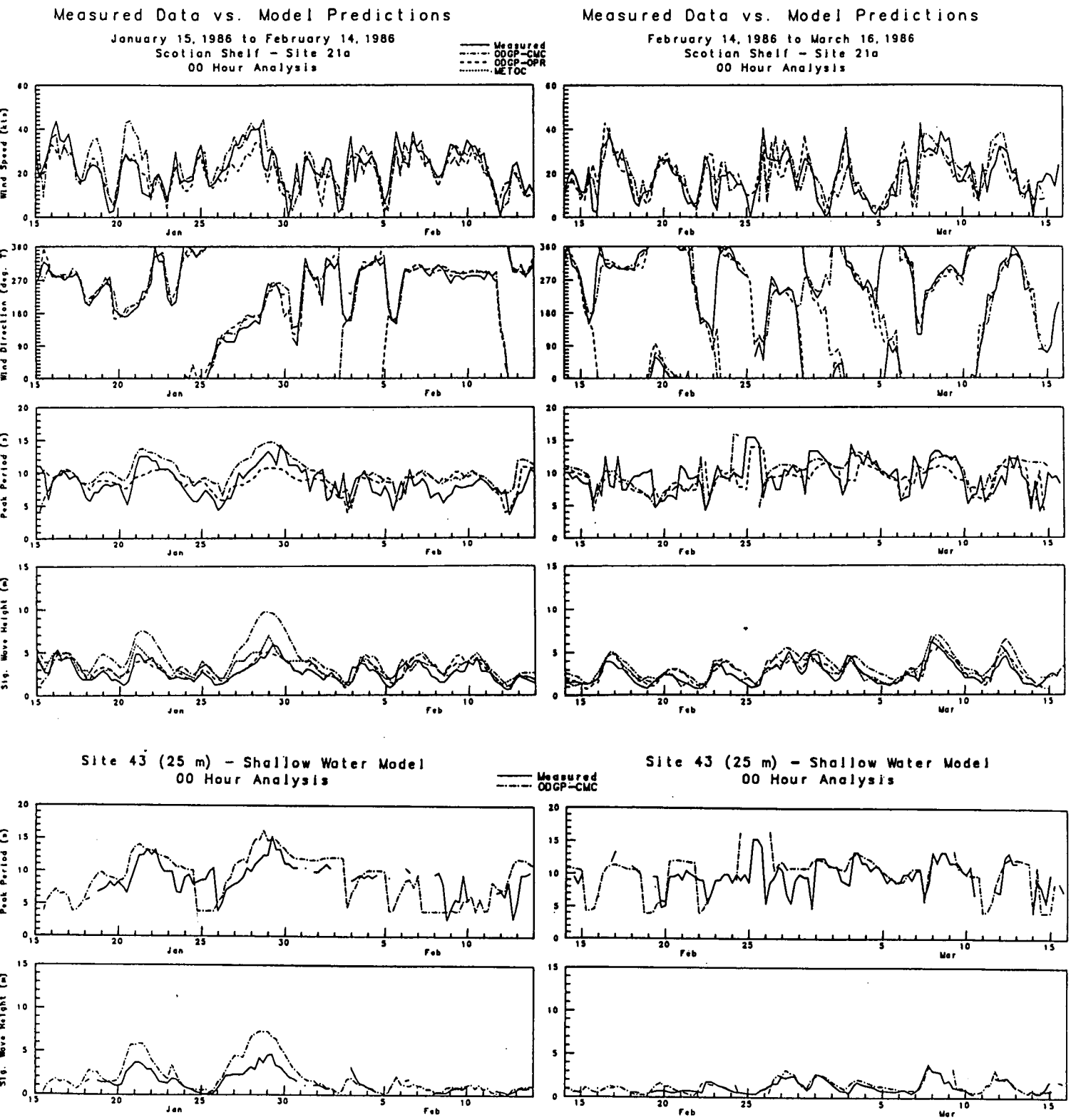
Measured Data vs. Model Predictions
January 15, 1986 to February 14, 1986
Scotian Shelf - Site 21a
00 Hour Analysis
Measured
ODGP-CMC
ODGP-OPR
METOC
Measured Data vs. Model Predictions
February 14, 1986 to March 16, 1986
Scotian Shelf - Site 21a
00 Hour Analysis
Wind Speed (kts)
Wind Direction (deg. T)
Peak Period (s)
Sig. Wave Height (m)
Jan
Feb
Mar
Site 43 (25 m) - Shallow Water Model
00 Hour Analysis
Measured
ODGP-CMC
Site 43 (25 m) - Shallow Water Model
00 Hour Analysis

FIGURE 5

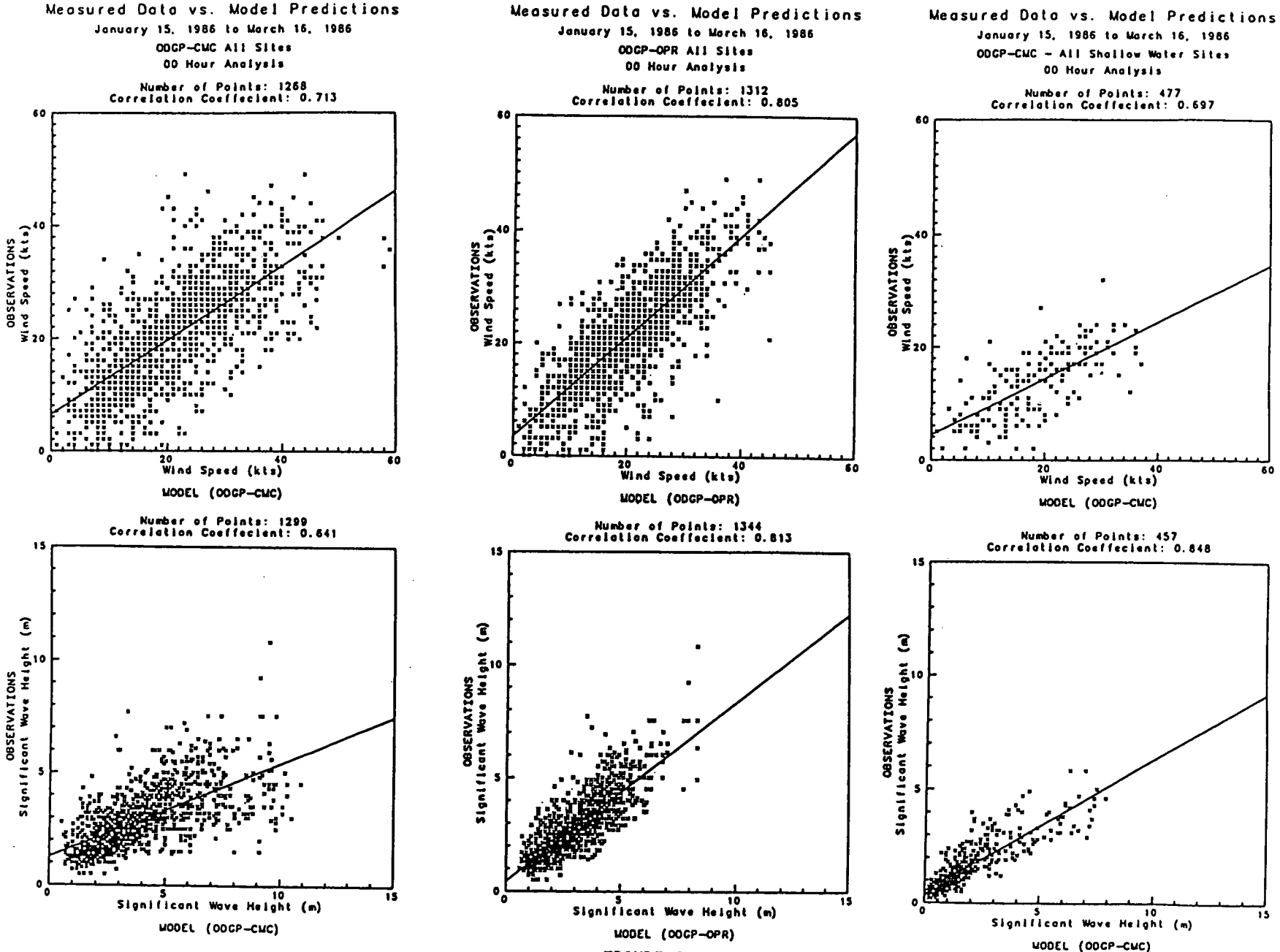
Measured Data vs. Model Predictions
January 15, 1986 to March 16, 1986
ODGP-CMC All Sites
00 Hour Analysis
Number of Points: 1268
Correlation Coeffecient: 0.713
OBSERVATIONS Wind Speed (kts)
Wind Speed (kts)
MODEL (ODGP-CMC)
Measured Data vs. Model Predictions
January 15, 1986 to March 16, 1986
ODGP-OPR All Sites
00 Hour Analysis
Number of Points: 1312
Correlation Coeffecient: 0.805
OBSERVATIONS Wind Speed (kts)
Wind Speed (kts)
MODEL (ODGP-OPR)
Measured Data vs. Model Predictions
January 15, 1986 to March 16, 1986
ODGP-CMC - All Shallow Water Sites
00 Hour Analysis
Number of Points: 477
Correlation Coeffecient: 0.697
OBSERVATIONS Wind Speed (kts)
Wind Speed (kts)
MODEL (ODGP-CMC)
Number of Points: 1299
Correlation Coeffecient: 0.641
OBSERVATIONS Significant Wave Height (m)
Significant Wave Height (m)
MODEL (ODGP-CMC)
Number of Points: 1344
Correlation Coeffecient: 0.813
OBSERVATIONS Significant Wave Height (m)
Significant Wave Height (m)
MODEL (ODGP-OPR)
Number of Points: 457
Correlation Coeffecient: 0.848
OBSERVATIONS Significant Wave Height (m)
Significant Wave Height (m)
MODEL (ODGP-CMC)

FIGURE 6

TABLE 3 SUMMARY OF ERROR STATISTICS FOR SHALLOW WATER SITES

| PRODUCT | PARAMETER | January 15 - March 15 Forecast Time | | | | | February 2 - March 15 Forecast Time | | | | |
|---|---|---|---|---|---|---|---|---|---|---|---|
| | | 00 | 12 | 24 | 36 | 48 | 00 | 12 | 24 | 36 | 48 |
| Wind Speed | Bias (knot) | 4.48 | 6.66 | 6.83 | 6.18 | 6.56 | 4.75 | 6.94 | 7.15 | 6.36 | 6.75 |
| | M. Abs. Er. | 5.88 | 7.62 | 8.20 | 8.06 | 8.44 | 5.81 | 7.60 | 8.36 | 8.12 | 8.49 |
| | RMSE (knot) | 7.45 | 9.51 | 10.74 | 10.76 | 12.00 | 7.46 | 9.6 | 10.99 | 10.97 | 12.20 |
| | SI (%) | 56 | 72 | 81 | 82 | 91 | 56 | 73 | 84 | 84 | 93 |
| Sig-Ht | Bias (m) | 0.30 | 0.37 | 0.41 | 0.41 | 0.49 | 0.00 | 0.10 | 0.15 | 0.14 | 0.25 |
| | M. Abs. Er. (m) | 0.57 | 0.61 | 0.68 | 0.74 | 0.82 | 0.37 | 0.42 | 0.49 | 0.58 | 0.70 |
| | RMSE (m) | 0.90 | 0.93 | 1.02 | 1.13 | 1.23 | 0.51 | 0.58 | 0.79 | 0.95 | 1.15 |
| | SI (%) | 55 | 57 | 63 | 69 | 76 | 35 | 40 | 54 | 65 | 79 |
| Peak Period | Bias (sec) | 0.62 | 0.62 | 0.79 | 0.78 | 0.78 | 0.42 | 0.42 | 0.67 | 0.65 | 0.69 |
| | M. Abs. Er. (sec) | 1.63 | 1.68 | 1.74 | 1.86 | 1.99 | 1.61 | 1.68 | 1.75 | 1.91 | 2.13 |
| | RMSE (sec) | 2.33 | 2.39 | 2.41 | 2.56 | 2.72 | 2.4 | 2.47 | 2.51 | 2.69 | 2.92 |
| | SI (%) | 26 | 26 | 27 | 28 | 30 | 27 | 27 | 28 | 30 | 33 |

TABLE 4: Verification of Central Pressure and Position
LFM/NGM, OPR and CMC Forecasts in Selected CASP Storms

| Parameter | Tau (hrs) | LFM/NGM[2] Mean[1] | LFM/NGM[2] Std. Dev. | LFM/NGM[2] No. | OPR[3] Mean[1] | OPR[3] Std. Dev. | OPR[3] No. | CMC[4] Mean[1] | CMC[4] Std. Dev. | CMC[4] No. |
|---|---|---|---|---|---|---|---|---|---|---|
| Pressure (mb) | 12 | 5.0 | 3.9 | 25 | 1.0 | 4.1 | 23 | 5.2 | 3.6 | 24 |
| | 24 | 6.2 | 6.6 | 25 | 1.1 | 5.4 | 23 | 6.0 | 6.4 | 22 |
| | 48 | 8.9 | 8.4 | 25 | 3.7 | 7.4 | 23 | 6.7 | 7.2 | 23 |
| Latitude (deg. N) | 12 | 0.1 | 1.8 | 25 | 0.1 | 1.5 | 23 | .4 | 1.8 | 24 |
| | 24 | 0.0 | 2.2 | 25 | 0.7 | 1.8 | 23 | 1.5 | 2.6 | 22 |
| | 48 | 0.1 | 2.2 | 25 | 0.3 | 2.6 | 23 | 1.6 | 2.7 | 23 |
| Longitude (deg. W) | 12 | 1.8 | 1.7 | 25 | 1.9 | 3.4 | 23 | 2.5 | 3.8 | 24 |
| | 24 | 1.9 | 1.9 | 25 | 2.1 | 3.6 | 23 | 1.8 | 3.3 | 22 |
| | 48 | 1.8 | 3.1 | 25 | 2.0 | 4.1 | 23 | 1.8 | 3.8 | 23 |

[1]Mean errors: forecast minus observed
[2]NOAA Limited Area Fine Mesh (LFM) Model to February 7, 1986; Nested Grid Model (NGM) after February 7, 1986.
[3]OPR: MacLaren Plansearch/Oceanweather operation forecast system
[4]CMC: AES Canadian Meteorological Centre Spectral atmospheric numerical forecast model

No. is number of comparisons - They are different due to missing of some facsimile transmissions.

# ACCURACY OF NUMERICAL WEATHER PREDICTION WINDS AND SOME CONSEQUENCES FOR WAVE PREDICTION

by

Donald O. Hodgins, Ph.D.
Sandra L.M. Hodgins, M.A.Sc.

Seaconsult Marine Research Ltd.
Vancouver, British Columbia, Canada

## Abstract

Forecast winds derived from the Canadian Meteorological Centre's spectral model are shown to have relatively small biases (less than 3 kts in speed and 10° in direction for lead times out to 24 h) when compared with observed winds proximate to Sable Island and averaged over an interval containing many different weather systems. However, the error statistics exhibit large scatter and temporally coherent wind speed errors of 15 to 20 kts were found in certain storms that seemed to be poorly modelled throughout their history. Error bounds on wave heights corresponding to systematic perturbations of storm parameters are then established through wave hindcasting. Over the NE Pacific Ocean bounds of 100% to 200% in $H_s$ are associated with storm trajectory errors of the order of 5° of longitude and central pressure errors of ± 10 to 15 mb. Errors of this magnitude, typically representing 4 to 6 m in reference sea states of the same order, can be roughly equated with forecasting lead times of 40 to 60 h.

## 1.0 Introduction

Operational ocean wave forecasting requires a time sequence of two-dimensional overwater wind fields $\mathbf{U}(\mathbf{x},t)$ to drive the wave prediction model. The accuracy of the wave forecast depends primarily on the accuracy of these wind fields, which are generally derived from numerical weather prediction (NWP) models run on hemispherical or global scales (see for example Mihok and Kaitala, 1976; Daley et al., 1976). Through the use of boundary layer models (e.g. Delage, 1985) the NWP winds may be specified at whatever reference level (10 m, 19.5 m, etc.) is required by the wave model.

Results of a comparison between NWP winds, generated by the Canadian Meteorological Centre's (CMC's) spectral primitive equation model at a vertical sigma coordinate level of 0.998, with measurements at Sable Island (44°N 60°W) and nearby anemometer winds from an offshore drilling rig are presented in this paper. These comparisons serve to quantify the error characteristics of the NWP winds at a given location; this information is valuable in its own right but proves to be difficult to relate to associated wave field errors.

In order to give a measure of expected error bounds in forecast wave height, a number of storm scenarios were then hindcast using a spectral wave model. The storm scenarios were designed to represent "worst case" differences in such parameters as trajectory, central low pressure, rate of deepening and filling, and horizontal scale that could be expected to occur in NWP winds. The results of this new work are discussed in terms of error characteristics in significant wave height. This leads to a recommendation for a more comprehensive study of prognostic wave height errors, both punctual and spatial in nature, that can be related to limitations in the numerical prognosis of severe weather systems.

## 2.0 Accuracy of NWP Winds

### 2.1 Data Sources

The NWP winds at Sable Island were derived from the CMC spectral primitive equation model described by Daley et al. (1976) and Creswick (1983). This model is run operationally twice per day. Three-hourly forecasts from 00 to 30 hours were obtained for runs commencing at 00 GMT and 12 GMT each day at a sigma level of 0.998. For typical oceanic variations in surface pressure and air density this corresponds to a reference height of (16 ± 10) m. Because of this uncertainty, these winds were not corrected to a reference height but were compared directly with measurements made at elevations in this range.

The 3-hourly sampling interval for CMC winds corresponds approximately with the minimum resolvable wave in the spectral model (C. Girard, CMC, pers. comm., 1986). The NWP winds were not smoothed, only extracted at the 3-hour time step and compared with the measured time-series of wind.

Measured data were obtained as follows (Fig. 1):

| | | |
|---|---|---|
| (1) | ROWAN GORILLA jack-up rig<br>W. Olympia O-51 | September 09 to November 10, 1985 |
| | anemometer height | 113 m MSL |
| | averaging time | 1 min |
| | recording interval | 3 h |
| (2) | Sable Island weather station | September 09 1985 to February 28, 1986 |
| | anemometer height | 13 m MSL |
| | averaging time | 1 min |
| | recording interval | 1 h (approx.) |

The rig winds were reduced to 10 m accounting for air column stability using the method published by Delage (1985). This procedure corresponds to the CMC method for boundary layer adjustment of the spectral NWP winds (C. Girard, CMC, pers. comm., 1985). Wind direction was modified according to Yamada (1976). No correction for wind flow modification around the jack-up leg was attempted.

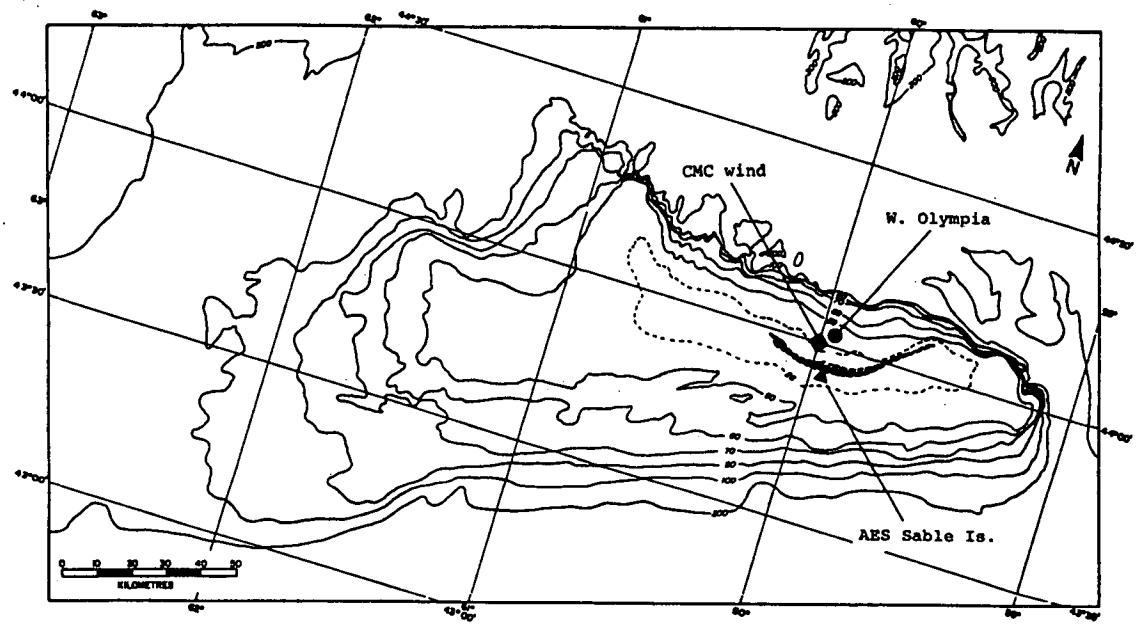


Fig. 1. Relationship of wind comparison locations near 44°N 60°W.

It is expected that winds measured at the Sable Island weather station will be affected by the topography of the central island. In fact, the anemometer is only a few metres higher than dunes that lie within 500 m of the station itself. Transfer functions were derived between the wind speed pairs measured at the weather station and at the ROWAN GORILLA rig (after reduction to 10 m) to correct the Sable Island winds for sheltering. These functions, which were derived as linear regressions of speed in four directional sectors, are:

| Wind Direction (°T from) | Overwater Wind Speed (knots) | Transfer Function |
|---|---|---|
| N | U | $1.12\ U_S + 1.9$ |
| E | | $1.33\ U_S + 0.5$ |
| S | | $1.37\ U_S + 1.1$ |
| W | | $1.08\ U_S + 3.7$ |

where $U_S$ = Sable Island wind speed in knots. These transfer functions were derived from the overlapping data collected in this study; the total number of data pairs was 555. These functions were then applied to the September 1985 to February 1986 measured wind series to give the equivalent overwater wind. No directional adjustment was made.

The accuracy of this calibration is discussed by Hodgins and Hodgins (1986). It appears that it is suitable to give a useful overwater wind with which to characterize errors in CMC-NWP winds. However, it is recognized that both the adjusted Sable Island and ROWAN GORILLA winds lack the precision of a true 10-m overwater wind estimated with an averaging time more closely matched to the synoptic scales of the spectral model.

## 2.2 Discussion of Results

Fig. 2 shows a representative time-series comparison between the NWP wind and the adjusted Sable Island wind. During this period three comparatively severe weather systems produced peak winds ranging from 40 to 50 knots. As can be seen in Fig. 2(a) the NWP analysis winds (shown by the diamonds) capture the trends reasonably well but occasionally exhibit quite large, 15 to 20 knot errors. However, the very short term prognosis winds at 03, 06, and 09 hours do show consistent differences of 5 to 10 knots and individual errors exceeding 20 knots. Interestingly the prognosis winds exhibit deviations that in some cases support the sense of the 00 hour forecast differences, but are opposite at other times.

In this particular time-series it can be seen that the NWP winds are overestimating the storm sequence from December 2 to 12, whereas they are in somewhat better agreement with observations from December 17 to 20. At forecast periods of 21, 24, 27 and 30 h in Fig. 2(b) temporally coherent errors of 10 to 15 knots characterize winds throughout the December 2 to 12 period. In the later system between December 17 and 20 the differences, or errors, are not too different from those at prognosis times ranging from 03 to 09 hours.

It is expected that the type of wind speed error seen here between December 2 and 12 is not only temporally coherent but spatially coherent as well. Consequently one would expect forecast waves during this period to be severely overestimated, but by an amount related in a complicated fashion to the weather system structure, its speed of advance and its position relative to the continental land mass.

Standard error statistics consisting of mean error, mean absolute error, RMS error and scatter index SI (defined as RMS error divided by the mean of the observed wind speeds) of wind speed were computed at 00, 12 and 24 hours. The mean errors were defined as observed minus forecast, and air temperature and atmospheric pressure were included in the calculations.

These error statistics are summarized in Table 1. We find, as expected, that the accuracy of wind deteriorates slightly as a function of lead time. The 00 hour forecast refers to the time-zero prognosis field generated by the spectral model; it is initialized through an objective analysis of observations as described by Creswick (1983). As can be seen in Table 1 there is a small overprediction bias in wind speed ($\sim$1 to 3 knots) and a clockwise bias in direction ranging from 10° at 00 h to 30° at 24 h. SI values for wind speed range from 20% to 42% indicating considerable dispersion about the correct values.

Atmospheric pressure exhibits a small bias (less than 1 mb) and an RMS error ranging from 2 mb at 00 h to 2.6 mb at 24 h. Air temperatures tend to be underestimated by about 1°C at 00 h and slightly overestimated by approximately 0.2°C at 24 h. RMS temperature errors range from 1.2 to 1.4°C.

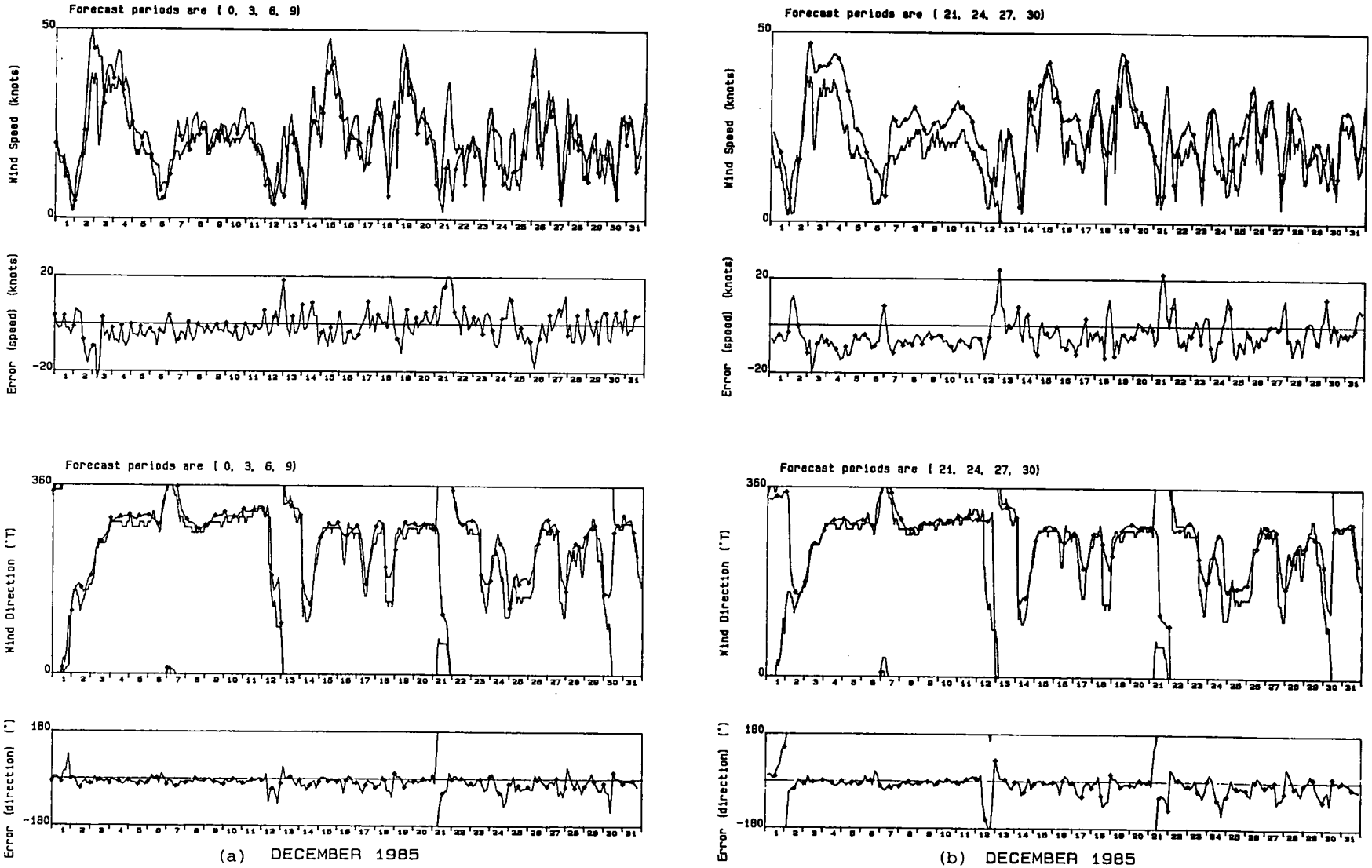


Fig. 2. Time-series comparison of wind speed and direction and errors in wind speed and direction at lead times (a) between 00 and 09 h and (b) between 21 and 30 h. The diamonds indicate the CMC wind series at 00 h in (a) and at 24 h in (b).

Scatter diagrams of CMC wind speed versus the measured rig winds, and of the errors in wind speed and direction as functions of wind speed are shown in Fig. 3 for 00 h and 24 h. The increase in the scatter of observations at 24 h compared with 00 h is evident, as is the considerable degree of dispersion even at 00 h. Wind speed error is not a strong function of wind speed, although the direction errors do tend to decrease with increasing wind speed. The trends observed in this figure carry over to the much longer database of adjusted Sable Island winds in which, however, it was noted that occasional, very large errors in wind speed (up to 30 knots) were found for individual points.

The error statistics presented above reflect conditions at one location off the eastern North American seaboard. They are based on a comparatively short database although extending the data record would not likely alter the bias statistics significantly. It must also be recognized that the "errors" described above are based on treating the observed values as perfect although this cannot be strictly true due to the applied transformations that will introduce errors. Perhaps more seriously, the measurements are based on averaging times that contain mesoscale wind effects. The NWP spectral model operates primarily at synoptic scales, and any sub-synoptic scale effects such as fronts would be highly smoothed (C. Girard, CMC, pers. comm., 1986; Creswick, 1983). Thus we expect that some of the scatter arises from introduced errors and some from inherent variability at scales below those resolved in the CMC model.

Nevertheless, the dispersion in these statistics indicates that at times comparatively large wind speed errors do occur. Inspection shows, in fact, that at such times the weather system may be poorly modelled with the wind field distortion being both temporally and spatially coherent. In a careful hindcast of four NE Pacific storms using CMC and regional weather analyses as separate inputs to a wave model, Hodgins and Nikleva (1986) have shown that routine differences in the wind fields can lead to spatially coherent wave height errors of up to 60% of sea states approaching 10 m in $H_s$.

**Table 1**

**Error Statistics in CMC Meteorological Variables Using Rig Observations as True Values**

00 Hour Forecast

| | Rate (knots) | Direction (deg.T) | Pressure (mb) | Temperature (deg.C) |
|---|---|---|---|---|
| Error | -.93 | -9.09 | 1.09 | .71 |
| Abs Error | 3.38 | 16.17 | 1.39 | .96 |
| RMS Error | 4.42 | 27.07 | 1.91 | 1.21 |
| Avg Value | 15.50 | n.a. | 1017.30 | 12.69 |
| S.I. | 28.55% | | | |

12 Hour Forecast

| | Rate (knots) | Direction (deg.T) | Pressure (mb) | Temperature (deg.C) |
|---|---|---|---|---|
| Error | -1.98 | -12.94 | .10 | .04 |
| Abs Error | 4.22 | 22.54 | 1.40 | .92 |
| RMS Error | 5.49 | 31.61 | 1.99 | 1.17 |
| Avg Value | 15.57 | n.a. | 1017.27 | 12.65 |
| S.I. | 35.27% | | | |

24 Hour Forecast

| | Rate (knots) | Direction (deg.T) | Pressure (mb) | Temperature (deg.C) |
|---|---|---|---|---|
| Error | -2.77 | -11.32 | -.38 | -.19 |
| Abs Error | 5.20 | 24.67 | 1.97 | 1.14 |
| RMS Error | 6.59 | 36.73 | 2.64 | 1.43 |
| Avg Value | 15.57 | n.a. | 1017.27 | 12.65 |
| S.I. | 42.33% | | | |

A careful diagnostic study of error characteristics in storms that have been modelled poorly by CMC and the consequences for wave forecasting has not yet been attempted. One expects, however, that such storms are misrepresented in terms of location and trajectory, speed of advance, horizontal scales, and temporal variations in pressure. In order to establish some bounds on wave height errors associated with errors in modelling these storm system parameters, a wave hindcast was made using a number of idealized storm wind inputs. These results are discussed in the next section.

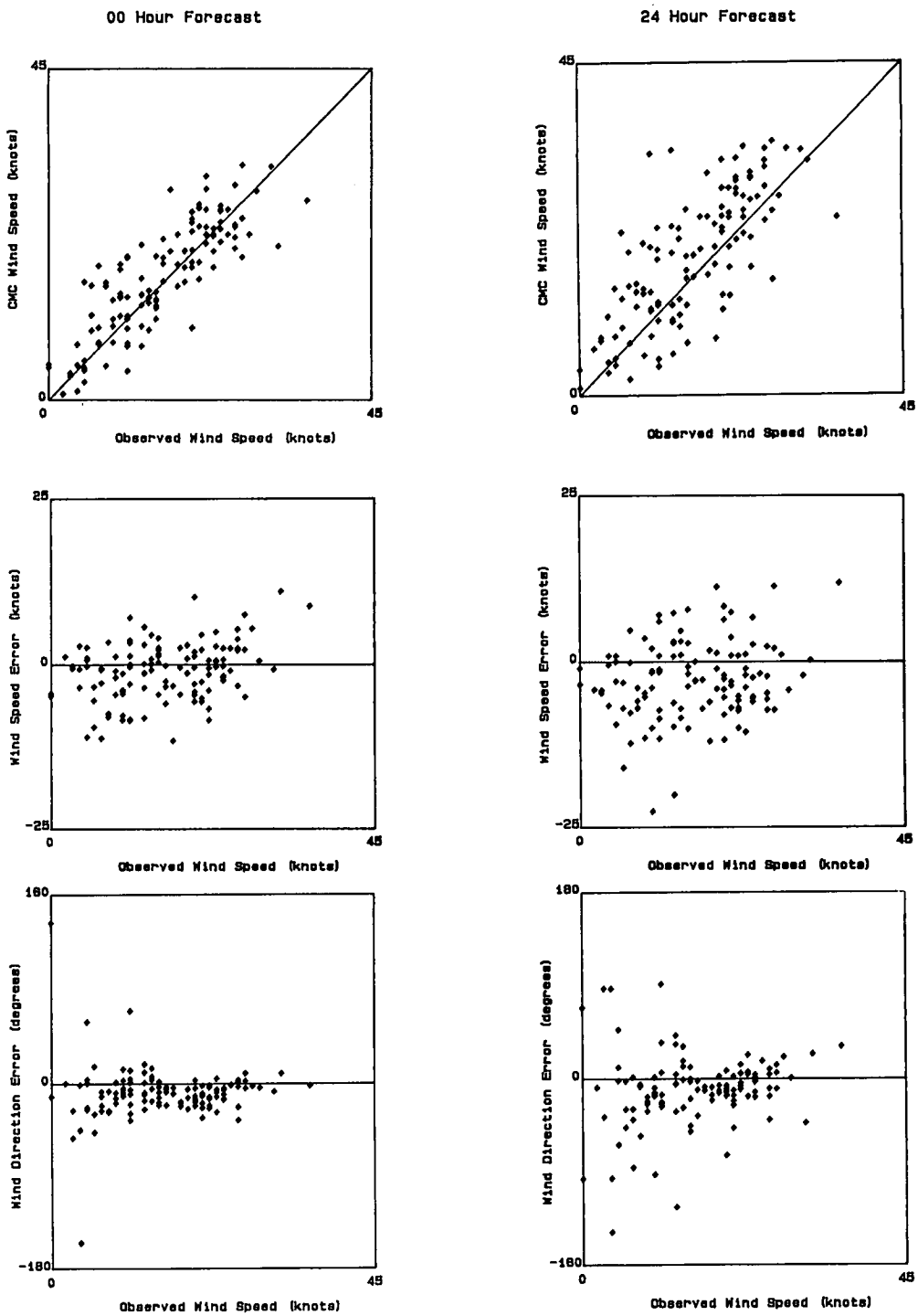


Fig. 3. Scatter diagrams of CMC wind versus anemometer winds from the ROWAN GORILLA reduced to 10 m.

Upper panel: CMC forecast speed versus observed speed.
Middle panel: Wind speed error versus observed speed.
Lower panel: wind direction error versus observed speed.

## 3.0 Wave Prediction Errors

### 3.1 Hindcast Approach

Based on a storm classification presented by Lewis and Moran (1985) for severe weather systems in the NE Pacific Ocean, a southwest frontal low storm was selected as the reference system to establish the expected sea states. Fig. 4 shows the composite prototype storm trajectories, and the idealized trajectory adopted for this reference storm. Table 2 summarizes the defining parameters in relation to the idealized trajectory; the values shown here are medians derived from the Lewis and Moran study. Systematic varia-

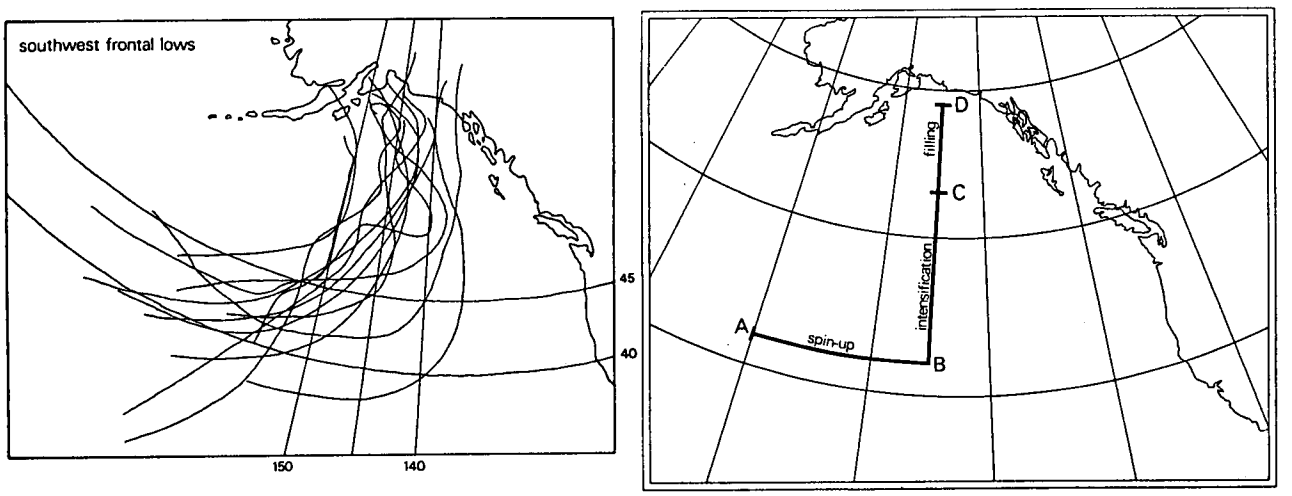


Fig. 4 Prototype southwest frontal low trajectories (left panel) and the idealized trajectory for this class of storm (right panel).

**Table 2**

**Surface Pressure Parameter Definitions for the Idealized Reference Storm Trajectory**

| Point | Leg | Latitude Longitude | Length (km) | Time YYMMDDHH | Duration (h) | $\Delta X_o/\Delta t$ (km/h) | $P_o$ (mb) | $\Delta P_o/\Delta t$ (mb/h) |
|---|---|---|---|---|---|---|---|---|
| A | | 42°N 160°W | | 86010100 | | | 984 | |
| | A-B | | 1238 | | 24 | 52 | | -0.6 |
| B | | 42°N 145°W | | 86010200 | | | 969 | |
| | B-C | | 1223 | | 18 | 68 | | -0.6 |
| C | | 53°N 145°W | | 86010218 | | | 958 | |
| | C-D | | 667 | | 18 | 37 | | +0.7 |
| D | | 59°N 145°W | | 86010312 | | | 970 | |

$X_o$ = path of the central low $P_o$ = central low pressure

tions in the following parameters were then made to derive six new storms representative of **worst-case** errors that could be expected in a numerical forecast:

| | | | |
|---|---|---|---|
| (i) | trajectory error | - | 5° eastward legs BC, CD; |
| (ii) | central low pressure | - | +16 mb, -14 mb; |
| (iii) | rate of intensification | - | explosive deepening -1.8 mb/h; |
| (iv) | advection rate | - | stall for 24 h in northern Gulf of Alaska; |
| (v) | horizontal scale | - | 33% increase in characteristic radius. |

Each storm was described by a 6-hourly sequence of radially symmetric surface pressure distributions defined by the three parameter function

$$P(\mathbf{x},t) = P_o(\mathbf{x}_r,t) + \Delta P \exp(-R/r) \qquad (1)$$

where $P_o$ is the central pressure, $\Delta P$ is the pressure gradient, and R is a radial scale parameter such the $r = R$ at $P = P_o + 0.37\Delta P$. Gradient winds were calculated from $P(\mathbf{x},t)$ and reduced to $\mathbf{U}(\mathbf{x},t)$ at 10 m with the boundary layer model described in Hodgins and Nikleva (1986) for neutral stability. The result was a 6-hourly sequence of surface wind fields defined on a 1°x1° latitude-longitude grid for input to the wave hindcast model.

The wave model (Hodgins and Nikleva, 1986; Hodgins, 1986) used in this hindcast was a discrete spectral code applied on the grid shown in Fig. 5. A spectral discretization of 16 frequencies and 16 directions was adopted. Each storm was modelled to give 3-hourly fields of significant wave height $H_s$, peak period $T_p$ and mean wave direction. Winds were linearly interpolated in time between the 6-hourly fields for input to the wave model, which ran on a 30 min time step.

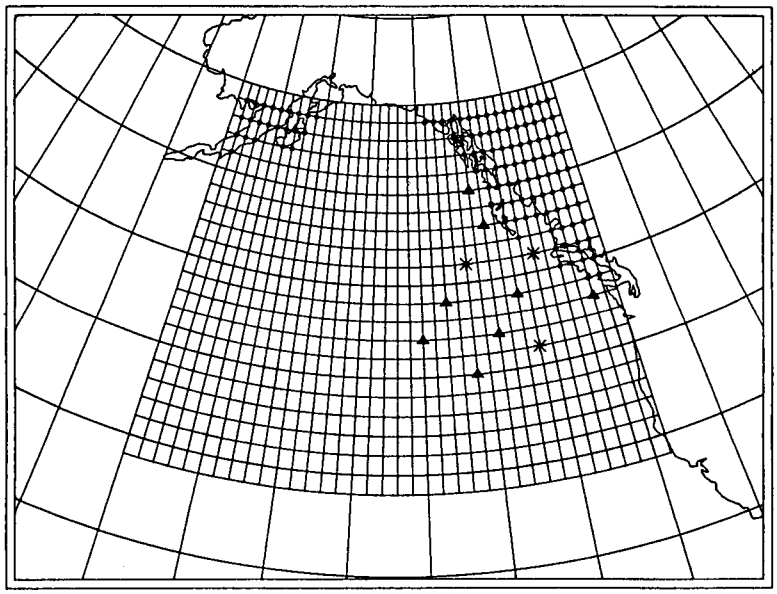

Fig. 5

Wave hindcast grid for NE Pacific Ocean, 1°x1° latitude-longitude spacing.

Further details of the storm definitions and hindcasting procedures are reported by Hodgins, 1986.

### 3.1 Discussion of Results

For the type of weather system modelled here the influence of trajectory emerged as the single most important parameter affecting wave heights ($H_s$). The contour map of $H_s$ at the peak of the reference storm is shown in Fig. 6. The results for a 5-degree eastward shift of the central low on its northward leg produced a corresponding shift in the $H_s$-field. It is easy then to appreciate that spatially coherent errors in $H_s$ amounting to 5 to 6 m in reference sea states of 3 to 4 m are obtained about 5° of longitude closer to the coast.

After trajectory, the parameters governing storm intensity emerged as the important factors. The spatially differenced $H_s$-fields at the storm peak (perturbed storm minus

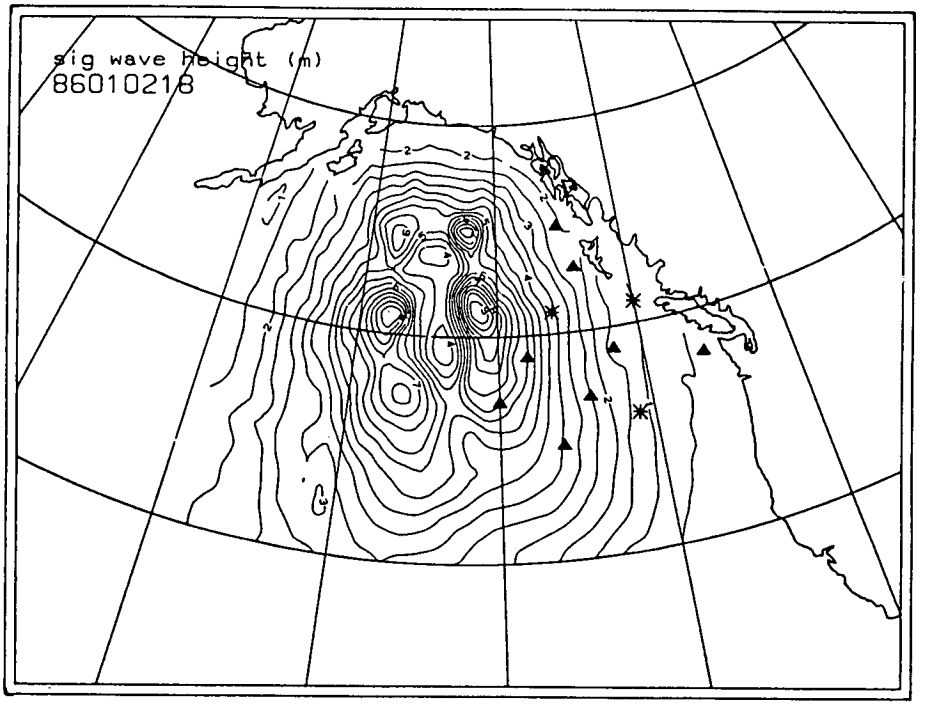


Fig. 6 Significant wave height field contoured in 0.5 m intervals at point C (Fig. 4) for reference storm conditions.

reference storm) are shown in Fig. 7 representing extreme ranges in central pressure. As shown here $H_s$-errors of 4 to 5 m in sea states of 7 to 9 m are associated with these central pressure differences (+16 mb; -14 mb). Explosive deepening to the same final central pressure as the reference storm had less severe consequences for waves, giving lower seas than the more slowly developing system. This is consistent with the growth of wave under strong winds sustained for longer durations.

The stalling of the weather system in the Gulf of Alaska for 24 h with no filling (corresponding with conditions observed, for example, on January 20-22, 1981 as reported by Lewis and Moran, 1985) also produced differences in $H_s$ amounting to 6 to 7 m in sea states of the same order. By comparison the wave heights varied far less for changes in the scale parameter R (~10%).

In each case the change of parameters made to the reference storm produced differences in peak sea states at times from 36 to 60 h following identification of the weather system at point A in Fig. 4. Roughly, then, these characteristic errors in $H_s$ can be equated to those that could result from NWP winds for storms that are poorly handled in the spectral model at lead times of about 40 to 60 h. One would expect, of course, that the such errors would diminish with shorter lead times.

## 4.0 Conclusions

The analysis of NWP wind errors has shown that CMC prognostic winds derived from the operational spectral model have relatively small bias errors when averaged over intervals that contain many weather systems, but statistically exhibit much scatter. Large wind speed errors seem to be associated with individual weather systems that are not well modelled, and as a result are temporally coherent. Although not presently well quantified, these errors are likely to be coherently distributed in space also. As a result, corresponding wave height errors are expected to be large.

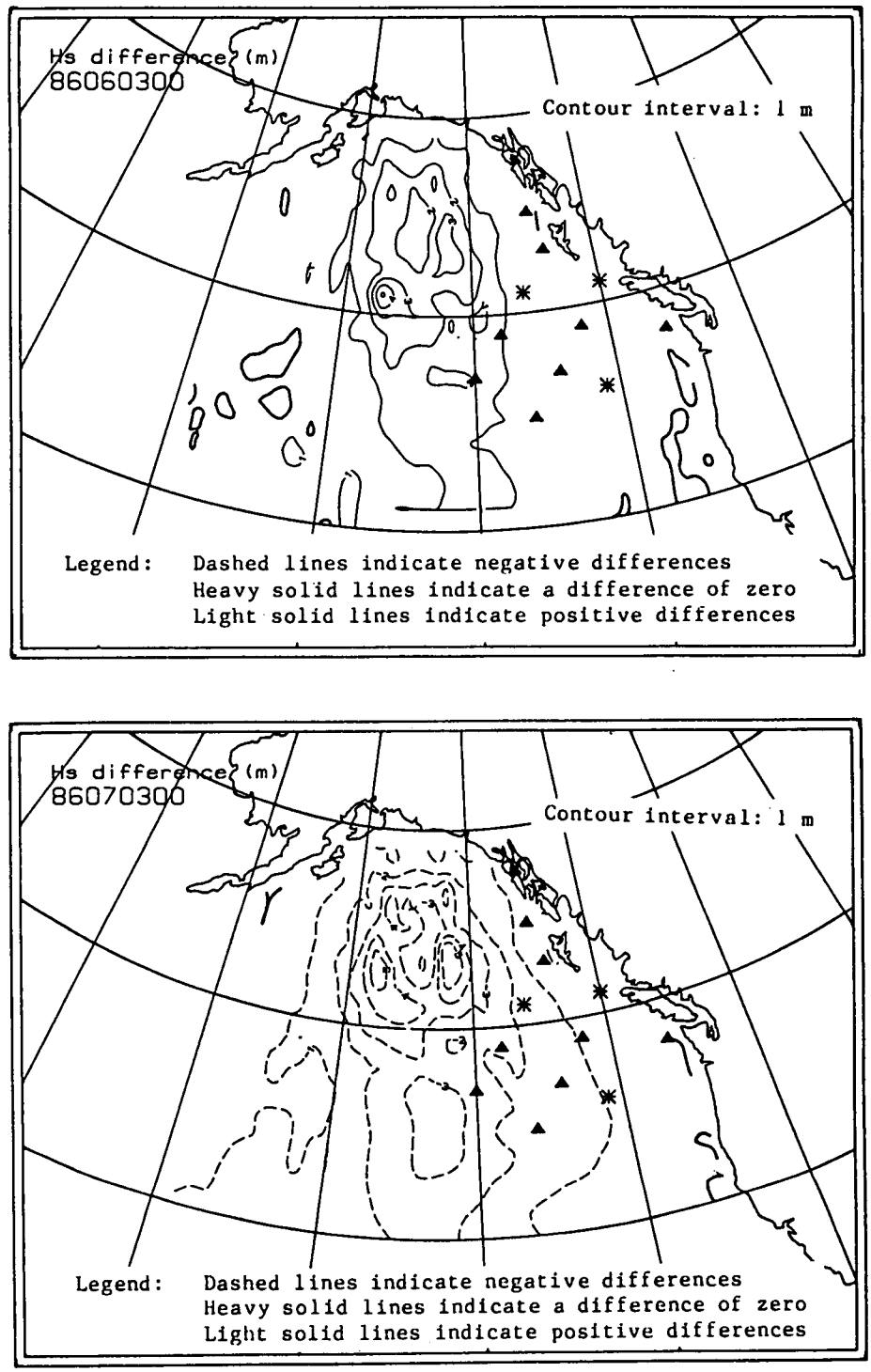


Fig. 7 Significant wave height difference fields (perturbed storm minus reference storm) for a central low pressure lowered by 14 mb (upper panel) and raised by 16 mb (lower panel) at peak sea state response.

Attempts to quantify significant wave height errors through hindcasting that could be associated with errors in NWP winds at lead times of 40 to 60 h have produced the following results:

| storm parameter | error in $H_s$ (% of reference sea state) |
|---|---|
| trajectory error | 100 - 200% |
| intensity errors (central pressure) | 80 - 100% |
| advection errors (stall) | 100 - 200% |
| scale of storm | 10 - 20% |

These are worst-case errors corresponding with extreme perturbations observed in weather systems over the Pacific Ocean; nevertheless, they are large with potentially important consequences for operational wave forecasting and the user community.

It remains to establish to what extent storm systems that are poorly modelled numerically do indeed give rise to wind errors causing wave height errors of these magnitudes, and with what frequency of occurrence. The next obvious hurdle to be overcome is dealing with combined errors in parameters such as trajectory and pressure variations in a manner that does not obscure the cause-and-effect relationships between pressure (and ultimately wind) and waves. To achieve this goal a systematic study of wave height field errors derived from the use of prognostic CMC winds in a spectral wave model is now required. The purpose would be to characterize and understand those synoptic situations in which the NWP winds perform poorly, to quantify the corresponding wave height errors, and to establish how frequently large errors occur over the course of a given year.

**Acknowledgements**

This work was supported in part by the Environmental Studies Revolving Funds Study Number 311-30-08 and in part by Seaconsult Marine Research Ltd. The assistance of CMC in providing the prognostic wind data and Mobil Oil Canada, Ltd. for providing the Rowan Gorilla rig wind data are gratefully acknowledged.

**References**

Creswick, W.S., 1983. The CMC Operational Spectral Forecast Model. CMC Information, 22-38, May 1983.

Daley, R. C. Girard, J. Henderson and I. Simmonds, 1976. Short-Term Forecasting with a Multi-Level Spectral Primitive Equation Model. Part I--Model Formulation. Atmosphere, 14(2), 98-116.

Delage, Y., 1985. Surface Turbulent Flux Formulation in Stable Conditions for Atmospheric Models. Mon. Wea. Rev., 113.

Hodgins, D.O., 1986. Evaluation of Two Shallow Water Spectral Wave Models on Sable Island Bank, Canada. Proc. Intern. Workshop on Wave Hindcasting and Forecasting. September 23-26, 1986, Halifax, N.S.

Hodgins, D.O. and S. Nikleva, 1986. On the Impact of New Observing Sites on Severe Sea State Warnings for the B.C. Coast. Unpublished technical report prepared for Fisheries & Oceans Canada by Seaconsult Marine Research Ltd., Vancouver.

Hodgins, S.L.M., 1986. Wave Hindcast Sensitivity to Wind Forcing. M.A.Sc. Thesis, University of British Columbia.

Lewis, C.J. and M.D. Moran, 1985. Severe Storms Off Canada's West Coast: A Catalogue Summary for the Period 1957 to 1983. Canadian Climate Centre Unpublished Report No. 85-7.

Mihok W.F. and J.E. Kaitala, 1976. U.S. Navy Fleet Numerical Weather Central Operational Five-Level Global Fourth-Order Primitive-Equation Model. Mon. Weather Rev., 104(12), 1527-1550.

Yamada, T. 1976. On the Similarity Functions A, B, and C of the Planetary Boundary Layer. J. Atmos. Sci., 23, 781-793.

# AN INTERCOMPARISON STUDY OF OCEAN WAVE MODELS DURING THE CANADIAN ATLANTIC STORMS PROGRAM (CASP) - SOME PRELIMINARY RESULTS

M.L. Khandekar[1], B.M. Eid[2] and V. Cardone[3]

## 1. INTRODUCTION

The CASP (Canadian Atlantic Storms Program) was an intensive observational program aimed at studying the evolution of winter storms that affect the Canadian Atlantic provinces. A large amount of meteorological and oceanographical data was collected during the CASP field project (15 January - 15 March 1986) over the Scotian Shelf and the Grand Banks area. In conjunction with the data collection program, two spectral wave models were tested in an operational mode during the CASP field project; both these wave models were driven by winds obtainable from the operational weather prediction model at the Canadian Meteorological Centre (CMC) in Montreal. The wave products (analyzed as well as forecast) from these two models were evaluated against wind and wave data collected during the CASP field project. In addition, wind and wave products from the U.S. Navy's Global Spectral Ocean Wave Model (GSOWM) were accessed during the CASP field project and were also included in the intercomparison study. Some preliminary results of this intercomparison study are presented in this paper. Brief details of the models used in this study are presented in the following section.

## 2. THE MODELS

The two spectral models used in the operational mode during the CASP field project were the ODGP and the WAVAD models. The ODGP (Ocean Data Gathering Program) model was derived by Cardone et al. (1974) following the development of the U.S. Navy's SOWM (Spectral Ocean Wave Model) and is based on the well-known spectral energy balance equation in which each spectral component is assumed to grow independent of all other components in accordance with an essentially linear input source function until it approaches its limiting 'saturation' level. The Pierson-Moskowitz (P-M) spectrum is used to model transition from the growing sea to the fully developed sea. The ODGP model uses 24 direction bands and 15 frequency bands to express the energy spectrum at any given point. The ODGP model uses a nested grid as seen in Figure 1, the grid spacing being 1.25° latitude by 2.5° longitude in deep water and half of that spacing in the nearshore region. To simulate the shallow-water effects, a one-dimensional grid (lower half of Figure 1) is set up and is aligned along the shallow-water wave array where special wind and wave observations were collected during the CASP field project. Along this one-dimensional grid, the shallow-water effects, namely bottom friction, refraction and shoaling are modelled. This ultra-fine grid has a spacing of 1 nautical mile and a time-step of 90 s is used for numerical integration along this grid. More details of the ODGP model are given in MacLaren Plansearch (1985).

The WAVAD is a spectral model applicable to arbitrary water depths and has been developed by Resio as an extension of his deep-water model (Resio, 1981). The WAVAD model uses a new theory of equilibrium spectral shapes in waters of arbitrary depth;

---

[1] Atmospheric Environment Service, Downsview, Ontario, Canada
[2] MacLaren Plansearch Ltd., Halifax, Nova Scotia, Canada
[3] Oceanweather Inc., Cos Cob, Connecticut, U.S.A.

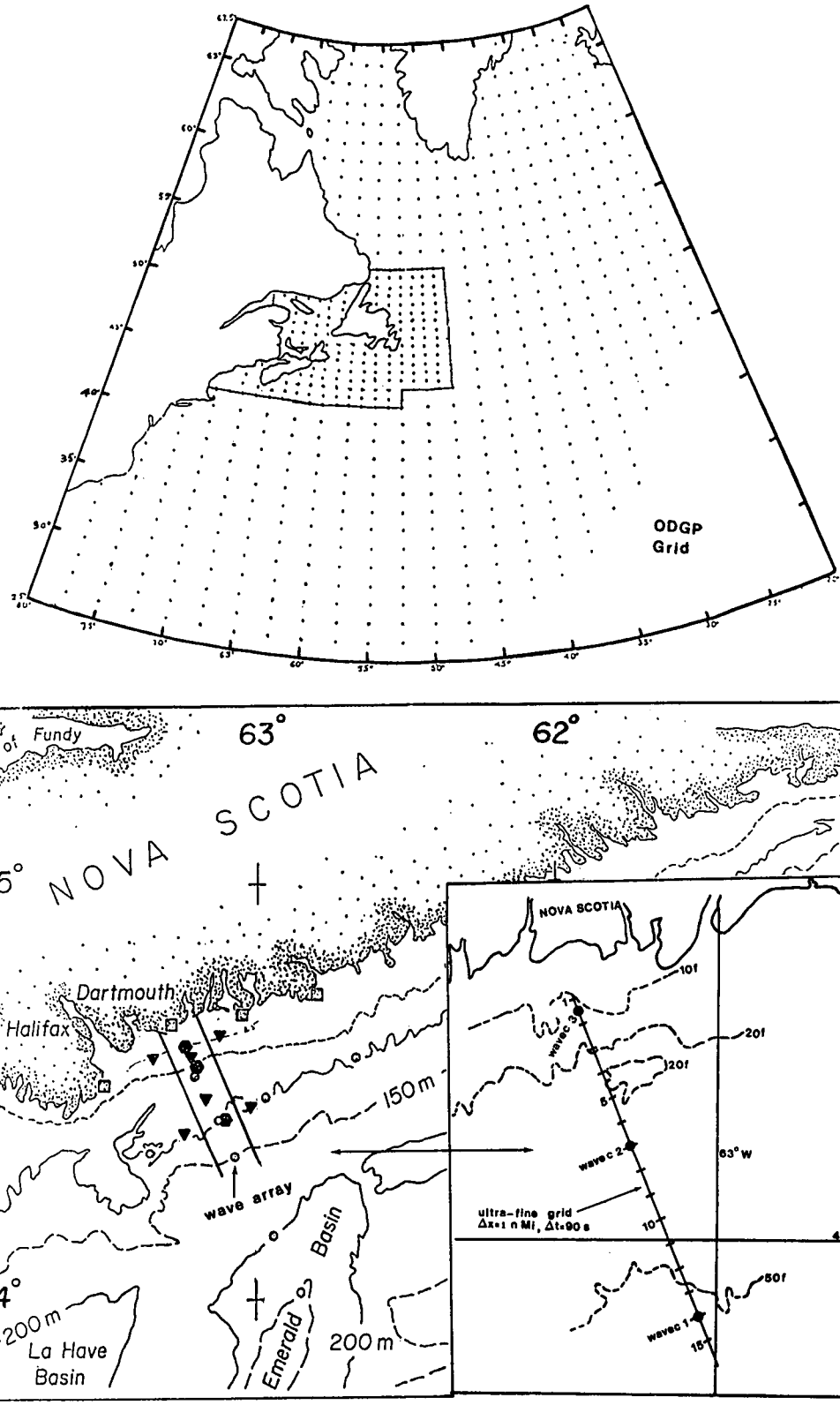


Figure 1: Top: The ODGP nested grid. Bottom: CASP wave array (left) and the ultra-fine grid of the ODGP model.

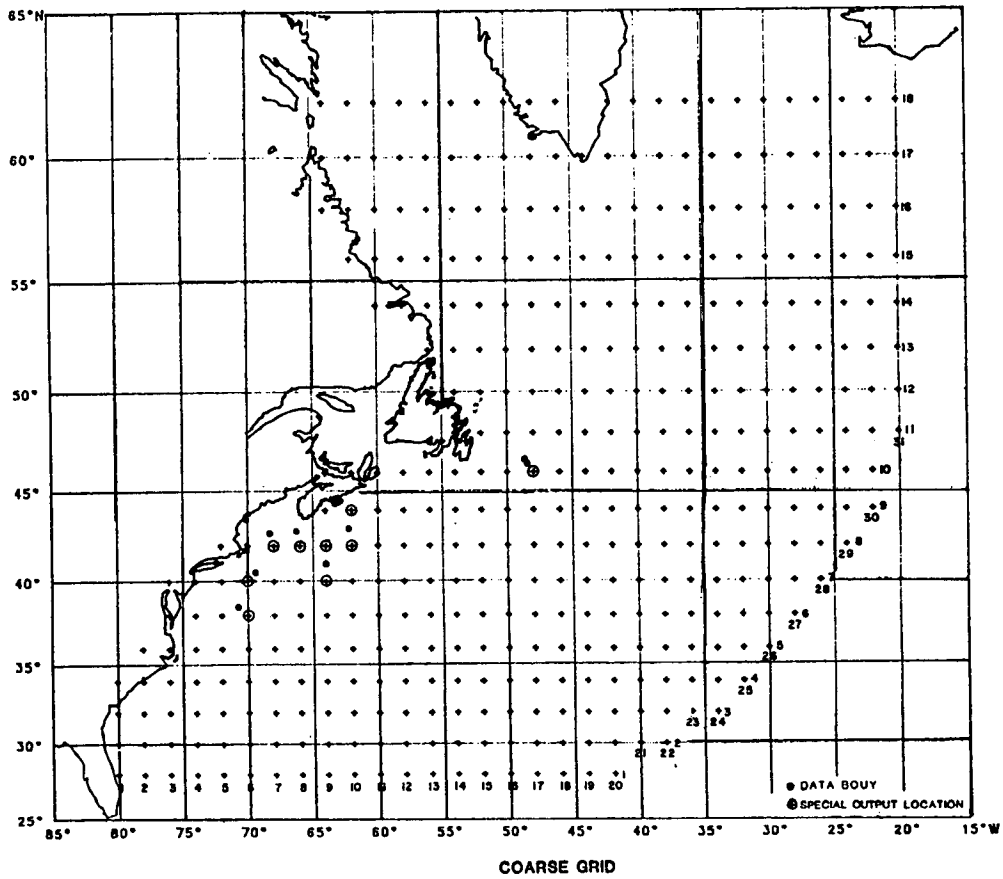


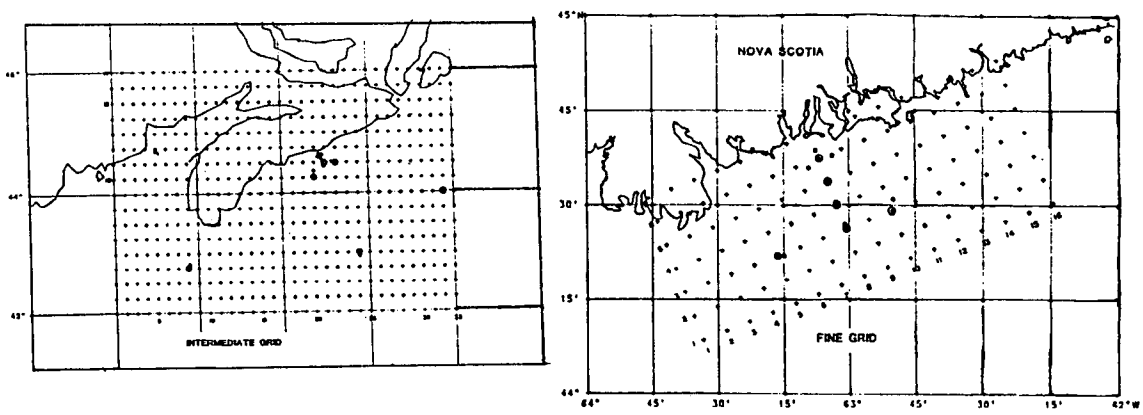


**WAVAD Grid**

Figure 2: Top: The coarse grid for the WAVAD model
Bottom: The intermediate and the fine grid for WAVAD model.

these equilibrium shapes are maintained by a mechanism which provides a strong flux of energy towards high frequencies where it is lost due to wave breaking. A dynamic balance between wind input and nonlinear flux dominates the shape of the spectrum and controls energy level and energy loss in waves propagating to water depths of 10 m or less. The bottom friction is considered as a free parameter in the model and is included only for long period swell waves with little or no wind. A coarse grid (grid spacing 2° latitude by 2° longitude) covering western North Atlantic Ocean, together with two nested grids covering the Scotian Shelf region, was designed for operational running of the WAVAD model during the CASP field project. Of the two nested grids, the intermediate grid had a spacing of 0.25° in latitude and longitude while the fine grid had a spacing of 4 nautical miles and extended approximately 4 nautical miles offshore from the Nova Scotia coastline and about 30 nautical miles on both sides of the CASP shallow-water array. Figure 2 shows the coarse and the two nested grids of the WAVAD model.

The GSOWM is the global operational spectral wave model of the U.S. Navy and has evolved from its predecessor the SOWM (Spectral Ocean Wave Model). The GSOWM has 24 direction bands (compared to 12 for the SOWM) while both the SOWM and the GSOWM use 15 frequency bands. The GSOWM operates on a 2.5° latitude by 2.5° longitude spherical grid on a global band extending from 77.5°N to 72.5°S. Both the SOWM and the GSOWM use the linear and the exponential wave growth terms and include the P-M spectrum to model transition from the growing sea to the fully developed sea; further, the wave energy in both the models is propagated along great circle paths at the frequency-dependent group velocity for deep-water waves. Additional details of the GSOWM can be seen in Clancy et al. (1986).

## 3. RESULTS AND DISCUSSION

The model products were evaluated over three deep-water regions (see Figure 3) and over shallow waters along the CASP wave array (region 4 of Figure 3). Wave plots

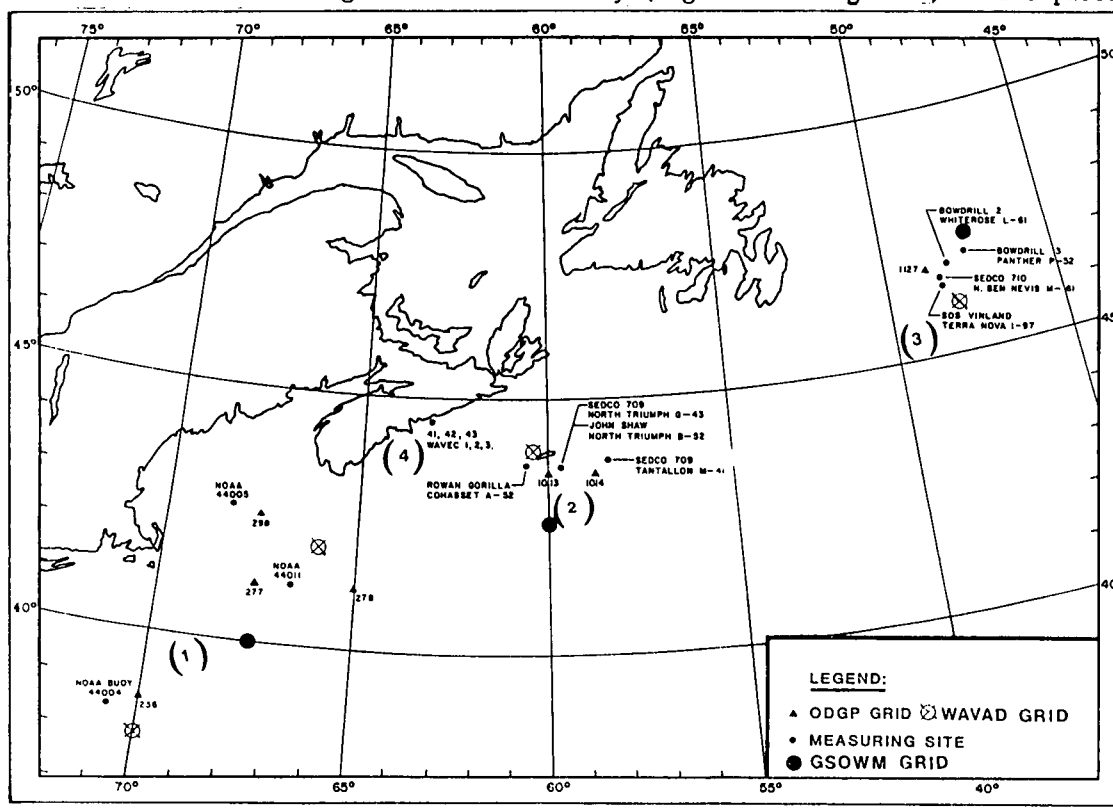


Figure 3. Map showing the 3 deep-water regions, the shallow-water region 4 and locations of measuring sites and model grid points.

(showing variation of significant wave height) and scatter diagrams (model versus observed values) were prepared for deep-water as well as shallow-water locations. For a quantitative evaluation, error statistics like Root Mean Square Error (RMSE) and Scatter Index (SI) were calculated. A few of these results are presented and discussed below.

## 3.1 Deep-water Results

Figure 4 is a sample wave plot for region 1 showing variation of significant wave height from 14 February to 16 March 1986 for four models, namely, ODGP-CMC, ODGP-OPR, WAVAD and GSOWM. The models ODGP and WAVAD were driven by CMC winds extracted at 0.998 sigma-level which is approximately 17 m above the ocean surface in a standard atmosphere. These 0.998 sigma-level winds were suitably interpolated to the models' grids before being used. These winds were used without any modification to drive both the models; however, for the WAVAD model, the drag coefficient was adjusted to neutral stability. The wave products from these two models were designated as ODGP-CMC and

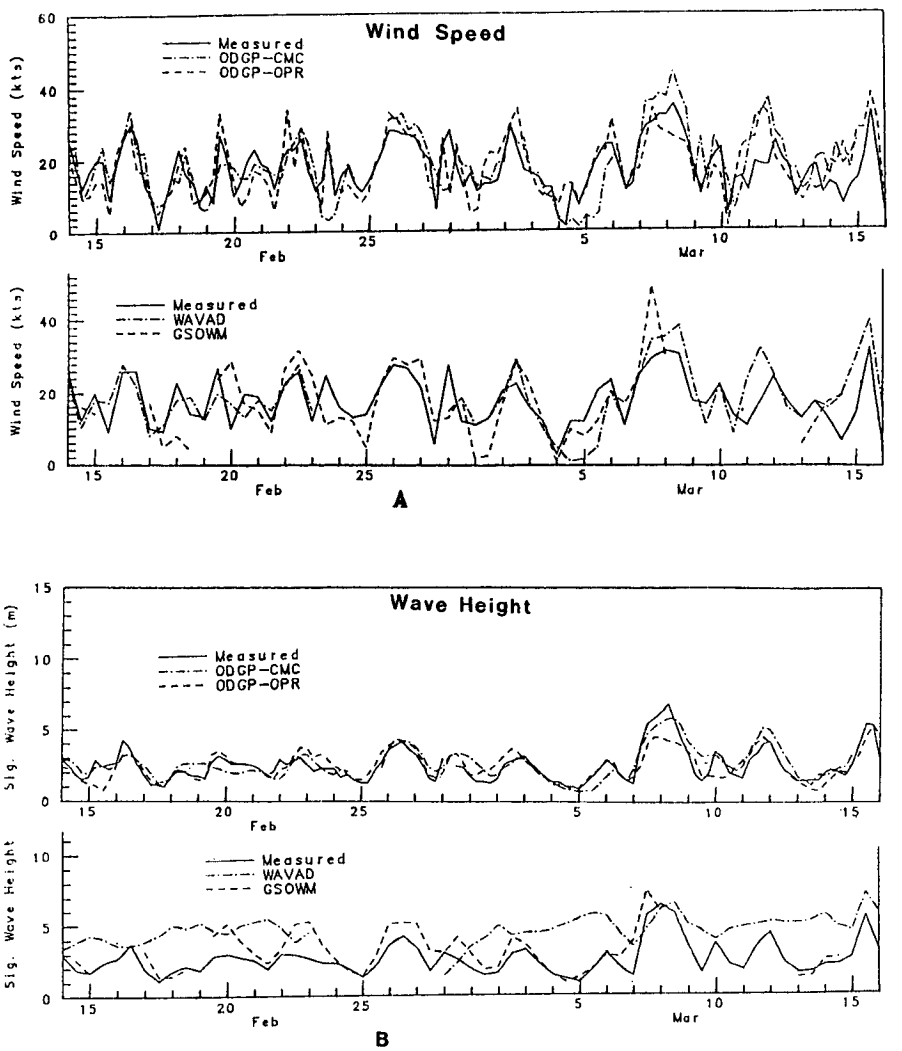


Figure 4: Wind speed and significant wave height plots for the four models covering the period 14 February - 16 March, 1986. The measured wind speed (kts) and significant wave height (m) refer to the NOAA buoy 44004 location.

WAVAD respectively. The ODGP is an operational model at the Oceanweather Inc. where it is driven by winds which are based on LFM (Limited-area Fine Mesh) model analysis prepared at the National Meteorological Center, Washington, U.S.A. These LFM winds are subjectively adjusted and a boundary layer model is applied to generate effective neutral winds at 20 m level; the wave products obtained by using these winds were designated as ODGP-OPR. The wave plot labelled GSOWM shows wave height variation at a GSOWM grid point in region 1. These model products are compared against wind and wave measurements at the NOAA buoy 44004 location. (See Figure 3). Besides the wave height variation, Figure 4 also shows the wind speed variation for the four models compared against measured wind speed at the NOAA buoy 44004 location. In general, the model values show reasonable agreement with measured wind and wave values. Figure 5 shows scatter diagrams of model versus observed values of wind speed and significant wave height for the four models. These scatter diagrams include two months of data (15 January - 16 March, 1986) at all deep-water sites and the model values correspond to analysis time (zero hour forecast). The Figure also shows N, the number of data points for each of the four models together with the magnitude of the linear correlation coefficient (r) between model and observed values and the corresponding regression line. The model ODGP-OPR appears to provide the best initial wind input (with correlation coefficient of 0.80 between model and observed values) and consequently the closest agreement between model and observed significant wave heights; this may be due to the man-machine mix which seems to provide better initial wind specification for the model ODGP-OPR. The models ODGP-CMC and the GSOWM both appear to provide similar scatter between model and observed wind and wave height values; this may be due to the fact that both these models have similar governing equations and both are driven by winds directly extracted from operational weather prediction models.

In order to evaluate the model performance in a forecast mode, scatter diagrams between observed and (model) predicted values at different forecast times were prepared. Figure 6 shows scatter diagrams between observed and model predicted wave heights at 24 hour forecast time. Besides the four models discussed above, wave heights extracted from the daily wave charts prepared at METOC (Meteorology and Oceanography) Centre in Halifax were also included in the intercomparison study and Figure 4E shows the scatter diagram for the METOC model. The closest agreement between observed and predicted wave heights is provided by the model ODGP-OPR with a correlation coefficient of 0.76 between observed and predicted values. Both the ODGP-CMC and the GSOWM models appear to have similar scatter in predicted wave heights although the ODGP-CMC appears to produce increased scatter when the significant wave height is more than 5 m. For the WAVAD model, the correlation coefficient between observed and model wave heights has increased from 0.32 (for 00 hour forecast) to 0.51 (for 24 hour forecast) suggesting perhaps that the WAVAD model appears to provide improved wave products when used in a forecasting mode.

To make a quantitative assessment, error statistics like RMSE and SI have been calculated for all models and Table 1 shows these values at analysis time as well as at forecast time out to 36 hours.

The Table reveals several interesting features of the intercomparison study. In general it is found that model winds with lower error statistics produce better wave products; thus better wind specification at analysis as well as at forecast times produces wave products which are in closer agreement with observed values. The ODGP-OPR model which is driven by winds based on a man-machine mix appears to provide the best error statistics for significant wave height out to 36 hours. At analysis time, the METOC charts appear to provide the closest agreement with the observed wave heights with a correlation coefficient of 0.83 between the two. This may be due to the fact that the METOC charts are based on observed wave data and that the wave heights from the METOC charts are extracted at the measuring sites, whereas the other model products are extracted at the respective model grid locations which are some distance away from the measuring sites. However, in a forecast mode, the ODGP-OPR model provides better results when measured in terms of the RMSE, the scatter index and the correlation coefficient. The METOC forecast wave charts are based on an empirical procedure, hence their forecast wave heights show a smaller skill than that attainable by a spectral wave model. Finally, the WAVAD and the GSOWM error statistics seem to suggest that these two models provide slightly better wave products at forecast times than at analysis time.

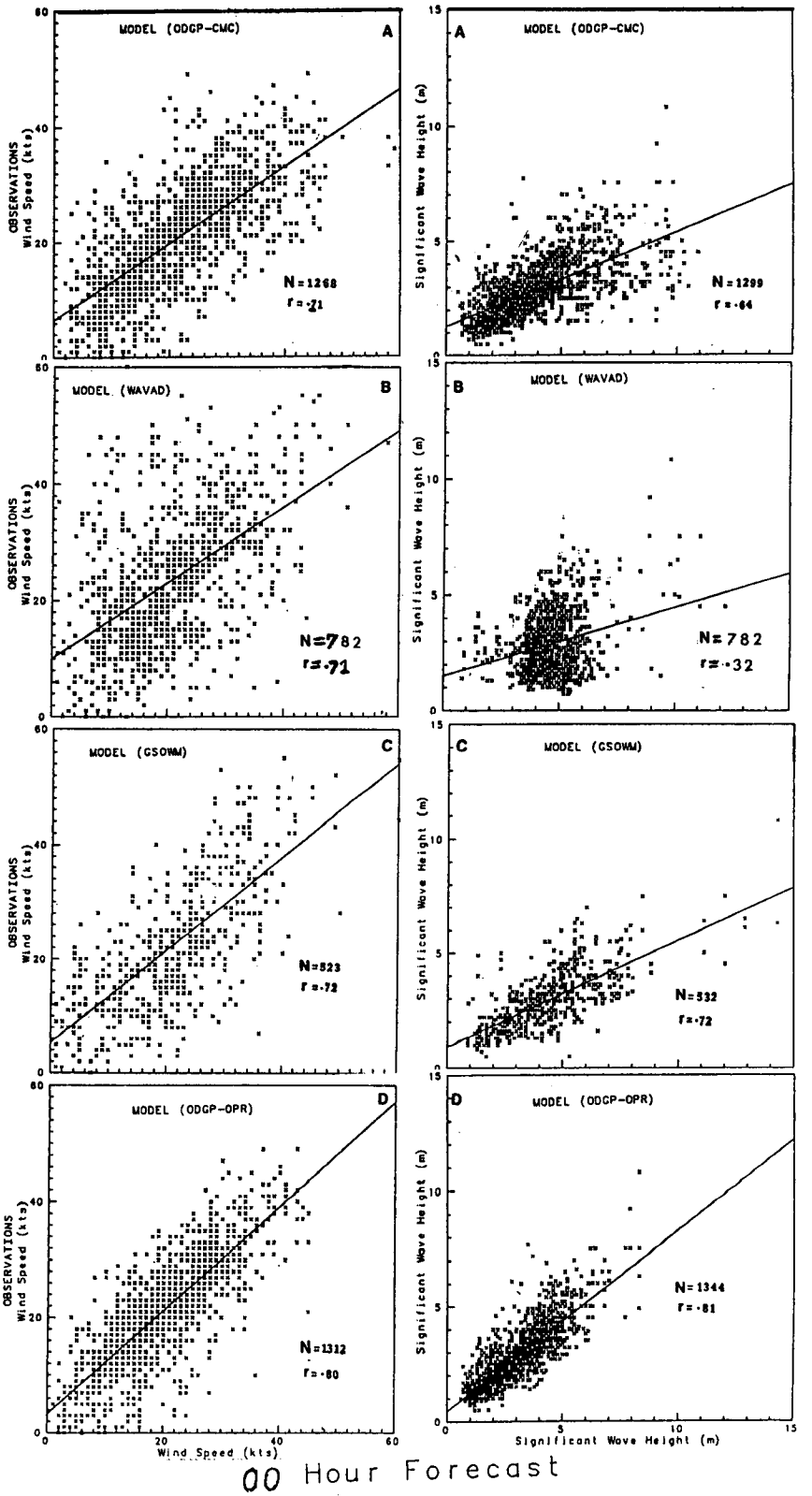


Figure 5. Scatter diagram between observed and model wind speed (left) and between observed and model significant wave height (right) at analysis time (00 hour forecast) at all deep-water sites covering the two-month period.

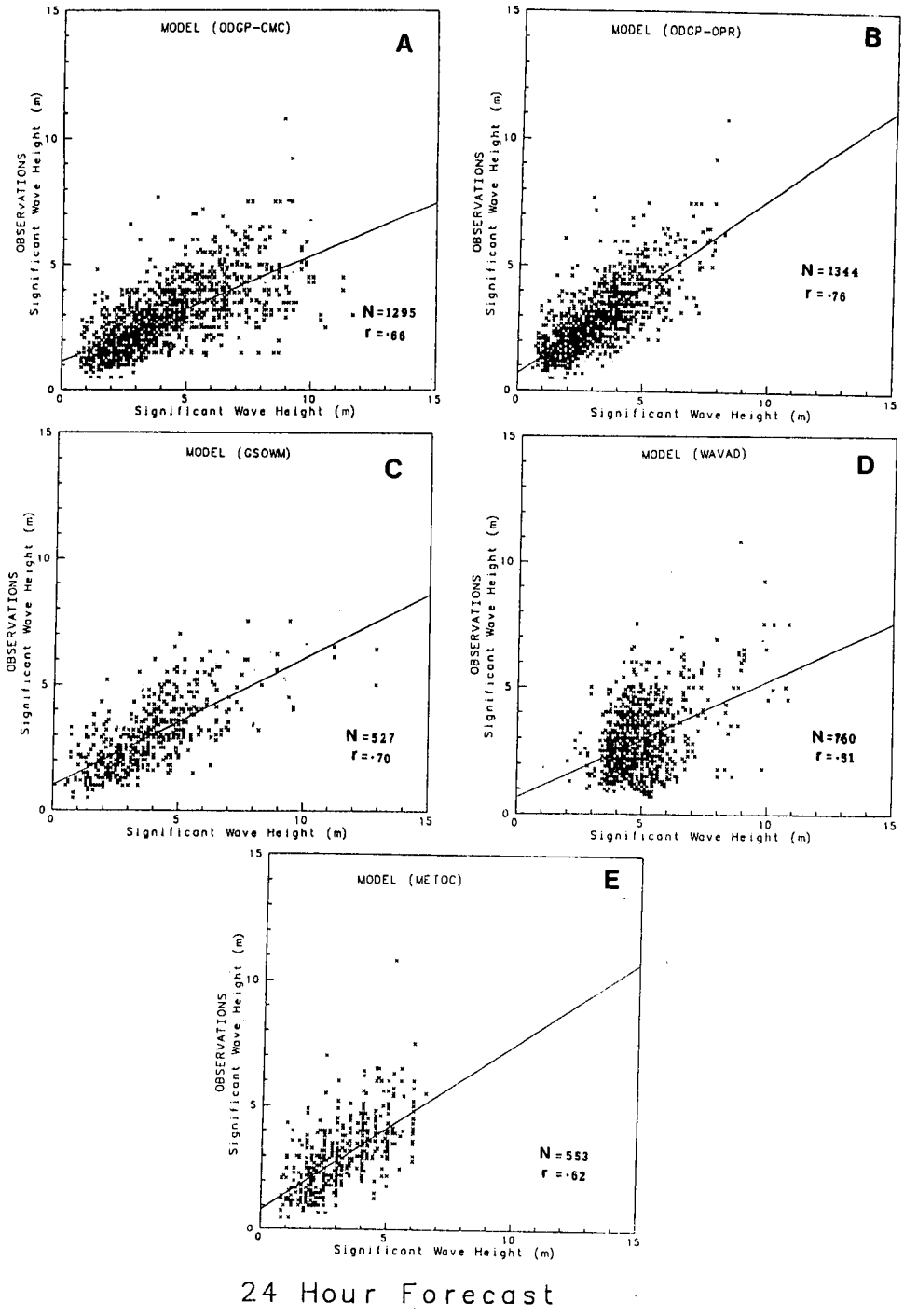


Figure 6. Scatter diagrams between observed and predicted significant wave heights at 24-hour forecast time for five models. Data for all deep-water sites covering the two-month period are included.

TABLE 1: Evaluation of various wave models

Summary of Error Statistics (All Deep-Water Sites)

| Model | Parameter | WIND SPEED (Knots) Forecast Time 00 hr | 12 | 24 | 36 | WAVE HEIGHT (Metres) Forecast Time 00 hr | 12 | 24 | 36 |
|---|---|---|---|---|---|---|---|---|---|
| ODGP CMC | RMSE | 7.59 | 8.17 | 8.55 | 9.32 | 1.88 | 1.91 | 1.96 | 1.97 |
| | MAE | 5.74 | 6.09 | 6.40 | 7.00 | 1.33 | 1.37 | 1.43 | 1.46 |
| | SI | 36 | 39 | 41 | 45 | 65 | 66 | 69 | 70 |
| | r | 0.71 | 0.70 | 0.67 | 0.60 | 0.64 | 0.65 | 0.66 | 0.66 |
| | N | 1268 | 1270 | 1268 | 1260 | 1299 | 1299 | 1295 | 1285 |
| WAVAD | RMSE | 7.24 | 8.25 | 8.71 | 9.30 | 2.31 | 2.38 | 2.36 | 2.38 |
| | MAE | 5.48 | 6.21 | 6.58 | 7.10 | 1.92 | 2.00 | 2.05 | 2.08 |
| | SI | 35 | 40 | 42 | 44 | 81 | 84 | 83 | 83 |
| | r | 0.71 | 0.69 | 0.65 | 0.59 | 0.32 | 0.44 | 0.51 | 0.52 |
| | N | 782 | 771 | 761 | 750 | 782 | 770 | 760 | 749 |
| GSOWM | RMSE | 8.40 | 9.75 | 10.93 | 11.66 | 1.96 | 1.66 | 1.52 | 1.49 |
| | MAE | 6.69 | 7.42 | 8.31 | 8.92 | 1.51 | 1.25 | 1.13 | 1.13 |
| | SI | 37 | 43 | 48 | 51 | 68 | 58 | 53 | 52 |
| | r | 0.72 | 0.67 | 0.54 | 0.47 | 0.72 | 0.73 | 0.70 | 0.64 |
| | N | 523 | 519 | 518 | 515 | 532 | 528 | 527 | 523 |
| ODGP OPR | RMSE | 5.89 | 7.22 | 7.93 | 8.39 | 0.85 | 0.92 | 0.98 | 1.06 |
| | MAE | 4.54 | 5.58 | 6.16 | 6.59 | 0.65 | 0.70 | 0.74 | 0.80 |
| | SI | 28 | 35 | 38 | 40 | 30 | 32 | 34 | 37 |
| | r | 0.81 | 0.69 | 0.62 | 0.58 | 0.81 | 0.79 | 0.76 | 0.72 |
| | N | 1312 | 1312 | 1312 | 1312 | 1344 | 1344 | 1344 | 1344 |
| METOC | RMSE | For the METOC model, only wave height charts were evaluated, hence no error statistics for wind speed were generated. | | | | 0.83 | 1.20 | 1.15 | 1.23 |
| | MAE | | | | | 0.62 | 0.88 | 0.89 | 0.95 |
| | SI | | | | | 28 | 41 | 39 | 42 |
| | r | | | | | 0.83 | 0.62 | 0.62 | 0.56 |
| | N | | | | | 537 | 543 | 553 | 553 |

RMSE = Root Mean Square Error; MAE = Mean Absolute Error

$$SI = \text{Scatter Index} = \frac{\text{RMSE}}{\text{Mean Observed value}} \times 100$$

r = Linear correlation coefficient between model and observed value

N = number of data points

### 3.2 Shallow-water Results

As mentioned earlier, the models ODGP-CMC and WAVAD included shallow-water effects explicitly and generated wave products at three WAVEC buoy locations (see Figure 1). As before, error statistics in terms of RMSE, SI, etc. were worked out for all shallow-water locations; also scatter diagrams between model and observed wind speed and wave height values were prepared at analysis as well as at forecast times. Some of these results are presented in Table 2 and in Figure 7. Table 2 presents the error statistics for all three shallow-water sites for the two models ODGP-CMC and WAVAD. Here, the various parameters RMSE, MAE, etc., are defined the same way as in Table 1. Both the ODGP-CMC and the WAVAD models were driven by the CMC winds; accordingly, the wind speed statistics for the two models have only minor differences which may be attributed to the different interpolation schemes used in the two models to generate winds at the shallow-water grid points. However, the wave height statistics are distinctly different for the two models. The ODGP-CMC model provides wave heights which appear to be in good agreement with observed wave height at analysis as well as at forecast times. The ODGP-CMC model uses the TMA spectrum (see Bouws et al., 1985) to model shallow-water transformation: this seems to provide an excellent agreement between model and observed wave heights with an RMSE of 0.5 and a scatter index of 35. The large scatter in wave heights for the WAVAD model (see Figure 7) appears to suggest that the WAVAD model needs to be tuned to the shallow-water locations over the Scotian Shelf.

TABLE 2: Evaluation of the Wave Models at Shallow-water Sites

Summary of Error Statistics

| Model | Parameter | WIND SPEED (Knots) Forecast Time 00 hr | 12 | 24 | 36 | WAVE HEIGHT (Metres) Forecast Time 00 hr | 12 | 24 | 36 |
|---|---|---|---|---|---|---|---|---|---|
| ODGP CMC | RMSE | 7.46 | 9.60 | 10.99 | 10.97 | 0.51 | 0.58 | 0.79 | 0.95 |
| | MAE | 5.81 | 7.60 | 8.36 | 8.12 | 0.37 | 0.42 | 0.49 | 0.58 |
| | SI | 56 | 73 | 84 | 84 | 35 | 40 | 54 | 65 |
| | r | 0.70 | 0.70 | 0.55 | 0.44 | 0.85 | 0.86 | 0.84 | 0.77 |
| | N | 477 | 444 | 449 | 450 | 457 | 460 | 463 | 463 |
| WAVAD | RMSE | 6.55 | 10.19 | 11.05 | 10.78 | 1.81 | 1.83 | 1.79 | 1.81 |
| | MAE | 5.28 | 8.30 | 8.71 | 8.26 | 1.57 | 1.57 | 1.52 | 1.55 |
| | SI | 51 | 79 | 85 | 83 | 122 | 124 | 120 | 121 |
| | r | 0.71 | 0.68 | 0.63 | 0.59 | 0.28 | 0.25 | 0.33 | 0.36 |
| | N | 447 | 441 | 435 | 429 | 342 | 338 | 334 | 331 |

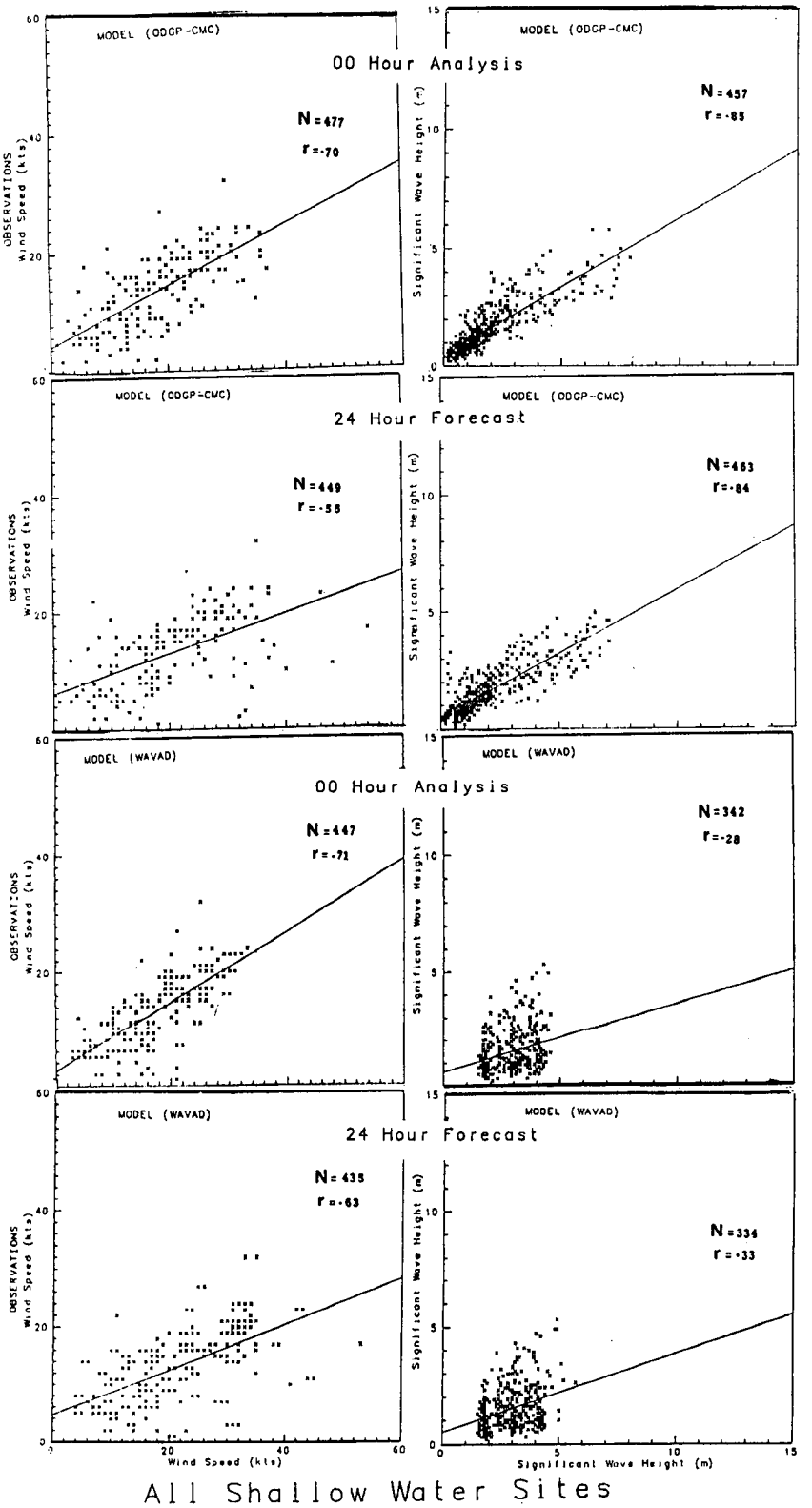


Figure 7: Scatter diagrams between observed and model wind speed (left) and between observed and model significant wave height (right) at all shallow-water sites covering the two-month period.

## 4. CONCLUDING REMARKS

The results presented in this paper are based on a preliminary evaluation of the model products against the CASP wind and wave data. A detailed analysis and evaluation based on selected storm cases is in progress at present; hopefully, this may provide an insigt into the model physics and the way it influences the model performance.

## 5. ACKNOWLEDGEMENTS

The operational testing of the ODGP model during the CASP field project was done by MacLaren Plansearch Ltd., Halifax, Nova Scotia, on contract from the Environmental Studies Revolving Fund, Ottawa. The operational testing of the WAVAD model was done by NORDCO Ltd., St. John's, Newfoundland, on contract from the Meteorological Services Research Branch (MSRB) of the Atmospheric Environment Service, Downsview, Ontario.

## REFERENCES

Bouws, E., H. Günther, W. Rosenthal and C.L. Vincent, 1985: Similarity of the wind wave spectrum in finite depth water; I. spectral form. J. Geoph. Research, 90, C1, 975-986.

Cardone, V. et al. (1974): Development of wave hindcasting methods applicable to hurricanes, Final Report, Ocean Data Gathering Program - Analysis Phase, Submitted to Shell Development Company, July 1974.

Clancy, R.M., J.E. Kaitala and L.F. Zambresky, 1986: The Fleet Numerical Oceanography Centre global spectral ocean wave model. Bulletin Amer. Meteor. Society, Vol. 67, No. 5, 498-512.

MacLaren Plansearch, 1985: Evaluation of the Spectral Ocean Wave Model (SOWM) for supporting real-time wave forecasting in the Canadian east coast offshore. Report prepared for Meteol. Services Res. Branch (MSRB), Atmospheric Environment Service, Downsview, Ont. 159 pp + Appendices. January 1985.

Resio, D.T.: The estimation of wind-wave generation in a discrete spectral wave model. J. Physical Oceanography, Vol. 11, 510-525.

# ON THE UTILITY OF SATELLITE SENSED WIND DATA FOR OCEAN WAVE ANALYSIS AND MODELLING

R. Lalbeharry, S. Peteherych, and M.L. Khandekar

Atmospheric Environment Service
Downsview
Ontario

## 1. INTRODUCTION

The short-lived satellite SEASAT (28 June - 10 October 1978) provided valuable wind/wave data for approximately 100 days over the North Atlantic Ocean. On board the satellite an oblique-viewing microwave radar, known as SEASAT-A Satellite Scatterometer was used to sense high resolution over-water winds in approximately 1400 km swaths extending across the sub-satellite tracks.

The radar measures back-scattered energy from centimetre scale capillary-gravity waves with wavelengths ~ 1-5 cm. The back-scattered energy is anisotropic and this allows directional information to be derived from measurements at different azimuths using fore and aft antennae. The wind vectors are measured indirectly at a height of 19.5 metre for a neutrally stratified atmosphere through use of an empirically derived model function, Schroeder et al. (1982). The sinusoidal nature of the model function provides the estimation of one wind speed but up to four possible directions based on the co-location of a pair of SASS cells measured from the fore and aft beams.

Numerous techniques have been used to dealias the SASS winds before incorporation into any data assimilation scheme. Objective dealiasing methods can be found in Yu and McPherson (1984), Baker et al (1984), and Levy and Brown (1986), while the subjective method is described by Wurtele et al. (1982).

Several studies to evaluate the usefulness of SASS wind data on weather prediction have been reported. For example, Yu and McPherson (1984), and Duffy et al. (1984) found negative or rather small impact of Seasat wind data on numerical weather prediction, although the impact was larger in southern hemisphere analysis and smaller in northern hemisphere analysis. Anthes et al. (1983) used SASS winds in a series of model simulations to predict the QE II storm and found significant improvement when supplementary data were added to the initial conditions. Cane and Cardone (1981) pointed out the potential impact of SASS winds on the QE II storm while Duffy and Atlas (1986) showed that when subjectively dealiased SASS winds were allowed to influence the upper levels of the atmosphere a large positive impact was found.

The objective of this study is to create a wind field appropriate for driving a spectral ocean wave model using SASS winds, and a blend of these winds with conventional ships' winds, and to assess their usefulness for wave hindcasting and forecasting.

A discrete spectral model developed by Resio (1981) is used in the present study. This is a deep water model with a specially designed spherical orthogonal grid. Resio re-analyses the non-linear wave-wave interaction term and obtains an expression which involves the square of the wind speed. Further Resio neglects the linear growth term so that the net source term consists of the exponential growth term and the parameterized non-linear wave-wave interaction term.

## 2. DATA

The data sets used in this study are:

(i) subjectively dealiased SASS winds described by Wurtele et al. (1982) for the period 12Z, 8 September - 00Z, 13 September 1978.

(ii) Marine surface winds and wave data from ocean weather ships, ships of opportunity, and buoys taken at the main synoptic hours for the same period.

(iii) Surface geostrophic winds from which the first guess field is derived for use in the interpolation technique. This data set is described by Moran and Alp (1985).

Satellite data are generally asynoptic. Pierson (1983) pointed out that the average time it takes for an eddy to be advected by the mean wind, $\overline{u}$, over a distance, D, is given by $T_e = D/\overline{u}$. The SASS winds with resolution of the order of 100 km and a mean wind speed of 10 m/s would be equivalent to an averaging time of about 2.8 hours so that the winds are synoptic if they fall within the time window of ± 1.4 hours of the analysis time. However, the SASS winds are considered to be synoptic if measured within ± 3.0 hours of analysis time. Time weights are applied to the winds between ± 3.0 hours and ± 5.0 hours. For SASS times up to ± 3.0 hours a weight of 1.0 is applied and this is reduced to .6 for a SASS time of ± 5.0 hours from analysis time.

## 3.0 DATA ANALYSIS TECHNIQUE

### 3.1 Interpolation Method

The data are interpolated onto a rectangular grid using the successive correction method (SCM) of Cressman (1959). The grid is a polar stereographic projection with grid length of 277.7 km in each direction (true at 60N) and includes the area of the North Atlantic Ocean bounded by 30N and 70N latitudes and 20W and 70W longitudes, the region of wind input into the Resio wave model. The gridded data are then transformed onto a spherical orthogonal grid (SOG). The SOG values are obtained by bi-linear interpolation of the four rectangular grid points surrounding each SOG point.

The essential steps of the SCM are described by Seaman (1983) and will not be repeated here. The influence function in this study is given by

$$\begin{aligned} b_i &= \left[(R^2 - d_i^2)/R^2 + d_i^2)\right]^4 \quad , d_i < R \\ &= 0 \qquad\qquad\qquad\qquad , d_i \geq R \end{aligned} \tag{3.1}$$

where $d_i$ is the distance between the observation point and the grid point and R is a prescribed scan radius which decreases with iteration. The weighting function $b_i$, used also by Levy and Brown (1986), weights the closer data points more heavily, the weights diminishing to .13 for d/R = .5. It is most likely to prevent undesired smoothing in data sparse areas at large scan radii.

The first guess field is obtained from the surface geostrophic winds through use of a reduction/rotation model. The geostrophic wind is reduced by a constant factor and rotated counter-clockwise a constant number of degrees to provide an estimate of the preliminary wind at the 19.5 metre level. Inclusion of the various ageostrophic terms are not made since the latter gives marginal improvements to wind hindcasts over the oceans, Moran and Saulesleja (1985). This reduction/rotation method is a simple model of the Ekman effect in the boundary layer. Studies have indicated that for open-water wind approximation, the geostrophic wind speed can be reduced by 15% and the direction rotated by 20° to obtain the surface winds at the 19.5 m level.

### 3.2 Interpolation Error Analysis

Let the superscript A, i, o, P denote respectively the analysed, interpolated, observed, and first guess values and the subscripts i, g, respectively the observed point and the grid point. Given the observed field, $F_i^o$, at irregularly spaced points and the first guess field, $F_g$, at grid points, the standard interpolation theory, Gandin (1963), gives an estimate of the grid point value from the equation

$$F_g^A = F_g + \sum_{i=1}^{n} w_i \, (F_i^o - F_i^{iP}) \; ; \quad f_g^A = \sum w_i \, (f_i + e_i) \tag{3.2}$$

where $f_i$ is the true increment between the observed value and the interpolated guess field at the ith observation point, $e_i$, the observational error, $w_i$, a non-iterative weight, and n, the number of observations influencing the grid point. Eq. (3.2) states that the correction to the first guess field can be expressed as a linear combination of the difference between the observed value and the interpolated value at the observation point. The interpolation error is given by

$$E_g = f_g - f_g^A \tag{3.3}$$

where $f_g$ is the true grid point correction. The mean square interpolation error (Seaman, 1983, Bergman and Bonner, 1976) is given by

$$[E_g^2] = [f_g^2] - 2 \sum_{i=1}^{n} w_i \, [f_g \, f_i] + \sum_{j=1}^{n} \sum_{i=1}^{n} w_i \, w_j \, [f_i \, f_j] + \sum_{i=1}^{n} w_i^2 \, [e_i^2] \tag{3.4}$$

where [ ] denotes an ensemble average $[e_i \, e_j] = 0$ for $i \neq j$, $[f_g \, e_i] = [f_i \, e_j] = 0$. Let $s^2 = [f_g^2]$ be the variance of the initial guess value from the true value at the grid point and assume homogeneity of variance, that is, $s^2 = s_{f_i}^2 = s_{f_j}^2$. A measure of the interpolation error is given by

$$[E_g^2]/s^2 = 1 - 2 \sum w_i \, u_{gi} + \sum \sum w_i \, w_j \, u_{ij} + \sum w_i^2 \, \lambda^2 \tag{3.5}$$

where $\lambda^2 = [e_i^2]/s^2$ is constant and represents the fraction of the natural variance due to observational errors, $u_{gi}$, the correlation coefficient between the grid point and the observation point, and $u_{ij}$, that between observation points. Assuming homogeneity and isotropy the coefficients can be expressed as a function of separation distance only. In this study the auto-correlation function chosen is Gaussian in form and is given by

$$u = \exp(-q^2/2L^2) \tag{3.6}$$

where q is the separation distance between pairs of observations and between a grid point and an observation point and L defines a separation distance in which isotropy is maintained. A correlation study of winds over the west North Atlantic (R. Brown, 1986, Atmospheric Environment Service) indicates that approximate isotropy is obtained for separation distance of about 450 km and hence a value of L = 450 km is chosen.

The non-iterative weights, $w_i$, are computed using the SCM. For a given scan the normalized weight is determined and the contribution by the ith observation to the grid point correction is found. The process is repeated for each scan using the same observed value but with the updated first guess field. Since no smoothing is performed, the algebraic sum of the corrections for all passes gives the contribution of the ith observation to the grid point correction. This allows the resultant weight (non-iterative) corresponding to the ith observation to be determined for the interpolation method employed. The process is repeated for all observations falling inside the maximum scan radius for each grid point. The weights, $w_i$, are then normalized for use in Eq. (3.6).

### 3.3 Field Blending

Consider the analysed grid point SASS winds $X_g^A$ and the conventional ships' winds $Y_g^A$. An estimate of the blended value at the grid point location can be given by

$$Z_g^A = aX_g^A + bY_g^A \tag{3.7}$$

where a and b are appropriate weighting factors. For unbiased estimates $[Z_g] = [Z_g] = [X_g^A] = [Y_g^A]$ and from Eq. (3.7) a + b = 1. $Z_g$ is the true grid point value and $[Z_g]$ can be considered as the norm. Removal of the norm reduces Eq. (3.8) to

$$z_g^A = ax_g^A + by_g^A \tag{3.8}$$

The mean square error is given by

$$[E_z^2] = s^2 - 2s\,(as_1 R_1 + bs_2 R_2) + a^2 s_1^2 + b^2 s_2^2 + 2abs_1 s_2 r \tag{3.9}$$

Here $R_1$ is the correlation coefficient between $z_g$ and $x_g^A$, $R_2$ that between $z_g$ and $y_g^A$, and r that between $x_g^A$ and $y_g^A$, $s^2$ is the variance of the blended field, $s_1^2$, that of the SASS wind field, and $s_2^2$, that of the ships' wind field. For homogeneous variance $s^2 = s_1^2 = s_2^2$. Minimization of the mean square error (Thompson, 1977) gives a and b in terms of $R_1$, $R_2$, and r and Eq. (3.9) reduces to

$$[E_z^2]/s^2 = 1 - 2R_1 R_2/(1 + r), \quad \text{for } R_1 \sim R_2 \tag{3.10}$$

For the SASS wind data set

$$[E_x^2] = 2s_1^2 (1 - R_1) \tag{3.11}$$

Similarly, for the ships' wind data set

$$[E_y^2] = 2s_2^2 (1 - R_2) \tag{3.12}$$

Normalization of a and b gives

$$\begin{aligned} a' &= (R_1 - R_2 r)/[(R_1 + R_2)(1 - r)] \\ b' &= (R_2 - R_1 r)/[(R_1 + R_2)(1 - r)] \end{aligned} \tag{3.13}$$

If the norm is considered as the initial guess field, then Eq. (3.8) can also be expressed as

$$z_g^A = \sum_{i=1}^{n} w_i (x_i + e_i) + \sum_{k=1}^{m} c_k (y_k + e_k) = \sum_{i=1}^{n+m} p_i (x' + e_i') \tag{3.14}$$

where both data sets are mixed and $x_i'$ is either $x_i$ or $y_i$ and $e_i'$ the corresponding observational error. Eq. (3.14) is of the same form as Eq. (3.2). Using Eq. (3.5), $[E_z^2]/s^2$, $[E_x^2]/s^2$, and $[E_y^2]/s^2$ can be estimated. Substitution of these values in Eqs. (3.10) - (3.12) gives $R_1$, $R_2$, and r and using Eq. (3.13) a' and b' are estimated. The objectively derived weighting factors are then used to blend the gridded values of SASS winds and ships' winds.

## 4. RESULTS AND DISCUSSION

Eq. (3.5) is used to tune the SCM to obtain the optimal scan radii and the error specification as given in Table 1.

Table 1. Optimal scan radii in grid units (1 grid unit = 277.7 km) and error specification for each scan radius.

| Scan radius | 3.7 | 3.7 | 3.7 | 2.7 | 1.8 | 1.0 |
|---|---|---|---|---|---|---|
| Error (m/s) | 15 | 15 | 10 | 10 | 5 | 5 |

Table 2 gives the result based on interpolation error analysis, in which the weighting factors $a'$ and $b'$ are objectively derived for fractional error variance of 0, .10, and .25 respectively. It is seen that $a'$ is slightly lower than $b'$ and this may be due to the large inter-pass gaps causing greater interpolation error.

Table 2. Correlation coefficients ($R_1$, $R_2$, r) and weighting factors ($a'$, $b'$) for SASS winds and ships' winds for specified observational errors. The values are for u-component of the wind only, with similar values for the v-component (not shown).

| Date | $\lambda^2$ | $R_1$ | $R_2$ | r | $a'$ | $b'$ |
|---|---|---|---|---|---|---|
| 12Z, 9 Sept. 1978 | 0.0 | .82 | .85 | .81 | .41 | .59 |
| | .10 | .81 | .84 | .85 | .40 | .60 |
| | .25 | .80 | .82 | .82 | .44 | .56 |
| 12Z, 10 Sept. 1978 | 0.0 | .85 | .86 | .90 | .45 | .55 |
| | .10 | .84 | .84 | .88 | .50 | .50 |
| | .25 | .83 | .82 | .86 | .62 | .38 |
| 12Z, 11 Sept. 1978 | 0.0 | .84 | .86 | .81 | .45 | .55 |
| | .10 | .83 | .84 | .79 | .47 | .53 |
| | .25 | .83 | .82 | .81 | .53 | .47 |

A value of .5 is chosen for both $a'$ and $b'$, that is, the SASS winds are given the same weight as the conventional marine winds. The weighting factors can be perturbed about the value .5 to assess the impact of weighting one data set more than the other.

Figure 3.1 shows the track of the QE II storm for the period 09/12Z - 13/00Z and the locations #1-3 relative to the track. The approximate position of the Oceanliner QE II at 11/12Z is also shown. The QE II was battered with waves of about 12 metres high. Emphasis is being placed on the results for 12Z, 11 Sept. 1978. Location #1 was generally under the influence of northerly flow and locations #2-3 that of southwestererly flow. The model wave heights are obtained for input based on gridded values of (i) SASS winds only, (ii) surface marine winds only, (iii) weighted grid point values of SASS winds and surface marine winds. The weights are obtained from interpolation error analysis.

Figure 3.2 shows the subjectively dealiased SASS winds used in the interpolation over the North Atlantic. Large inter-pass gaps exist. If no SASS winds influence a grid point, the first guess field remains unchanged so that specification of the latter field close to the observed field is important when only SASS winds are used to obtain grid point values.

The interpolated SASS wind field is shown in Figure 3.3a and the blended field in Fig. 3.3b. The SASS winds are capable of reproducing the circulation pattern given a reasonable first guess field. The centres of circulation are well defined and in good agreement with the observed circulation (see Fig. 6, Cane and Cardone, 1981). The blending of the SASS winds with the marine winds tends to produce a somewhat smoother field with the main circulation features remaining intact. The centre of the storm is located near 51.5N, 43.0W and agrees well with the observed location.

The Resio wave model is initialized with zero wave energy. The hindcast wave heights valid at 11/18Z are presented in Figs. 3.4a - 3.4c after a spin-up time of 48 hours. A warm-up period of about 48 hours appears to be adequate to bring the wave field into equilibrium with the input wind field. Fig. 3.5 is METOC's significant wave height analysis valid at 11/12Z.

Wave heights due to SASS winds (Fig. 3.4a) are generally in good agreement with those shown in Fig. 3.5. The lower values between the two cut-off areas may be due to the large inter-pass gap in this region. Hindcast waves greater than 8m are obtained

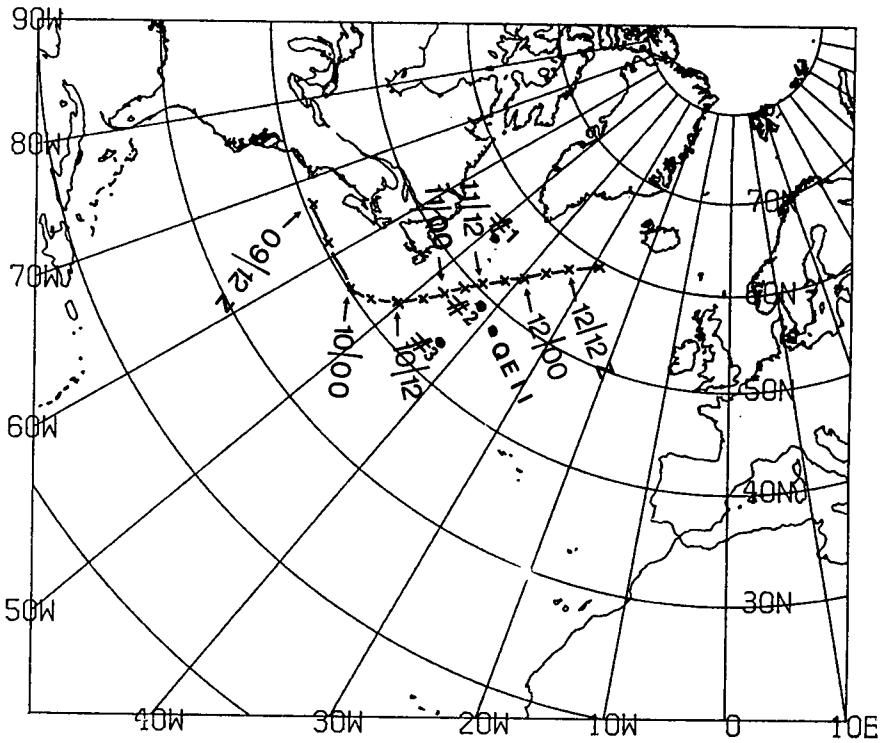


Fig. 3.1 Track of the QE II storm for the period 09/12Z - 12/18Z, Sept. 1978. Location #1-3 used in the discussion and the position of the Oceanliner QE II on the 11th at about 12Z are also shown.

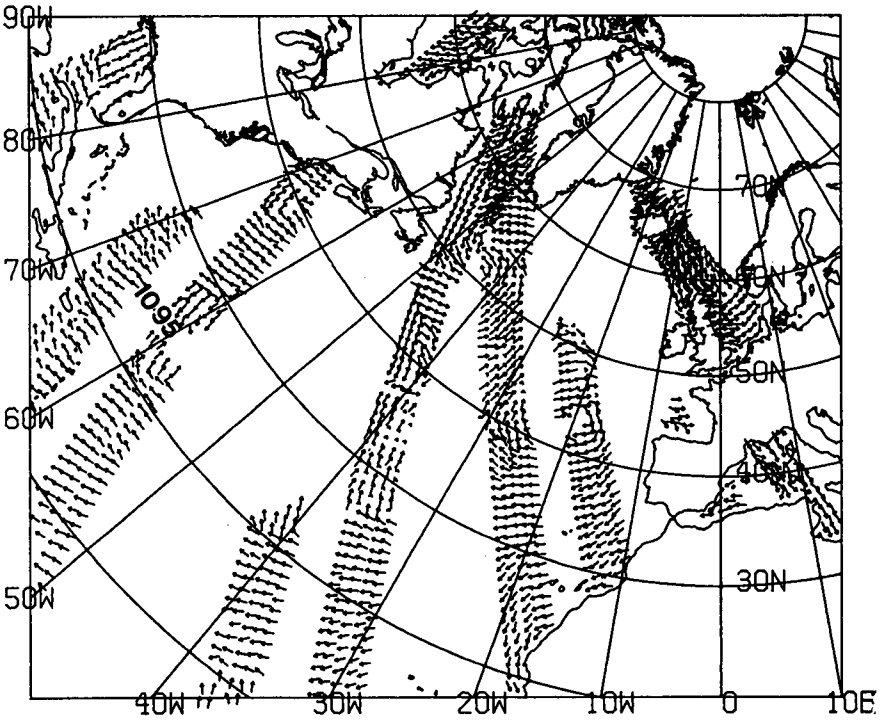


Fig. 3.2 Subjectively dealiased SASS winds over the North Atlantic centred at analysis time 12Z, 11 Sept. 1978, for orbits 1092 - 1096 covering the time period 0822Z - 1530Z.

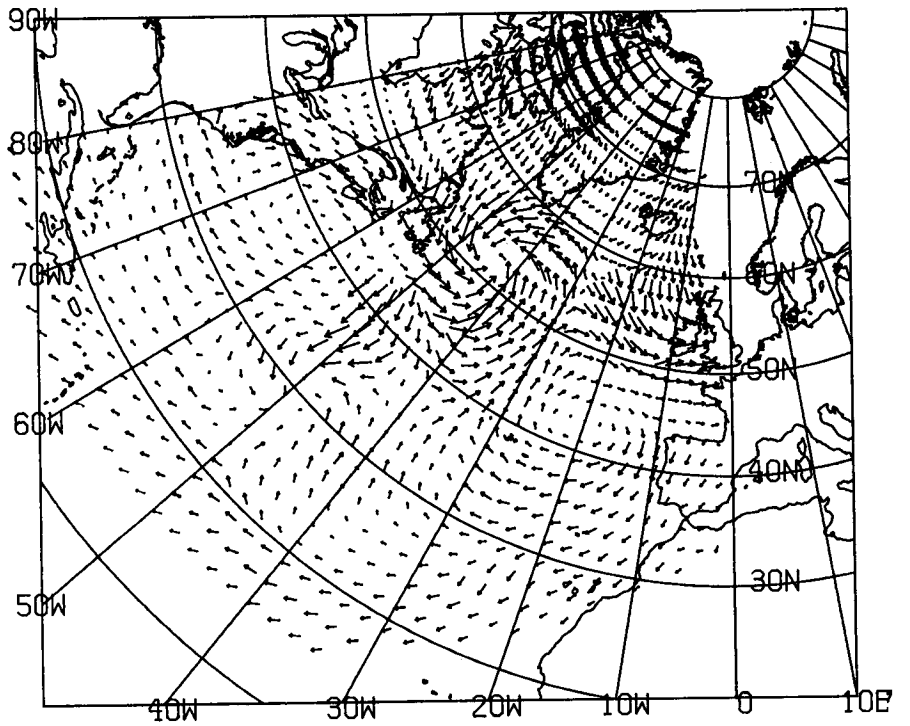


Fig. 3.3a The analysed gridded wind vector for 12Z, 11 Sept. 1978 using SASS wind only. The vector length is proportional to wind speed (.02 cm = 1 m/s) and the arrows point toward the direction of flow.

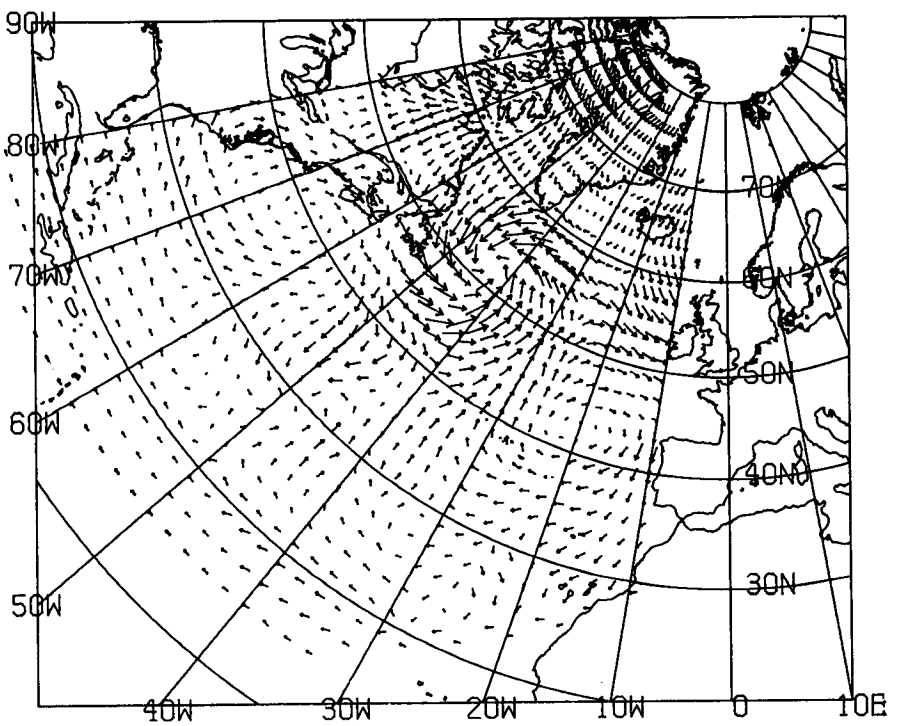


Fig. 3.3b Same as Fig. 3.3a but for blended winds. A weight of .5 is given to SASS winds and .5 to ships' winds.

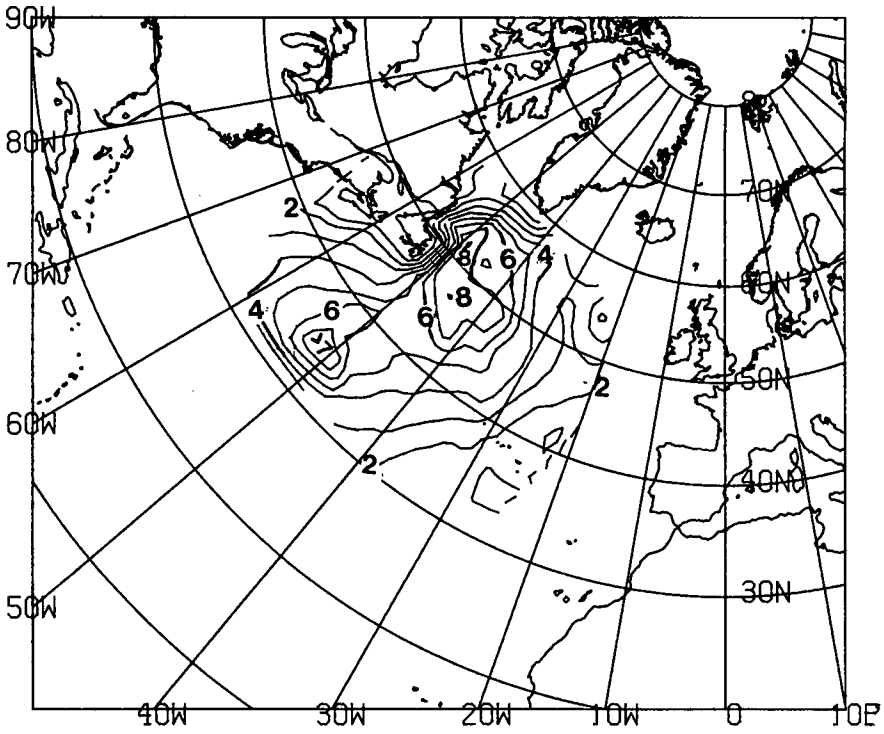


Fig. 3.4a Hindcast wave heights (metres) valid at 18Z, 11 Sept. 1978, based on SASS winds only, with initial wind input at 12Z, 09 Sept. 1978, and zero wave energy.

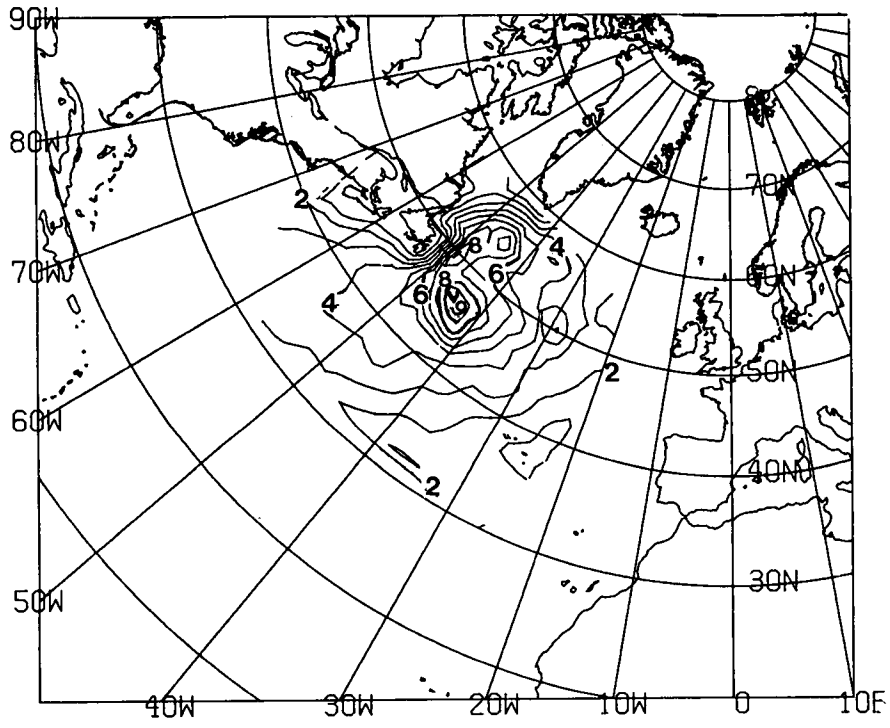


Fig. 3.4b Same as Fig. 3.4a but for ships' winds.

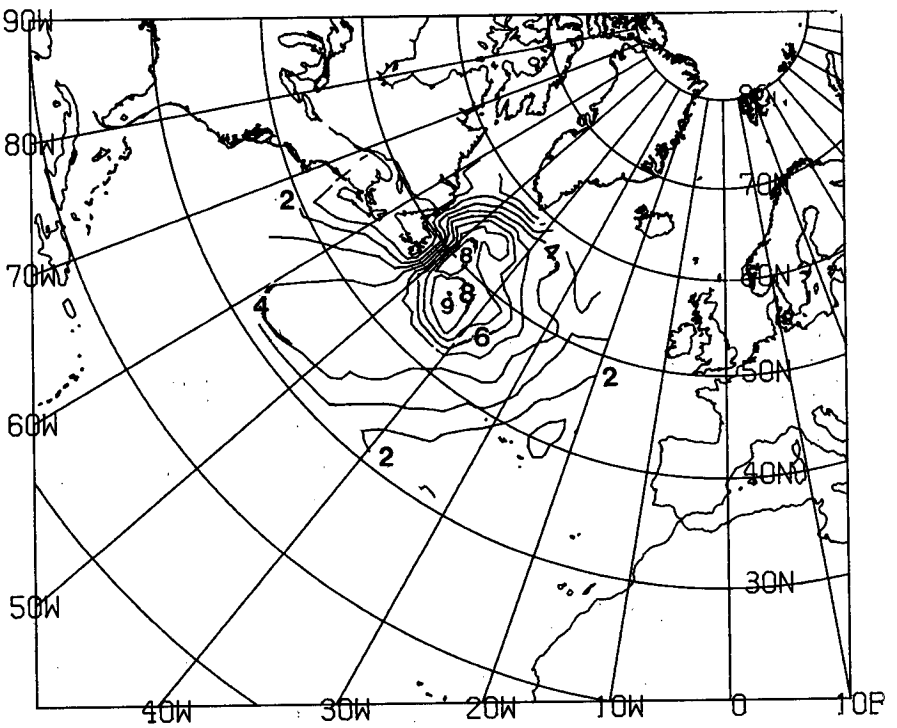


Fig. 3.4c Same as Fig. 3.4a but for blended winds. The weighting is .5 for SASS winds and .5 for ships' winds.

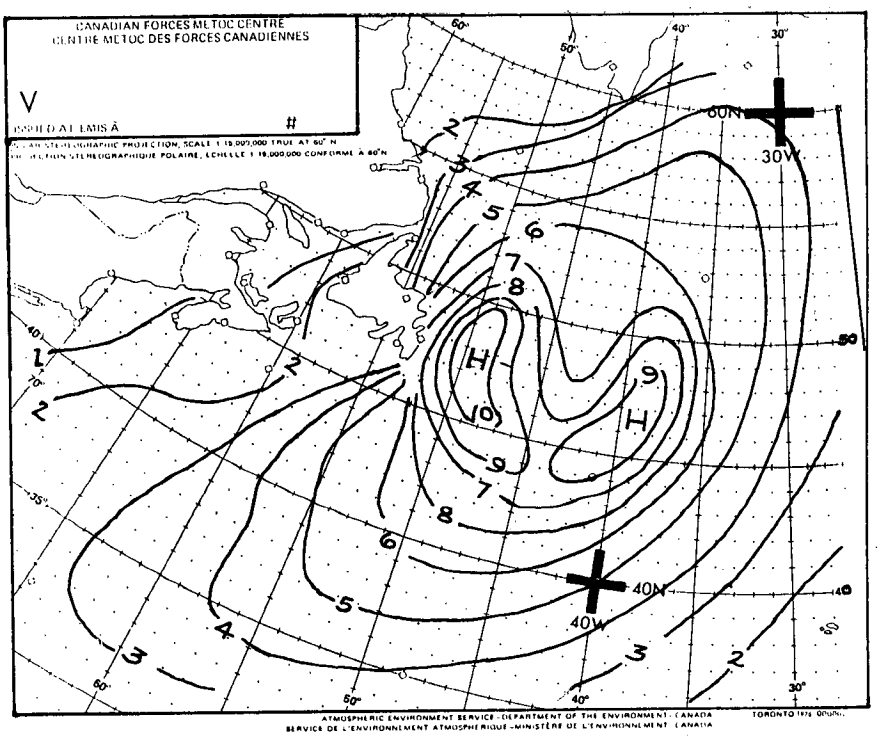


Fig. 3.5 METOC's subjective wave height analysis valid at 12Z, 11 Sept. 1978. Height contours are in metres.

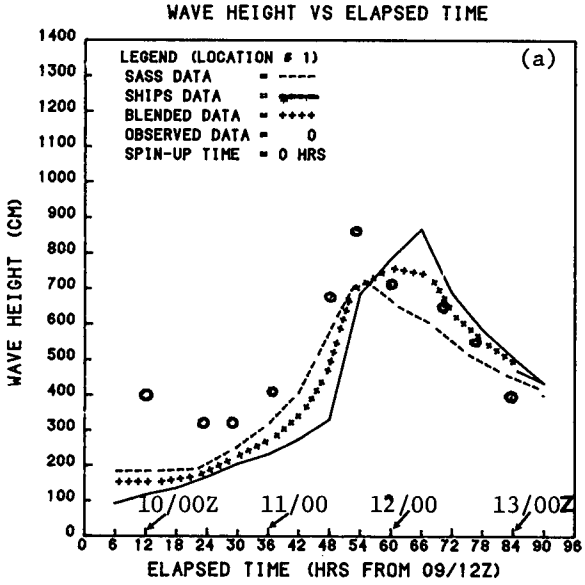


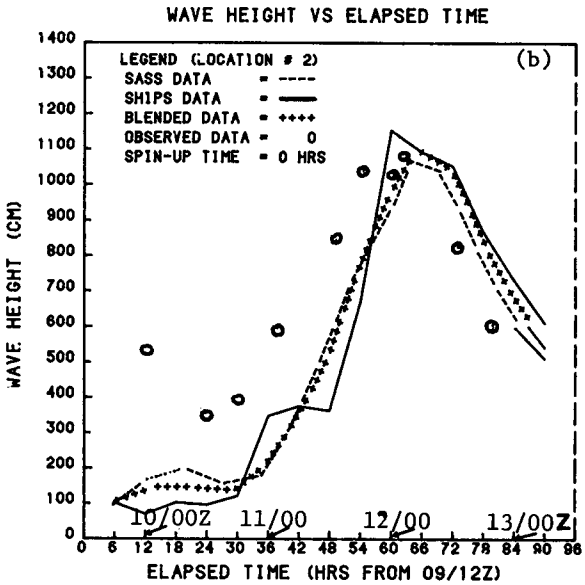


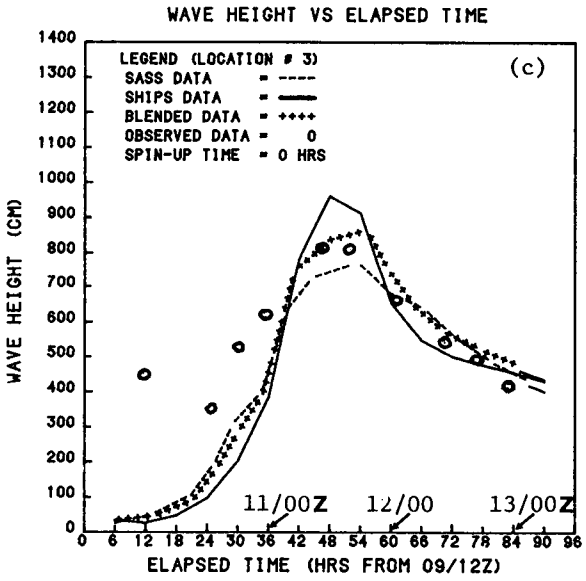


Fig. 3.6a Time evolution of hindcast wave heights in response to SASS, ships', and blended wind data with initial wind input at 12Z, 09 Sept. 1978, and zero wave energy at location #1 (54.5N, 49W). Observed heights are shown in open circles.

Fig. 3.6b Same as Fig. 3.6a but for location #2 (49.2N, 41.3W).

Fig. 3.6c Same as Fig. 3.6a but for location #3 (44.3N, 42W).

with waves greater than 7m near the location of the QE II. The ships' data produce waves greater than 9m in the same region. The SASS data are centred around analysis times 00Z and 12Z, while ships' data are available every six hours. The model requires wind input every six hours and hindcast waves generated are valid 6 hours following wind input using the wave field generated by the previous wind inputs. The difference between the SASS and the ships' hindcast wave fields may be partly due to linear time interpolation of the 00Z and 12Z SASS winds to obtain the 06Z ansd 18Z data and to a more even spatial distribution of ships' data and to the somewhat higher winds observed by the ships. The blended field shows waves over 8m and good synoptic agreement between the model heights and METOC's wave height analysis. Similar trends are observed when other times are examined. The main result is that SASS data are capable of generating the wave field just as well as the conventional marine winds. Greater accuracy can be achieved given greater frequency of observation and a more even spatial distribution of remotely-sensed winds.

The evolution of wave heights in response to the application of SASS, ships' and blended wind data is illustrated in Figs. 3.6a - 3.6c at three locations relative to the storm track shown in Fig. 3.1. Wind input commences at 09/12Z with zero wave energy. The frequency of wind input is every six hours and the elapsed time is the time after the first wind input at which the hindcast waves are valid based on all previous inputs.

For the locations shown the fetches are long and this allows the significant wave height to be proportional to the square of wind speed. The agreement in wave fields due to SASS and ships' data is reasonably good. Differences may be due to reasons already given. At location #2 waves reached a height near 7m at 11/12Z and rose to over 10m by 12/06Z. The QE II was in the vicinity and experienced waves near 12m. These Figures also indicate that a warm-up time of about 36-48 hours is required. The hindcast waves due to the blended field appear to be in closer agreement with the observed wave height with a tendency of peak heights of the former to lag those of the latter. The dissipation rates following storm peak are similar to, and appear to somewhat lag, the observed rates.

The validation is somewhat crude since the observed wave heights are interpolated to the locations #1-3 using the ships' swell and sea wave height data. It should be pointed out that these are visual observations and are subject to errors. Nevertheless, there is a fair agreement between model and observed wave heights.

## 5. CONCLUSIONS

The results are preliminary but, nevertheless, demonstrate that SASS winds can provide useful input for validating wave models in a hindcast or in a forecast mode, if the forecast field is used as the first guess field. The model wave heights generated are of comparable values with observed values given the required model warm-up time. If the time window of ± 3 hours from analysis time is used to define synopticity, then SASS winds can be assimilated into an objective interpolation scheme given adequate spatial distribution and frequency of observation. The gridded values can be blended with gridded values obtained from conventional data and the weighting factors can be objectively derived using interpolation error analysis.

Greater accuracy can be achieved with improved interpolation scheme. This would require detailed study of the auto-correlation function and the corresponding weighting factors. An analysis of the auto-correlation function is in progress. Also the wave model validation will be extended to other periods for which wave height data are available.

## ACKNOWLEDGEMENTS

Special thanks are due to Norbert Driedger for providing computer support and to Bea McKay for typing the manuscript.

REFERENCES


Anthes, R.A., Ying-Hwa Kuo, and John R. Gyakum: Numerical simultations of a case of explosive marine cyclogenesis, Mon. Wea. Rev., 111, 1174-1188, 1983.

Baker, W.E., R. Atlas, E. Kalnay, M. Halem, P.M. Woiceshyn, S. Peteherych, and D. Edelman: Large-scale analysis and forecast experiments with wind data from Seasat-A scatterometer, J. Geophys. Res., 89, 4927-4936, 1984.

Bergman, K.H. and W.D. Bonner: Analysis error as a function of observation density for satellite temperature soundings with spatially correlated errors, Mon. Wea. Rev., 104 1308-1316, 1976.

Cane, M. A., and V.J., Cardone: The potential impact of scatterometry on oceanography: A wave forecasting case, in Oceanography from Space, edited by J.F.R. Gower, pp 587-595, Plenum Press, New York, 1981.

Cressman, G.P.: An operational objective analysis system, Mon. Wea. Rev., 87, 367-374, 1959.

Duffy, D., R. Atlas, T. Rosmond, E Baker, and R. Rosenberg: The impact of Seasat scatterometer winds on the Navy's operational model, J. Geophys. Res., 89, 7238-7244, 1984.

---- and R. Atlas: The impact Of Seasat-A scatterometer data on the numerical prediction of the Queen Elizabeth II storm, J. Geophys. Res., 91, 2241-2248, 1986.

Gandin, L.S.: Objective analysis of meteorological fields [Translated (1965) by Israel Programme for Scientific Translations, Jerusalem, 242 pp ], 1963.

Levy, G. and R.A. Brown: A simple objective analysis scheme for scatterometer data, J. Geophys. Res., 91, 5153-5158, 1986.

Moran, M.D. and S. Alp: Optimization of offshore hindcast winds: Phase I Report, CCC Report No. 85-2, Canadian Climate Centre, Downsview, Ontario, 94 pp, 1985.

---- and A. Saulesleja: Optimization of hindcast surface winds, Proceedings International Workshop on Offshore Winds and Icing, Halifax, Nova Scotia, 1985.

Pierson, W.J.: The measurement of synoptic scale wind over the ocean, J. Geophys. Res., 88, 1683-1708, 1983.

Resio, D.T.: Estimation of wind-wave generation in a discrete spectral model, J. Phys. Oceanogr., 11, 510-525, 1981.

Seaman, R.S.: Objective analysis of statistical interpolation and successive correction schemes, The Sixth Conference on Numerical Weather Prediction, Am. Meteorol. Soc., Omaha, Nebr., 1983.

Schroeder, L.C., D.H. Boggs, G. Dame, I.M. Halberstam, W.L. Jones, W.J. Pierson, and F.J. Wentz: The relationship between wind vector and normalized radar cross-section used to derive Seasat-A satellite scatterometer winds, J. Geophys.Res., 87, 3318-3336 1982.

Thompson, P.D.: How to improve accuracy by combining independent forecasts, Mon. Wea. Rev., 105, 228-229, 1977.

Wurtele, M. G., P.M. Woiceshyn, S. Peteherych, M. Barowski, and W.S. Appleby: Wind direction removal studies of SEASAT scatterometer derived winds, J. Geophys. Res., 87, 3365-3377, 1982.

Yu, T.W. and R.D. McPherson: Global data assimilation experiments with scatterometer winds from Seasat-A, Mon. Wea. Rev., 112, 368-376, 1984.

# A THIRD GENERATION OCEAN WAVE MODEL

G.J. Komen and L. Zambresky*

KNMI, De Bilt, The Netherlands

Abstract: We summarize and explain the basis for third generation wave models. The WAM model, the first of this type, is briefly described. After a review of early results of the model we focus on recent progress concerning

(i) dependence of predictions on wind field quality
(ii) a comparison with SIR-B observations of the North Sea

## 1. The basis

A weakly varying wave field can be described by the energy transfer equation

$$\left(\frac{\partial}{\partial t} + \underset{\sim}{c}_g \frac{\partial}{\partial \underset{\sim}{x}} + \frac{\partial \omega}{\partial \underset{\sim}{x}} \frac{\partial}{\partial \underset{\sim}{k}}\right) F = S_{in} + S_{nl} + S_{wc} + S_{bt} \qquad (1)$$

Here, the conventions are the usual ones: $F = F(k; x, t)$ is the wave spectrum, as a function of wave number k, position x and time t; $c_g$ is the group velocity and $\omega$ denotes frequency. On the right we have source terms, specific functionals of the spectrum, which describe wind input, nonlinear transfer, and dissipation through white capping and interaction with the bottom. The evolution of our understanding of equation (1) is interesting; a full account would easily fill a monograph of several hundred pages. Here, we can only indicate gross features. We will be unable to quote important contributions by many individuals.

The left hand side of equation 1 describes propagation effects. It can be derived for any dispersive wave problem: slowly varying wave trains follow wave rays with the appropriate group velocity.

The input term, describing the transfer of energy from wind to waves seems to be dominated by shear flow instability. This problem is a difficult one for the coupled, turbulent air-sea system. Modern research was started by Miles (1957). His study was followed by many others. Through a combination of analytic, numerical and experimental methods a rough consensus has been reached. However, details of the process are still insufficiently understood.

* On leave of absence from Fleet Numerical Oceanography Center, Monterey, CA.

The nonlinear transfer term represents resonant four-wave interactions, which play a role in nearly any branch of physics. For surface gravity waves it was calculated from first principles by Klaus Hasselmann (1962) who obtained a representation in terms of a complicated 6 dimensional integral over triple products of F. The fast and accurate evaluation of this so-called Boltzmann integral (in analogy with a similar integral in molecular physics) has been a challenge until recently, and even now there is room for improvement. Physically the nonlinear transfer significantly contributes to the migration of the spectral peak with fetch, in fetch-limited growth, to wind-sea swell interaction, and to directional relaxation in turning winds. Its poor representation in most current wave models is responsible, in part, for the discrepancies between these wave models, as found in the SWAMP (1985) study.

Dissipation through white capping is fairly complicated, because white capping is a strongly nonlinear process. An estimate of the dissipation source term has been given by Hasselmann (1974). Bottom dissipation in shallow water is caused by friction, percolation and other processes.

A detailed study of the energy balance, which results when all source terms are working simultaneously, had to wait until a fast numerical algorithm for the Boltzmann integral became available. Although several people had written valuable integration programs, they could only be applied to a few spectra, for lack of computer resources. Recently, Hasselmann and Hasselmann (1985) developed an efficient integration code, which they implemented on several CRAY-1 computers. Using the best known expressions for the other source terms, one-dimensional, fetch limited simulation runs were performed, integrating equation 1 from a near flat sea to full development. The results were analyzed and compared with experimental lore (Komen, Hasselmann and Hasselmann, 1984).

A next step was the full 2-D integration of equation 1 for an arbitrary time history of the wind field. This was going to be the third generation model (as distinct from second generation models, which have a (simple) parameterization of the nonlinear transfer, and first generation models, which have no explicit non-linear transfer at all). It could only be achieved after further progress with the efficient estimate of the Boltzmann integral (Hasselmann, Hasselmann, Allender and Barnett, 1985).

## 2. The WAM model

The program that integrates equation 1 for general geometry and general winds, with an explicit representation for each source term has become known as the WAM model, because work was carried out within the so-called WAM (= WAve Modelling) group. The foundations were laid at the Max-Planck Institut für Meteorologie, where the deep water version was developed, but many members of the WAM group also made their contribution.

The model is available in a global and a regional version. The equation is solved in either geographical or Cartesian coordinates. The spectrum has a discrete representation with 26 frequencies and 12 directions. In most applications propagation has been done with a first-order, up wind finite difference scheme, but a second order scheme has also been tested. Time stepping is done with an implicit integration scheme. The model has been implemented on various CRAY computers, in particular on the CRAY-X-MP of the European Centre for Medium Range Weather Forecasting (ECMWF) in Reading, U.K. A Cyber-205 implementation is envisaged.

Early results of the model have been reported in Brighton and Maryland (Komen, 1985a and b). A full account of the model is in preparation (Hasselmann et al, 19..). The early results comprised, besides the usual tests,

(i) a global run (2 days)
(ii) regional hindcasts
  a) 6 extratropical storms ('WHIST')
  b) 3 hurricanes

For lack of time (and space) we have to refer to the original publications for details, but we will show one result from each exercise to give the reader a feeling for their quality. Fig. 1 gives the global sea state after 2 days of simulation. So far, these

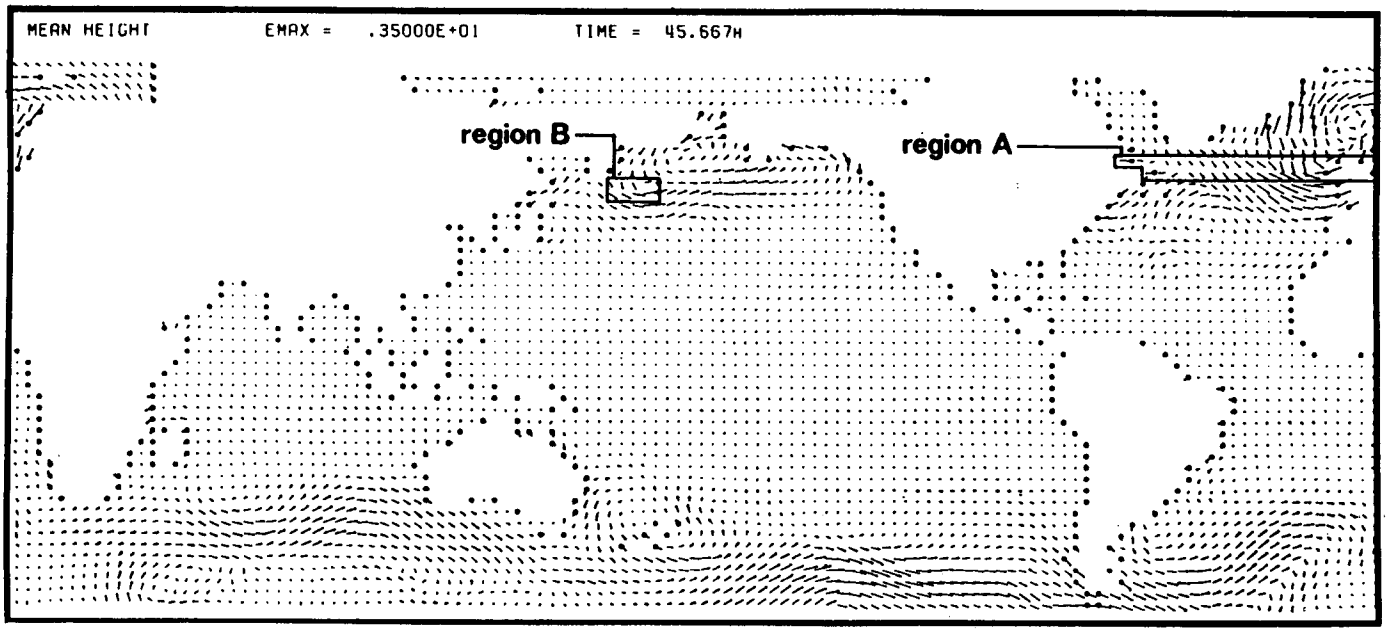


Fig. 1. Significant wave height and direction at 8.00, Oct. 15, 1983, 46 hours after initial time.

results have not been validated, but they give a good idea of the global applicability of the model. The figure gives only significant wave height and mean direction. However, the full 2-D spectra are available in each grid point, when needed. For the extensive regional hindcast, on the other hand, a comprehensive comparison with observations has been made (Bertotti, Guillaume and Janssen, 1985). The results were quite good, as can been seen from table 1, which gives summary statistics for all storms and two groups of stations: Euro, IJmuiden and K13, being shallow (depth 20 - 30 m) and Ekofisk, Brent and Statfjord, being typical deep water stations.The shallow water stations, all located in the southern North Sea, measured a mean wave height of 3.2 m; the model results were on average 16 cm too low, whereas the Scatter Index (rms error/mean observed value) was only 16%.

Table 1

| | $H_s^{obs}$(m) | $\Delta H_s$(m) | SI |
|---|---|---|---|
| EURO<br>IJMUIDEN<br>K13 | 3.2 | 0.16 | 16% |
| EKOFISK<br>BRENT<br>STATFJORD | 5.5 | 0.30 | 15% |

Table 1. Mean observed wave height, WAM model bias and scatter index for typical shallow (EURO, IJMUIDEN, K13), and deep water stations in the North Sea, in a hindcast of 6 storms.

The hurricane hindcast has been made by Vince Cardone and coworkers. Using best available wind fields this led to results as in figure 2, (the measurement device broke down at the height of the hurricane) indicating the current performance of the model in complicated turning wind situations.

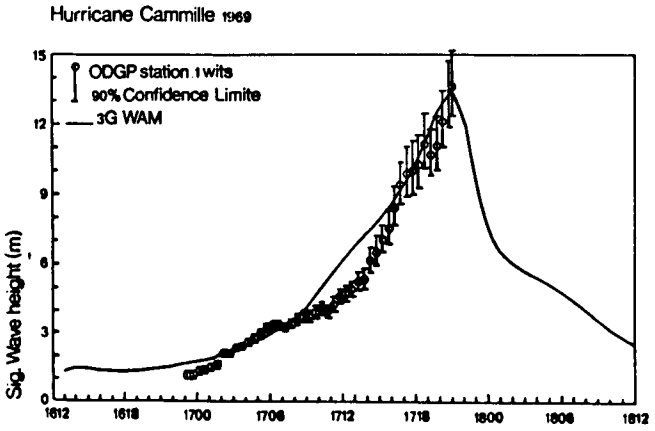


2 A comparison of calculated and observed wave heights during hurricane Camille. At the height of the storm the wave sensor broke down.

## 3. Recent results

### 3.1. Wind field dependence.

The hindcasts of the WHIST storms, mentioned in section 2 were performed with high quality wind fields which were based on fine mesh products and which had been reanalyzed at the (British) Meteorological Office. Since the wave model runs on the CRAY X-MP of ECMWF, most conveniently with winds from the ECMWF numerical atmospheric model, we compared runs when the WAM model was driven by different ECMWF surface wind fields. Although ECMWF forecast products are of good quality in general, wind fields over sea have not been evaluated in detail.

The period of interest is 1-5 Jan 1984, one of the regional hindcast periods discussed in Sec. 2. This was a stormy time over the European Continental Shelf. Isoline plots of significant wave height on 2 Jan 00 GMT are shown which were computed from each of the four wind fields (see figures 3a-d). It is worthwhile to recognize the similarities and differences which these wind fields can introduce in wave model results. One of the wind

fields was the 19.5 m surface wind from the (British) Meteorological Office (BMO) in Bracknell. The other three wind fields came from ECMWF. These were the 1000 mb, the 10 m and the surface stress winds.

The isoline plot of waves computed from BMO winds (fig. 3a) shows four major distinct wave systems: a 10 m system northwest of Ireland, a 5.5 m system north of the Shetland Islands, a 5.0 m system in the North Sea and a 9.0 m system off the coast of Norway. These winds and waves were considered to be the most accurate.

The wave field most similar to this is the one computed from the ECMWF 1000 mb winds (fig. 3b). All of the four major features are present in this field although, in every case except in the North Sea, the maxima are less. The wave field generated by the ECMWF winds shows a 8.0 m system northwest of Ireland, a 4.0 m system north of the Shetland Islands, a 5.0 m system in the North Sea and a 7.0 m system off the coast of Norway.

The next wave field to consider is the one computed from the ECMWF 10 m winds (fig. 3c). This field shows a 8.0 system northwest of Ireland, a broad sea of 3 m north of the Shetland Islands, 6.0 m waves in the North Sea and a 6.0 m system off the coast of Norway. A wave observation of 5.2 m at Ekofisk implies that these 6.0 m waves in the North Sea were a little high. The waves at Ekofisk produced by the BMO and ECMWF 1000 mb winds verified exactly.

The final wave field to study is the one produced from the ECMWF surface stress fields (fig. 3d). The isoline plot shows the wave field to be broad and featureless. Out of the four distinct wave systems present in the wave field produced from the BMO winds, only one is clearly present in the wave field computed from the surface stress winds. This is the 6.0 m system north of Ireland. The isoline plot also shows 2.0 m waves north of the Shetlands, 3-4 m waves in the North Sea and 4 m waves off the coast of Norway. All of these waves are much lower than those produced by the other wind fields. A positive average error for waves computed from the stress fields reveal the waves to be consistently too low, when compared to observations.

What can be concluded from this study is that it is likely even a very good wave model will require data assimilation for both wind and wave fields in order to produce the best possible quality results.

3.2. A comparison with SIR-B observations.

In the first half of this section we have seen how sensitive wave models are to wind field quality. It is for this reason that the idea of data assimilation of wave observations is receiving growing attention. This possibility will get maximum scope when in the next decade satellites will routinely observe the sea state. As a first step in a program along these lines, in order to gain insight into the usefullness of radar observations from space, we have hindcasted the WAM model during the period of the SIR-B mission over the North Sea, using wind fields from two centers. One set is the 19.5 m winds from BMO; the other is the ECMWF 1000 mbar winds.

Surface observations of 2-D wave spectra are presented here at two different times (Alpers et al, 1986). On October 6, 1984 an observation was made at $53^{o}36.67'N$, $5^{o}52.7'E$ by a wave rider buoy. The mean wave direction was obtained by visual observation and by analyses of X-band real aperture radar images. This observation can be seen in figure 4a. The WAMS

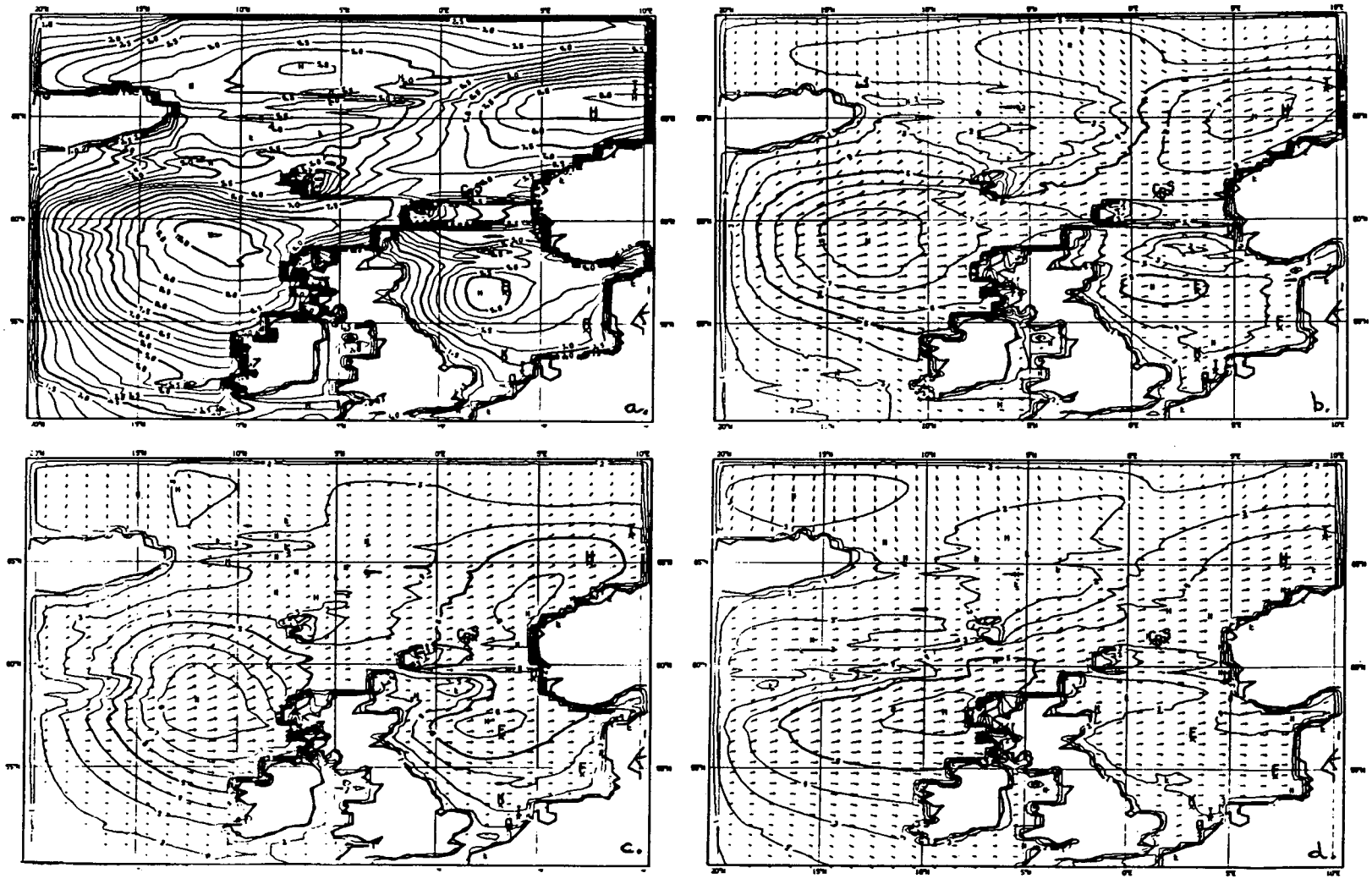


3. Significant waveheight and direction at midnight, Oct. 2, 1984 when the WAMS model is driven by (a) BMO 19.5 m winds, (b) ECMWF 1000 mb winds, (c) ECMWF 10 m winds and (d) ECMWF surface stress winds.

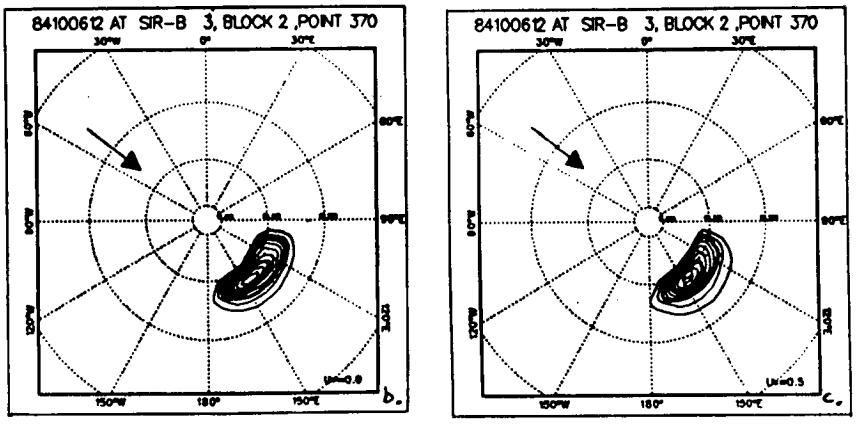


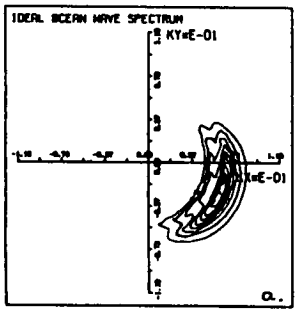


Fig. 4. 2-D wave spectra on Oct. 6, 1984 near (53.5°N, 6-E) from (a) surface observation, (b) WAMS driven by ECMWF 10 m winds and (c) WAMS driven by BMO 19.5 m winds.

model spectrum at this location computed from the ECMWF winds can be seen in figure 4b and the spectrum computed from the BMO winds is seen in figure 4c. The numerical values for significant wave height ($H_s$), mean wave direction ($\theta$), peak frequency ($f_p$), wind speed (u) and wind direction ($\phi$) are presented in table 2. Note that the abscissa for the observed wave spectra is located along the flight path and is not in the true east-west direction. The agreement in $H_s$ and $\theta$ is very good. The difference between observed and modeled $f_p$ is only half the model frequency bandwidth in the case of ECMWF winds.

Table 2.

Comparison between observed and modeled spectra on Oct. 6, 1984.

| | $H_s$(m) | $\theta$ | $f_p$(Hz) | U(m/s) | $\phi$ |
|---|---|---|---|---|---|
| OBS | 3.1 | 140° | .125 | 15 | 120 |
| WAMS (BMO) | 3.2 | 139° | .108 | 13 | 129 |
| WAMS (ECMWF) | 3.4 | 136° | .119 | 15 | 128 |

The surface observation of a pitch and roll buoy of the two dimensional spectrum on Oct. 8, 1984 at 54°51.56'N, 7°2.52'E is presented in figure 5a. The WAMS model wave spectrum for each of the winds is shown in figure 5b-c. The numerical values are presented in table 3.

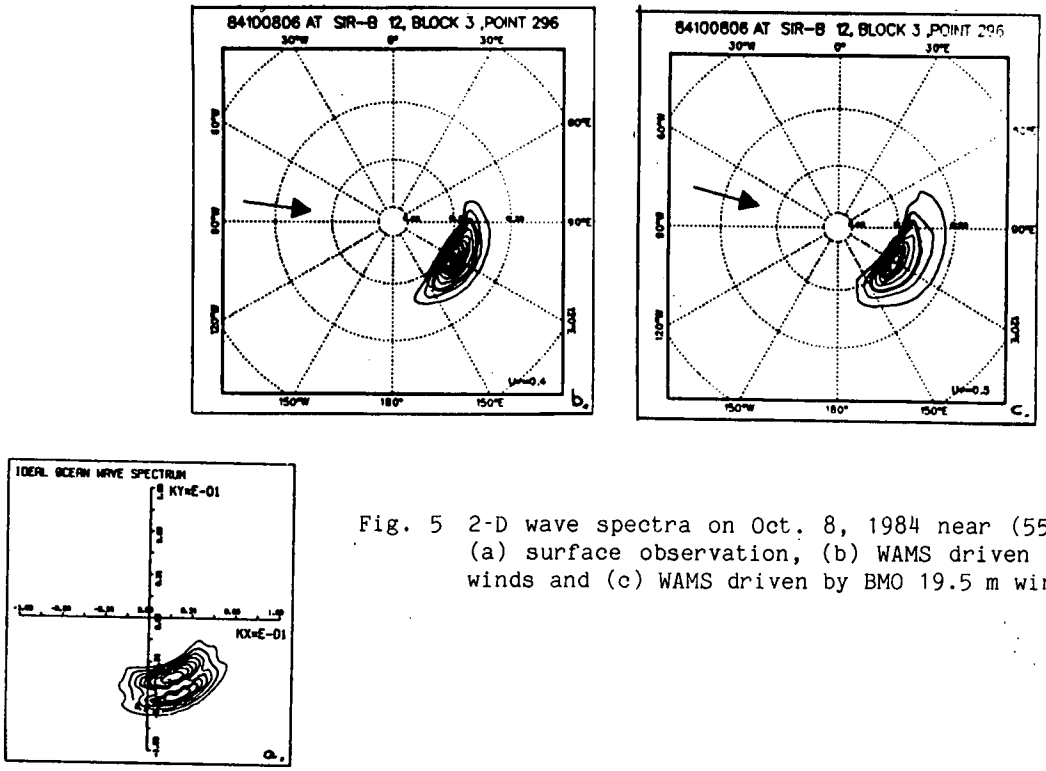


Fig. 5 2-D wave spectra on Oct. 8, 1984 near (55°N, 7°E) from (a) surface observation, (b) WAMS driven by ECMWF 10 m winds and (c) WAMS driven by BMO 19.5 m winds.

Table 3.

Comparison between observed and modeled spectra on Oct. 8, 1984.

| | $H_s$(m) | θ | $f_p$(Hz) | U(m/s) | φ |
|---|---|---|---|---|---|
| OBS | 2.3 | 135° | .109<br>.125 | 8.5 | 110° |
| WAMS(BMO) | 2.9 | 116° | .108 | 12.2 | 105° |
| WAMS(ECMWF) | 2.3 | 117° | .108 | 9.6 | 97° |

For this day, the agreement between the observed and modeled spectra is not as good as on Oct 6. $H_s$ computed from ECMWF winds agrees exactly with the observations, but $H_s$ computed from the BMO winds is high. This is because the BMO winds were high. The difference between observed and modeled wave direction is 18°-19°. This difference is about half the model directional bin width of 30°. The modeled $f_p$ agrees with the lowest peak observed, but the modeled spectrum is not showing the second peak that has been observed. It is unlikely that the buoy observation with 36 degrees of freedom is capable of actually resolving the two frequency peaks. These two peaks should probably be smoothed into one.

## Conclusion

The WAM model is a third generation model based on our best known estimate for the different source terms in the energy balance equation. The model is fairly flexible, and it has been shown to produce reliable results.

We have, once again, illustrated, how important the wind field quality is for getting accurate wave forecasts.

In view of this, the possibility of data assimilation of wave observations in models should be seriously investigated.

## Acknowledgements:

We would like to thank the many individuals that have contributed to the WAM project. The project received financial support from NATO grant SA 9.9.03(0523/85). Computer time was made available by ECMWF under a 'special project' arrangement.

## References

Alpers, W., C. Bruening and K. Richter (1986), Comparison of Simulated and Measured Synthetic Aperture Radar Image Spectra with Buoy-Derived Ocean Wave Spectra During the Shuttle Imaging Radar B Mission, IEEE Trans Geosc. Rem Sens, GE24, p 559

Bertotti, L., A. Guillaume and P.A.E.M. Janssen, (1986), The WAMS project; first test of a shallow water third generation model against data. Unpublished, to be obtained from KNMI, P.O. Box 201, 3730 AE De Bilt, The Netherlands.

Hasselmann, K., (1962), On the Nonlinear Energy Transfer in a Gravity Wave Spectrum, Part 1. General Theory, JFM, Vol. 12, pp. 481-500.

Hasselmann, K., (1974), On the spectral dissipation of ocean waves due to white capping. Boundary Layer Met. 6, 107-127.

Hasselmann S., and K. Hasselmann, (1985), Computations and Parameterizations of the Nonlinear Energy Transfer in a Gravity-Wave Spectrum, Part I: A New Method for Efficient Computations of the Exact Nonlinear Transfer Integral, JPO 15, 1369-1377.

Hasselmann S., K. Hasselmann, J.H. Allender and T.P. Barnett, (1985), Computations and parameterizations of the nonlinear energy transfer in a gravity wave spectrum, Part II: Parameterizations of the nonlinear energy transfer for application in wave models, J. Phys. Ocean 11, 1378-1391.

Hasselmann S., K. Hasselmann, P.A.E.M. Janssen, G.J. Komen, L. Bertotti, A. Guillaume, V.J. Cardone, A. Greenwood, M. Reistad and J.A. Ewing, The WAM model, a third generation ocean wave prediction model. In preparation.

Komen G.J., (1985a), Activities of the WAM (Wave Modelling) Group in Advances in Underwater Technology. Ocean Science and Offshore Engineering, Vol. 6 Oceanology p 121-127, Graham and Trotman, Ltd.

Komen G.J., (1985b), Recent results with a third generation ocean wave model in Proceedings of a Symposium on Measuring Ocean Waves from Space., APL, Maryland, to appear.

Komen G.J., S. Hasselmann, K. Hasselmann, (1984), On the existence of a fully developed wind-sea spectrum, JPO 14, 1271-1285.

Miles J.W., (1957), On the generation of surface waves by shear flow., J. Fluid Mech. 3, 185-204.

The SWAMP Group: J.H. Allender, T.P. Barnett, L. Bertotti, J. Bruinsma, V.J. Cardone, L. Cavaleri, J. Ephraums, B. Golding, A. Greenwood, J. Guddal, H. Günther, K. Hasselmann, S. Hasselmann, P. Joseph, S. Kawai, G.J. Komen, L. Lawson, H. Linné, R. B. Long, M. Lybanon, E. Maeland, W. Rosenthal, Y. Toba, T. Uji, W.J.P. de Voogt, (1985), Ocean Wave Modelling, Part I, The Sea Wave Modelling Project (SWAMP). An intercomparison study of wind wave prediction models, principal results and conclusions. Plenum Press.

# OBSERVATIONS OF VELOCITIES BENEATH WIND-DRIVEN WAVES

M.A. Donelan and K.K. Kahma*

National Water Research Institute
867 Lakeshore Road
Burlington, Ontario, Canada, L7R 4A6

## ABSTRACT

The National Water Research Institute's tower in Lake Ontario provides an ideal site for observing the behaviour of steep (fetch-limited) wind-generated waves. The statistical properties of these waves are akin to those of the steep (duration-limited) storm waves that are applicable to the design of offshore structures. It is clear that the incidence of whitecapping in these waves will affect the statistics of the near-surface velocity components. This paper describes measurements of some statistics of horizontal and vertical velocity components with reference to the expected forces on cylindrical structural members.

## INTRODUCTION

The design of offshore structures depends critically on the expected wave orbital velocities, accelerations and pressures. Very few measurements have been made of actual velocities beneath natural wind-generated waves and the design engineer generally relies on linear wave theory to derive appropriate design forces from a suitable climatology of wave (surface elevation) information. Laboratory tests with regular and irregular (non-breaking) paddle-generated waves generally find that linear theory yields surprisingly good estimates of orbital velocites derived from measured surface elevation (see, for example, Vis, 1980). However, in an actively wind-driven sea, waves periodically break producing whitecaps and injecting an impulse of momentum to the underlying current structure (Donelan, 1978). In addition, the wind-driven current near the surface alters the velocity pattern from that which would be expected based on linear theory. These differences from linear theory might be important in the calculation of forces on offshore structures - all the more so because the forces are related to the square of the velocity and to the acceleration of the fluid. Thus sudden increases in fluid velocity caused by whitecapping at the crest of a wave, where the orbital velocity is a maxiumum, produce disproportionately large increases in the drag force on the structure. The scale of the velocity fluctuations introduced by whitecapping is much smaller than the scale of the wave itself (wavelength), so that these relatively small fluctuations, advected past the structure by the substantial orbital velocities, may produce significantly different local accelerations from those expected by linear theory. Furthermore, rapid variations with Reynolds number of the drag characteristics of bluff bodies emphasize the importance of good velocity statistics in design.

In view of the expected differences between statistics of velocities in laboratory paddle-generated (albeit irregular) waves and those encountered in a natural wind-driven sea, an observational program in Lake Ontario was designed to explore the statistics of velocities beneath wind-driven waves.

*Present affiliation: Institute of Marine Research, Helsinki, Finland

## EXPERIMENTAL ARRANGEMENTS

A fixed tower provides the ideal platform for measurements of sub-surface velocities and that of the National Water Research Institute in Lake Ontario is particularly well suited to this purpose. Having been designed expressly for wave measurements, the tower is free of cross-bracing in the vicinity of the water surface. The location of the tower (Figure 1) is indicated in Figure 2. The tower is supplied with power via underwater cables and 48 channels of data, sampled at 20 Hz by computer, are transmitted by cable to shore where another computer accepts the information and writes it to disk for eventual transferal to tape. Further details of the research site are given in Donelan et al. (1985).

The instruments used for measuring both vertical and horizontal components of velocity were "drag spheres", in which the fluid force on a sphere yields a measure of the velocity components (Donelan and Motycka, 1977). There were three drag spheres mounted on a rotatable mast, the "fifth leg" (Figure 1) of the tower at depths of about 1.2 m, 2.0 m and 4.0 m with the axis of symmetry of the instrument aligned horizontally. The mast could be rotated by control from the shore station so that the axes of the drag spheres were aligned normal to the mean wave direction. The instruments thus yielded vertical and horizontal (down-wave) velocity components. The size of the drag spheres (4 mm) was such that they responded essentially to drag and not to inertial effects (Donelan and Motycka, 1977) in the range of wave heights and periods expected. Since the drag response is non-linear (almost precisely a square law in the Reynolds number range used), the instruments were zeroed mechanically before and after each measurement episode by means of pneumatically activated sleeves that shielded the drag spheres from the ambient flows. The drag spheres were carefully calibrated both before and after field exposure. Calibration was accomplished by towing the instruments in the 120 m towing tank of the National Water Research Institute.

## BACKGROUND

The incremental horizontal force (per unit length) exerted by a moving fluid on a fixed vertical cylinder is generally estimated from "Morison's equation" (Morison et al., 1950):

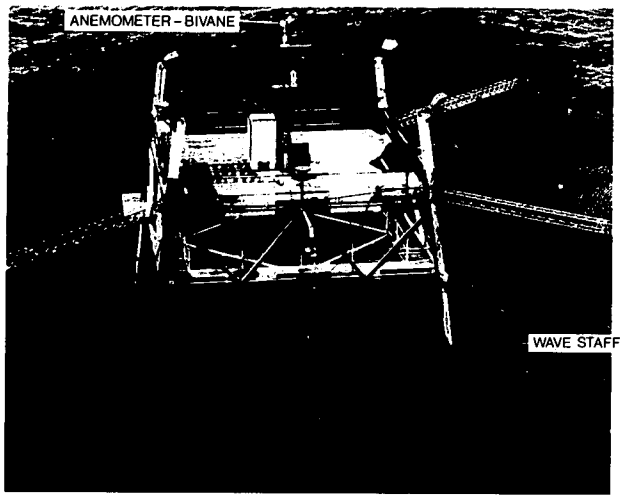


Figure 1. Photograph of the National Water Research Institute's offshore tower showing the rotatable mast on which the drag spheres and wave staffs are mounted. Meteorological instruments are installed at about 11 m on the central mast. The deck area is square with a side of 10 m.

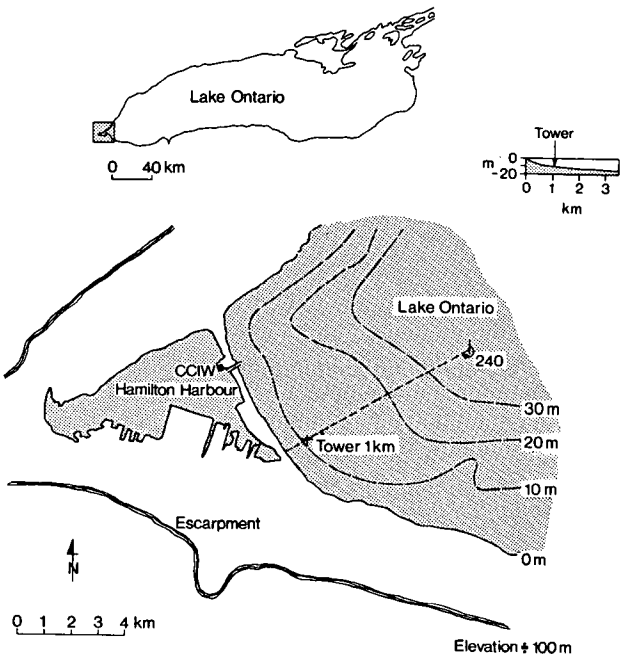


Figure 2. Map showing the location of the tower in Lake Ontario and the shore-normal profile in the vicinity of the tower.

$$F(t) = C_D \rho r\, u(t)\, V(t) + C_M \rho \pi r^2 \dot{u}(t) \qquad (1)$$

where $\rho$ is the fluid density, r is the radius of the cylinder, $C_D$ and $C_M$ are drag and inertia coefficients, u(t) and $\dot{u}(t)$ are horizontal fluid velocity and acceleration and V(t) is the magnitude of the velocity vector. $C_D$ and $C_M$ are functions of the Reynolds number $R_e = 2|u|r/\nu$, the relative surface roughness (k/2r) and the Keulegan-Carpenter number $N_{KC} = AT/2r$, where $\nu$ is the fluid kinematic viscosity, k is the average roughness diameter, A is the velocity amplitude of the oscillatory part of the flow, and T is its period.

Morison's equation ignores wave drag, which occurs if the cylinder is at or near density interfaces, and skin drag. Nonetheless, for most engineering applications the form drag and inertial resistance modelled by Morison's equation are the dominant forces. Laboratory measurements of the in-line (with horizontal velocity) force on vertical cylinders seem to agree well with that deduced from Morison's equation (Bearman et al., 1985). As pointed out by Chaplin (1985), Morison's equation is applicable to planar oscillatory flow, i.e., flow in which the instantaneous velocity and acceleration vectors are colinear. In circular oscillatory flow, characteristic of deep water surface gravity waves, the instantaneous acceleration and velocity vectors are mutually perpendicular and additional inertial terms need to be included in Morison's equation.

The behaviour of the drag and inertial coefficients with Reynolds and Keulegan-Carpenter numbers has been the subject of many investigations (see for example, Batchelor, 1967; Mogridge and Jamieson, 1976; Sarpkaya, 1976; Yamamoto and Nath, 1976; Garrison et al., 1977; Holmes and Chaplin, 1978; Koterayama, 1980). Most of these investigations have been done in laboratories under idealized conditions of uni-directional, planar oscillatory or circular oscillatory flows. Strong Reynolds number and Keulegan-Carpenter number dependencies of the drag and inertial coefficients imply that the standard practice of using constant values for these coefficients for force calculations over the entire length of vertical cylinders in irregular waves is fraught with error (Ramberg and Niedzwecki, 1979). An additional source of error arises in the calculation of orbital velocities from observed surface elevations through a theoretical model. It is to this aspect of force calculations on engineering structures that this paper is directed. Furthermore, the strong Reynolds number dependences of the drag and inertia coefficients underscore the need for accurate information on the actual velocities in a wind-driven sea.

## RESULTS

Over one hundred hours of data were gathered in episodes of 80 minutes duration. A small sub-set (four episodes) of these data is presented here. Table 1 summarizes the ambient conditions during the four episodes. In each case the analysis was done on the first 27.3 minutes of data.

**TABLE 1**

Summary of Runs

| Run | $\bar{U}$ m/s | WD deg. | Fetch km | $H_{1/3}$ m | $T_p$ s | $\bar{U}/C_p$ |
|---|---|---|---|---|---|---|
| 85111 | 1.2 | 80 | 300 | 0.7 | 4.8 | 0.2 |
| 85105 | 10.6 | 87 | 300 | 1.9 | 6.7 | 1.0 |
| 85145 | 14.1 | 70 | 280 | 2.6 | 6.8 | 1.3 |
| 85159 | 17.4 | 240 | 1.2 | 0.6 | 2.5 | 4.5 |

$\bar{U}$ is the average measured wind speed, WD is the wind direction, $H_{1/3}$ is the characteristic wave height and $T_p$ is the period of the spectral peak.

In the following we illustrate some of the temporal and spectral characteristics of the wave height and velocity data of these four runs. The first three runs listed correspond to long fetch (easterly wind) conditions. The parameter $\bar{U}/C_p$ (the ratio of wind speed to the phase speed of the waves at the spectral peak) reflects the state of development of the waves. The first case ($\bar{U}/C_p = 0.2$) corresponds to "swell", i.e., over-developed waves, produced by an earlier higher wind. The second case is nearly fully developed, while the third is under-developed. The last case, corresponding to strong westerly winds over a short fetch, yields very young (undeveloped) and strongly forced waves with intense whitecapping.

Figure 3a shows a section of the time series of observed surface elevation, $\eta$ and horizontal (downwave) and vertical velocities, u and w at a depth of 1.25 m beneath the mean water level. The top curve, uV, with $C_D$ assumed constant, illustrates the temporal dependence of the first term of Morison's equation (1). Because of the quadratic nature of the drag force, strong events, such as the group near 50 seconds, are accentuated and the intergroup small waves are relatively unimportant. These waves are over-developed so that there is very little whitecapping and this is reflected in the smooth traces of horizontal (u) and vertical (w) velocity. The high frequency wavelets, evident in the surface elevation ($\eta$) traces, are rapidly attenuated with depth and therefore do not appear in the velocity traces.

Figures 3b, c and d illustrate the changes in the observed velocities and uV product as the waves are more and more strongly forced. The surface elevation becomes more

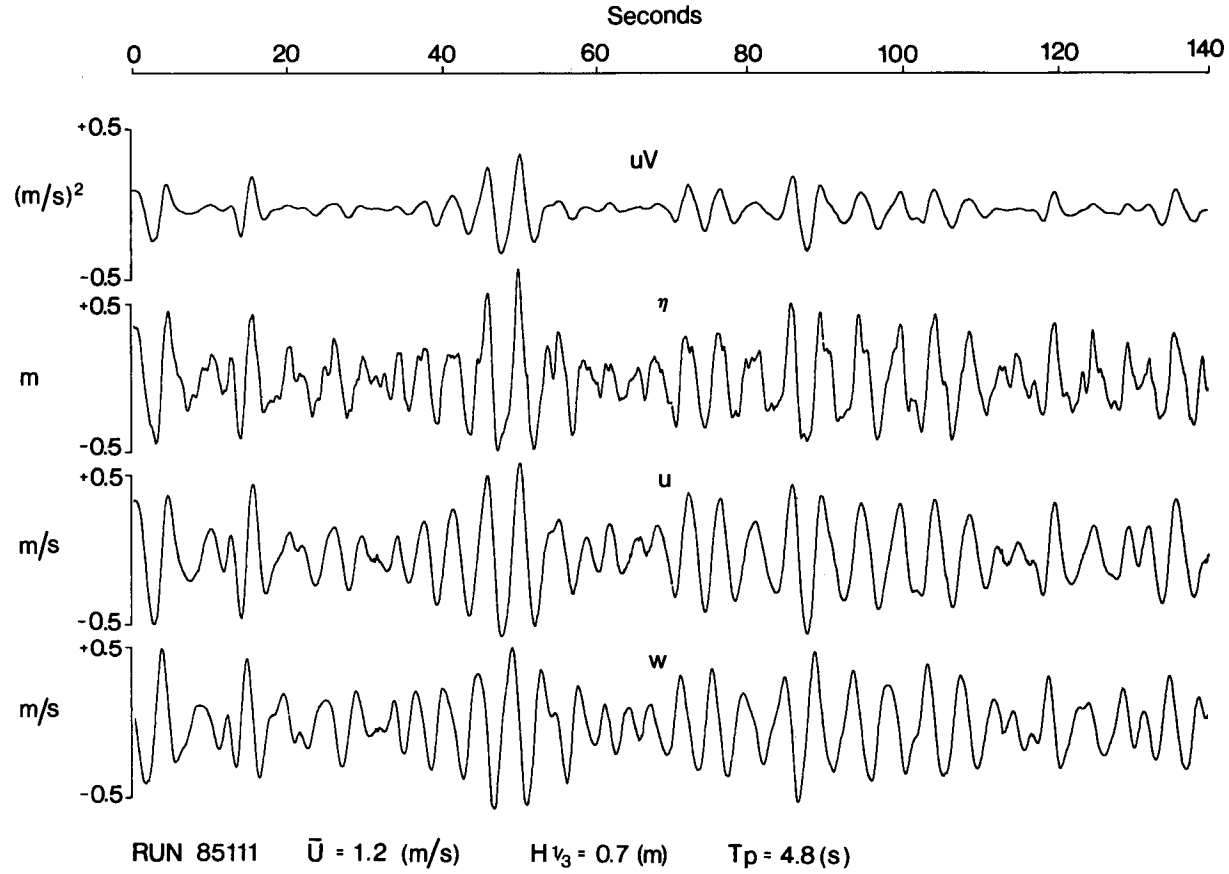


Figure 3a. A section of the time series of the measured surface elevation ($\eta$), horizontal (u) and vertical (w) velocity components at 1.25 m depth. The top curve (uV) is the instantaneous product of the horizontal velocity and the magnitude of velocity vector. This figure is drawn from the case of recent swell, run 85111 - over-developed.

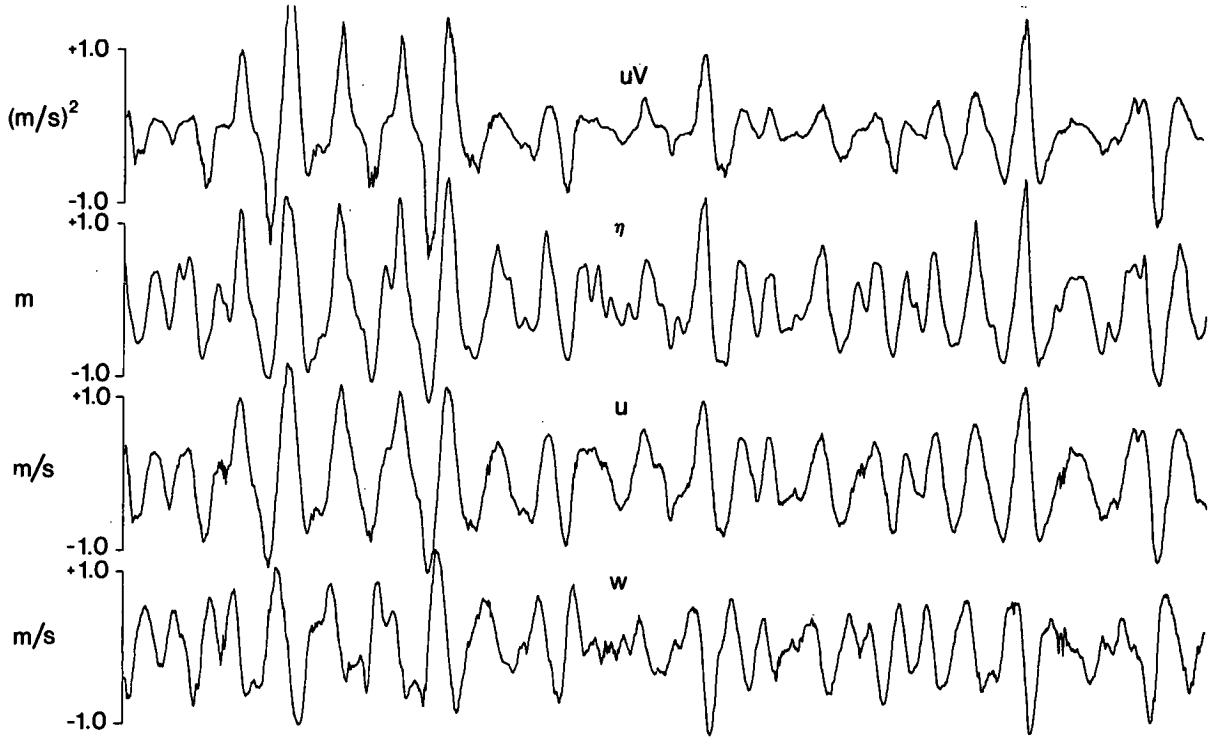


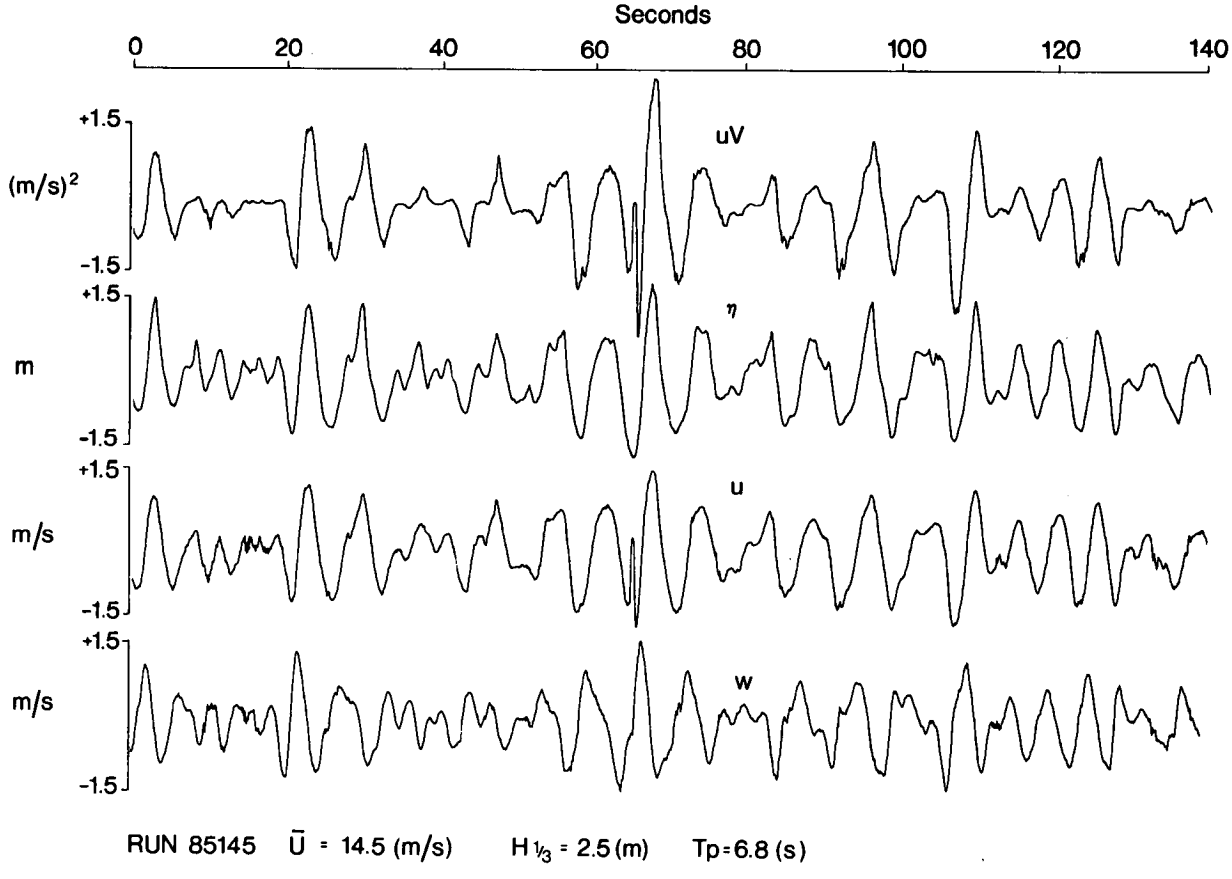


Figure 3b. The same as for Figure 3a but for run 85105 - nearly fully developed.
Figure 3c. The same as for Figure 3a but for run 85145 - under-developed.

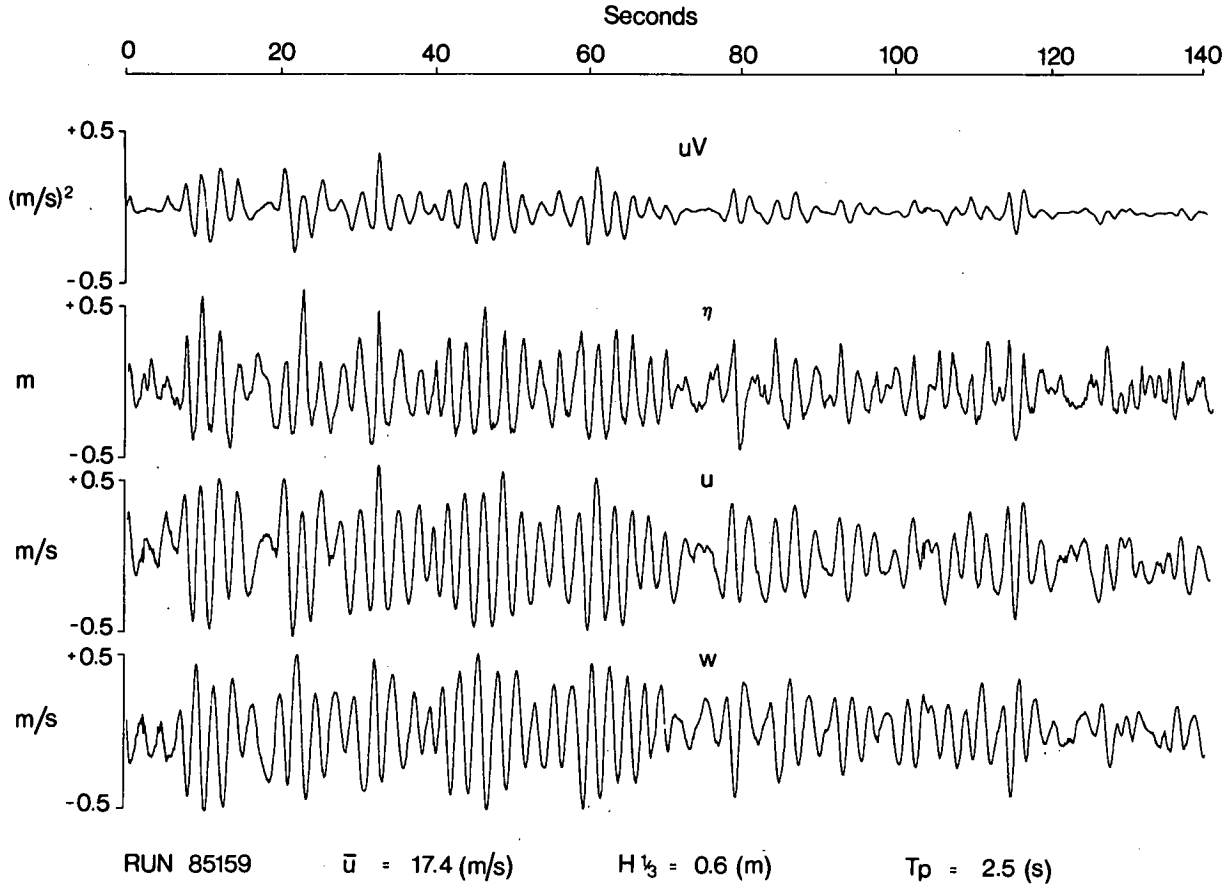


Figure 3d. The same as for Figure 3a but for run 85159 - strongly wind-generated or very underdeveloped.

positively skewed and evidence of small scale turbulence can be seen in the velocity traces. Occasional deep troughs in run 85145 cause the drag sphere to break the surface and the horizontal velocity signal to change abruptly from strongly negative (orbital velocity under the trough) to weakly positive (wind above surface). An example of this is seen around 65 seconds in Figure 3c. Increasing skewness in the uV product is also apparent in the progress through the panels of Figure 3.

For brevity, sample spectra for two runs only are shown in Figures 4 and 5. These are the two extreme cases of Table 1. Each spectrum is computed from 32768 samples in blocks of 1024. The spectra cover up to seven decades in the range of spectral densities. To avoid contamination of the low spectral densities, through window leakage from the peak, a 4-term Blackman-Harris taper (Harris, 1978) was applied to the separate blocks. The spectral estimates are averaged in pairs so that each plotted point has 128 degrees of freedom corresponding to 90% confidence limits of 1.23 and 0.82.

The spectra of surface elevation are graphed in Figure 4 with a straight line of slope -4 (Donelan et al., 1985) added. The line is fitted to the high frequency part of Figure 4b and redrawn on Figure 4a to demonstrate the sensitivity of the rear face (high frequency part) of the spectrum to wind speed (Donelan et al., 1985).

Figure 5 illustrates the spectra of horizontal velocity fluctuations and compares the observed spectra with calculations from the surface elevation spectra using linear long-crested theory. The deviations from linear theory are most obvious at high frequencies in both cases and at low frequencies also in the strongly forced case (Figure 5b). Away from the peak (and several decades lower in spectral density) the deviations are caused by turbulence generated by the wind-driven sheared current and by wave breaking (Donelan, 1978; Kitaigorodskii, et al., 1983) as modified by the advection of the orbital

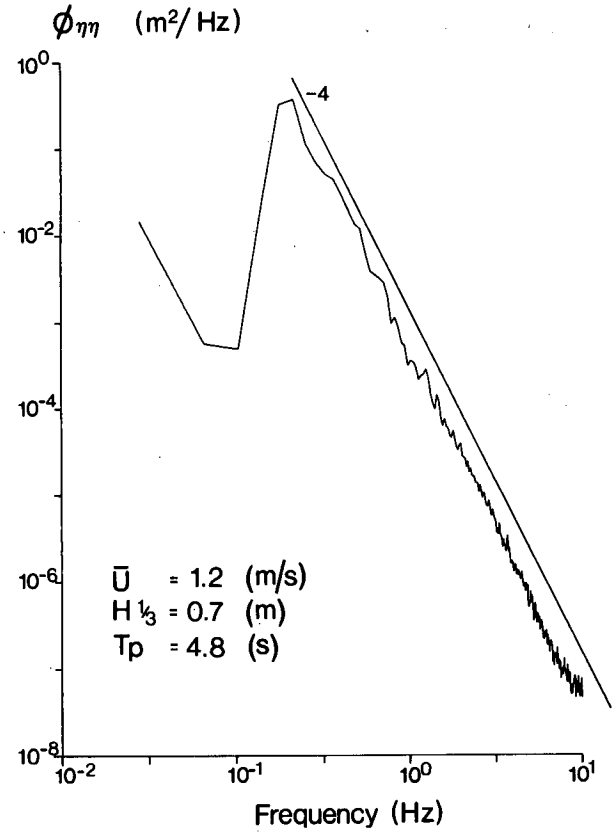


RUN 85111

Figure 4a. The spectrum of surface elevation for the case of recent swell. The -4 power law fitted to Figure 4b is also shown here.

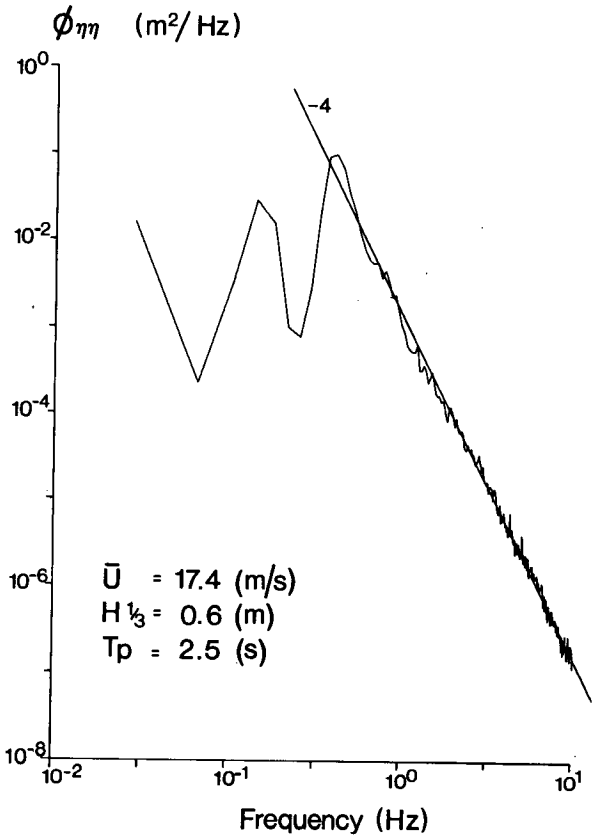


RUN 85159

Figure 4b. The spectrum of surface elevation for the strongly wind-generated case. Above the peak, the spectrum conforms to a -4 power law (Donelan et al, 1985).

velocities (Lumley and Terray, 1983). For purposes of calculation of forces on structures these differences are less important than the differences near the peak (especially in Figure 5a) at substantially higher energy levels.

An exploration of the source of these differences is beyond the scope of this preliminary paper. However, it is important to note that differences of this magnitude may have significant effects on the higher order statistics. For example a strictly linear model, in which the wave components are independent (in random phase) and freely propagating, necessarily yields no skewness of either the surface elevation or the underlying velocity field. Figure 6 illustrates the dependence of the skewness $[\overline{x^3}/(\overline{x^2})^{3/2}]$ of the uV product on the skewness of surface elevation $\eta$. The skewness of $\eta$ and the skewness of uV both increase as the waves are more and more strongly forced. However, although the skewness of $\eta$ is always positive (crests sharper than troughs) as expected, the skewness of uV is positive only for the very strongly forced case. Negative skewness of uV corresponds to generally larger (in magnitude) velocities under the troughs than under the crests. Similar results have been noted by Vis (1980) in the laboratory. Differences (observations versus theory) in skewness and kurtosis $[\overline{x^4}/(\overline{x^2})^2]$ of uV reflect differences in the symmetry and extremes of fluid forces on structures that may have important consequences in establishing engineering design parameters.

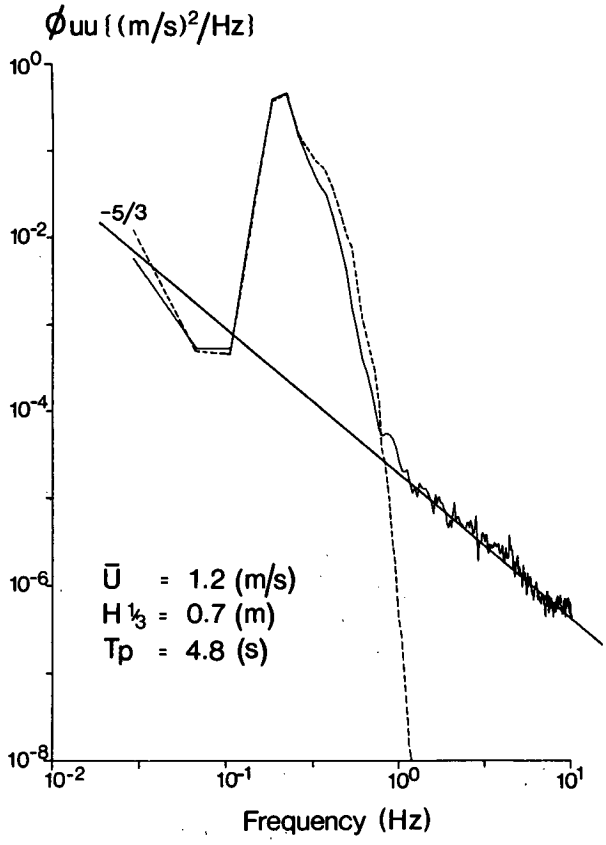


RUN 85111

Figure 5a. The spectrum of horizontal velocity for the case of recent swell. The solid line is for the measured horizontal velocity and the dotted line is the calculated spectrum from the spectrum of surface elevation through linear long-crested theory. The -5/3 line shown corresponds to the inertial sub-range of isotropic turbulence (Lumley and Terray, 1983).

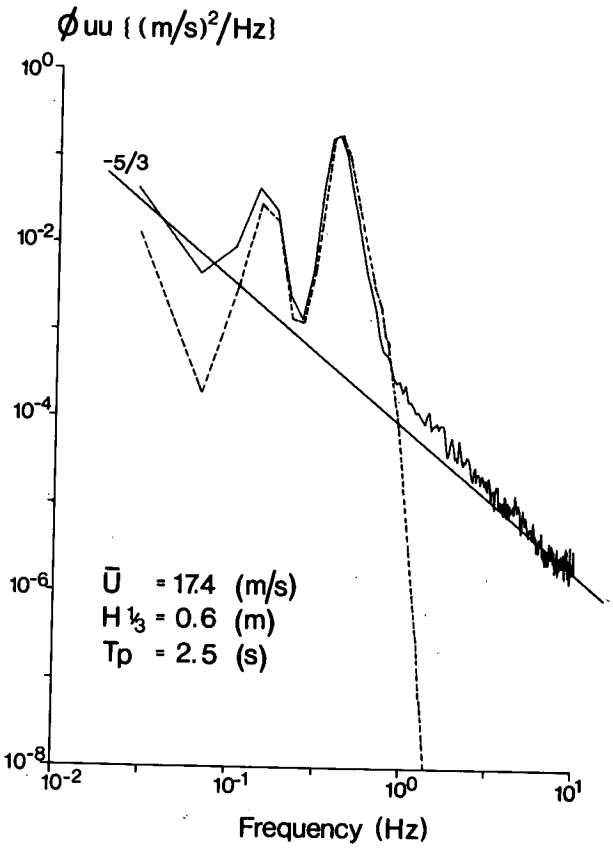


RUN 85159

Figure 5b. The same as for Figure 5a but for the case of strongly wind-generated waves.

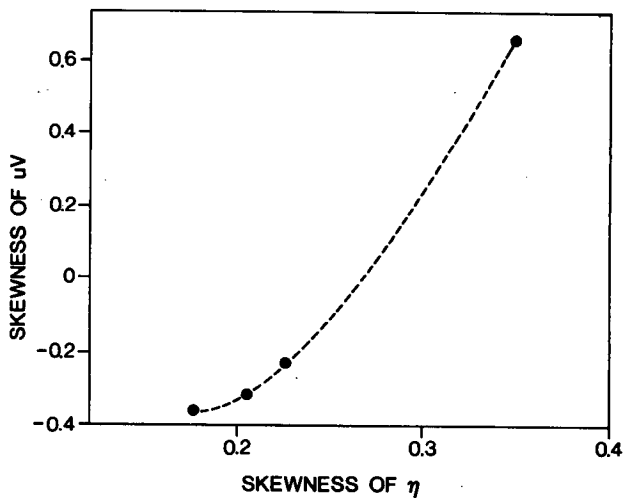


Figure 6. Skewness of uV versus skewness of η.

## CONCLUDING REMARKS

These preliminary results have demonstrated the ability of our observational method to explore the velocity field beneath breaking waves. It is clear that calculations from linear theory are unable to account for the observed velocities. However, considerably more analysis must be completed before we can recommend suitable corrections to current design practices for the calculation of wave-induced loadings on structures in a wind-driven sea.

## ACKNOWLEDGEMENTS

Many members of the staff of the National Water Research Institute contributed to this study. We acknowledge, in particular, S. Beal, D. Beesley, Y. Desjardins, R. Desrosiers, J. Dolanjski, J. Field, J. Hodson, N. Madsen, M. Pedrosa, D. Robertson, H. Savile, M. Skafel, N. Snelling and J. Valdmanis.

We also thank C. Bishop, E. Terray and M. Skafel for useful criticisms of the manuscript.

The experiment was supported in part by the Panel for Energy Research and Development under OERD project number 62114.

One of the authors, K. Kahma was supported by the National Sciences and Engineering Research Council of Canada on a Post-Doctoral Visiting Fellowship. He would like to thank the National Water Research Institute for its hospitality while this work was carried out.

## REFERENCES

Batchelor, G.K., 1967: An Introduction fo Fluid Dynamics. Cambridge University Press, Cambridge, U.K. 615 pp.

Bearman, P.W., J.R. Chaplin, J.M.R. Graham, J.K. Kostense, P.F. Hall and G. Klopman, 1985: The loading on a cylinder in post-critical flow beneath periodic and random waves. Behaviour of Offshore Structures. Elsevier Science Publishers B.V., Amsterdam, 213-225.

Chaplin, J.R., 1985: Morison inertia coefficients in orbital flow. J. Waterway, Port, Coastal and Ocean Eng., ASCE, III, 201-215.

Donelan, M.A., and J. Motycka, 1978: A miniature drag sphere velocity probe Rev. Sci. Instrum., 49, 298-304.

Donelan, M.A., 1978: Whitecaps and momentum transfer. Turbulent Fluxes Through the Sea Surface, Wave Dynamics and Prediction, Plenum Press, New York and London, 273-287.

Donelan, M.A., J. Hamilton and W.H. Hui., 1985: Directional spectra of wind-generated waves. Phil. Trans. R. Soc. Lond. A, 315, 509-562.

Garrison, C.J., J.B. Field and M.D. May, 1977: Drag and inertia forces on a cylinder in periodic flow. J. Waterway, Port, Coastal and Ocean Div., ASCE, 103, 193-204.

Harris, F.J., 1978: On the use of windows for harmonic analysis with discrete Fourier transform. Proc. IEEE, 66, 51-83.

Holmes, P., and J.R. Chaplin, 1978: Wave loads on horizontal cylinders. Proc. 16th Coastal Eng. Conf., Hamburg, 3, 2449-2460.

Kitaigorodskii, S.A., M.A. Donelan, J.L. Lumley and E.A. Terray, 1983: Wave-turbulence interactions in the upper ocean. Part II: Statistical characteristics of wave and turbulent components of the random velocity field in the marine surface layer. J. Phys. Oceanogr., 13, 1988-1999.

Koterayama, W., 1980: Wave forces acting on a submerged horizontal circular cylinder in oblique waves and on a vertical cylinder in deep waves. Ocean Engineering, 7, 399-412.

Lumley, J.L., and E.A. Terray, 1983: Kinematics of turbulence convected by a random wave field. J. Phys. Oceanogr., 13, 2000-2007.

Mogridge, G.R., and W.W. Jamieson, 1976: Waveloads on large circular cylinders: a design method. Hydraulics Laboratory, Nat. Res. Council of Canada, No. 15827, 34 pp.

Morison, J.R., M.P. O'Brien, J.W. Johnson and S.A. Schaaf, 1950: The force exerted by surface waves on piles. Petroleum Trans., AIME, 189, 149-154.

Ramberg, S.E., and J.M. Niedzwecki, 1979: Some uncertainties and errors in wave force computations. Proc. 11th Annual Offshore Technology Conference, Houston. 2091-2102.

Sarpkaya, T., 1976: Forces on rough-walled circular cylinders in harmonic flow. Proc. 15th Coastal Eng. Conf., Hawaii. 2301-2320.

Vis, F.C., 1980: Orbital velocities in irregular waves. Delft Hydraulics Laboratory, No. 231, 13 pp.

Yamamoto, T., and J.H. Nath, 1976: High Reynolds number oscillating flow by cylinders. Proc. 15th Coastal Eng. Conf., Hawaii. 2321-2340.

# WAVE MODELING RESEARCH NEEDS

Charles L. Vincent
Senior Scientist

Coastal Engineering Research Center
U.S. Army Engineer Waterways Experiment Station
P.O. Box 631
Vicksburg, MS 39180-0631

## Introduction

The U.S. Army Corps of Engineers (USACE) requires coastal wave information for the shorelines of the United States. Primary needs include extreme wave data for project design and day-to-day wave climate information for sediment transport calculations. In the mid-1970's USACE recognized that wave climates based on measured wave data were unlikely to be available over sufficiently large areas or time spans in the foreseeable future. USACE turned to wave hindcasting as an alternative to synthetically derive a wave climate from historical weather information as a cost effective method to obtain climate estimates over the regions of need using state-of-the-art hindcast methods. Use of hindcast methods was made in knowledge of imperfections of the technology but in recognition that a consistently derived oceanic wave climatology represented an advance over extrapolations from ship records, limited gage information, or site specific hindcasts performed by a range of differing techniques.

Since establishment of the hindcast program, wave climates for the Atlantic, Pacific, and Gulf of Mexico coasts have been generated for the period 1956-1975. Hurricane hindcasts are under way and Great Lakes hindcasts will be initiated in the coming year. The 20 years of data are stored on an interactive data base system accessible by USACE local offices with directional spectra available indirectly on tape.

As a consequence of this project and in part of a continuing effort to keep the models used at the state of the art, evaluations of the gaps in our understanding of wave modeling have been made and are a base for research efforts in this area conducted by the U.S. Army Engineer Waterways Experiment Station's Coastal Engineering Research Center (CERC). This paper reviews where gaps or unknowns exist and where progress is needed to reconfirm our current understanding or replace it.

As a general statement relative to the CERC deep- and shallow water spectral models, which in present technical terminology are both second generation models, both models reproduce general spatial and temporal patterns of wave height and peak spectral periods and, when the height and period are accurately predicted, the frequency spectrum lies within acceptable bounds of the observed spectrum. Recent comparisons of directional properties follow similar trends. However, hindcasts are rarely perfect. Examples of problems can include: time shifts in the occurrence of peak conditions happen; the observed wave trains generally exhibit more variability than the predicted; and there is insufficient high quality directional spectra to make adequate directional comparisons. The same sorts of differences are seen in published results of other models. Many of the differences can be attributed to inaccurate wind information, but it is only rational to expect that part of the error lies within the wave models.

## Deep-water Wave Models

Many of the advances in wave models in the last 15 years can be related to the development of the wave-wave interaction source term of Hasselmann (1962) and measurements of fetch limited wave growth (Hasselmann et al., 1973). Yet there are still questions concerning the rate of wave growth with fetch and its variation with stability. The variation of peak frequency of the spectrum with fetch has been related to a -0.25 power by Phillips (1977) rather than the -0.33 from JONSWAP, as an example. The JONSWAP spectrum (Hasselmann et al., 1973) has proven to be a very useful concept in wave modeling and for calculations of the source term contributions in the spectrum. However, other evidence (Toba, 1973) very strongly suggests that the frequency power law used in the JONSWAP spectrum is physically inconsistent (-5, rather than -4), although from a curve fitting point of view adequate.

At a minimum, a good review of basic fetch limited data or repetition of the experiment needs to be made in light of the advances in intrumentation and physical understanding in the past 10 years. Spectral shapes should be based on a more physically realistic power law, and the analysis of the spectral parameter data performed simultaneously to meet consistency constraints.

The variation with the momentum input to the wave field with growth stage and boundary layer stability still remains an area in which many numerical models differ. Often intercomparisons of functioning wave models are hampered by these differences (SWAMP, 1981). This remains one area in which production models have over the years been tuned to particular wind models. Since this is vital to wave growth calculation, an accurate specification should be a first foundation for modeling.

Most of the detailed measurements of wave growth and spectral evolution have been made under simple conditions. Extrapolation of wave models to more complex generation and decay scenarios is usually accomplished by appeal to particular theories of wave behavior. Definitive work, theoretical and field measurements, are needed to specify the interaction of sea and swell wave trains, the effect of a freshening wind over old swell, and the effect of an opposing wind on swell. These problems are difficult but are more representative of real wave modeling problems.

Finally, evolution of the directional aspects of the wave spectrum remains an area in which there are almost no high quality measurements and little to go on but extrapolations of theory. Since the theories have little confirmation with respect to direction, reliance upon theory is a great expression of faith. The directional properties of the sea surface become important as input to shallow water wave models and for waves transecting a current, as well as for problems related to ship response and remote sensing.

With the few problems listed above, it is not unexpected that there continues to be uncertainty over the physics dominating wave evolution in varying parts of the spectrum (Kitaigorodskii, 1983 and Phillips, 1985).

## Shallow Water Modeling

To a large degree, shallow water wave models follow the lead of deep-water wave models with addition of source terms to represent the presence of a bottom boundary layer and other bottom related effects. The development of the empirical TMA-extension to the JONSWAP spectrum has provided a shallow water analog for a limiting shallow water spectrum shape (Bouws et al., 1985). All of the difficulties discussed above in deep water to a large degree carry over to shallow water wave models. To this list must be added a few problems peculiar to shallow water.

First, it is not clear that the Miles mechanism formulation for wind input can be directly extended to shallow water waves. As the depth becomes small relative to wave length, wave shape changes and wave propagation become more directly determined by the depth. Airflow over the waves may become quite different from the deep-water case.

In less shallow water, larger waves may break due to limited depth in regions farther offshore from the traditional breaker zone. Breaking induced by depth and the effect of depth upon the whitecapping source term are not understood. Phillips and Banner (1974) have shown that steep swell waves can eradicate a short wind sea. Propagation of sea and swell over complex topography may produce areas where such effects are significant.

The shallow water suite of source terms, such as they are, has not been rigorously evaluated with measured data. Data sets are not available that accurately define wind evergy input and provide measurements of the bottom boundary layer. Hence, modelers have sufficent options to tune the source terms to produce models that are reasonably reflective of conditions on sand beaches but appear at considerable theoretical variance to each other.

Most spectral models are run on spatial grid meshes that are relatively coarse. Most models are based on linear monochromatic propagation procedures. Near coasts and often in areas of interest, the bathymetry can be very complex. Linear wave theory has been shown to be inadequate for strong topographic curvatures. Evaluation of the adequacy of the linear approach is needed in regions of significant convergence. It seems inadequate to perform detailed spectral hindcasts of wave conditions using weak, nonlinear interactions to couple wave components and then convert the answer into a monochromatic wave for propagation across the irregular topography. Generalized procedures for refracting, shoaling, and diffracting a weakly coupled spectrum are needed.

## Waves on Currents

The deficiencies noted for shallow water wave modeling are mirrored for the case of waves on a current. For the presence of a current, the propagation problems become difficult if the current is spatially and time varying. There is no spectral shape expression similar to the JONSWAP. The characteristics of the weak, nonlinear interactions have not been established for a current, much less the appropriate dissipation source terms. In deep water, variation of the flow with depth may need consideration while in shallow water the propagation problem must consider both depth and current effects.

## Discussion

The questions raised in the preceding paragraphs represent some of the obvious gaps in our understanding of wave growth and decay processes. In spite of these questions, the general experience of the wave forecast/hindcast community as represented by any number of published studies over the past few years indicates that present wave models can perform well in a wide range of circumstances. Often poor model performance can be attributed to poor wind field definition. However, considering the size of the oceans and the variability of the weather systems, relatively few high quality wave measurements are available, and probably few wave models have been subjected to sufficient comparisons to determine what part of the difference from observation can be truly attributed to the winds; indeed, such an assessment may be impossible to make.

To a large degree the measurements and theoretical analyses of the late 1960's and early 1970's have been replaced by an explosion of numerical models incorporating the physics of the earlier efforts. A natural sequence of events must be a questioning of the models and their physics which will need high quality data sets beyond the capabilities of individual investigators. With the advent of increased satellite coverage and availability of more measured data, it is time to try and assemble major data sets oceanic in scale of both wave and wind information, carefully analyzed and made available to the wave model community worldwide. In areas of characteristic complexity and interest, special experiments could be made to gather data to supplement more continuous observations. Through such comparisons a better definition of the adequacies of present day wave models can be made and a basis for improvement established.

Acknowledgment

The research was sponsored under the Coastal Program of the USACE by CERC. The Wave Information Studies are funded under the Coastal Field Data Collection Program of the Chief of Engineers. Permission was granted by the Chief of Engineers to publish this information.

References

Bouws, E., Gunther, H., Rosenthal, N., and Vincent, C. 1985. "A Similarity Based Spectral Form for Finite Depth Water: Part I - Spectral Form," Journal of Geophysical Research, Vol 90, pp. 975-986.

Hasselmann, K. 1962. "On the Nonlinear Energy Transfer in a Gravity Wave Spectrum, Part 1. General Theory, "Journal of Fluid Mechanics, Vol 12, pp. 481-500.

Hasselmann, K., Barnett, T. P., Bouws, E., Carlson, H., Cartwright, D. E., Enke, K., Ewing, J. A., Gienapp, H., Hasselmann, D. E., Kruseman, P., Meerburg, A., Muller, P., Olbers, D. J., Richter, K., Sell, W., and Walden, H. 1973. "Measurements of Wind-Wave Growth and Swell Decay During the Joint North Sea Wave Project JONSWAP," Deutsch Hydrogr. Zeith., Vol 8, (Suppl A8), No. 12, p. 95.

Kitaigorodskii, S. A. 1983. "On the Theory of the Equilibrium Range of the Spectrum of Wind-Generated Gravity Waves," Journal of Physical Oceanography, Vol 13, pp. 816-827.

Phillips, O. M. 1977. The Dynamics of the Upper Ocean, Second Edition, Cambridge University Press, Cambridge, U.K., p. 162.

Phillips, O. M. 1985. "Spectral and Statistical Properties of the Equilibrium Range in Wind-Generated Gravity Waves," Journal of Fluid Mechanics, Vol 156, pp. 505-531.

Phillips, O. M. and Banner, M. L. 1974. "Wave Breaking in the Presence of Wind Drift and Swell," Journal of Fluid Mechanics, Vol 66, pp. 625-640.

SWAMP (Sea Wave Modeling Project). 1981. An Intercomparison Study of Wind Wave Prediction Models, Symposium on Wave Dynamics and Radio Probing of Ocean Surface, Miami, FL, Plenum Press.

Toba, Y. 1973. "Local Balance in the Air-Sea Boundary Processes, II, Partition of Wind Stress to Waves and Currents," Journal of the Oceanographic Society of Japan, Vol 20, pp. 20-25.

# WAVE GROWTH IN SCATTERED SEA-ICE

Diane Masson
and
Paul H. Leblond

Department of Oceanography
University of British Columbia
Vancouver, British Columbia
Canada, V6T 1W5

## ABSTRACT

We present a model for the growth of wind waves in a sparse field of floating ice-floes. Wave growth is modeled using Hasselmann and Hasselmann's (1985 b) discrete spectral model. Wave scattering by an idealized cylindrical floe is represented in terms of far field potentials and the combined effect of a homogeneous field of floes is expressed in terms of the Foldy-Twersky integral equation (Ishimaru, 1978), under the single-scattering approximation. The formulation of the model is explained and preliminary results presented.

## 1) INTRODUCTION

The Marginal Ice Zone (MIZ) includes wide areas of scattered ice in which floes are isolated from each other and free to respond to wave motion. The dimensions of such areas (up to 100 km. across) are generally small enough, compared to those of the adjacent open ocean areas, that they may be neglected in regional wave climate studies. However, within and near the scattered ice zone itself, wave conditions are significantly affected by the presence of ice floes. Wadhams (1975, 1978, 1983 b) has studied the decay of swell entering the ice pack from the open sea, and shown how scattering by ice floes could account for the loss of energy. More recently, Wadhams et al. (1986) have examined the modification of the directional properties of wind wave spectra entering the MIZ. When the wind blows from the land, or from the solid ice pack, towards the open sea, wave generation occurs within the zone of dispersed ice floes. Growing wind waves are scattered by the ice; their directional spread is increased and their spectral characteristics modified. The waves also push the ice into banded structures at right angles to the wind (Martin et al., 1983; Wadhams, 1983 a). This coupled wave-ice problem, which is an important factor in both wave conditions and ice configurations in the MIZ, is addressed here.

## 2) BASIC PHYSICS

A sea state is commonly represented in terms of its two-dimensional

spectrum of surface displacement variance $F(\underset{\sim}{k};\underset{\sim}{x},t)$ which specifies the distribution of energy among plane waves of wavenumber $\underset{\sim}{k}$. In the presence of ice, the spectrum evolves in time (t) and space ($\underset{\sim}{x}$) according to the modified radiative transfer equation:

$$\frac{\partial F}{\partial t} + \underset{\sim}{C_g} \cdot \underset{\sim}{\nabla} F = S = S_{in} + S_{nl} + S_{ds} + S_{ice} \qquad (1)$$

where $\underset{\sim}{C_g}$ is the group velocity and S includes all source and sink terms: $S_{in}$, the rate of energy exchange with the atmosphere, $S_{nl}$, the nonlinear redistribution of energy between spectral components, and $S_{ds}$, the dissipation rate, mostly through wave breaking. The term $S_{ice}$ is introduced here to represent the effects of ice floes on the wave field. The roles of the first three terms are by now well known and a variety of formulations, based on theoretical and observational grounds, have been proposed to express $S_{in}$, $S_{nl}$, and $S_{ds}$ (SWAMP Group, 1985).

Freely floating ice floes endeavour to follow the displacements of the supporting water surface within limits imposed by their rigidity and inertia. Under equilibrium conditions, they re-radiate incident wave energy, slightly diminished by dissipative effects in the water and within the ice itself. This scattering process tends to broaden the angular distribution and to decrease the energy content of the wave field. Wadhams et al. (1986) have found that, in the presence of a compact ice cover, a wind wave spectrum broadens to near isotropy soon after entering the MIZ. The term $S_{ice}$ in (1) will thus include a certain amount of dissipation, adding to $S_{ds}$, and, more importantly, it will cause spectral redistribution, tending to spread out the energy over a broader range of directions. One might thus expect that the growth rate as well as the equilibrium shape of the directional spectrum could be significantly affected in proportion to the degree of ice cover.

Waves also exert a net horizontal force on the floes (wave radiation pressure), pushing them ahead. The rate of ice drift, $\underset{\sim}{u}$, will then depend on the wind, the local currents and the waves. In the absence of sources or sinks, the ice floe concentration, C, obeys

$$\frac{\partial C}{\partial t} + \nabla . \underset{\sim}{u}\, C = 0 \qquad (2)$$

Supposing that wave energy increases as the floe concentration decreases and that floe drift increases with wave energy, it becomes evident that any inhomogeneity in the initial concentration, C (x, 0), will tend to be amplified. This is basically the mechanism advanced by Martin et al. (1983) and Wadhams (1983 a) to account for the formation, movement and decay of ice bands.

The radiative transfer (1) and ice concentration (2) equations are thus coupled through $S_{ice}$ and u. A quantitative understanding of wave and ice conditions in the MIZ would thus require their simultaneous solution. We shall limit our attention to the uncoupled problem at this stage, examining the growth of purely time-limited waves in a uniform concentration of ice floes.

## 3) MODEL FORMULATION

### 3.1) The Radiative Transfer Equation

The wave spectrum is given in terms of the frequency f (in deep water, $f = g|k|/2\pi$) and wave direction $\theta$ measured counterclockwise from that of the wind ($\theta = \tan^{-1}(k_y/k_x)$ with $k_x$ along the wind direction and $k_y$ normal to it).

Since the medium is assumed unbounded and uniform, the spectrum $F(f,\theta;t)$ depends only on time, and the advection term, $\underset{\sim}{C}g \cdot \nabla F$, is dropped from (1). The specific model used for the source terms $S_{in}$, $S_{ds}$ and $S_{nl}$ is that described by Hasselmann and Hasselmann (1985 a,b) who kindly provided a copy of their software. The input source term, $S_{in}$, follows from Snyder et al. (1981):

$$S_{in}(f,\theta) = \max\left[0., 0.25\ \rho_a/\rho_w \left(\frac{28u^*}{C}\cos\theta - 1\right) 2\pi f\ F(f,\theta)\right] \qquad (3)$$

where $\rho_a$ and $\rho_w$ are the densities of air and water, respectively, $u^*$ the friction velocity and $C$ the wave phase velocity. In (3), the direct dependence on the wind speed ($U_5$, the wind speed at 5m.) of the original expression derived by Snyder et al. has been replaced by a similar dependence on $u^* = U_5/28$.

The dissipation term $S_{ds}$ follows that of Komen et al. (1984):

$$S_{ds}(f,\theta) = -3.2\pi\ f^2\ \bar{f}^{-1}\ \tilde{\alpha}^2\ F(f.\theta) \qquad (4)$$

where $\bar{f}$ is defined as $E^{-1}\int\int F(f,\theta) f\ df d\theta$, and $\tilde{\alpha} = (2\pi)^4 \bar{f}^4 g^{-2} E$ with $E = \int\int F(f,\theta) df d\theta$, the total wave energy. Because waves can neither be generated nor dissipated in that fraction, $f_r$, of the sea surface covered by ice, both $S_{in}$ and $S_{ds}$ are reduced by a factor $(1 - f_r)$ from their ice-free values given above.

The nonlinear wave-wave interaction terms are calculated via the Boltzmann integral

$$S_{nl}(\underset{\sim}{k}_1) = \int\int\int Co\ \delta(\underset{\sim}{k}_1 + \underset{\sim}{k}_2 - \underset{\sim}{k}_3 - \underset{\sim}{k}_4)\ \delta(f_1 + f_2 - f_3 - f_4)\ x$$
$$[n_3 n_4 (n_1 + n_2) - n_1 n_2 (n_3 + n_4)]\ d\underset{\sim}{k}_2\ d\underset{\sim}{k}_3\ d\underset{\sim}{k}_4 \qquad (5)$$

where $Co(\underset{\sim}{k}_1, \underset{\sim}{k}_2, \underset{\sim}{k}_3, \underset{\sim}{k}_4)$ is a coupling coefficient and $n_i = F(\underset{\sim}{k}_i)/2\pi f_i$ is the wave-action density. The integral is estimated by the method described by Hasselmann and Hasselmann (1985 a) which involves a symmetrical treatment of the resonant interactions among wavenumber quadruplets. This is achieved by using the invariance of the coupling coefficient Co with respect to permutations of the wavenumbers and the principle of detailed balance by which the computation of the change in action density for one wavenumber $\underset{\sim}{k}_1$ gives also the identical action changes for $\underset{\sim}{k}_2$, $\underset{\sim}{k}_3$ and $\underset{\sim}{k}_4$ (Hasselmann and Hasselmann, 1981). Furthermore, an important reduction in computing time can be obtained by filtering out the regions of the interaction phase space where the contributions to the integral are not significant. These techniques make it possible to evaluate the exact nonlinear transfer expression for any wave spectrum, which is essential, in this work, due to the unusual spectral shape of the wave field. The ice-interaction term, $S_{ice}$, will be introduced in a different fashion, as explained below.

## 3.2 The Ice Model

The sea surface is assumed to be covered uniformly and sparsely by a random distribution of rigid ice floes, the fraction of the surface covered by ice, $f_r$, not exceeding 25%. For simplicity, the floes are modeled as circular cylinders of radius $a$ ($7 \leq a \leq 25$ m.) and draft $h$ ($1 \leq h \leq 4$ m.). Each discrete component of the spectrum of frequency and direction $(f_n, \theta_n)$ is assumed to interact independently with the ice

floes. The total wave field then consists of the linear superposition of incident and scattered wave components of all frequencies and directions.

We first consider the interaction of a plane wave with a single cylindrical floe. This wave is in part diffracted, as if the floe was a rigid obstacle, and partly modified by the motion of the ice induced by the incident and diffracted waves. A purely symmetrical floe will respond in three modes: a surge, back and forth in the direction of $\underset{\sim}{k}$; a heave, up and down; and a pitch, about an axis parallel to wave crests (Fig. 1).

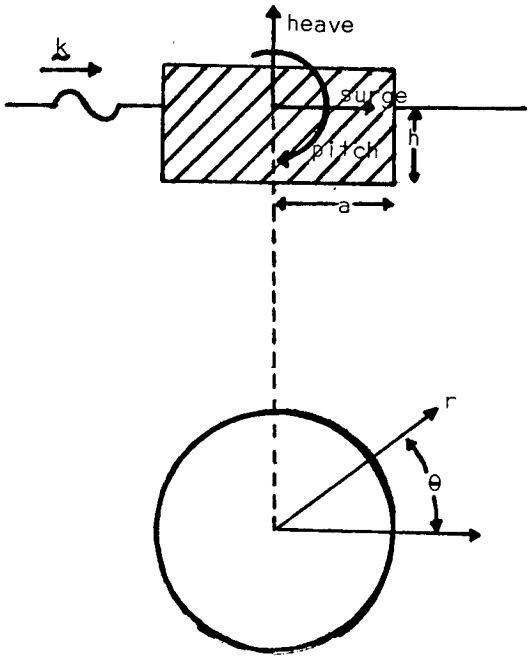


FIG. 1 - Cylindrical floe with the three modes of motion: heave, surge and pitch.

The complete wave field associated with the scattering of one single incident plane wave may then be written in terms of the velocity potential (e.g. Isaacson, 1982):

$$\phi(\underset{\sim}{x},t) = [\phi_i(\underset{\sim}{x}) + \phi_4(\underset{\sim}{x}) + \sum_{k=1}^{3} \xi_k \phi_k(\underset{\sim}{x})]e^{-i\omega t}, \qquad (6)$$

where $\phi_i$ is the undisturbed part of the incident wave potential; $\phi_4$, the diffracted wave potential; and $\phi_k$, the forced wave potential due to each mode of motion of amplitude $\xi_k$. The diffracted and forced potentials are obtained using the Green's function method with the unknown potentials, $\phi_k$, expressed as:

$$\phi_k(\underset{\sim}{x}) = \frac{1}{4\pi} \int_{S_o} f_k(\underset{\sim}{X})\, G\,(\underset{\sim}{x},\underset{\sim}{X})\, dS \quad \text{for} \quad k=1,2,3,4 \qquad (7)$$

where $f_k(\underset{\sim}{X})$ is a source strength distribution function; $\underset{\sim}{X}$, a point on $S_o$ (the equilibrium body surface); and $G(\underset{\sim}{x},\underset{\sim}{X})$, a Green's function for the general point, $\underset{\sim}{x}$, due to a source of unit strength at $\underset{\sim}{X}$. The amplitudes of motion, $\xi_k$, and the source strength functions, $f_k(\underset{\sim}{X})$, are obtained using a method described by Isaacson (1982),

valid for large axisymmetric bodies, in which the various functions are expressed as Fourier series in the angle about the body's vertical axis and the problem solved by an integral equation method. Figure 2 presents the amplitude of the three modes of motion, as a function of ($|\underset{\sim}{k}|a$), for a typical ice floe.

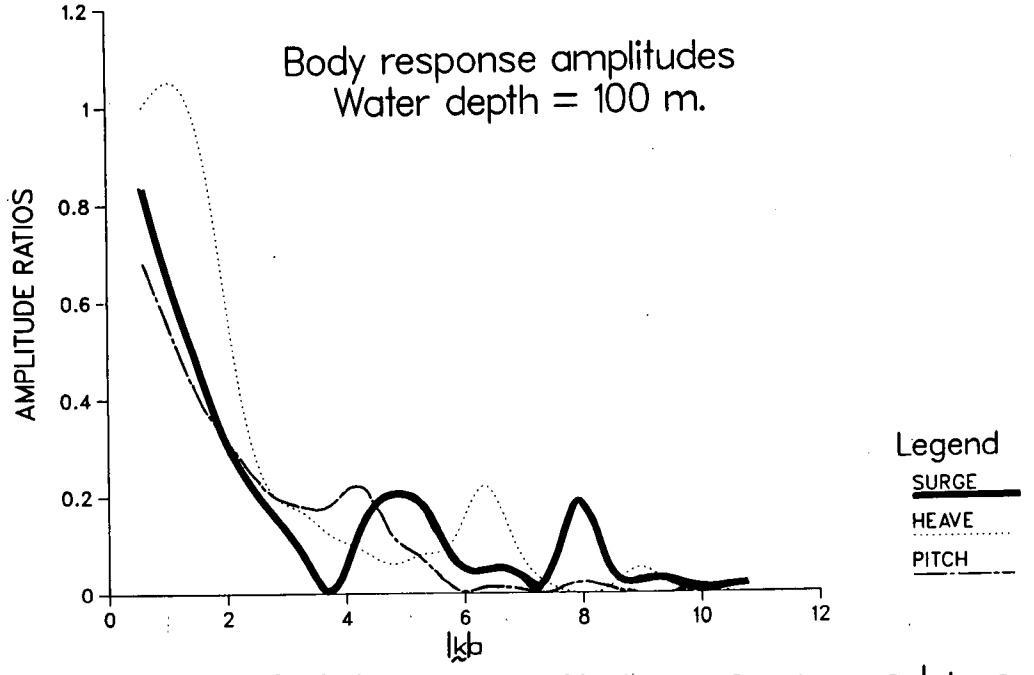


FIG. 2 - Heave, surge and pitch response amplitudes as functions of $|K|a$ for an incident wave of unit amplitudes (1 m.) in a water depth of 100 m. For heave and surge, the response is given as the ratio of the amplitude in m. over the incident amplitude and, for pitch, as (L/360) x the amplitude in degress (with L, the wavelength) over the incident amplitude.

Adequate expressions for the potentials are obtained by using the Green's function derived by John (1950) in the case of deep water. Finally, substituting those results in (6) and (7), an expression for the scattered potentials are obtained which, at large distance from the body, takes the form (at the water surface):

$$\varepsilon_k \phi_k(r,\theta) = (RA)\ r^{-1/2} e^{ikr} D_k(\theta) \quad (\varepsilon_4=1)\ k = \text{for } 1,2,3,4 \qquad (8)$$

with r measured radially from the object's centre and the angle, $\theta$, from the incident wave direction (see Fig. 1). A is the amplitude of the incident wave potential and the factor R is introduced to conserve energy, as explained below. The potentials in (8) represent waves propagating outward from the scatterer with angular distribution $D_k(\theta)$.

The wave potential due to scattering by a whole field of ice floes may be written in terms of the Foldy-Twersky integral (eg. Ishimaru, 1978), under the single scattering approximation

$$< \emptyset\ (\underset{\sim}{x},t) > = [\emptyset_i(\underset{\sim}{x}) + \iint_{\underset{\sim}{r}} (\emptyset_4 + \sum_{k=1}^{3} \varepsilon_k \emptyset_k)_s\ (\underset{\sim}{x})\ \rho(\underset{\sim}{r}) d\underset{\sim}{r}]\ e^{-i\omega t} \qquad (9)$$

The spatially averaged wave field (< >) at a point $\underset{\sim}{x}$ on the water surface consists of the incident wave field, $\emptyset_i(\underset{\sim}{x})$, at that point plus the integrated contribution from all waves scattered by each scatterer s, with a distribution $\rho(\underset{\sim}{r})$ (number of scatterers per unit surface) around that point. A decay of the "number density", $\rho(\underset{\sim}{r})$, with distance from the point of observation is included to account for shading of remote scatterers by nearby floes and to prevent divergence of the integral.

The wave intensity resulting from an incident plane wave is expressed as (Ishimaru, 1978, p. 268):

$$<|\emptyset(\underset{\sim}{x},t)|^2> = |\ <\emptyset(\underset{\sim}{x},t)>\ |^2 + [\iint_{\underset{\sim}{r}} <|(\emptyset_4 + \sum_{k=1}^{3} \varepsilon_k\ \emptyset_k)_s(\underset{\sim}{x})|^2>\rho(\underset{\sim}{r})d\underset{\sim}{r}] \qquad (10)$$

The energy distribution resulting from the scattering of one component ($f_n$, $\theta_n$) of the incident spectrum is obtained from (10), using the spatially averaged wave field expression given by (9):

$$<|\emptyset(\underset{\sim}{x},t)|^2> = [\,|RA|^2(1 + |\ \alpha\ |^2 + \beta \sum_{k=1}^{4} \int_0^{2\pi} |D_k(\theta)|^2 d\theta] \qquad (11)$$

The scattered wave then consists of: 1-a component identical to the unscattered incident wave, but of reduced amplitude RA; 2- an isotropic term, $|\ \alpha\ |^2$, due to the $\theta$ - independent terms in (9), with energy equally distributed in all directions; 3- directional scattering contributions with intensity apportioned as $|D_k\ (\theta)|^2$. A specific example will be worked out below.

Since the problem is homogeneous in space, (11) holds everywhere. In addition, since we have chosen symmetric scatterers, (11) will also hold for any angle of incidence, provided that $\theta$ is referred to that direction when using the result rather than to some fixed direction in space. For chosen floe dimensions, a and h, the scattering coefficients $\alpha$, $\beta$, R, and $D_k(\theta)$ need to be calculated only once for the range of frequencies of interest.

## 4) INTEGRATION PROCEDURE

The evolution of the spectrum is obtained from the procedure outlined in Fig. 3. The numerical integration of the radiative transfer equation proceeds following a simple first-order forward-difference method. Time steps are dynamically adjusted, starting with $(\Delta t)_n = t_{n-1}/2$ and reducing it by a factor 2 in case of too large $\Delta F/F$'s. A simple first-order integration scheme is considered adequate since $\Delta t$ is determined by the rapidly responding high frequency region of the spectrum, leading to very small $\Delta F$ in the energetically relevant region of the spectral peak (Komen et al., 1984). The frequency direction spectrum is specified for $0.125 < f < 0.8$, beyond which a high frequency $f^{-5}$ decay is assumed (adjusted independently for each direction).

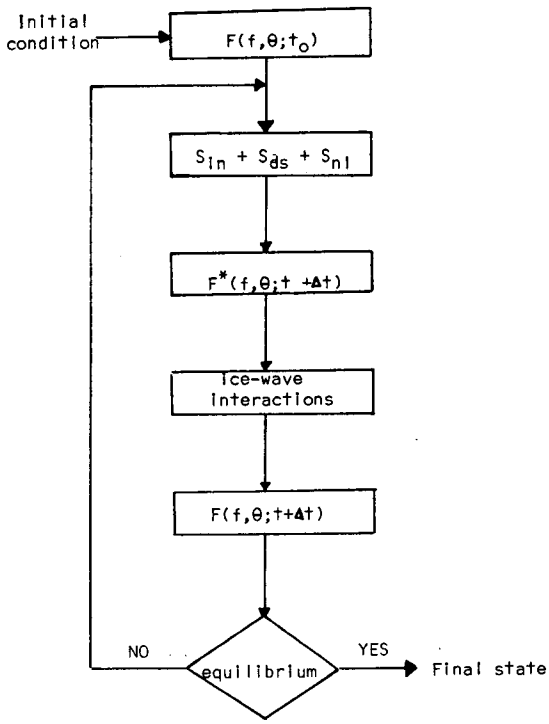


FIG. - 3 Integration scheme for wind wave generation in presence of ice floes.

The initial wavefield specified is a JONSWAP spectrum with low wave amplitude, corresponding to $f_{peak} = 0.4\ s^{-1}$ and $H_s = 0.5m$. The source terms $S_{in}$, $S_{ds}$ and $S_{nl}$ are computed for that spectrum and an intermediate spectrum $F^*(f,\theta)$ is obtained which does not yet include the influence of scattering by the ice floes.

For a sparce floe field, the travel time of deep water waves between floes (of the order of tens of seconds) is much smaller than the adjustment time of the wind wave spectrum (20 minutes or so). Therefore we consider the scattering process to be instantaneous. After every time step, the energy of each spectral component of $F^*(f,\theta)$ is redistributed between the incident, isotropic and angular dependent terms of (11). If A is the amplitude of a plane wave of frequency $f_n$ and direction $\theta_n$ in the $F^*(f,\theta)$ spectrum, then energy conservation applied to (11) determines the factor R:

$$R = \left[1 + |\alpha|^2 + \beta \sum_{k=1}^{4} \int_0^{2\pi} |D_k(\theta)|^2 d\theta + f_d\right]^{-1/2} \qquad (12)$$

To account for energy dissipation upon scattering by such factors as wave breaking on floes or internal stresses in the ice, we have included a factor $f_d$ which is the fraction of energy lost in the scattering process.

The procedure is then repeated until a near equilibrium is reached. The final spectrum obtained corresponds to the equilibrium sea-state, for infinite fetches, expected in the decoupled problem with the ice cover and wind speed given and the parameters used.

## 5) DETAILED SCATTERING OF A SINGLE COMPONENT

In this example, we chose an ice coverage, $f_r$, of 10% with floes of dimension a = 15 m. and h = 3 m. Taking into account the shading effects, this results in a "number density" of floes:

$$\rho(r) = [1.42 \times 10^{-4} \ (1.145)^{-0.033r}] \ m^{-2}$$

An incident wave of unit amplitude travels in the direction of the wind ($\theta = 0^0$) with a frequency $f = 0.182 s^{-1}$ and in a water depth of 100 m. From those values, the body motion amplitudes are there computed (see fig. 2, $|\underset{\sim}{k}|a = 2.0$):

| | Surge (m.) | Heave (m.) | Pitch (rad.) |
|---|---|---|---|
| Amplitude | 0.3110 | 0.5792 | 0.0412 |

In order to obtain the scattered spectrum, we first have to compute the different angular distributions, $D_k(\theta)$, for the 4 modes, as a function of ($0 \leq \theta \leq \pi$ rad.). Figure 4 and table 1 present the scattering coefficients, $|D_k(\theta)|$, obtained in this particular case.

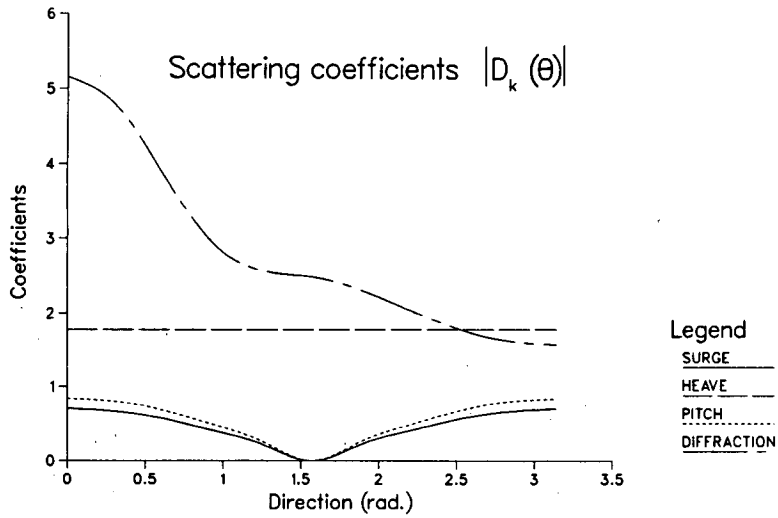


FIG. - 4 Scattering coefficients, $|D_k(\theta)|$, for the three modes of motion (k=1,2,3) and for diffraction (k=4) as a function of direction, $\theta$ (rad.).

| DIRECTION (DEG.) | 1 (SURGE) | 2 (HEAVE) | 3 (PITCH) | 4 (DIFFRACTION) |
|---|---|---|---|---|
| 0.0 | .71E+00 | .18E+01 | .84E+00 | .52E+01 |
| 18.0 | .67E+00 | .18E+01 | .80E+00 | .48E+01 |
| 36.0 | .57E+00 | .18E+01 | .68E+00 | .38E+01 |
| 54.0 | .41E+00 | .18E+01 | .49E+00 | .29E+01 |
| 72.0 | .22E+00 | .18E+01 | .26E+00 | .26E+01 |
| 90.0 | .89E-06 | .18E+01 | .11E-05 | .25E+01 |
| 108.0 | .22E+00 | .18E+01 | .26E+00 | .23E+01 |
| 126.0 | .41E+00 | .18E+01 | .49E+00 | .20E+01 |
| 144.0 | .57E+00 | .18E+01 | .68E+00 | .18E+01 |
| 162.0 | .67E+00 | .18E+01 | .80E+00 | .16E+01 |
| 180.0 | .71E+00 | .18E+01 | .84E+00 | .16E+01 |

TABLE 1 - Scattering coefficients, $|D_k(\theta)|$, as a function of direction, $\theta$ (deg.).

Finally, the energy distribution of the scattered spectrum is determined by the computed values of the 3 terms involved in eq. (11):

$$\alpha = 0.0251$$
$$\beta = 3.168 \times 10^{-2} \quad m^{-3}$$
$$R = 0.5336$$

with $f_d$ assumed to be 0. Figure 5 shows the resulting angular distribution of the energy after scattering. A significant fraction of the energy, as measured from the departure of R from unity, is thus redistributed in direction in a single scattering event. Successive application of this process will thus be an important factor in the evolution of the wind-wave spectrum in the presence of ice floes.

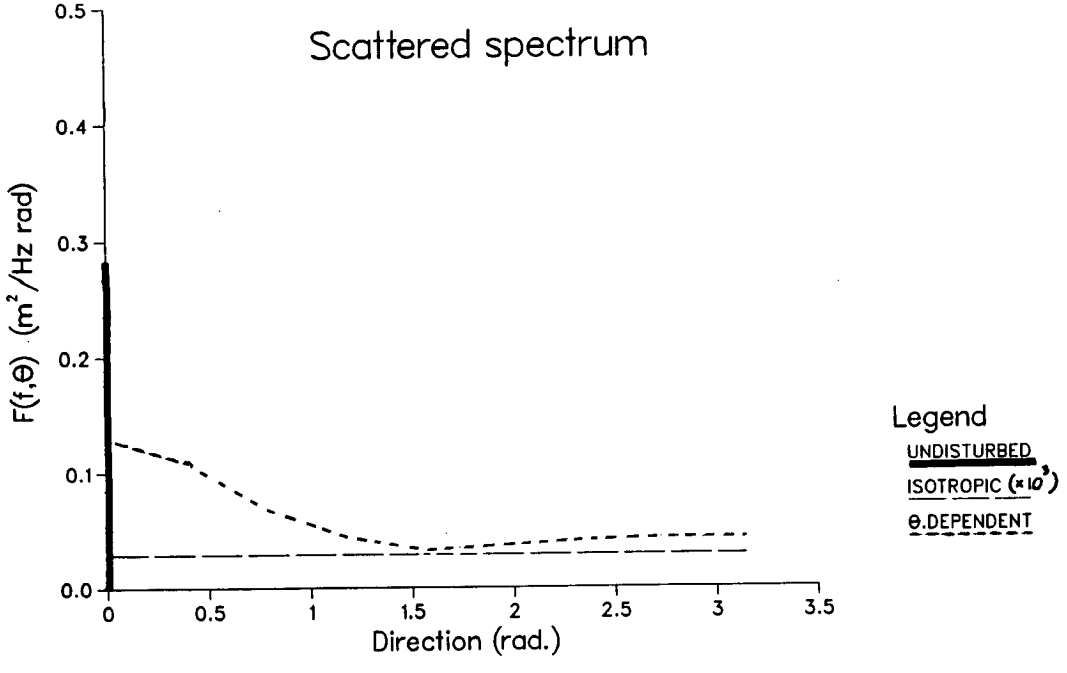


FIG. - 5 Energy distribution after scattering of one component with unit amplitude as obtained from the three terms of eq. (11) (with the isotropic contribution, $|\alpha|^2$, increased by a factor $10^3$).

References

Hasselmann, S. and K. Hasselmann, 1981. A symmetrical method of computing the nonlinear transfer in a gravity-wave spectrum. Hamb. Geophys. Einzelschriften, Reihe A:Wiss. Abhand., 52, 138.

Hasselmann, S. and K. Hasselmann, 1985a. Computations and parameterizations of the nonlinear energy transfer in a gravity-wave spectrum. Part I: A new method for efficient computations of the exact nonlinear transfer integral. J. Phys. Oceanogr., 15, 1369-1377.

Hasselmann, S. and K. Hasselmann, 1985b. The wave model EXACT-NL. Ocean wave modeling, (The SWAMP group). Plenum, 256pp.

Isaacson, M. de St. Q., 1982. Fixed and floating axisymmetric structures in waves. J. Waterway Port Coastal and Ocean Div., ASCE, 108(WW2), 180-198.

Ishimaru. A., 1978. Wave propagation and scattering in random media, Vol. 2., Academic Press, New York, 572pp.

John, F., 1950. On the motion of floating bodies II. Comm. Pure Appl. Math., 3, 45-101.

Komen, G.J., S. Hasselmann and K. Hasselmann, 1984. On the existence of a fully developed wind sea spectrum. J. Phys. Oceanogr., 14, 1271-1285.

Martin, S., P. Kauffman and C. Parkinson, 1983. The movement and decay of ice-edge bands in the winter Bering Sea. J. Geophys. Res., 88 (C5), 2803-2812.

Snyder, R.L., F.W. Dobson, J.A. Elliot and R.B. Long, 1981. Array measurements of atmospheric pressure fluctuations above surface gravity waves. J. Fluid Mech., 102. 1-59.

SWAMP group, 1985. Ocean wave Modeling. Plenum Press, New York, 256pp.

Wadhams, P., 1975. Airborne laser profiling of swell in an open ice field. J. Geophys. Res., 80(33), 4520-4528.

Wadhams, P., 1978. Wave decay in the Marginal Ice Zone measured from a submarine. Deep-Sea Res., 25, 23-40.

Wadhams, P., 1983a. A mechanism for the formation of ice edge bands. J. Geophys. Res., 88(C5), 2813-2818.

Wadhams, P., 1983b. The seasonal ice zone, in NATO advanced study institute on air-sea-ice interactions, Plenum, New York.

Wadhams, P., V.A. Squire, J.A. Ewing and R.W. Pascal, 1986. The effect of the marginal ice zone on the directional wave spectrum of the ocean. J. Phys. Oceanogr., 16, 358-376.

# THE ESTABLISHMENT OF A SEVERE STORMS DATA BASE FOR THE PREDICTION OF EXTREME ENVIRONMENTAL CONDITIONS FROM HINDCAST DATA

O. Brink-Kjær [1], J.B. Nielsen [1] and L. Watson [2]

[1] DANISH HYDRAULIC INSTITUTE
DK-2970 Hørsholm
Denmark

[2] Phillips Petroleum Company Norway
N-4056 Tananger
Norway

## ABSTRACT

The present paper describes the successive development of a data base of hindcast wind and wave conditions during severe North Sea storms and its latest application for re-assessing the extreme wave conditions at the Ekofisk Field (Lat. 56°30'N, Long. 03°15'E) in the Central North Sea. Also a computerized method for correct storm ranking is described, this being of importance for extreme value analyses based on the peaks-over-threshold method.

## 1. INTRODUCTION

In June 1985 Phillips Petroleum Company Norway authorized Danish Hydraulic Institute (DHI) to carry out a re-assessment of extreme wave conditions for the Ekofisk area. The study formed part of a general assessment of the consequences of the seabed subsidence which had been identified for the Ekofisk Field.

The Ekofisk Field is located in the southernmost part of the Norwegian North Sea sector. The water depth is approx. 70 m. Larger water depths are found towards the north. Smaller water depths are found towards the south in the Danish, German, Dutch and southern U.K. sectors.

DHI had on earlier occasions carried out a number of North Sea wave hindcast studies which have contributed to the description of shallow water effects in the North Sea. The Ekofisk Field appeared to be located in the transition zone between the higher deep-water waves experienced at more northerly locations in Norwegian and U.K. waters and the much lower waves experienced in Danish, German, Dutch and southern U.K. waters. Much data was already available at DHI since several previous hindcast studies had been carried out by the same methodology.

The present paper describes the successive development of the severe storms data base held by DHI, some elements of the prehistory of the assessment of the wave conditions at Ekofisk, the validity of the hindcast data, a computerized methodology by which to perform accurate storm ranking by a learning process which can make use of hindcast data, and the re-assessment of design wave conditions at Ekofisk.

## 2. SUMMARY OF DHI EXPERIENCE

DHI has been active in wave modelling since 1976, on a commercial basis since 1978. Some 30 wave studies have been carried out for waters all over the world, this including a number of North Sea studies.

The very first DHI North Sea wave study was carried out in 1980 for Dansk Olie og Naturgas A/S. The study dealt with design wave conditions for the 220 km long west-east oriented pipeline from the Tyra Field to the coast of Denmark, an alignment with water depths lower

than 50 m. The study outcome turned out to be of great practical significance because it allowed for savings worth some 25 mill. US Dollars, when compared to the costs arising from the basic design. To some extent the basic design relied on the much more comprehensive Norwegian experience which, however, had all been gained for deeper waters. This study helped to generate increased interest in the reassessment of environmental design conditions in the Central North Sea. It relied on other study techniques than later studies and the results are not presented in this paper. Some elements of the study are described in Sand et al (1981).

In 1982 the DHI Wind Wave Modelling System, SYSTEM 20, was upgraded from being a first generation to become a second generation shallow water discrete frequency model. Much experience has been gained with this model. The basic study methodology and the model calibration have remained constant throughout these applications. In this manner it has always been possible to extend rather than to replace the outcome of earlier studies.

The second North Sea wave study was carried out in 1982/83 for Mærsk Olie og Gas A/S. The study comprised the hindcasting of wave conditions during 53 severe storms from the period 1966-1982. The wind fields were set up by combining objective and manual analyses in a manner also maintained in later studies. Design wave conditions were established for the westernmost part of the Danish sector, primarily with water depths within the range of 35 to 55 m. In the discussions leading to the approval of DHI's results, the adequacy of the applied storm selection criteria was an important point. The successive refinements in the documentation of the storm selection procedure are summarized in Chapter 5. The general outcome of the study including model validation is described in Brink-Kjær et al (1984).

Mærsk Olie og Gas A/S kindly allowed DHI to make use of the hindcast wind and wave data base for subsequent studies.

The third North Sea Study was carried out in 1984 for Hamilton Brothers Oil and Gas Ltd. The study dealt with environmental design conditions for the Esmond Complex in the southern UK sector. The study greatly relied on the former study, but was extended to include by same techniques the simulation of wave conditions during severe easterly storms. In addition, a number of current/water level simulations driven by a subset of the established wind fields were carried out with the DHI Hydrodynamic Modelling System, SYSTEM 21. The ultimately accepted environmental design conditions lead to significant savings in costs compared to those following from earlier assessments. Also, the study outcome lead to a useful discussion with approving authorities on the distinction between central estimates of certain extreme events and corresponding design conditions.

The fourth North Sea study was carried out in 1985 as a joint research project with British Petroleum International. The study dealt with locations further to the north than so far investigated. The study therefore dealt with the establishment of criteria from which to decide on new relevant storms, for correct ranking of storm severity and on the adequacy of certain model area extensions with subsequent rehindcasting of wind and wave conditions. The study outcome was very well guided by the long-term wind and wave measurements from West Sole and Forties which British Petroleum International made available to DHI for this purpose. This is described in further detail in Nielsen (1986) and Nielsen et al (1986). Upon completion of study the area of model validity had been extended northwards from latitude 56°N to latitude 59°N, that is from the south to the north of the Ekofisk Field.

## 3. PREHISTORY OF ASSESSMENT OF WAVE CONDITIONS AT EKOFISK

When oil was first discovered at Ekofisk, there was no specific record of the environmental conditions since there were no permanent facilities there from which to collect measurements. In fact, back in the 1960's, the best available information about any offshore environment was ship observations as they were estimated by the eye of the ship's officers. Such observations were the only information - and as such extremely valuable - from which to make predictions on extreme conditions. When it comes to wave conditions, it is very difficult to provide an accurate estimate of the sea state by eye. Consequently, some conservatism was included in arriving at the original design individual wave height of 23.77 m to ensure that the platforms would be sufficiently safe when installed.

During the 1970's more wave data was collected by weather ships on location in the northern North Sea in waters deeper than those at Ekofisk. After reviewing this information, it was decided to design future platforms at Ekofisk to the more severe wave height of 26.00 m.

Clearly it was desirable to collect information directly at Ekofisk. In 1980 the Ekofisk Data Aquisition System (EDAS) was installed with instrumentation located on the platform 2/4 Hotel, on the platform 2/4 Charlie, and on the bridge connecting these platforms, see Fig. 3.1.

EDAS uses two devices to measure wave heights, a Datawell Waverider buoy deployed two kilometers from the 2/4 Hotel and a Plessey radar monitor mounted on the bridge.

The data from EDAS has been collected continuously from June 1980. The two measuring devices provide almost identical measures of the significant wave height, both indicating from their cumulative frequency distribution a hundred year significant wave height $H_{m0}$ of the order of 13 m.

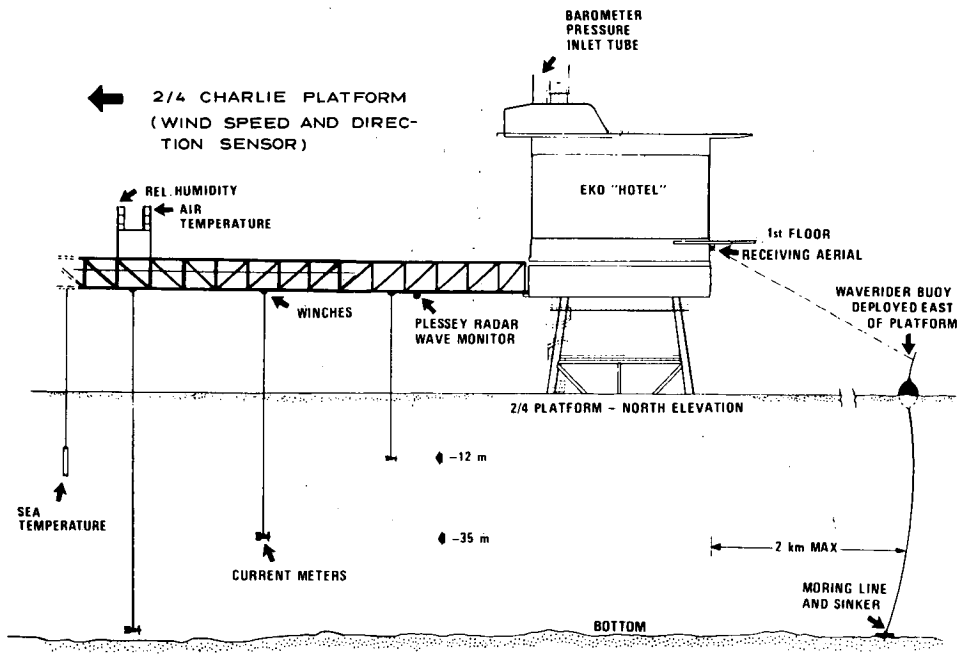


Fig. 3.1 Location of Meteorological and Oceanographical Measuring Instruments. From Loginfo (1984).

As discussed by Nolte (1972), a time period as short as 5 years should preferably not be used directly for determining extreme conditions because of the unaddressed influence of short term climatic variations. The approach taken by Phillips Petroleum Company Norway therefore was that of making use of the measured data for validating a wave model and then to apply this model to establish data from a much longer time span. In this manner not only the problems associated with short term variations in climate are resolved, the error bounds of the central estimates of the extreme events also are reduced because of the access to much more data of only slightly reduced quality compared to good measurements.

On this background DHI was contracted by Phillips Petroleum Company Norway to conduct a new evaluation of wave conditions at Ekofisk using the EDAS information and DHI's SYSTEM 20.

## 4. MODEL VALIDATION

Altogether wave conditions have been hindcast by same methodology during 85 storms covering the period 1966-1985.

### 4.1. General Validation of North Sea Wave Model

Measurements of wave conditions have been available for validation of the wave model from a total of 13 locations distributed in all the different national sectors of the North Sea. From some of these locations only very little data has been available, while long series of data have been available from a few locations. The best data coverage has been established for Forties in the northern part of the model area, for Ekofisk in the Central North Sea, and for West Sole in the Southern North Sea. The 13 stations are located in areas with water depths of between 20 and 110 m. The 13 locations are shown in Fig. 4.1.

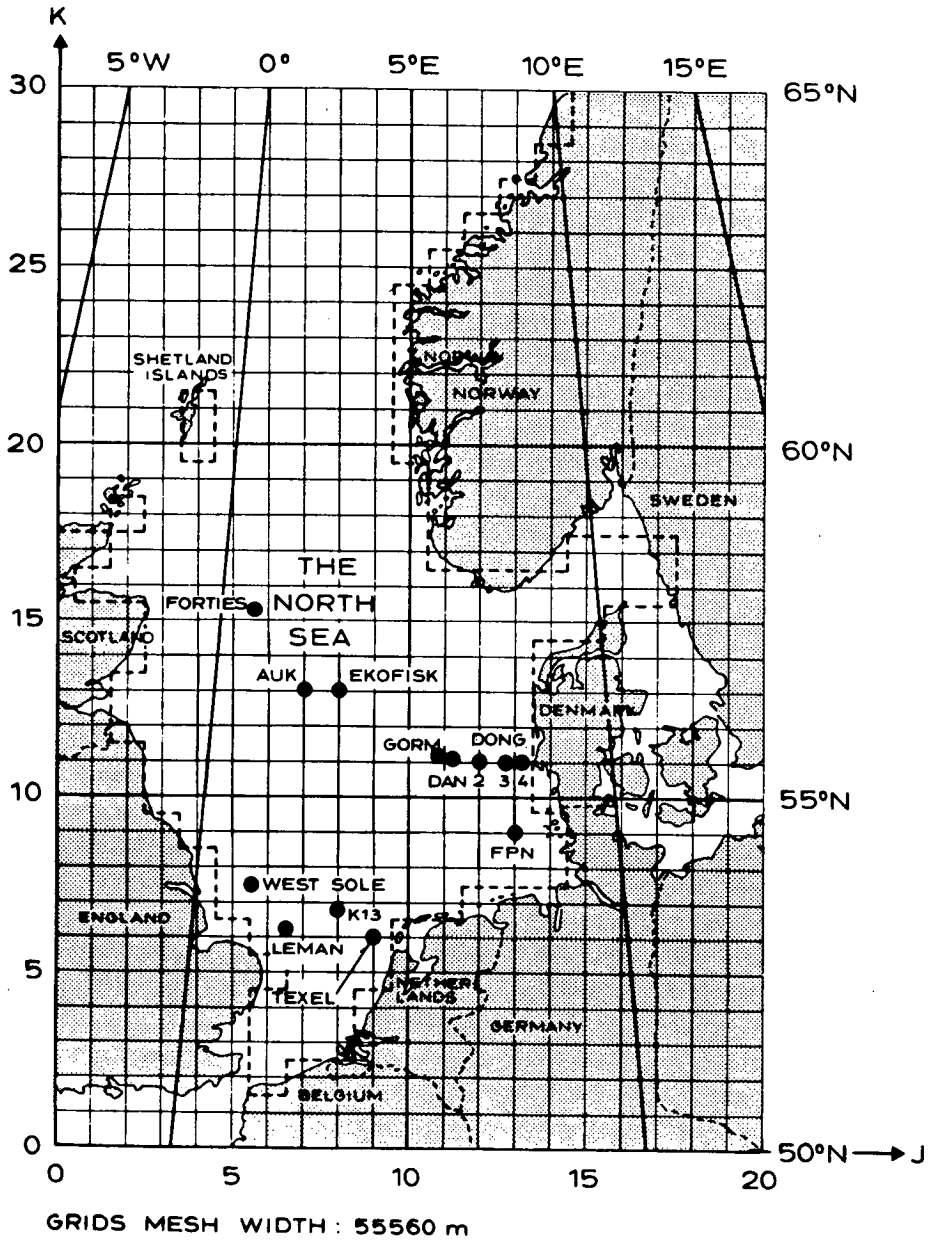


Fig. 4.1 Locations of Validation Stations in the Model Area.

Data has been gathered from 82 storm peak events. The number of events during a single storm goes with the number of stations from which measured data is available. Fig. 4.2 shows a comparison against the corresponding hindcast peak significant wave heights for all 82 events.

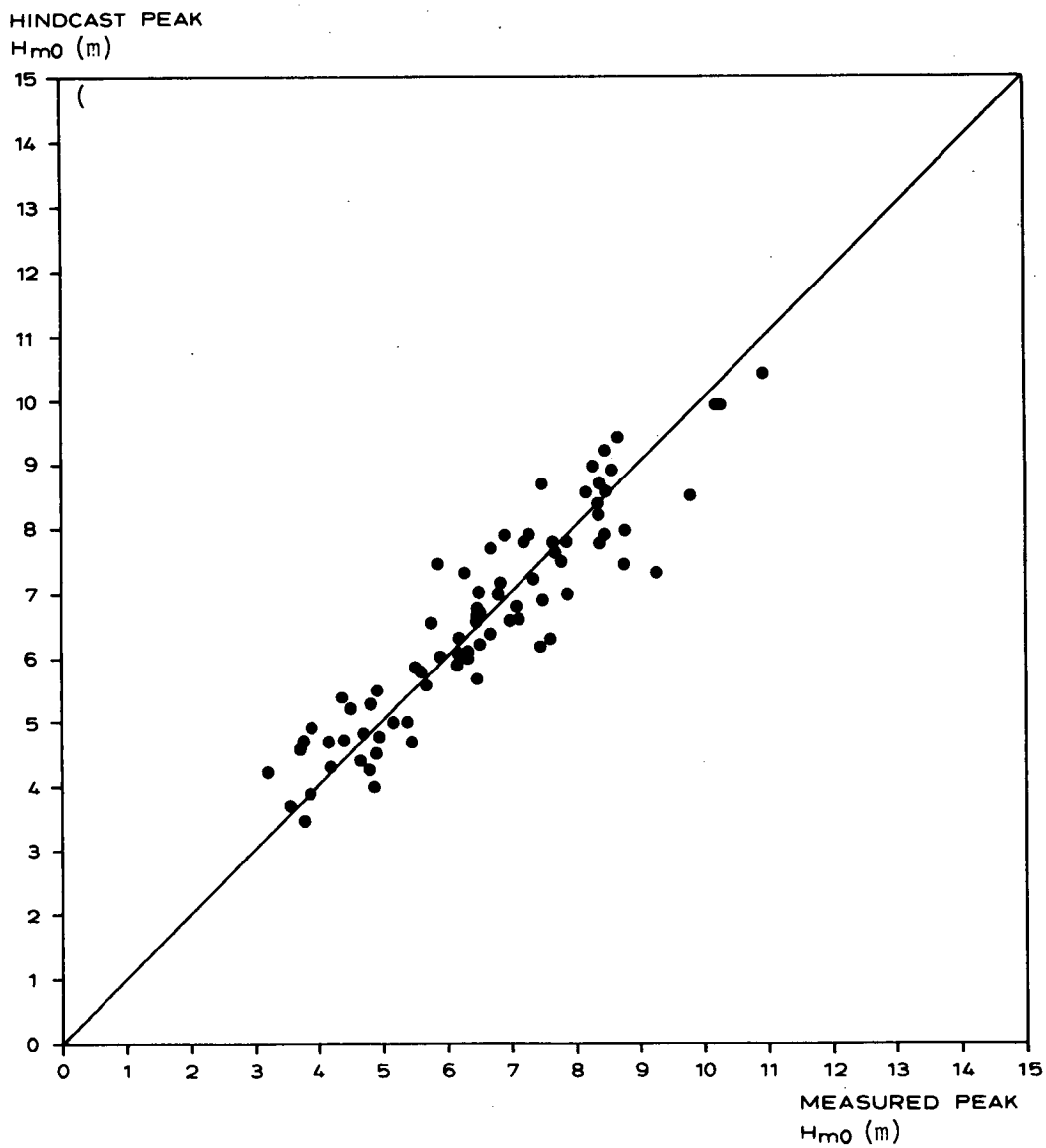


Fig. 4.2 Comparison of Measured and Hindcast Peak $H_{m0}$-Values for 82 Validation Storm Peak Events.

The comparison in Fig. 4.2 shows that no bias is present in the comparison between measurements and hindcast results. The best fitting line through origon of the coordinate system has a slope of 0.993, i.e. the bias is less than 1%, or for all practical purposes non-existent. The overall rms-error of the wave model is found to be 0.71 m.

The abilities of the wave model to predict correctly peak values of $H_{m0}$ in the entire North Sea is further illustrated in Fig. 4.3. This figure shows isolines of hindcast peak $H_{m0}$-values in the entire North Sea for two severe storms, which occured on 19-21 April 1980 and 23-25 November 1981, respectively. For these two storms measurements are available from 5 respectively 6 different locations. The peak values from these measurements are also shown in the figure.

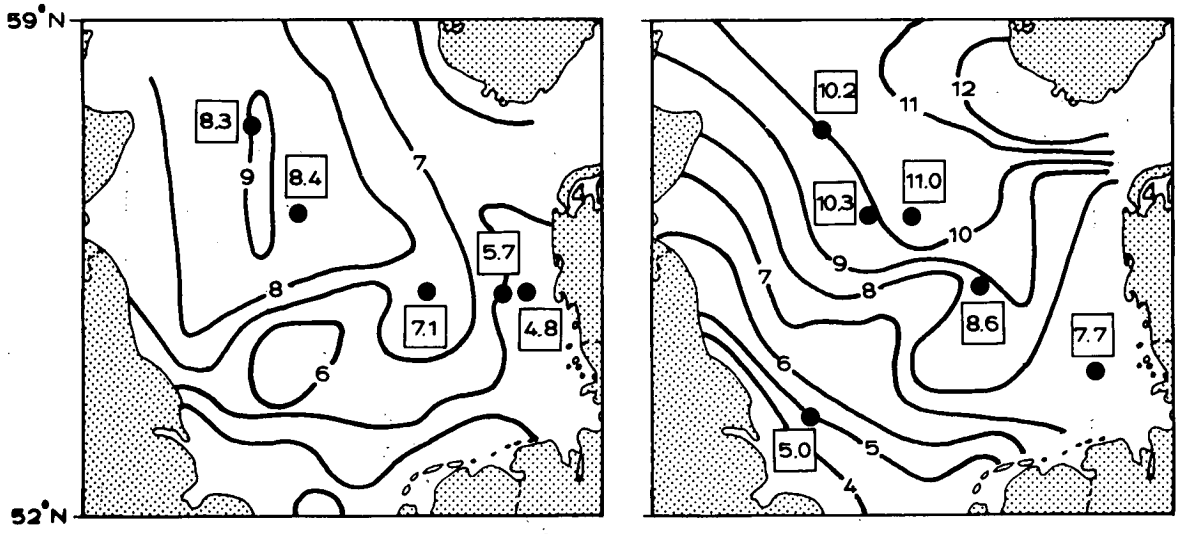


Fig. 4.3 Comparisons between Measured (Single Values (m)) and Hindcast (Isolines (m)) Peak $H_{m0}$-Values for Two Severe Storms.

Fig. 4.3 also demonstrates the importance of the shallow water effects. For both storms, the wave heights tend to decrease towards the southern parts of the North Sea, although the free fetch over which the wind is blowing from the west and north in fact increases towards the south. The effects of decreasing water depths towards the south totally dominates over those of increased fetch, and the wave model reproduces this depth modified pattern correctly.

Finally, Fig. 4.3 also serves to illustrate the severity of the storm of 23-25 November 1981. Peak values of $H_{m0}$ higher than 12 meters are hindcast in the deep water areas closer to the southern coasts of Norway. This indication of the extreme severity of the storm of 23-25 November 1981 is further supported by water level measurements from Esbjerg, which reached the highest level ever recorded over the period of more than 100 years for which measurements exist.

## 4.2 Validation of North Sea Wave Model against EDAS Data

Radar measurements and waverider measurements from EDAS were available from 27 and 23 (a subset of the 27) storm peak events, respectively. These events have been identified from 21 storm periods of which 16 contributed each with 1 peak event, 4 each with 2 distinctly different peak events, and 1 with 3 distinctly different peak events.

For comparison against hindcast peak data, the time series of radar and waverider measurements were averaged and the peak value identified. Fig. 4.4 shows the comparison between measured and hindcast peak values of the significant wave height.

When evaluated from Ekofisk data only, the best fitting line through origon has a slope of 0.984 with an rms-error of 0.76 m.

It could be argued that the Ekofisk subset of validation data expose a variation towards the hindcast values being on the high side for peak sea states less than 7.35 m and on the low side for peak sea states higher than 7.35 m. The best fitting line which is not restricted to pass through origon is shown in Fig. 4.4 also.

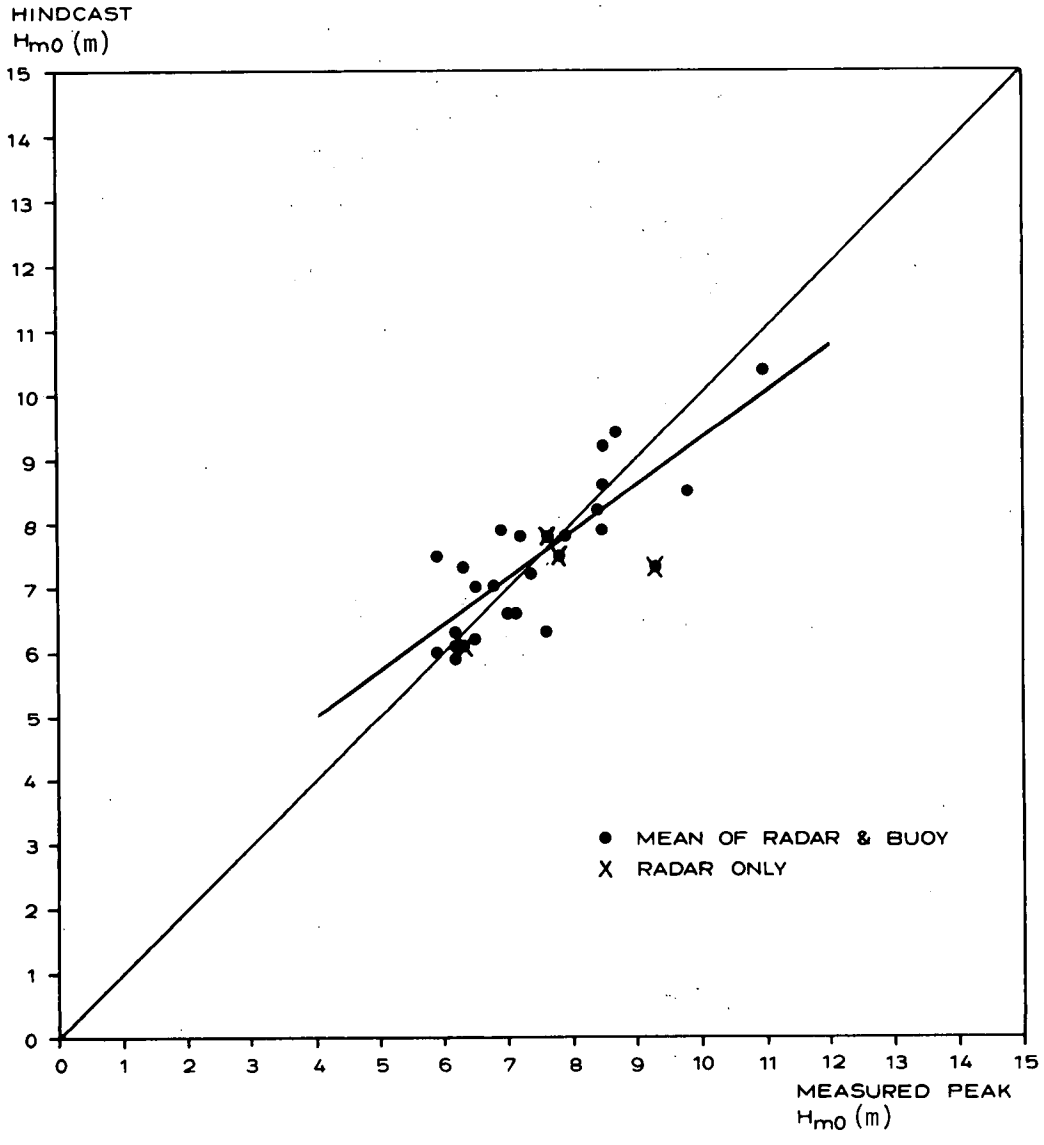


Fig. 4.4 Comparison of Measured and Hindcast Peak $H_{m0}$-Values for 27 Validation Storm Peak Events at Ekofisk.

In the subsequent analyses, the consequences of accepting either regression line were investigated. In order to pay maximum respect to the very site-specific validation data, the more conservative approach was given much weight.

Fig. 4.5 shows some examples of measured and hindcast time series of the significant wave height at Ekofisk. Similar comparisons which demonstrate the capability of the model to resolve correctly the entire time series of the significant wave height, have been presented for other locations at earlier occasions, see e.g. Brink-Kjær and Rodenhuis (1983), Brink-Kjær et al (1985).

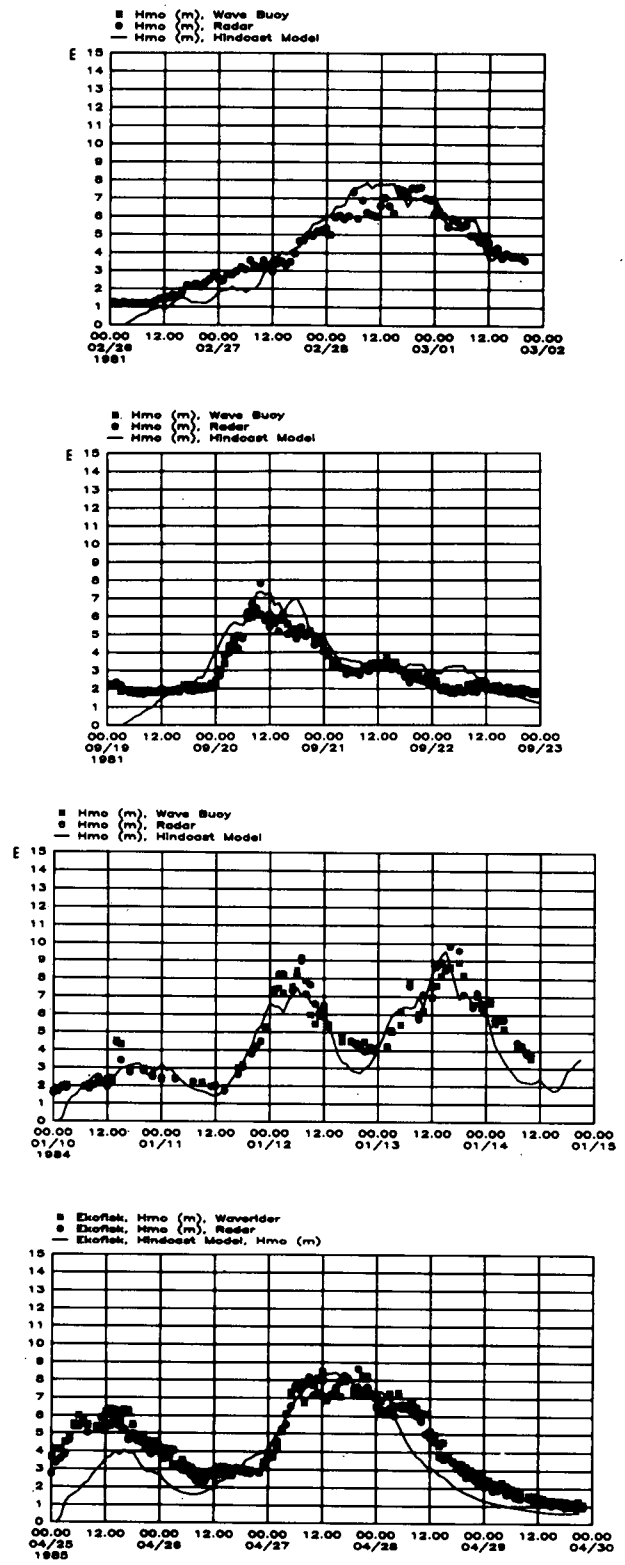


Fig. 4.5 Measured and Hindcast $H_{m0}$ Time Series at Ekofisk during 4 Storms.

## 5. VALIDATION OF STORM SELECTION CRITERIA

The selection of the storms to be included in a wave hindcast study forms a non-trivial task. If at all possible, the process should be guided from data which is available in uniform quality throughout the period of investigation. As a starting point, no or very little wave data (measured or hindcast) may be available for which reason the process of establishing an adequate selection criterion may well become an iterative or learning process as illustrated in Fig. 5.1.

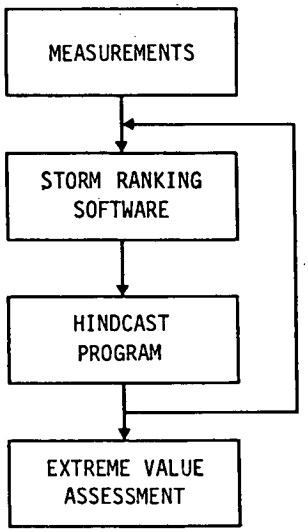


Fig. 5.1 The Learning Process

The storm selection criteria applied during the initial phases of the study for Mærsk Olie og Gas A/S relied on

- 12 hourly wave hindcasts produced on a routine basis by the Royal Dutch Meteorological Institute, KNMI
- wind time series from a Danish North Sea Light Vessel for the early part of the period of investigation
- wave measurements from the area of interest for the later part of the period of investigation

Clearly, this data formed a valuable entry, but the thorough documentation was not established until the hindcast sea states were correlated to a combined measure of regional and local severity as expressed by

- a gale index as defined by Jenkinson and Collison (1977), but centered 5 degrees more easterly at latitude 55°N, longitude 5°E
- the peak water level at the Port of Esbjerg which displays a positive surge for storms with westerly wind components

The two latter measures were of objective nature and available in uniform quality throughout the period of investigation, but their usefulness was restricted to the application in question, see Brink-Kjær et al (1985).

In fact the original number of 40 production storms was extended by 13 through the introduction of the latter criteria.

Later efforts in the study undertaken jointly with British Petroleum International showed that a fully computerized procedure of good predictive capability could be established on the basis of digitized atmospheric surface pressure fields, see Nielsen (1986) and Nielsen et al (1986). For the North Sea, such a data base is maintained by the Norwegian Meteorological Institute. The data is held on a six-hourly basis from 1955 to 1981. The area and grid of digitization are shown in Fig. 5.2.

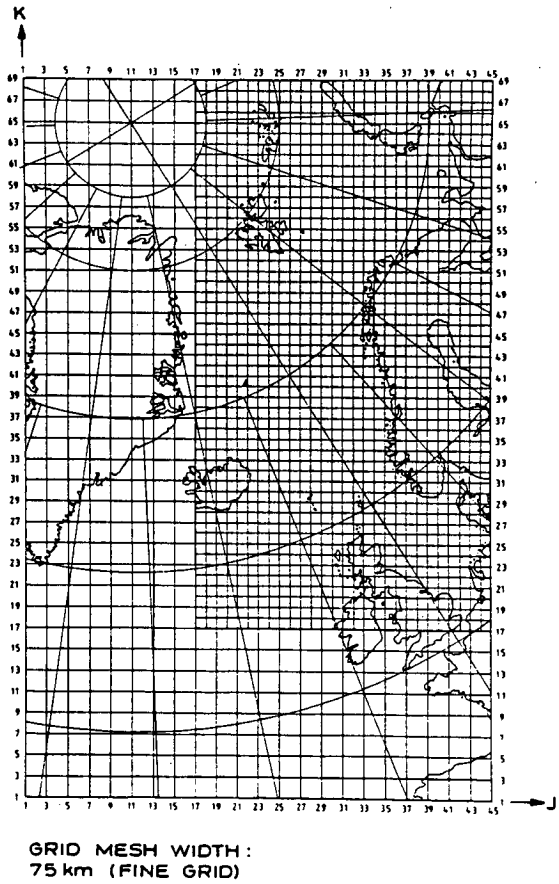


Fig. 5.2 Area and Grid of the Pressure Data Base of the Norwegian Meteorological Institute.

From such a data base it is possible to compute numerous different parameters which express storm severity. The applied approach was that of a generalization of the gale index method of Jenkinson and Collison (1977) as it basically operates with the same definitions of geostrophic flow and vorticity, but makes it possible to apply measures of different horizontal scale from several locations and from different times.

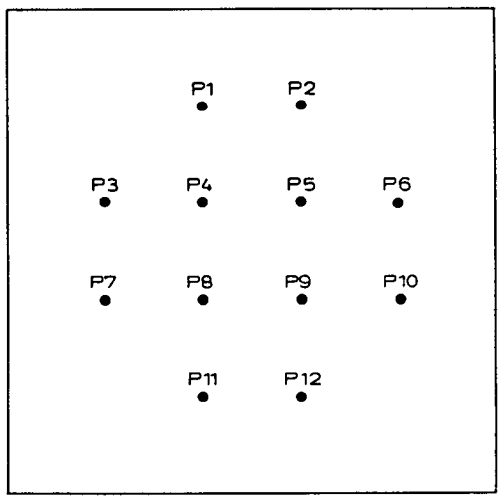


Fig. 5.3 Twelve Point Grid for Computation of Geostrophic Flow and Vorticity

The definitions (units and scales left out) of flow and vorticity follows from the pressure values at the 12 points of Fig. 5.3 by the following equations:

"East-west" flow component:
$FW = (P7 + 2P8 + 2P9 + P10 - P3 - 2P4 - 2P5 - P6)/6$

"North-south" flow component:
$FS = (P2 + 2P5 + 2P9 + P12 - P1 - 2P4 - 2P8 - P11)/6$

$FLOW = \sqrt{FW^2 + FS^2}$

"East-west" vorticity component:
$ZW = (P11 + P12 - P8 - P9 - P4 - P5 + P1 + P2)/2$

"North-south" vorticity component:
$ZS = (P6 + P10 - P5 - P9 - P4 - P8 + P3 + P7)/2$

$VORTICITY = \sqrt{ZW^2 + ZS^2}$

The problem can then be formulated as that of relating the daily peak significant wave height above a certain threshold level at a given location to corresponding values of a number of expressions for geostrophic flow or vorticity at same or other locations at same or other times, termed GI1, GI2, ..., GIn. The optimum solution is one which optimizes the values of the coefficients $a_1$, $a_2$, ..., $a_n$ in the expression

$$H_{pred} = a_1 x GI1 + a_2 x GI2 + \ldots + a_n x GIn$$

or a similar (linear or non-linear) expression with respect to the rms-value of the error of the prediction versus measured or hindcast significant wave height.

The technique applied for this purpose is that of "hill-climbing" as described by Rich (1983). It consists of a number of steps which are repeated until an optimum solution is found. From a given set of initially assumed values of the coefficient $a_1$, $a_2$, ... $a_n$ these steps are:

1) A small value is added to one of the coefficients.

2) The rms-error of $H_{pred}$ is calculated using the new set of coefficients. The value is stored.

3) The same small value is instead subtracted from the same coefficient.

4) The rms-error is again calculated and stored.

5) Steps 1-4 are repeated for all other coefficients.

6) The coefficients corresponding to the smallest rms-error are defined as "new" coefficients, i.e. only one coefficient has been changed slightly up or down.

7) Steps 1-6 are repeated until no improvement (no decrease in the rms-error) is found. Then the "small" value is divided by 2 and then procedure is resumed.

8) When the "small" value is smaller than a specified minimum value then the coefficients are considered to be the best possible set and the corresponding rms-error of $H_{pred}$ has been minimized.

Improved accuracy can be obtained when only little measurements are available by using hindcast wave conditions for comparison and minimization of prediction errors. This iterative or learning process can be carried out with little extra effort because all steps have already been computerized. This means that the ultimate ranking of production storms should be considered being a working process running parallel to that of hindcasting these storms.

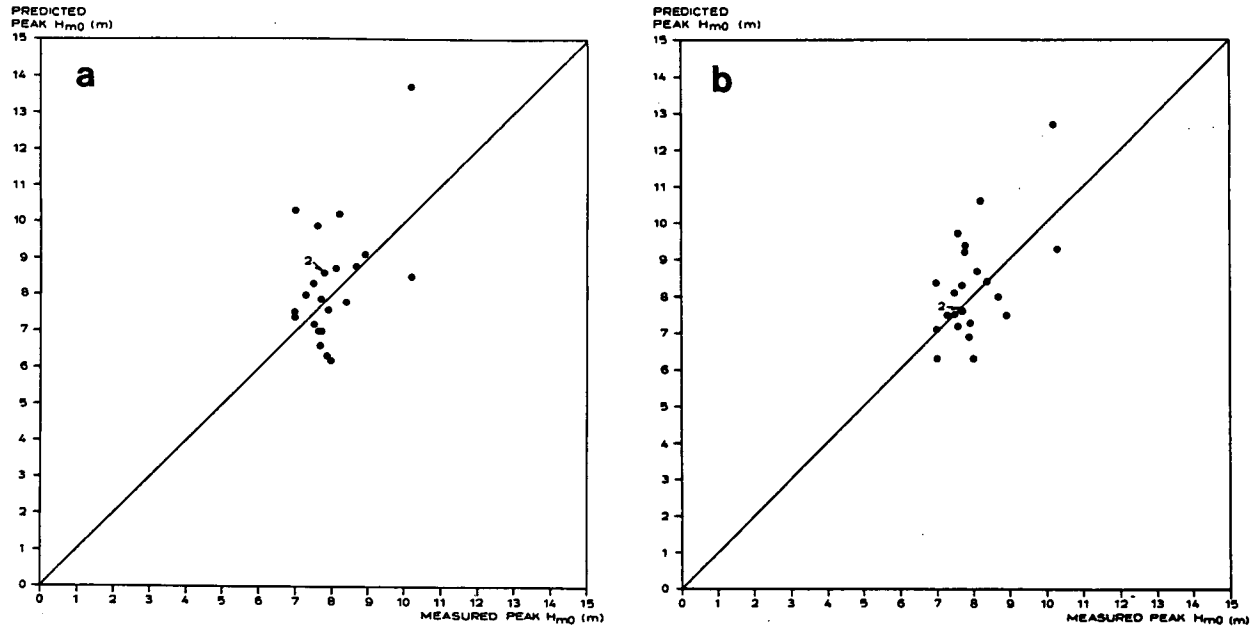


Fig. 5.4 Comparison of Measured and Predicted Peak $H_{m0}$-Values at Forties. Applied Treshold is 7 m. a) Non-Directional Model. b) Directional Model.

Fig. 5.4a shows a comparison between measured and predicted significant wave height at Forties. The prediction is based on expressions for flow and vorticity, irrespective of directional characteristics, and referred to as a non-directional model.

Fig. 5.4b shows a corresponding comparison for a directional model which can react to fetch-limitations and thereby provide better accuracy.

The rms-errors of the two predictive models are 1.3 m and 1.1 m, respectively.

The computational efforts of applying such predictive methods are much smaller than those of applying state-of-the-art wave models. Their use for continuous screening of a long period of time for all events of possible interest is, accordingly, very feasible as done in the latest performed studies for British Petroleum International and Phillips Petroleum Company Norway.

## 6. CONCLUSIONS

Hindcast wind and wave data from 85 severe historical North Sea storms have been established during the course of a number of studies carried out by Danish Hydraulic Institute for Mærsk Olie og Gas A/S, Hamilton Brothers Oil and Gas Ltd., British Petroleum International, and Phillips Petroleum Company Norway.

The results have proven to be of practical significance for the re-assessment of design wave conditions at several locations in the North Sea, mainly so because of the accurate resolution of shallow water effects. When supplemented with documentation on the adequacy of storm selection criteria, the comprehensive data base makes it possible to arrive at central estimates of extreme conditions with narrow error bounds. The above described major studies have in fact been succeeded by a number of smaller studies for same clients during which additional use of this data base has been made for new locations in the U.K., German, Danish and Norwegian North Sea sectors.

When supplemented with hindcast current/water level data which have already been established for some 45 of the 85 storms, the data base allows for the assessment of the effects of the joint probability of occurrence of severe wind, wave and current conditions. Although this subject is beyond the scope of this presentation, it is mentioned for its future potential importance.

For the Ekofisk Field, the extreme value analyses based on the more conservative interpretation of model validation lead to a central estimate of the 100 year significant wave height of 12.45 m with a corresponding value of the individual wave height of 23.00 m, this latter value to be compared against the earlier estimates of 23.77 m and 26.00 m. Clearly, when compared against the latter value of 26.00 m, the outcome of the study described in this paper is of importance when evaluating the urgency of remedial action to be taken by Phillips Petroleum Company Norway to account for the subsidence at the Ekofisk Field.

## 7. REFERENCES


Brink-Kjær, O., Knudsen, J., Rodenhuis, G.S. and Rugbjerg, M., Extreme Wave Conditions in the Central North Sea, Proc. 1984 Offshore Technology Conference, Paper OTC 4809, pp. 283-293, 1984.

Brink-Kjær, O. and Rosenhuis, G.S., Environmental Design Aspects of Marine Pipelines for the Danish Part of the North Sea, Proc. Workshop Meeting on the Application of Joint Probability of Metocean Phenomena in the Oil Industry's Structural Design Work, E&P Forum, London, June 1983.

Brink-Kjær, O., Lyngberg, B. and Nielsen J.B., Direct Assessment of Environmental Forces from Hindcast Time Series of Environmental Parameters, Proc. Workshop Meeting on the Application of Joint Probability of Metocean Phenomena in the Oil Industry's Structural Design Work, E&P Forum, London, November 1985.

Jenkinson, A.F. and Collison, F.P., An Initial Climatology of Gales over the North Sea, Met.O. 13, Branch-Memorandum No. 62, England, 1977.

Loginfo A/S, Environmental Conditions at the Ekofisk Field, Yearly Report July 1983-June 1984, Report Prepared for Phillips Petroleum Company Norway, 1984.

Nielsen, J.B., A Learning System for the Identification and Ranking of Severe Storms, Proc. 1st International Conference on Applications of Artificial Intelligence in Engineering Problems, Southhampton, U.K., April 1986.

Nielsen, J.B., Grant, C.K., Webb, R.M., and Brink-Kjær, O., Investigation of the Importance of Joint Probability and Directionality of Environmental Data for Platform Design, Proc. 1986 Offshore Technology Conference, pp. 499-510, 1986

Nolte, K.G., Statistical Methods for Determining Extreme Sea States, Proc. Second International Conference on Port and Ocean Engineering under Arctic Conditions, pp. 705-742, 1972.

Rich, E., Artificial Intelligence, McCraw Hill Series in Artificial Intelligence, 1983.

Sand, S.E., Brink-Kjær, O. and Nielsen, J.B., Directional Numerical Models as Design Basis, Proc. International Conference on Wind and Wave Directionality, Paris, 1981.

# IDENTIFICATION OF SEVERE WAVE-PRODUCING STORMS AFFECTING COASTAL AREAS OF EASTERN CANADA

R.D. Brown[1], P. Roebber and K. Walsh

The MEP Company
Markham, Ontario

V.R. Swail

Atmospheric Environment Service
Downsview, Ontario

## 1. Introduction

The design and construction of coastal and offshore structures requires a comprehensive knowledge of all of the forces to which the structure will be subjected. The predominant contribution to environmental forces on offshore installations comes from water waves. One of the most important requirements for design is an estimate of the extreme wave height and associated period for a given level of risk, usually given as a return period. It is this wave which is assumed to develop the maximum loads on the structure as a whole and on some, or all, of its principal elements. The maximum crest level of this wave will be required to calculate the clearance height for the superstructure (UKDOE, 1984). The requirement in Canadian waters is for the 100-year return period value of wave height.

Ideally the values to be used in the design of structures should be calculated from long time series of wave heights measured at the location in question. However, to calculate the 100-year return period value with reasonable reliability would require at least 25 years of measured data. Typically, the longest available time series of measured wave data at offshore locations in Canadian waters are less than 5 years. Time series from individual drilling locations often have durations less than 1 year.

The accepted solution to this problem is to use hindcast wave data, derived from wave models run with historical wind fields computed from surface pressure analyses. Several major hindcasts have been completed, including the U.S. Navy Spectral Ocean Wave Model (SOWM) described by Cummins and Bales (1980), and the U.S. Army Wave Information Study (WIS) described by Corson et al. (1982). These hindcasts have been produced for large ocean areas. Detailed analysis suggests that they may not be sufficiently reliable for extrapolation to 100-year return period values in areas of offshore exploration in Canadian waters (Wilson and Baird, 1984).

Resio (1982), Baird and Readshaw (1981), and Wilson and Baird (1984) all recommended that a set of 20-30 of the largest storms be selected, the winds re-analyzed, and the waves re-hindcast to form the basis for design wave information for all Canadian Atlantic areas. As a result, the Environmental Studies Revolving Fund (ESRF) contracted the MEP Company to produce a list of the 30-35 most severe wave-producing storms off the Canadian east coast. The study area was divided into 7 separate regions, shown in Figure 1 (Brown et al., 1986), based on physiography and generally accepted regional definitions. By pre-selecting the meteorology, it is possible to perform the much more detailed hindcasts required for extreme value analysis. Precise ice cover can be included for each case, and subjective input from meteorologists can be included in the production of the wind fields, which are the largest source of error in the hindcast procedure (Cardone and Szabo, 1985). Future wave hindcasts in each of the regions considered will be based on the storms selected in this study.

[1] Present affiliation: Atmospheric Environment Service, Downsview, Ont.

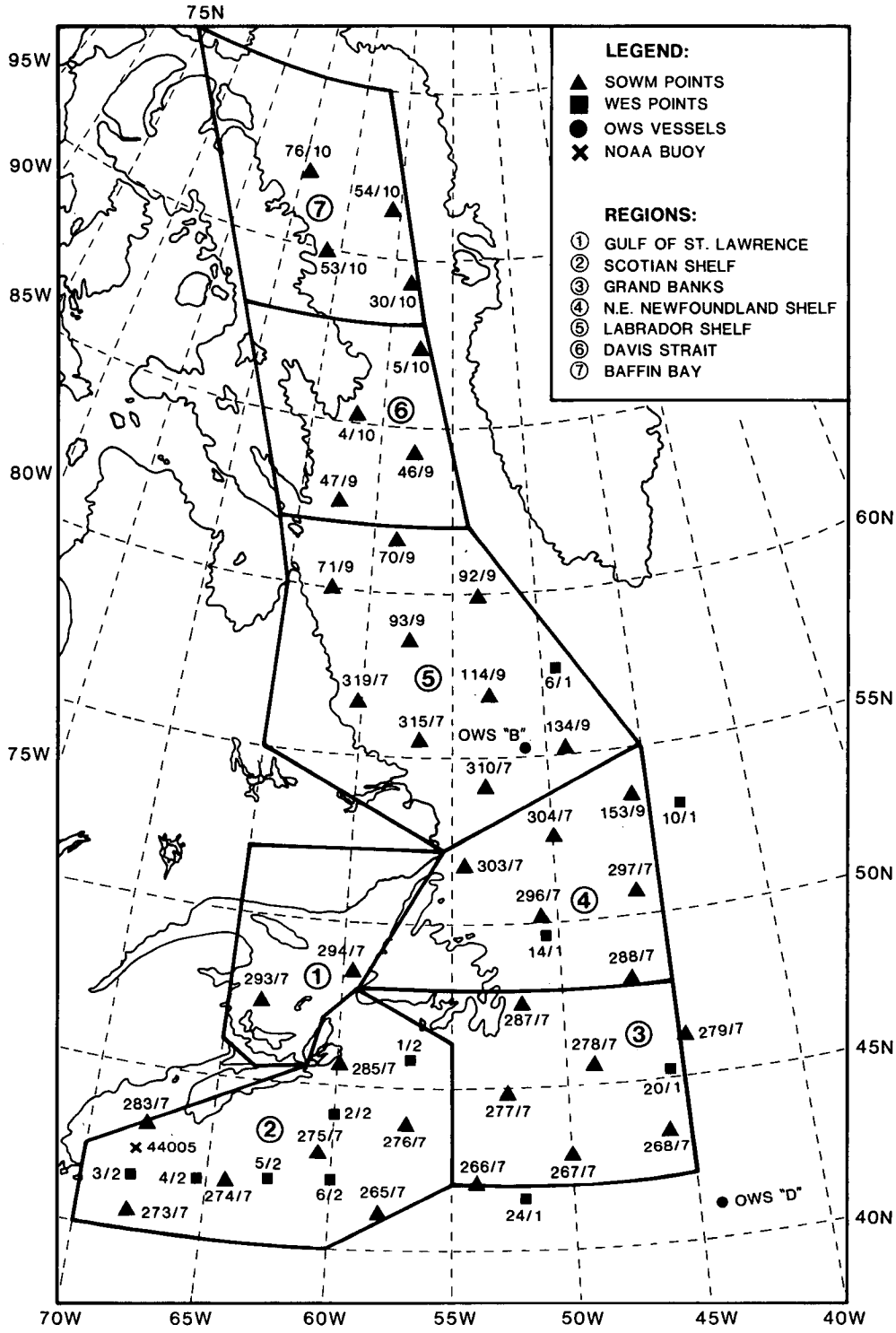


Figure 1. Location of study regions and SOWM and WES wave hindcast points. After Brown et al. (1986).

## 2. DATA SOURCES

A variety of data sources are available for the identification of significant wave-producing storms. These can be generalized into two basic categories: explicit sources that provide wave information directly (ie. observed, measured and hindcast wave data), and implicit sources such as wind data from which wave data can be inferred. The data sources used in this study are described briefly below.

### 2.1 Measured Wave Data

A continuous record of measured wave data in each study area would simplify the task of selecting extreme wave-producing meteorological events. Unfortunately, the spatial and temporal coverage of measured wave data off the Canadian east coast is such that it severely restricts its use for this purpose. Waverider buoy measurement programs in deeper water regions have usually been related to offshore oil exploration activities, which results in highly variable coverage in both spatial and temporal terms. A summary of available waverider data in each of the study regions is given in Brown et al. (1986). However, the waverider buoy may not necessarily be located in the area of maximum wave heights within a region. A further problem with the waverider buoy data is that data recovery is often less than 100%. Thus, data gaps exist in the period of record.

Only one National Oceanographic and Atmospheric Administration (NOAA) buoy (#44005) was located in the study area. However, its position close to Cape Cod meant that it did not experience waves greater than about 6 metres.

### 2.2 Spectral Ocean Wave Model (SOWM) Hindcast

The U.S. Navy has produced a 20-year hindcast for the Atlantic Ocean based on the Spectral Ocean Wave Model (SOWM) for the period 1956-75. The hindcast is described by Bales (1984). The wave model was evaluated and described in detail by MacLaren Plansearch (1984). A brief description of the model and the input wind fields is given below.

The SOWM is a deep water wave model based on the Pierson-Moskowitz (PM) spectrum for a fully-developed sea (Pierson and Moskowitz, 1964). It is a discrete spectral wave model, essentially a linear theory where each spectral component is assumed to grow independent of all other components in accordance with a linear input source function until it approaches its limiting "saturation" level. The wave growth and spectral form is dominated by the wind input rather than non-linear energy transfer by wave-wave interaction.

Winds are input to the SOWM model at a level of 19.5 m. The winds are derived from historical archives of the National Climatic Data Center in Asheville, N.C. Land and ship observations are included. The data are derived through the field-by-information-blending technique described by Holl and Mendenhall (1971).This involves adding a modified gradient wind velocity to the geostrophic values and adjusting them for lower level atmospheric stability and air-sea temperature difference to an effective "neutral" wind at the required height according to the method originally developed by Cardone (1969). A description of the wind algorithm is given by Lazanoff and Stevenson (1978).

The resulting wave hindcast is produced at 6-hour intervals on a gnomonic icosahedral grid, where grid points are spaced 90 to 180 nautical miles apart. The distribution of SOWM grid points on the Canadian east coast is shown in Figure 1.

Lazanoff and Stevenson (1975) compared SOWM and wave data measured by NOAA buoys, and showed that significant wave heights computed by the SOWM were generally higher than buoy-derived significant wave heights. The comparison study concluded that SOWM wave spectra had 20% excess energy, and suggested that the cause was a lack of strong decay coefficients in the low frequency range. A comparison of SOWM and significant wave heights from waverider buoys on the Grand Banks and Scotian shelf by MEP (1982) found that the SOWM tended to over-predict higher waves.

The coarse resolution of the SOWM land/sea boundaries severely restricts the performance of the model in enclosed areas such as the Gulf of St. Lawrence and Baffin Bay. The SOWM also does not incorporate shallow water effects on wave growth and decay, which limits its performance in the vicinity

of the Magdalen Islands in the Gulf of St. Lawrence. The effects of ice cover on wave development, propagation and decay are similarly not taken into account, which has important consequences for the identification of severe events.

2.3 U.S. Army Waterways Experiment Station (WES) Hindcast

The U.S. Army Corps of Engineers Waterways Experiment Station has produced a 20-year hindcast (1956-75) for the east coast. The wave model and the hindcast are described in detail by Corson et al. (1982), Resio et al. (1982), and Resio (1981).

The WES model is a deep-water discrete spectral model that approximates the similarity-based fetch and duration growth characteristics of the Hasselmann et al. (1976) parametric model. The fundamental physics of the model consists of three parts: a new parameterization of the wave-wave interaction source term, an exponential atmospheric input term, and a variable energy density level in the range of frequencies above the spectral peak. The dominant source term is the non-linear wave-wave interaction, unlike the SOWM model, which relies on atmospheric input as the wave growth mechanism.

Derivation of the WES winds has been described by Resio et al. (1982), and evaluated by Swail et al. (1984). The winds were derived from Fleet Numerical Oceanography Center (FNOC) pressure fields, into which National Weather Service (NWS) pressures were blended for a finer mesh grid along the eastern seaboard. The blending was only carried out for intense storms, and was intended to compensate for the tendency of the original FNOC pressures to underestimate the depth of lows along the western Atlantic Ocean. The input winds consisted of geostrophic winds modified in several ways. The geostrophic winds calculated at each grid point had an isallobaric component added to them if the local rate of pressure change was high. A gradient wind estimate was used in place of the geostrophic wind in low pressure areas if the isobars had tight curvatures, because the centrifugal accelerations would force greater deviations from the true geostrophic values. A thermal wind component was added by integrating the thermal wind equation up to 1 km. The resultant winds were then reduced to the 19.5 m level and blended with approximately 7.4 million independent ship wind speed measurements (neglecting directions).

The resulting wave hindcast was produced on a spherical orthogonal grid, with 222 km spacing, at 6 hour intervals for the U.S. coast and the Scotian shelf. However, north of this only selected points were archived. The distribution of WES grid points on the Canadian east coast is shown in Figure 1.

The study of Resio (1982) indicated that, given accurate wind fields, the WES model will produce reasonably reliable wave fields. The WES hindcast data, however, appear to be reasonably reliable only in the U.S. coastal regions. Resio (1982) recommended not using the WES hindcasts for the Scotian shelf area because of problems with the pressure fields, and consequently the winds input to the wave hindcast. In other areas off the Canadian east coast, the WES study appeared to be acceptable in providing at least a general description of the wave climate. This is in general agreement with a study by Baird and Readshaw (1981), which concluded that, while the WES hindcast does not provide an accurate description of the sea state at any given hour on the Grand banks or Scotian shelf, the hindcast data might provide an accurate representation of the wave climate at grid points to the south and east of these areas. Wilson and Baird (1984) concluded that the WES data, while probably more reliable than the SOWM hindcast, are not sufficiently reliable for the estimation of extreme events (eg. the 100-year return period storm). Like the SOWM, the WES hindcast does not include shallow water effects, or the effects of ice cover on wave growth and decay.

2.4 Meteorological and Oceanographic Centre (METOC) Wave Data

Every 12 hours, METOC issues significant wave height analysis and prognosis fields for the Canadian east coast area and northwestern Atlantic. The area of coverage includes all regions within the study area except Davis Strait and Baffin Bay. The analyzed fields are based on available wave observations, including reports from ships and oil rigs, together with subjectively-derived wave information from Sverdrup-Munk-Bretschneider (SMB) techniques applied to analyzed pressure fields and wind speed observations. These analysis charts, containing significant wave height isopleths at 1 m intervals, have been digitized by METOC for the period 1972-82 to give the highest significant wave height and its associated period and direction for each $5^0$ latitude-longitude square. The METOC data

include seasonal ice cover effects: areas of ice cover greater than six-tenths concentration are assumed to be equivalent to land surfaces with respect to wave growth, propagation and decay.

### 2.5 Forecast Wave Data (NEDN)

Forecast wave data from the FNOC operational spectral model (SOWM) are archived at the Atmospheric Environment Service (AES). This data set is referred to as the Naval Environmental Data Network (NEDN). The model output is produced at a 6-hourly interval based on model runs at 0000Z and 1200Z. Values of significant wave height, period and direction are available. The data cover the period June 1974 to July 1984, but there are missing or incomplete months. The model characteristics are similar to those for the SOWM hindcast. However, the use of real time wind fields results in less reliable wave height values than contained in the hindcast.

### 2.6 Observed Wave Data

A large volume of ship-based observations of wave height is contained in the marine weather reports archived at AES. Although marine weather observations go back to the late 1800s in all east coast regions, sea wave observations were not reported regularly until 1949, and swell wave observations did not begin until 1959. Observed wave data have two main disadvantages for the identification of severe wave events. First, the temporal and spatial coverage of ship observations is highly variable, and will likely include a fair weather bias. Secondly, ship observations are inconsistent in terms of data quality. Jardine (1979) showed good agreement between observed and measured wave data at Ocean Weather Station 'I' in the North Atlantic. However, those observations were made by trained observers who, no doubt, had feedback from the shipborne wave recorder in operation at OWS 'I' over the same period that Jardine's comparison was carried out. An example of an inconsistency in observed wave data is particularly visible at OWS Bravo in the Labrador Sea, where the reported wave heights exhibited a well-defined upper limit of 9.5 m. During 24 years of wave observations, only 37 observations of waves greater than 9.5 m were reported, whereas over 260 observations of waves equal to 9.5 m were reported. The maximum reported wave height was 12.5 m.

### 2.7 Wind Data

Ship observations of wind speed and direction are available from the late 1800s in all of the regions in the study domain. These may be more reliable than wave observations, as many ships were equipped with wind measuring devices. However, according to Shearman, quoted in Swail and Mortsch (1984), more than 90% of wind observations are estimates based on the Beaufort scale. Even for the Hibernia location for recent years the percentage is about 75%. These data suffer from problems of spatial and temporal coverage, and probable fair-weather bias as well. Extreme value listings of ship winds were used to identify potentially severe storms for later verification. Wind and wave data from Ocean Weather Stations (OWS) Bravo (1945-72) and Delta (1946-73) were also used.

Measured wind data from island and coastal stations are potentially useful for severe storm identification, in that the data form a complete time series. Many of these stations have digitized wind records back to 1953. However, local influences can have a significant impact on observed winds. For this reason, only data from the three island stations (Grindstone, Sable and Belle Isle) were used in this study.

The AES has derived a 33-year geostrophic wind climatology (1946-78) for Canada and adjacent marine areas. The winds are derived from FNOC surface pressure data on a 381 km grid (Swail, 1985). Swail et al. (1984) found that the wind speeds in this data set were too low compared to true geostrophic winds, due to the documented under-representation of the pressure gradients (Corson et al., 1982) in the FNOC pressure data. The result is that the winds produced are close to "true" surface winds. Wind speeds at OWS "Bravo" were, on average, about 10% less than the geostrophic wind speed values. This data set has been widely used for climatological analyses and applications such as oil spill scenarios and current modeling. These winds were used in this study to determine potential severe wave events.

## 3. METHODOLOGY FOR SELECTION OF SEVERE STORMS

### 3.1 Wave Hindcasts

The SOWM and WES hindcasts were the main data sets used for this task. To summarize the hindcast data into storm events, a suitable definition of a storm had to be determined. According to Readshaw and Baird (1981), the usual practice is to define a storm as an independent event producing waves above a predetermined threshold condition. The main problem with such storm definitions is how to ensure independence. In some cases, arbitrary separations of 24 or 36 hours are specified to ensure independence. However, Readshaw and Baird (1981) considered this procedure unsatisfactory over the Canadian Atlantic continental shelf, as storms can stall there for several days. They indicated that the only satisfactory procedure was to refer to synoptic charts to determine the independence of sequential storms. Bearing these points in mind, it was decided to use 18 hours as the time period separating "independent events". Eighteen hours corresponds to 2 hindcast values below the storm threshold wave height, and was selected instead of 12 hours (the minimum separation possible), to take into account the possibility of spurious values or "spikes" in the wave hindcast record. It should be noted that this will identify independence of surface characteristics, but not necessarily of larger scale atmospheric controls. In the above context, the word "independent" refers to the meteorological independence of the severe storms. However, for extreme value analysis, the statistical independence of the storms must also be determined.

The choice of a particular threshold value is important, in that it will affect the number of storms identified in a particular region. In this study, a threshold value for significant wave height of 6.0 m was employed over all regions except Baffin Bay, where a threshold value of 4.0 m was required to identify a sufficient number of storms.

### 3.2 Ice Cover Effects

All the regions included in the study domain experienced seasonal ice coverage to some extent. However, neither the SOWM nor the WES hindcasts included ice cover effects; the models assumed open water conditions year round. One solution to this problem would have been to determine average ice cover periods at each hindcast grid point, and to consider only extreme wave events which occurred during the defined open water period. This methodology has two weaknesses. First, even though one location is ice free, ice cover remaining within a region may affect wave development and propagation considerably. Secondly, the annual variability displayed by seasonal ice cover, particularly in the more southerly regions, is significant enough that major wave-producing events could be screened out by using averaged ice cover information.

It was, therefore, decided to ignore ice cover in the selection of potential severe storms in all regions except Baffin Bay, as these regions could experience significant areas of open water throughout the winter. Baffin Bay exhibited a high probability of complete ice cover in the period December to June (Markham, 1981). Severe storms from this region were, therefore, restricted to the period from July to November.

It must be noted that ice cover effects will have to be taken into account when determining return periods associated with large wave heights. This problem is complicated by the fact that the spatial distribution of ice concentration is not independent of the storms producing larger waves. Thus, joint probability statistics apply; the application of such statistics is more difficult, and requires further investigation.

Storm files were generated for every SOWM and WES point within a region and sorted by maximum wave height and storm severity index (SSI). The SSI was calculated as the product of the mean storm significant wave height and storm duration. The top 30 storms from each sorted file were then merged and sorted to form regional files of potentially severe storms. A considerable amount of overlap existed in the regional storm files from several points picking up the same storm. This overlap was eliminated manually, and a final set of potentially severe storms was obtained from combining storms ranked 30 or above with respect to either maximum significant wave height or SSI. This yielded about 45-50 potential storms per region. During this final selection process, an additional criterion was imposed: storms with durations of less than, or equal to, 6 hours were rejected to take into account possible "spikes" in wave model output.

3.3 Other Sources

The other sources used for identification of potentially severe storms, in order of importance, were:

. METOC maximum significant wave height data
. AES geostrophic winds
. NEDN data set
. wind and wave observations from ships
. historical records

METOC maximum significant wave data and the NEDN data set were the main sources used to extend the hindcast identified up to 1982, the end date for the study period. Ranked listings of the METOC and NEDN wave data by month and by region were scanned manually, and storms selected that exceeded a determined threshold height. The selection of this height was based on the region under consideration, and the range of storm wave height values exhibited in the METOC and NEDN data. Several NEDN-identified storms were found to be spurious, with no corresponding wind speeds greater than 20 knots. In most regions, the NEDN-selected storms compared reasonably well with the METOC derived storms. However, it did not seem to perform well in the Gulf of St. Lawrence or Labrador Shelf regions.

The main source for identification of potentially severe storms prior to 1956 was the AES geostrophic wind data set. Ranked listings of wind speeds above 48 knots were obtained for each region, and extreme events selected manually. These were then used with the Bretschneider nomogram (CERC, 1977) to hindcast storm wave heights. Storms with hindcast wave heights falling in the range exhibited by the SOWM and WES-identified potential storms were then selected for inclusion in the final set of potential severe storms.

Wind and wave observations from ships were less useful for identification of severe events because of their variable spatial and temporal coverage. However, data from OWS Bravo and OWS Delta were found to be of more use. Ranked listings of wind speeds greater than 48 knots and wave observations greater than 8.0 m were generated for all regions. A lower wave threshold of 4.0 m was used for the Gulf of St. Lawrence, Davis Strait and Baffin Bay. These listings were then scanned manually for extreme wind speeds and wave heights. Quality control had to be applied during this process, as many of the extreme observations were the result of coding errors.

Copies of the Marine Observer (1924 to date), and the Mariner's Weather Log (1957 to date) were scanned for reports of severe storms and vessel sinkings. Early reports of severe weather events in these sources were found to be of limited value because of highly subjective reporting of wind and wave conditions. Storms reported prior to 1946 could not be verified by other available sources. For this reason, the study period was defined to start in 1946.

4. STORM VERIFICATION

Storm verification was carried out at two levels. First, intercomparisons were carried out between all available data sources to establish the validity of a potentially severe storm. Secondly, during the process of obtaining the surface pressure charts for potential storms, the meteorologists involved were able to judge whether the meteorological conditions were sufficient to generate an extreme wave event.

At the first level, tables were constructed to allow cross comparisons between data sources for each significant storm identified. All available data sources were used, and storms were rejected if they were unable to be confirmed by more than one source. This procedure had to be relaxed for pre-1956 storms, as the AES wind hindcast was often the only regularly available data source. Following initial verification, surface pressure charts were obtained for each potentially severe storm. For the period 1957 to 1982, Canadian Meteorological Centre surface pressure charts at 6-hourly intervals were used. Prior to 1957, surface pressure charts from the U.S. Daily Series of Synoptic Weather Maps were used. Severe wave events were confirmed by investigation of pressure gradients. Most of the identified severe storms were associated with significant low pressure systems. However, there were a few potential events where the analyzed pressure field showed little or no evidence of the pressure gradients and fetch-duration requirements needed to produce major wave events. These storms were subsequently deleted from the

list of severe events. The meteorological independence of the various storms was also established at this time.

## 5. RANKING SEVERE STORMS

It had originally been proposed to use a multiple ranking system based on SOWM and WES storm wave heights and SSI rankings to determine the final ranked sets of 30-35 worst storms in each region. However, this approach later proved to be impractical, as many of the storms identified did not have corresponding hindcast information, and because of a low correlation between SOWM and WES-identified severe storms. The only solution to this problem was to hindcast maximum wave heights for all storms.

Hindcasting was performed using the Bretschneider nomogram (CERC, 1977) with geostrophic winds derived manually from the surface pressure charts collected during the verification phase. The resulting wave hindcast values should not be considered accurate representations of actual wave conditions for several reasons. First, surface winds can differ significantly from geostrophic flow. Secondly, hindcasting with the daily series pressure charts (pre-1957) involved considerable subjective interpolation of wind speed, duration and fetch information. Thirdly, the hindcasting technique does not consider swell, which can have a considerable effect on storm wave heights. However, the main aim of this hindcasting exercise was to provide values for ranking purposes. Here, relative magnitudes are more important than absolute accuracy. Provided the hindcast procedures are applied consistently, the results should provide reasonable indications of the relative severities of the various storms. More appropriate values of the wave height will be obtained when the storms from the final list are hindcast using a particular wave model, with consistent, high-quality wind input.

## 6. DISCUSSION OF STORM SELECTION BY REGION

### 6.1 GRAND BANKS

The SOWM was found to perform well in identifying storms in this region, with 19 of the top 30 height-ranked SOWM storms making the final selection. The WES, although it did not perform as well as the SOWM, was most successful in this region, with 14 of the top 30 storms making the final severe storm set. This may be due in part to the greater number of SOWM points in the region (7 as opposed to 2). The degree of overlap between the two sets was surprisingly low, with only 11 storms common to both, out of the top 30 height-ranked storms. A total of 69 potentially severe storms were obtained for this region. A breakdown of these by data source is given in Table 1.

The SOWM storm results for this region exhibited a strong bias towards point 279/7, where 70% of the 30 top height-ranked storms were found. WES results were more or less evenly divided between the two points in the region, with point 20/1 being associated with a greater number of storm events. These results are not surprising, since the points in question are located at the eastern edge of the region. Mortsch et al. (1985) and Naval Oceanography Command (1983) show a strong gradient of wave height, increasing from west to east in this region.

### 6.2 SCOTIAN SHELF

This region included six WES hindcast points and 7 SOWM points, and is the only region where the regional storm selection capabilities of each hindcast can be fairly assessed. There was little overlap between severe storms identified by the two hindcasts. Of the top 30 height-ranked storms, only 10 cases overlapped. According to Resio (1982), there were problems with the pressure field specification over the Scotian shelf area, which produced spurious overpredictions by WES. The December 1973 and March 1974 cases were cited by Resio as examples of this problem. Problems with the pressure field may explain the low number of WES-identified storms which made it into the final set of severe storms. Only 9 of the WES-identified storms made the final list, compared with 15 from the SOWM. A total of 56 storms were verified as being potentially severe events on the Scotian shelf. The breakdown of these by data source is given in Table 1. No additional NEDN storms were obtained for this region, as these storms all coincided with the METOC-selected storms.

The hindcast-identified potentially severe storms exhibited some degree of spatial preference. For the SOWM, 33% of the top 30 height-ranked storms were associated with point 276/7, whereas 50% of

the WES top 30 storms were associated with point 6/2. Naval Oceanography Command (1983) show a gradient of increasing wave height towards the northeast along the Scotian shelf.

TABLE 1

Breakdown of Verified[2] Severe Storms by Data Source

| | Gulf | Scotian Shelf | Grand Banks | NE Nfld Shelf | Labrador Shelf | Davis Strait | Baffin Bay |
|---|---|---|---|---|---|---|---|
| SOWM | 32 | 21 | 43 | 42 | 44 | 41 | 34 |
| WES | NA | 9 | 14 | 5 | 1 | NA | NA |
| METOC | 6 | 14 | 3 | 1 | 10 | NA | NA |
| AES-GWC | 9 | 12 | 7 | 11 | 7 | 12 | 4 |
| NEDN | 3 | - | 2 | 1 | 3 | 1 | 1 |
| OWS 'B' | NA | NA | NA | NA | 7 | NA | NA |
| SHIPS | - | - | - | - | - | 9 | 1 |
| WAVERIDER | - | - | - | - | - | 1 | - |
| MAXWELL | NA | NA | NA | NA | NA | NA | 13 |
| GR'STONE | 16 | NA | NA | NA | NA | NA | NA |

## 6.3 NORTHEAST NEWFOUNDLAND SHELF

This region included six SOWM points and 2 WES points (note that even though WES point 10/1 lay outside the defined region, it was included for the purposes of severe storm identification). The SOWM performed well at identifying severe storms, with 19 of the top 30 SOWM storms being included in the final ranking. Only 7 WES storms were included, and the degree of overlap between the SOWM and the WES, eight storms, was the lowest of those regions containing WES data. As previously noted, the WES points are probably too few to adequately represent the extreme storm climate of the large areas included in the regions.

An interesting observation about this region is that the top-ranked SOWM storm (22.8 m for 25 January 1957), also ranked sixth by WES, did not make the final set. This storm produced 60 knot winds from the northwest over the region, but these were not maintained long as the system moved rapidly eastward. However, it is likely that strong winds (75 knots) to the south of the region during 24 January generated a significant swell which propagated into this region. These more complex situations could not be dealt with adequately using the Bretschneider methodology, which may explain why this storm did not make the final selection. This particular case was noted for discussion, as it represented the greatest storm wave height hindcast by SOWM for the entire study domain.

A total of 60 potentially severe storms were identified in this region for further verification, as shown in Table 1. The low number of METOC storms reflects a high degree of overlap between hindcast-identified and METOC-identified storms.

In terms of the spatial distribution of severe storms, the top 30 height-ranked SOWM storms did not show as marked a bias toward a single point as for the Grand Banks region. Severe storms were most

[2] Initial verification from other sources.

frequently associated with point 153/9 (33%), followed by points 304/7 (23%), 288/7 (20%), and 297/7 (17%). Only 2 of the top 30 SOWM storms were associated with point 303/7, and no storms with point 296/7. The severe storms identified by WES were dominated by point 10/1, as would be expected.

### 6.4 LABRADOR SHELF

A total of 72 verified potentially severe storms were identified for this region, as shown in Table 1. As in other regions, there was a low degree of overlap between the hindcasts (9 storms). In terms of performance, the SOWM worked well in this region, with 20 of the top 30 height-ranked storms making the final selection set. Spatially, SOWM point 134/9 dominated the severe storms (43%), followed by point 310/7 (20%). This is indicative of an increase in storm wave heights toward the south and east of the region (Mortsch et al., 1985; Naval Oceanography Command, 1983).

The severe storm of 12 March 1974, identified by Neu (1982) as producing the highest wave in the Labrador Sea over the period 1970-80, was ranked second by SOWM, but did not appear in the top 30 WES storm list. As for the northeast Newfoundland shelf region, the storm of 25 January, 1957 was identified as having the highest waves by SOWM. Due to inadequacies in the Bretschneider technique, this storm did not make the final selection. However,it would be advisable to consider this storm for more detailed hindcasting.

### 6.5 GULF OF ST. LAWRENCE

The Gulf of St. Lawrence was one of the more difficult regions for identifying potentially severe storms, in that the SOWM hindcast results were found to be unreliable. Therefore, greater reliance had to be placed on the AES wind hindcast and Grindstone Island winds.

Part of the SOWM's problem in this region is related to the coarse resolution used in the specification of land and sea boundaries, which has a significant effect on fetch definitions within the Gulf. However, there also appeared to be a problem with the SOWM surface winds in this region. More than 60% of the SOWM-identified severe storms did not have corresponding winds of 48 knots or greater at Grindstone Island, and 20% of the storms were not confirmed by AES hindcast winds of 48 knots or greater. This contrasts with other regions, where nearly all SOWM-identified severe storms had corresponding AES hindcast winds above that threshold. The 2 SOWM points in the Gulf showed little bias in the spatial variation of storms, with 60% identified at point 293/7, and the remainder at point 294/7.

Very few ship observations of wave height 4.0 m or greater were found for the final list of storms. This is a reflection of the fact that 10 of the 32 selected storms occurred during the months of February and March, when the mean ice concentration in the Gulf is about six-tenths or greater (Markham, 1980). If the ice cover season is extended to include January and April, then 21 of the 32 severe storms have a high probability that ice cover affected wave development. Verification of ice cover conditions for individual storms was not included in the work scope for this study. However,this will have to be addressed if these storms are to be hindcast at a later date. This process may well show a need to include additional storms in the set provided for this region.

### 6.6 DAVIS STRAIT

Selection of severe storms in this region was more biased toward the SOWM, in that the WES and METOC data sources were not available. Prior to 1956, AES hindcast winds were the main source for storm identification. Very few ship observations were found for this period. From 1976 to 1982, AES hindcast winds, NEDN wave forecast data, ship wave observations, and available waverider data were used to identify significant storms. Of these data sources, the AES wind hindcast was found to be the most successful at identifying severe wave events. A total of 64 potentially severe storms were identified, as shown in Table 1. Of the top 30 height-ranked storms in SOWM, 19 made the final list. There was a marked bias toward point 47/9 (83%), located in the southern portion of the region.

### 6.7 BAFFIN BAY

The Baffin Bay region was the most difficult for storm selection, as much of the data used in other regions was not available. The SOWM hindcast and the AES wind hindcast were the main data sources

used, supplemented by NEDN wave forecast data, ship observations and a catalogue of severe storms provided by Maxwell et al. (1980). The latter storms had been identified based on geostrophic winds derived from Arctic Weather Centre pressure analyses. A total of 53 potentially severe storms were identified for this region. Twenty-three of the top 30 SOWM storms were included in the final storm set. There was no marked spatial bias in the SOWM-identified storms. The greatest numbers of storms were associated with points 30/10 (37%),and 53/10 (30%).

This region differed from the others in that an "ice-free" period was specified from July to November in the storm selection process. However, the 5 worst SOWM storms occurring during the ice cover period are also appended to the storm list.

## 7. SUMMARY AND CONCLUSIONS

A requirement has been identified for detailed hindcasts of waves for the purpose of adequately defining extreme events such as the 100-year return period wave height, its associated period and direction. Existing data do not satisfy this requirement. The first step toward accomplishing this goal is to produce a set of about 30 of the most severe wave producing storms. That was the intent of this study. This paper has dealt mainly with the storm selection methodology for identifying potentially severe storms. Details of the climatology of these storms, including storm tracks, seasonal and annual distributions of storms, storm classification and storm location at the time of maximum intensification and maximum wave height can be found in Brown et al. (1986).

The main data sources used in the identification of potentially severe storms were the two major hindcasts for the North Atlantic Ocean - the SOWM hindcast and the WES hindcast. Other data used included measured wave data, data observed from ships, forecast wave data, hindcast winds, observed winds from island stations and ships, and historical records.

The study area comprised the marine areas off the east coast of Canada, subdivided into seven separate regions according to bathymetry, physiography, environmental conditions and offshore activity. The period over which storms were selected was 1946-1982. Prior to 1946 there were insufficient data to adequately define storms; for the period after 1982 much of the data had not yet become available.

In general, the SOWM hindcast was more successful in producing verifiable storms than the WES. This is not to say that the wave height values produced by the SOWM are more reliable than those from the WES, in general or for a particular storm. This is primarily because the SOWM provides better spatial coverage in most regions considered. Also, the WES hindcast appears to have some problems related to the specification of the pressure grid, particularly over the Scotian Shelf, which leads to the production of anomalously high waves which are not supported by other data sources.

The hindcasts were not the main data source for the Gulf of St. Lawrence, since the WES is not available for that region, and the SOWM had problems, mainly due to the poor resolution of the land/sea boundary in that area.

The next step in the procedure is to perform detailed hindcasts on the storms contained in the list to produce a set of wave height values for input to a suitable extreme value analysis model. Careful attention must be paid to generating accurate input wind fields, using all available data on surface pressures, measured surface wind speeds and directions, and atmospheric stability. Kinematic analysis of the surface wind fields is strongly recommended. Consideration must also be taken of ice cover effects. Ice cover maps must be obtained for each individual storm, and adequately incorporated into the wave model. This may change the rankings presently assigned to the storms, and may reduce the number of storms to some degree. In the Gulf, it is possible that additional storms may need to be identified. Efforts must be made to better reflect the land/sea boundaries of the area under consideration in the wave models. This is particularly true for the Gulf, but applies to parts of the Scotian Shelf and Grand Banks as well.

Only when such a subset of storms is hindcast with careful attention to these details will a reliable estimate of extreme wave events be possible.

## 8. REFERENCES


Baird, W. F. and J. S. Readshaw, 1981: A comparison of hindcast and recorded wave data. Prepared for Canada, Dept. of Fisheries and Oceans, Marine Environment Data Services Branch, Ottawa, Ont. by W. F. Baird & Associates, Coastal Engineers Ltd., Ottawa, Ont., 102 p

Bales, S.L., 1984: Development and application of a deep water hindcast wave and wind climatology. Proceedings of the International Symposium on Wave and Wind Climate Worldwide, London, England, April 12-13, 1984.

Brown, R.D., P. Roebber and K. Walsh, 1986: Climatology of severe storms affecting coastal areas of eastern Canada. Environmental Studies Revolving Funds. Report 020. Ottawa, Ontario. 233 p.

Cardone, V. J., 1969: Specification of the wind distribution in the marine boundary layer for wave forecasting. New York, NY: New York University, School of Engineering, Research Division, Technical Report TR69-1, 131 p.

Cardone, V.J. and D. Szabo, 1985: Impact of uncertainty in measurements of offshore wind on accuracy of wave hindcasts and forecasts. Proceedings of the International Workshop on Offshore Winds and Icing, Halifax, N.S., October 7 - 11, 1985, p. 42-56.

CERC. 1977. Shore protection manual. Volume I. U.S. Army Coastal Engineering Research Center. Washington, D.C.

Corson, W. D., D. T. Resio and C. L. Vincent, 1982: Wave information study for U.S. coastlines. Report I: Surface pressure field reconstruction for wave hindcasting purposes. Vicksburg, MS: U.S. Army Engineer Waterways Experiment Station, Technical Report HL-80-11, 24 p.

Cummins, W. E. and S. L. Bales, 1980: Extreme value and rare occurrence wave statistics for northern hemispheric shipping lanes. In: Spring meeting/STAR symposium of the Society of Naval Architects and Marine Engineers, Coronado, CA, June 4 - 6, 1980, p. 219 - 239.

Jardine, T. P., 1979: The reliability of visually observed wave heights. Coastal Engineering, 3(1):33 - 38.

Hasselmann, K., D.B. Ross, P.Muller and W. Sell, 1976: A parametric wave prediction model. Journal of Physical Oceanography. 6: 200-228.

Holl, M. M., and B. R. Mendenhall, 1971: The FIB methodology and application: fields by information blending sea level pressure version. Project M-167, Meteorology International Incorporated. Prepared for Fleet Numerical Weather Central, Monterey, Calif. under contract N66314-70-C-5226, 65 p.

Lazanoff, S. M. and N. M. Stevenson, 1975: An evaluation of a hemispheric operational wave spectral model. Monterey, CA: Fleet Numerical Weather Central Technical Note 75-3.

Lazanoff, S. M. and N. M. Stevenson, 1978: A twenty year northern hemisphere wave spectral climatology. In: Turbulent fluxes through the sea surface, wave dynamics and prediction, A. Favre and K. Hasselmann, eds. New York: Plenum Press, p. 547 - 563.

MacLaren Plansearch Ltd., 1984: Evaluation of the spectral ocean wave model for supporting real-time wave forecasting in the Canadian east coast offshore. Prepared under contract for the Atmospheric Environment Service, Downsview, Ontario. 87 p.

Markham, W.E., 1980: Ice Atlas. Eastern Canadian Seaboard. Atmospheric Environment Service. Downsview, Ontario. 96 p.

Markham, W.E., 1981: Ice Atlas. Canadian Arctic Waterways. Atmospheric Environment Service. Downsview, Ontario. 198 p.

Maxwell, J. B., 1980: The climate of the Canadian Arctic Islands and adjacent waters. Volume 1. Ottawa, Ont.: Environment Canada. Atmospheric Environment Service. Climatological Studies No. 30, 532 pp.

Meteorological and Environmental Planning Company, 1982: Operability analysis for the drillship Petrel on the Nova Scotia shelf. Report prepared for Canterra Energy Ltd.

Mortsch, L.D., T.Agnew, A.Saulesleja and V.R. Swail, 1985: Marine Climatological Atlas - Canadian East Coast. Downsview, Ontario: Atmospheric Environment Service, Canadian Climate Centre Report 85-11, 432 pp.

Neu, H. J. A., 1982: 11-year deep-water wave climate of Canadian Atlantic waters. Dartmouth, N.S.: Bedford Institute of Oceanography, Fisheries and Oceans Canada, Canadian Technical Report on Hydrography and Ocean Science 13, 41 p.

Pierson, W.J. and L. Moskowitz, 1964: A proposed spectral form of fully developed wind seas based on the similarity theory of S.A. Kitaigorodskii. Journal of Geophysical Research 69: 5181-5190.

Readshaw, J. S. and W. F. Baird, 1981: A discussion of procedures to estimate extreme wave heights over the Canadian Atlantic Continental Shelf. Ottawa, Ont.: Dept. of Fisheries and Oceans, Marine Environmental Data Service, Report No. 3, 76 p.

Resio, D. T., 1981: Estimation of wind-wave generation in a discrete spectral model. J. of Physical Oceanography, 11(4):510 - 525.

Resio, D. T., 1982: Assessment of wave hindcast methodologies in the Scotian Shelf, Grand Banks and Labrador Sea areas. Ottawa, Ont.: Dept. of Fisheries and Oceans, Marine Environmental Data Services Branch, Canadian Contractor Report of Hydrography and Ocean Sciences 4, 125 p.

Resio, D. T., C. L. Vincent and W. D. Corson, 1982: Wave information study for U.S. coastlines, Report 4: Objective specification of Atlantic Ocean wind fields from historical data. Vicksburg, MS: U.S. Army Engineer Waterways Experiment Station, 55 p.

Swail, V.R., L.D.Mortsch and D.A.Carr, 1984: Intercomparison of marine wind data sets. Downsview, Ontario: Atmospheric Environment Service, Canadian Climate Centre Report No. 84-15, 84 p.

Swail, V.R., and L.D. Mortsch, 1984: A review of the state- of-the-art in marine climatology on the east coast of Canada. Downsview, Ontario. Atmospheric Environment Service. Climatological Studies Number 36, 82 p.

Swail, V. R., 1985: Geostrophic wind climatology of Canadian marine areas. Downsview, Ontario: Atmospheric Environment Service. Canadian Climate Centre Report 85-9, 52 pp.

United Kingdom. Dept. of Energy, 1984: Offshore installations: guidance on design and construction. London: Her Majesty's Stationery Office.

United States. Naval Oceanography Command Detachment, 1983: U.S. Navy hindcast spectral ocean wave model climatic atlas: North Atlantic Ocean. Washington, DC: U.S. Government Printing Office, Report No. NAVAIR 50-1C-538, 375 pp.

Wilson, J.R. and W.F.Baird, 1984: An assessment of the state of knowledge of east coast offshore wave climatology. Prepared for the Royal Commission on the Ocean Ranger Marine Disaster. 87 p.

# THE NORTH EUROPEAN STORM STUDY (NESS)

P.E. Francis

(Meteorological Office, Bracknell, United Kingdom)

Project Manager, and representative of the NESS Contracting Consortium

## 1. Introduction

Numerical modelling techniques for waves, surges and currents have reached a level of accuracy which for most purposes makes hindcast data (ie obtained by running models to represent past events), superior to measured data for purposes of extreme value estimation and climate definition. Hindcast data can cover long time period and wide geographical areas, in contrast with the presently available intermittent and sparse measured data. Thus it is possible to establish an acceptable data base for the assessment of design environmental condition in any sea area. The measured data can however be used for validation purposes, thus extending their value beyond their limited duration and restricted spatial coverage. Properly constituted hindcast data carry information of importance for the estimation of environmental conditions, by resolving phenomena that are not easily detected by the examination of short periods of in situ measurements of waves and currents. For example, by correct physical modelling it is possible to detect the effects of topographic variation in a manner impossible to match without very large numbers of instruments in a wide spread network.

## 2. The Project

The North European Storm Study (NESS) is a major computer hindcast study, designed to generate a data base from which an accurate assessment can be made of environmental conditions on the European Shelf and in adjacent waters. The project is sponsored by a group of oil companies and European governmental organisations. In order to obtain a hindcast data base which would be generally acceptable within the European operating area, it has been necessary to gather a broadly based international team of experienced modellers, drawn from governmental agencies and scientific institutes with much experience in the running of hindcast studies and operational (real time) services. The wind modelling tasks are being performed by the United Kingdom Meteorological Office (MO) and the Norwegian Meteorological Institute (DNMI), using well established techniques for pressure field and wind field analysis. The wave modelling task is under the direction of experienced modellers of the Danish Hydraulics Institute (DHI) and the GKSS Forschungszentrum, Geesthact GMBH (in the Federal Republic of Germany), who will tailor an existing wave model of high scientific merit (the HYPA-S model) into a system best adapted for the project. Two well known hydraulics institutes, DHI and the Delft Hydraulics Laboratory (DHL), are jointly responsible for the surge and current hindcast task, using a versatile and much used system from DHI (the System 21). The Royal Netherlands Meteorological Institute (KNMI) is highly experienced in the gathering and interpretation of wave data, and hence is qualilfied to perform the validation assessment of the project wave model. DHL are again involved, being responsible for the statistical processing of the resultant data base. The entire project is to be managed by a small team (MO as leader, assisted by DHI and DHL), backed by the joint experience and scientific knowledge of all the key personnel.

The objective of the project is to prepare a data base of hindcast winds, waves, surge elevations and depth integrated currents over the entire North European operating area, and to use these data to develop a uniform and sound basis for design and operational criteria

in that area.

The hindcast time period will initially include the winter seasons of 1966/67 to 1985/86 and, in addition, will cover the major storm event in January-February 1953. The selection of periods to be hindcast (on average 6 months per season) will use a proven storm selection procedure to identify all major storm events during the entire 20 years, 1966/67-1985/86. In the event that storms outside of the continuous winter hindcast periods are identified by the storm selection procedure, these will be included in the data base (by individual running), up to a maximum of 40 such storms. Wave hindcasts will be continuous for the winter periods, plus the discrete storm events. Surge elevation/ current hindcasts will be performed for 200 storms.

The project will be enhanced in stages if sufficient extra funding becomes available at a later date, ie if other oil companies join the group of the funding agencies. Possible additional features would be:-

a) extending the hindcast period by up to 10 more winter seasons
b) adding up to 5 summer periods in order to obtain normal condition statistics
c) increasing the number of the significant storms that lie outside the winter seasons
d) performing continuous hindcasts for surge elevation and depth integrated currents

The basic data to be archived are required at 3-hourly intervals, covering both the coarse and fine grid areas of wave and surge models. The data include information on wind speed and direction, significant wave height, representative wave periods, dominant wave direction and directional spread. Additionally more detailed, spectral, wave information will also be archived; but the amount of data implied, if stored for every grid point, is extremely large. From the surge modelling activity the total, the tidal and the residual values of currents and surface elevations will be stored.

Extreme value statistics will be generated on data produced in the individual storms and the continuous months. These statistics will include data for 70 selected grid points, concentrating on events when wave heights exceeded 5 m. Joint occurrence tables and correlations of selected pairs of parameters will also be produced. Direction analysis will also be included, based on either or both of eight equal (45°) sections or 4 (unequal) sections identified for each of 10 sea areas. Both the 'peak over threshold' and the 'asymptotic extreme value' method of analysis for extremes will be considered. An optional analysis of equivalent design currents is also to be made available if required.

## 3. Methods - wind field preparation

In order to obtain hindcasts of sea state it is necessary first of all to adequately define the surface wind field throughout the period of study. The requirement is for two time series of wind vector fields, at 3-hourly intervals covering the chosen period, with spatial resolutions of 150 km in the North Atlantic and 30 km on the European continental shelf. The procedure to generate the wind fields consists of two main sections. Firstly to establish surface pressure fields by means of analysing available synoptic data, with the aid of suitable background numerical fields. Secondly to compute surface wind vectors from the pressure fields, using the geostrophic wind relationship and taking into account observed synoptic wind data.

The necessary data are available mainly from collections already established at the Norwegian Meteorological Institute (DNMI) and the United Kingdom Meteorological Office (MO). A variety of sources for background numerical pressure fields have already been identified (United States National Weather Service, World Meteorological Organisation, DNMI, MO and the European Centre for Medium Range Weather Forecasting).

Synoptic observations of surface pressure, surface wind, surface air temperature and sea surface temperature, are to be collated into a unified data bank for input into the various numerical analysis routines. Data for the area of previous Norwegian (DNMI) pressure analyses have already been so organised. Additional data will be collected and organised into a similar data bank.

It may be necessary to digitise a number of hand drawn synoptic surface pressure charts, in order to expand the information available from some areas where professional insight as well as observed data yields the final picture. Data from such a source can be merged with observed data during the numerical analysis. A series of charts for the Barents Sea have been analysed in this way by DNMI in an earlier exercise. An inventory of hurricane data is also available for reference, as required.

A modified Cressman scheme will be used in order to analyse the surface pressure fields. The background fields will thus be modified by the influence of weighted functions of the observed values.

From the analysis on the coarse (150 km resolution grid), a time series of pressure fields will be available from which the wind fields can be directly derived, at the correct resolution in space. Temporal interpolation will however be required, since these fields will only be analysed at 12-hourly intervals, the frequency of the background fields. A polynomial interpolation technique which ensures continuity and intensity of the pressure pattern will be employed. The final product will be at 6-hourly time intervals.

The finer mesh pressure fields are already obtainable at DNMI, with the exception of the most recent years. These fields are at 75 km resolution, at 6-hourly intervals, covering an area larger than that required for the fine mesh models. The generation of pressure fields for the surge model, at a higher spatial and temporal resolution, will be achieved by using a polynomial fitting and interpolation technique, designed to ensure the continuity of the pressure patterns.

A numerical scheme for the calculation of surface wind fields has been devised, based on well proven techniques, which uses both the digital pressure fields and the synoptic data banks assembled and processed by DNMI.

The first step in the process is the calculation of the geostrophic wind, by direct spatial differentiation of the pressure field. This process is performed numerically by transforming the differential operator into an acceptably accurate finite difference form. The next stage is to extrapolate the geostrophic wind (ie the wind in the free atmosphere, unaffected by frictional and certifugal effects) to the surface by means of well established relationship (Findlater et al, 1966).

The next step is to numerically improve these first guess wind fields by performing a single variable analysis for each of the wind components. The analysis technique has been used operationally at Bracknell for many years (up till late 1982) and is well documented (Flood 1977, Hall 1977). The wind observations from the Norwegian data bank are used to "correct" the first guess fields and produce final values which are an optimal blend of observations and pressure related winds.

In order that 3-hourly time series are obtained, and to interpolate from the intermediate to the final mesh grid, the polynomial fitting procedures of the analysis scheme are used (Flood 1977, Hall 1977). These schemes ensure continuity and intensity in space and time.

The objectively analysed winds will be subjected to a process of manual intervention, concentrating on the major storm periods. Basic checks will be carried out to ensure that the objective analyses form a realistic continuous series, and that significant features are corrected represented. Major storms will be identified during the procedure used to define the winter seasons. Up to 350 such storms will be carefully assessed, by reference to newly plotted and manually analysed charts. Continuity of analyses will be closely observed through twelve hours either side of the peak wind event in each storm. Any differences between the manual and automatic products will be reconciled by means of recalculating the numerically analyses, using additional 'bogus' observations in areas where the human analyst has decided on different interpretations of the available data.

A test of this procedure will be based on a comparison between wind fields derived as outlined above and selected manual analyses performed during the NORSWAM study (NORSWAM, 1977). Additionally, available instrumental data for 20 storms will be used in a validation exercise, incorporating both speed and direction.

The selection of stormy winter months, as well as major 'summer' storms, will be based on the so-called gale index method. The technical details of this approach are given in an accompanying paper in this workshop (Brirk-Kjaer and Nielson, 1986).

Following approval of the wind fields produced in the above trial, the main production runs will be carried out. Surface pressure, with surface wind speed and direction, will be archived for all grid points of the coarse and fine mesh wind grids at a frequency of every 3 hours.

## 4. Methods - wave hindcasts

It is proposed to use the HYPA-S wave model as a basis for the NESS wave modelling task. The HYPA (Hybrid Parametric) model for deep water has been described in Gunther et al (1979a,b) and Gunther et al (1981). The extension to shallow water is described in Gunther and Rosenthal (1983). The shallow water varsion has been previously assessed in Gunther et al (1984) and in SWIM (1985).

The proposed study involves several distinct tasks, much work being necessary before the actual hindcasts can be performed. The appropriate coarse mesh (Atlantic) and fine mesh (Continental Shelf) grids have first to be defined, and the model correctly specified to pass boundary values into the inner (fine mesh) grid. An even finer grid (10 km) has also been requested, for a trial model that covers an area of the southern North Sea. The spectral resolution of the model is to be set at 16 equally spaced directions and 14 frequencies for the non-parametric (ie swell) calculation. A variable ice edge in the North Atlantic will be taken into account by means of monthly updating the appropriate boundaries of the model. As accurate a bathymetry as possible will be established for the fine mesh model.

The accuracy of the hindcast model is to be established by comparing model variables against measurements for 20 storms, in the manner described in Bouws et al (1985). As much data as possible, from a wide variety of sources, has to be identified and collected, including spectral data since the direectional behaviour of the model is a initial factor affecting validity of the final statistical analyses. The sensitivity of the model to the forcing wind field will also be investigated at this stage, continuing the assessment of the wind field analyses against NORSWAM data as described in Section 3. The wave model will be run on both sets of winds (ie those from NORSWAM and those from the proposed NESS procedure) and then the individual results compared with available measurements.

The funding agencies will select 6 storms by which to evaluate possible errors occurring in the shallow southern North Sea, where the spatial resolution of the fine grid model may be less satisfactory. This evaluation will be made possible by using the hyperfine grid model. It is assumed that the 6 storms are included in the main production periods. Wave parameters, including directional information, will be compared at the common grid points of the fine and hyperfine grid models, using available instrumental data as a reference standard. In the event that application of a hyperfine grid in production simulations is beneficial, and its use agreed on, it is recommended that such a grid be used only for the simulation of peak sea states.

Both coarse and fine grid models, if deemed satisfactory after the validation trials, will then be run for the production phase of the project, using the winds prepared by the method described in Section 3. Three-hourly values of significant wave height, 3 period estimations, dominant wave direction, directional spreading parameter, and 2-dimensional wave spectra will be archived for every grid point of both models. In addition 3-hourly time histories of directional wave spectra for 70 pre-chosen grid points, at which statistics are to be developed during the project, are to be sequentially archived as a seperate process.

## 5. Methods - surge and current hindcasts

A depth integrated 2-dimensional model will be employed to hindcast currents and surface elevations generated by the hindcast pressure and wind fields, as well as by astronomical forcing. The model will be used to compute the total non-linear combination of meteorological and astronomical forcing as well as the tidal current and water level

variations generated by the astronomical forcing alone. The residual fields, being the difference between these two data sets, can be readily derived.

It is proposed to use SYSTEM 21 (developed by DHI) as the basis for the NESS surge/current modelling. The modelling package has the change-of-scale capability which is of practical significance for the cost-effective modelling of current conditions in the southern North Sea and in the Channel. SYSTEM 21 has already been extensively applied in earlier hindcast studies in the North Sea, and detailed model verifications have been made for the Central and Southern parts of the area of interest. The system has been used in more than 100 engineering projects.

Some modifications of SYSTEM 21 are needed to meet the Technical Specifications of the project, but there are assessed to be within the joint capabilities of the experienced staff at DHL and DHI.

The modelling system can operate fully interactively on two grids for which the mesh width of the embedded fine grid is 3 times smaller than that of the surrounding coarse grid. Mesh width of 10 and 30 km for the two grids have been selected in compliance with the technical specifications.

The simulations on the two grids will be performed simultaneously, thereby allowing full exchange of computational information between the grids. For a given time step, the model produces results of comparable accuracy at a water depth of 900 m in the coarse grid and 100 m in the fine grid. The implicit nesting of grids allows focusing on a relatively shallow area using a minimum of computational resources.

The basic structure thus becomes one that covers the European North Atlantic Shelf and part of the Atlantic Ocean with a coarse grid with a mesh width of 30 km, and the waters off Northern Norway, the North Sea and the Channel with a fine grid with a mesh width of 10 km.

The model meteorological input will consist of surface pressure and surface wind stress. The latter will be calculated using the formulation of Smithe and Banks (1975). Other input is required in the form of conditions at coarse grid open boundaries, tidal potential and bottom shear stress throughout the whole model area, and the location of the ice edge. The most recent literature on global tidal models will be examined in order to assess how to determine the tidal height and current constituents at the open boundaries. At these open boundaries weakly reflective boundary conditions will be used. The basic formulation for including the tidal potential will be according to the most recent developments in this area.

The bottom shear stress is related to the average-over-depth current speed by a quadratic law. The default Manning number before model calibration is taken as 32 $m^{1/3}/s$ throughout the model area. In earlier North Sea applications this value, with some local variations found through calibration, has been proven to provide a good reproduction of bottom shear. The influence of ice within the model area will be taken into account by neglecting the influence of wind forcing in ice covered areas. The propagation of tidal waves and pressure surges is assumed to be unaffected by the presence of ice.

An important feature of the study is the proposed validation exercise for the surge/current model. As much measured data as possible will be gathered for this purpose. The total simulation will be verified first, calibration consisting only of changes in bottom friction and boundary conditions. The validation simulation will have a minimum duration of 28 days. The tidal consitituents will be derived at 20 selected grid points from this simulation. The tidal analysis will - in addition to the 2 diurnal and 4 semi-diurnal constituents which drive the model - as a starting point make use of 15 shallow water constituents which are resolvable from a record with a duration of 28 days. A minimal set of constituents will be established which is capable of reproducing the original model time series with average RMS errors no greater than 5 per cent at any of the 20 locations studied. The ultimate set of constituents will be used to analyse all relevant grid points of the fine grid. A listing will be prepared for sites at which model constituents are to be compared with constituents derived from measurements. The number of

sites will not exceed 50 for either sea level or current comparisons.

Comparisons between model results and tidal predictions from measurements will be made for each of the individual constituents at the specified sites. Comparisons at the current meter sites will be in terms of depth mean tidal amplitude and phase for each velocity component, and depth mean tidal ellipse parameters.

In order to form the dpeth mean tidal constants from the measured currents, adjustments will be made for velocity shear in the data. The basis for these adjustments will be clearly identified.

For each of the specified sites, time history plots will be prepared which compare the total tidal signal (elevation or current as appropriate) generated from the tidal constants deduced from the measurements and those deduced from the model results. The time histories will be at least 28 days long.

The surge calculations will then be verified against measurements from 4 storms nominated by the funding agencies. The results will be analysed into their tidal and residual components using the previously established tidal constituents at each grid point.

Model residuals will be compared to residual surface elevation and current observations by plotting measured and modelled time histories. Current comparisons will be presented in terms of the north and east components. Cross correlations will be made between measured and modelled (total) surface elevations and current components. This will include both coherence squared and phase. In the case of currents, the cross correlations will be based on the rotary spectra.

Progress to the production stages of the surge/current hindcast wind only be made when the funding agencies are satisfied as to the performance of both the tidal and surge elements of the model. During production runs (a total of 200 storms in the 20 year period) an agreed procedure will be followed.

From the established tidal constituents at each grid point, the residuals will be calculated. The residuals are defined as the difference between the total signal (elevation, current component) and the tidal signal at a given time.

The simulation results will be dumped directly on to one set of archiving tapes. Isoline level plots and current field plots ("arrow plots") will be produced at regular time intervals together with plotted time series of surface elevations, current velocities and current directions in a number of selected grid points. This graphical output will be generated as a parallel activity partly as a documentation of the production simulations, but primarily as a quality control measure ensuring proper model performance and data conversion and storage. The plotted output will be analysed for any unexpected variations.

Archiving will comprise hourly total values (ie tidal plus storm signal) of elevation and two current velocity components, ie a total of 9 numbers per active grid point (water points).

For each archive tape this information will be supplemented with the information on tidal constituents at all grid points. The tidal constituents will occupy about 5-6 per cent of each tape.

6. Methods - statistical analysis

According to the hindcast procedure outlined in the previous sections, wind, wave, and surge conditions on the European North Atlantic Shelf will be simulated in a (semi)-continuous and summer storm mode for the period 1966-1985, with the addition of the storm event in January-February 1953. Summarized wind-, wave-, current-, and surge conditions (extracted from the complete hindcast data set) will be available for statistical analyses for 70 grid points, 10 in each of seven primary areas. The complete statistical analysis procedure proposed, consists of the development and archiving of extreme value statistics for wind, wave, currents and surges, for 70 grid points, from the summer storms and the continuous wintermonths hindcast. Both for all directions and 8 angular sectors of 45°.

The core of this task deals with (i) the omnidirectional analysis of all 3-hourly sea-states exceeding 5 m significant wave height by means of joint occurrence tables and non-linear regression analyses with respect to 13 storm parameter-pairs, and (ii) the omnidirectional and directional analysis of all peak sea-states exceeding a certain threshold (to be specified by the sponsors) by means of the determination of Risk diagrams for height, wind and current parameters using both the Peaks Over Threshold (POT) and Asymptotic Extreme Value (AEV) method.

For the POT-method 3 candidate Probability Distribution Functions (PDFs) will be considered (later on one will be selected for each primary area), ie Log Normal, Gumbel and Weibull (2 parameter). For the core, with the AEV-method, it is proposed to select no intervals within the wintermonths period, and to use the so-called multi-dimensional Gumbel distribution.

Three Options are proposed in addition to the core,

- Option 1: To consider a 3-parameter Weibull distribution instead of a 2-parameter for the POT-method.

- Option 2: To consider 3 intervals within the wintermonths period for the AEV-method, and to apply a compounded Gumbel distribution.

- Option 3: As Option 2, but now with the application of a compounded General Extreme Value (GEV) distribution.

The project sponsors will meet at a date within the project duration in order to decide finally on the exact form of the statistical analysis.

Results will be displayed in summary tables and computer plots. The results will be stored on two magnetic tapes and copies supplied to all sponsors as a listing of the summary hindcast parameters, the joint occurrence tables, the coefficients for the joint occurrence correlations and the extreme statistics fit parameters, for the 70 grid points considered in the statistical analysis. The software necessary to read these tapes and regenerate tables, plots and estimates of risk for given return periods, plots and estimates of risk for given return periods, will also be provided.

An enlarged statistical analysis will become possible if more sponsors join the funding group after the start of the project. In particular the addition of complete summer seasons to the hindcast periods would allow the derivation and archiving of normal condition statistics for winds and waves. Additionally there may be sufficient interest from a sub-group of sponsors in the development and archiving of equivalent design current statistics. Both these analysis would be carried out on the time series of data written up for the 70 previously selected grid points mentioned above.

## 7. Archiving arrangements

The Technical Specification from the sponsors emphasised the subject of the creation, maintenance and access for the resultant archive of NESS data. Two copies of the archive were requested, one of which the Consortium propose to keep at the Meteorological Office, the other copy to be kept at a seperate central computing facility. The Specification requests that one copy of the archive is kept in the original data format, ie arranged in a time series of geographical fields, while the other copy is re-arranged (as far as is economically possible) to give time series at individual geographical locations. Some of the data (surface pressure, wind components, integrated wave parameters) can be fully re-arranged during the production runs, but a major component (wave spectra and hourly surge/current data) can probably only be partially sorted during the production process. (In any event a fully sorted set of 70 data points will be produced for statistical processing). The Consortium intend to explore the most cost effective way of sorting the archive during the opening months of the project, when data bases of the size and complexity of those to be sorted will become available for processing.

The sponsors intend to maintain the confidentiality of the archive for 10 years from the completion of the project, allowing the Consortium access for purposes of scientific

study. The whole software ensemble used during the project is also to be archived, so that extra work of an exactly compatible nature can be commissioned if required. Further statistical processing of other data subsets is expected to be requested.

References:

Bouws, E., Komen, G.J., van Moerkerken, R.A., Peeck, H.H. and Saraber, M.J.M. 1985 "An evaluation of operational wave forecasts on shallow water". To appear in: Proc. IUCRM Synopsium on wave dynamics and radio probing of the ocean surface, Miami, 1981. Plenum Press.

Brink-Kjaer, O. and Nielson, J.B. (1986) "The establishment of a severe storms data base for the prediction of extreme environmental conditions from hindcast data".

Findlater, J., Harrower, T.N.S., Howkins, G.A. and Wright, H.L. (1966) "Surface and 900 mb wind relationships" Meteorological Office Scientific Paper No. 23. HMSO London.

Flood, C.R. (1977) "The Meeteorological Office operational objective analysis system" Meteorological Office (Met O 2b) Technical Note No. 41. (Unpublished, copy available in the National Meteorological Library, Bracknell).

Gunther, H., Rosenthal, W., Weare, T.J., Worthington, B.A., Hasselmann, K. and Ewine, J.A. (1979a) "A hybrid parametrical wave prediction model" J. Geophys. Res. 84,C9,5257-5738.

Gunther, H., Rosenthal, W. and Richter, K. (1979b) "Application of the parametric wave prediction model to rapidly varying wave fields during JONSWAP 1973" J. Geophys. Res. 84,C8,4855-4864.

Gunther, H., Rosenthal, W. and Dunckel, M. (1981) "The response of surface gravity waves to changing wind direction" J. Phys. Oceanogr. 11,No.8,718-728.

Gunther, H. and Rosenthal, W. (1983) "Shallow water surface wave model based on the TEXEL-MARSEN-ARSLOE (TMA) wave spectrum". Proceedings of the 20th Congress of the International Association for Hydraulic Research. Marlow, 1983.

Gunther, H., Komen, G.J. and Rosenthal, W. (1984) "A semioperational comparison of two parametrical wave prediction models". Dt.Hydrogr.Z. 37,89-106.

Hall, D.C. (1977) "A single variable analysis program package". Meteorological Office (Met O 2b) Technical Note No.46. Revised version 1979. (Unpublished, copy available in the National Meteorological Library, Bracknell).

NORSWAM, Numerical wave climate study for the North Sea (1977). Report No.EX 775, Hydraulics Research Station, Wallingford.

Smith, S.P. and Banke, E.G. (1975) "Variation of the sea surface drag coefficient with wind speed". Quart. J.R. Met. Soc. 101,665-673.

The SWIM Group (1985) "A shallow water intercomparison of three numerical wave prediction models, (SWIM)" Quart. J.R. Met. Soc. 111,1087-1112.

# ON THE ADEQUACY OF HINDCAST DATA IN STRUCTURAL DESIGN

Sverre Haver
Statoil, R&D Department
Stavanger, Norway

## ABSTRACT

The adequacy of the Norwegian hindcast data base is considered for Statfjord and Tromsøflaket. Emphasis is given to the wave data but the accuracy of the generated wind fields is also commented upon. Data quality is evaluated by comparing distribution functions estimated from simultaneous measurements and hindcast values. The hindcast quality is shown to depend on both season and direction. The present study shows that extreme values predicted from hindcast data generally have to be corrected before they can be applied for design purposes. Due to this a simple correction procedure is proposed. The hindcast wave data are adjusted according to this scheme and the distribution functions estimated from these values are found to be of reasonable accuracy.

## NOMENCLATURE

The symbols are generally explained as they first appear, but the meaning of the most commonly used notations is given below;

| | |
|---|---|
| $F_X(x)$ | - distribution function for X |
| $H_{mo}$, h | - significant wave height |
| $T_p$ ,t | - spectral peak period |
| $x_m$ | - observed value of a variable X |
| $x_{hc}$ | - hindcast value of X |
| $\bar{x}$ | - mean value of X |
| v | - wind speed |
| $\theta$ | - wind direction |
| $\rho$ | - coefficient of correlation |

## INTRODUCTION

The offshore oil and gas activities have resulted in a major requirement for accurate wave data. This is aimed at either by making measurements or by running a numerical model based on historical measurements of air pressure. The advantage of using numerical models is that long data series can be produced cheaply for wide areas whereas corresponding observation programs are quite expensive. On the other hand observations are generally expected to reflect the underlying processes more accurately.

Subsequently, emphasis will be given to the needs in a possible design situation, where both ultimate loads and fatigue damage are to be considered. In these cases a long term method yielding the long term distribution functions for the actual response quantities is preferable. Such an analysis is at present possible for linear structural systems only. The basic principles of this method are given in Battjes (1979) and a possible interpretation is outlined in Haver and Nyhus (1986).

A crucial part of the long term method is the availability of a reliable estimate for the joint distribution of the significant wave height, the spectral peak period, and, possibly, the spectral peak direction. An adequate measure of hindcast quality is therefore the accuracy of the estimated distribution functions. If hindcast data should be used in design we must require that the relative frequencies of at least the most

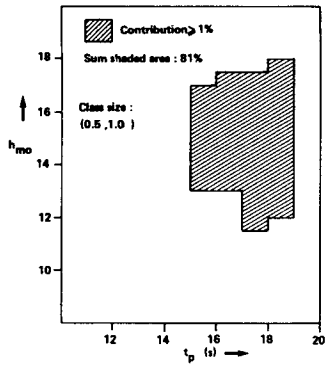


Fig. 1. The most important sea states for the shear force at mudline of a typical concrete gravity platform.

important sea states are reasonably well reproduced. The most important sea states will vary with varying response quantities, but concerning ultimate loads of todays structures the most important seas are usually those of highest waves. For the shear force at mudline of a concrete gravity based structure, this is indicated in Fig. 1 by shading the sea state classes whose contribution to the probability of exceeding the 100-year value is larger than 1 %.

## THE NORWEGIAN HINDCAST DATA BASE

### Hindcast procedure

The hindcast procedure consists of the following main steps;

- establish pressure fields for the actual area
- generate the corresponding wind fields
- generate the combined wave conditions i.e. wind sea plus swell

The area for which pressure and wind fields are established covers the North Sea, the Norwegian Sea, the Barents Sea, and the eastern part of the Atlantic Ocean. For the area of main interest a grid size of 75 km is used.

Pressure fields are established by involving both numerical models and the subjective judgement of trained meteorologists, Eide et al. (1985). The wind fields are thereafter generated by means of a geostrophic model followed by a correction procedure in order to account approximately for frictional effects. This correction procedure is tuned against measurements from the weatherships "Famita", "Mike", and "Ami", Eide et al. (1985).

The wave model used in the present study is a discrete spectral model especially modified for the actual application, Cardone (1984). A spatial resolution of 75 km is adopted for the North Sea, the Norwegian Sea and the Barents Sea, while a resolution of 150 km is used for the included part of the Atlantic Ocean. For further documentation of the wave model reference is made to Cardone (1984).

### The data base

Hindcast values for wind and waves are stored for every 6th hour during the years 1955-1985. The wave spectrum is stored only for a limited number of grid points, whereas the main characteristics are kept for all. Thus, for each grid point the data base is structured as vector time series with a time increment of 6 hours. The elements are the following characteristics:

- wind speed
- wind direction
- significant wave height (wind sea plus swell)
- spectral peak period (wind sea or swell)
- spectral peak direction (wind sea or swell)
- significant wave height for the wind sea
- spectral peak period for the wind sea
- spectral peak direction for the wind sea
- significant wave height for swell
- spectral peak period for swell
- spectral peak direction for swell

Since these parameters are available for all grid points every 6th hour during 30

years, the data base represents a unique data source for the actual waters. The potential for engineering applications is very large if the data are of sufficient accuracy.

Limitations

The adopted wave model is essentially a deep water model and shallow water effects are not properly accounted for. Model data might therefore be inaccurate in shallow waters, e.g. the southern part of the North Sea.

Concerning the model wind field, the poorest accuracy should be expected close to the coast lines because the land topography and its effect on the wind are not properly modelled. As a consequence, model waves generated in these waters should also be considered as rather rough estimates.

DATA QUALITY ASSESSMENT

Sources of uncertainties

Both bias - and random errors may be introduced at each step of the hindcast procedure. Herein emphasis is given to the bias errors and to an identification of conditions for which the data are likely to be related with such errors.

For offshore waters, the most important sources concerning bias errors are expected to be;

* imperfect wind model
* imperfect wave model
* coarse grid resolution

Although both the wind and wave models rest on theoretical foundations, they were modified empirically against observations Thus, typical situations are usually reproduced reasonably well, but this is not necessarily true for more rare meteorological events. This indicates that model adequacy should be investigated conditionally with respect to meteorological characteristics. This is also the case concerning effects of grid size since the spatial resolution is of primary importance when wind and waves are generated near narrow frontal zones.

A thorough conditional consideration is out of scope of this study. Thus, the the present work is restricted to a discussion of data quality versus season and wind direction, assuming that this will result in a certain similarity in the main characteristics.

Methods for quality assessment

Two fundamentally different approaches might be selected for an assessment of hindcast quality;

* time domain approach, i.e. simultaneous measurements and hindcast values are compared directly
* probability domain approach, i.e. the statistical properties estimated from the hindcast data are compared to those estimated from simultaneous measurements.

Methods of the first kind are the strongest ones and should be preferred if the underlying physical reasons for errors are to be identified and understood. This will be necessary if the hindcast models themselves should be improved, either in terms of the idealized mathematical models or the involved parameters.

The aim of this study is to evaluate the adequacy of an already existing data base. For such a purpose the latter approach is very convenient. It will provide information which is useful for a wide range of engineering applications of the data. In addition, input information for a more thorough consideration of model accuracy is obtained because it indicates under which situations the results are likely to be biased.

Available observations

In this project hindcast data are compared with observations from four different

locations in the North Sea and the Norwegian Sea;

* Ekofisk (1980-1985)
* Statfjord (1975-1981)
* Halten (1980-1985)
* Tromsøflaket (1976-1981)

In this paper we will briefly review the results from Statfjord and Tromsøflaket. For further details on all locations reference is made to Haver(1986).

The observed wind is the 10 minutes sustained wind velocity reduced to a height of 10 m above mean sea level. With respect to waves, the characteristics are estimated from time series of about 20 minutes duration. For both sites, the time series were achieved by means of an anchored Waverider buoy. Both wind- and wave measurements are ideally available for every third hour.

In view of the averaging times of 10 and 20 minutes, respectively, it is clear that the observations correspond to a better resolution in time than the hindcast data for which the typical averaging period is of the order of two hours. Accordingly, the measurements will show somewhat more statistical fluctuations than the hindcast data when time traces are compared. For the actual comparison these differences are not likely to affect the results too much. In a time domain approach, however, this inconsistency should be accounted for.

It should also be kept in mind that whereas observations provide estimates for values at a nearly fixed point, the hindcast procedure yields spatially averaged estimates. This might affect the results if the underlying processes are inhomogeneous.

In the future one should aim at obtaining observations being consistent with hindcast realizations regarding the lengths of averaging both in time and space. This will result in a more consistent tuning procedure or, as for the present study, a more consistent quality assessment.

## ADEQUACY OF HINDCAST DATA FOR STATFJORD AND TROMSØFLAKET

### Time domain comparison

As an introduction some results from a time domain approach are given below. Concerning wind speed, significant wave height, and spectral peak period, attention is given to the correlation coefficient and to a measure of relative deviation given as follows;

$$r_x = \frac{1}{n} \sum_{i=1}^{n} \frac{|x_{hc}^{(i)} - x_m^{(i)}|}{x_m^{(i)}} \qquad (1)$$

hc indicates hindcast value, m denotes measurement, and n is the number of simultaneous realizations. Wind direction is also considered and the time domain adequacy is indicated by the mean absolute deviation, i.e.

$$d_\theta = \frac{1}{n} \sum_{i=1}^{n} \min \left\{ |\theta_{hc}^{(i)} - \theta_m^{(i)}|, 360 - |\theta_{hc}^{(i)} - \theta_m^{(i)}| \right\} \qquad (2)$$

The result are summarized in Table 1. It is seen that the correlation coefficient, $\rho$, for wind speed and wave height is found to be 0.78 and 0.84, respectively, when all simultaneous value are included. In view of the rather large statistical variability of the observations, these values are most probably as good as we can expect for a long lasting routine run. As a threshold level is introduced the correlations are seen to

Table 1. Time domain comparison for the northern North Sea.

| Variable | No.of obs. | $\rho$ | $r_x$ | $d_\theta$ | Mean value Hc | Mean value O |
|---|---|---|---|---|---|---|
| Wind speed | | | | | | |
| all obs. | 7228 | 0.78 | 0.36 | | 9.25 | 9.40 |
| $v_m$>10 m/s | 3040 | 0.57 | 0.20 | | 12.56 | 13.92 |
| Wind direct. | | | | | | |
| $v_m$>10 m/s | 3040 | | | 18 | | |
| $v_m$>20 m/s | 185 | | | 14 | | |
| Wave height | | | | | | |
| all obs. | 6150 | 0.84 | 0.26 | | 2.75 | 2.68 |
| $h_m$ >3m | 2048 | 0.61 | 0.19 | | 4.20 | 4.38 |
| Wave period | | | | | | |
| all obs. | 6150 | 0.54 | 0.19 | | 9.09 | 9.40 |
| $h_m$ >3m | 2048 | 0.51 | 0.15 | | 10.62 | 10.74 |

decrease significantly. This is most probably a consequence of the abovementioned inconsistency between hindcast and observations with respect to the averaging period.

For the spectral peak period a rather low correlation coefficient is observed. This is mainly caused by difficulties in reproducing combined seas. Due to a rather limited frequency resolution in the hindcast spectrum, the hindcast procedure underestimates the number of swell dominated seas (i.e. sea states where the peak period is associated with a swell system). In such cases a large difference is found between the peak periods and, consequently, the correlation is reduced.

Regarding the wind direction, a mean absolute deviation of about $15^{\circ}$ is observed. Because this quantity is always larger than 0, a mean value as low as $15^{\circ}$ indicates that the wind direction is on the average reasonably well reproduced by the model.

Finally, Table 1 shows that the mean values fit very well for all variables. When all simultaneous values are included the deviations are less than some few percent.

In the context of the present time domain discussion, we will also briefly consider errors in the wind speed versus errors in the significant wave height. If a significant deviation is observed in the wind field, a corresponding deviation in the generated wave field is to be expected as well. This should be reflected in a rather high correlation between the errors in the generated wind and wave fields, at least if the generation and growth of waves are accurately modelled. The errors are given by:

$$d_w = \frac{U_m^{(i)} - U_{hc}^{(i)}}{U_{hc}^{(i)}} \qquad (3)$$

$$d_h = \frac{h_m^{(i)} - h_{hc}^{(i)}}{h_{hc}^{(i)}}$$

The deviations between averaged storm characteristics were considered for 42 storm events. Characteristic parameters were obtained by averaging over 24 hours centered around the storm maximum, i.e. averaging over 4 individual estimates. The storm characteristics are given in Table 2 and the results concerning $d_w$ and $d_h$ are shown in Table 3. The correlations are rather low, especially for southern winds. This indicates that the errors in waves can only be partly explained by the errors in the wind speed. Accordingly, the hindcast quality of wind and waves should be assessed separately.

Table 2. Wind speed and significant wave height of 42 storm periods.

| Date | Wind speed | | Wave height | | Direction |
|---|---|---|---|---|---|
| | Hc | O | Hc | O | |
| 8.12-75 | 17.65 | 23.20 | 7.62 | 8.38 | NW |
| 27.12-75 | 19.19 | 12.10 | 6.82 | 5.89 | W |
| 13.01-76 | 12.88 | 13.15 | 5.73 | 7.11 | NW |
| 15.01-76 | 6.42 | 12.55 | 3.54 | 8.48 | S-W |
| 22.01-76 | 13.54 | 11.58 | 6.63 | 6.20 | N-NW |
| 24.01-76 | 18.57 | 17.95 | 7.57 | 7.31 | N |
| 29.01-76 | 17.87 | 18.82 | 4.27 | 6.38 | S |
| 23.02-76 | 20.00 | 23.08 | 6.39 | 7.51 | S |
| 25.02-76 | 19.39 | 19.33 | 6.91 | 7.13 | W |
| 20.03-76 | 14.90 | 19.50 | 2.80 | 7.13 | S |
| 28.11-76 | 20.22 | 20.50 | 6.12 | 6.58 | S-SW |
| 7.12-76 | 11.93 | 17.48 | 3.35 | 6.28 | S-SE |
| 1.04-76 | 16.72 | 25.23 | 6.02 | 9.72 | S |
| 15.09-77 | 15.64 | 15.56 | 6.25 | 6.99 | NW |
| 21.11-77 | 17.27 | 18.10 | 7.67 | 6.46 | N |
| 11.12-77 | 16.77 | 25.38 | 6.20 | 7.68 | S-SE |
| 5.02-78 | 15.63 | 22.58 | 4.55 | 5.77 | S-SE |
| 17.02-78 | 10.72 | 18.80 | 4.52 | 5.53 | N |
| 23.02-78 | 15.46 | 20.73 | 3.12 | 4.77 | S-SE |
| 20.03-78 | 18.10 | 30.45 | 4.28 | 9.54 | S |
| 17.09-78 | 22.40 | 22.20 | 7.03 | 7.60 | W |
| 3.03-79 | 17.54 | 15.48 | 5.88 | 5.58 | W-SW |
| 25.10-79 | 14.28 | 19.83 | 4.48 | 6.02 | S |
| 31.10-79 | 15.71 | 24.20 | 5.40 | 8.19 | S |
| 3.11-79 | 20.99 | 20.95 | 5.96 | 7.10 | S |
| 5.12-79 | 21.54 | 21.53 | 7.20 | 6.97 | W-NW |
| 13.12-79 | 19.00 | 24.03 | 6.07 | 8.51 | S |
| 4.01-80 | 18.63 | 18.50 | 3.74 | 8.54 | S-SE |
| 14.01-80 | 15.98 | 15.50 | 6.94 | 7.49 | N |
| 21.01-80 | 14.37 | 18.38 | 4.01 | 5.70 | S |
| 21.02-80 | 16.85 | 17.21 | 5.04 | 6.25 | S |
| 2.03-80 | 15.44 | 13.80 | 5.74 | 5.89 | NW-N |
| 12.03-80 | 17.11 | 15.80 | 5.27 | 7.47 | S |
| 19.04-80 | 17.53 | 19.45 | 6.56 | 7.91 | N |
| 28.02-81 | 13.68 | 12.71 | 4.31 | 5.92 | S-SE |
| 28.03-81 | 17.92 | 15.31 | 4.37 | 7.27 | S-SE |
| 30.04-81 | 19.73 | 21.69 | 8.56 | 6.91 | NW |
| 4.11-81 | 21.28 | 17.00 | 7.73 | 8.29 | W |
| 13.11-81 | 18.23 | 14.49 | 6.50 | 6.06 | W |
| 24.11-81 | 26.42 | 24.19 | 9.46 | 8.27 | NW |
| 5.12-81 | 17.70 | 12.72 | 7.27 | 6.49 | NW |
| 20.12-81 | 21.00 | 20.13 | 4.57 | 8.16 | S-SE |

## Wind statistics

The quality of hindcast wind speed is indicated by showing some percentage points

Table 3. Characteristics of $d_w$ and $d_h$

| Direction | $d_h$ Mean | $d_h$ Std | $d_w$ Mean | $d_w$ Std | $\rho$ | No.of obs. |
|---|---|---|---|---|---|---|
| All | 0.13 | 0.29 | 0.31 | 0.43 | 0.55 | 42 |
| SW-SE | 0.25 | 0.29 | 0.59 | 0.42 | 0.39 | 22 |
| NW-N | 0.06 | 0.24 | 0.02 | 0.14 | 0.51 | 13 |

versus direction in Fig. 2. The accuracy is seen to vary clearly with direction. For Statfjord a significant underestimation of wind speed is observed for wind from south-southeast and to some extent for wind from northwest. At Tromsøflaket the model seems to overestimate wind from south to west, whereas the median for wind from north seems to be underestimated.
The observed underestimations may be a result of an insufficient spatial resolution but further work is necessary before the deviations are completely understood.

Finally, the number of observations versus direction are compared in Fig. 3. It is clear from these figures that the model reproduces these distributions with reasonable accuracy.

Joint distribution of wave characteristics.

Since available wave measurements do not include wave direction, emphasis is subsequently given to the joint distribution

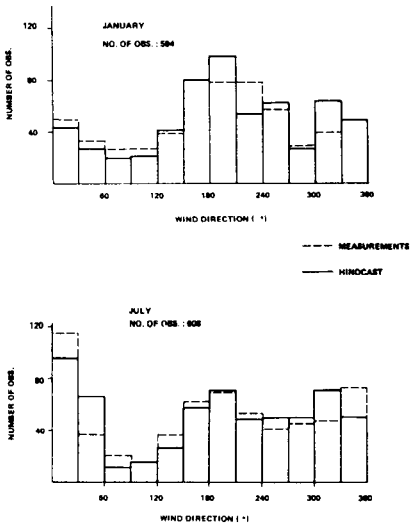


Fig. 3. Histograms for wind direction at Statfjord.

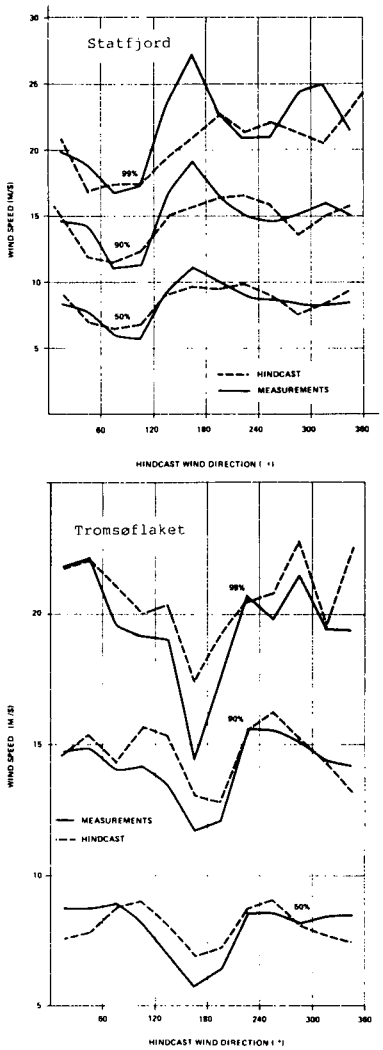


Fig. 2. Percentage points for the wind speed versus direction.

of significant wave height, $H_{mo}$, and spectral peak period, $T_p$. This distribution is conveniently written;

$$F_{H_{mo}T_p}(h,t) = F_{H_{mo}}(h)\, F_{T_p|H_{mo}}(t|h) = F_{T_p}(t)\, F_{H_{mo}|T_p}(h|t) \quad (4)$$

$F_X(x)$ denotes the marginal distribution of a variable X and $F_{Y|X}(y|x)$ denotes the conditional distribution of a variable Y given X.

The marginal distribution functions for $H_{mo}$ and $T_p$ are shown in Figs. 4 and 5,

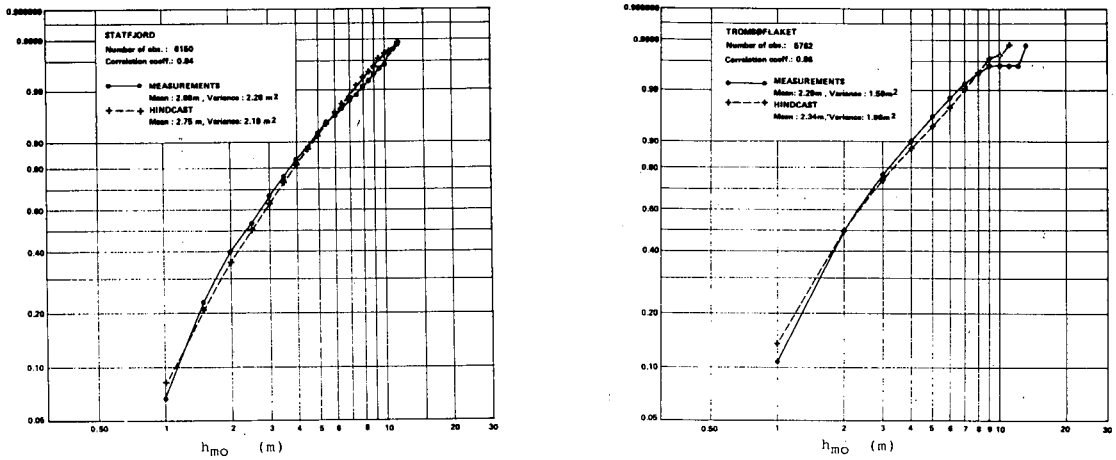


Fig. 4. Distribution functions for the significant wave height

respectively. Regarding the wave height, a reasonable good fit is obtained for both locations. However, for both sites the relative frequencies of events with h >8 m seem to be slightly underestimated and this might affect a possible extreme value prediction. The discrepancies are on the other hand so small that their importance is limited for engineering applications like preliminary design,comparative studies of structural concepts, etc..

With respect to the spectral peak period a reasonable fit is obtained for a central 80 % interval. The lower tail region is seen to be reproduced somewhat less accurately, whereas for the long periods the hindcast distributions deviate very much from those estimated from observations. This was also indicated by the time domain approach (p. 5) and the deviations are explained previously. The largest deviation is observed for the northern North Sea. This seems reasonable

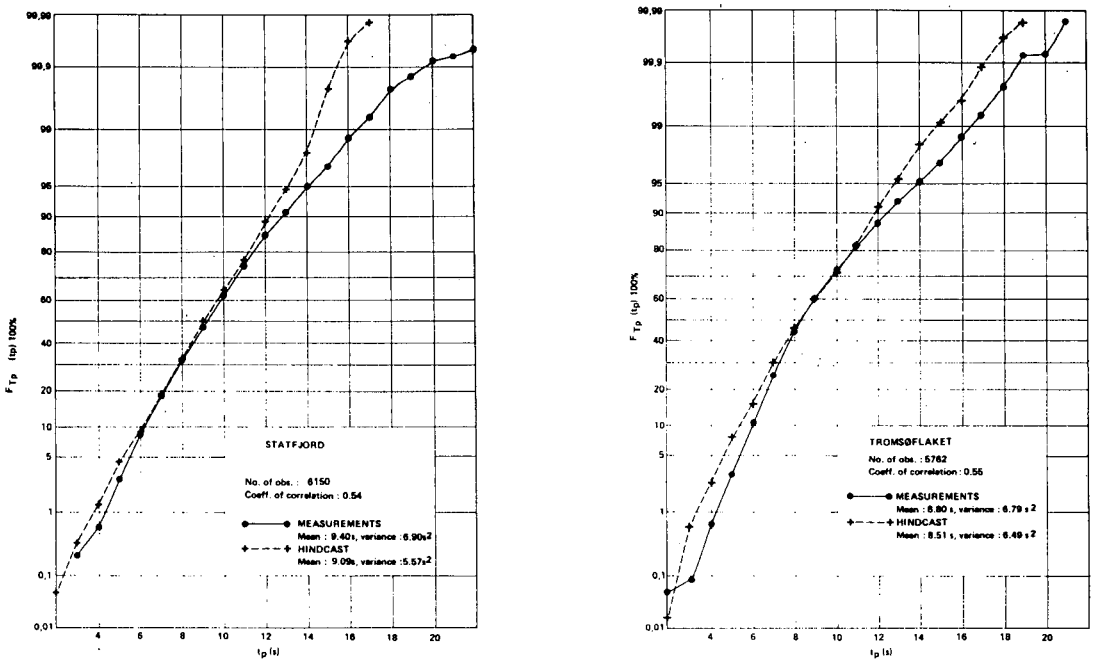


Fig. 5. Distribution functions for the spectral peak period.

since this area is frequently exposed to wind sea from the south and swell from the Atlantic.

This bias is mainly pronounced for low and to some extent moderate seas since these frequently are of a combined nature. It is not too important concerning design, which typically involves the most extreme sea states. The most important seas in this connection are furthermore often located well inside a central range of the conditional distribution of $T_p$ given $H_{mo}$, see Fig. 1. The fit within this range can be indicated by considering the conditional mean for the spectral peak period shown in Fig. 6. For Tromsøflaket a very good fit is observed, while for Statfjord the conditional mean period of severe seas seems to be slightly overestimated. This overestimation is most probably smaller than 1 s but in many applications it has to be accounted for if an optimum design shall be achieved.

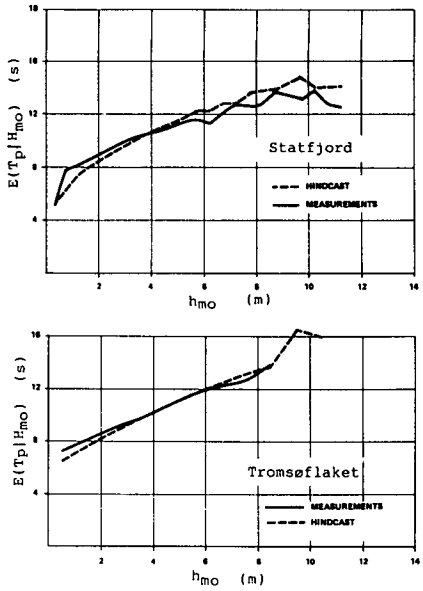


Fig. 6. Conditional mean for the spectral peak period.

Wave height versus wind direction and season

The varying data quality with respect to season and wind direction is indicated by Figs. 7 and 8. In order to reduce the random errors, the data were pooled into wider sectors, within which the bias errors were assumed to be more or less constant. For the locations included in this study, the following sectors seem to be a reasonable choice, Haver (1986);

* Northern North Sea
  - $30^o$-$120^o$
  - $120^o$-$210^o$
  - $210^o$- $30^o$
* Tromsøflaket
  - $0^o$-$120^o$
  - $(120^o$-$210^o) \cup (300$-$360^o)$
  - $210^o$-$300^o$

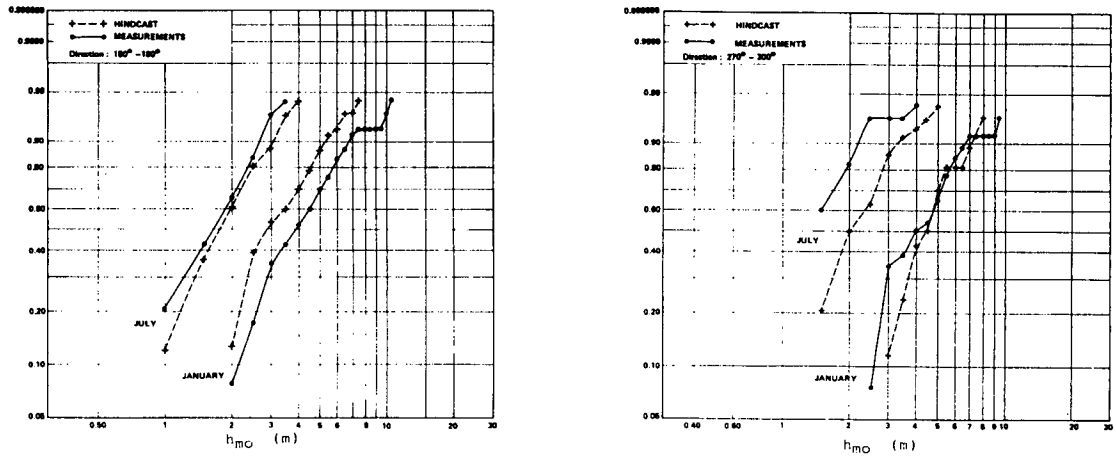


Fig. 7. Distribution functions for the significant wave height for various directions and seasons. Statfjord.

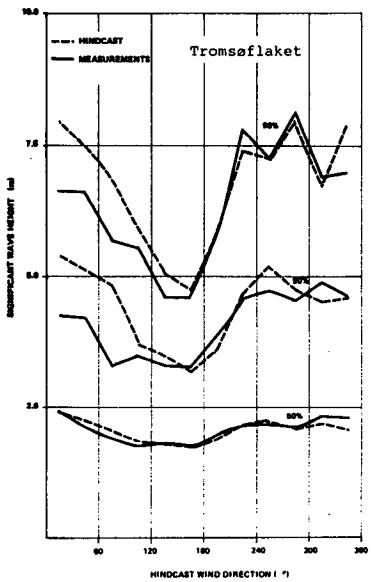


Fig. 8. Percentage points for the significant height versus direction.

Monthly means for the significant wave height for these sectors are given in Table 4. From Table 4 the most important results are;

* on the average the significant wave height is overestimated within the summer season
* for Statfjord seas from south are significantly underestimated during the cold season
* at Tromsøflaket seas from North to East are significantly overestimated, while seas form south and northwest are slightly underestimated during the winter season.

## ADJUSTED HINDCAST VALUES

### Adjusting procedure

The errors in means indicated by Table 4 are of course affected by random errors and the aforementioned inconsistency between hindcast and measurements. However, in cases where the same tendency is found over a range of neighbouring months, it is reasonable to assume that the deviation is of a systematic nature.

In order to reduce the random errors and correct the data for the bias errors, smoothed correction factors are also given in Table 4. Hindcast values corrected for the deviations in means are then obtained by;

$$\hat{h}_{hc} = h_{hc} / c \qquad (6)$$

where $h_{hc}$ is the original hindcast and c is the correction factor given in Table 4.

In general a simple mean value correction, Eq.(6), will not be enough if an accurate fit shall be obtained. The variances of hindcast values and observations may differ significantly. If so it has to be accounted for if a reasonable fit shall be obtained in the tail regions of the distribution functions.

For the locations considered in this paper, Eq.(6) seems to result in distribution functions of reasonable accuracy except for the one describing seas from south during the cold season at Statfjord. For this case the following additional correction is obtained by comparing corresponding

Table 4. Monthly means for the significant wave height.

STATFJORD:

| Month no. | 30 - 120° | | | c | 120 - 210° | | | c | 210 - 390° (30°) | | | c |
|---|---|---|---|---|---|---|---|---|---|---|---|---|
| | $\bar{h}_m$ | $\bar{h}_{hc}$ | $\bar{h}_{hc}/\bar{h}_m$ | | $\bar{h}_m$ | $\bar{h}_{hc}$ | $\bar{h}_{hc}/\bar{h}_m$ | | $\bar{h}_m$ | $\bar{h}_{hc}$ | $\bar{h}_{hc}/\bar{h}_m$ | |
| 1 | 3.10 | 3.02 | 0.97 | 1.00 | 3.81 | 3.08 | 0.80 | 0.81 | 4.16 | 4.19 | 1.01 | 1.00 |
| 2 | 2.33 | 2.28 | 0.98 | | 3.52 | 2.92 | 0.83 | | 3.38 | 3.46 | 1.02 | |
| 3 | 3.01 | 2.75 | 0.91 | 0.95 | 3.68 | 3.25 | 0.88 | 0.93 | 3.28 | 3.47 | 1.06 | 1.09 |
| 4 | 1.89 | 1.78 | 0.94 | | 2.46 | 2.41 | 0.98 | | 2.77 | 3.04 | 1.10 | |
| 5 | 1.39 | 1.61 | 1.16 | 1.15 | 1.84 | 2.08 | 1.13 | 1.13 | 1.99 | 2.36 | 1.19 | 1.18 |
| 6 | 1.27 | 1.49 | 1.17 | | 1.41 | 1.56 | 1.11 | | 1.85 | 2.08 | 1.12 | |
| 7 | 1.23 | 1.37 | 1.11 | | 1.52 | 1.75 | 1.15 | | 1.66 | 2.05 | 1.23 | |
| 8 | 1.38 | 1.53 | 1.11 | | 1.65 | 1.53 | 0.93 | | 1.79 | 1.93 | 1.08 | |
| 9 | 2.10 | 1.92 | 0.91 | 0.95 | 2.50 | 2.69 | 1.08 | 0.93 | 3.00 | 3.25 | 1.08 | 1.09 |
| 10 | 2.26 | 2.30 | 1.02 | | 3.08 | 2.79 | 0.91 | | 3.03 | 3.51 | 1.16 | |
| 11 | 2.72 | 2.89 | 1.06 | 1.00 | 3.34 | 3.09 | 0.93 | | 3.87 | 4.16 | 1.07 | |
| 12 | 2.55 | 2.42 | 0.95 | | 3.96 | 3.34 | 0.84 | | 3.80 | 4.21 | 1.11 | |

TROMSØFLAKET:

| Month no. | 0 - 120° | | | c | 210 - 300° | | | c | (120-210°)∪(300-360°) | | | c |
|---|---|---|---|---|---|---|---|---|---|---|---|---|
| | $\bar{h}_m$ | $\bar{h}_{hc}$ | $\bar{h}_{hc}/\bar{h}_m$ | | $\bar{h}_m$ | $\bar{h}_{hc}$ | $\bar{h}_{hc}/\bar{h}_m$ | | $\bar{h}_m$ | $\bar{h}_{hc}$ | $\bar{h}_{hc}/\bar{h}_m$ | |
| 1 | 3.16 | 3.49 | 1.10 | 1.10 | 3.17 | 3.19 | 1.01 | 1.00 | 3.24 | 3.02 | 0.93 | 0.92 |
| 2 | 2.77 | 2.91 | 1.05 | | 3.31 | 3.49 | 1.05 | | 2.70 | 2.47 | 0.91 | |
| 3 | 2.60 | 2.70 | 1.04 | 1.00 | 2.77 | 2.63 | 0.95 | 1.00 | 2.59 | 2.49 | 0.96 | 0.95 |
| 4 | 2.36 | 2.43 | 1.03 | | 2.41 | 2.35 | 0.98 | | 2.22 | 2.02 | 0.91 | |
| 5 | 1.72 | 1.74 | 1.01 | 1.09 | 1.98 | 2.02 | 1.02 | 1.14 | 1.63 | 1.57 | 0.96 | 1.07 |
| 6 | 1.66 | 1.79 | 1.08 | | 1.85 | 2.11 | 1.14 | | 1.57 | 1.65 | 1.05 | |
| 7 | 1.34 | 1.46 | 1.09 | | 1.19 | 1.36 | 1.14 | | 1.15 | 1.24 | 1.08 | |
| 8 | 1.43 | 1.43 | 1.00 | 1.00 | 1.46 | 1.58 | 1.08 | 1.04 | 1.38 | 1.38 | 1.00 | 1.00 |
| 9 | 2.08 | 2.00 | 0.96 | | 1.85 | 1.79 | 0.97 | | 1.89 | 1.87 | 0.99 | |
| 10 | 2.53 | 2.63 | 1.04 | 1.16 | 2.67 | 2.82 | 1.06 | 1.00 | 2.43 | 2.50 | 1.03 | 0.97 |
| 11 | 2.80 | 3.30 | 1.18 | | 3.98 | 3.99 | 1.00 | | 2.43 | 2.45 | 1.01 | |
| 12 | 3.05 | 3.47 | 1.14 | | 2.97 | 2.91 | 0.98 | | 2.76 | 2.59 | 0.94 | |

percentage points, Haver(1986);

$$\hat{\hat{h}}_{hc} = 1.52\,\hat{h}_{hc} - 0.7\,\bar{h}_{hc}/c \quad ; \quad h_{hc}/\bar{h}_{hc} > 1.4 \qquad (7)$$

where $\bar{h}_{hc}$ and c are taken from Table 4.

The adjusting procedure is formulated under the requirement that the fit of the marginal distribution of $H_{mo}$ should at least be as good as the one obtained for the original hindcast data. For Statfjord, the distribution function estimated from the adjusted hindcast values is compared to the one from observations in Fig. 9. It is seen by consulting Fig. 4 that the fit has been slightly improved by application of the adjusting procedure.

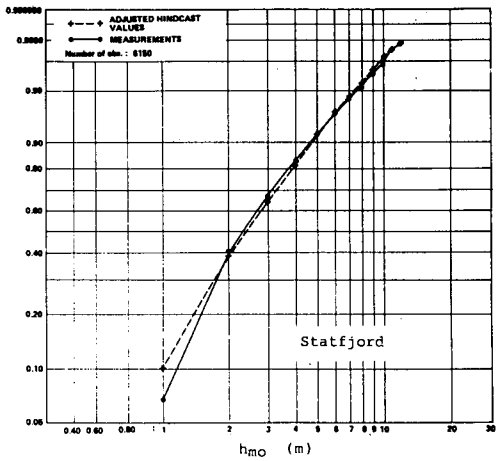


Fig. 9. Distribution functions for the significant wave height.

Extreme sea states

In this section the adequacy of the adjusted hindcast data is considered briefly by predicting 100-year values for the significant wave height under various conditions. To which extent the actual samples are representative for the long term wave conditions is not considered herein and too much attention should not be given to the absolute values. The extremes are obtained by fitting a Weibull model to the upper tail of the estimated distribution functions. The results are given below where O and Ahc denotes observations and adjusted hindcast values, respectively.

* Marginal extremes

| | Statfjord | Tromsøflaket |
|---|---|---|
| O | 14.9 m | 13.2 m |
| Ahc | 14.5 m | 13.0 m |

* Seasonal extremes

- Winter (November - February)

| | Statfjord | Tromsøflaket |
|---|---|---|
| O | 14.3m | 12.5-13.5m |
| Ahc | 13.9-14.5m | 12.5-13.0m |

- Summer (May - August)

| | Statfjord | Tromsøflaket |
|---|---|---|
| O | 8.0-8.8m | 7.8-8.2m |
| Ahc | 7.6-9.0m | 8.0-8.2m |

- Spring/Autumn

| | Statfjord | Tromsøflaket |
|---|---|---|
| O | 11.0-14.0m | 9.8-10.5m |
| Ahc | 12.0m | 9.7-10.6m |

* Seasonal extremes for given directions

Two sectors with respect to the hindcast wind direction are included; $135^{o}$-$225^{o}$ (south) and $270^{o}$-$360^{o}$ (northwest). For the winter in the southern sector the distribution functions are shown in Fig. 10. It is encouraging to observe that a reasonable good fit is obtained by means of the rather simple correction procedure, Eqs.(6 and 7). This is also indicated by the predicted 100-year values for $H_{mo}$ which are given below.

- $135^{o}$-$225^{o}$ (Statfjord)

| | Summer | Winter | Spring/Autumn |
|---|---|---|---|
| O | 5.8m | 14.6m | 13.1m |
| Ahc | 6.3m | 15.0m | 12.8m |

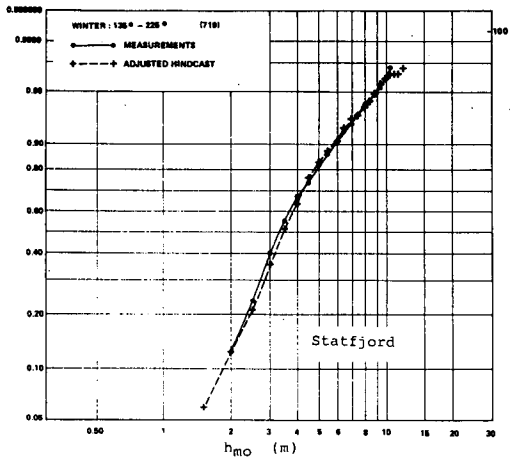


Fig. 10. Distribution functions for the significant wave height.

- $270^{o}$-$360^{o}$ (Statfjord)

| | Summer | Winter | Spring/Autumn |
|---|---|---|---|
| O | 8.7m | 12.5m | 11.2m |
| Ahc | 9.7m | 12.5m | 11.2m |

CONCLUSIONS

The accuracy of hindcast data generated for Statfjord and Tromsøflaket is considered. Emphasis is given to a comparison of the distribution functions estimated from simultaneous observations and hindcast values, respectively. However a time domain comparison is included as an extended introduction.

The main results of the present study may be summarized as follows;

* For both sites the correlation coefficient between observed and hindcast wind speeds is found to be 0.78. In view of the rather large statistical variability in the observations due to the 10 min. averaging time , this indicates that most of the main wind variations are reflected by the model.

* For Statfjord a significant underestimation of the wind speed is observed from a south - southeasterly sector and to some extent from a northwesterly sector. At Tromsøflaket the model overestimates winds from south to west.

* The statistical properties of wind direction are reproduced with an accuracy being sufficient for most practical applications.

* A rather low correlation is observed between the error in wind speed and the error in significant wave height, indicating that errors in the wave fields are only partly caused by errors in the wind fields.

* The marginal distribution functions for the significant wave height are reproduced quite well. However, the relative frequencies of severe seas (h >8 m) seem to be slightly underestimated. This together with a slight overestimation of the percentage points corresponding to moderate seas, results in biased estimates for the extremes.

* For Statfjord the conditional mean for the spectral peak period given the significant wave height seems to be overestimated with about 1 s for the most severe seas. At Tromsøflaket the deviation is most probably somewhat smaller. The scatter around the mean is typically underestimated by the model due to an underestimation of the number of swell dominated seas (i.e. cases where the maximum measured spectral density is associated with a swell system). Fortunately, the bias is most clearly pronounced for rather low seas which are not so important in structural design.

* The adequacy of the hindcast wave height is found to vary both with direction and season. Typically;

- seas are overestimated during the summer
- seas from south are significantly underestimated during the cold season at Statfjord
- seas form north to east are significantly overestimated at Tromsøflaket.

* Application of a rather simple correction procedure seems to produce distribution functions of sufficient accuracy for most practical applications. This is a very encouraging result concerning the future use of the data base because of the implied possibility to combine the "true" information included in relatively short time series of observations with the long term information included in the hindcast data.

In view of these findings it can be concluded that without corrections hindcast data are not accurately enough for final structural design. For such purposes the value of the hindcast data base is primarily that it reduces the need of long-lasting observation programs.

REFERENCES

Battjes, J.A. (1979): "Long Term Wave Statistics", Second WEGEMT Course, The Norwegian Institute of Technology, Trondheim.

Cardone, V. (1984): "WINCH2 - User's Guide", (Unpublished), Oceanweather Inc./ The Norwegian Meteorological Institute.

Eide, L.I., Reistad, M. and Guddal, J. (1985): "Hindcast database of wind- and wave parameters for the North Sea, the Norwegian Sea, and the Barents Sea", (in Norwegian),The Norwegian Meteorological Institute, Oslo/Bergen

Haver, S. (1986): "On the Adequacy of the Norwegian Hindcast Database for Ekofisk, Statfjord, Haltenbanken and Tromsøflaket", (Restricted), Statoil, R&D-dep., Stavanger.

Haver, S. and Nyhus, K.A. (1986): "A Wave Climate Description for Long Term Respons Calculations", Proceedings from the 5th International Offshore Mechanics and Arctic Engineering Symposium, Tokyo.

## F-5 The Specification of Univariate Extremes and Multivariate Scenarios from Spatial Fields

*Donald T. Resio*

In recent years considerable emphasis has been placed on the acquisition and interpretation of environment data fields using remote sensing technology and/or numerical models; however, little effort has been spent on the quantitative analysis of these data sets in terms of climatological statistics. A new technique has been developed explicitly for the statistical analysis of data from spatial fields and has been successfully applied to the analysis of extreme waves in hurricanes (Resio and Berek, 1985) and extreme winds in extratropical storms (Resio, 1985). In this paper, the new technique is explained and analyzed in terms of major differences between extremes predicted by this technique and those predicted by analyses of data from an individual site. Discussion is also given of the implications of mixed populations due to samples taken from different regions of a storm in site-by-site analyses. A variation of the analysis of univariate extremes is shown to permit a nonlinear multivariate analysis of environmental data fields. This multivariate technique is quite data adaptive and can provide substantial insight into the natural organization of simultaneously occurring parameters. To demonstrate this statistical tool, an analysis of wave heights, periods and directions, and coincident wind and current speeds and directions in hurricanes will be given.

### References

Resio, D.T., 1985: A new technique for the estimation of extreme wind speeds. *Proc., International Workshop on Offshore Winds and Icing*, Halifax, 329-338.

Resio, D.T., and E.P. Berek, 1985: Joint probability estimation of oceanographic and meteorologic conditions in hurricanes. Presented at The Oil Industry International Exploration & Production Forum, Workshop Meeting on the Application of Joint Probability of Metocean Phenomena in the Oil Industry's Design Work, London, England.

# A REVIEW OF EXTREME WAVE HEIGHT STUDIES FOR THE CANADIAN BEAUFORT SEA

M.A. Murray[+], M.A. Maes[+] and L.R. Muir[*]

+ Det norske Veritas (Canada) Ltd., Calgary

* Environmental Protection Branch, Canada Oil and Gas Lands Administration, Ottawa

## INTRODUCTION

During the past 25 years or so, the Beaufort Sea has been the scene of much hydrocarbon exploration activity. These efforts have been supported by a constantly improving description of all of the environmental hazards confronting safe operations. Although ice is generally regarded as posing the greatest threat of disruption to activities, recent experience has shown that wave action is also of considerable importance, affecting not only structural adequacy, but also installation procedures and the selection of operational equipment. For example, severe storm-induced waves caused the temporary evacuation of the Tarsiut site in July 1982 and eroded a 1-m depth of gravel fill at the base of the caisson. More recently in the late summer of 1985, a complete drilling rig was lost due to storm seas at the Minuk I-52 well site. Both of these events emphasize the need for a sound knowledge of the wave climate to ensure safe economic construction and operation of offshore exploration and, eventually, production facilities in the area.

A number of studies have been undertaken during the past 15 years to quantitatively describe the wave climate in the Beaufort Sea in order to establish suitable design criteria. However, there is a wide disparity in the results obtained in these studies, in particular the values of extreme significant wave height associated with different return periods. Broadly speaking the disparities are largely due to the use of different data bases and methods to arrive at extreme values. Of the six publicly available studies all but one used parametric hindcasting methods, the exception being a SeaConsult study Hodgins et al (1981) which adopted a spectral approach in conjuction with an assumed prototype storm. A pictorial comparison of extreme value distributions of significant wave height for all six studies is shown in Figure 1 where it can be seen that the difference between the SeaConsult results and the closest parametric model is almost as large as the difference within the group of parametric studies. In fairness Hodgins (1983), in the course of a review of available studies, made a number of recommendations in respect of the 1981 SeaConsult study that he contended would reduce their estimates by 30%. Given the differences in methodologies and extreme wave estimates the Environmental Studies Revolving Fund commissioned a study whose objective was to identify shortcomings and uncertainties associated with the best of the parametric studies and the 1981 SeaConsult study and suggest possible improvements. This study by Murray and Maes (1985) forms the basis of the present paper.

## THE BASIS FOR THE COMPARISON

The 1980 Hydrotechnology study (Baird and Hall, 1980) is widely regarded as the best of the publicly available parametric studies not only because of the longer data base of wind records available to it at the time that the study was performed, but also the care with which the hindcasting was implemented. In reviewing the Hydrotechnology and SeaConsult studies it is important to recognise that they differed in their terms of reference as well as their means of execution. Hydrotechnology were commissioned by Gulf Canada Resources to develop a wind wave hindcast procedure to improve the definition of the normal wave conditions in the Beaufort Sea. The extreme wave analysis given for six locations (shown as A - F in Figure 2), appears to have been a by-product rather than the principal objective of their study. SeaConsult on the other hand were commissioned by Esso Canada Resources to provide an estimate of the upper bounds of wave heights and storm surge levels at ten locations (labelled 1-10 in Figure 2) with return periods of 10, 50 and 100 years. This study was conducted as a joint effort between SeaConsult and the Danish Hydraulic Institute (D.H.I), who were responsible jointly for

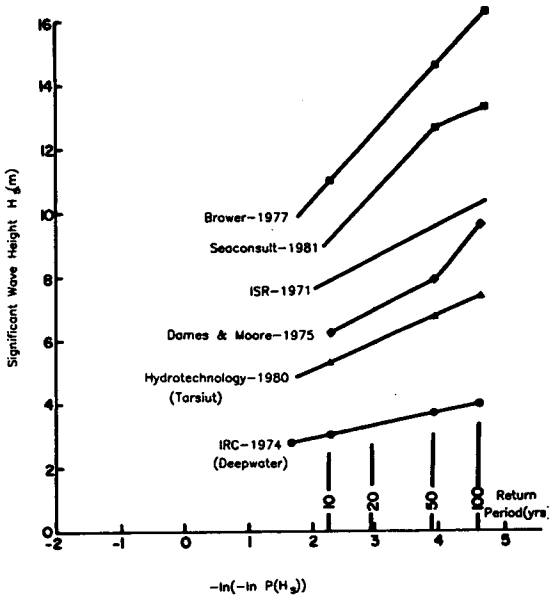


**Figure 1 Comparison of Extreme Value Distribution of Significant Wave Heights for the Canadian Beaufort Sea from Various Hindcast Studies**

the water level hindcasting, while the Meteorological and Environmental Planning Company Ltd. (M.E.P) had responsibility for the meteorological hindcasting.

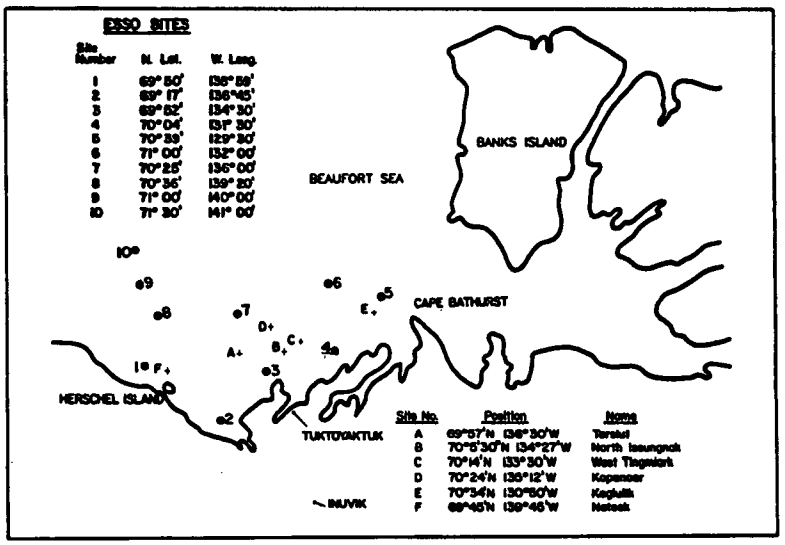


**Figure 2 The Location of the 6 Hydrotechnology sites (A - F) and 10 SeaConsult Locations (1 - 10)**

Despite the differing objectives of the studies it is possible to compare them by examining five distinct aspects of wave hindcasting namely:

- storm/event selection
- wind-field methodology
- wave model application
- verification effort
- statistical estimation techniques

Each of these aspects directly affects, by varying amounts, the accuracy of the extreme wave height estimate. Accordingly, following a brief summary of the respective study methodologies, each aspect is discussed in turn before an attempt is made to quantify the magnitude of any errors or uncertainties associated with them.

**SUMMARY OF THE HYDROTECHNOLOGY APPROACH**

Hydrotechnology hindcast the ten open water seasons 1970-79 for six different sites using the dimensionless Bretschneider (1973) wave hindcasting equations. These equations have the form;

$$\frac{gH}{U^2} = 0.283 \tanh\left[0.530\left(\frac{gd}{U^2}\right)^{0.75}\right] \tanh\left[\frac{0.0125\left(\frac{gF}{U^2}\right)^{0.42}}{\tanh\left[0.530\left(\frac{gd}{U^2}\right)^{0.75}\right]}\right] \quad \text{(Eq.1)}$$

$$\frac{gT}{2\pi U} = 1.20 \tanh\left[0.833\left(\frac{gd}{U^2}\right)^{0.375}\right] \tanh\left[\frac{0.077\left(\frac{gF}{U^2}\right)^{0.25}}{\tanh\left[0.833\left(\frac{gd}{U^2}\right)^{0.375}\right]}\right] \quad \text{(Eq.2)}$$

and

$$t_{min} = 2 \int_0^{F_{min}} \frac{1}{C_o}\, dx \quad \text{(Eq.3)}$$

where H is the significant wave height, T is the peak period, U the windspeed, F the fetch and t the duration of the windspeed. The significant wave height and wave period are calculated using the lesser value of the actual topographic fetch length or the equivalent duration limited fetch.

In order to provide the best estimates of the overwater wind-fields to the model, hourly windspeed and direction time histories measured at Tuktoyaktuk Airport were modified by the careful application of overland to overwater scaling factors to obtain spatially homogenous wind-fields for each hour during each open water season. These scaling factors were obtained, initially, using a procedure developed by Atmospheric Environment Service (AES) whereby specific overwater measurements at Kopanoar and Ukalerk, adjusted for height, were compared with contemporaneous overland measurements. Hydrotechnology however claimed that the AES scaling factors were erroneous and overestimated the overwater wind speed with the error accentuated for the lower winds speeds. They decided to develop a new set of ratios based on the frequency of occurrence of wind-speed intervals for the data sets at Tuktoyaktuk, Kopanoar, and Ukalerk.

Having first corrected the onshore and offshore wind-speed records to be at the same height using a 1/7th power law, they constructed histograms of the data (Figure 3) and used the shape of these to establish a transfer function between the data sets for Tuktoyaktuk and the offshore sites. The goodness of fit between the onshore Tuktoyaktuk and the modified, offshore wind distributions were obtained by visual inspection of the histograms. These histograms are marginal distributions because wind speed and directions are bivariate, although, for this purpose, wind direction appears to have been treated as being constant.

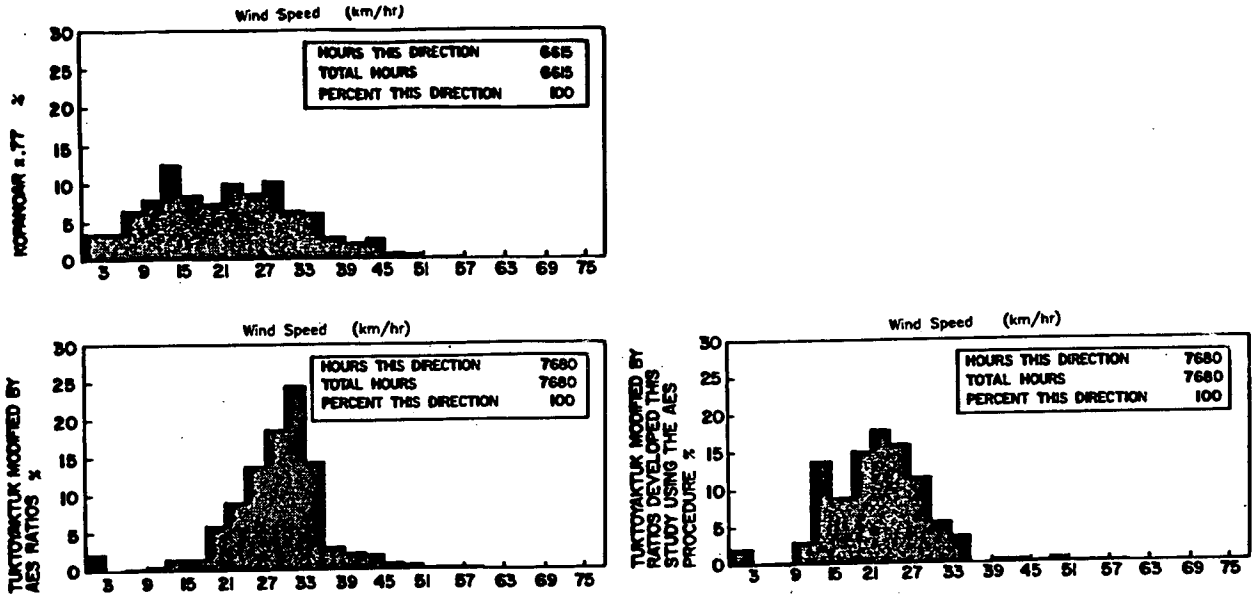


**Figure 3 Marginal Distributions for Wind Speed at Kopanoar, Ukalerk and Tuktoyaktuk**

Strictly speaking the Bretschneider equations are only applicable for winds of constant speed blowing from one direction over a long period of time. To overcome this limitation Hydrotechnology used a nine point running average method to effectively smooth the wind direction changes, thus enabling slowly varying windfields to be used.

The wave model was run continuously for all ten open-water seasons (1970-79), with the ice limits specified by the position of the average monthly limits of the one-tenth ice cover. Fetch lengths were computed as the actual straight line distances from the hindcast point to the land edge or the limit of the one-tenth ice cover. The position of the ice edge was defined using the "Current Ice Condition Charts" prepared by Ice Forecasting Central of Atmospheric Environment Service (AES). These charts are based on observations made by aircraft and ships in the area, shore ice reports, and since 1976, Satellite imagery. In most instances the leading edge of the ice is not very diffuse, with its position also depending upon the wind conditions. The time period during which the ice edge progresses and retreats can vary significantly from year to year. In the ten seasons covered by the Hydrotechnology study, the period of open water varied from a maximum of four months (July - October) in some years, to an essentially no ice-free period in 1974.

It is not immediately obvious from the Hydrotechnology study how shallow water effects, such as refraction or bottom friction, were taken into account. However, they do include a table of refraction and shoaling coefficients, inferring that these were applied to the hindcast results at the shallow sites. The form of the Bretschneider equation also implicitly contains a constant bottom-friction factor of 0.01. The height wave occurring in each of the ten years was used to form the data sample from which the extreme wave height estimates were made.

**SUMMARY OF THE SEACONSULT APPROACH**

The wave hindcasting technique selected in this study was fundamentally different from that used in any previous hindcast for the area in that a spectral modelling approach was adopted. This model, the system 20, developed by the DHI, computes the spatial and temporal variations in the directional wave height spectrum. The technique

used is based upon the conservation of wave energy over space and time, and includes terms for empirical energy growth and decay. Refraction, shoaling, and wave height decay effects were also included within the model. Basically the model is similar to that described by Inoue (1967) which permits the spectral form to grow, up to the limit of a Pierson Moskowitz spectrum.

A second major difference in the SeaConsult approach was the development of a hypothetical extreme storm hindcast using a prototype storm suitably intensified to provide wind speeds with the required return periods. Thus a 10 year storm was defined as one which would produce the 10 year return wind speed, a 50 year storm for the 50 year return wind speed, that is to say, wind speed durations and fetch lengths for wave generation were not considered in the selection process. Thus, the n-year wave was postulated to correspond to the n-year storm.

Meterological and Environmental Planning Ltd. (MEP) were responsible for providing the wind-field descriptions to the SeaConsult hindcast model. In the first instance, they compiled a data base of mean sea-level pressures over an extended area of the Beaufort Sea, Alaska, Northwest Territories, and northern Alberta for the ten-year period 1969-78 using the six hourly CMC synoptic weather charts, which have a 381-km coarse grid. They then used this pressure information to estimate geostrophic winds, which were subsequently reduced using a planetary, boundary-layer model to produce wind speeds at a 19.5-m reference height. In the actual hindcast study, it was argued, using observed data from one site, that the geostrophic winds themselves, and not the reduced wind speeds which provided better agreement with the observations. Consequently, derived geostrophic winds were used in the estimation of wind-speed recurrence intervals.

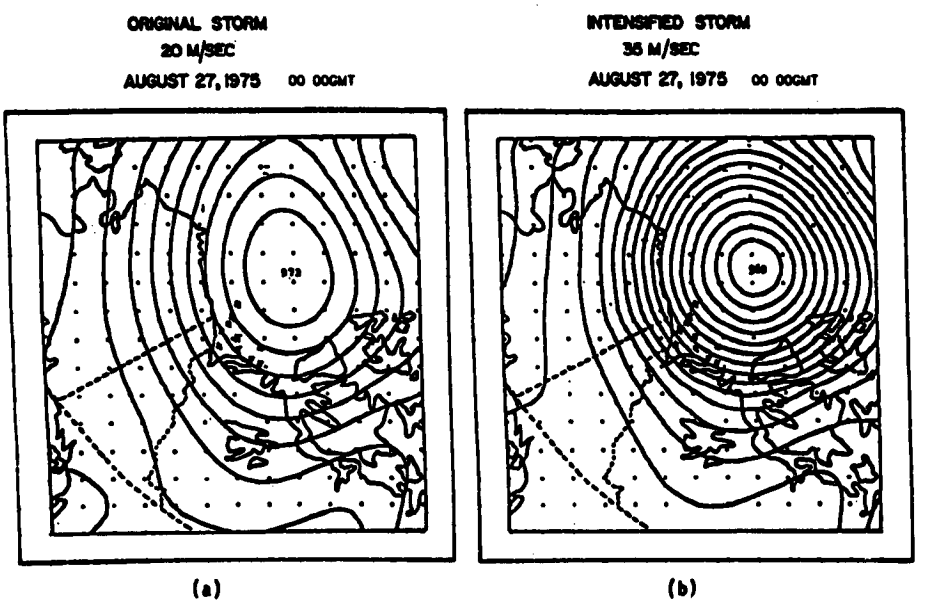


**Figure 4 Comparison of Surface Pressure Charts for an Actual and "Intensified" Storm**

The extreme wind-speeds for each of the ten sites of interest was derived by fitting a Gumbel distribution to the ten hindcast annual maxima (irrespective of wind direction) and by extrapolating the fitted distribution to provide wind speeds having an expectancy of return of 50 years and 100 years.

The process by which SeaConsult arrived at the selection of a "prototype" storm appears to be one of default in an attempt to find a storm with sufficient contemporaneous measured wind and wave data to provide verification. After studying six storms in the period 1970-79 they selected the storm of 26-28 August, 1975 as the prototype. The four synthetic storms used in the hindcast were constructed by intensifying the prototype storm so as to match the desired maximum wind speed associated with return periods of 1, 10, 50 and 100 years. The description of the intensification procedure indicates that the low-pressure system was intensified and broadened, increasing its zone of influence (see Figure 4), which probably has the consequence of characterizing the storms with higher wind speeds by longer durations.

The windfields used in the model were based on estimates of the overwater wind-fields available at hourly intervals throughtout the open water season. The intensified wind-field was then input to the spectral wave model which describes the sea state at any given time in terms of a directional-frequency energy spectrum. This spectrum is described in such a way as to permit the simulation of energy flow into and out of 240 spectral elements; that is, 15 frequency bands and 16 angular intervals. The basic equation used assumes that the wave energy in the spectrum is propagated at the wave group velocity.

SeaConsult chose to define the open-water area as that bounded by the land and the nine-tenths (9/10) ice edge at the maximum extent of open water that had ever been observed (Brower et al 1977). This definition placed the ice edge west of Point Barrow, permitting westerly winds to have an effective fetch length in excess of 850 km, that is of comparable order to the scale lengths of the storm. A single ice edge was thus used with all the extreme storms, and the effect of fetch limitation was removed from them by implying that wave growth was essentially duration-limited. However, no attempt was made to verify that such was the case. Because the return periods were based solely on wind fields and the open water conditions have their own probability of occurrence, SeaConsult noted that their return period designations were "slightly conservative".

## COMPARISON OF THE STUDIES

Because the two studies had quite different terms of reference and approached the problem of estimating extreme wave-height in a fundamentally different manner, discrepancies exist between the results they produced (see Table 1). Referring specifically to the 100 year return period significant wave heights, a commonly used measure for comparing extreme waves, one finds that for water depths less than 30 m, there is reasonably good agreement between the studies. However, in deeper water and at locations which are less than 30 km apart (Kopanoar and Site 7 in the SeaConsult study), Hydrotechnology estimate a significant wave height of 7.3 m whereas SeaConsult's estimate is almost double that at 13.2 m. As a general observation, the extreme wave heights estimated by SeaConsult show a much greater dependence on water depth than do the Hydrotechnology results.

To provide a rational basis for assessing the results of the studies both in relative and absolute terms a critical assessment of each is made in this section under the five distinct aspects of hindcasting listed previously.

## STORM AND EVENT SELECTION

As a rough rule of thumb, n-years of wave measurements at a fixed site can provide a reasonable estimate of wave heights for recurrence intervals up to about 2n years (Borgman, 1975). However, even a limited set of data such as 10 years of wind records used in both studies can be usefully employed to estimate an extreme event with a 100 year return period and assign confidence levels to it. The key issue in deciding the extent of the extrapolation is whether the width of the confidence levels is acceptable or not. Clearly, the longer the estimated recurrence interval in comparison with the length of the data record, the greater will be the associated uncertainties.

**Table 1**

**Summary of extreme wind speed and significant wave height estimates**

| | Return period (yrs) | Hydrotechnology Sites A | | D | SeaConsult Sites 3 | 7 |
|---|---|---|---|---|---|---|
| Hourly Average Wind speed (knots) | 10 | 44 | | 44 | 45[1] | 46[1] |
| | 20 | 49 | | 49 | | |
| | 50 | 56 | | 56 | | |
| | 100 | 59 | | 59 | 59 | 61 |
| Significant wave height $H_s$(m) | 10 | (4.5)[3] | 4.2 | 4.8 | (5.00)[3] | 5.5[2] | 9.2 |
| | 20 | (5.0) | 4.8 | 5.5 | (5.60) | | |
| | 50 | (5.6) | 5.7 | 6.5 | (6.35) | 5.5 | 12.8 |
| | 100 | (6.0) | 6.2 | 7.3 | (6.90) | 5.5 | 13.2 |

1 Source Meteorological and Environmental Planning Ltd. (MEP) (1982).
2 Wave heights were depth-limited for all storms at this site.
3 Wave heights based on Challenor's maximum likelihood estimators (this paper).

It is tempting to suppose that the relatively scanty data base could be augmented through the generation of synthetic "prototype" storms, however, the relevant physics describing such Arctic storms is beyond the present state of knowledge. SeaConsult's usage and description of a prototype storm in terms of a single scalar variable-wind speed complicated the situation by introducing additional unknowns into the determination of recurrence intervals. The concept of a prototype storm is however quite a useful one provided a means of adequately characterising and describing a multi dimensional vector wind-field can be found. The construction of an abstract, probabilistic set of storms should follow from a careful, thorough study of storm behaviour, since variations in storm wind fields in both time and space can produce significant variations in the maximum hindcast wave heights.

In a probabilistic sense, a scalar random quantity, such as wave height, can be produced by a large range of storm wind fields (for example: very high wind speeds with short durations or with short fetches, or lower wind speeds with longer durations or fetches). By the same token the inverse problem, that of reconstructing a storm field from a single parameter (wind speed), as attempted by SeaConsult, is ill-posed. In a formal sense, if one were to attempt to derive a parametric-abstract set of storms to hindcast, all the possible sources of variation in the wind fields and fetches would have to be considered to obtain a joint probability estimate of all of these parameters. This has been done in joint probability method studies of hurricane surge levels (Myers 1954), where the probability space consists of five parameters. The storm wind fields in the Beaufort Sea however are more complex than a tropical storm and would be much more difficult to describe prametrically; nevertheless it is worth consideration.

## FORMULATION OF A PROBABLISTIC REPRESENTATION OF A STORM

If the wind field, which is spatially and temporally varying, and the open-water areas were specified completely for one storm by some vector of parameters x, then the hindcast method could be expressed as a function H(x), for the maximum, significant wave height generated by that storm.

The probabilistic description of storms should include their arrival rate and the joint probability distribution of the parameters describing the spatial and temporal distribution of the wind field within a random storm, $f_{\underset{\sim}{X}}(\underset{\sim}{x})$. Ideally, the parameters used to describe a storm should be sufficient to specify completely the spatial and temporal variations in the wind field throughout its history. The vector of parameters for one storm might include the wind speed, the duration of the storm, and the scale of the spatial variations in the wind field. Of course, a complete description would require a large number of parameters, so some subjectivity must be introduced to make the procedure tractable.

Like the wind field, the extent of open water during a storm is probabilistic. Ideally, its description should include the correlation between the area of open water and the wind field int he form of a joint probability distribution. If the vector of parameters used to describe a storm, "X", is expanded to include the parameters to describe the open-water area, then $f_{\underset{\sim}{X}}(\underset{\sim}{x})$ is the joint probability distribution of the wind field and open-water area through one random storm.

Assuming that the wave height, H, can be calculated from x using the relationship $H = (\underset{\sim}{x})$, and its inverse can be obtained from $\underset{\sim}{x} = H^{-1}(h)$ then the probability of the calculated significant wave height exceeding a specified height, h, in a given storm is given by:

$$Pr(H > h) = \int_{\underset{\sim}{H}^{-1}(h)}^{\infty} f_{\underset{\sim}{X}}(x)\, d\underset{\sim}{x} \qquad \text{(Eq.4)}$$

If the average frequency per unit time, or the arrival rate, is denoted $\lambda$, the expected number of storms, n(h), with a significant wave height greater than h in a unit of time is given by,

$$n = \lambda \int_{\underset{\sim}{H}^{-1}(h)}^{\infty} f_{\underset{\sim}{X}}(x)\, d\underset{\sim}{x} \qquad \text{(Eq.5)}$$

Thus the expected time period between storms which exceed h, or the return period denoted R(h) is given by 1/n, or:

$$R(h) = 1/n \qquad \text{(Eq.6)}$$

That is to say, the return period associated with a given wave height is the inverse of the product of the frequency of storms, and the probability that the maximum wave height in one random storm would exceed that height. The probability that the maximum wave height in one random storm would exceed a given height is the sum of the probabilities of occurrence of all combinations of wind-field and open-water area parameters, which would generate wave heights in excess of that value. This procedure is followed later in the paper, when a sensitivity analysis is described.

In n-years of waves are hindcast at a site, then the resulting data set, if the hindcast is accurate, is roughly equivalent to n-years of measurements at that site. These hindcasts should provide, inherent in their results, all of the nonlinear interactions among different wind fields and fetches that are suppressed in the simplistic single parameter "prototype" storm methodology, as applied in the SeaConsult report. This methodology appears to be more direct, given our present knowledge of storms in the Beaufort sea.

It is difficult to quantify the error of extreme wave height magnitudes resulting from overly short record lengths, except under restrictive assumptions (independent storms, homogeneous population, etc.). Resio (1978) addressed some of the complicating factors from both long and short-term climatic fluctuations and concluded that the more important influences on extreme wave heights were related to short-term (5-10 years) fluctuations. Based on this, a sample length of at least 20 years should produce a reasonably stable estimate, in a climatic though not necessarily a statistical sense, of longer term recurrence intervals.

**WIND FIELD METHODOLOGY**

Neither the Hydrotechnology nor SeaConsult studies appeared to address the problem of wind-field specification in a manner commensurate with its importance to wave hindcasting; clearly without accurate wind estimates, it is impossible to obtain accurate wave estimates. This should not imply that the accuracy of the wave model need be no greater than that to which the wind speeds are estimated, for such reasoning would only lead to a compounding of the error by contributing additional bias and random errors to those already present in the wind-field estimates.

The hindcast model used in the Hydrotechnology study assumed the usage of spatially uniform wind-fields and in addition did not take into account possible wave attenuation due to the low ice concentrations within the open water area. There are also uncertainties introduced by the assumption that a modification of the onshore wind data at one location Tuktoyaktuk would be representative of the winds over the Southern Beaufort. It is clear from Table 2 that considerable differences of opinion exist on the values of the transfer function(s) to be used for overland/overwater conversions in general, while as will be noted later, there have been several alternative transfer functions proposed for the Beaufort Sea.

Physical effects such as atmospheric stability, relative heights of anemometers, sheltering, direction of wind, and general roughness scales surrounding the land station can affect the ratio of overwater-to-overland wind speeds. With the exception of anemometer height, Hydrotechnology did not address these factors in their study. Wind events tend to have particular correlations between wind directions and stabilities, so it is possible that ratios derived from histograms might be misleading. Interestingly, many of these concerns have been addressed by Hydrotechnology as part of an intensive investigation within the proprietary study APOA 203 (1983).

**Table 2**

| SPEED / STUDY | KILOMETRES PER HOUR | | | | | | | | | | | | | |
|---|---|---|---|---|---|---|---|---|---|---|---|---|---|---|
| | 2 | 6 | 10 | 14 | 18 | 22 | 26 | 30 | 34 | 38 | 42 | 46 | 50 | |
| HYDROTECHNOLOGY (1980) | | 1.0 | 1.0 | 1.02 | 1.07 | 1.11 | 1.15 | 1.13 | 1.08 | 1.05 | 1.04 | 1.03 | 1.03 | 1.03 |
| RESIO[1] MODIFIED BY BAIRD | | 1.04 | 1.11 | 1.3 | 1.42 | 1.45 | 1.44 | 1.4 | 1.36 | 1.31 | 1.27 | 1.24 | 1.22 | 1.21 |
| RESIO[1] | | 2.34 | 2.0 | 1.8 | 1.6 | 1.6 | 1.5 | 1.42 | 1.36 | 1.31 | 1.28 | 1.25 | 1.23 | 1.22 |
| RICHARD – 1970[1, 3] | | 2.65 | | | 1.55 | | | 1.26 | | | 1.02 | | | |
| AES 1975[2, 3] LAND TO WATER | | 3.17 | | | 1.82 | | | 1.42 | | | 1.2 | | | |
| AES 1975[2, 3] WATER TO LAND | | 3.26 | | | 1.72 | | | 1.28 | | | 0.95 | | | |

NOTES:

1. GREAT LAKES
2. BEAUFORT SEA
3. AVERAGE WEIGHTED VALUES FROM STUDIES THAT CONSIDER STABILITY

As SeaConsult recognised, the 381 Km grid spacing on the CMC synoptic charts used to establish their wind fields was too coarse. In addition the six hour sampling time filtered out short duration effects such as storm peaking which leads to underestimating peak wind speeds. Of perhaps even greater significance the poor spatial resolution of the charts can cause significant small scale intense disturbances, designated by Hodgins (1983) as "Arctic instability lows", to be completely missed. These disturbances could be akin to similar systems found in the Southern Norwegian Sea which have hurricane strength winds associated with depressions having a horizontal extent ranging from 150 - 300 Km. These cyclonic polar lows are difficult to detect and differ from more common frontal systems not only in their size but also in their general lack of a pronounced frontal structure. A number of such storm systems have been documented (Rabbe, 1975, Tryggestad et al 1983) and observations made from the weather station AM1 indicates that high waves can be generated quite rapidly. According to the MEP study these "missed" storms could cause wind speeds several times greater than those they deduced from their large grid point pressure pattern.

**WAVE MODEL APPLICATION**

It is difficult for a parametric wave model to represent the various types of propagation and sheltering effects found in coastal areas. In addition, there are difficulties in defining fetch lengths and in dealing with changing wind directions. A spectral model, however, should be able to account for these effects in a more accurate manner. Neither of the studies examined the effects of partial ice cover on wave growth and decay. However, this aspect may not be critical when considering the estimation of extreme wave height, since extreme waves can be generated only in fairly ice-free conditions. When the ice edge and significant partial ice cover are near a site, it is reasonable to suppose that extremely large waves are not generated.

**VERIFICATION EFFORTS**

A thorough verification effort is a prerequisite to placing confidence in hindcast results. It has a twofold purpose, first to demonstrate the validation of each of the steps which make up the hindcast methodology, and secondly to obtain quantitative estimates of the errors inherent in the approach taken. Neither the Hydrotechnology nor the SeaConsult studies achieved these goals. Even a cursory review of their comparison of modelled and measured winds would indicate that neither methodology was verified successfully. SeaConsult were perhaps the more remiss in this aspect since they concluded that their modelled windfields were not accurate enough to be used to calibrate the wind wave model results against measured wave data. They chose instead to use measured winds at NCC Camp 208 for the period of the chosen storm event. Thus the wind methodology used in the verification is not the same as that used in their production runs.

Hydrotechnology compared a number of time series of wave heights and periods at selected hindcast points to measurements taken from wave buoys. No quantification of the deviations between the two time series was included in their report, however descriptive comments would indicate that in a large number of cases, "good" agreement was obtained. It is important to note that the complete hindcast methodology used in the verification comparisons was identical to that used in all production runs; consequently, deviations between measured and hindcast wave conditions can be regarded as characteristic of the actual errors inherent in the production hindcasts.

A further verification was included in the form of comparisons between histograms of measured and hindcast wave heights and wave periods. Although this is very important for verifying the validity of their methodology for operational conditions, it does not, however, provide much information on the validity of the methodology for the purposes of estimating extremes.

**STATISTICAL ESTIMATION TECHNIQUES**

The uncertainty in predicting a future value of wave height results from several causes. For the purposes of statistical analysis, two main areas are identified:

- shortness of the data record; and
- scatter in the data.

To estimate the return periods associated with extreme wave heights, Hydrotechnology selected as their sample the highest wave occurring in each of the ten years studied.

The usual technique in analysis of significant wave height extremes is to plot a function of the cumulative distribution F(y), (or in the case of the Gumbel, double exponential extremal distribution of extremes, $-\ln(-\ln F(y))$, against significant wave height. The cumulative values are estimated from the data. A straight line should result and it is then necessary to estimate the location and scale parameters of $\alpha$ and $\beta$, defining the line that is

$$y = \alpha(x - \beta)$$

from the plot. Results obtained by Hydrotechnology for the Tarsiut site is shown in Figure 5(a); the best-fit line presumably being obtained (because the methodology is not stated) by least squares regression. The use of least squares is not criticized here, however, the authors believe that, as regards confidence intervals, the methodology used by Hydrotechnology is inappropriate for two reasons.

a) It is based on a technique developed by Gumbel (1958, p.214) to compute the distribution of the mth order statistics ($x_m$) in N observations. No account is taken of the scatter of the obtained data points; in other words, the same standard error is obtained for data points with large and small scatter.

b) The methodology was developed for a value of m approximately equal to (N/2), that is, near the central value.

Under these conditions, an approximate, normal distribution of $x_m$ is found. However, this is not suitable for extrapolation near the ends or outside the data range. Challenor (1979) has presented a method based on maximum likelihood estimators and given standard deviations and confidence intervals for the location and scale parameters. Using the Hydrotechnology data sample with the Challenor methodology results in the graph shown in Figure 5(b) for the Tarsiut. These are 90% confidence intervals based on parameter uncertainty. For comparative purposes, the most likely value calcuated using the Challenor tables have been included in Table 1. The values of the location and scaling parameters and for Tarsiut were found to be 8.243; 1.6355. Clearly, these results differ from those obtained by Hydrotechnology as would be expected, because the latter have uncertainty in the underlying process.

As pointed out earlier in the SeaConsult study, the n-year "prototype" storm was assumed to produce the n-year wave. Confidence intervals of the estimated wave heights were derived somewhat subjectively by selecting additional prototype storms which were taken to represent the confidence bounds on wind speed at each recurrence interval. Extreme wave heights can only be generated during strong wind storms. Therefore, it is appropriate to treat the extreme wave-height generation problem as being made up of discrete events, such as is the case with earthquakes and ice invasions. In practice, environmental characteristics, such as wind speed or wave height, can be treated as random quantities <u>given</u> a storm event. The extremes can subsequently be derived as the maximum of a random number of random quantities. It is also important to examine whether all of the extreme wave-producing storms are of a homogeneous storm type or if they are of differing types which require subgrouping before perforing the analysis of extremes (Muir and El Shaarawi 1986). A step forward would be to establish a set of criteria for a critical storm definition, such as strength and duration of the wind and

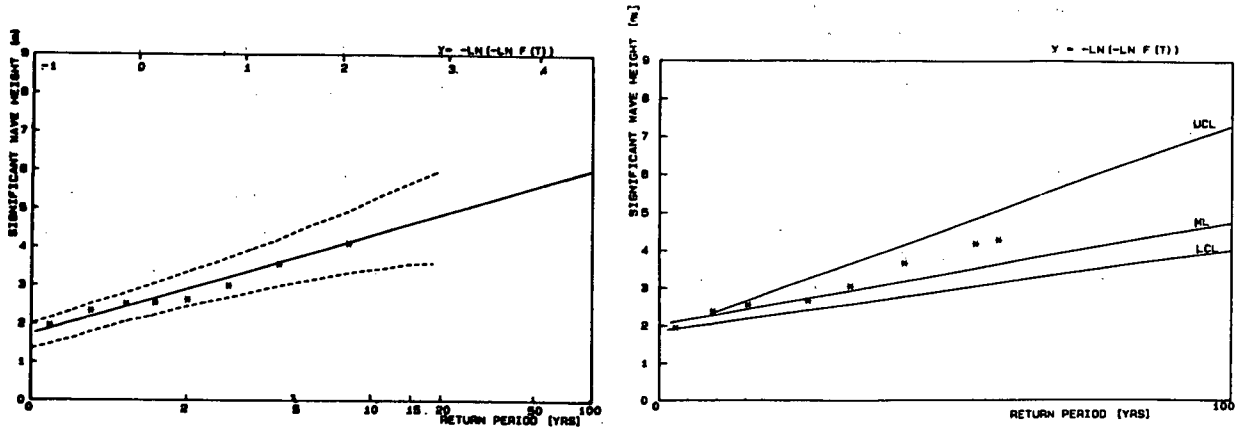


**Figure 5(a) and (b) Extreme Value Distributions for Significant Wave Height at Tarsiut**

the extent of the open-water area. The definition of what constitutes a critical storm, however, is of less importance than ensuring that all storms which could generate high waves are included within the definition.

**SOURCES AND QUANTIFICATION OF ERRORS**

There are four principal factors governing the hindcast estimation of extreme wave height in deep water, namely:

- the temporal and spatial description of the wind field (defining duration, wind speed, and directionality);
- the definition of the open-water area (defining the effective fetch length);
- the hindcast procedure adopted; and
- the method of associating a return period with a wave height.

Each of these factors were reviewed for both studies in Murray and Maes (1985) with a view to quantifying the effects of the various simplications and assumptions on the extreme wave height estimations. Space limitations precludes a detailed description of this effort here so that a summary of the findings must suffice. Potential sources of error were identified for each approach and in both cases the means of describing the wind fields received close attention. The determination of the overwater/overland transfer function is critical to the Hydrotechnology results for example and requires the accurate contemporaneous measurement of the mean hourly wind speed and direction at difference locations and their reduction to a common reference height. The three cup U2A type anemometers in common use in the area have a stated accuracy upon calibration of $\pm$ 1.5 m/s for wind speeds in excess of 30 m/s. A greater potential source of error, however, lies in accurately establishing the heights at which the offshore readings have

been taken and the possible sheltering effects caused by superstructures and derricks. The use of a $^{1}/_{7}$th power scaling law while appropriate when the vertical wind component is weak is, however, suspect under Arctic storm conditions. In all, the water/land speed ratios of 1.0 to 1.15 for the speeds of interest used by Hydrotechnology are markedly different from those subsequently derived in the APOA 203 study which contained a further 2 years of wind data and an exhaustive attempt to repair wind records at Tuktoyaktuk and offshore, referring them to a common reference height. Both Fissel and Birch (1984) and Danard and Gray (1982) produced scaling factors which were on average 20% higher than the Hydrotechnology results over the range of interest. As was noted earlier, it is difficult for a parametric model to represent the various types of sheltering and propagation effects that are present in coastal areas. The changing wind patterns and the complex geometry of the coastal edge make it difficult to estimate fetch lengths and duration times accurately. The errors introduced to the modelling process from these sources, however, are unknown.

In the Beaufort Sea, the fetch lengths are also affected by the position of the polar pack ice and fetches of great length in comparison to their width are quite common. This effect inhibits energy transfer from the winds into the waves, with the result that the wave heights generated under such circumstances are lower than would be expected in less-restricted waters. The width effect is not considered in the Hydrotechnology parametric model, although the absolute effect of its omission is unknown. Since the completion of the Hydrotechnology 1980 study, the Coastal Engineering Research Centre (CERC) of the U.S. Army Corps of Engineers have revised the original Bretschneider hindcasting equations. These revisions have been based on a detailed review and analysis of the data used in the preparation of the original empirical equations and results, obtained from JONSWAP (Hasselmann et al. 1973). These revised equations (basically a change in exponent from 0.42 to 0.5 in equations (1) and (2) were used in the hindcast modelling which forms part of the Sensitivity Analysis described in this paper.

In comparison to the parametric or significant wave model, the spectral wave approach is considerably more complex, although that in itself does not make it more prone to errors. The crucial elements were the selection of the prototype storm, the derivations of the surface winds from the synoptic pressure charts, and the energy transfer mechanism within the waves, particularly for shallow water conditions.

An accurate measurement of grid station pressures and their subsequent reduction to mean level pressure is essential to the preparation of accurate weather mapping. MEP identified pressure measurement as the least significant source of error ascribing to it a maximum value of 0.2 mbar. The Beaufort Weather Office, however, notes that misreadings of between 0.5 and 1.0 mbar are not uncommon in reports from drillships. It is expected, though, that noticeable pressure discrepancies of the latter type would be detected and not used in the determination of grid point pressures.

Mean sea level pressure is analysed after each six-hourly interval at CMC, and the pressures are stored for all 381-km grid points. In general, the level of error contained in the computer analyses of these grid point pressures is in the order of 0.2 mbar. The probability of larger errors increases for regions of sparse data reports, such as the Beaufort Sea, where the position and central pressures of systems often are difficult to assess. In such circumstances, the error in the grid point pressures over a localized area could be about $\pm 4$ mbar, which is sufficient to cause a significant change in the derived wind speeds for the region affected.

The derivation of the surface winds from synoptic charts contains several possible sources of error among which are:

- surface roughness or frictional effects;
- atmospheric stability;
- curvature of the isobars in the vicinity of well-developed lows (or highs); and
- isallobaric (rate of change of pressure) effects.

These latter effects at a conservative estimate could modify derived windspeeds by the order of 5 - 10%. The variability of the position of the ice edge, and the intensity and duration of the storm record are important elements in the spectral wave approach. In the SeaConsult study the intensification process was carried out until the peak storm winds matched the required recurrent windspeed. This leads to two possible sources of error; that the storm movement is constant and that deepening the low will also cause it to broaden.

**SENSITIVITY ANALYSIS**

Having established a number of potential sources of error in both studies an attempt has been made to quantify their effect on extreme wave height estimation. A proprietary wind storm/wave hindcast parametric model developed by Canmar as part of APOA study 205 was used in conjunction with the methodology described earlier for characterising Arctic storms and their return periods. The wind data based used in the sensitivity modelling was identical to that in the APOA study 203 (1983) which is essentially the Hydrotechnology data augmented by a further two years of records.

The nub of the methodology involved the characterization of a wind storm and the development of storm statistics, as the statistical description of fetch lengths had been obtained from the available monthly AES ice charts. The wind data of storms for the 12-year period 1970-82, was established by searching out wind speeds in excess of 40 km/hr with peak wind speeds exceeding 50 km/hr. The 40 km/hr threshold speed enabled storm durations to be ascertained; with the exception of tolerating short lulls (of less than two hours), the storms were deemed to end when the wind speed dropped below 40 km/hr. Storms with a duration of less than one hour were ignored when compiling the statistics. Subsequent study of the storm analysis data showed that within the 12 years of records (13 drilling seasons), there were nine storms exhibiting wind speeds greater than 55 km/hr, all emanating from the northwest. Two populations were discernable in those storms having peak wind speeds in the range 50-55 km/hr, storms from the northwest and from the northeast. The northeasterly storms were rejected from the storm population set, because such storms in the region move the ice edge closer to the shore, hence reducing fetch.

The wind storms were characterized by a simple bilinear symmetrical shape defined in terms of the peak, mean, and threshold wind speeds, and the storm duration. The peak wind was assumed to be reached at the halfway point of the storm duration, while the wind speed was assumed to build up linearly from the threshold speed at the start of the storm until the mean wind speed was reached. The time at which this speed was reached was selected so that the area under the measured wind-speed history equalled the product of the man wind speed and the storm duration. The left-hand flank of the idealized wind-speed history was completed by assuming a linear increase in speed until peak value was reached. Statistics of storm duration and peak and mean wind speeds were compiled in the form of probability of exceedance tables. Checks on storm duration and fetch established that these were independent of wind speeds.

To derive the distribution of peak significant wave height in a single random storm, sets of peak wind speeds, average wind speeds, wind durations, and fetches were selected which had equally spaced probabilities of exceedance and the peak signficant wave heights were calculated for all combinations of the parameters. The validity of the model was checked by testing whether the proposed method would yield height estimates close to those obtained in the SeaConsult and Hydrotechnolgy studies. Using the same fetch and storm durations as SeaConsult and a distribution of extreme wind speeds similar to those used in both the SeaConsult and Hydrotechnology studies, the 25 year and 100 year return-period wave heights were estimated to be 11.0 and 12.8 m respectively, which is quite close to the predictions made by SeaConsult for deep-water locations. However, when the distributions of fetch and duration based on the observed wind records over ten years were used as input, the 25 year and 100 year return-period wave heights were found to be 6.3 and 7.7 m, respectively, which are similar to estimates from the Hydrotechnology study for deep-water locations. Both of these comparative exercises provided the necessary confidence in the adequacy of the model to perform the sensitivity analyses. They emphasized that the assumptions of one extreme

fetch and one extreme duration are inappropriate when estimating the return periods of extreme wave heights. In addition, they support the view that most of the discrepancies in the results produced in the two studies can be explained by the use of the extreme fetch and duration assumed by SeaConsult.

Since there was reason to believe that the Hydrotechnology windspeeds were on the low side, it was decided to test the sensitivity of the estimated wave height relative to the base case of a 20% increase in wind speeds used by Hydrotechnology. This exercise resulted in about a 20% increase in wave heights for all the return periods compared. Further, a 20% increase in the storm durations over the base case resulted in an increase of about 10% in the estimated wave heights. The percentage increases chosen were incorporated into the model by scaling the distributions by the appropriate amount. Interestingly, a 20% increase in the fetch distribution produced only a slight increase (3%) in the extreme wave heights, indicatiang that the storms most likely to cause an extreme wave are duration-limited, rather than fetch-limited or fully developed.

**CONCLUSIONS**

Both the studies reviewed were of high technical quality and contained a good deal of fresh thinking on the subject of extreme wave height estimation. SeaConsult was the more conservative of the two with their decision to use an extreme ice edge position effectively removing the important influence of fetch from their estimate. An equally serious deficiency was the inability of their derived windfields to reflect the spatial and temporal effects of severe storms.

The major reasons for the difference in results from the two studies are contained int he issues of fetch and the description of the windfield. The authors recommend, therefore, that a careful reconstruction fo the wind fields from all available data sources be undertaken, for the largest 20 or so storms over the past 15 years which have storm tracks in a predominantly west-northwesterly direction over the open water of the Beaufort Sea. There should be sufficient information in these wind fields to enable good-quality estimates to be made of the wind stress, wind speed, and direction obtained for averaged hourly intervals at a fixed reference height. This effort will require a careful blending of kinematic analyses and derived wind conditions.

A number of sensitivity analyses were performed as part of this study, using a simple extreme wave height prediction method which takes account of the joint probability distributions for wind speeds, duration, and fetch lengths. The validity of the approach was tested by running separate satisfactory comparisons with the SeaConsult and Hydrotechnology results. The sensitivity of the model to variations in wind speed, storm duration, and fetch length was assessed. In three separate analyses, the wind speeds, durations, and fetch distributions were increased by 20% above the base case. The estimated wave heights were found to be most sensitive to the variation in wind speed: the 20% increase producing a 20% increase in wave height over all return periods. The effect of the 20% increase in the storm duration was to increase wave heights by 10%. The least sensitive paramater was fetch distribution, with the increase in fetch producing only aslight increase in the extreme wave height. As a consequence, we conclude that the extreme wave heights are associated with duration-limited rather than fetch-limited storms. Applying the wind speed sensitivity to the Hydrotechnology results, and assuming that the wind speeds used in their study are 10% lower than they should be, their estimate of extreme wave height would be upwardly adjusted to about 8 m at the Kopanoar site.

It appears, therefore, that, with the suggested downward adjustment of the SeaConsult estimates and a moderate change to the Hydrotechnology results to account for an underestimation of wind speeds, an extreme wave height in the range of 8-9 m is appropriate for deep-water conditions in the area. In the much shallower water conditions, that is less than 12 m, the waves may be depth-limited, in which case there is little point in using analysis of extremes, becasue the wave height will be determined by the wave breaking-limited height. This circumstance would not be true of the large body of water existing between the 12-m and deep-water locations where it would be appropriate to take proper account of shallow water adjustments.

## REFERENCES


Arctic Petroleum Operator's Association. 1983. Beaufort Sea hindcast study 1970-1982. APOA Study 203, Prepared by Gulf Canada Resources Inc., Calgary, Alberta.

Arctic Petroleum Operator's Association. 1984. Design criteria for arctic offshore production platforms. APOA Study 205, Prepared by Dome Petroleum Ltd., Calgary, Alberta. 170 p. plus appendices.

Atmospheric Environment Service. 1984. Beaufort Weather Office Report. AES, Western Region, Edmonton, Alberta. 171 p.

Baird, W.F. and C.W. Glodowski. 1978. Estimation of wave energy using a wind wave hindcast technique. Paper F3, British Hydromech. Research Association International Symposium on Wave and Tidal Energy, Canterbury, England. pp.39-54.

Baird, W.F. and K.R. Hall. 1980. Wave hindcast study, Beaufort Sea. Report by Hydrotechnology Ltd., Ottawa, Ontario, for Gulf Canada Resources Inc., Calgary, Alberta. (Available from Pallister Resources Management Ltd., Calgary, Alberta, T2C 2B3, as Beaufort EIS Report RWE 28). 81 p. (with appendices).

Berry, M.O., P.M. Dutchak, M.E. Lalonde, J.A.W. McCulloch, and I. Savdie. 1975. Weather, waves and icing in the Beaufort Sea. Beaufort Sea Project, Department of the Environment, Victoria, British Columbia. Beaufort Sea Technical Report No. 21. 179 p.

Borgman, L.E. 1975. Extremal statistics in ocean engineering. Proceedings American Society of Civil Engineers. Civil Engineering in the Oceans III, Washington, D.C.: pp.117-133.

Bretschneider, C.L. 1973. Prediction of waves and currents. Look Lab/Hawaii, 3(1): 1-17.

Brower, W.A. Jr., H.W. Searby, and J.L. Ulise. 1977. Climatic atlas of the outer continental shelf waters and coastal regions of Alaska, VO.III, Chukchi and Beaufort Sea. U.S. Department of Commerce, NOAA/OCSEAP, 3:409.

Challenor, P.G. 1979. Confidence limits for extreme value statistics. Institute of Oceanographic Sciences, Godlming England, Report No. 82. 25 p.

Coastal Engineering Research Centre. 1981. Technical notes I5, I6 and I7. Shore Protection Manual, Department of the Army Corps of Engineers, Fort Belvoir, Virginia.

Dames & Moore (Consulting Engineers). 1975. Extreme wave hindcast study for the Beaufort Sea. Prepared for Atmospheric Environment Services, Environment Canada, Canada. 18 p.

Danard, M., and M. Gray. 1984. Extreme wind stresses over the Beaufort Sea as determined from Tuktoyaktuk winds. Unpublished report by Atmospheric Dynamics Corp., Victoria, British Columbia for Institute of Ocean Sciences, Sidney, British Columbia.

Fissel, D.B. and J.R. Birch. 1984. Sediment transport in the Canadian Beaufort Sea. Report by Arctic Sciences Ltd., Sidney, British Columbia for Atlantic Geoscience Centre, Bedford Institute of Oceanography, Dartmouth, Nova Scotia. 165 p.

Meteorological and Environmental Planning Ltd. (MEP). 1982. Beaufort Sea water level hindcast study, meteorological section. Report for Esso Resources Canada Limited, Calgary, Alberta. 76 p.

Muir, L.R. and A.H. El-Sharrawi. 1985. On the calculation of extreme wave heights -a review. Ocean Engineering, 13(1): 93-118

Myers, V.A. 1954. Characteristics of United States Hurricanes pertinent to levee design for Lake Okeechobee, Florida. Hydrometeorological Report No. 32, U.S. Weather Bureau and Corps. of Engineers, Washington, D.C. 46 p.

Murray, M.A. and M. Maes. 1986. Beaufort Sea extreme wave studies assessment. Environmental Studies Revolving Fund Report Series No. 023. Ottawa. 97 p.

Gumbel, E.J. 1958. Statistics of extremes. Columbia University Press, New York. 375 p.

Hasselmann, K., R.P. Barnett, E. Bouws, H. Carlson, D.E. Cartwright, K. Enke, J.A. Ewing, H. Gienapp, D.E. Hasselmann, P. Kruseman, A. Meerburg, P. Muller, D.J. Olbers, K. Richter, W. Sell, and H. Walden. 1973. Measurements of wind-wave growth and swell decay during the Joint North Sea Wave Project (JONSWAP). Deutsche Hydrographische Zietschrift, Supplement, A8:12:1-75.

Hodgins, D.O. 1983. A review of extreme wave conditions on the Beaufort Sea. Report by SeaConsult Marine Research Ltd., Vancouver, British Columbia, for Marine Environmental Data Service, Department fo Fisheries and Oceans, Ottawa. 160 p.

Hodgins, D., P.H. LeBlond, and O. Brink-Kjaer. 1981. A hindcast study of extreme water levels in the Beaufort Sea. Report by SeaConsult Marine Research ltd., Vancouver, British Columbia, for Esso Resources Canada ltd. (Available from Pallister Resources Management Ltd., Calgary, Alberta, T2C @B3 as Beaufort EIS Report RWE 36.), 231 p.

Hsu, S.A. 1984. Improved formulas for estiamting offshore winds. Proceedings A.S.C.E. Coastal Engineering Conference, Houston, Texas. pp.2220-2231.

Inoue, T. 1967. On the growth of the spectrum of a wind-generated sea according to a modified Miles-Phillips mechanism and its applciation to wave forecasting. New York University, School of Engineering and Science, New York. Report GSL-67-5.

Institute for Storm Research. 1971. Winds, waves and storms in the souther Beaufort Sea. Report for ELF Oil Exploration adn Production (Canada) Ltd.

Intersea Research Corporation. 1974. Normal and extreme winds and waves in the Canadian southern Beaufort Sea. Report for Imperial Oil Company Ltd. (3 Volumes).

Rabbe, A. 1975. Arctic instability low. Norwegian MET Institute, 6(11): 11-21.

Resio, D.T. 1978. Some aspects of extreme wave prediction related to climatic variations. Proceedings Offshore Technology Conference, Paper OTC 3278, 1967-1980.

Resio, D.T. and C.L. Vincent. 1977. Estimation of winds over the Great Lakes. Journal of Waterways, Harbours and Coastal Engineering Division, American Society of Civil Engineers. 130:265-283.

Tryggestad, S., K.A. Orvik, S. Haver and L.I. Gide. 1983. Environmental conditions at Tromsoflaket, Report No. 8. Prepared by the River and Harbour Laboratory, Trondheim for the Norwegian Petroleum Directorate. July 1983, 247 p. (with appendices).

## SUMMARY OF DISCUSSIONS AND RECOMMENDATIONS

Session A - Wave Measurement

Chairman: Dr. J. R. Wilson

Rapporteur: Dr. M. L. Khandekar

Papers Presented:

A-1 The Canadian Atlantic Storms Program: An Overview. The Oceanographic Component - C. Anderson; the Meteorological Component - R. Shaw.

A-2 The CASP ESRF WOTAN Evaluation. F. Dobson, D. D. Lemon and D. M. Farmer.

A-3 The Distribution of Surface Winds over the Scotian Shelf. P. C. Smith.

A-4 Wave Field Properties and a Comparison of Two Directional Wave Buoys. B. Juszko, B. de Lange Boom, D. R. Green and R. Brown.

A-5 Wave Climate Study, Northern Coast of British Columbia. J. Harper.

The questions that arose following the presentations in this session centred mainly on the quality of wave measurements rather than on any of the wave climatological information presented.

It was agreed that WOTAN systems seem to provide reliable wind measurements in most oceanic water depths, but that they must be individually calibrated to be sufficiently accurate to be useful as input for wave modeling.

Ice loading on wave buoys was mentioned as a problem in Canadian coastal waters in the winter months. It was mentioned that the data collected by Waveriders could be contaminated by buoy icing whereas data from WAVECs would not. Observations of ice loading on various buoys showed that Waveriders tilt beyond the range within which the internal gimbaled accelerometers can accommodate, but that the distribution of floatation on WAVEC buoys does not allow ice buildup to cause buoy tilts. Icing becomes significant when the air temperature is less than -10C and water temperature is less than -1C.

It was agreed that there are systematic differences between winds at Sable Island and those measured onboard ships in the vicinity. Ship winds are consistently about 20% higher than those measured on Sable Island.

It was pointed out that the difference between sea waves and swell is not always easy to detect with buoy measurements like those from Waveriders or WAVECs. If the separation of sea from swell becomes critical (and there was disagreement on this point) then other techniques for analysis or measurement will need to be developed.

Session B - Shallow Water Effects

Chairman: M. Coolen

Rapporteur: D. Bliss

Papers Presented:

B-1 Evaluation of two Shallow Water Spectral Wave Models on Sable Island Bank, Canada. D. O. Hodgins.

B-2 Forecasting Wave Conditions Under the Influence of Currents and Bottom Topography. Y. Y. Chao.

B-4 A Second Generation Shallow Water Resio Wave Model. W. Perrie, B. Toulany and W. Rosenthal.

B-5 Modeling the CASP Wave Data Set. F. Dobson and W. Perrie.

During the discussion following the presentations, a great deal of time was spent debating the adequacy of these models. Although it was recognized that these models generate hindcasts which are adequate for engineering use, it is not clear if they have universal application. The effects of different bottom types and growth rates and relaxation rates of the wave field are unknown and are often assumed to have small or negligible effects. The third generation models which are presently being developed will attempt to account for the non-linear effects.

It was generally agreed that in order to account properly for these effects, the actual physical processes have to be more clearly understood. It is the lack of understanding of the physics which is limiting the proper mathematical description of the non-linear shallow water effects. The physical processes of the effect of bottom friction, wave-current and wave-wave inter-action should be investigated for coupled and non-coupled waves and for equilibrium and non-equilibrium states. The changes in the spectral shapes associated with these conditions should be examined. It was felt that the changes occurring in the spectral shape in a wave-current interaction have not been properly addressed and that there is work to be done in this area.

There was some discussion on whether the source terms in the models could or could not be separated and what in fact were the correct source terms.

The drawback of the TMA approach to shallow water wave modeling was agreed to be that it is not based on physical principles but makes some assumptions, particularly concerning the equilibrium of the wave state. The TMA scaling which has been based on a kinematic approach must be improved, particularly to account for the differences expected between the wave state at a location that is being actively generated at that spot, and that which is not being generated but has waves travelling in from another location.

An empirical approach should be taken to test the models under various conditions to make comparisons. This approach, although not as elegant as a purely deterministic approach based on physics, will indicate specific situations where models do not perform adequately. For example, to study the effects of bottom friction, a series of field experiments should be performed in areas where there is a hard rock bottom and in other areas where there are layers of highly viscous ooze.

There was general agreement that better and more accurate wind information is needed to improve confidence in the models.

The data from CASP hopefully will show changes of the spectra for changing situations and changing winds. CASP data will be analysed to examine the growth of waves and the effect of changing wind direction. Data from CASP soon will be available from BIO for other experimenters.

A final note in the discussion was a restatement of Murphy's Law applied to experimental programs like CASP:

> "If an atmospheric parameter is thought to have a marginal, insignificant effect on wave growth, then measure it. If you do not measure the parameter, then someone in the next ten years will discover it to be the important parameter for predicting waves."

Session C1 - Operational Forecasting

Chairman: W. Appleby

Rapporteur: R. Shaw

Papers presented:

C1-1 The Meteorological Office Operational Sea State Forecasting System. P.E. Francis.

C1-2 Development of a Global Scale Ocean Wave Forecasting Model for Marine Guidance. D. Esteva and H. Chin.

C1-3 Incremental Enhancement of Wave Forecasting Capabilities by an Operational Spectral Wave Model. S.K. Lally, N. Stevenson and D. Fu.

C1-4 The Operational Wave Forecasting Program of the Canadian Forces Meteorological and Oceanographic (METOC) Centre, Halifax, N. S., W.G. Lumsden and R.K. Cross.

C1-5 The AES Parametric Ocean-Wave Forecast System. K.A. Macdonald and S. Clodman.

There was general agreement that waves observed from ships were not too useful to operational forecasters since ships' reports have too little accuracy and too much variance to be assimilated meaningfully into the forecast. The length of the ship and its direction of motion apparently affect the period and wave height reported by the shipboard observer. It was stated that wave heights reported from closely clustered ships varied greatly among themselves and that ship reports explain less than 30% of the variance in wave height. One participant felt that one bad ship report caused less of a problem for initializing a model than did a bad initial wind field.

It was generally felt that objectively measured waves are more useful than visual observations. These measurements could be made from offshore drilling platforms, buoys and satellites. However, where the density of observations is sufficiently great, it may be worthwhile to attempt to assimilate observations into forecasts. A study is underway at present in the United Kingdom to examine ways of using observations of waves and wind at the same time and place at selected points in the North Sea. Satellite-borne scatterometers should be a copious source of wind data by the 1990's. Due to the great spatial extent of of the data collected in a short time frame, these data may be more usefully assimilated into a centrally located model rather than into a number of smaller regional ones.

Attempts are being made to incorporate sea ice into forecast models. In the UK, the sea ice boundaries will be input via a terminal. At the U.S. National Meteorological Centre, a scheme is being developed to treat ice as a time dependent land boundary.

It was pointed out that tuning a model must be done in a careful and systematic way in order to avoid it becoming a random exercise. It was noted that it is wise to avoid overfitting the model to data whose accuracy may not be completely known.

There was discussion about the apparent slowness of operational implementation of new wave models. Participants pointed out the considerable programming necessary to marry a wave model to an atmospheric model for the purpose of producing both wind and wave forecasts and the difficulty in transporting model code from the computer for which it was designed to any other machine. Part of the delay was also attributed to the mixture of research and

operational, government and private contract people who must work together to achieve useful results.

Although smaller computers often have sufficient power to run large forecast models, the models in general run too slowly to be useful for local forecasting except in limited fetch cases such as the Great Lakes or the Beaufort Sea.

It was widely agreed that better wind forecasts were a major factor in improving operational wave forecasts. These winds would be provided by improved atmospheric models operating on time and space scales relevant to the wave forecasting problem.

A man-machine mix which would allow the forecaster to assimilate wind and wave observations into the forecast cycle may bring about significant improvements in the forecasts. This interaction would allow the forecaster some judgment, based on experience,to accept or reject the data. There was some disagreement as to whether the man-machine interaction should take place at a central computer or at regional terminals.

Session C2 - Wave Model Evaluation

Chairman: L. Muir

Rapporteur: B. Toulany

Papers presented:

C2-1 A Sensitivity Study of Spectral Wave Growth Algorithms. V.J. Cardone and J.A. Greenwood.

C2-2 Ocean Wind and Wave Model Comparison With GEOSAT Satellite Data. R.L. Pickett, D.A. Burns and R.D. Broome.

C2-3 A Comparison of Hindcast Studies with (1) A Coupled Discrete Wave Model and (2) A Coupled Hybrid Wave Model. L.I. Eide, M. Reistad and J. Guddal.

Although the papers presented in this session were about wave model evaluation, the discussion following concentrated on wave model improvement.

The inclusion of wind gustiness was discussed as a potential improvement in wave models. It was concluded that mesoscale gustiness was probably more important than turbulence scale gustiness which is normally left out of wave models since the time scale of mesoscale variability is closer to that of wave growth. To assess the relative importance and usefulness of gustiness in wave models, it will be necessary to answer the following questions:

How much difference will it make?

How does it affect the wave growth rate?

Can it be parameterized? (in terms of wind speed, atmospheric stability or surface stress?)

How can it be measured in an operational sense?

How can it be included in wave models?

One participant mentioned that the more sophisticated wave models could act as a practical tool to validate other, simpler wave models.

The use of GEOSAT data to improve wave forecasts is not possible in real time due to the time required for the sensor footprint to get over a particular location, but is possible in near-real time.

As well as the gustiness issue, several topics for further work in wave model development were discussed. It was suggested that:

Spin-up and spin-down of storm wind fields at sea has not been adequately addressed and needs to be.

Improvements in the forecasts of winds in unusual meteorological conditions such as explosive cyclogenesis storms need to be made.

Spatially coherent error in specification of the wind field is an apparent problem in wave forecasting, in comparison to randomly distributed error which is effectively filtered out by the wave model. Tests with introduced spatially coherent errors in the wind field are needed to verify this assumption.

The relationship between wind conditions and growth curves needs to be investigated. This investigation may be done by stratifying all existing marine wind and wave data to determine what wind condition is associated with what growth curve.

Does $u*$ or $u_{10}$ govern the growth rate?

Session D - Model Development

Chairman: V. J. Cardone

Rapporteurs: D. Szabo

Papers presented:

D-1 The Incorporation of Real-Time Wave Measurements into Wave Forecasts. D.T. Resio.

D-2 Real-Time Spectral Wave Forecasting Model Test During CASP. B.M. Eid, V.J. Cardone, J.A. Greenwood and J. Saunders.

D-3 Accuracy of Numerical Weather Prediction Winds and Some Consequences for Wave Prediction. D.O. Hodgins and S.L.M. Hodgins.

D-4 An Intercomparison Study of Ocean Wave Models During the Canadian Atlantic Storms Project (CASP) - Some Preliminary Results. M.L. Khandekar, B.M. Eid and V.J. Cardone.

D-5 On the Utility of Satellite Sensed Wind Data for Ocean Wave Analysis and Modeling. R. Lalbeharry, S. Peteherych and M.L. Khandekar.

The apparent deficiency in accuracy of CMC winds during CASP was a major point of discussion in this session. No remedy for the problem was agreed upon, but these points were noted:

CMC has not yet been approached to clarify the problem.

The errors were worse on the Grand Banks than on the Scotian Shelf.

The apparent improvement in wind quality after two storms early in the CASP period has not been verified.

CMC winds have been noted to have a positive bias also on the west coast of Canada.

Hodgins' results on the effects of wind input errors on wave model outputs led to the apparent conclusion that errors of 100- 200% were possible in combination. The reality of the magnitude of the expected meteorological errors was discussed, and it was agreed that the imposed errors were the maximum conceivable and the worst case of resulting errors were those reported. Errors in combination would not possibly happen simultaneously in the worst conceivable case. Therefore, expected errors in practice would be much lower.

Wind direction as an important parameter for wave hindcasting was discussed. The lack of direction information from satellite scatterometer measurements, although a problem, was not seen as a serious deficiency in the measurement technique, since global wind speed information will identify characteristic high wind speed zones, which, coupled with directional analysis, will improve definition of high wave areas. Normal errors in wind direction were not thought to pose a major problem either, since energy in wave generation models is spread directionally and is smeared over a directional range by wind turning.

The use of METOC sea state analyses as initial state input for wave forecast models was discussed, and was believed to be useful provided the charts show sufficient skill. Their inclusion of swell however, posed a problem, since numerical diffusion of swell in wave

models is an unresolved problem.

The utility of the shallow water results from CASP as critical tests of shallow water wave models was questioned, since the meteorological forcing was complex as were the resulting wave regimes. The poor results of the WAVEAD model operated in CASP by NORDCO was discussed and attributed by the model's author to the inexperience of the operator rather than to inadequacies in the model itself.

Session E - Theory

Chairman: D. T. Resio

Rapporteurs: W. Perrie and F. Dobson

Papers presented:

E-1 A Third Generation Ocean Wave Model. G.J. Komen and L. Zambresky.

E-2 Observations of Velocities Beneath Wind-Driven Waves. M.A. Donelan and K.K. Kahma.

E-3 Wave Modeling Research Needs. C.L. Vincent.

E-4 Wave Growth Under Scattered Sea Ice. D. Masson and P.H. Leblond.

There was general questioning and justification of the third generation (3G) approach as compared to the first generation (1G) approach to wave prediction. Operational 1G models work well, and the 3G models don't appear to do much better. However, it was agreed that the use of 3G models is justified because they put the physics up front, where it can be tested; they should be better at handling out-of-the-ordinary situations (rapidly turning wind vectors, resonant growth in rapidly moving storms); they are only now becoming operational and so haven't been tuned to the extent the earlier ones have and they are more sensitive to errors in the data. Standards are required for reporting model error statistics.

There was a call for more carefully designed measurement and theoretical programs to improve our understanding of the wind in-put and dissipation source functions (particularly the latter). They are so poorly known that although included in the 3G models, it is hardly fair to call their inclusion "physics" over the full parameter range.

There was a call to the meteorological numerical and forecast modelers to provide precise definitions of the products they produce. In particular, surface winds need to be defined.

The modelers requested copious high-quality experimental data in order to carry out the critical tests required in order to go beyond the model intercomparison experiments like SWAMP and SWIM.

They need copious field data to give them statistics to overcome geophysical variability. The experimental data must be accurate and must be searched carefully for the special cases needed for the critical tests. Further field tests should be designed specifically with the modelers' needs in mind.

The need to predict dangerous events was expressed. Although some such events were mentioned, no workable general strategy was outlined for doing so.

The experimental work of Donelan and Kahma and the theoretical work of Masson and Leblond were discussed in some detail. Both were recognized as important contributions to the field: the water velocity work because it led into a more precise definition of wave induced forces and understanding dissipation by breaking; and the theoretical work because of its central relevance to existing efforts to develop the ice-infested high-latitude continental shelf regions.

Linwood Vincent announced plans to set up and be the founding chairman of a wave measurement, modeling, hindcasting and prediction society. International recognition of this society will be needed for it to be useful.

The group expressed optimism for the future, based on the present level of well-directed and active research and development.

Session F - Hindcasting

Chairman: K. Sato

Rapporteur: T. Agnew

Papers presented:

F-1 The Establishment of a Severe Storms Data Base for the Prediction of Extreme Environmental Conditions from Hindcast Data. O. Brink-Kjaer, J.B. Nielsen, and L. Watson.

F-2 Identification of Severe Wave-Producing Storms Affecting Coastal Areas of Eastern Canada. R.D. Brown, P. Roebber, K. Walsh and V. Swail.

F-3 The North European Storm Study (NESS). P.E. Francis.

F-4 On the Adequacy of Hindcast Data in Structural Design. S. Haver.

F-5 The Specification of Univariate Extremes and Multivariate Scenarios from Spatial Fields. D.T. Resio.

F-6 A Review of Extreme Wave Height Studies for the Canadian Beaufort Sea. M.A. Murray, M.A. Maes and L.R. Muir.

There was some discussion concerning the adequacy of wave hindcast databases and user requirements. It was noted that hindcasts performed for one purpose may not provide results acceptable for another. While the NESS program is taking great care to provide a general hindcast data set that will be widely accepted by the European community, the hindcasts done on the Canadian East Coast and in the Beaufort Sea for specific engineering purposes did not provide results of general utility.

While it was agreed that extreme waves could be predicted from a selection of severe storm hindcasts, it was less well accepted that 100 year waves could be modeled by extrapolating severe storms to predict a 100 year storm, and then use that storm to hindcast the waves. There was also some discussion about the usefulness of extreme storm wave predictions when in fact, with smaller, more compliant structures, repeated occurrence of waves whose periods were close to periods of structural resonance might in the long term be more severe for the structure.

The stationarity of time series was brought into question. Since offshore meteorological time series in Canada are, at best 30 years long, decadal variability might not be sufficiently resolved to allow for proper extreme value analysis. Long period variability in Beaufort Sea ice cover and in East Coast iceberg counts were also discussed in this manner.

The existence of the several generations of wave models led to a discussion of the criteria for the selection of one model over another. The relevant criteria were:

Quality of input data (good, poor, copious or sparse)
User requirements (spectral or parametric)
Physical situation being modeled (fetch limited or not).

Session G - Summary Discussion

Chairman: V. R. Swail

Rapporteur: J. R. Buckley

Rapporteurs' presentations:

Session A: M. L. Khandekar

Session B: D. Bliss

Session C1: R. Shaw

Session C2: B. Toulany

Session D: D. Szabo

Session E: F. Dobson

Session F: T. Agnew

Discussion started with a question about the apparent inadequacy of existing hindcasts in Canada. In defence of the existing hindcasts it was noted that they were all performed for specific engineering projects, and were acceptable for those projects. The point was made that the offshore industry is experienced in offshore structure design and has a good safety record. Any inadequacies in wave hindcasts are accounted for by being conservative in the engineering of the structures. Thus waiting for the "best" science can be avoided. It was noted that the hindcasts performed for Mobil's East Coast development projects would eventually become public.

The interest shown in the workshop for marine wind research was noted and was attributed to the fact that winds cause waves and therefore are an important part of wave research. Bad winds give bad wave predictions but good winds do not necessarily give good waves. Numerical weather prediction is optimized to serve land-based and aviation, not marine, operations. The apparent lack of appreciation by weather forecast centres for the importance of surface wind predictions for waves was noted. The example was given of how in the middle of CASP the U.S. NMC pulled its LFM wind model out of its east coast weather prediction system in favour of the NGM, which, in terms of the adequacy of surface winds for wave prediction, was a step backwards. To obtain more useful and consistent surface wind predictions, there must be an increased interaction between wind and wave forecasters.

It was also noted, in defence of the wind modelers that there are almost no measurements of marine winds for modelers to calibrate models against. Therefore there is a task for the oceanographers to provide the wind forecasters with research quality marine wind data.

One type of wind input that the oceanographers thought was important, and that was a problem for the numerical weather predictors, was the specification of the marine wind field on very short spatial scales (5-10km) in the coastal zone. Our lack of ability to differentiate between the accuracy of output of the various wave models in mid-ocean was pointed out and attributed to the lack of observations. The use of satellite data was suggested to remedy this situation.

The utility of investigating systematic errors in wind forecast models and the relative improvement offered by a man-machine mix was discussed. It was suggested that such an investigation might not be useful since the wind models often changed, sometimes subtly, sometimes dramatically. It was pointed out that, in any case, the machine should be relied upon to provide the best possible advice to the forecaster, who then is forced to make an even better guess.

Discussion continued on the topic of wave physics. It was noted that in carefully run experiments such as JONSWAP, the wind data have little scatter, but there is a large scatter in the Peak Enhancement Factor. Therefore something may be missing in the physics. The suggestion was made that perhaps too much blame has been placed on poor winds for the sometimes inadequate performance of wave models. It was noted that ONR has a new Wave Dynamics Initiative that will critically examine the wave physics specifically in the areas of the importance of wave-wave interaction, wave-current interaction, coupling between source functions, and wave breaking as a function of wave growth.

All generations of wave models work in an operational sense. The fact that 1G and 2G models employ different source functions, but may be tuned to give the same results is an indication that they shed little light on the essential physics of waves but a lot on the mechanics of model tuning. The 3G models produce good results by physics. There was a suggestion that the 1G and 2G models actually worked better than the 3G model, but the older models will perform worse under extreme conditions since they have not been tuned for them, whereas the physics in the 3G model will help it perform.

There was a renewed controversy over which one of u or $u_*$ is the appropriate input term for wave generation. Both cannot be right. Kitaigorodskii raised the problem first in 1961 and it still hasn't been adequately addressed. The possibility of interpreting a WOTAN measurement as $u_*$ was raised. It was stated that CASP couldn't afford to measure $u_*$.

The wave-in-ice work of Masson and Leblond was noted to have importance operationally for the Canadian East Coast where pack ice is seasonally present.

The general state of the art of wave modeling was applauded, and the suggestion was made that it was time to start to use the output from wave models to work on the larger problems of the ocean-atmosphere system. Suggestions included looking at the contributions of waves to mixed-layer dynamics. This suggestion and the expectation of WOCE that wave models would provide predictions of momentum input to the ocean were deemed beyond the state of the art at this time.

A note of caution was introduced on using different models to discriminate between physical principles in wave dynamics, since computer programmes are subject to programming errors. Carefully designed experiments were recommended as superior discriminators of the essential physics in models.

The accuracy of estimates of $H_{max}$ was questioned since the entire discussion had involved only $H_S$. It was pointed out that, since wave models are inherently spectral, they produce $H_S$ directly but $H_{max}$ only statistically.

There was a recommendation that Canada become involved in the NESS program in order to get the data which the model generated for the Canadian offshore. Part of this involvement must include an attempt to ensure that the quality of analysis is uniform across the grid so that the results are useful for Canada.

It was recommended that C.L. Vincent's call for an international wave working group be heeded. The contribution of the WAM group was noted but it was thought that SCOR should be approached to sponsor a group. It was also noted that there was a WMO group on waves chaired by J. Guddal. He stated that there would be a global conference in 1988 on the scientific aspects of wave modeling and on the assimilation of satellite data. There was the offer of opportunity for Canadian participation.

The wave modelers thought that such a group was not necessary for themselves, since they talked frequently among themselves anyway, but thought it was a useful idea in order to communicate with others. It was also suggested that the group be separate from WAM, since there was little financial support in North America for basic research of the sort done by WAM. The best that could be done is to collect North American ideas together and contribute them to WAM.

A discussion on the usefulness of field experiments yielded the following points:

- A focus on field data is necessary in order to reveal the weaknesses in 3G models.
- Experiments to date have been done without sufficient care in the meteorology.
- Model comparisons themselves don't prove anything about differences in wave physics.
- Instrumental data alone may not be enough to distinguish between u and $u_*$.
- Satellite data will overcome the problems inherent in site specific data collection, although there is still a need to measure $u_*$ in a site specific sense.
- Certain aspects of wave models can be tested with existing wave instrumentation but they are probably not sufficient to distinguish between models.
- It was pointed out that radar is capable of making the best surface wave measurement and that a recent JPO article described the calibration of a surface contouring radar against buoys and the bettering of those measurements by internal consistency checks.

Areas suggested for further work were:

- The surface wind stress and the stage of wave development apparently regulate the partition of momentum: i.e. $c_D$ changes with stage of wave development. This change needs to be investigated.
- Satellite-borne scatterometers will provide winds, but more work needs to be done on the corrections applied to the computed wind fields due to the presence of waves.
- How does shallow water dissipation affect the modeling process, since it is apparently possible to get good results with no bottom friction?
- Studies of wave transformations in shallow water, in as far as the surf zone in both the space and time domains are needed to guide modelers.

- Shallow water kinematics needs a proper parameterization of forces and loads.
- Shallow water versions of wave-structure and wave-current need to be developed.
- The traditional engineering approach of combining loading effects leads to structural overdesign. A statistical approach needs to be developed.

**APPENDIX 1**
**POSTER/DISPLAY SESSION**

- **The Operational Ocean Wave Forecasting Program of the Canadian Forces Meteorological and Oceanographic (METOC) Centre, Halifax, Nova Scotia**

  Presented by: W.G. Lumsden
  Officer-in-Charge
  Canadian Forces METOC Centre
  Halifax, Nova Scotia

  R.K. Cross
  Senior Staff Officer
  Scientific Services
  Canadian Forces Weather Service
  Ottawa, Ontario

- **Remote Sensing of Currents by HF Radar**

  Presented by: D.J. Lawrence
  Department of Fisheries and Oceans
  Bedford Institute of Oceanography
  Dartmouth, Nova Scotia

  Shore-based groundwave HF radar (CODAR) has been employed by DFO/BIO in three oceanographic experiments since 1983. Current maps with a spatial resolution of 1.2 km are obtained. CODAR gives an average vertically over a range comparable with the surface wave height, of order 1 metre. The CODAR velocities are here compared with Eurlerian velocities from near surface moored current meters and Lagrangian velocities derived from surface drifters.

- **A Graphics Display of Wind Information Derived from Satellite Passive Microwave Data**

  Presented by: Ph.D. Associates Inc.
  Rexdale, Ontario

- **Results from Recent Wave Data Measurement and Analysis Projects; Real-Time Wave Data Collection/Spectral Analysis Computer System and Software**

  Presented by: Dobrocky Seatech
  St. John's, Newfoundland

- **Potential Accuracy of a Lake Wave Model Tested on Lake Huron and the Beaufort Sea**

  Presented by: S. Clodman, S. Venkatesh
  Meteorological Services Research Branch
  Atmospheric Environment Service
  Downsview, Ontario

  and

  B. Eid
  MacLaren Plansearch
  Halifax, Nova Scotia

# POTENTIAL ACCURACY OF A LAKE WAVE MODEL

# TESTED ON LAKE HURON AND THE BEAUFORT SEA


| Stephen Clodman | Bassem Eid | S. Venkatesh |
|---|---|---|
| Atmospheric Environment Service<br>Downsview, Ontario | MacLaren Plansearch<br>Halifax, Nova Scotia | Atmospheric Environment Service<br>Downsview, Ontario |


## 1. INTRODUCTORY SUMMARY

The modelling of waves on the surface of the Great Lakes and the Beaufort Sea has been studied as part of a project to implement an operational forecast procedure. This report is a synopsis of work done, and a discussion of its potential significance. It will discuss how accurately one can simulate and forecast waves on the Great Lakes and the Beaufort Sea, what the main sources of error are and how one might overcome them. A proposal to improve the model will be demonstrated.

The model for Beaufort Sea cases in use is an Eulerian momentum balance non-spectral model developed by Dr. Mark Donelan of the Canada Centre for Inland Waters. An improved version developed by the U.S. Great Lakes Environmental Research Laboratory (GLERL) as documented in Schwab et al. (1984) is used for the Great Lakes. In this model, the input is the wind velocity interpolated to each time step and grid point. The wind impacts an increment of momentum to the wave at each time step at each grid point. The increment may increase or decrease the magnitude of the momentum, and may change its direction. Once the wave momentum is calculated, wave direction, period and height are derived. Shallow water effects — bottom drag and refraction — might be introduced later if desired.

We will discuss the following questions:

- Deep water approximation. The "deep water" approximation is suitable for most general purpose modelling on the Great Lakes but there are circumstances in which it is inaccurate.

- Form of input wind. Accurate local winds, such as from a data buoy, are best. Other forms, such as numerical model winds, are suitable within limits.

- Planetary boundary layer. Seasonal statistics show the tendency of wave heights to be greater in unstable conditions. The current model version allows for this.

- Wave development with wind. Increasing the forcing applied to build the wave obtains a more realistic result. Altering the form of the wave drag equation may also lead to future improvement in the modelling.

## 2. DEEP WATER APPROXIMATION

Shallow conditions alter (usually reduce) wave height, reduce wave period, and turn the wave towards shore by refraction. The principles of compensating for shallow water effects are known. However, it is easier and cheaper to run a model without these effects. The problem is to determine when it is acceptable to make such a deep water assumption.

The relative importance of shallow water effects increases with decreasing D/L or decreasing D/H. (Here D is the water depth, L the significant wavelength, H the significant wave height). A scale analysis would show that the shallow water effect is substantial for D/L below .35 or D/H below 10. A consequence is that shallow water effects increase with windspeed and lake size, since these factors lead to larger waves.

The specific lakes are considered using scale analysis, model test runs, and examination of bathymetric charts. Typical storm conditions are assumed, with winds blowing along the long axis of the lake.

- Lake Ontario is comparatively small, with depth fairly large except for the northeast corner -- deep water assumption holds except in northeast corner.

- Lake Erie is fairly small, but the depth is also small especially in the west -- shallow water effects are significant, especially in the west. However, deep water calculations will give a reasonable upper bound to the wave height.

- Georgian Bay is small, with depth moderate away from the irregular shoreline — deep water approximation applies if well away from shore.

- Lake Huron is a medium sized lake of mostly moderate depth, except for shallow Saginaw Bay and some 30 m shoals — deep water approximation marginally satisfactory.

- Lake St. Clair, although very small, is also very shallow — the deep water assumption is not valid. Fortunately shallow water effects should be relatively simple here since the bottom is flat and wave heights small.

- Lake Michigan is medium sized (but elongated) and deep except in the northeast corner — deep water values correct except in northeast corner.

- Lake Superior is large and, though deep on average, has many islands and shoals and a large peninsula — deep water assumption correct over most of lake but will fail locally.

- Beaufort Sea is very large but highly variable in size due to the ice boundary. It has a shallow sloping shelf at the southern shore dropping off to great depth seaward — deep water approximation is accurate well offshore but may fail nearer the shore.

Overall, it is acceptable to neglect shallow water effects on the Great Lakes and the Beaufort Sea for general purpose wave forecasting away from shore, provided a moderate overestimate of the wave and sonic inaccuracy in its direction is permissible. For the rest of this paper, the deep water assumption is used.

## 3. INPUT WIND

We now consider the input wind. As with most wave prediction models, wind is the basic input variable. Wave observations are used only for verification. Experience shows that the quality of the input wind is the most important determinant. Accurate input winds are necessary for accurate results. If accurate input winds are available, accurate results are usually obtained.

Initially runs were made with input winds from the lowest level of the Canadian Meteorological Centre (CMC) forecast model. These are historical cases and analyzed, rather than forecast, winds are used. Tests were done on various lakes and the Beaufort Sea. Also model runs were made using buoy winds as input.

These runs used an older version of the wave model, a modification of earlier work by Donelan. (The improved version will be discussed later). This version had a "fossil" wave, a simple substitute for a swell wave; but this is ignored in the results to be shown. To empirically correct for a low wave bias, the wind speed was multiplied by 1.2 for the CMC wind and by 1.5 for the observed wind. Observed wave heights are

here rounded to 0.5 m. The input and verification data are at buoy 45003 (45.3°N, 82.8°W) of the U.S. National Data Buoy Center. Figures 1 and 2 show respectively wave height comparisons for the CMC and buoy input winds.

The important thing to note is that the wave height hindcast with buoy winds is more highly correlated to that observed than is that using CMC winds. Wave height peaks are either missing (2, 9 November) or flattened (3, 6 November) in the version using the CMC wind input; but these are all accounted for in the buoy wind input.

In the Beaufort Sea portion of the study (MacLaren Plansearch, 1986) a similar comparison was made. Here no empirical increases were made to the windspeed. The verification observations were 25 July - 5 October 1981 at several stations concentrated about 70.5°N, 135°W; the input wind station (Kopanoar) was near this point.

The Beaufort Sea statistical average results were for runs using CMC observations: RMSE 1.06 m, bias -0.39 m, correlation 0.34. Comparable buoy observation input results were: RMSE 0.81 m, bias +0.20 m, correlation 0.70, which is considerably better. An examination of day-by-day results (not shown) shows that wave height peaks are usually missing or flattened in the CMC wind run but much better identified in the observed wind run.

The CMC numerical weather prediction model is that current at the time of the cases (1981 or 1982). It is possible that more recent versions of the CMC model would give better results, but that remains to be tested. Numerical models in use by other countries have not been tested in this study, but it is likely that they would give similar results.

Certain conclusions are possible. First of all, it is best to use buoy wind observations whenever possible to compute wave analyses. Second, it is important to improve the accuracy of surface wind forecasts. In general one can say that wind forecast errors rather than wave model limitations are the most important constraint on potential wave forecast accuracy.

## 4. BOUNDARY LAYER AND SHORELINE EFFECTS

So far, the wind has been input unaltered into the wave model. However, two types of planetary boundary layer adjustment are needed to refine the input wind. First of all, the anemometer height must be corrected for. We take 10 m as the standard height. The Great Lakes data buoys have a 5 m anemometer height; therefore, their windspeed must be increased to give a 10 m standard. The Beaufort Sea anemometers are at heights from 27 to 65 m; their windspeeds must be reduced. Secondly, the effective wind must be found at the actual sea surface; this is not the same as the 10 m wind.

To do this, some boundary layer profile method must be used, for example a friction velocity calculation. This takes into account static stability as expressed by the air-water temperature difference. For a given observed wind, unstable conditions give a higher effective wind than stable conditions, and thus higher waves also.

The effect of static stability can be roughly estimated from Table 1. It can be seen that as the season advances, conditions proceed from stable to unstable, the wave height increases much more rapidly than the wind speed. By comparison, Sverdrup-Munk-Bretschneider (SMB) wave theory, for a 200 km fetch gives $H = 0.32$ m for $U = 3.4$ m $s^{-1}$ (the May value) and $H = 0.95$ m for $U = 6.3$ m $s^{-1}$ (the November value). It can be seen that even for average conditions static stability is of some importance.

It is intended to study in some detail the effect of allowing for static stability and anemometer height in wave predictions, both on the Great Lakes and the Beaufort Sea. The results of a preliminary investigation on the Beaufort Sea were calculated for the Kopanoar station (70.5°N, 135°W), over the 1981 period, for observed input winds. The RMSE was reduced from 0.87 to 0.83 m. Since the bias was altered from 0.20 m to -0.40 m, the random RMSE (of variation about the mean) was reduced from 0.85 to 0.73, a moderate decrease. Correlation coefficient increased from 0.61 to 0.70. Since improvements to be discussed in the next section will tend to increase the wave height forecast, the bias will be decreased in the long run.

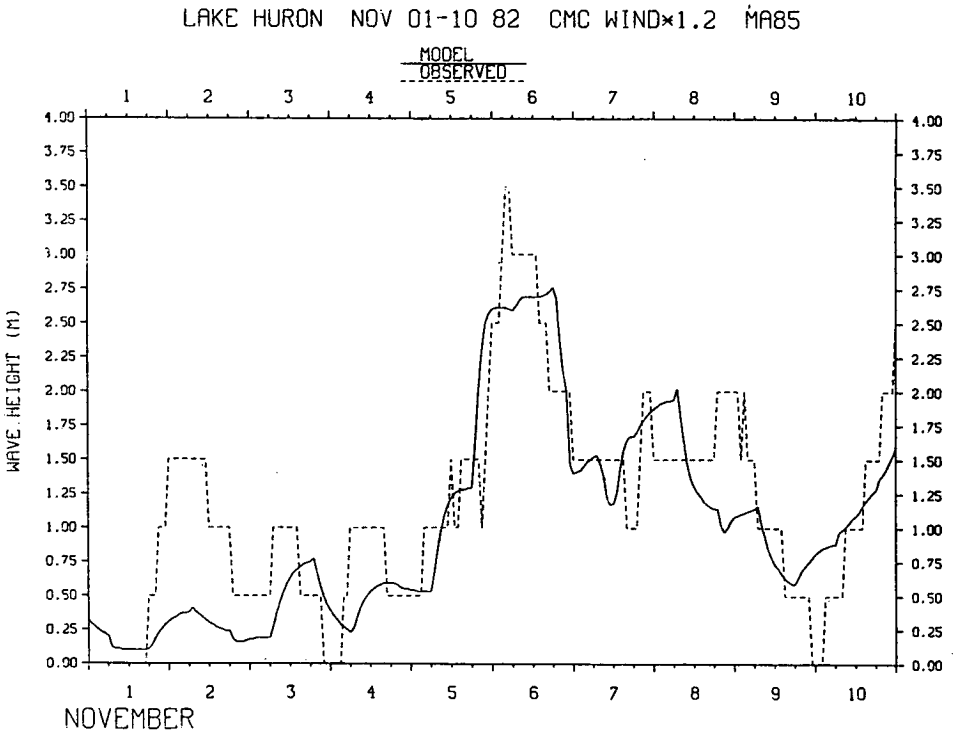


Fig. 1. Model hindcast wave height against observed. Model uses CMC wind input. Old version of model used. CMC wind speed multiplied empirically by 1.2 to correct bias. Wave height observations rounded to 0.5 m. Location of forecast and observation is NDBC Buoy 45003 (45.3°N, 82.8°W).

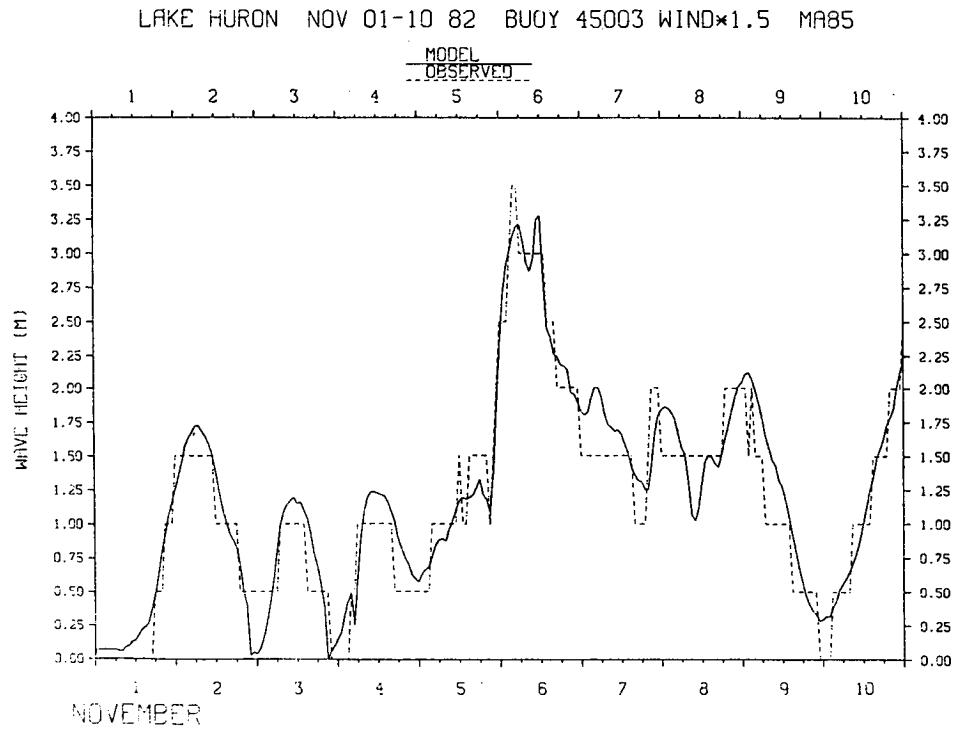


Fig. 2. As in Fig. 1, but model uses buoy observed input winds, empirically multiplied by 1.5.

Table 1: Monthly averages of significant wave height (H), air-water temperature difference (DT) and wind speed (U) observed by buoy; also CMC U at buoy location (Lake Huron buoy NDBC 45003 - 45.3°N, 82.8°W - 1982

| | H (m) | DT (°C) | U ($m\ s^{-1}$) | $CMC_1$ U ($m\ s^{-1}$) |
|---|---|---|---|---|
| May | .24 | 2.9 | 3.4 | 4.9 |
| June | .27 | 3.0 | 3.5 | 4.8 |
| July | .38 | 3.0 | 3.5 | 4.7 |
| August | .63 | 0.6 | 4.1 | 5.2 |
| September | .76 | 0.8 | 4.7 | 6.4 |
| October | 1.05 | -0.8 | 5.6 | 7.2 |
| November | 1.26 | -2.3 | 6.3 | 7.4 |

The newer (GLERL) version of the model, now being run on the Great Lakes, has an allowance for wave dispersion. Some wave energy from points with larger wave energy disperses laterally across the direction of wave motion to points with lower wave energy. This prevents shoals and peninsulas (e.g. Keewinaw Peninsula of Lake Superior) from casting an excessively sharp "shadow" of low wave values. The dispersion does have the effect of reducing slightly the overall strength of fetch-limited waves.

The Beaufort Sea, and sometimes also the Great Lakes, are affected by variations in ice boundary. For a specific late summer case, Figure 3 gives the actual ice boundary and its climatological variation. Figure 4 illustrates a hindcast for Kopanoar for that case. It can be seen that the effect is an important one.

## 5. WAVE RESPONSE TO WIND

Figure 2 shows that the wave responds qualitatively correctly to the wind. However, since the input windspeed had to be multiplied by 1.5 it must be said that the wave was being underforecast. In addition, details of the forecast might be improved. Accordingly, a program of study and improvement of the wave response function is underway, using Lake Huron cases. A complete archive of buoy data was obtained, with wave heights to 0.1 m and periods to 0.1 s.

So far, conversion to the new version of the program has the following effects: Wave dispersion slightly reduces the average forcing for fetch dependent cases. Allowing for anemometer height (5 m) moderately increases forcing. Static stability (air-water temperature difference) increases forcing for unstable cases (such as Figs. 1 - 2) and decreases it for stable cases. The overall effect is to somewhat increase the strength of wave forcing and the average height obtained, but not sufficiently to eliminate all bias.

Ideally, both average and peak waves should be accurately forecast, and changes should be properly timed. In simple terms, as seen in Figure 5, there are four situations to be handled: constant, developing, decaying and turning waves.

Increasing the empirical fraction of the stress retained by the waves from .028 to .100 obtains a hindcast that is in general very good, without needing any artificial multiplication of the input windspeed (the 1.5 factor above). See Figure 6. Errors both at average and peak wave heights are small and the wave buildup is accurately timed. Wave decay rate tends to be moderately overestimated. Also wave height decay when the wind turns is exaggerated. Wave period forecasts are not quite as good; the correlation against observed period is quite high, but the up and down swings are exaggerated.

To obtain further improvement it is necessary to consider altering the form of the wave forcing equations. The forcing function in the Schwab et al. (1984) model is

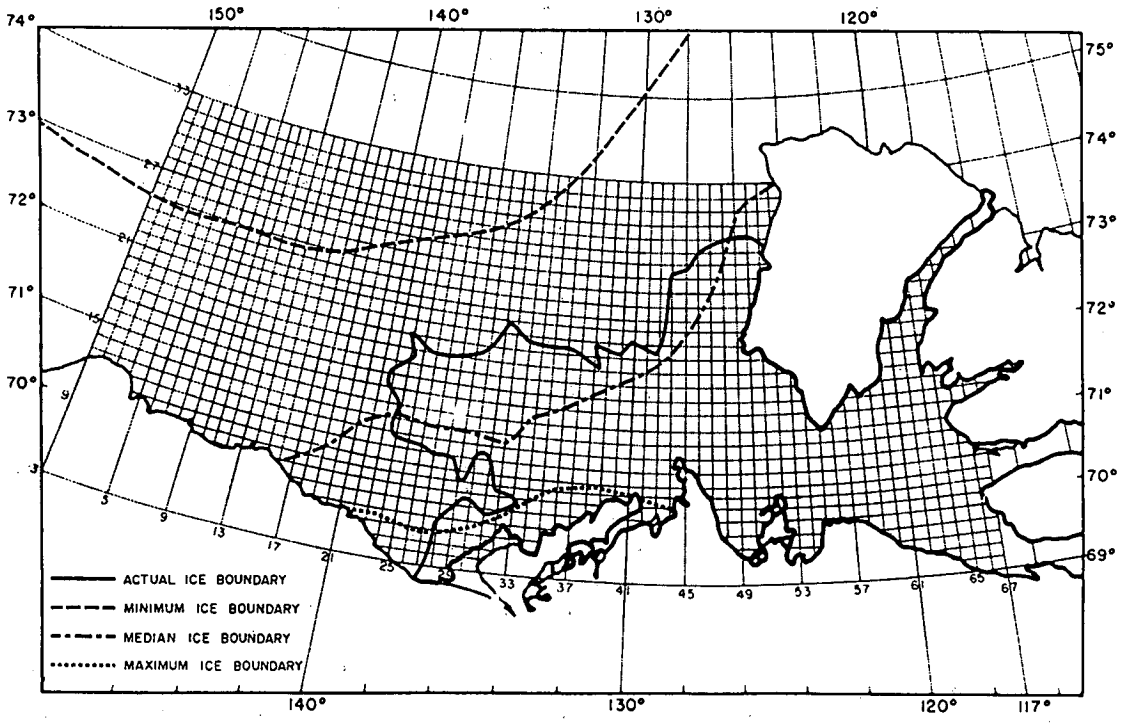


Fig. 3. Map of Beaufort Sea. Observed ice boundary for Aug. 28 - Sept. 3 1981 case shown. Also range of climatological ice boundaries for that date shown.

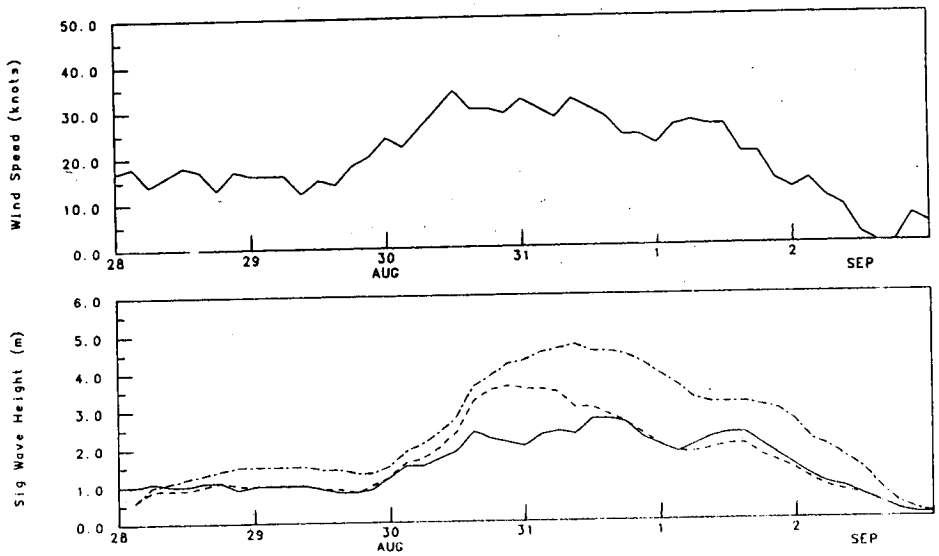


Fig. 4. Wave height hindcast for Kopanoar (70.5°N, 135°W) in the Beaufort Sea, in 1981. Solid line - observed ice boundary used. Dashed line, dash-dot line - median and minimum climatological ice boundaries used. Station is on ice at climatological maximum. See Fig. 3 for boundaries. Wind speed also shown.

based on a form drag concept and is proportional to $(U - .83\ C)^2$ where U is the wind velocity and C the wave phase velocity. This type of equation has the effect of making the final convergence of the wave to its fully developed value too slow, especially for lighter wind cases.

Accordingly, experiments have been conducted with a linear U - .83 C type of forcing, which can be thought of as a sort of skin drag. See Figure 7. This more nearly resembles the forcing function usually used in spectral models. It has the advantage of non-dimensionalizing the forcing; i.e., the development curves as in Figs. 7.4 - 7.7 of SWAMP (1985) are independent of the magnitude of U. Figure 8 is an adaptation of their Fig. 7.6. Initial results with this type of equation are also very good. The optimum forcing strength is close to that of the more strongly forced of the models discussed in SWAMP (1985). Further study will be done of the merits of this type of forcing.

## 6. APPLICATIONS AND CONCLUSIONS

The model is now being used as operational guidance in wave height forecasts. The Ontario Weather Centre of the Atmospheric Environment Service (AES) is using a version of the older program of Donelan as operational guidance in Great Lakes forecasting. In addition, the Centre is using a microcomputer version of the original GLERL code as a backup (the Hydrometeorology Division of the AES participated in this development). Certain U.S. National Weather Service forecast offices are using the GLERL version of the model for operational guidance. It is intended to use the present study to further improve the operational use of the model.

This study has used systematic consideration of water depth, static stability, the wave forcing function and other factors to demonstrate that this type of modelling can forecast Great Lakes and Beaufort Sea wind waves accurately. It should be possible to obtain insight into the general behaviour of waves. Moreover, with accurate forecast winds, accurate wave forecasts for operational use can be obtained.

## REFERENCES

MacLaren Plansearch, 1986: Forecasting Beaufort Sea wind waves by a momentum balance method. Contract report, file 48933, MacLaren Plansearch, Halifax, N.S.; 180 pp + appendices.

Schwab, D.J., J.R. Bennett, P.C. Liu and M.A. Donelan, 1984: Application of a simple numerical wave prediction model to Lake Erie. J. Geoph. Res. V89, No. C3, pp 3586-3592.

SWAMP Group, 1985: Ocean wave modelling. Plenum Press, New York, 256 pp.

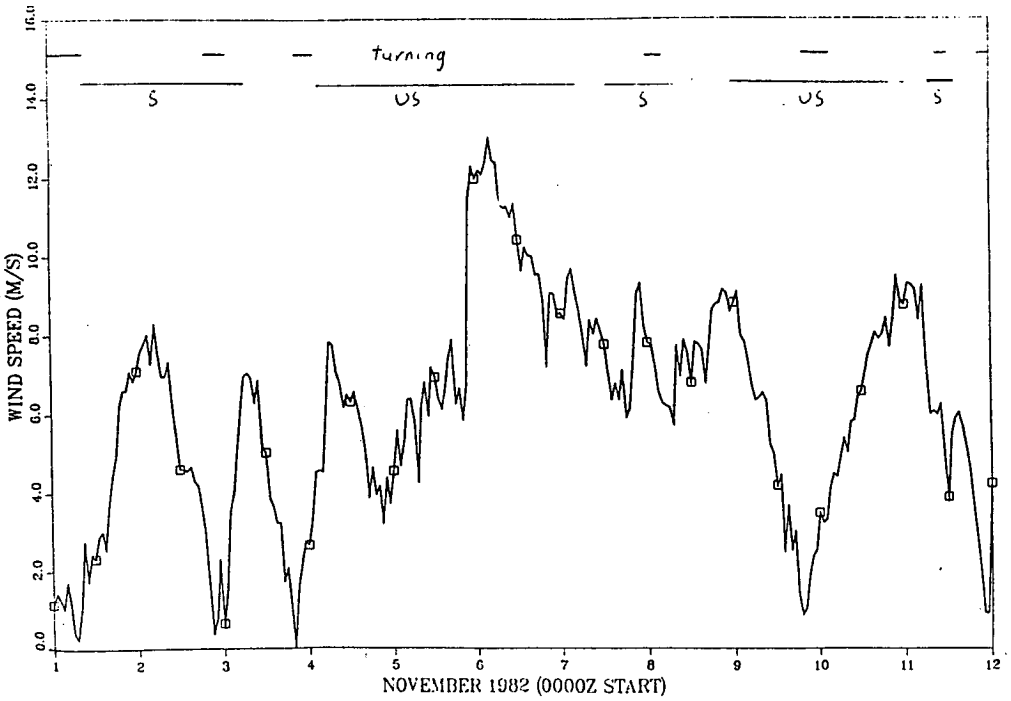


Fig. 5. Wind speed observations, from NDBC Buoy 45003 145.3°N, 82.8°W). These buoy winds are used as input to the model forecasts. Periods of rapid wind turning, and of stable (S) and unstable (US) conditions indicated.

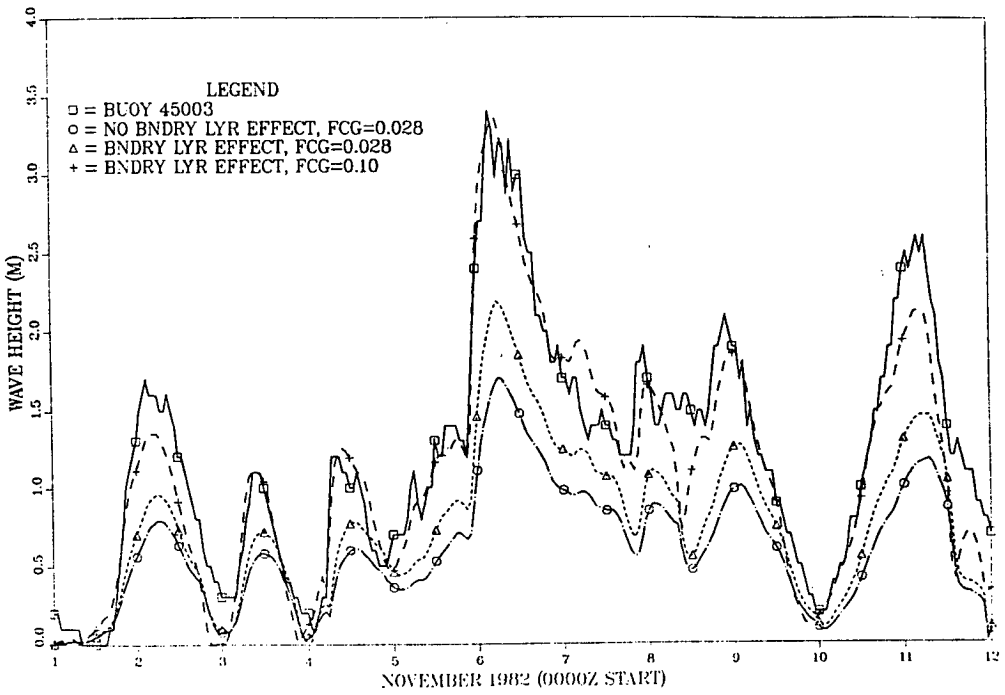


Fig. 6. Wave height hindcast, using winds as in Fig. 5. Boundary layer effect and wave forcing coefficient discussed in text. Buoy 45003 curve is verification observations.

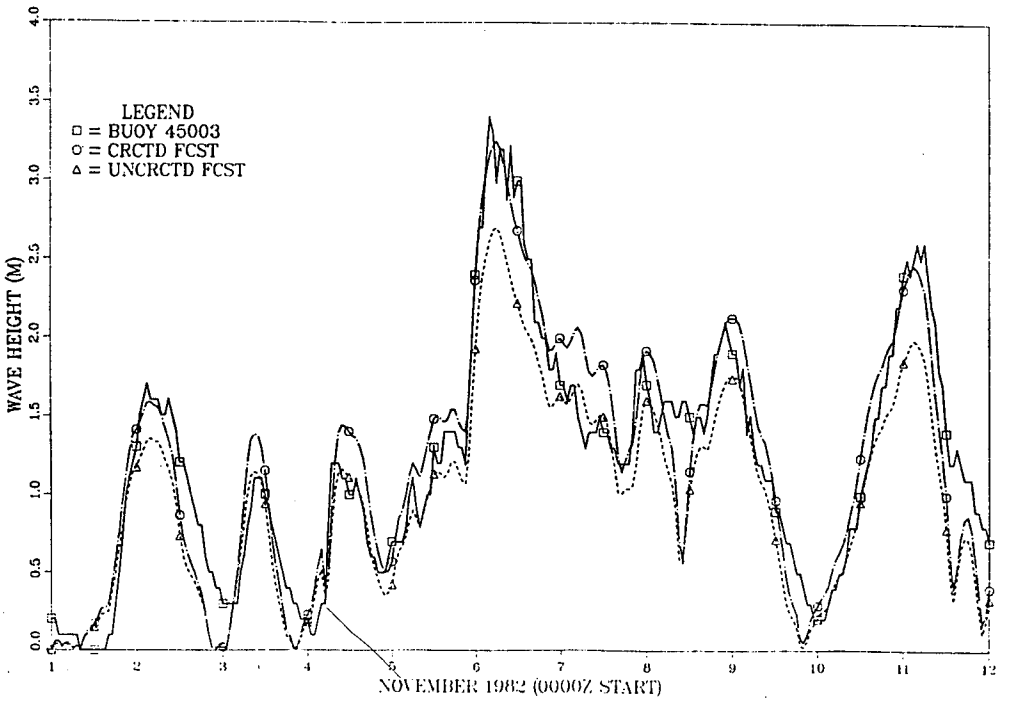


Fig. 7. Wave height hindcast, using Fig. 5 winds. Forcing function varies as U-.83 C (see text). Corrected forecast has boundary layer calculation; uncorrected does not.

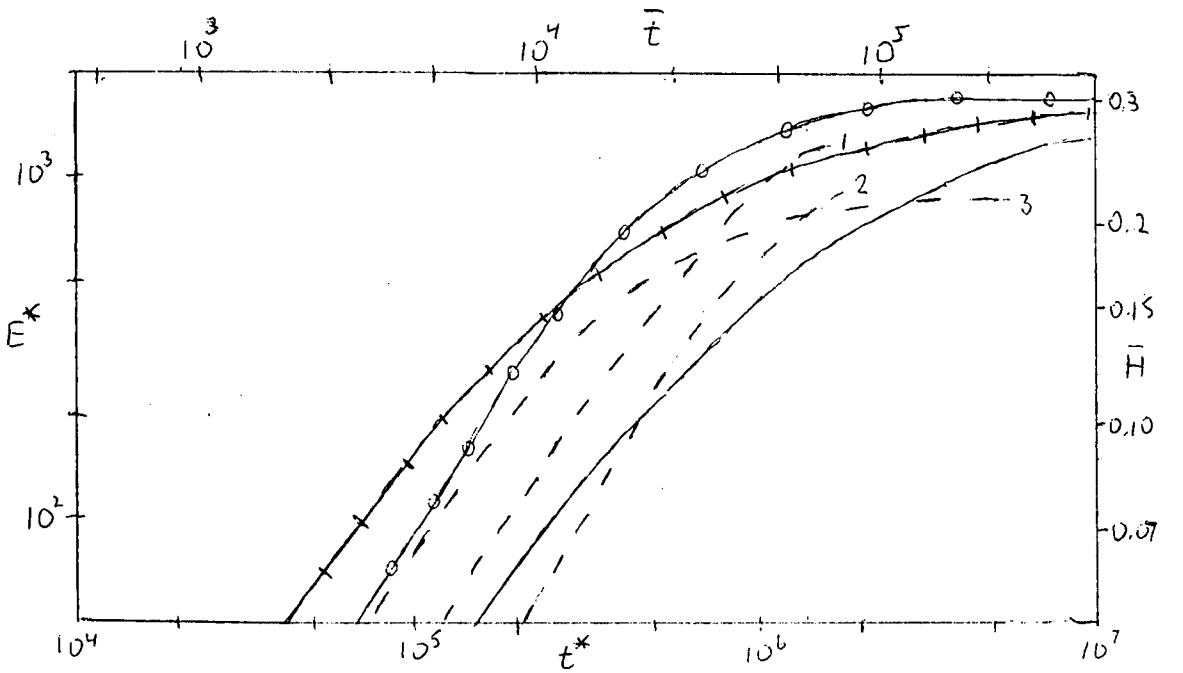


Fig. 8. Wave build up curves. Assume wind unidirectional at constant speed from time zero. Solid line: standard model forcing 0.028, U = 10 m $s^{-1}$. Solid line with tick marks: forcing 0.10, U = 10 m $s^{-1}$. Solid line with circles: momentum change varies as U-.83C. Dashed lines: typical spectral models 1 BMO, 2 TOHOKU, 3 GONO. Nondimensional values of time $\bar{t} = tgU^{-2}$, $t^* = tg(u_*)^{-2}$; of wave height $\bar{H} = g^2HU^{-2}$, of wave energy $E^* = g^2E(u_*)^{-4}$. $u_*$ is friction wind speed.

**APPENDIX 2**

**LIST OF PARTICIPANTS**


Tom Agnew
Atmospheric Environment Service
4905 Dufferin Street
Downsview, Ontario
M3H 5T4

Hubert Allard
Atmospheric Environment Service
Department of Environment
2121 North Service Road
Suite 504, T.C.H.
Dorval, Quebec
H9P 1J3

Carl Anderson
Fisheries & Oceans Canada
Bedford Institute of
Oceanography
P.O. Box 1006
Dartmouth, Nova Scotia
B2Y 4A2

Bill Appleby
Canada Oil and Gas Lands
Administration
355 River Road
Ottawa, Ontario
K1A 0E4

Susan Bales
David Taylor Naval Ship
R&D Centre
Bethesda, Maryland 20084-5000
U.S.A.

Robert C. Beal
John Hopkins Applied Physics
Lab.
Laurel, Maryland 20707
U.S.A.

Alan Bealby
Atmospheric Environment Service
Department of Environment
4905 Dufferin Street
Downsview, Ontario
M3H 5T4

Dr. V. Barthel
National Research Council
Montreal Road, Bldg. M-32
Ottawa, Ontario
K1A 0R6

Stephen R. Blackwell
Atmospheric Environment
Service
Department of Environment
4905 Dufferin Street
Downsview, Ontario
M3H 5T4

R.D. Brown
Atmospheric Environment
Service
Department of Environment
4905 Dufferin Street
Downsview, Ontario
M3H 5T4

J.R. Buckley
2526 Dalhousie Street
Victoria,
British Columbia
V8R 2H7

David G. Burley
Canada-Newfoundland
Offshore Petroleum Board
5th. Floor, TD Place
140 Water Street
St. John's, NF
A1C 6H6

John O. Bursey
Atmospheric Environment
Service
Department of Environment
1496 Bedford Highway
Bedford, Nova Scotia
B4A 1E5

V.J. Cardone
Oceanweather Inc.
5 River Road
Cos Cob, CT 06807
U.S.A.

Dr. Yung Y. Chao
NOAA/NOS/OPC
World Weather Building
5200 Auth Road
Washington, D.C. 20233
U.S.A.

Stephen Clodman
Atmospheric Environment Service
Department of Environment
4905 Dufferin Street
Downsview, Ontario
M3H 5T4

M.E. Coolen
Mobil Oil Canada Ltd.
Suite 1004
1809 Barrington Street
Halifax, Nova Scotia
B3J 3K8

Robert Cross
DND-Canadian Forces Weather Service
101 Colonel By Drive
Ottawa, Ontario
K1A 0K2

William F. Cross
Office of Naval Research
800 N. Quincy Street
Arlington, Virginia 22217-5000
U.S.A.

T.A. Danks
METOC Centre
FMO Halifax
Halifax, Nova Scotia
B3K 2X0

Bodo deLange Boom
Seakem Oceanography Ltd.
2045 Mills Road
Sidney, B.C.
V8L 3S1

Jose Enrique de Luis Guillen
Programa de Clima Maritimo
Y Banco de Datos Oceanograficos
Direccion General de Puertos y Costas
747M.O.P.U.
P. Castellana, 16-28046 MADRID

Sylvain de Margerie
ASA Consulting Ltd.
P.O. Box 2025
Dartmouth East
Dartmouth, Nova Scotia
B2W 3X8

Dr. W.J.P. De Voogt
Delft Hydraulics Laboratory
P.O. Box 152
Emmeloord, Netherlands
8300 AD

Dr. F.W. Dobson
Ocean Circulation Division
Department of Fisheries & Oceans
P.O. Box 1006
Dartmouth, Nova Scotia
B2Y 4A2

Mark Donelan
National Water Research Institute
867 Lakeshore Road
Burlington, Ontario
L7R 4A6

B.M. Eid
MacLaren Plansearch Limited
Suite 701, Purdy's Wharf Tower
1959 Upper Water Street
Halifax, Nova Scotia
B3J 3N2

Mona El-Tahan
Fenco Newfoundland Ltd.
P.O. Box 248, Stn. C
St. John's, NF
A1C 5J2

T. Colleen Farrell
METOC Centre
FMO Halifax
Halifax, Nova Scotia
B3K 2X0

David Fissel
Arctic Sciences Ltd.
100 Ilsley Avenue,
Unit AA
Dartmouth, Nova Scotia
B3B 1L3

Dr. P.E. Francis
Meteorological Office
London Road, Bracknell
Berkshire RG12 2S7
United Kingdom

Dr. Nelson G.S. Freeman
RADARSTAT Project Office
110 O'Connor Street, Suite 200
Ottawa, Ontario
K1A 5M9

Scott Glenn
Shell Development Company
P.O. Box 481
Houston, Texas
U.S.A.

David Green
Seakem Oceanography Ltd.
Argo Building
Bedford Institute of
Oceanography
Box 696
Dartmouth, Nova Scotia
B2Y 3Y9

J. Arthur Greenwood
Oceanweather Inc.
5 River Road
Cos Cob, CT 06807
U.S.A.

Johananes Guddal
Norwegian Met. Institute
Allegt. 70, 5000 Bergen
Bergen, Norway

Dr. John Harper
Dobrocky Seatech Ltd.
9765 West Saanich Road
P.O. Box 6500
Sidney, B.C.
V8L 4M7

Sverre Haver
Statoil
P.O. Box 300
N4001 Stavanger, Norway

Donald O. Hodgins
Seaconsult Marine
Research Ltd.
820-1200 W 73rd Avenue
Vancouver, B.C.
V6P 6G5

Ralph Horne
Atmospheric Environment
Service
Department of Environment
10 Wellington Street
Hull, Quebec

Dr. Norden E. Huang
ONR/NASA
ONR 1122PO
800 North Quincy Street
Arlington, VA 22217-5000
U.S.A.

Stephen Johnson
METOC Centre
FMO Halifax
Halifax, Nova Scotia
B3K 2XO

M.L. Khandekar
Atmospheric Environment
Service
Department of Environment
4905 Dufferin Street
Downsview, Ontario
M3H 5T4

Dr. G.J. Komen
Royal Netherlands Met.
Institute
P.O. Box 201
3730 AE De Bilt
The Netherlands

Roop Lalbeharry
Atmospheric Environment
Service
Department of Environment
4905 Dufferin Street
Downsview, Ontario
M3H 5T4

Dr. P. Leblond
University of British Columbia
Oceanography Department
Vancouver, B.C.
V6T 1W5

Wayne Lumsden
METOC Centre
FMO Halifax
Halifax, Nova Scotia
B3K 2X0

Ken MacDonald
Atmospheric Environment Service
Maritimes Weather Centre
1496 Bedford Highway
Bedford, Nova Scotia
B4A 1E5

Hugh McPherson
Oceanroutes Canada
1469 Bedford Highway
Bedford, Nova Scotia
B4A 1E5

Dr. C.S. Mason
Coastal Oceanography Division
Department of Fisheries & Oceans
P.O. Box 1006
Dartmouth, Nova Scotia
B2Y 4A2

David Milburn
Canada Oil and Gas Lands
Administration
355 River Road
Ottawa, Ontario
K1A 0E4

James Moir
Esso Resources Canada Ltd.
339 50th. Avenue SE
Calgary, Alberta
T2G 2B3

Dr. Langley R. Muir
Canada Oil and Gas Lands
Administration
355 River Road
Ottawa, Ontario
K1A 0E4

Jorgen Bo Nielsen
Danish Hydraulic
Institute
Agern Alle 3-5
DK 2970 Horsholm
Denmark

John P. O'Reilly
Environment Canada
Ontario Weather Centre
P.O. Box 159
Toronto, AMF, Ontario
L5P 1B1

Dr. W. Perrie
Coastal Oceanography
Division
Department of Fisheries &
Oceans
P.O. Box 1006
Dartmouth, Nova Scotia
B2Y 4A2

R.L. Pickett
Department of the Navy
Naval Ocean Research and
Development Activity
NSTL Station, MS 38529
U.S.A.

John Readshaw, P. Eng.
W.F. Baird and Associates
Ltd.
Suite 150
38 Antares Drive
Ottawa, Ontario
K2E 7V2

Magnar Reistad
Norwegian Met. Institute
Allegt. 70, 5000 Bergen
Bergen, Norway

Dr. Donald T. Resio
Offshore & Coastal
Technologies Inc.
911 Clay Street
Vicksburg, Mississippi
39180
U.S.A.

Kathryn J. Resio
Offshore & Coastal
Technologies Inc.
911 Clay Street
Vicksburg, Mississippi
39180
U.S.A.

William Richards
Atmospheric Environment
Service
Department of Environment
1496 Bedford Highway
Bedford, Nova Scotia
B4A 1E5

David W. Robinson
Lloyd's Register of Shipping
71 Fenchurch Street
London, England

Paul Roebber, M.Sc.
The MEP Company
7050 Woodbine Ave., Suite 100
Markham, Ontario
L3R 4G8

Irene Rubinstein
Ph.D. Associates
4700 Keele Street
North York, Ontario
M3J 1P3

Dr. Ken Sato
Canada Oil and Gas Lands
Administration
355 River Road
Ottawa, Ontario
K1A 0E4

A. Saulesleja
Atmospheric Environment Service
Department of Environment
4905 Dufferin Street
Downsview, Ontario
M3H 5T4

Hassan M. Shabib
ARAMCO/Saudi Career Dev.
9009 W. Loop South
P.O. Box 53211
Houston, Texas 77096
U.S.A.

Rod Shaw
Fisheries & Oceans Canada
Bedford Institute of
Oceanography
P.O. Box 1006
Dartmouth, Nova Scotia
B2Y 4A2

P.C. Smith
Fisheries & Oceans Canada
Bedford Institute of
Oceanography
P.O. Box 1006
Dartmouth, Nova Scotia
B2Y 4A2

Ted Spearing
Chevron Canada Resources
Ltd.
500 5th. Avenue S.W.
Calgary, Alberta
T2P 0L7

Norman Stevenson
Oceanroutes Inc.
3260 Hillview Avenue
Palo Alto, California
94304
U.S.A.

Ming-Yang Su
NORDA, Code 331
NSTL, Mississippi 39529
U.S.A.

Val R. Swail
Atmospheric Environment
Service
Department of Environment
4905 Dufferin Street
Downsview, Ontario
L3Y 3R9

David Szabo
Mobil R & D
Offshore Engineering
P.O. Box 819047
Dablo, Texas 75381-9047
U.S.A.

Bechara Toulany
Coastal Oceanography Division
Department of Fisheries & Oceans
P.O. Box 1006
Dartmouth, Nova Scotia
B2Y 4A2

Charles L. Vincent
U.S. Army Engineer
Waterways Experimental Station
Coastal Engineering Research
Centre
P.O. Box 631
Vicksburg, Mississippi 39180
U.S.A.

Ronald K. Watanabe
Martec Limited
5670 Spring Garden Road
Halifax, Nova Scotia
B3J 1H6

Dr. J.R. Wilson
Marine Environmental Data
Service
Department of Fisheries & Oceans
200 Kent Street
Ottawa, Ontario
K1A 0E6

Liana F. Zambresky
Fleet Numerical Oceanography Centre
Code 42
Monterey, California 9390
U.S.A.